eman ta zabal zazu

Universidad del País Vasco
Euskal Herriko Unibertsitatea

Reproductive constraints and gonadal alterations in fish locally exposed to pollutants: how life history shapes exposure

International PhD Thesis

ANTHONY NZIOKA MUTUA

Under the supervision of

Ibon Cancio Uriarte

and

Oihane Diaz De Cerio Arruabarrena

2023

Plentziako Itsas Estazioa
Estación Marina de Plentzia

eman ta zabal zazu
Universidad del País Vasco
Euskal Herriko Unibertsitatea

ZIENTZIA ETA TEKNOLOGIA FAKULTATEA
FACULTAD DE CIENCIA Y TECNOLOGÍA

DEPARTMENT OF ZOOLOGY AND ANIMAL CELL BIOLOGY

CELL BIOLOGY IN ENVIRONMENTAL TOXICOLOGY AND ONE HEALTH (CBET+) RESEARCH GROUP

Reproductive constraints and gonadal alterations in fish locally exposed to pollutants: how life history shapes exposure

International PhD Thesis submitted by

ANTHONY NZIOKA MUTUA

For the degree of

Philosophiae Doctor

Leioa, December 2023

Cover image credits:

Cover artwork design by Marisa Hudlin

Thesis Director 1: Prof. Ibon Cancio Uriarte

Thesis Director 2: Dr. Oihane Diaz de Cerio Arruabarrena

Recommended citation:

Nzioka, A., 2023. Reproductive constraints and gonadal alterations in fish locally exposed to pollutants: how life history shapes exposure. PhD Thesis. Department of Zoology and Animal Cell Biology, University of the Basque Country, 296 pp.

"Bahari haivukwi kwa kuogelea."

"The ocean is not crossed by swimming."

Swahili Proverb

This work was funded by:

- The University of the Basque Country (UPV/EHU) pre-doctoral grant (PIF17/172) to Anthony Nzioka Mutua.

- The Spanish Ministry of Science, Innovation and Universities and EU-FEDER/ERDF (ATREoVO AGL2015-63936-R and BORN2bEGG PGC2018-101442-B-I00).

- The Basque Government (Grants to consolidated research groups IT1302-19 and IT1743-22).

- The Association of European Marine Biological Laboratories Expanded (ASSEMBLE Plus) Horizon-2020 project through the Transnational Access (TNA) programme mobility grant (ASSEMBLE Plus no. 730984) to Anthony Nzioka Mutua.

- Partial support from the Strategic Funding UID/Multi/04423/2019 through national funds provided by FCT and European Regional Development Fund (ERDF), in the framework of the program PT2020.

Acknowledgements

I would like to convey my sincere thanks to the many people who contributed significantly to the research and completion of this thesis. Their continuous support and invaluable advice were essential in making this endeavour a reality. It brings me great pleasure to acknowledge and appreciate all who have contributed to this accomplishment.

I'd like to thank my two supervisors for their contributions to my successful completion of my PhD studies as an international student. Prof. Ibon Cancio deserves a special thanks for taking the effort to promote my candidature in the Marine Environment and Resources (MER) doctoral program while I was in Kenya. Furthermore, I would like to express my heartfelt gratitude to Dr. Oihane Diaz de Cerio for her constant assistance and encouragement throughout my candidacy. I am extremely grateful for their persistent support. Their unwavering commitment to scientific research and meticulous approach to every aspect of their work has greatly contributed to my growth as both a scientist and a writer. I am eternally grateful for the priceless knowledge and abilities I have gained as a result of their mentoring.

I'd like to thank Prof. Ionan Marigómez, the coordinator of the Postgraduate MER program, for accepting me into the doctoral program. Further thanks go to Prof. Miren Carajaville, former head of the Cell Biology in Environmental Toxicology and One Health (CBET+) research group, for accepting me into the research group. My warmest thanks go to everyone in the CBET+ research group who helped collect samples, gave guidance, and made me feel welcome. This includes everyone at the UPV/EHU Leioa Campus and the Plentzia Marine Station (PiE-UPV/EHU), as well as the excellent contributions of all the students and the current head of the CBET+ research group, Dr. Maren Ortiz-Zarragoitia who was instrumental in guiding my sampling strategies. Thank you, Dr. Xabier Lecube, for granting access to samples in the Biscay Bay Environmental Biospecimen Bank (BBEBB), and thank you, Dr. Urtzi Izaguirre, for being the "mullet whisperer". Without you, no sampling program would have been effective. Beñat, thank you for your insights in various aspects of histology and immunohistochemistry techniques. Tamer, Aitor, Erik, Laura, Denis, Tiff, Joy, Markel, Txema, Ainara, Endika, Luisma, Nagore, Irune, Lupe, Christopher, Hossain, Priyanka, and Gourab, thank you for your assistance during sampling campaigns. Dr. Maria Korta (AZTI) kindly donated samples acquired from commercial fishing vessels, and Dr. Lambros Kokoris (International Hellenic University) kindly gave samples from Greece. I thank you both for this, as well as your comments on drafts of chapters 1 and 3.

I would like to thank colleagues from the Genetics Lab (FCT-UPV/EHU) for contributing their expertise to the improvement of immunoblotting or western blot analysis techniques.

I'd like to thank the Systematics, Biogeography, and Population Dynamics (SystBioGen) Research Group for hosting me in their lab for three months, especially Dr. Maria José

Madeira for sharing her extensive knowledge of population genetics and her efforts while performing and analysing microsatellite loci investigations. Thank you for teaching me how to genotype microsatellite loci. During my stay, I had the opportunity to learn a great deal from you.

Further thanks are extended to the Interdisciplinary Centre of Marine and Environmental Research (CIIMAR) in Porto, Portugal, and Dr. Alberto Teodorico Correia, leader of the Ecophysiology Team at CIIMAR, for allowing me to join his team as part of my international experience. He trained me on otolith shape and microchemistry analyses, which included otolith sectioning for age determination and laser-ablation ICP-MS and made sure my stay went smoothly. Dr. Rafael Schroeder in Alberto's Lab, your expertise in analysing digitized otolith images with the R package *ShapeR*, as well as your advice on Canonical Analysis of Principal (CAP) coordinates, was invaluable. Thank you for your valuable time. To Dr. Paulo Almeida, thank you for sharing your knowledge while we polished otoliths together. Dr. Edgar Pinto and Dr. Agostinho Almeida (Associated Laboratory for Green Chemistry (LAQV) of the Network of Chemistry and Technology (REQUIMTE), University of Porto) deserve special thanks. Your assistance and support in carrying out the otolith microchemical elemental analyses was invaluable, and to Ruiz Azevedo, thank you for your technical assistance and invaluable insights while using the ICP-MS.

Dr. Ana Mendez-Vincente (Scientific Technical Support (SCT/STS) service of the Environmental Testing Unit, University of Oviedo, Mieres Campus) was especially helpful in performing and analysing laser-ablation ICP-MS. Your knowledge was invaluable, and I would have been lost without it. Together with your colleagues, you made certain that my stay in Mieres went smoothly. I'd also like to thank Dr. Felipe Daros (São Paulo State University – International (UNESP), Brazil) for sharing his expertise in reconstructing life history patterns from laser-ablation ICP-MS data and for providing invaluable advice on the use of Change-Point Analysis (CPA).

I would like to thank Prof. James Njiru, Chief Executive Officer of Kenya Marine and Fisheries Research Institute (KMFRI), as well as the KMFRI management for providing me with the opportunity to pursue my doctoral studies. All those at KMFRI who have provided their support, I thank you too.

To all my friends and colleagues who cheered me on silently and openly, inspiring my final push despite the challenges and enormous work pressures, Matt, James, Xabi, Macs, Pete, Marisa, Holly... the list is long, thank you for keeping me sane outside of academia. Erik, Tamer, Ainara, Nacho, Tiff, Joy, Nagore, Iratxe, Alberto, Txema, Nerea, Ada, Eva, Lupe, Sonia, Noemi, Mar, Camila, Gaybrielle, Argellia... thank you for all the coffees and the good laughs.

Last but not least, I'd like to express my gratitude to my family. This journey would not have been possible without your unwavering love and support.

RESUMEN

La presencia global de contaminantes y sustancias químicas contaminantes en el medio acuático supone una amenaza para los organismos expuestos, lo que recibe una atención cada vez mayor tanto por parte de la comunidad científica como del público en general. Algunas de estas sustancias químicas pueden alterar potencialmente las vías endocrinas que controlan la reproducción en los animales expuestos, dando lugar, en el caso de la exposición a xenoestrógenos, a un aumento de la atresia ovárica, una alteración del desarrollo gonadal y la feminización de los peces. Esta tesis investigó los mecanismos moleculares y celulares que subyacen a la atresia en dos especies, la merluza europea (*Merluccius merluccius*) y el muble (*Chelon labrosus*), así como el modo en que las alteraciones gonadales observadas en los mújoles de labios gruesos que habitan entornos cargados de xenoestrógenos en algunos estuarios del sur del Golfo de Vizcaya están determinadas por sus rasgos vitales. Los mecanismos moleculares que regulan las alteraciones gonadales se estudiaron en ambas especies a nivel de transcripción génica y expresión proteica mediante métodos estándar de qPCR e inmunotransferencia, respectivamente. La mayoría de los ovarios de ambas especies presentaban folículos atrésicos, independientemente de la fase de desarrollo, y los mecanismos que regulan la atresia folicular parecen implicar respuestas tanto apoptóticas como autofagocíticas. Se utilizaron marcadores de microsatélites para evaluar la estructura genética y la conectividad de los mubles con el fin de conocer el nivel de flujo genético, mientras que la forma de los otolitos y la química elemental se emplearon para evaluar la estructura de la población, la conectividad del hábitat y los atributos del ciclo biológico de la misma especie a partir de peces recogidos en dos estuarios con distinta carga de xenoestrógenos, Gernika y Plentzia (sin xenoestrogenicidad). Los resultados del análisis de marcadores microsatélites hallaron indicios de diferenciación genética entre individuos o localidades, revelando una única población genética de *C. labrosus* en todas las localidades muestreadas. *C. labrosus* mostró una amplia homogeneidad genética y panmixia en toda la zona muestreada, abarcando las cuencas atlántica y mediterránea. La forma de los otolitos y el análisis elemental de los mubles estudiados recogidos en los dos estuarios de Gernika y Plentzia mostraron distintas agrupaciones de subpoblaciones locales con una conectividad limitada entre los dos estuarios cercanos. La reconstrucción de la historia migratoria de los mubles entre los dos estuarios utilizando firmas químicas elementales de secciones transversales de otolitos reveló dos historias vitales principales y distintas en los peces estudiados con diferentes comportamientos de movimiento diádromo al comparar ambos estuarios: residentes estuarinos y migrantes marinos. La mayoría de los individuos de Gernika fueron siempre residentes estuarinos y probablemente nunca desovaron en comparación con todos los individuos de Plentzia que migraron al océano después de pasar sus primeros 2 - 3 años en el estuario, posiblemente para desovar. Esta tesis demuestra que, a pesar de la presencia de panmixia en los mubles del sur de Europa, los individuos que migran al mar para reproducirse parecen regresar a su estuario de origen y que los efectos xenoestrogénicos que resultan en la condición intersexual y la atresia observada en estuarios contaminados como Gernika es muy probablemente el resultado de la exposición a xenoestrógenos durante toda la vida y la incapacidad de madurar reproductivamente de forma adecuada, e impidiendo que los individuos participen en la migración reproductiva anual para desovar en mar abierto.

MUHTASARI

Uwepo mkubwa wa uchafuzi wa kemikali katika mazingira ya majini ni tishio kwa viumbe vya majini na wanyama wenye uti wa mgongo, na hii imepata tahadhari kuongezeka kutoka kwa jamii ya kisayansi na umma kwa ujumla. Baadhi ya kemikali hizi zinaweza kuvuruga njia za endocrini ambazo zinadhibiti uzazi katika wanyama waliowachwa wazi, na kusababisha kesi ya mfiduo ya kemikali nakala ya estrojeni, kuongezeka kwa atresia ya ovari, mabadiliko ya maendeleo ya gonadi na uke au uume ya samaki kulingana na jinsia ya awali. Tasnifu hii ilichunguza taratibu za molekuli na seli zinazotokana na atresia katika spishi mbili, hake ya Ulaya (*Merluccius merluccius*) na aina ya mkizi yenye midomo-minono (*Chelon labrosus*), na pia vile jinsi mabadiliko ya gonadi katika mikizi zinazoishi katika mazingira yaliyojaa kemikali nakala ya estrojeni katika baadhi ya mito ya kusini mwa Ghuba ya Biscay imeundwa na sifa za historia ya maisha yao. Mifumo ya molekuli inayodhibiti mabadiliko ya gonadi ilichunguzwa katika spishi zote mbili katika unukuzi wa jeni na viwango vya kujieleza kwa protini kwa kutumia qPCR ya kawaida na mbinu za immunoblotting, kwa mtiririko huo. Ovari nyingi za spishi zote mbili zilionyesha kukabiliwa na atresia bila kujali hatua ya ukuaji, na taratibu za udhibiti wa atresia ya folikoli ilionekana kuhusisha mwitikio wa apoptosis na autophagocytosis. Alama za satelaiti ndogo zilitumika kutathmini muundo wa kijenetiki na muunganisho katika mikizi ili kuelewa kiwango cha mtiririko wa jeni, wakati umbo la otolith na vipengeli vya kemikali katika otolith zilitumiwa kutathmini muundo wa idadi ya samaki hii, muunganisho wa makazi na sifa za historia ya maisha ya spishi hii kutoka kwa samaki waliokusanywa kutoka kwa mito miwili yenye mizigo tofauti za kemikali nakala ya estrojeni, Gernika na Plentzia (hakuna athari za kemikali nakala ya estrojeni). Matokeo kutoka kwa uchanganuzi wa alama za satelaiti ndogo haukupata ushahidi wa tofauti za kijeni kati ya mikizi au maeneo yaliyofanyiwa utafiti, ikifichua idadi moja ya kinasaba ya *C. labrosus* katika maeneo yote yaliyofanyiwa utafiti. *C. labrosus* ilionyesha usawa wa kijenetiki ulioenea na panmixia katika eneo lililotolewa sampuli, ikianzia bahari ya Atlantiki mpaka Mediterania. Uchanganuzi wa umbo la otolith na vipengele vya kemikali katika otolith za mikizi zilizochunguzwa na zilizokusanywa kutoka kwa mito miwili ya Gernika na Plentzia ulionyesha vikundi tofauti vya wakazi wa eneo hilo, na muunganisho mdogo kati ya mito hayo miwili ya karibu. Kuunda upya historia ya uhamaji wa mikizi kati ya mito hayo miwili kwa kutumia saini za kemikali za kimsingi zilizopimwa katika sehemu za “otolith” kulifunua historia mbili kuu na tofauti za maisha katika samaki waliochunguzwa, pamoja na tabia tofauti za harakati wakati wa kulinganisha mito yote miwili: wakaazi wa mito na wahamiaji wa baharini. Samaki wa kutoka mto wa Gernika walikuwa daima wakaaji wa mto huo na kuna uwezekano ya kua hawakuwahi zaa ikilinganishwa na samaki wote kutoka Plentzia ambao walihamia baharini baada ya kukaa miaka yao 2 - 3 ya kwanza kwenye mlango wa mto, labda kwa ajili ya kuzaa. Tasnifu hii inaonyesha kwamba, licha ya kuwepo kwa panmixia katika mikizi kutoka kusini mwa Ulaya, mikizi wanaohamia baharini kwa ajili ya kuzaliana wanaonekana kurudi kwenye mto wao wa asili. Athari za kemikali nakala ya estrojeni zinazosababisha hali ya jinsia tofauti na atresia kuonekana katika samaki wanaoishi katika mito iliyochafuliwa na kemikali, kama vile Gernika, inaonyesha kuna uwezekano mkubwa kuwa ni matokeo ya mfiduo wa muda mrefu wa kemikali nakala ya estrojeni na kutokuwa na uwezo wa kukomaa kwa uzazi ipasavyo, pamoja na kuzuia samaki binafsi kushiriki katika uhamaji wa uzazi wa kila mwaka na kuzaa katika bahari ya wazi.

SUMMARY

The global presence of chemical pollutants and contaminants in the aquatic environment poses a threat for the organisms exposed and this receives increasing attention from both the scientific community and the public in general. Some of these chemicals may potentially disrupt endocrine pathways that control reproduction in exposed animals, resulting in the case of exposure to xenoestrogens, to increased ovarian atresia, altered gonadal development and the feminisation of fish. This thesis investigated the molecular and cellular mechanisms underlying atresia in two species, European hake (*Merluccius merluccius*) and thicklip grey mullets (*Chelon labrosus*), as well as how gonad alterations observed in thicklip grey mullets inhabiting xenoestrogen-loaded environments in some estuaries of the southern Bay of Biscay (SBB) are shaped by their life history traits. The molecular mechanisms regulating gonadal alterations were studied in both species at the gene transcription and protein expression levels using standard qPCR and immunoblotting methods, respectively. Most ovaries of both species displayed atretic follicles irrespective of developmental stage and the mechanisms regulating follicular atresia seem to involve both apoptotic and autophagocytic responses. Microsatellite markers were used to evaluate the genetic structure and connectivity in mullets to understand the level of gene flow, while otolith shape and elemental chemistry was used to assess population structure, habitat connectivity and life history attributes of the same species from fish collected from two estuaries with distinct burdens of xenoestrogens, Gernika and the Plentzia (no xenoestrogenicity). The results from microsatellite marker analysis found no evidence of genetic differentiation among individuals or locations, revealing a single genetic population of *C. labrosus* in all sampled locations. *C. labrosus* displayed widespread genetic homogeneity and panmixia across the sampled area, spanning the Atlantic and Mediterranean basins. Otolith shape and elemental analysis of the studied mullets collected from the two estuaries of Gernika and Plentzia showed distinct local subpopulation groupings with limited connectivity between the two close estuaries. Reconstructing the migratory history of mullets among the two estuaries using elemental chemical signatures of transverse otolith sections revealed two main and distinct life histories in the studied fish with different diadromous movement behaviours when comparing both estuaries: estuarine residents and marine migrants. Most individuals from Gernika were always estuarine residents and likely never spawned compared to all individuals from Plentzia that migrated to the ocean after spending their first 2 – 3 years in the estuary, possibly for spawning. This thesis demonstrates that, despite the presence of panmixia in thicklip grey mullets from southern Europe, individuals migrating to the sea for reproduction appear to return to their estuary of origin and that the xenoestrogenic effects resulting intersex condition and atresia observed in contaminated estuaries such as Gernika is most likely the result of life-long exposure to xenoestrogens and incapacity to reproductively mature properly, and preventing individuals from participating in the annual reproductive migration to spawn in the open ocean.

TABLE OF CONTENTS

I. GENERAL INTRODUCTION

Abbreviations

BPA, bisphenol A
BFT, bluefin tuna
CEC, chemicals of emerging concern
CWT, coded wire tags
DDT, dichlorodiphenyltrichloroethane
DNA, deoxyribonucleic acid
DST, data storage tags
E_2, oestradiol
ED, endocrine disruptors
EDC, endocrine disrupting chemicals
EE_2, ethinylestradiol
EFD, elliptic Fourier descriptors
EPA, Environmental Protection Agency
ER, oestrogen receptor
GC, granulosa cells
GtH, gonadotropin-releasing hormone
HPG, hypothalamus-pituitary-gonadal
HPT, hypothalamus-pituitary-thyroid
INDELS, insertion-deletions
LA-ICP-MS, laser ablation-inductively coupled plasma-mass spectrophotometry
lcWGS, low-coverage whole genome sequencing
MES, multi-elemental signatures
mrPAT, mark-report satellite tags
mtDNA, mitochondrial DNA
NGS, next generation sequencing
PCB, polychlorinated biphenyls
PCB, polychlorinated biphenyls
PFAS, polyfluoroalkyl substances
PIT, passive integrated transponder tags
POC, postovulatory complexes
POP, persistent organic pollutants
PPCP, pharmaceuticals and personal care products
PSAT, pop-up satellite archival tags
RAD-seq, restriction site-associate DNA sequencing
RFID, radio frequency identification
RNA, ribonucleic acid
rRNA, ribosomal ribonucleic acid
SB-ICP-MS, solution based-inductively coupled plasma-mass spectrophotometry
SNP, single nucleotide polymorphisms
SSLP, simple sequence length polymorphisms
SSR, simple sequence repeats
STR, short tandem repeats
T3, triiodothyronine
T4, thyroxine
TBT, tributyltin
TCDD, tetrachlorodibenzo-p-dioxin
TH, thyroid hormone
Vtg, vitellogenin
WGS, whole genome sequencing

1. Pollutant exposure in the marine environment

The increase in human activities have led to the contamination and subsequent pollution of varied ecosystems including the highly fragile, complex and diverse estuarine areas. Pollution reaches the aquatic environment through a variety of routes (Figure 1), which include both point and non-point (diffuse) sources (Frid and Caswell, 2017). Aquatic environments act as sinks, accumulating anthropogenic chemical and solid contaminants from both urban and industrial wastes, altering the physical and chemical characteristics of the environment and threatening the health of living aquatic life and ecosystem services (Borja et al., 2010; Halpern et al., 2007).

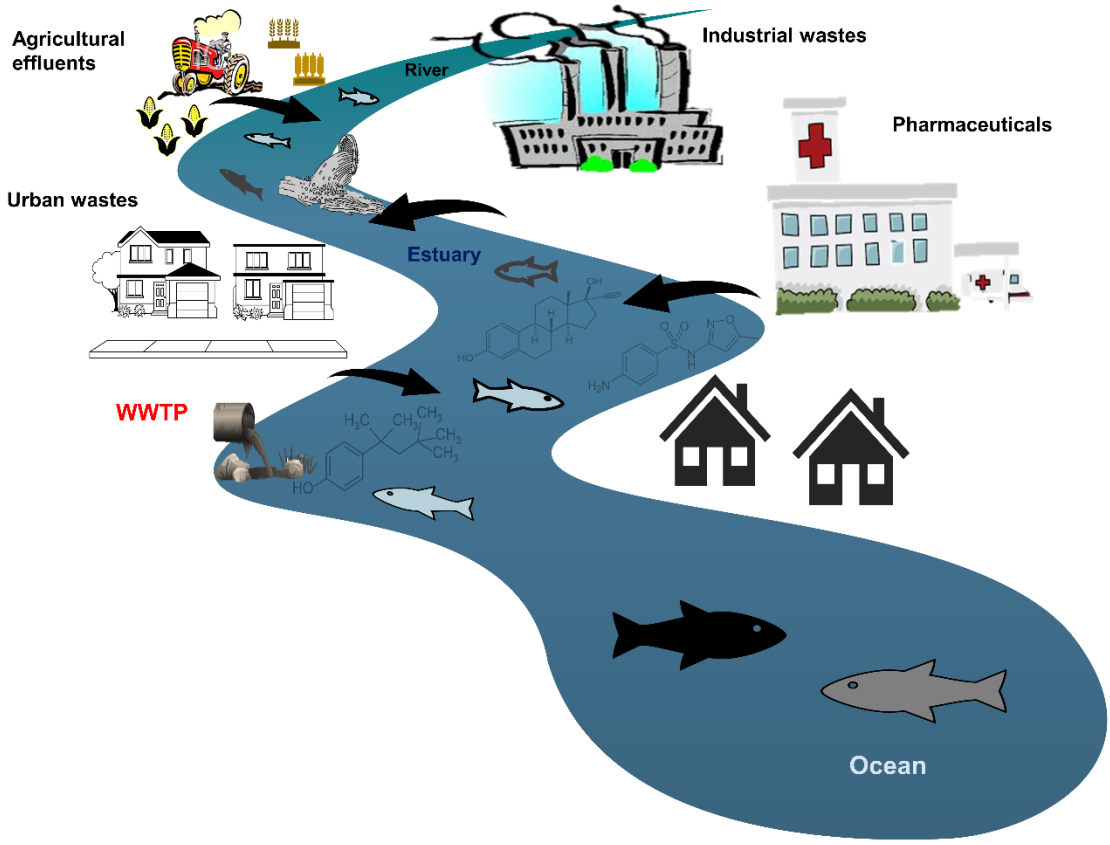

Figure 1
Point and non-point (diffuse) sources of pollution and the movement of pollutants into the aquatic environment.

Historically, aquatic pollution is as old as the history of the planet and the history of life (Frid and Caswell, 2017); however, it did not receive the significant consideration it deserved until a threshold level was reached and adverse outcomes on ecosystems and living organisms, including humans, became evident (Frid and Caswell, 2017; Halpern et al., 2007; Shahidul Islam and Tanaka, 2004). In recent decades, the global presence of chemical pollutants and contaminants in the aquatic environment has received increasing attention

from both the scientific community and the general public (Li, 2014; Petrie et al., 2015; Sörengård et al., 2019). Although the discharge of oil containing naturally occurring hazardous substances, widespread heavy metal pollution and the presence of persistent organic pollutants (POPs) such as PCBs (polychlorinated biphenyls) and DDT (dichlorodiphenyltrichloroethane) is an ongoing problem, emerging pollutants or chemicals of emerging concern (CECs) that include nanoparticles, pharmaceuticals and personal care products (PPCPs), industrial chemicals, per- and polyfluoroalkyl substances (PFASs), agrochemicals and pesticides have potential bio-accumulative and toxic characteristics (Golovko et al., 2021; Ismail et al., 2017; Meyer et al., 2019; Petrie et al., 2015; Sörengård et al., 2019) that have brought them into the spotlight. These CECs contaminate the aquatic environment and some of which may potentially disrupt the endocrine system of aquatic organisms.

CECs that disrupt the normal functioning of the endocrine system in animals are classified as endocrine disruptors (ED) or endocrine disrupting chemicals (EDC) (Figure 2). Several definitions of an ED in terms of both the mode of action (ability to interfere with hormone action) and the ability to cause harm, have been proposed. The United States Environmental Protection Agency (EPA) defines an EDC as “an exogenous agent that interferes with the synthesis, secretion, transport, binding, action and elimination of natural hormones in the body, that are responsible for the maintenance of homeostasis, reproduction, development and/or behaviour” (EPA, 2001). A simpler version of the EPA definition proposed by Zoeller et al. (2012) defined an ED to be an exogenous chemical, or mixture of chemicals that interferes with any aspect of hormone action. EDCs interact with the endocrine system, interfering with the neuroendocrine and/or endocrine functions involved in embryo development and reproduction (Carnevali et al., 2018), thereby compromising the survival of exposed individuals and populations (Hachfi et al., 2012; Jiang et al., 2016, 2015a, 2015b; Zoeller et al., 2012).

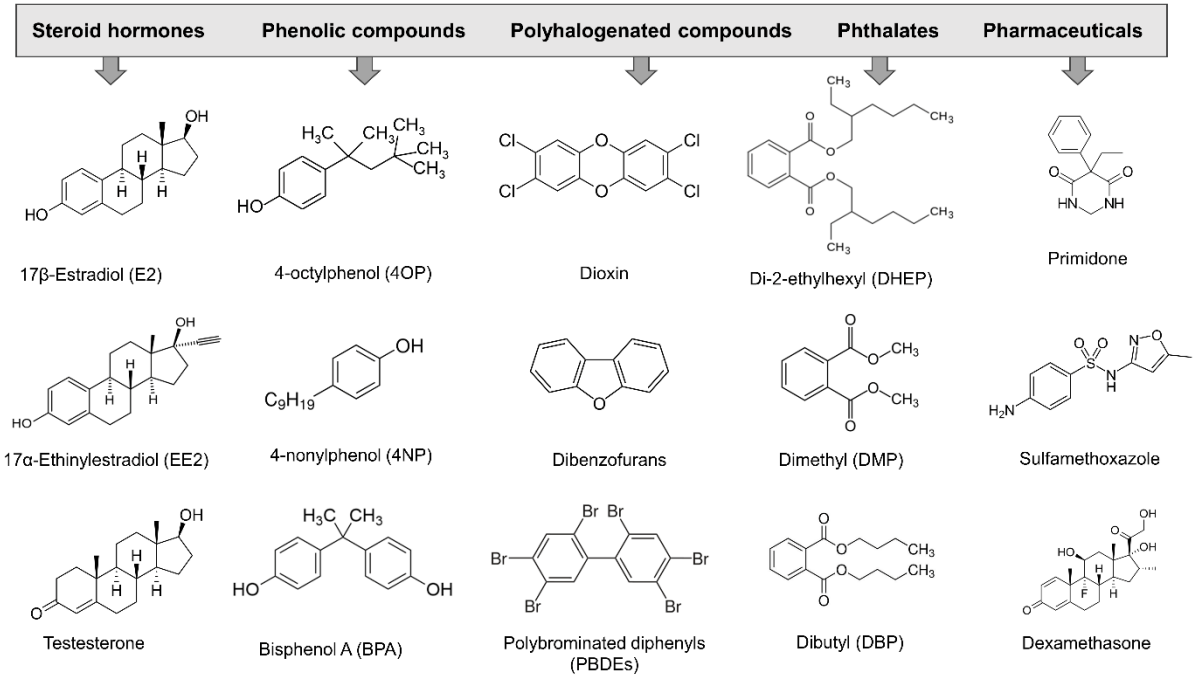

Figure 2
Molecular structure of some endocrine disrupting compounds present in the aquatic environment (modified from Ismail et al., 2017).

2. Effects of endocrine disruption effects on marine organisms

The impact of early exposures to EDCs has been linked to a variety of effects in fish (Figure 3), including altered growth and development profiles, impacted immune function, modified gene expression and altered DNA methylation, decreased egg production, increased ovarian atresia, altered gonadal development and feminisation or masculinisation of fish populations (Delbes et al., 2022; Hinck et al., 2007; Major et al., 2020; Schug et al., 2016). Immediate EDC effects may be observed shortly after exposure, but it is also possible that the phenotypic consequences of molecular responses are visible only later after exposure or during the development of exposed animals (Delbes et al., 2022). In complex mixtures, EDCs can interact and enhance (or reduce) their potency and biological activity, and are thus able to act in an agonistic, antagonistic and/or synergistic manner, altering endocrine pathways, including those that control reproduction (Brander, 2013; Goksøyr, 2006).

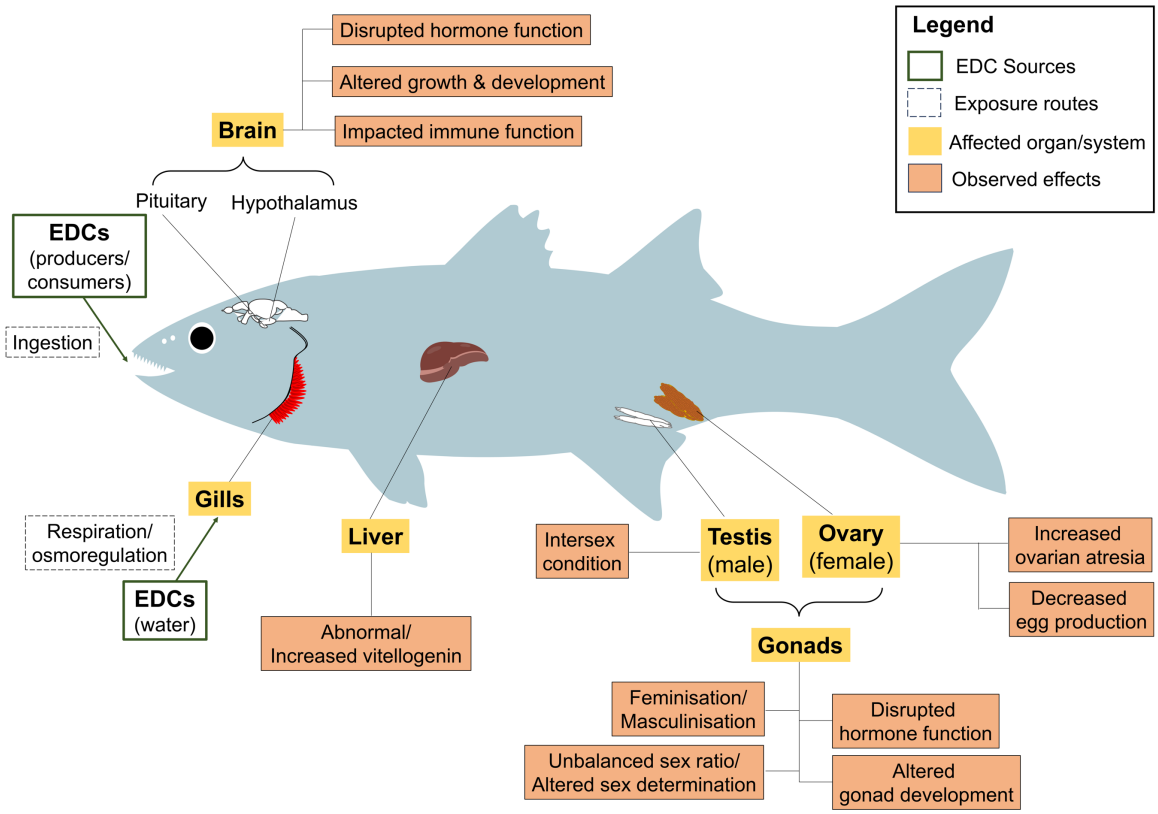

Figure 3
A summary some of the common exposure routes and potential effects of endocrine disrupting chemicals (EDCs) in wild fish (modified from Ismail et al., 2017).

In marine gastropods, tributyltin (TBT), an organotin biocide, is known to disrupt the endocrine control of sexual development resulting in the masculinisation of females or resulting in what it is known as the imposex condition (Beyer et al., 2022; Laranjeiro et al., 2018; Schøyen et al., 2019). Its banning from use in marine antifouling paints has led to reproductive health recovery in marine gastropod populations globally (Schøyen et al., 2019). Exposure to TBT and oestrogenic ethinylestradiol (EE_2), either separately or together, has also been shown to disrupt the morphological and behavioural developmental patterns of juvenile, black-striped pipefish *Syngnathus abaster*, affecting their early survival and having profound implications for population structure, from a decrease in recruitment to disruption of sexual selection (Sária et al., 2011).

Many of the EDCs have the potential to disrupt thyroid hormone (TH) function along the hypothalamus-pituitary-thyroid (HPT) axis in vertebrates, including aquatic organisms (Campinho et al., 2015). The thyroid gland produces TH, which comprises of the prohormone thyroxine (T4) and the active hormone triiodothyronine (T3), both of which are critical and necessary in regulating post-embryonic development (Campinho, 2019). Post-

embryonic metamorphosis in amphibians and teleosts is dependent on TH signalling to mediate the morphological changes seen in vertebrate early development during the transition from larvae to juvenile (Campinho, 2019; Campinho et al., 2015; Thambirajah et al., 2019). In *Xenopus laevis* tadpoles (and most teleosts), TH analogs in a variety of PPCPs (methimazole, ibuprofen, triclosan, etc) and industrial chemical products (PCBs, BPAs, Phthalates, etc) can act as thyroid-disrupting compounds and can disrupt TH synthesis (through deiodination of T4 to T3), transport (through interference with plasma distributing proteins), or metabolism of thyroid hormones along the HPT axis, resulting in delayed and/or inhibited natural progression of metamorphosis (Noyes and Stapleton, 2014; Thambirajah et al., 2019). In pleuronectid fish (flatfishes), symmetric larvae normally develop into asymmetric juveniles, which are distinguished by the migration of one eye to the opposite side of the head and the tilting of the body axis towards the migrating eye side (Campinho, 2019; Campinho et al., 2015). Thus, in the presence of EDCs such as methimazole which acts as a TH analog, metamorphosis has been observed to be blocked in larvae of Senegalese sole *Solea senegalensis* and the migration of the eye impaired (Campinho et al., 2015).

2.1. Xenoestrogenicity in wild fish populations

Mechanistically, xenoestrogen compounds mimicking the female hormone oestradiol (E_2) can bind to the oestrogen receptor (ER) in vertebrates and regulate transcription of downstream oestrogenic response genes. E_2 is a major oestrogen in oviparous vertebrates that stimulates hepatic ERs to induce transcription of vitellogenin (Vtg), an egg-yolk precursor protein (Meucci and Arukwe, 2006). Vtg is naturally expressed in mature females by oestrogen induction, but under xenoestrogenic exposure, it can be expressed in both males and immature juveniles (Arukwe and Goksøyr, 2003; Matthiessen, 2003; Tyler and Jobling, 2008). Several studies have reported an increase in hepatic levels of Vtg synthesis in immature and male fishes exposed to natural oestrogens and xenoestrogens (Bahamonde et al., 2013; Jobling et al., 1998; Kidd et al., 2007; Lindholst et al., 2000; Prado et al., 2014; Scott et al., 2007; Sumpter and Jobling, 1995). For example, persistent exposure to alkyl phenolic compounds that are weak ER agonists have been shown to elevate Vtg synthesis and inhibit testicular growth in rainbow trout (Jobling et al., 1996), while chronic exposure to the potent synthetic oestrogen EE_2 can promote Vtg mRNA upregulation, and the continued production of Vtg protein in females beyond their normal reproductive season as observed in the fathead minnow *Pimephales promelas* (Kidd et al., 2007). As such, the

induction of Vtg has been used widely as a biomarker for the presence of xenoestrogens in the environment.

EE_2 is also known to down-regulate enzymes responsible for androgen production in several fish species and to decrease testicular development in male fish (Cabas et al., 2011; Filby et al., 2007; Liarte et al., 2011; Szwejser et al., 2017). One of the best described effects of xenoestrogens (including EE_2) on aquatic organisms is the feminization of juvenile and male fish (Arukwe and Goksøyr, 2003; Bizarro et al., 2014; Goksøyr, 2006; Tyler and Jobling, 2008). The generation of ovotestis (or intersex condition) occurs when oocytes differentiate within the normal testicular tissue in gonochoristic fish species (Bahamonde et al., 2013; Bizarro et al., 2014; Matthiessen, 2003). Intersex condition in both freshwater and marine fish has been related to chemical exposure in highly to moderately contaminated areas (Bizarro et al., 2014; Ortiz-Zarragoitia et al., 2014). The exposure to both natural and synthetic oestrogens may disrupt the hypothalamus-pituitary-gonadal (HPG) axis at low level concentrations, altering the physiological production and/or release of sex hormones and associated feedback mechanisms (Decourten et al., 2020). This can alter gametogenesis and cause gonadal alterations that can be transitory or permanent (Luzio et al., 2016). This may in turn disrupt reproduction leading to possible population decline over time (Decourten et al., 2020; Decourten and Brander, 2017; Kidd et al., 2007; White et al., 2017).

Intersex males display lower reproduction capacity than normal males, with logical consequences in the sustainability of wild fish populations (Harris et al., 2011; Jobling et al., 2002b; Jobling and Tyler, 2006). However, assessing the impacts of chronic exposure through the monitoring of wild fish populations is difficult, considering that fish populations are characterized by natural fluctuations resulting from complex interactions with multiple biotic and abiotic factors (Hamilton et al., 2016). This is especially true, considering that the reasons behind significant population declines observed in salmonids (Borsuk et al., 2006; Kroglund and Finstad, 2003; Lobón-Cerviá, 2009) or in the European eel *Anguilla anguilla* (Dekker, 2003), with possible contribution of pollution, are not well understood (Hamilton et al., 2016). Tyler and Jobling (2008) hypothesized that the feminization of wild fish may result in adverse population-level effects. A study that looked at the impacts of feminization in wild roach *Rutilus rutilus* indicated that the presence of severely intersex fish could have adverse effects for the fish population in question, whereas the presence of mildly intersex fish appears likely to have little to no effects (Harris et al., 2011). As such,

short-term population crashes on the scale demonstrated in prior long-term EDC exposure studies where chronic exposure led to the collapse of the fathead minnow population (Kidd et al., 2007) are highly unlikely in the presence of mildly intersex feminised males (Harris et al., 2011). In a study that assessed how EDCs affect population dynamics (White et al., 2017), a "mating function" model that examines the relationship between sex ratio and reproductive success was tested on wild populations of estuarine inland silverside *Menida beryllina*. According to this model, masculinization was found to be more detrimental to fish populations than feminization, reducing reproductive success that can lead fish populations to experience population decline. However, in species that have an almost 50:50 sex ratio, such as the inland silverside, feminization and masculinization have been shown to be detrimental (White et al., 2017). Androgenic responses to chemicals are less understood than oestrogenic responses. In turn, androgenicity, or better-said masculinisation and sex reversal female to male is better understood in an aquaculture context under temperatures outside normal developmental ranges (Devlin and Nagahama, 2002; Piferrer and Anastasiadi, 2021).

In addition to their agonistic effects on ERs, xenoestrogenic compounds exert their endocrine-disrupting effects when they tamper with steroidogenesis and how sex steroid hormones (androgens and oestrogens) regulate the normal development and functioning of male and female reproductive organs. ERs mediate the biological effects of sex steroid hormones, thus play important roles in sex differentiation and reproduction, particularly in the development and expression of male and female phenotypic traits (Devlin and Nagahama, 2002; Nelson and Habibi, 2013; Ogino et al., 2018). In gonads of developing embryos/larvae, the expression of steroidogenic enzymes related genes by steroid-producing cells (theca, granulosa and Leydig cells) results in the differential synthesis of their respective sex steroids that are easily detectable prior to gonadal morphological differentiation (Devlin and Nagahama, 2002). The transcription factor Forkhead Box L2 (Foxl2) preferentially expressed in ovary granulosa cells (GCs) is thought to be responsible for the maintenance of the GC through the repression of testis-specific genes and the regulation of cytochrome P450 aromatase (*cyp19a1a*), a key enzyme involved in oestrogen synthesis and EDC target. Transcription of *foxl2* promotes the activation of *cyp19a1a* transcription while repressing *amh* (anti-Mullerrian hormone), *dmrt1* (dsx- and mab-3-related transcription factor 1) and *sox9* (SRY-box9) transcription (Yang et al., 2017; Zhang et al., 2017). Most vertebrates have a single P450 aromatase encoding *cyp19* gene, while

most teleost fish have two structurally distinct isoforms or paralog *cyp19* genes that arose from genome duplication, gonadal *cyp19a1a* and brain *cyp19a1b* (Blázquez and Piferrer, 2004; Lin et al., 2020). P450 aromatase encoded by the *cyp19a1a* gene catalyses the conversion of androgens into oestrogens and plays an important role in sex differentiation and gonad development, whereas P450 aromatase encoded by the *cyp19a1b* gene is involved in the development of the central nervous system and reproductive behaviour (Fernandino et al., 2013; Lin et al., 2020; Nelson and Habibi, 2013). Considering the close relationship between androgens and oestrogens, *cyp19a1a* seems to be important during ovarian differentiation due to its role in coordinating their synthesis and catalyse the final step of E_2 biosynthesis (Fernandino et al., 2013; Zhang et al., 2017).

2.2. Ovarian follicular atresia in wild fish populations

In vertebrate ovaries, follicular atresia is a common phenomenon during which the number of ovarian follicles recruited into the vitellogenic pool fail to complete maturation and ovulation resulting in their degeneration and reabsorption (Guraya, 1986; Saidapur, 1978). Ovarian follicle development in vertebrates is a dynamic process that involves the sequential development of primordial follicles into first primary, then secondary and finally mature follicles through different recruitment and selection steps (Bhardwaj et al., 2022; Qiang et al., 2021). In mammals, a large number of primordial follicles are produced, more than those that will be required for maturation, with most follicles arresting development and degenerating after a certain age or stage along oogenesis through atresia (Bhardwaj and Sharma, 2012; Krysko et al., 2008; McGee and Horne, 2018). In fish, irrespective of their reproductive strategy, ovarian development follows annual cycles which in many species and during early oogenesis results in the recruitment into vitellogenesis of more oocytes than those that will finally be spawned (Kjesbu, 2009). Mitotic oogonia are maintained for life in teleost's contrary to the situation in mammals where the pool of primordia that could develop into mature eggs is established during foetal development with no mitotic oogonia available after birth.

The fish oocytes in vitellogenesis that cannot be spawned each reproductive cycle go to atresia, facilitating the absorption and re-distribution of energy-rich yolk material (Janz and Van Der Kraak, 1997; Miranda et al., 1999; Wood and Van Der Kraak, 2003, 2001). Follicular atresia and follicle resorption seem to be more important in teleost fish than in other vertebrates due to the large number of primary oocytes that initiate maturation in each

reproductive cycle and the large amount of yolk accumulation that this entails (Cassel et al., 2017). It is thus an important physiological process essential for the maintenance of ovarian homeostasis in fish, just like in all other vertebrates (Bhardwaj and Sharma, 2012; Corriero et al., 2021; Krysko et al., 2008) This is so because it allows the fish to interrupt its normal reproductive cycle by skipping a batch of oocytes during their recruitment thereby adjusting the number of eggs produced to the affordable amount of stored energy (Kennedy et al., 2009; Kjesbu, 2009).

In spawned ovaries, the remaining structures from mature follicles known as postovulatory complexes (POCs) that were ovulated during the spawning season are also reabsorbed (Cassel et al., 2017; Morais et al., 2016; Thomé et al., 2006). POCs, formerly known as postovulatory follicles (POFs), show little to no hormonal activity in most teleost species, but their elimination appears to be critical for new follicle recruitment (Cassel et al., 2017; Kumar and Joy, 2015; Thomé et al., 2006). Follicular atresia in teleosts has been observed irrespective of the differentiation stage between previtellogenesis and final maturation in the follicles (Sardul S Guraya, 1986; Janz and Van Der Kraak, 1997; Miranda et al., 1999; Rizzo and Bazzoli, 1995; Wood and Van Der Kraak, 2001). It has been morphologically described in previtellogenic and vitellogenic follicles of captive *Prochildus affinis* (Rizzo and Bazzoli, 1995), *Astyanax bimaculatus lacustris* and *Leporinus reinhardti* (Miranda et al., 1999). Generally, four main stages can be differentiated during ovarian atresia; (1) oocyte fragmentation and hypertrophy of follicles or granulosa cells, (2) invasion of the ooplasm with follicular/phagocytic cells and elimination of cell residues, (3) degeneration of the granulosa cells and changes in pigmentation and, (4) degeneration of the follicle (Corriero et al., 2021; Habibi and Andreu-Vieyra, 2007; Lubzens et al., 2010). However, the molecular and cellular mechanisms responsible for the observed morphological changes remain poorly understood (Lubzens et al., 2010).

Although a physiological phenomenon notably observed at the end of the spawning season, atresia in fish ovaries is usually impacted by environmental stress (starvation, contaminant exposure, confinement, unfavourable temperature or photoperiod regimes, sub-optimal water quality) or changes in hormonal levels (Corriero et al., 2021; Guzmán et al., 2013; Serrat et al., 2019; Yamamoto et al., 2016). With regard to pollutants and contaminant exposure, follicular atresia has been reported in several fish species exposed to pesticides (Chukwuka et al., 2019; Mohapatra et al., 2021), pharmaceuticals (Jiang et al.,

2019; Madureira et al., 2011) and heavy metals (Driessnack et al., 2017a, 2017b). In a recent review of atresia in ovarian follicles of fish, follicular atresia as a result of contaminant exposure was observed to occur from the disruption of the HPG axis via an inhibitory effect on the release of gonadotropin-releasing hormone (GtH) and subsequent impairment of steroid production (Corriero et al., 2021) when E_2 plasma levels were low (Aguilar et al., 2007; Au, 2004; Jobling et al., 2002a; Mayon et al., 2006). Xenoestrogens induce atresia in fish ovaries by not only preventing the release of GtH, but also through apoptotic cell death of theca and granulosa cells, thus exposure to chemicals may cause consequential damage to the ovaries by reducing the number of follicular cells accessible for steroid production (Corriero et al., 2021 and references therein). Polychlorinated dibenzodioxins such as 2,3,7,8-tetrachlorodibenzo-p-dioxin (TCDD) have the ability to inhibit E_2 synthesis in zebrafish ovaries, decreasing hepatic Vtg synthesis and preventing previtellogenic follicles from transitioning to the vitellogenic stage follicles, eventually leading to follicular atresia (Corriero et al., 2021; King Heiden et al., 2006). On the contrary, many other species inhabiting waters contaminated with xenoestrogens have displayed atresia in ovaries when E_2 plasma levels were high (Agbohessi et al., 2015; Janz and Van Der Kraak, 1997). In the presence of xenoestrogens, transcription of genes encoding steroidogenic enzymes might be either up- or down-regulated, implying that xenoestrogenic effects on E_2 synthesis and follicular atresia is species-specific (Corriero et al., 2021 and references therein).

Follicular atresia is a complex process involving both processes of apoptosis and autophagy (Corriero et al., 2021; Miranda et al., 1999; Morais et al., 2012; Yang et al., 2022). In mammals, apoptotic cell death has long been considered the main molecular mechanism responsible for ovarian follicular atresia (Matsuda et al., 2012; Tiwari et al., 2015). Apoptosis, an evolutionarily conserved process, involves biochemical and morphological changes that remodel tissues to maintain cell and organ homeostasis (Krysko et al., 2008; Steller, 1995; Tilly, 1996). The role of apoptosis in follicular atresia has been studied in teleosts (Janz and Van Der Kraak, 1997; Wood and Van Der Kraak, 2001) and the evidence excludes the possibility of apoptosis being the main or only mechanism. Autophagy is an alternative mechanism that contributes to the efficient elimination of all cell types conforming the ovarian follicle in vertebrates (Bhardwaj et al., 2022; Cassel et al., 2017; Corriero et al., 2021; Morais et al., 2012; Sales et al., 2019; Santos et al., 2008; Thomé et al., 2009). Nutrients from degraded cell organelles in the follicle can be recycled

through autophagocytosis, providing the much-needed energy required for future oocyte production (Bhardwaj et al., 2022).

Currently, atresia in fish is classified into alpha (α), beta (β), gamma (γ) and delta (δ) stages (Figure 4), a widely accepted classification scheme (Corriero et al., 2021). In the α-atretic stage, the nuclear envelope lyses, dispersing the nuclear content into the cytoplasm, while yolk granules and lipid droplets fuse as the shape of the oocyte becomes irregular. At the same time, while a small fraction of follicular cells degenerates by apoptosis, there is fragmentation and breakdown of the *zona radiata* and invasion of enlarged granulosa cells into the oocyte to phagocytize the liquefied yolk granules (Corriero et al., 2021). The follicles then enter the β-atretic stage where a thin layer of theca cells and blood vessels surround the follicular cells that appear disorganized and having vacuoles that may or may not be empty. The β-atretic follicle may either progress through gamma (γ) and delta (δ) stages, be completely reabsorbed at the β-atretic stage, or skip the γ-atretic stage and directly progress to the δ-atretic stage. It is worth mentioning that extensive apoptosis of follicular cells has been observed in late β-atretic follicles (Morais et al., 2012). In the γ-atretic stage, follicles are much smaller than those in β-atresia, and the granulosa cells present with irregular-shaped nuclei and light-yellow flocculent material in the cytoplasm. Furthermore, phagocytosis of oocyte components by follicular cells is still active and a reduction in the number of theca cells and blood vessels surrounding the granulosa cells can be observed (Corriero et al., 2021). The number of granulosa cells drastically reduce in the δ-atretic stage and contain yellow-brownish pigments (lipofuscins and melanin). The atretic process ends when theca cells and blood vessels no longer surround the granulosa cells (Corriero et al., 2021).

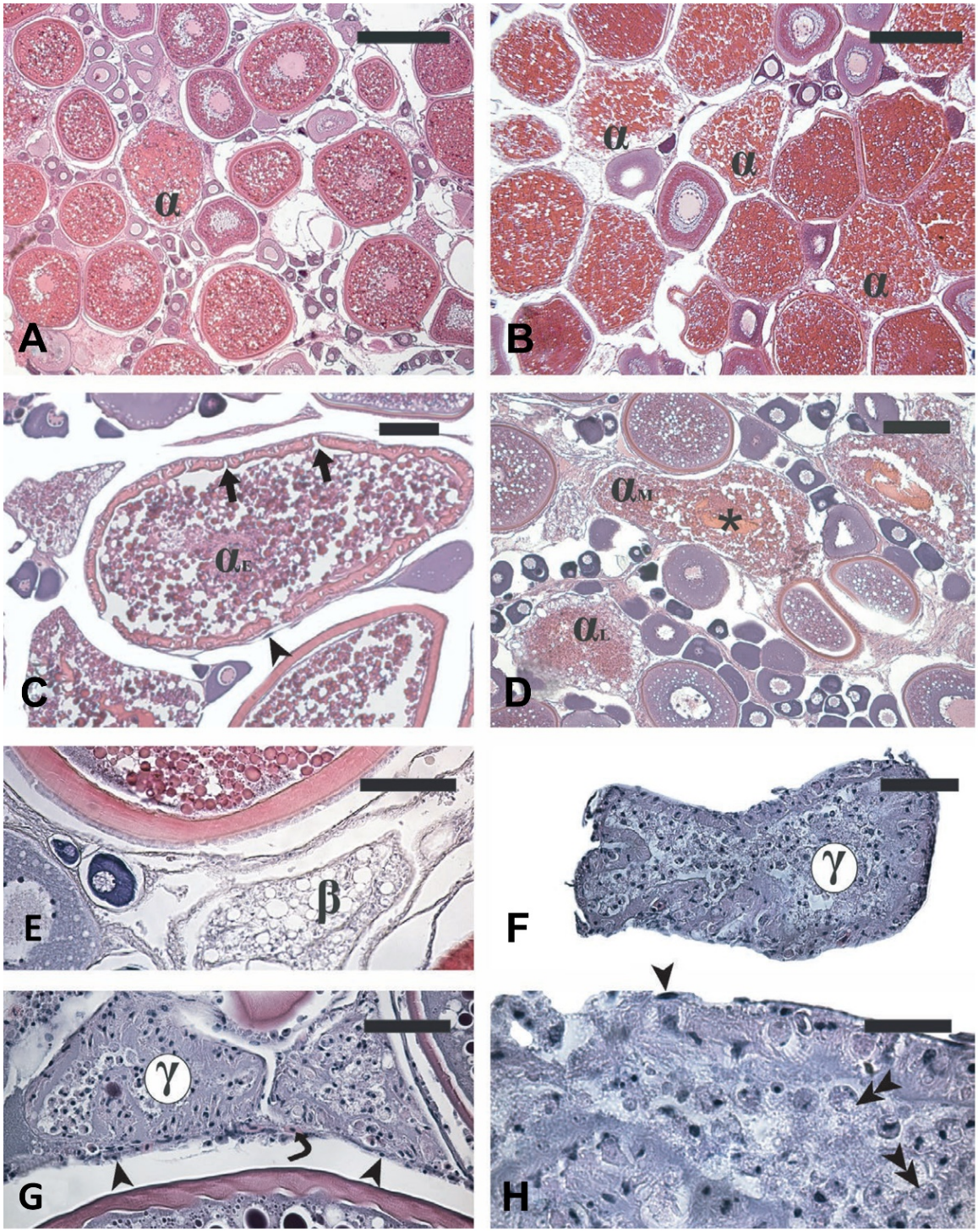

Figure 4
Ovarian histology showing atresia classification into alpha (α), beta (β), gamma (γ) and delta (δ) stages in adult (A, B, F, G and H) Atlantic bluefin tuna Thunnus thynnus, (E) swordfish Xiphias gladius and (C and D) greater amberjack Seriola dumerili in different reproductive developmental stages. Magnification bars: 400 µm in (A) and (B); 100 µm in (C) and (E); 150 µm in (D); 50 µm in (F) and (G); 30 µm in (H). α, α-atretic vitellogenic follicle; β, β-atretic follicle; γ, γ-atretic follicle; arrow, zona radiata breakdown; arrowhead, thecal cell; double arrowhead, follicular cell in active phagocytosis; asterisk, residual zona radiata under digestion; curved arrow, blood vessel (plate reprinted from Corriero et al. 2021).

A recent review of the literature identified a list of 25 different genes (Table 1) that play a potential role in ovarian follicular atresia in teleost fish either through lipid metabolism, oxidative metabolism and immune cell processes, but also through apoptotic and autophagic mechanisms (González-Kother et al., 2020). Sequential activation of caspases has been observed to be important for proteolytic cleavage and apoptosis-mediated cell death during follicular atresia in fasted coho salmon (Yamamoto et al., 2016). In the freshwater fishes *Astyanax bimaculatus, Leporium obtusidens* and *Prochilodus* argenteus, the overexpression of apoptotic (*caspase-3, bcl2, bax*) and autophagocytotic (*beclin-1, cathepsin D*) genes have been demonstrated in ovarian follicular and theca cells during atresia (Morais et al., 2012). In the Japanese flounder *Paralichthys olivaceus*, the phosphatase and tensin homolog B (*ptenb*) gene has been implicated in the process of follicular atresia through its relationship with Beclin-1 and the initiation of autophagy and apoptosis (Li et al., 2020). p53, a regulator of both apoptotic and autophagic pathways (Levine et al., 2006; Levine and Oren, 2009; Vousden and Prives, 2009), plays a very important role in controlling the fate of ovarian follicles in teleost fishes. This has been demonstrated in fasted coho salmon (Yamamoto et al., 2016), the spotted knifejaw *Oplegnathus punctatus* (Du et al., 2017) The role of p53 is for instance very clear during zebrafish sex differentiation. All zebrafish develop a juvenile ovary after hatching which in genetic males, regresses to allow the formation of testis in a process that is regulated through the activation of p53 to trigger the resorption of immature oocytes (Rodríguez-Marí et al., 2010).

Table 1
Summary of 25 potential molecular marker genes of follicular atresia in teleost fish (adapted and modified from Gonzalez-Kother et al., 2020).

Gene function	Gene	Gene identification	Relation with atresia	Fish species	Reference
Apoptosis	*bax*	Bcl-2 Associated X-protein	High protein expression during late atresia	*Astyanax bimaculatus* *Leporium obtusidens* *Prochilodus argenteus*	Morais et al., 2012
	bcl2	B-cell leukaemia/lymphoma 2 protein	High protein expression in early and advanced atresia than in late atresia	*Astyanax bimaculatus* *Leporium obtusidens* *Prochilodus argenteus*	Morais et al., 2012
	casp3	Caspase 3	High gene expression during late atresia	*Astyanax bimaculatus* *Leporium obtusidens* *Prochilodus argenteus*	Morais et al., 2012
			High gene expression in vitellogenic ovaries during atresia	*Merluccius merluccius*	Nzioka et al., 2023
	casp8	Caspase 8	Increased gene expression in fasted fish with severe atresia	*Oncorhynchus kisutch*	Yamamoto et al., 2011
	casp9	Caspase 9	Increased gene expression in fasted fish with severe atresia	*Oncorhynchus kisutch*	Yamamoto et al., 2011
	pdcd4	Programmed cell death protein 4	Potential early marker of apoptosis/atresia	*Oncorhynchus kisutch*	Yamamoto et al., 2016
	litaf	Lipopolysaccharide-induced tumour necrosis factor (TNF)-alpha factor	High gene expression in fasted fish leading to increased atresia incidence	*Oncorhynchus kisutch*	Yamamoto et al., 2016
	klf6	Kruppel-like factor 6	Potential early marker of apoptosis/atresia	*Oncorhynchus kisutch*	Yamamoto et al., 2016
	mdm2	Mouse double minute 2 homolog/ E3 ubiquitin-protein ligase	High protein expression in vitellogenic ovaries during atresia	*Merluccius merluccius*	Unpublished data (this thesis)
	p53	Tumour protein p53	High gene expression in vitellogenic ovaries during atresia	*Merluccius merluccius*	Nzioka et al., 2023
			High protein expression in previtellogenic ovaries during atresia	*Chelon labrosus*	Unpublished data (this thesis)
	rpl11	Ribosomal protein L11	High protein expression in previtellogenic ovaries during atresia	*Chelon labrosus*	Unpublished data (this thesis)
			High protein expression in vitellogenic ovaries during atresia	*Merluccius merluccius*	Unpublished data (this thesis)
Autophagy	*becn1*	Beclin-1	High protein expression in advanced atresia	*Astyanax bimaculatus* *Leporium obtusidens* *Prochilodus argenteus*	Morais et al., 2012

Table 1 continued…

Gene function	Gene	Gene identification	Relation with atresia	Fish species	Reference
			High gene expression during atresia irrespective of ovarian developmental stage	*Merluccius merluccius*	Nzioka et al., 2023
	dapk1	Death-associated protein kinase 1	High gene expression in vitellogenic ovaries during atresia	*Merluccius merluccius*	Nzioka et al., 2023
	ptenb	Phosphatase and tensin homolog B	High gene expression during atresia and activation of autophagy	*Paralichthys olivaceus*	Li et al, 2020
			High gene expression during atresia irrespective of ovarian developmental stage	*Merluccius merluccius*	Nzioka et al., 2023
Apoptosis/ Autophagy	*ctsd*	Cathepsin D	Increased protein expression in early and advanced atresia than in late atresia	*Astyanax bimaculatus* *Leporium obtusidens* *Prochilodus argenteus*	Morais et al., 2012
			High gene expression in vitellogenic ovaries during atresia	*Merluccius merluccius*	Nzioka et al., 2023
Anti-apoptotic function	*s100a10*	S100 calcium binding protein A10	Gene up-regulated in atretic ovaries	*Solea senegalensis*	Tingaud-Sequeria et al., 2009
Apoptosis-related functions	*fst*	Follistatin	Potential marker of ovarian age	*Oryzias latipes*	Herpin et al., 2013
	krt79	Type 2 keratin k 8b (S2)	Potential early marker of altered ovarian follicular growth	*Oncorhynchus kisutch*	Yamamoto et al., 2016
	s8	Type 1 keratin s8	Gene down-regulated in fasted fish ovaries	*Oncorhynchus kisutch*	Yamamoto et al., 2016
	thbs	Thrombospondin	Gene up-regulated in atretic ovaries	*Solea senegalensis*	Tingaud-Sequeria et al., 2009
Lipid metabolic processes	*apoc1*	Apolipoprotein C1	Gene up-regulated in atretic ovaries	*Solea senegalensis*	Tingaud-Sequeria et al., 2009
	amh	Anti-Mullerian hormone	Increased gene expression in atretic ovaries causing reduction of healthy ovarian follicles	*Oncorhynchus kisutch*	Yamamoto et al., 2016
	all	Alveolin	Gene expression in previtellogenic atretic ovaries in fasted fish	*Oncorhynchus kisutch*	Yamamoto et al., 2016
	fabp11	Fatty acid-binding protein 11	Gene strongly up-regulated in somatic cells surrounding atretic follicles	*Solea senegalensis*	Agullero et al., 2007
	hsd3b	hydroxy-delta-5-steroid dehydrogenase 3 beta	Altered gene expression prior to atresia becoming evident	*Oncorhynchus kisutch*	Yamamoto et al., 2016

The analysis of atresia has important implications from the point of view of the analysis of fish fecundity, with implications in the scientific assessment of fish stock dynamics. In the case of the European hake (*Merluccius merluccius*, Linnaeus, 1758), it has been established to be a batch spawner with indeterminate fecundity, that is, oocyte development is asynchronous (oocytes of all stages are simultaneously present in reproductively active ovaries) within the main spawning season (Korta et al., 2010; Murua et al., 2006; Murua and Motos, 2006). Recently, early oocyte recruitment patterns with direct consequences for the resulting egg production was observed this meaning that hake show a determinate, rather than indeterminate, fecundity type (Serrat et al., 2019). In addition, hake in the Bay of Biscay and Galician waters was shown to have a protracted spawning season (spawning activity observed all year round) characterized by three spawning peaks (Serrat et al., 2019). The highest egg production is usually observed in the winter-spring spawning season peak, followed by an intermediate peak in summer and finally a lower autumn peak. In this sense, egg production is thought to invest in a buffer stock that would be spawned depending on the fluctuating environmental conditions (García-Fernández et al., 2020; Serrat et al., 2019).

The mechanisms of atresia are entitled to differential regulation depending on the ovarian developmental pattern (whether synchronic or asynchronic) and spawning behaviour (batch spawners or single spawners). For hake, intense atretic activity has been reported in ovaries at the end of each spawning season, except for the summer spawning peak (Serrat et al., 2019). This suggested fecundity could be modulated by environmental conditions; thus, facilitating the removal of under-developed oocytes by atresia once spawning is over (Serrat et al., 2019). Hake can additionally experience periods of a high incidence of follicular atresia linked to environmental changes as it was for instance during the Prestige oil spill in 2002 (Díez et al., 2011; Murua and Motos, 2006). Therefore, when studying the population dynamics of fish species, knowledge of the reproductive biology and estimation of fecundity and egg production is fundamental because they are the basis to quantify reproductive capacity at individual and population levels (Murua and Motos, 2006).

3. Thicklip grey mullet *Chelon labrosus*: a sentinel of pollution exposure

The thicklip grey mullet *Chelon labrosus* (Risso, 1827) is a member of the family Mugilidae (grey mullets), which consists of approximately 25 genera and 80 species widely distributed around the world in tropical and temperate regions (Xia et al., 2016). It is a long-lived and slow-growing euryhaline demersal fish species broadly distributed along the eastern Atlantic Ocean from southern Scandinavia and Iceland to Senegal and Cape Verde, and across the Mediterranean and Black Seas (Crosetti and Blaber, 2016; Freyhof and Kottelat, 2008; Froese and Pauly, 2022). It occupies inshore areas, estuaries, coastal lagoons and seas, thereby supporting artisanal and recreational fisheries (Crosetti and Blaber, 2016; Freyhof and Kottelat, 2008; Froese and Pauly, 2022).

Thicklip grey mullets are gonochoristic species with separate sexes. Females are bigger than males and sexual dimorphism is lacking, at least externally (Crosetti and Blaber, 2016). Male testes are internal, longitudinal and paired organs that lie lateral to the gas bladder suspended by mesenteries, whereas the female ovaries are hollow and paired ovarian lobes separated by a septum and joined together near the urogenital pore (Crosetti and Blaber, 2016). In a study of the flathead mullet *Mugil cephalus*, most undifferentiated juveniles (83%) had become sexually differentiated on attaining a size > 200 mm, though no definitive morphological characteristic that would enable sexual determination was present (McDonough et al., 2005). In males, the germ cell tissue located at the periphery portions of each lobe elongate and expand to form lobules, with spermatogonia beginning to line the lobules as part of the germinal epithelium. Female sexual differentiation on the other hand involves the organization of germ-cell tissue into balls of 8-10 cells each that will line along the lateral periphery of the lobe and eventually give rise to oogonia (McDonough et al., 2005).

Grey mullets are capable of spending part or most of their life in fresh or brackish water, taking advantage of available rich resources and shelter from predators, hence they have a short marine phase that is mostly related to the larval stage and spawning period of their life (Crosetti and Blaber, 2016). A pattern of migration for grey mullets, that is, young grey mullets living predominantly in brackish waters, moving to the open sea to complete maturation and spawn, onshore migration of larvae and settlement in surf zones as juveniles, and the movement of juvenile schools to coastal lagoons or estuarine waters has generally been acknowledged (Crosetti and Blaber, 2016). It should be noted that, although mullets

perform their annual spawning migration from estuarine and coastal waters into the open sea, and that the spawning grounds for most mullet species remain poorly documented (Crosetti and Blaber, 2016), some individuals of *M. cephalus* have been observed to remain in estuaries without migrating to spawn, while permanent marine-living populations have also been observed to exist (Whitfield et al., 2012).

C. labrosus exhibits a high degree of residency within estuarine and coastal systems (Figure 5), using estuaries as nursery areas or foraging habitats, migrating daily up and down of the estuaries with the tidal regime (Froese and Pauly, 2022; Whitfield, 2020). It spawns yearly at sea in coastal surface waters during the winter season (December – February), and pelagic eggs hatch in 3-4 days, with the pelagic larval stage lasting approximately four weeks (Besbes et al., 2020; Boglione et al., 1992). In the open ocean, movements of adult spawning shoals and spawning areas are unknown, but in coastal environments, juveniles form dense schools, migrating to inshore coastal waters and shallow estuaries, that in the Mediterranean Sea, occurs during the first and second month of life (Crosetti and Blaber, 2016; Hickling, 1970; Mićković et al., 2010).

In estuarine-associated marine fishes, evidence suggests that early juveniles use olfactory cues as a primary means to find estuarine nursery areas and once inside an estuary, sediment composition, turbidity and salinity preferences play a role in determining the exact regions and habitats occupied by juvenile mullets (Crosetti and Blaber, 2016). They are capable of either actively swimming into the estuaries against outgoing currents or using the flood tidal transport system to assist with movement upstream with juveniles (Crosetti and Blaber, 2016). However, the process through which *C. labrosus* juveniles are incorporated into estuaries along the Basque coast where they are highly predominant remains unknown. Furthermore, it remains unclear as to whether populations *C. labrosus* along the Basque coast exhibit panmixia or whether a metapopulation structure exists, with different populations linked to specific or geographically close estuaries. In a recently concluded study on *Chelon ramada* (Risso, 1827), the absence of significant genetic structure supported the existence of a metapopulation with high gene flow and suggested that *C. ramada* displays high dispersal capacity (Pereira et al., 2023). According to the study, the maintenance of a single *C. ramada* genetic group is possibly due to a continuous habitat availability and low exploitation that favours the presence of large population numbers, a scenario that may as well be replicated by *C. labrosus* in Basque estuaries.

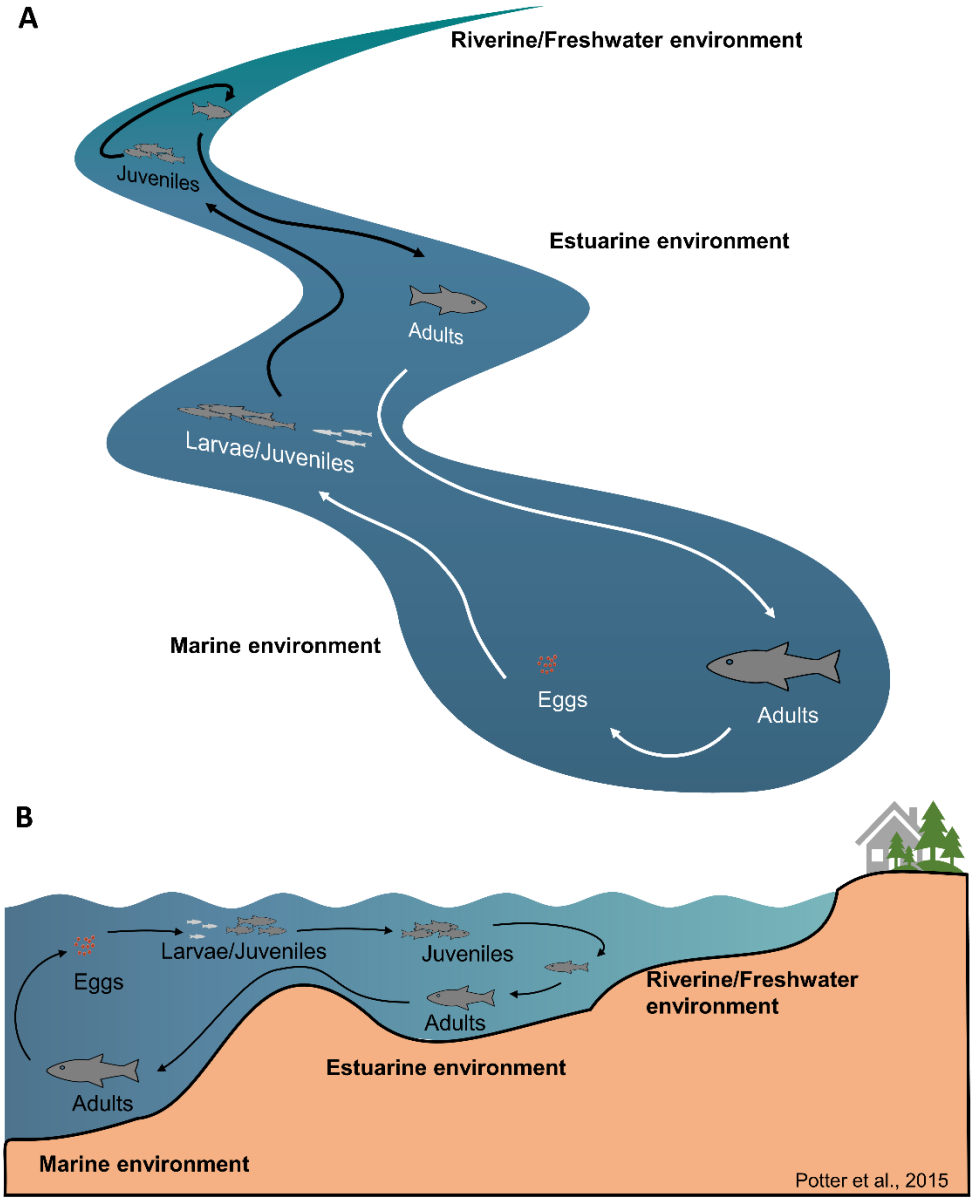

Figure 5
Life history of euryhaline thicklip grey mullet Chelon labrosus in estuarine and marine environments. Thicklip grey mullets very seldom inhabits fully freshwater environments (Cardona, 2006; Whitfield et al., 2012). (A) Birds eye view and (B) Cross section view with image illustration adopted and modified from Potter et al. (2015).

3.1. Xenoestrogenic effects in Chelon labrosus from the Basque coast

Along the Basque coast, strong xenoestrogenic effects have been reported in *C. labrosus* individuals from contaminated estuaries, mainly linked to exposure to alkylphenols, pesticides and other xenoestrogens coming principally from WWTPs effluents (Bizarro et al., 2014; Diaz De Cerio et al., 2012; Ortiz-Zarragoitia et al., 2014; Puy-Azurmendi et al., 2013; Valencia et al., 2017). This exposure has been reported to result into the development of intersex individuals. An abnormally high number of intersex testes (up to 83%) has been

identified in *C. labrosus* males sampled in the Urdaibai estuary near Gernika. These individuals have also shown bile accumulation of xenoestrogenic compounds such as bisphenol A (up to 177.5 ng mL^{-1}), oestradiol (up to 27.0 ng mL^{-1}) and nonylphenol (up to 1,142.0 ng mL^{-1}) (Bizarro et al., 2014; Ortiz-Zarragoitia et al., 2014; Puy-Azurmendi et al., 2013; Ros et al., 2015). Additionally, varying prevalence of intersex condition have been reported in *C. labrosus* males captured from Bilbao (Nerbioi-Ibaizabal estuary) near the WWTP of Galindo (up to 9%) and the Arriluze marina (10%), the fishing port of Ondarroa (50%), the port of Deba (20%) and the industrial harbour of Pasaia (up to 56%) at the mouth of Oiartzun river (Bizarro et al., 2014; Diaz De Cerio et al., 2012; Ortiz-Zarragoitia et al., 2014; Puy-Azurmendi et al., 2013; Ros et al., 2015; Valencia et al., 2017). However, mullets sampled from the leisure port of Plentzia have shown normally developing testes with no incidences of intersex condition (Bizarro et al., 2014; Ortiz-Zarragoitia et al., 2014; Ros et al., 2015). The development of intersex condition thus appears to be estuarine-specific depending on the pollution load present in each estuary.

The effects of xenoestrogens on the expression of various genes related to reproduction have been evaluated in *C. labrosus* individuals (Table 2). Mullets from Basque estuaries have shown signs of endocrine disruption that include the hepatic expression of *Vtg* genes and upregulation of *cyp19a1b* gene in both male and intersex individuals (Bizarro et al., 2014; Valencia et al., 2017). The upregulation of *foxl2* has also been observed in male and intersex mullets, while *cyp19a1a* was observed to be downregulated in female individuals inhabiting estuaries exposed to xenoestrogenic compounds (Valencia et al., 2017). The 5S ribosomal RNA (5s rRNA) and its transcription factor (general transcription factor 3A, *gtf3a*) were also found to be present in intersex mullets and expressed similarly to ovaries (Diaz De Cerio et al., 2012). 5S rRNA plays an important role in oocyte development, producing new ribosomes that will be required for protein synthesis during early embryonic development after successful fertilization of the oocyte (Diaz De Cerio et al., 2012). In this case, there appears to be an inhibitory effect of xenoestrogens on oestrogenic regulation of ovarian oocyte growth while at the same time, promoting testis feminization in males (Devlin and Nagahama, 2002; Valencia et al., 2017).

Table 2
Genes directly involved in sex determination and differentiation in Chelon labrosus individuals inhabiting estuaries with a high burden of xenoestrogenic exposure and presenting intersex condition.

Gene	Transcription patterns and relation with intersex	Reference
42sp43	Increased gene expression in gonads of intersex individuals than males, similar to females	Diaz de Cerio et al., 2012
5S rRNA	Increased gene expression in gonads of intersex individuals than males, similar to females	Diaz de Cerio et al., 2012
cyp11b	No differences in gonad transcription levels but high variability in males	Sardi et al., 2015; Valencia et al., 2017
cyp19a1	No differences in gonad transcription levels, higher variability in intersex	Puy-Azurmendi et al., 2013
cyp19a1a	No differences in gonad transcription levels	Sardi et al., 2015; Valencia et al., 2017
cyp19a1b	No differences in gonad transcription levels, higher transcript levels in brain of males similar to females and high variability in brain of intersex individuals	Bizarro et al., 2015; Valencia et al., 2017
cyp19a2	No differences in gonad transcription levels	Valencia et al., 2017
dmrt1	No differences in gonad transcription levels but high variability in males	Valencia et al., 2017
er	No differences in gonad, brain and liver transcription levels	Bizarro et al., 2015; Puy-Azurmendi et al., 2013
foxl2	No differences in gonad and brain transcription levels	Valencia et al., 2017
gtf3a	No differences in gonad transcription levels	Valencia et al., 2017
importin α1	No differences in gonad transcription levels, higher variability in males	Diaz de Cerio et al., 2012
importin α2	No differences in gonad transcription levels	Diaz de Cerio et al., 2012
importin β2	No differences in gonad transcription levels	Diaz de Cerio et al., 2012
piwil 1	No differences in gonad transcription levels	Diaz de Cerio et al., 2012
piwil 2	No differences in gonad transcription levels	Diaz de Cerio et al., 2012
rxr	No differences in gonad, brain and liver transcription levels	Bizarro et al., 2015; Puy-Azurmendi et al., 2013
star	No differences in gonad transcription levels	Sardi et al., 2015
sult	No differences in gonad transcription levels	Sardi et al., 2015
tfiiia	Increased gene expression in gonads of intersex individuals than males, similar to females	Diaz de Cerio et al., 2012
ugt	No differences in gonad transcription levels	Sardi et al., 2015
vtg	Detectable transcription in liver but no differences in transcription levels	Bizarro et al., 2015; Valencia et al., 2017

3.2. Disrupted gonad development in Chelon labrosus

Early sex differentiation in *C. labrosus* occurs in continental waters, and in polluted estuaries in close contact to xenoestrogens when they are bioavailable. Temperature is an environmental factor that is most related to fish sex differentiation and normally, unusually high temperatures can result in masculinisation (Devlin and Nagahama, 2002). In most fish species tested, the offspring of sex reversed neomales show higher sensitivity to

masculinising temperatures, suggesting some kind of epigenetic mechanism such as DNA methylation of sex control genes that would render the offspring of these neomales more susceptible to sex reversal (Piferrer and Anastasiadi, 2021). Over time DNA hypermethylation of some regions of the genome could lead to accumulation of mutations due to the propensity of methylated cytosines to spontaneously mutate into thymine's. Whether this occurs in xenoestrogen driven intersex individuals is not known, but it has multiple implications depending on whether the thicklip grey mullets maintain fidelity to their estuary of origin and their larvae too.

Exposure to chemicals may lead to genetic changes within fish populations. Certain contaminants can cause mutations as well as alter the contributions of individual fish to subsequent generations. This can result in the alteration of the genetic composition of a population, reduction in genetic diversity, increased genetic variability or even emergence of specific gene traits within the population without necessarily affecting the population size (Hamilton et al., 2016). This is especially important when through migration, populations exposed to contaminants are linked with populations from less contaminated sites resulting in either the maintenance of a healthy population in contaminated areas, or the development of genetic structuring within a species (Hamilton et al., 2016). In the three-spined stickleback *Gasterosteus aculeatus*, Lind and Grahn, (2011) observed that although pulp mill effluents acted as selective agents on natural populations, there was a convergence of genotypic changes at multiple sites in an open environment. Microsatellite analyses on populations of the fathead minnow *Pimephales promelas* exposed to EE_2 clearly demonstrated that post-recovery fish reproductively linked to unexposed populations can recover from EE_2 exposure at the biochemical and population level (Blanchfield et al., 2015). These studies suggest that populations exposed to contaminants are often linked through migration thus helping in the maintenance of a healthy population (Hamilton et al., 2016). Gene flow between the polluted and unpolluted waters could help to compensate for potential loss of genetic variation in the polluted waters. As such, knowledge of the population genetic structure of *C. labrosus*, could be critical to the understanding of how chemicals impact populations, providing information on the level of exposure and the geographical scale at which changes in population sizes are likely to occur.

4. Estimating migration patterns, population structure and connectivity in teleosts

Several methods including the measurement of different intrinsic biological markers (body morphometrics, meristics, otoliths, scales, presence of parasites, population genetic structure) or external markers (mark-recapture, mark and teletracking) have been used to identify and discriminate fish, life traits and population dynamics (Cadrin et al., 2014; Ferreira et al., 2019; Marengo et al., 2017; Moreira et al., 2020). More recently, a combination of complimentary analytical methods has been used to provide knowledge on the levels of genetic diversity and population structure of wild fish populations (Marengo et al., 2017). This is observed to be more effective since the efficacy of single markers can vary across different spatial, temporal, and evolutionary scales, and also between species (Moore, 2011; Ovenden et al., 2015). Adopting a multidisciplinary holistic approach combining techniques may resolve limitations of each method, increasing the chances of identifying differences between spatially distinct (sub)populations within a species (Begg and Waldman, 1999; Cadrin et al., 2014; Marengo et al., 2017).

4.1. Application of marking and teletracking techniques

The study of the migration patterns of fish, the most adequate methodological approach applying physical tagging (implanted internal or external tags) of juveniles and adults. Conventional tag-recapture methods have been used to understand the movement and dynamics of fish populations, as individual fish move from one place to another (Hall, 2014; Thorstad et al., 2014). Fish can be marked upon capture in a geographically discrete area such as a spawning ground to follow their migration and determine whether they eventually encounter and mix with other individuals and/or spawning groups. The fish can also be marked on fishing grounds to investigate dispersal patterns to spawning areas (Hall, 2014; Nanami et al., 2015; Pepping et al., 2020).

Following individual fish often requires utilisation of traditional mechanical tags such as anchor T-bar tags, plastic-tipped dart tags and coded wire tags (CWTs) to be recaptured (Figure 6). The T-bar anchor tags (which are similar to clothing tags) remain the most popular because of the easy delivery mechanism that minimizes the tag entry wound while maximizing anchor strength, especially in small organisms (invertebrates included); however, the plastic-tipped dart tags are better designed for larger fish > 25 cm in length (Hall, 2013). External dart tags have been used to study spawning migration of fish species

such as the white-streaked grouper *Epinephelus ongus* in order to provide information for designing effective management strategies (Nanami et al., 2015). Such tags have been recovered even more than 20 years later in perfectly readable states after having been used to tag a wide variety of other fish species, as it was the case for the southern bluefin tuna (Hall, 2014). CWTs injected into the nasal cartilage of fish combined with an adipose fin clip have been used to tag hatchery-reared trout and salmon destined to be released into the Laurentian Great Lakes prior to stocking, in order to track the survival of stocked fish and the contribution of stocked adults to the restoration of local fish populations (Bronte et al., 2012). However, these traditional mark-recapture tagging methods only provide snapshot information, leaving several gaps about the continuous long-term behaviour, dispersal and habitat use of the fish (Dzul et al., 2021; Thorstad et al., 2014). These methods depend on recapturing a large number of tagged fish to obtain data on movement patterns, a process highly influenced by fishing effort (Dzul et al., 2021; Nanami et al., 2015; Thorstad et al., 2014). Information on the individual fish between the time of first capture/tagging and recapture cannot be obtained, nor can any information be provided for fish not recaptured (Dzul et al., 2021; Thorstad et al., 2014).

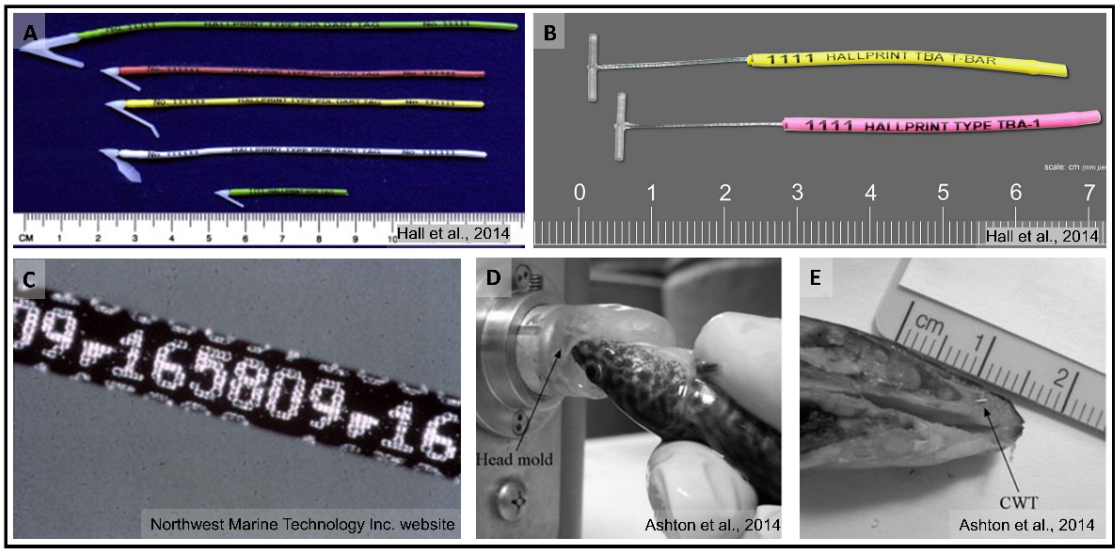

Figure 6
Traditional mechanical tags used to mark fish to be recaptured. (A) Plastic-tipped dart tags, (B) Anchor T-bar tags, (C) Individual coded wire tag (CWT) from a spool of wire, (D) Automatic CWT tag injector fitted with a customized head mould, and (E) Sagittal section of the head with a CWT injected in the nasal cavity. Image sources (Ashton et al., 2014; Hall, 2014).

Other "tag and trace" techniques that have been used to monitor and track fish migration routes take advantage of advances made in animal tracking technology (telemetry) that allow for the collection of detailed data on individual fish movements, physiology and/or environmental parameters from each individual (Hussey et al., 2015; Klimley et al., 2013;

Nielsen et al., 2009; Thorstad et al., 2014). Fish telemetry (teletracking or biotelemetry) include the use of electronic tags such as acoustic and radio tags, data storage tags (DST, also known as archival tags), pop-up satellite archival tags (PSAT) and passive integrated transponder tags (PIT-tag) (Figure 7) (Nielsen et al., 2009; Thorstad et al., 2014). Many of these electronic tags have been used to study migrating Atlantic salmon *Salmo salar* smolt and European eel *Anguilla anguilla* (Baker et al., 2021; Leander et al., 2021, 2020; Rohtla et al., 2022), Atlantic bluefin tuna (Cermeño et al., 2015; Fromentin and Lopuszanski, 2014), brown trout *Salmo trutta* (Saboret et al., 2021) and estuarine fishes such as the mummichog *Fundulus heteroclitus* and pinfish *Lagodon rhomboides* (Kimball and Mace, 2020). Electronic tags are attached to fish internally through surgical implantation in the body cavity, gastric insertion via the mouth, or as an external attachment (Thorstad et al., 2014), and are often used in combination with deployed receivers or antennas (Figure 8) placed in and around the water bodies to detect signals emitted by the tagged fish (Hussey et al., 2015; Jepsen et al., 2015; Lennox et al., 2017). However, potentially negative effects include inflammations, infections, tag repulsion, altered behaviour, decreased swimming performance, reduced feeding and growth and increased mortality (Thorstad et al., 2014).

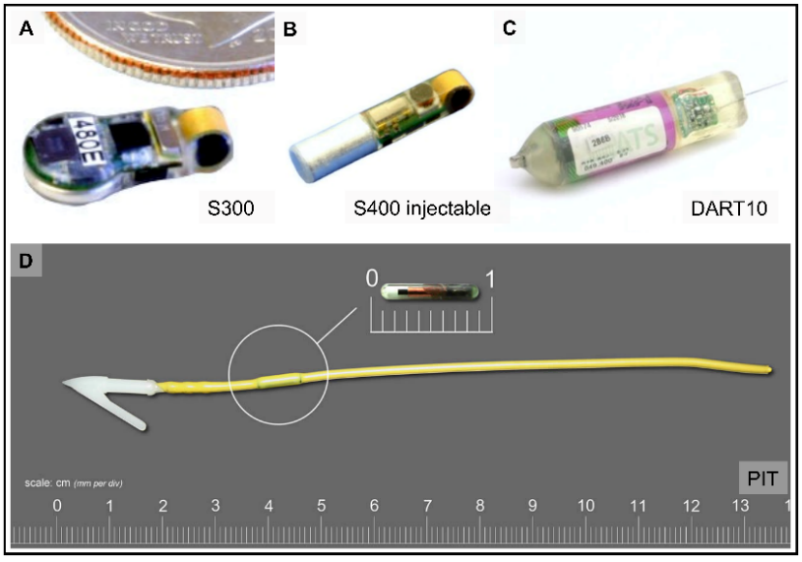

Figure 7
Main types of active electronic tags often used in fish telemetry studies that can collect detailed data on fish movements, physiology and/or environmental parameters. (A) S300 acoustic tag (Advanced Telemetry Systems, Inc.) and (B) S400 injectable acoustic tag (ATS, Inc.), (C) DART10 Dual Acoustic Radio Transmitter tag (ATS, Inc.), and (D) RFID Passive Integrated Transponder (PIT) tag. (Image sources: Advanced Telemetry Systems, Inc. (https://atstrack.com) and Hallprint fish tag (https://hallprint.com).

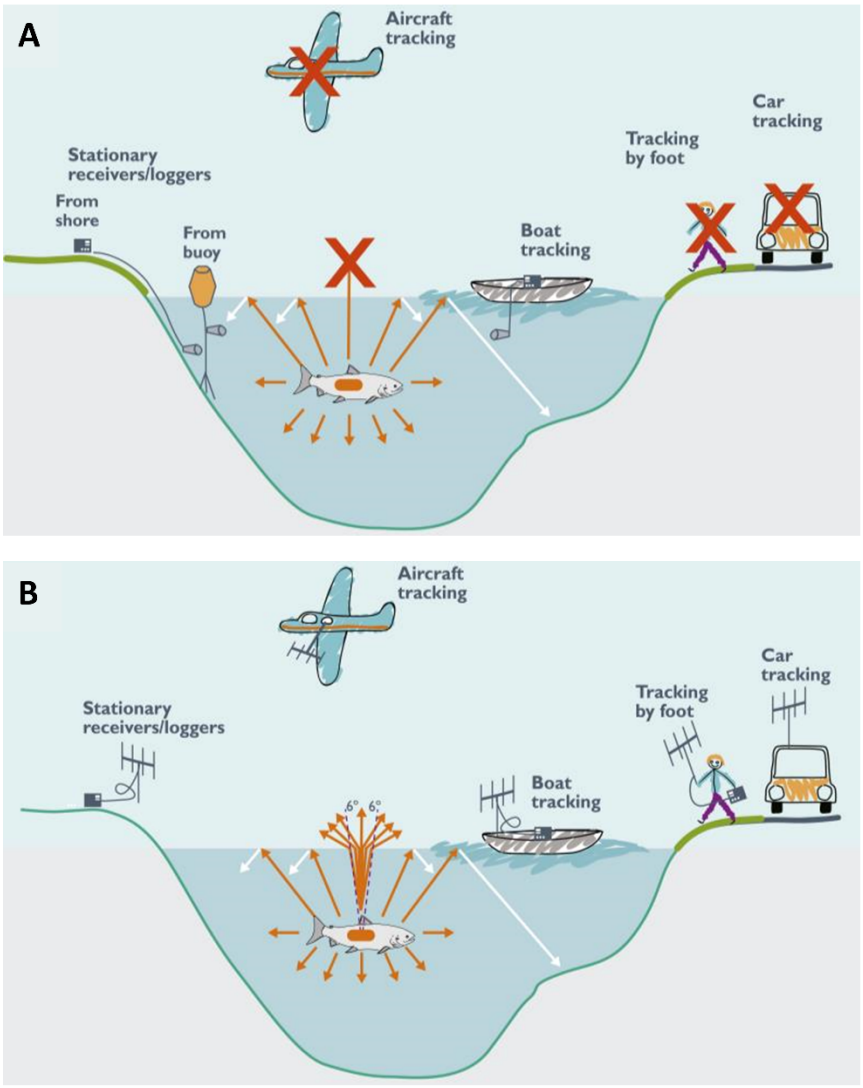

Figure 8
(A) acoustic and (B) radio telemetry fish tracking methods in action. Acoustic transmitters are only recorded by hydrophones in water, while aerial antennas record fish tagged with radio transmitters with tracking by foot, car, boat, aircraft or using stationary loggers on shore being feasible. (Image source: Thorstad et al., 2013).

The use of acoustic, radio or PIT-tags (Figure 8) would help in identifying episodic exit and entry of *C. labrosus* into estuaries where permanent antennas or network of receivers have been deployed (Cooke et al., 2022; Hussey et al., 2015; Lennox et al., 2017), though information on spawning ground locations and mixing of individuals and/or spawning groups would be lacking. Internally implanted tags that require recapture of individual or pop-up archival tags that are intended to be washed onto the shore would be useful in identifying spawning locations or provide knowledge of spawning behaviour but are difficult to recover in coastal areas where rocky shores and cliffs predominate as it is like in the case of the Basque coast. While pop-up satellite archival tags (PSAT) may solve this problem (Figure 9) they are normally suitable for larger species as they may impact fish

performance due to their size (Hedger et al., 2017; Musyl et al., 2011); though latest advancements in miniaturization of PSATs have led to the introduction and use of one of the smallest and more affordable PSATs, the mark-report satellite tags (mrPAT; Wildlife Computers Ltd., Redmond, WA, USA) on small migratory marine fishes with a fork length of approximately 45 cm (Naisbett-Jones et al., 2023).

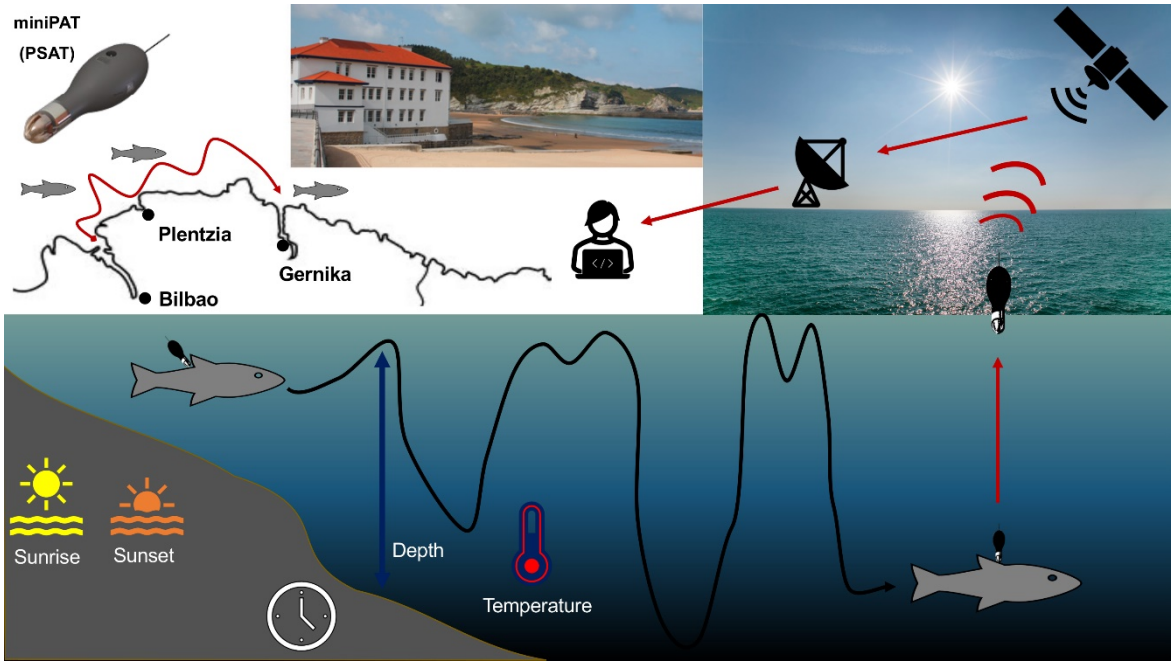

Figure 9
Principle of tracking fish ("teletracking") with pop-up satellite archival tags (PSAT). Depth, water temperature and light intensity is collected and stored by the tag as the fish migrates in the ocean. Every time the receiver pops up to the surface, the position is recorded and stored data transferred to ARGOS satellites. The stored data can then be used to retrospectively calculate migration routes of the fish (Image adopted and modified from Thorstad et al., 2013).

4.2. Application of genetic markers to analyse population structure

Genetic approaches have long been recognized for their usefulness in defining fish population structure (Cadrin et al., 2014). Population genetics analyses and quantifies the distribution of alleles within and across populations thus, allocating genetic diversity (Crosetti and Blaber, 2016). Genetic diversity may help predict a species or population ability to evolve and adapt to local selection pressures and future changes in environmental conditions (Hamilton et al., 2016; Martinez et al., 2018). Reproductive isolation, geographic distance, biogeographic barriers, specific behavioural traits such as fidelity to spawning grounds or even exposure to contaminants or stressful environmental conditions may result in population genetic differences within a species (Gandra et al., 2021). Thus, through the

study of the population genetic structure we could partially infer how a population has historically responded to adapt to environmental stress (Martinez et al., 2018).

Considerable progress made over the last few decades in the field of molecular biology has aided in the development of a variety of molecular genetic markers through advancements in nucleic acid hybridization, polymerase chain reaction (PCR) and DNA sequencing techniques that have significantly improved the resolution and utility of DNA markers. Molecular genetic markers such as those analysed by restriction fragment length polymorphism (RFPLPs) (Karaiskou et al., 2004), mitochondrial DNA (mtDNA) (Colín et al., 2020; Moreira et al., 2019a; Ragauskas et al., 2014), DNA microsatellites (Moreira et al., 2020; Pereira et al., 2023) and single nucleotide polymorphisms (SNPs) or INDELS using restriction site-associate DNA sequencing (RAD-sequencing or RAD-seq) (Gong et al., 2019) or low-coverage whole genome sequencing (lcWGS) (O'Donnell and Sullivan, 2021) have been widely used to study fish populations and differentiate stocks (Gandra et al., 2021). These are often referred to as neutral markers since studied loci are not under selection.

In population genetics, one of the most widely studied genetic markers is mtDNA (Durand et al., 2013, 2012; Xia et al., 2016). Its relatively rapid mutation rates and consequent high levels of polymorphism and divergence make mtDNA useful for providing information about the ancient history of populations and their evolutionary processes (Antoniou and Magoulas, 2014; Durand et al., 2013). The maternal inheritance pattern of mtDNA combined with the lack of recombination facilitates the assessment of intraspecific genetic variation, meaning that samples of individuals taken from different areas or from the same area but at different times may possibly belong to the same population should they present the same type of mtDNA molecules or haplotypes of similar frequencies (Antoniou and Magoulas, 2014). For instance, mtDNA has been used to test and confirm panmixia in the European eel *Anguilla anguilla*, where sequence variation of the mtDNA D-loop was virtually non-existing, demonstrating lack of genetic differentiation (Ragauskas et al., 2014). In the striped mullet *Mugil cephalus* both the mtDNA cytochrome oxidase subunit I (COI) and D-loop regions were used to investigate population genetic structure and philopatric behaviour where individual mullets returning to their natal origin or adopted location that they may or may not have been initially recruited to (Colín et al., 2020). When three mtDNA regions (COI, cytochrome *b* and D-loop regions) were used to study the genetic structure and diversity of the blue jack mackerel *Trachurus picturatus* in the North-

East (NE) Atlantic Ocean and the Mediterranean Sea, the absence of population genetic structuring was indicated by all the markers (Moreira et al., 2019a). However, mtDNA represents a single nonrecombining locus and may be an unreliable indicator of species relationships or demographic history. The smaller effective population size of mtDNA compared to nuclear DNA may result in the different lineages of mtDNA not accurately reflecting true species relationships especially when different mitochondrial genes present different allelic histories due to incomplete sorting of ancestral mtDNA haplotype polymorphisms under drift (Antoniou and Magoulas, 2014).

To obtain information on current or immediate population processes, nuclear markers such as microsatellites provide great resolution and allow identifying population structure due to their abundance in the genome and high degree of polymorphism (Durand et al., 2013; Ward, 2000). Microsatellites (also known as Short Tandem Repeats, STRs, Simple Sequence Repeats, SSRs, or Simple Sequence Length Polymorphisms, SSLPs) are highly variable tandemly repeated nucleotide sequences that can provide current estimates of migration (e.g., gene flow, effective population size), have a high statistical power to distinguish relatively high rates of migration from panmixia, and can estimate the relatedness of individuals (Selkoe and Toonen, 2006). For instance, multi-locus allele frequency data from > 10 microsatellites can provide information on the number of populations present and which populations individuals came from (Pearse and Crandall, 2004; Selkoe and Toonen, 2006). However, fewer microsatellite loci could be sufficient if a species migration rates are low and/or populations are small (Selkoe and Toonen, 2006). Highly polymorphic microsatellite data can also inform on whether a population has recently grown or shrunk, as well as whether historical and contemporary populations differed in size. Furthermore, genetic relationships between individuals, migrations and clones of individuals can be determined with microsatellites (Pearse and Crandall, 2004; Selkoe and Toonen, 2006).

The power of microsatellites in resolving fine-scale population structure has been illustrated in many studies. Microsatellites have been used to provide support for the panmixia hypothesis in the European eel *A. anguilla* (Dannewitz et al., 2005; Palm et al., 2009) and the Japanese eel *Anguilla japonica* (Yu et al., 2020), the migratory marine sparid *Acanthopagrus australis* from Australia (Roberts and Ayre, 2010), the minke whale *Balaenoptera physalus* from the NE Atlantic (Quintela et al., 2014) and most significantly in the catadromous mugilid *C. ramada* (Pereira et al., 2023), among many other marine

species. In addition, microsatellite loci have also revealed population genetic structure in the Norway lobster *Nephrops norvegicus* in the NE Atlantic (Gallagher et al., 2022), the blue and red shrimp *Arristeus antennatus* (Heras et al., 2019), the chub mackerel *Scomber japonicus* in the Northwestern Pacific (Cheng et al., 2015) and albacore tuna *Thunnus alalunga* populations in the North Atlantic and the Mediterranean Sea (Montes et al., 2012).

As next generation sequencing (NGS) technologies get faster and cheaper, the analyses of SNPs have become more popular in population genetics and molecular ecology (Ekblom and Galindo, 2011). SNPs are genome-wide markers that are based on the substitution of one nucleotide in a specific position of the DNA, and since they are dispersed throughout the genome, are more abundant than microsatellites. Their use allows for the simultaneous genotyping of hundreds of markers with low scoring errors (Cuéllar-Pinzón et al., 2016). In general, SNP detection in non-model organisms usually involves sequencing the targeted individuals' genomic regions or randomly sequencing the genomic regions, followed by the identification of segregating SNPs (Slate et al., 2009). SNPs analysis has provided insights into the worldwide population structure of the Atlantic bluefin tuna *Thunnus thymus* (Atlantic BFT) and the albacore tuna *T. alalunga*, revealing a high level of differentiation between stocks in addition to discriminating two major spawning areas for the Atlantic BFT (Albaina et al., 2013). In the Bay of Biscay, transcriptome analysis of 456 exonic SNPs identified neutral and adaptative evolutionary processes underlying the differentiation between offshore and coastal populations of European anchovy *Engraulis encrasicolus* (Montes et al., 2016). SNPs have also been used to study population mixing and ecological adaptation of Atlantic cod *Gadus morhua* in the Baltic Sea, successfully assigning individuals to their respective eastern or western Baltic cod stock and highlighting the species' potential for ecological adaptation at small geographical scales (Weist et al., 2019).

The advantages of SNPs over other markers are that, not only does having a large number of SNPs provide a large amount of statistical power to detect biologically meaningful genetic differences between populations, but SNP assays are also reproducible in any laboratory without the need to standardize allelic variants thus allowing for meta-analyses across regions or international boundaries, suitable for simulation models and can be used to analyse both neutral and adaptive genetic variations (Albaina et al., 2013; Krück et al., 2013). However, SNPs are diallelic (*i.e.*, they can have at least two different alleles existing at a given locus), hence less informative than microsatellites, thus requiring a considerable large number of SNPs to achieve the same amount of information (Krück et

al., 2013). Nonetheless, in virtually every scenario, SNPs are at least as powerful as microsatellite markers (Flanagan and Jones, 2019), and NGS technologies now have the capacity to detect a large number of SNPs alongside microsatellites (Krück et al., 2013).

High-throughput sequencing methods in NGS typically often results in the collection of extremely large data sets from large and complex genomes, resulting in the development of simpler technology for SNP discovery (Ekblom and Galindo, 2011; Liu et al., 2020; Slate et al., 2009). RAD-Seq is one such technology that reduces genome-complexity by sequencing the same loci across individuals' genomes, allowing for comparisons, and reducing costs (Liu et al., 2020). RAD-seq has been successful in SNP discovery in many species, such as the European eel (Pujolar, 2013), the Japanese eel (Gong et al., 2019; Liu et al., 2020), the flathead grey mullet (Krück et al., 2013), the Atlantic mackerel *Scomber scombrus* (Rodríguez-Ezpeleta et al., 2016) and the red snapper *Lutjanus campechanus* (Portnoy et al., 2022). In situations where selection and adaptive divergence signatures that are highly localized in the genome may be missed with RAD-seq, whole genome sequencing (WGS) has proven to be effective, despite being cost-prohibitive (Therkildsen and Palumbi, 2017). More recently, lcWGS has emerged as a powerful cost-effective solution that allows for screening of the entire genome at a population-level scale while retaining information of an individual (Lou et al., 2021). For instance, the evaluation of the population genetic structure of the Atlantic cod *Gadus morhua* using lcWGS revealed molecular markers for spawning season and sex identification (O'Donnell and Sullivan, 2021).

Despite their effectiveness in detecting genetic variations in populations, molecular genetic techniques may be inadequate in unravelling the underlying causes of the molecular genetic patterns observed, especially where low and inconsistent levels of genetic differentiation exist (Marengo et al., 2017; Moreira et al., 2019a; Ward, 2000; Ward et al., 1994). This is because they tend to focus more on the power of the technique (Belfiore, 2001). For marine species that experience high gene flow due to lack of physical geographical barriers, molecular genetic techniques cannot inform us on the life history of the fish in the absence of genetic differentiation. According to Lowe and Allendorf (2010), it is important to make a distinction between genetic and demographic connectivity and avoid the misconceptions associated with the use of genetic indices to provide information about population connectivity. Other approaches such as those studying otolith shape and/or elemental signatures might be useful to make inferences on demographic connectivity and distinguish geographically separated populations by discriminating the environmental

conditions the fish has lived in (Correia et al., 2012; Moreira et al., 2020, 2019b; Moura et al., 2020; Schroeder et al., 2021; Soeth et al., 2019).

4.3. Use of otolith shape indices and elemental signatures

Otoliths are paired metabolically inert bio-mineralized crystalline-organic complex structures found in the inner ears of teleost fishes and are used for balance and hearing (Campana, 1999). They are mainly composed of calcium carbonate (~98%) and an organic matrix (~2%), and grow incrementally, resulting in conspicuous growth bands generated by seasonal variations in the calcium carbonate to organic matrix ratio as they grow (Hüssy et al., 2021). In the inner ear of fish, three pairs of otoliths are contained in otolith organs, *sagittae* (the largest) in the saccule, *astericii* in the lagena and *lapilli* in the utricule, all which aid fish in balance and hearing (Popper et al., 2022; Popper and Lu, 2000; Thomas et al., 2017). The term "otolith" will be used solely to refer to sagittal otoliths, which are the most widely studied.

The sagittal otoliths in fish comprise of aragonite crystals on the otolith surface which require the presence of calcium (Ca^{2+}) and bicarbonate (HCO_3^-) ions in the endolymph (Thomas et al., 2017). Calcium carbonate ($CaCO_3$) is accreted into the otolith when free Ca^{2+} ions in the blood plasma diffuse along a concentration gradient into the endolymphatic epithelium and are transported into the endolymph (Hüssy et al., 2021; Thomas et al., 2017). Active transport across the endolymphatic epithelium promotes the supersaturation of the endolymph with carbonate (CO_3^{2-}) ions relative to blood plasma, resulting in the precipitation of $CaCO_3$ crystals (biomineralization) in otoliths (Hüssy et al., 2021). Extrinsic (salinity, temperature, oxygen) and intrinsic (ontogeny, growth/diet, reproduction/maturation) factors may affect the accretion of otolith $CaCO_3$, and this has been hypothesized to affect otolith elemental composition. For instance, whereas higher salinities may have no effect on otolith biomineralization, a doubling of otolith biomineralization rates has been observed with every 10°C increase within the optimal range of a species (Hüssy et al., 2021). Moreover, anaerobic stress due to hypoxic water conditions significantly reduced biomineralization rates, and otolith resorption may even take place during extreme anaerobic stress (Walther et al., 2010).

Otoliths remain the most widely utilized age and growth estimates and validation technique when evaluating life history traits in fish (Begg et al., 2005; Campana, 2005;

Thomas and Swearer, 2019). The incremental nature of otolith growth is critical to otolith age estimation (Green et al., 2009). The alternating opaque and transparent ring-like structures (annuli) in otoliths are thought to represent annual slow (opaque) and fast (transparent) growth segments (Siskey et al., 2016). Validation of the periodicity of annuli formation in otoliths, and hence their use for ageing, is often done through mark-recapture tagging of individuals (wild or cultured) or artificially "tagging" otoliths by injecting the fish with the antibiotic oxytetracycline (or tetracycline) that ends up incorporated into the otolith within a short time of injection. Tetracycline fluoresces under ultraviolet light thus allowing for examination of post-marking increments from the time of injection (Green et al., 2009).

Apart from the ability to read age from otolith structure, the shape of otoliths has become increasingly important to study fish spatial and temporal structure, populations, and spawning aggregations (Hüssy, 2008; Neves et al., 2021). Otolith shape is species-specific and the variability in shape that is often attributed to ontogenetic, genetic and environmental influences (Berg et al., 2018; Vignon, 2015, 2012; Vignon and Morat, 2010). Fish that have spent much of their lives in different geographical regions can be distinguished from other fish of the same species (Marengo et al., 2017; Neves et al., 2021; Soeth et al., 2019). Otolith shape is often analysed using two main methods, landmark analysis (Cadrin et al., 2014) and outline analysis (Stransky, 2014). Outline analysis is more commonly used and involves quantifying boundary shapes so that patterns of shape variation within and among groups can be studied (Stransky, 2014). This is often achieved by taking photographs of the otoliths, extracting the outline using statistical software and using elliptic Fourier descriptors (EFD) to analyse the otolith shape (Libungan et al., 2015; Libungan and Pálsson, 2015).

In several studies, the use of otolith shape has proven successful in resolving fish stock structure and indirectly inferring connectivity among stocks occupying different geographic regions, even in the presence of limited genetic heterogeneity (Correia et al., 2012; Marengo et al., 2017; Moreira et al., 2019a). For instance, otolith shape has been used as a population marker for Atlantic herring *Clupea harengus* populations, successfully distinguishing individuals spawning at different locations in the North-East and North-West Atlantic Ocean (Libungan et al., 2015). According to the same study, despite seasonal mixing of some *C. harengus* populations in the NE Atlantic, natal homing, larval recruitment in distinct areas and life-history strategies may have resulted in different trajectories during

early developmental stages, preserving otolith diversity among populations (Libungan et al., 2015). In the catadromous and panmictic European eel *Anguilla anguilla*, otolith shape differences in adult individuals have been attributed to variability in environmental factors, with local population units being successfully separated into brackish water estuarine and riverine freshwater population units in Italy (Capoccioni et al., 2011) and in waters of the North-West Iberian Peninsula (Moura et al., 2022).

During growth, otoliths incorporate different elements from the local environment in which a fish dwells, even if transiently, during its lifetime, thus providing a record of their life history and habitat characteristics (Campana et al., 2000; Hüssy et al., 2021; Moura et al., 2020). As such, otolith chemistry (elemental composition of otoliths) can be a valuable tool for reconstructing fish stock dynamics, migration patterns and connectivity between habitats. At least 50 different elements have been detected in fish otoliths (Hüssy et al., 2021). Most studies using otolith chemistry as tracers of environmental history have focused on strontium (Sr), barium (Ba) and manganese (Mn) since they substitute for calcium (Ca) in the otolith (Doubleday et al., 2014; Hüssy et al., 2021). Sr and Ba show strong relationships between environmental and otolith concentrations, with ambient Sr concentrations accounting for > 70% of its content in otoliths and 80 – 90% in the case of Ba (Hüssy et al., 2021). Whereas Sr and Ba are often used to track fish movements across salinity gradients, Sr concentrations are typically lower in freshwater and higher in ocean water, while Ba tends to show an inverse pattern increasing with transition from marine waters to freshwaters (Hüssy et al., 2021). Otolith Mn has also been shown to be positively related to surrounding concentrations often included in studies as an environmental indicator of estuarine habitats since Mn water concentrations tend to decrease with increasing distance from the coastline to the open ocean (Aschenbrenner et al., 2016; Laugier et al., 2015) and, it has been reported to be elevated in the otolith core, suggesting maternal transfer (Hüssy et al., 2021). Aluminium (Al), cadmium (Cd), cobalt (Co), copper (Cu), iron (Fe), lithium (Li), magnesium (Mg), zinc (Zn) and other elements that may be randomly trapped in the $CaCO_3$ crystal matrix may also reflect environmental availability and thus serve as useful geographical markers (Hüssy et al., 2021; Izzo et al., 2018; Thomas et al., 2017).

The ability to reconstruct the environmental history of fish from otolith chemistry using mass spectrometry techniques relies on the concentration of elements in otoliths changing

predictably manners with environmental variables (Correia et al., 2021, 2014; Elsdon and Gillanders, 2004; Macdonald et al., 2020; Moreira et al., 2018). This is based on the idea that elements are incorporated into otoliths at proportions roughly proportionate to those in the surrounding environment, although this is not often the case (Hüssy et al., 2021; Izzo et al., 2018; Sturrock et al., 2015). Solution based-inductively coupled plasma-mass spectrophotometry (SB-ICP-MS) has been used to measure multi-elemental signatures (MES) and potentially distinguish population based on Sr:Ca and Ba:Ca ratios in whole otoliths (Correia et al., 2021, 2014; Hoff et al., 2022; Schroeder et al., 2022; Soeth et al., 2020). The application of different techniques combining shape (EFD) and elemental composition (MES) have revealed intra-specific geographic variations and discriminated fish stocks of the tub gurnard *Chelidonichthys lucerna* (Ferreira et al., 2019) and the Atlantic mackerel *Scomber scombrus* (Moura et al., 2020) in the North Atlantic Ocean. In addition, otolith core-to-edge transects using laser ablation-inductively coupled plasma-mass spectrophotometry (LA-ICP-MS) have been successfully used to study the lifetime movement patterns of fish (Figure 10), including mugilids such as *M. liza* (Callicó Fortunato et al., 2017; Lemos et al., 2017), *M. cephalus* (Callicó Fortunato et al., 2017) and *M. curema* (Avigliano et al., 2020; Mai et al., 2018).

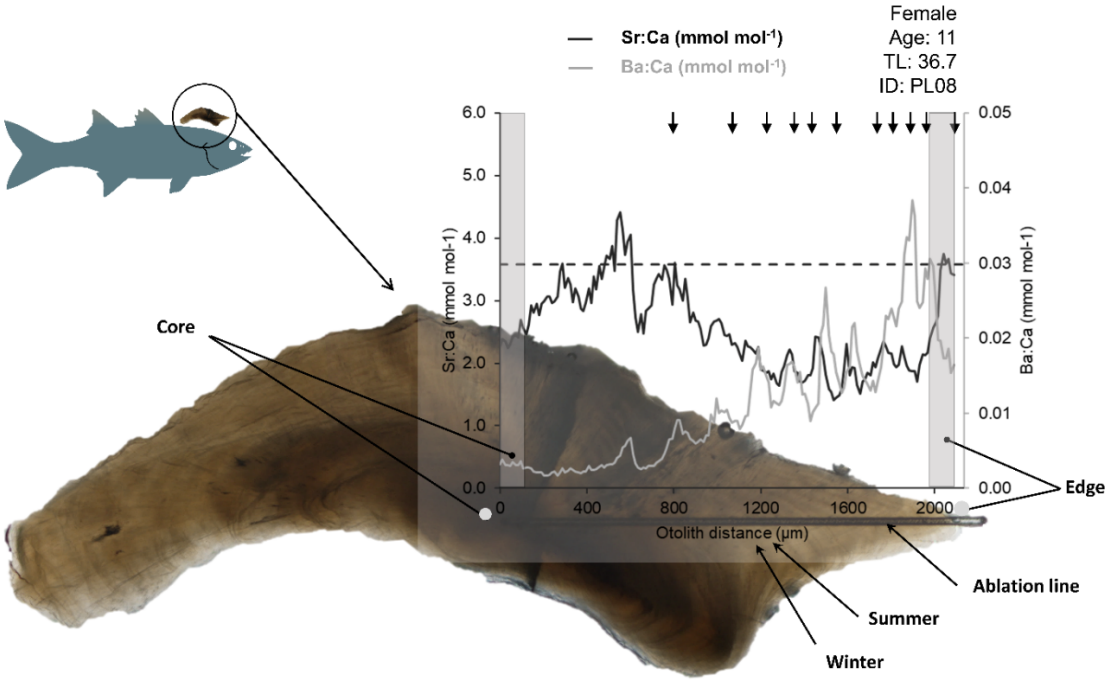

Figure 10
Overlay of a LA-ICP-MS strontium (Sr) and barium (Ba) distribution in otoliths of Chelon labrosus (Source: present PhD thesis).

Although otolith chemistry is more successful in identifying different population groups where there is little to no genetic heterogeneity, disregarding information from either otolith or genetic markers might lead to misconceptions about fish population connectivity (Marengo et al., 2017). Because numerous biophysical processes shape connectivity patterns in marine fish, it is difficult to predict connectivity from early life history features and dispersal potential. Therefore, to provide robust information, it is necessary to synthesize data from various markers, including teletracking approaches, and gather relevant information at different spatio-temporal scales (Reis-Santos et al., 2018).

References

Agbohessi, P.T., Imorou Toko, I., Ouédraogo, A., Jauniaux, T., Mandiki, S.N.M., Kestemont, P., 2015. Assessment of the health status of wild fish inhabiting a cotton basin heavily impacted by pesticides in Benin (West Africa). Science of the Total Environment 506–507, 567–584. https://doi.org/10.1016/j.scitotenv.2014.11.047

Aguilar, C., González-Sansón, G., Hernández, I., MacLatchy, D.L., Munkittrick, K.R., 2007. Effects-based assessment in a tropical coastal system: Status of bicolor damselfish (*Stegastes partitus*) on the north shore of Cuba. Ecotoxicol Environ Saf 67, 459–471. https://doi.org/10.1016/j.ecoenv.2006.05.004

Albaina, A., Iriondo, M., Velado, I., Laconcha, U., Zarraonaindia, I., Arrizabalaga, H., Pardo, M.A., Lutcavage, M., Grant, W.S., Estonba, A., 2013. Single nucleotide polymorphism discovery in albacore and Atlantic bluefin tuna provides insights into worldwide population structure. Anim Genet 44, 678–692. https://doi.org/10.1111/AGE.12051

Antoniou, A., Magoulas, A., 2014. Application of Mitochondrial DNA in Stock Identification, in: Stock Identification Methods. Elsevier, pp. 257–295. https://doi.org/10.1016/B978-0-12-397003-9.00013-8

Arukwe, A., Goksøyr, A., 2003. Eggshell and egg yolk proteins in fish: Hepatic proteins for the next generation: Oogenetic, population, and evolutionary implications of endocrine disruption. Comp Hepatol 2, 1–21. https://doi.org/10.1186/1476-5926-2-4

Aschenbrenner, A., Ferreira, B.P., Rooker, J.R., 2016. Spatial and temporal variability in the otolith chemistry of the Brazilian snapper *Lutjanus alexandrei* from estuarine and coastal environments. J Fish Biol 89, 753–769. https://doi.org/10.1111/jfb.13003

Ashton, N.K., Anders, P.J., Young, S.P., Cain, K.D., 2014. Coded Wire Tag and Passive Integrated Transponder Tag Implantations in Juvenile Burbot. N Am J Fish Manag 34, 391–400. https://doi.org/10.1080/02755947.2014.882458

Au, D.W.T., 2004. The application of histo-cytopathological biomarkers in marine pollution monitoring: A review. Mar Pollut Bull 48, 817–834. https://doi.org/10.1016/j.marpolbul.2004.02.032

Avigliano, E., Ibañez, A., Fabré, N., Callicó Fortunato, R., Méndez, A., Pisonero, J., Volpedo, A. V., 2020. White mullet *Mugil curema* population structure from Mexico and Brazil revealed by otolith chemistry. J Fish Biol 97, 1187–1200. https://doi.org/10.1111/JFB.14500

Bahamonde, P.A., Munkittrick, K.R., Martyniuk, C.J., 2013. Intersex in teleost fish: Are we distinguishing endocrine disruption from natural phenomena? Gen Comp Endocrinol 192, 25–35. https://doi.org/10.1016/j.ygcen.2013.04.005

Baker, N.J., Wright, R.M., Cowx, I.G., Murphy, L.A., Bolland, J.D., 2021. Downstream passage of silver European eel (*Anguilla anguilla*) at a pumping station with a gravity sluice. Ecol Eng 159, 106069. https://doi.org/10.1016/j.ecoleng.2020.106069

Begg, G.A., Campana, S.E., Fowler, A.J., Suthers, I.M., 2005. Otolith research and application: current directions in innovation and implementation. Mar Freshw Res 56, 477. https://doi.org/10.1071/MF05111

Begg, G.A., Waldman, J.R., 1999. An holistic approach to fish stock identification. Fish Res 43, 35–44. https://doi.org/10.1016/S0165-7836(99)00065-X

Belfiore, N., 2001. Effects of contaminants on genetic patterns in aquatic organisms: a review. Mutation Research/Reviews in Mutation Research 489, 97–122. https://doi.org/10.1016/S1383-5742(01)00065-5

Berg, F., Almeland, O.W., Skadal, J., Slotte, A., Andersson, L., Folkvord, A., 2018. Genetic factors have a major effect on growth, number of vertebrae and otolith shape in Atlantic herring (*Clupea harengus*). PLoS One 13, 1–16. https://doi.org/10.1371/journal.pone.0190995

Besbes, R., Benseddik, A.B., Kokokiris, L., Changeux, T., Hamza, A., Kammoun, F., Missaoui, H., 2020. Thicklip (*Chelon labrosus*) and flathead (*Mugil cephalus*) grey mullets fry production in Tunisian aquaculture. Aquac Rep 17, 100380. https://doi.org/10.1016/j.aqrep.2020.100380

Beyer, J., Song, Y., Tollefsen, K.E., Berge, J.A., Tveiten, L., Helland, A., Øxnevad, S., Schøyen, M., 2022. The ecotoxicology of marine tributyltin (TBT) hotspots: A review. Mar Environ Res 179, 105689. https://doi.org/10.1016/j.marenvres.2022.105689

Bhardwaj, J.K., Paliwal, A., Saraf, P., Sachdeva, S.N., 2022. Role of autophagy in follicular development and maintenance of primordial follicular pool in the ovary. J Cell Physiol 237, 1157–1170. https://doi.org/10.1002/JCP.30613

Bhardwaj, J.K., Sharma, R.K., 2012. Apoptosis and ovarian follicular atresia in mammals, in: García, M.-D. (Ed.), Zoology. IntechOpen, pp. 185–206.

Bizarro, C., Ros, O., Vallejo, A., Prieto, A., Etxebarria, N., Cajaraville, M.P., Ortiz-Zarragoitia, M., 2014. Intersex condition and molecular markers of endocrine disruption in relation with burdens of emerging pollutants in thicklip grey mullets (*Chelon labrosus*) from Basque estuaries (South-East Bay of Biscay). Mar Environ Res 96, 19–28. https://doi.org/10.1016/j.marenvres.2013.10.009

Blanchfield, P.J., Kidd, K.A., Docker, M.F., Palace, V.P., Park, B.J., Postma, L.D., 2015. Recovery of a wild fish population from whole-lake additions of a synthetic estrogen. Environ Sci Technol 49, 3136–3144. https://doi.org/10.1021/es5060513

Blázquez, M., Piferrer, F., 2004. Cloning, sequence analysis, tissue distribution, and sex-specific expression of the neural form of P450 aromatase in juvenile sea bass (*Dicentrarchus labrax*). Mol Cell Endocrinol 219, 83–94. https://doi.org/10.1016/j.mce.2004.01.006

Boglione, C., Bertolini, B., Russiello, M., Cataudella, S., 1992. Embryonic and larval development of the thicklipped mullet (*Chelon labrosus*) under controlled reproduction conditions. Aquaculture 101, 349–359. https://doi.org/10.1016/0044-8486(92)90037-L

Borja, Á., Elliott, M., Carstensen, J., Heiskanen, A.-S., van de Bund, W., 2010. Marine management – Towards an integrated implementation of the European Marine Strategy Framework and the Water Framework Directives. Mar Pollut Bull 60, 2175–2186. https://doi.org/10.1016/j.marpolbul.2010.09.026

Borsuk, M.E., Reichert, P., Peter, A., Schager, E., Burkhardt-Holm, P., 2006. Assessing the decline of brown trout (*Salmo trutta*) in Swiss rivers using a Bayesian probability network. Ecol Modell 192, 224–244. https://doi.org/10.1016/j.ecolmodel.2005.07.006

Brander, S.M., 2013. Thinking Outside the Box: Assessing Endocrine Disruption in Aquatic Life, in: Ahuja, S. (Ed.), Monitoring Water Quality. Elsevier, pp. 103–147. https://doi.org/10.1016/B978-0-444-59395-5.00005-4

Bronte, C.R., Walch, K.A., Dettmers, J.M., Gaden, M., Connerton, M.J., Daniels, M.E., Newcomb, T.J., 2012. A coordinated mass marking program for salmonines stocked into the Laurentian Great Lakes. American Fisheries Society Symposium 76, 27–42.

Cabas, I., Chaves-Pozo, E., Alcázar, A.G., Meseguer, J., Mulero, V., García-Ayala, A., 2011. Dietary intake of 17α-ethinylestradiol promotes leukocytes infiltration in the gonad of the hermaphrodite gilthead seabream. Mol Immunol 48, 2079–2086. https://doi.org/10.1016/j.molimm.2011.07.001

Cadrin, S.X., Karr, L.A., Mariani, S., 2014. Stock Identification Methods, in: Stock Identification Methods. Elsevier, pp. 1–5. https://doi.org/10.1016/B978-0-12-397003-9.00001-1

Callicó Fortunato, R., Benedito Durà, V., Volpedo, A., 2017. Otolith morphometry and microchemistry as habitat markers for juvenile *Mugil cephalus* Linnaeus 1758 in nursery grounds in the Valencian community, Spain. Journal of Applied Ichthyology 33, 163–167. https://doi.org/10.1111/jai.13291

Campana, S.E., 2005. Otolith science entering the 21st century. Mar Freshw Res 56, 485. https://doi.org/10.1071/MF04147

Campana, S.E., 1999. Chemistry and composition of fish otoliths: Pathways, mechanisms and applications. Mar Ecol Prog Ser 188, 263–297. https://doi.org/10.3354/meps188263

Campana, S.E., Chouinard, G.A., Hanson, J.M., Fréchet, A., Brattey, J., 2000. Otolith elemental fingerprints as biological tracers of fish stocks. Fish Res 46, 343–357.

Campinho, M.A., 2019. Teleost metamorphosis: The role of thyroid hormone. Front Endocrinol (Lausanne) 10, 1–12. https://doi.org/10.3389/fendo.2019.00383

Campinho, M.A., Silva, N., Roman-Padilla, J., Ponce, M., Manchado, M., Power, D.M., 2015. Flatfish metamorphosis: A hypothalamic independent process? Mol Cell Endocrinol 404, 16–25. https://doi.org/10.1016/j.mce.2014.12.025

Capoccioni, F., Costa, C., Aguzzi, J., Menesatti, P., Lombarte, A., Ciccotti, E., 2011. Ontogenetic and environmental effects on otolith shape variability in three Mediterranean European eel (*Anguilla anguilla*, L.) local stocks. J Exp Mar Biol Ecol 397, 1–7. https://doi.org/10.1016/j.jembe.2010.11.011

Cardona, L., 2006. Habitat selection by grey mullets (Osteichthytes: Mugilidae) in Mediterranean estuaries: The role of salinity. Sci Mar 70, 443–455. https://doi.org/10.3989/scimar.2006.70n3443

Carnevali, O., Santangeli, S., Forner-Piquer, I., Basili, D., Maradonna, F., 2018. Endocrine-disrupting chemicals in aquatic environment: what are the risks for fish gametes? Fish Physiol Biochem 44, 1561–1576. https://doi.org/10.1007/s10695-018-0507-z

Cassel, M., de Paiva Camargo, M., Oliveira de Jesus, L.W., Borella, M.I., 2017. Involution processes of follicular atresia and post-ovulatory complex in a characid fish ovary: a study of apoptosis and autophagy pathways. J Mol Histol 48, 243–257. https://doi.org/10.1007/s10735-017-9723-6

Cermeño, P., Quílez-Badia, G., Ospina-Alvarez, A., Sainz-Trápaga, S., Boustany, A.M., Seitz, A.C., Tudela, S., Block, B.A., 2015. Electronic tagging of Atlantic bluefin tuna (*Thunnus thynnus*, L.) reveals habitat use and behaviors in the Mediterranean Sea. PLoS One 10. https://doi.org/10.1371/journal.pone.0116638

Cheng, J., Yanagimoto, T., Song, N., Gao, T.-X., 2015. Population genetic structure of chub mackerel *Scomber japonicus* in the Northwestern Pacific inferred from microsatellite analysis. Mol Biol Rep 42, 373–82. https://doi.org/10.1007/s11033-014-3777-2

Chukwuka, A., Ogbeide, O., Uhunamure, G., 2019. Gonad pathology and intersex severity in pelagic (*Tilapia zilli*) and benthic (*Neochanna diversus* and *Clarias gariepinus*) species from a pesticide-

impacted agrarian catchment, south-south Nigeria. Chemosphere 225, 535–547. https://doi.org/10.1016/j.chemosphere.2019.03.073

Colín, A., Hernández-Pérez, Z., Guevara-Chumacero, L.M., Castañeda-Rico, S., Serrato-Díaz, A., Ibáñez, A.L., 2020. Are striped mullet (*Mugil cephalus*) philopatric? Mar Biol 167, 1–15. https://doi.org/10.1007/s00227-019-3622-1

Cooke, S.J., Brooks, J.L., Raby, G.D., Thorstad, E.B., Brownscombe, J.W., Vandergoot, C.S., Lennox, R.J., Bulte, G., Bino, G., Thiem, J.D., 2022. Electronic Tagging and Tracking of Animals in Inland Waters, in: Tockner, K., Mehner, T. (Eds.), Encyclopedia of Inland Waters, Second Edition. Elsevier, pp. 699–712. https://doi.org/10.1016/B978-0-12-819166-8.00061-X

Correia, A.T., Moura, A., Triay-Portella, R., Santos, P.T., Pinto, E., Almeida, A.A., Sial, A.N., Muniz, A.A., 2021. Population structure of the chub mackerel (*Scomber colias*) in the NE Atlantic inferred from otolith elemental and isotopic signatures. Fish Res 234, 105785. https://doi.org/10.1016/j.fishres.2020.105785

Correia, A.T., Ramos, A.A., Barros, F., Silva, G., Hamer, P., Morais, P., Cunha, R.L., Castilho, R., 2012. Population structure and connectivity of the European conger eel (*Conger conger*) across the North-Eastern Atlantic and Western Mediterranean: Integrating molecular and otolith elemental approaches. Mar Biol 159, 1509–1525. https://doi.org/10.1007/s00227-012-1936-3

Correia, A.T.T., Hamer, P., Carocinho, B., Silva, A., 2014. Evidence for meta-population structure of *Sardina pilchardus* in the Atlantic Iberian waters from otolith elemental signatures of a strong cohort. Fish Res 149, 76–85. https://doi.org/10.1016/j.fishres.2013.09.016

Corriero, A., Zupa, R., Mylonas, C.C., Passantino, L., 2021. Atresia of ovarian follicles in fishes, and implications and uses in aquaculture and fisheries. J Fish Dis 44, 1271–1291. https://doi.org/10.1111/JFD.13469

Crosetti, D., Blaber, S. (Eds.), 2016. Biology, ecology and culture of grey mullets (Mugilidae), 1st ed. CRC Press. https://doi.org/10.1201/b19927

Cuéllar-Pinzón, J., Presa, P., Hawkins, S.J., Pita, A., 2016. Genetic markers in marine fisheries: Types, tasks and trends. Fish Res 173, 194–205. https://doi.org/10.1016/j.fishres.2015.10.019

Dannewitz, J., Maes, G.E., Johansson, L., Wickström, H., Volckaert, F.A.M., Järvi, T., 2005. Panmixia in the European eel: A matter of time... Proceedings of the Royal Society B: Biological Sciences 272, 1129–1137. https://doi.org/10.1098/rspb.2005.3064

Decourten, B.M., Brander, S.M., 2017. Combined effects of increased temperature and endocrine disrupting pollutants on sex determination, survival, and development across generations. Sci Rep 7, 1–9. https://doi.org/10.1038/s41598-017-09631-1

Decourten, B.M., Forbes, J.P., Roark, H.K., Burns, N.P., Major, K.M., White, J.W., Li, J., Mehinto, A.C., Connon, R.E., Brander, S.M., 2020. Multigenerational and transgenerational effects of environmentally relevant concentrations of endocrine disruptors in an estuarine fish model. Environ Sci Technol 54, 13849–13860. https://doi.org/10.1021/acs.est.0c02892

Dekker, W., 2003. Status of the European Eel Stock and Fisheries. Eel Biology 237–254. https://doi.org/10.1007/978-4-431-65907-5_17

Delbes, G., Blázquez, M., Fernandino, J.I., Grigorova, P., Hales, B.F., Metcalfe, C., Navarro-Martín, L., Parent, L., Robaire, B., Rwigemera, A., Van Der Kraak, G., Wade, M., Marlatt, V., 2022. Effects of endocrine disrupting chemicals on gonad development: Mechanistic insights from fish and mammals. Environ Res 204. https://doi.org/10.1016/j.envres.2021.112040

Devlin, R.H., Nagahama, Y., 2002. Sex determination and sex differentiation in fish: an overview of genetic, physiological, and environmental influences. Aquaculture 208, 191–364. https://doi.org/10.1016/S0044-8486(02)00057-1

Diaz De Cerio, O., Rojo-Bartolomé, I., Bizarro, C., Ortiz-Zarragoitia, M., Cancio, I., 2012. 5S rRNA and accompanying proteins in gonads: powerful markers to identify sex and reproductive endocrine disruption in fish. Environ Sci Technol 46, 7763–7771. https://doi.org/10.1021/es301132b

Díez, G., Díaz, E., Arregi, L., Sagarminaga, Y., Irigoien, X., Álvarez, P., Cotano, U., Murua, H., Santos, M., Murillas, A., 2011. Impact assessment in the life cycle and demographic structure of commercial and ecological interest species after the Prestige oil spill. Revista de Investigación Marina (Marine Research Journal) 18, 92–133.

Doubleday, Z.A., Harris, H.H., Izzo, C., Gillanders, B.M., 2014. Strontium randomly substituting for calcium in fish otolith aragonite. Anal Chem 86, 865–869. https://doi.org/10.1021/ac4034278

Driessnack, M.K., Jamwal, A., Niyogi, S., 2017a. Effects of chronic waterborne cadmium and zinc interactions on tissue-specific metal accumulation and reproduction in fathead minnow (*Pimephales promelas*). Ecotoxicol Environ Saf 140, 65–75. https://doi.org/10.1016/j.ecoenv.2017.02.023

Driessnack, M.K., Jamwal, A., Niyogi, S., 2017b. Effects of chronic exposure to waterborne copper and nickel in binary mixture on tissue-specific metal accumulation and reproduction in fathead minnow (*Pimephales promelas*). Chemosphere 185, 964–974. https://doi.org/10.1016/j.chemosphere.2017.07.100

Du, X., Wang, B., Liu, Xiumei, Liu, Xiaobing, He, Y., Zhang, Q., Wang, X., 2017. Comparative transcriptome analysis of ovary and testis reveals potential sex-related genes and pathways in spotted knifejaw *Oplegnathus punctatus*. Gene 637, 203–210. https://doi.org/10.1016/j.gene.2017.09.055

Durand, J.D., Blel, H., Shen, K.N., Koutrakis, E.T., Guinand, B., 2013. Population genetic structure of *Mugil cephalus* in the Mediterranean and Black Seas: A single mitochondrial clade and many nuclear barriers. Mar Ecol Prog Ser 474, 243–261. https://doi.org/10.3354/meps10080

Durand, J.D., Shen, K.N., Chen, W.J., Jamandre, B.W., Blel, H., Diop, K., Nirchio, M., Garcia de León, F.J., Whitfield, A.K., Chang, C.W., Borsa, P., 2012. Systematics of the grey mullets (Teleostei: Mugiliformes: Mugilidae): Molecular phylogenetic evidence challenges two centuries of morphology-based taxonomy. Mol Phylogenet Evol 64, 73–92. https://doi.org/10.1016/j.ympev.2012.03.006

Dzul, M.C., Kendall, W.L., Yackulic, C.B., Winkelman, D.L., Van Haverbeke, D.R., Yard, M., 2021. Partial migration and spawning movements of humpback chub in the Little Colorado River are better understood using data from autonomous PIT tag antennas. Canadian Journal of Fisheries and Aquatic Sciences 78, 1057–1072. https://doi.org/10.1139/cjfas-2020-0291

Ekblom, R., Galindo, J., 2011. Applications of next generation sequencing in molecular ecology of non-model organisms. Heredity (Edinb) 107, 1–15. https://doi.org/10.1038/hdy.2010.152

Elsdon, T.S., Gillanders, B.M., 2004. Fish otolith chemistry influenced by exposure to multiple environmental variables. J Exp Mar Biol Ecol 313, 269–284. https://doi.org/10.1016/j.jembe.2004.08.010

EPA, 2001. Removal of endocrine disruptor chemicals using drinking water treatment processes. EPA/625/R-00/015. Washington, DC.

Fernandino, J.I., Hattori, R.S., Moreno Acosta, O.D., Strüssmann, C.A., Somoza, G.M., 2013. Environmental stress-induced testis differentiation: Androgen as a by-product of cortisol inactivation. Gen Comp Endocrinol 192, 36–44. https://doi.org/10.1016/j.ygcen.2013.05.024

Ferreira, I., Santos, D., Moreira, C., Feijó, D., Rocha, A., Correia, A.T., 2019. Population structure of *Chelidonichthys lucerna* in Portugal mainland using otolith shape and elemental signatures. Marine Biology Research 15, 500–512. https://doi.org/10.1080/17451000.2019.1673897

Filby, A.L., Thorpe, K.L., Maack, G., Tyler, C.R., 2007. Gene expression profiles revealing the mechanisms of anti-androgen- and estrogen-induced feminization in fish. Aquatic Toxicology 81, 219–231. https://doi.org/10.1016/j.aquatox.2006.12.003

Flanagan, S.P., Jones, A.G., 2019. The future of parentage analysis: From microsatellites to SNPs and beyond. Mol Ecol 28, 544–567. https://doi.org/10.1111/mec.14988

Freyhof, J., Kottelat, M., 2008. *Chelon labrosus*,Thicklip Grey Mullet [WWW Document]. IUCN Red List. https://doi.org/10.2305/IUCN.UK.2008.RLTS.T135689A4182365.en

Frid, C.L.J., Caswell, B.A., 2017. Marine Pollution. Oxford University Press. https://doi.org/10.1093/oso/9780198726289.001.0001

Froese, R., Pauly, D. (Eds.), 2022. *Chelon labrosus* summary page [WWW Document]. www.fishbase.org. URL https://fishbase.se/summary/Chelon-labrosus.html (accessed 6.15.22).

Fromentin, J.-M., Lopuszanski, D., 2014. Migration, residency, and homing of bluefin tuna in the western Mediterranean Sea. ICES Journal of Marine Science 71, 510–518. https://doi.org/doi:10.1093/icesjms/fst157

Gallagher, J., Lordan, C., Hughes, G.M., Jonasson, J.P., Carlsson, J., 2022. Microsatellites obtained using high throughput sequencing and a novel microsatellite genotyping method reveals population genetic structure in Norway Lobster, *Nephrops norvegicus*. J Sea Res 179, 102139. https://doi.org/10.1016/j.seares.2021.102139

Gandra, M., Assis, J., Martins, M.R., Abecasis, D., 2021. Reduced global genetic differentiation of exploited marine fish species. Mol Biol Evol 38, 1402–1412. https://doi.org/10.1093/molbev/msaa299

García-Fernández, C., Domínguez-Petit, R., Aldanondo, N., Saborido-Rey, F., 2020. Seasonal variability of maternal effects in European hake *Merluccius merluccius*. Mar Ecol Prog Ser 650, 125–140. https://doi.org/10.3354/meps13420

Goksøyr, A., 2006. Endocrine disruptors in the marine environment: Mechanisms of toxicity and their influence on reproductive processes in fish. J Toxicol Environ Health A 69, 175–184. https://doi.org/10.1080/15287390500259483

Golovko, O., Örn, S., Sörengård, M., Frieberg, K., Nassazzi, W., Lai, F.Y., Ahrens, L., 2021. Occurrence and removal of chemicals of emerging concern in wastewater treatment plants and their impact on receiving water systems. Science of the Total Environment 754, 142122. https://doi.org/10.1016/j.scitotenv.2020.142122

Gong, X., Davenport, E.R., Wang, D., Clark, A.G., 2019. Lack of spatial and temporal genetic structure of Japanese eel (*Anguilla japonica*) populations. Conservation Genetics 20, 467–475. https://doi.org/10.1007/s10592-019-01146-8

González-Kother, P., Oliva, M.E., Tanguy, A., Moraga, D., 2020. A review of the potential genes implicated in follicular atresia in teleost fish. Mar Genomics 50, 100704. https://doi.org/10.1016/j.margen.2019.100704

Green, B.S., Mapstone, B.D., Carlos, Gary., Begg, G.A., 2009. Tropical Fish Otoliths: Information for Assessment, Management and Ecology, 1st ed, Reviews: Methods and Technologies in Fish Biology and Fisheries. Springer Netherlands, Dordrecht. https://doi.org/10.1007/978-1-4020-5775-5

Guraya, Sardul S., 1986. The cell and molecular biology of fish oogenesis. Monogr Dev Biol, Monographs in Developmental Biology 18, 1–223.

Guraya, Sardul S, 1986. The cell and molecular biology of fish oogenesis. Karger, Basel. https://doi.org/10.1016/0165-7836(89)90071-4

Guzmán, J.M., Adam Luckenbach, J., Swanson, P., 2013. Molecular characterization and quantification of sablefish (*Anoplopoma fimbria*) gonadotropins and their receptors: Reproductive dysfunction in female captive broodstock. Gen Comp Endocrinol 193, 37–47. https://doi.org/10.1016/j.ygcen.2013.07.007

Habibi, H.R., Andreu-Vieyra, C. V., 2007. Hormonal regulation of follicular atresia in teleost fish, in: Babin, P.J., Cerdà, J., Lubzens, E. (Eds.), The Fish Oocyte: From Basic Studies to Biotechnological Applications. Springer Netherlands, pp. 235–253. https://doi.org/10.1007/978-1-4020-6235-3_9

Hachfi, L., Couvray, S., Simide, R., Tarnowska, K., Pierre, S., Gaillard, S., Richard, S., Coupé, S., Grillasca, J.-P., Prévot-D 'alvise, N., 2012. Impact of endocrine disrupting chemicals [EDCs] on Hypothalamic-Pituitary-Gonad-Liver [HPGL] axis in fish. World Journal of Fish and Marine Sciences 4, 14–30.

Hall, D.A., 2014. Conventional and Radio Frequency Identification (RFID) Tags, in: Stock Identification Methods. Elsevier, pp. 365–395. https://doi.org/10.1016/B978-0-12-397003-9.00016-3

Halpern, B.S., Silliman, B.R., Olden, J.D., Bruno, J.P., Bertness, M.D., 2007. Incorporating positive interactions in aquatic restoration and conservation. Front Ecol Environ 5, 153–160. https://doi.org/10.1890/1540-9295(2007)5[153:IPIIAR]2.0.CO;2

Hamilton, P.B., Cowx, I.G., Oleksiak, M.F., Griffiths, A.M., Grahn, M., Stevens, J.R., Carvahlo, G.R., Nicol, E., Tyler, C.R., 2016. Population-level consequences for wild fish exposed to sublethal concentrations of chemicals – a critical review. Fish and Fisheries 17, 545–566. https://doi.org/10.1111/faf.12125

Harris, C.A., Hamilton, P.B., Runnalls, T.J., Vinciotti, V., Henshaw, A., Hodgson, D., Coe, T.S., Jobling, S., Tyler, C.R., Sumpter, J.P., 2011. The consequences of feminization in breeding groups of wild fish. Environ Health Perspect 119, 306–311. https://doi.org/10.1289/ehp.1002555

Hedger, R.D., Rikardsen, A.H., Thorstad, E.B., 2017. Pop-up satellite archival tag effects on the diving behaviour, growth and survival of adult Atlantic salmon *Salmo salar* at sea. J Fish Biol 90, 294–310. https://doi.org/10.1111/jfb.13174

Heras, S., Planella, L., García-Marín, J.-L., Vera, M., Roldán, M.I., 2019. Genetic structure and population connectivity of the blue and red shrimp *Aristeus antennatus*. Sci Rep 9, 13531. https://doi.org/10.1038/s41598-019-49958-5

Hickling, C.F., 1970. A contribution to the natural history of the English grey mullets [Pisces, Mugilidae]. Journal of the Marine Biological Association of the United Kingdom 50, 609–633. https://doi.org/10.1017/S0025315400004914

Hinck, J.E., Blazer, V.S., Denslow, N.D., Echols, K.R., Gross, T.S., May, T.W., Anderson, P.J., Coyle, J.J., Tillitt, D.E., 2007. Chemical contaminants, health indicators, and reproductive biomarker responses in fish from the Colorado River and its tributaries. Science of The Total Environment 378, 376–402. https://doi.org/10.1016/J.SCITOTENV.2007.02.032

Hoff, N.T., Dias, J.F., Pinto, E., Almeida, A., Schroeder, R., Correia, A.T., 2022. Potential Anthropogenic Interferences and Allows Refinement.

Hussey, N.E., Kessel, S.T., Aarestrup, K., Cooke, S.J., Cowley, P.D., Fisk, A.T., Harcourt, R.G., Holland, K.N., Iverson, S.J., Kocik, J.F., Flemming, J.E.M., Whoriskey, F.G., 2015. Aquatic animal telemetry: A panoramic window into the underwater world. Science (1979) 348, 1255642. https://doi.org/10.1126/science.1255642

Hüssy, K., 2008. Otolith shape in juvenile cod (*Gadus morhua*): Ontogenetic and environmental effects. J Exp Mar Biol Ecol 364, 35–41. https://doi.org/10.1016/j.jembe.2008.06.026

Hüssy, K., Limburg, K.E., de Pontual, H., Thomas, O.R.B., Cook, P.K., Heimbrand, Y., Blass, M., Sturrock, A.M., 2021. Trace element patterns in otoliths: The role of biomineralization. Reviews in Fisheries Science and Aquaculture 29, 445–477. https://doi.org/10.1080/23308249.2020.1760204

Ismail, N.A.H., Wee, S.Y., Aris, A.Z., 2017. Multi-class of endocrine disrupting compounds in aquaculture ecosystems and health impacts in exposed biota. Chemosphere 188, 375–388. https://doi.org/10.1016/j.chemosphere.2017.08.150

Izzo, C., Reis-Santos, P., Gillanders, B.M., 2018. Otolith chemistry does not just reflect environmental conditions: A meta-analytic evaluation. Fish and Fisheries 19, 441–454. https://doi.org/10.1111/faf.12264

Janz, D.M., Van Der Kraak, G.J., 1997. Suppression of apoptosis by gonadotropin, 17β-estradiol, and epidermal growth factor in rainbow trout preovulatory ovarian follicles. Gen Comp Endocrinol 105, 186–193. https://doi.org/10.1006/gcen.1996.6820

Jepsen, N., Thorstad, E.B., Havn, T., Lucas, M.C., 2015. The use of external electronic tags on fish: An evaluation of tag retention and tagging effects. Animal Biotelemetry 3. https://doi.org/10.1186/s40317-015-0086-z

Jiang, J., Chen, Y., Yu, R., Zhao, X., Wang, Q., Cai, L., 2016. Pretilachlor has the potential to induce endocrine disruption, oxidative stress, apoptosis and immunotoxicity during zebrafish embryo development. Environ Toxicol Pharmacol 42, 125–134. https://doi.org/10.1016/j.etap.2016.01.006

Jiang, J., Wu, S., Liu, X., Wang, Y., An, X., Cai, L., Zhao, X., 2015a. Effect of acetochlor on transcription of genes associated with oxidative stress, apoptosis, immunotoxicity and endocrine disruption in the early life stage of zebrafish. Environ Toxicol Pharmacol 40, 516–523. https://doi.org/10.1016/j.etap.2015.08.005

Jiang, J., Wu, S., Wang, Y., An, X., Cai, L., Zhao, X., Wu, C., 2015b. Carbendazim has the potential to induce oxidative stress, apoptosis, immunotoxicity and endocrine disruption during zebrafish larvae development. Toxicology in Vitro 29, 1473–1481. https://doi.org/10.1016/j.tiv.2015.06.003

Jiang, Y.X., Shi, W.J., Ma, D.D., Zhang, J.N., Ying, G.G., Zhang, H., Ong, C.N., 2019. Dydrogesterone exposure induces zebrafish ovulation but leads to oocytes over-ripening: An integrated histological and metabolomics study. Environ Int 128, 390–398. https://doi.org/10.1016/j.envint.2019.04.059

Jobling, S., Beresford, N., Nolan, M., Rodgers-Gray, T., Brighty, G.C., Sumpter, J.P., Tyler, C.R., 2002a. Altered sexual maturation and gamete production in wild roach (*Rutilus rutilus*) living in rivers that receive treated sewage effluents. Biol Reprod 66, 272–281. https://doi.org/10.1095/biolreprod66.2.272

Jobling, S., Coey, S., Whitmore, J.G., Kime, D.E., Van Look, K.J.W., McAllister, B.G., Beresford, N., Henshaw, A.C., Brighty, G., Tyler, C.R., Sumpter, J.P., 2002b. Wild intersex roach (*Rutilus rutilus*) have reduced fertility. Biol Reprod 67, 515–524. https://doi.org/10.1095/biolreprod67.2.515

Jobling, S., Nolan, M., Tyler, C.R., Brighty, G., Sumpter, J.P., 1998. Widespread sexual disruption in wild fish. Environ Sci Technol 32, 2498–2506. https://doi.org/10.1021/es9710870

Jobling, S., Sheahan, D., Osborne, J.A., Matthiessen, P., Sumpter, J.P., 1996. Inhibition of testicular growth in rainbow trout (*Oncorhynchus mykiss*) exposed to estrogenic alkylphenolic chemicals. Environ Toxicol Chem 15, 194–202. https://doi.org/10.1897/1551-5028(1996)015<0194:IOTGIR>2.3.CO;2

Jobling, S., Tyler, C.R., 2006. Introduction: The ecological relevance of chemically induced endocrine disruption in wildlife. Environ Health Perspect 114, 7–8. https://doi.org/10.1289/ehp.8046

Karaiskou, N., Triantafyllidis, A., Triantaphyllidis, C., 2004. Shallow genetic structure of three species of the genus Trachurus in European waters. Mar Ecol Prog Ser 281, 193–205. https://doi.org/10.3354/meps281193

Kennedy, J., Gundersen, A.C., Boje, J., 2009. When to count your eggs: Is fecundity in Greenland halibut (*Reinhardtius hippoglossoides* W.) down-regulated? Fish Res 100, 260–265. https://doi.org/https://doi.org/10.1016/j.fishres.2009.08.008

Kidd, K.A., Blanchfield, P.J., Mills, K.H., Palace, V.P., Evans, R.E., Lazorchak, J.M., Flick, R.W., 2007. Collapse of a fish population after exposure to a synthetic estrogen. Proc Natl Acad Sci U S A 104, 8897–8901. https://doi.org/10.1073/pnas.0609568104

Kimball, M.E., Mace, M.M., 2020. Survival, Growth, and Tag Retention in Estuarine Fishes Implanted with Passive Integrated Transponder (PIT) Tags. Estuaries and Coasts 43, 151–160. https://doi.org/10.1007/s12237-019-00657-4

King Heiden, T., Carvan, M.J., Hutz, R.J., 2006. Inhibition of follicular development, vitellogenesis, and serum 17β-estradiol concentrations in zebrafish following chronic, sublethal dietary exposure to 2,3,7,8-tetrachlorodibenzo-p-dioxin. Toxicological Sciences 90, 490–499. https://doi.org/10.1093/toxsci/kfj085

Kjesbu, O.S., 2009. Applied fish reproductive biology: contribution of individual reproductive potential to recruitment and fisheries management, in: Jakobsen, T., Forgarty, M., Megrey, Bernard.A., Moksness, E. (Eds.), Fish Reproductive Biology: Implications for Assessment and Management. Wiley-Blackwell, pp. 293–332. https://doi.org/10.1002/9781444312133.ch8

Klimley, A.P., MacFarlane, R.B., Sandstrom, P.T., Lindley, S.T., 2013. A summary of the use of electronic tagging to provide insights into salmon migration and survival. Environ Biol Fishes 96, 419–428. https://doi.org/10.1007/s10641-012-0098-y

Korta, M., Murua, H., Kurita, Y., Kjesbu, O.S., 2010. How are the oocytes recruited in an indeterminate fish? Applications of stereological techniques along with advanced packing density theory on European hake (*Merluccius merluccius* L.). Fish Res 104, 56–63. https://doi.org/10.1016/j.fishres.2010.01.010

Kroglund, F., Finstad, B., 2003. Low concentrations of inorganic monomeric aluminum impair physiological status and marine survival of Atlantic salmon. Aquaculture 222, 119–133. https://doi.org/10.1016/S0044-8486(03)00106-6

Krück, N.C., Innes, D.I., Ovenden, J.R., 2013. New SNPs for population genetic analysis reveal possible cryptic speciation of eastern Australian sea mullet (*Mugil cephalus*). Mol Ecol Resour 13, 715–725. https://doi.org/10.1111/1755-0998.12112

Krysko, D. V., Diez-Fraile, A., Criel, G., Svistunov, A.A., Vandenabeele, P., D'Herde, K., 2008. Life and death of female gametes during oogenesis and folliculogenesis. Apoptosis 13, 1065–1087. https://doi.org/10.1007/s10495-008-0238-1

Kumar, R., Joy, K.P., 2015. Melanins as biomarkers of ovarian follicular atresia in the catfish *Heteropneustes fossilis*: biochemical and histochemical characterization, seasonal variation and hormone effects. Fish Physiol Biochem 41, 761–772. https://doi.org/10.1007/s10695-015-0044-y

Laranjeiro, F., Sánchez-Marín, P., Oliveira, I.B., Galante-Oliveira, S., Barroso, C., 2018. Fifteen years of imposex and tributyltin pollution monitoring along the Portuguese coast. Environmental Pollution 232, 411–421. https://doi.org/10.1016/j.envpol.2017.09.056

Laugier, F., Feunteun, E., Pecheyran, C., Carpentier, A., 2015. Life history of the Small Sandeel, *Ammodytes tobianus*, inferred from otolith microchemistry. A methodological approach. Estuar Coast Shelf Sci 165, 237–246. https://doi.org/10.1016/j.ecss.2015.05.022

Leander, J., Klaminder, J., Hellström, G., Jonsson, M., 2021. Bubble barriers to guide downstream migrating Atlantic salmon (*Salmo salar*): An evaluation using acoustic telemetry. Ecol Eng 160, 106141. https://doi.org/10.1016/j.ecoleng.2020.106141

Leander, J., Klaminder, J., Jonsson, M., Brodin, T., Leonardsson, K., Hellström, G., 2020. The old and the new: Evaluating performance of acoustic telemetry systems in tracking migrating Atlantic salmon (*Salmo salar*) smolt and European eel (*Anguilla anguilla*) around hydropower facilities. Canadian Journal of Fisheries and Aquatic Sciences 77, 177–187. https://doi.org/10.1139/cjfas-2019-0058

Lemos, V.M., Monteiro-Neto, C., Cabral, H., Vieira, J.P., 2017. Stock identification of tainha (*Mugil liza*) by analyzing stable carbon and oxygen isotopes in otoliths. Fishery Bulletin 115, 201–205. https://doi.org/10.7755/FB.115.2.7

Lennox, R.J., Aarestrup, K., Cooke, S.J., Cowley, P.D., Deng, Z.D., Fisk, A.T., Harcourt, R.G., Heupel, M., Hinch, S.G., Holland, K.N., Hussey, N.E., Iverson, S.J., Kessel, S.T., Kocik, J.F., Lucas, M.C., Flemming, J.M., Nguyen, V.M., Stokesbury, M.J.W., Vagle, S., Vanderzwaag, D.L., Whoriskey, F.G., Young, N., 2017. Envisioning the future of aquatic animal tracking: technology, science, and application. Bioscience 67, 884–896. https://doi.org/10.1093/biosci/bix098

Levine, A.J., Feng, Z., Mak, T.W., You, H., Jin, S., 2006. Coordination and communication between the p53 and IGF-1-AKT-TOR signal transduction pathways. Genes Dev 20, 267–275. https://doi.org/10.1101/gad.1363206

Levine, A.J., Oren, M., 2009. The first 30 years of p53: Growing ever more complex. Nat Rev Cancer 9, 749–758. https://doi.org/10.1038/nrc2723

Li, W., Guan, X., Sun, L., 2020. Phosphatase and tensin homolog (Pten) of japanese flounder—its regulation by miRNA and role in autophagy, apoptosis and pathogen infection. Int J Mol Sci 21, 1–18. https://doi.org/10.3390/ijms21207725

Li, W.C., 2014. Occurrence, sources, and fate of pharmaceuticals in aquatic environment and soil. Environmental Pollution 187, 193–201. https://doi.org/10.1016/J.ENVPOL.2014.01.015

Liarte, S., Cabas, I., Chaves-Pozo, E., Arizcun, M., Meseguer, J., Mulero, V., García-Ayala, A., 2011. Natural and synthetic estrogens modulate the inflammatory response in the gilthead seabream (*Sparus aurata* L.) through the activation of endothelial cells. Mol Immunol 48, 1917–1925. https://doi.org/10.1016/j.molimm.2011.05.019

Libungan, L.A., Óskarsson, G.J., Slotte, A., Jacobsen, J.A., Pálsson, S., 2015. Otolith shape: A population marker for Atlantic herring *Clupea harengus*. J Fish Biol 86, 1377–1395. https://doi.org/10.1111/jfb.12647

Libungan, L.A., Pálsson, S., 2015. ShapeR: An R package to study otolith shape variation among fish populations. PLoS One 10, 1–12. https://doi.org/10.1371/journal.pone.0121102

Lin, C.-J., Maugars, G., Lafont, A.-G., Jeng, S.-R., Wu, G.-C., Dufour, S., Chang, C.-F., 2020. Basal teleosts provide new insights into the evolutionary history of teleost-duplicated aromatase. Gen Comp Endocrinol 291, 113395. https://doi.org/10.1016/j.ygcen.2020.113395

Lind, E.E., Grahn, M., 2011. Directional genetic selection by pulp mill effluent on multiple natural populations of three-spined stickleback (*Gasterosteus aculeatus*). Ecotoxicology 20, 503–512. https://doi.org/10.1007/s10646-011-0639-8

Lindholst, C., Pedersen, K.L., Pedersen, S.N., 2000. Estrogenic response of bisphenol A in rainbow trout (*Oncorhynchus mykiss*). Aquatic Toxicology 48, 87–94. https://doi.org/10.1016/S0166-445X(99)00051-X

Liu, B.J., Li, Y.L., Zhang, B.D., Liu, J.X., 2020. Genome-wide discovery of single-nucleotide polymorphisms and their application in population genetic studies in the endangered Japanese eel (*Anguilla japonica*). Front Mar Sci 6, 1–11. https://doi.org/10.3389/fmars.2019.00782

Lobón-Cerviá, J., 2009. Why, when and how do fish populations decline, collapse and recover? the example of brown trout (*Salmo trutta*) in Rio Chaballos (Northwestern Spain). Freshw Biol 54, 1149–1162. https://doi.org/10.1111/j.1365-2427.2008.02159.x

Lou, R.N., Jacobs, A., Wilder, A.P., Therkildsen, N.O., 2021. A beginner's guide to low-coverage whole genome sequencing for population genomics. Mol Ecol 30, 5966–5993. https://doi.org/10.1111/mec.16077

Lowe, W.H., Allendorf, F.W., 2010. What can genetics tell us about population connectivity? Mol Ecol 19, 3038–3051. https://doi.org/10.1111/j.1365-294X.2010.04688.x

Lubzens, E., Young, G., Bobe, J., Cerdà, J., 2010. Oogenesis in teleosts: How fish eggs are formed. Gen Comp Endocrinol 165, 367–389. https://doi.org/10.1016/j.ygcen.2009.05.022

Luzio, A., Monteiro, S.M., Rocha, E., Fontaínhas-Fernandes, A.A., Coimbra, A.M., 2016. Development and recovery of histopathological alterations in the gonads of zebrafish (*Danio rerio*) after single and combined exposure to endocrine disruptors (17α-ethinylestradiol and fadrozole). Aquatic Toxicology 175, 90–105. https://doi.org/10.1016/j.aquatox.2016.03.014

Macdonald, J.I., Drysdale, R.N., Witt, R., Cságoly, Z., Marteinsdóttir, G., 2020. Isolating the influence of ontogeny helps predict island-wide variability in fish otolith chemistry. Rev Fish Biol Fish 30, 173–202. https://doi.org/10.1007/s11160-019-09591-x

Madureira, T.V., Rocha, M.J., Cruzeiro, C., Galante, M.H., Monteiro, R.A.F., Rocha, E., 2011. The toxicity potential of pharmaceuticals found in the Douro River estuary (Portugal): Assessing impacts on gonadal maturation with a histopathological and stereological study of zebrafish ovary and testis after sub-acute exposures. Aquatic Toxicology 105, 292–299. https://doi.org/10.1016/j.aquatox.2011.06.017

Mai, A.C.G., Santos, M.L. dos, Lemos, V.M., Vieira, J.P., 2018. Discrimination of habitat use between two sympatric species of mullets, *Mugil curema* and *Mugil liza* (Mugiliformes: Mugilidae) in the rio Tramandaí Estuary, determined by otolith chemistry. Neotropical Ichthyology 16, 1–8. https://doi.org/10.1590/1982-0224-20170045

Major, K.M., DeCourten, B.M., Li, J., Britton, M., Settles, M.L., Mehinto, A.C., Connon, R.E., Brander, S.M., 2020. Early life exposure to environmentally relevant levels of endocrine disruptors drive multigenerational and transgenerational epigenetic changes in a fish model. Front Mar Sci 7, 1–17. https://doi.org/10.3389/fmars.2020.00471

Marengo, M., Baudouin, M., Viret, A., Laporte, M., Berrebi, P., Vignon, M., Marchand, B., Durieux, E.D.H., 2017. Combining microsatellite, otolith shape and parasites community analyses as a holistic approach to assess population structure of *Dentex dentex*. J Sea Res 128, 1–14. https://doi.org/10.1016/j.seares.2017.07.003

Martinez, A.S., Willoughby, J.R., Christie, M.R., 2018. Genetic diversity in fishes is influenced by habitat type and life-history variation. Ecol Evol 8, 12022–12031. https://doi.org/10.1002/ece3.4661

Matsuda, F., Inoue, N., Manabe, N., Ohkura, S., 2012. Follicular growth and atresia in mammalian ovaries: Regulation by survival and death of granulosa cells. Journal of Reproduction and Development 58, 44–50. https://doi.org/10.1262/jrd.2011-012

Matthiessen, P., 2003. Endocrine disruption in marine fish. Pure and Applied Chemistry 75, 2249–2261. https://doi.org/10.1351/pac200375112249

Mayon, N., Bertrand, A., Leroy, D., Malbrouck, C., Mandiki, S.N.M., Silvestre, F., Goffart, A., Thomé, J.P., Kestemont, P., 2006. Multiscale approach of fish responses to different types of environmental contaminations: A case study. Science of the Total Environment 367, 715–731. https://doi.org/10.1016/j.scitotenv.2006.03.005

McDonough, C.J., Roumillat, W.A., Wenner, C.A., 2005. Sexual differentiation and gonad development in striped mullet (*Mugil cephalus* L.) from South Carolina estuaries. Fishery Bulletin 103, 601–619.

McGee, E.A., Horne, J., 2018. Follicle atresia, Second Edi. ed, Encyclopedia of Reproduction. Elsevier. https://doi.org/10.1016/B978-0-12-801238-3.64395-7

Meucci, V., Arukwe, A., 2006. Transcriptional modulation of brain and hepatic estrogen receptor and P450arom isotypes in juvenile Atlantic salmon (*Salmo salar*) after waterborne exposure to the xenoestrogen, 4-nonylphenol. Aquatic Toxicology 77, 167–177. https://doi.org/10.1016/j.aquatox.2005.11.008

Meyer, M.F., Powers, S.M., Hampton, S.E., 2019. An evidence synthesis of pharmaceuticals and personal care products (PPCPs) in the environment: imbalances among compounds, sewage treatment techniques, and ecosystem types. Environ Sci Technol 53, 12961–12973. https://doi.org/10.1021/acs.est.9b02966

Mićković, B., Nikčević, M., Hegediš, A., Regner, S., Gačić, Z., Krpo-Ćetković, J., 2010. Mullet fry (Mugilidae) in coastal waters of Montenegro, their spatial distribution and migration phenology. Arch Biol Sci. https://doi.org/10.2298/ABS1001107M

Miranda, A.C.L., Bazzoli, N., Rizzo, E., Sato, Y., 1999. Ovarian follicular atresia in two teleost species: a histological and ultrastructural study. Tissue Cell 31, 480–488. https://doi.org/10.1054/tice.1999.0045

Mohapatra, S., Kumar, R., Sundaray, J.K., Patnaik, S.T., Mishra, C.S.K., Rather, M.A., 2021. Structural damage in liver, gonads, and reduction in spawning performance and alteration in the haematological parameter of *Anabas testudineus* by glyphosate- a herbicide. Aquac Res 52, 1150–1159. https://doi.org/10.1111/are.14973

Montes, I., Iriondo, M., Manzano, C., Arrizabalaga, H., Jiménez, E., Pardo, M.Á., Goñi, N., Davies, C.A., Estonba, A., 2012. Worldwide genetic structure of albacore *Thunnus alalunga* revealed by microsatellite DNA markers. Mar Ecol Prog Ser 471, 183–191. https://doi.org/10.3354/meps09991

Montes, I., Zarraonaindia, I., Iriondo, M., Grant, W.S., Manzano, C., Cotano, U., Conklin, D., Irigoien, X., Estonba, A., 2016. Transcriptome analysis deciphers evolutionary mechanisms underlying genetic differentiation between coastal and offshore anchovy populations in the Bay of Biscay. Mar Biol 163, 205. https://doi.org/10.1007/s00227-016-2979-7

Moore, B.R., 2011. Movement, connectivity and population structure of a large, non-diadromous, tropical estuarine teleost (PhD thesis). James Cook University.

Morais, R.D.V.S., Thomé, R.G., Lemos, F.S., Bazzoli, N., Rizzo, E., 2012. Autophagy and apoptosis interplay during follicular atresia in fish ovary: a morphological and immunocytochemical study. Cell Tissue Res 347, 467–478. https://doi.org/10.1007/s00441-012-1327-6

Morais, R.D.V.S., Thomé, R.G., Santos, H.B., Bazzoli, N., Rizzo, E., 2016. Relationship between bcl-2, bax, beclin-1, and cathepsin-D proteins during postovulatory follicular regression in fish ovary. Theriogenology 85, 1118–1131. https://doi.org/10.1016/j.theriogenology.2015.11.024

Moreira, C., Correia, A.T., Vaz-Pires, P., Froufe, E., 2019a. Genetic diversity and population structure of the blue jack mackerel *Trachurus picturatus* across its western distribution. J Fish Biol 94, 725–731. https://doi.org/10.1111/jfb.13944

Moreira, C., Froufe, E., Sial, A.N., Caeiro, A., Vaz-Pires, P., Correia, A.T., 2018. Population structure of the blue jack mackerel (*Trachurus picturatus*) in the NE Atlantic inferred from otolith microchemistry. Fish Res 197, 113–122. https://doi.org/10.1016/j.fishres.2017.08.012

Moreira, C., Froufe, E., Vaz-Pires, P., Correia, A.T., 2019b. Otolith shape analysis as a tool to infer the population structure of the blue jack mackerel, *Trachurus picturatus,* in the NE Atlantic. Fish Res 209, 40–48. https://doi.org/10.1016/j.fishres.2018.09.010

Moreira, C., Presa, P., Correia, A.T., Vaz-Pires, P., Froufe, E., 2020. Spatio-temporal microsatellite data suggest a multidirectional connectivity pattern in the *Trachurus picturatus* metapopulation from the Northeast Atlantic. Fish Res 225, 105–499. https://doi.org/10.1016/j.fishres.2020.105499

Moura, A., Dias, E., López, R., Antunes, C., 2022. Regional population structure of the European eel at the southern limit of its distribution revealed by otolith shape signature. Fishes 7. https://doi.org/10.3390/fishes7030135

Moura, A., Muniz, A.A., Mullis, E., Wilson, J.M., Vieira, R.P., Almeida, A.A., Pinto, E., Brummer, G.J.A., Gaever, P.V., Gonçalves, J.M.S., Correia, A.T., 2020. Population structure and dynamics of the Atlantic mackerel (*Scomber scombrus*) in the North Atlantic inferred from otolith chemical and shape signatures. Fish Res 230, 105621. https://doi.org/10.1016/j.fishres.2020.105621

Murua, H., Lucio, P., Santurtún, M., Motos, L., 2006. Seasonal variation in egg production and batch fecundity of European hake *Merluccius merluccius* (L.) in the Bay of Biscay. J Fish Biol 69, 1304–1316. https://doi.org/10.1111/j.1095-8649.2006.01209.x

Murua, H., Motos, L., 2006. Reproductive strategy and spawning activity of the European hake *Merluccius merluccius* (L.) in the Bay of Biscay. J Fish Biol 69, 1288–1303. https://doi.org/10.1111/j.1095-8649.2006.01169.x

Musyl, M.K., Domeier, M.L., Nasby-Lucas, N., Brill, R.W., McNaughton, L.M., Swimmer, J.Y., Lutcavage, M.S., Wilson, S.G., Galuardi, B., Liddle, J.B., 2011. Performance of pop-up satellite archival tags. Mar Ecol Prog Ser 433, 1–28. https://doi.org/10.3354/meps09202

Naisbett-Jones, L.C., Branham, C., Birath, S., Paliotti, S., McMains, A.R., Joel Fodrie, F., Morley, J.W., Buckel, J.A., Lohmann, K.J., 2023. A method for long-term retention of pop-up satellite archival tags (PSATs) on small migratory fishes. J Fish Biol 102, 1029–1039. https://doi.org/10.1111/jfb.15351

Nanami, A., Ohta, I., Sato, T., 2015. Estimation of spawning migration distance of the white-streaked grouper (*Epinephelus ongus*) in an Okinawan coral reef system using conventional tag-and-release. Environ Biol Fishes 98, 1387–1397. https://doi.org/10.1007/s10641-014-0366-0

Nelson, E.R., Habibi, H.R., 2013. Estrogen receptor function and regulation in fish and other vertebrates. Gen Comp Endocrinol 192, 15–24. https://doi.org/10.1016/j.ygcen.2013.03.032

Neves, J., Silva, A.A., Moreno, A., Veríssimo, A., Santos, A.M., Garrido, S., 2021. Population structure of the European sardine *Sardina pilchardus* from Atlantic and Mediterranean waters based on otolith shape analysis. Fish Res 243. https://doi.org/10.1016/j.fishres.2021.106050

Nielsen, J.L., Arrizabalaga, H., Fragoso, N., Hobday, A., Lutcavage, M., Sibert, J. (Eds.), 2009. Tagging and Tracking of Marine Animals with Electronic Devices, 1st ed, Reviews: Methods and Technologies in Fish Biology and Fisheries. Springer Netherlands, Dordrecht. https://doi.org/10.1007/978-1-4020-9640-2

Noyes, P.D., Stapleton, H.M., 2014. PBDE flame retardants. Endocrine Disruptors 2, e29430. https://doi.org/10.4161/endo.29430

O'Donnell, T.P., Sullivan, T.J., 2021. Low-coverage whole-genome sequencing reveals molecular markers for spawning season and sex identification in Gulf of Maine Atlantic cod (*Gadus morhua*, Linnaeus 1758). Ecol Evol 11, 10659–10671. https://doi.org/10.1002/ece3.7878

Ogino, Y., Tohyama, S., Kohno, S., Toyota, K., Yamada, G., Yatsu, R., Kobayashi, T., Tatarazako, N., Sato, T., Matsubara, H., Lange, A., Tyler, C.R., Katsu, Y., Iguchi, T., Miyagawa, S., 2018. Functional distinctions associated with the diversity of sex steroid hormone receptors ESR and AR. Journal of Steroid Biochemistry and Molecular Biology 184, 38–46. https://doi.org/10.1016/j.jsbmb.2018.06.002

Ortiz-Zarragoitia, M., Bizarro, C., Rojo-Bartolomé, I., de Cerio, O.D., Cajaraville, M.P., Cancio, I., 2014. Mugilid fish are sentinels of exposure to endocrine disrupting compounds in coastal and estuarine environments. Mar Drugs 12, 4756–4782. https://doi.org/10.3390/md12094756

Ovenden, J.R., Berry, O., Welch, D.J., Buckworth, R.C., Dichmont, C.M., 2015. Ocean's eleven: A critical evaluation of the role of population, evolutionary and molecular genetics in the management of wild fisheries. Fish and Fisheries 16, 125–159. https://doi.org/10.1111/faf.12052

Palm, S., Dannewitz, J., Prestegaard, T., Wickström, H., 2009. Panmixia in European eel revisited: No genetic difference between maturing adults from southern and northern Europe. Heredity (Edinb) 103, 82–89. https://doi.org/10.1038/hdy.2009.51

Pearse, D.E., Crandall, K.A., 2004. Beyond FST: Analysis of population genetic data for conservation. Conservation Genetics 5, 585–602. https://doi.org/10.1007/S10592-003-1863-4/METRICS

Pepping, M.Y., O'Rourke, S.M., Huang, C., Katz, J.V.E.E., Jeffres, C., Miller, M.R., 2020. Rapture facilitates inexpensive and high-throughput parent-based tagging in salmonids. PLoS One 15, 1–17. https://doi.org/10.1371/journal.pone.0239221

Pereira, E., Mateus, C.S., Alves, M.J., Almeida, R., Pereira, J., Quintella, B.R., Almeida, P.R., 2023. Connectivity patterns and gene flow among *Chelon ramada* populations. Estuar Coast Shelf Sci 281, 108209. https://doi.org/10.1016/j.ecss.2022.108209

Petrie, B., Barden, R., Kasprzyk-Hordern, B., 2015. A review on emerging contaminants in wastewaters and the environment: Current knowledge, understudied areas and recommendations for future monitoring. Water Res 72, 3–27. https://doi.org/10.1016/j.watres.2014.08.053

Piferrer, F., Anastasiadi, D., 2021. Do the offspring of sex reversals have higher sensitivity to environmental perturbations? Review Article Sex Dev 15, 134–147. https://doi.org/10.1159/000515192

Popper, A.N., Hawkins, A.D., Sisneros, J.A., 2022. Fish hearing "specialization" – a re-evaluation. Hear Res 425, 108393. https://doi.org/10.1016/j.heares.2021.108393

Popper, A.N., Lu, Z., 2000. Structure–function relationships in fish otolith organs. Fish Res 46, 15–25. https://doi.org/10.1016/S0165-7836(00)00129-6

Portnoy, D.S., Fields, A.T., Puritz, J.B., Hollenbeck, C.M., Patterson, W.F., 2022. Genomic analysis of red snapper, *Lutjanus campechanus*, population structure in the U.S. Atlantic and Gulf of Mexico. ICES Journal of Marine Science 79, 12–21. https://doi.org/10.1093/icesjms/fsab239

Potter, I.C., Tweedley, J.R., Elliott, M., Whitfield, A.K., 2015. The ways in which fish use estuaries: a refinement and expansion of the guild approach. Fish and Fisheries 16, 230–239. https://doi.org/10.1111/faf.12050

Prado, P.S., Pinheiro, A.P.B., Bazzoli, N., Rizzo, E., 2014. Reproductive biomarkers responses induced by xenoestrogens in the characid fish *Astyanax fasciatus* inhabiting a South American reservoir: An integrated field and laboratory approach. Environ Res 131, 165–173. https://doi.org/10.1016/j.envres.2014.03.002

Pujolar, J.M., 2013. Conclusive evidence for panmixia in the American eel. Mol Ecol 22, 1761–1762. https://doi.org/10.1111/mec.12143

Puy-Azurmendi, E., Ortiz-Zarragoitia, M., Villagrasa, M., Kuster, M., Aragón, P., Atienza, J., Puchades, R., Maquieira, A., Domínguez, C., López de Alda, M., Fernandes, D., Porte, C., Bayona, J.M., Barceló, D., Cajaraville, M.P., 2013. Endocrine disruption in thicklip grey mullet (*Chelon labrosus*) from the Urdaibai Biosphere Reserve (Bay of Biscay, Southwestern Europe), Science of the Total Environment. Elsevier. https://doi.org/10.1016/j.scitotenv.2012.10.078

Qiang, J., Duan, X.J., Zhu, H.J., He, J., Tao, Y.F., Bao, J.W., Zhu, X.W., Xu, P., 2021. Some 'white' oocytes undergo atresia and fail to mature during the reproductive cycle in female genetically improved farmed tilapia (*Oreochromis niloticus*). Aquaculture 534, 736278. https://doi.org/10.1016/j.aquaculture.2020.736278

Quintela, M., Skaug, H.J., Øien, N., Haug, T., Seliussen, B.B., Solvang, H.K., Pampoulie, C., Kanda, N., Pastene, L.A., Glover, K.A., 2014. Investigating population genetic structure in a highly mobile marine organism: The minke whale *Balaenoptera acutorostrata acutorostrata* in the Northeast Atlantic. PLoS One 9, 108640. https://doi.org/10.1371/journal.pone.0108640

Ragauskas, A., Butkauskas, D., Sruoga, A., Kesminas, V., Rashal, I., Tzeng, W.-N.N., 2014. Analysis of the genetic structure of the European eel *Anguilla anguilla* using the mtDNA D-loop region molecular marker. Fisheries Science 80, 463–474. https://doi.org/10.1007/s12562-014-0714-1

Reis-Santos, P., Tanner, S.E., Aboim, M.A., Vasconcelos, R.P., Laroche, J., Charrier, G., Pérez, M., Presa, P., Gillanders, B.M., Cabral, H.N., 2018. Reconciling differences in natural tags to infer demographic and genetic connectivity in marine fish populations. Sci Rep 8, 1–12. https://doi.org/10.1038/s41598-018-28701-6

Rizzo, E., Bazzoli, N., 1995. Follicular atresia in curimatá-pioa *Prochilodus affinis* Reinhardt, 1874 (Pisces, Characiformes). Rev Bras Biol 55, 697–703.

Roberts, D.G., Ayre, D.J., 2010. Panmictic population structure in the migratory marine sparid *Acanthopagrus australis* despite its close association with estuaries. Mar Ecol Prog Ser 412, 223–230. https://doi.org/10.3354/meps08676

Rodríguez-Ezpeleta, N., Bradbury, I.R., Mendibil, I., Álvarez, P., Cotano, U., Irigoien, X., 2016. Population structure of Atlantic mackerel inferred from RAD-seq-derived SNP markers: effects of sequence clustering parameters and hierarchical SNP selection. Mol Ecol Resour 16, 991–1001. https://doi.org/10.1111/1755-0998.12518

Rodríguez-Marí, A., Cañestro, C., BreMiller, R.A., Nguyen-Johnson, A., Asakawa, K., Kawakami, K., Postlethwait, J.H., 2010. Sex reversal in zebrafish fancl mutants is caused by Tp53-mediated germ cell apoptosis. PLoS Genet 6, 1–14. https://doi.org/10.1371/journal.pgen.1001034

Rohtla, M., Moland, E., Skiftesvik, A.B., Thorstad, E.B., Bosgraaf, S., Olsen, E.M., Browman, H.I., Durif, C.M.F., 2022. Overwintering behaviour of yellow-stage European eel (*Anguilla anguilla*) in a natural marine fjord system. Estuar Coast Shelf Sci 276, 108016. https://doi.org/10.1016/j.ecss.2022.108016

Ros, O., Vallejo, A., Blanco-Zubiaguirre, L., Olivares, M., Delgado, A., Etxebarria, N., Prieto, A., 2015. Microextraction with polyethersulfone for bisphenol-A, alkylphenols and hormones determination in water samples by means of gas chromatography-mass spectrometry and liquid chromatography-tandem mass spectrometry analysis. Talanta 134, 247–255. https://doi.org/10.1016/j.talanta.2014.11.015

Saboret, G., Dermond, P., Brodersen, J., 2021. Using PIT-tags and portable antennas for quantification of fish movement and survival in streams under different environmental conditions. J Fish Biol 99, 581–595. https://doi.org/10.1111/jfb.14747

Saidapur, S.K., 1978. Follicular atresia in the ovaries of nonmammalian vertebrates, in: International Review of Cytology. Academic Press, pp. 225–244. https://doi.org/10.1016/S0074-7696(08)60169-2

Sales, C.F., Melo, R.M.C., Pinheiro, A.P.B., Luz, R.K., Bazzoli, N., Rizzo, E., 2019. Autophagy and Cathepsin D mediated apoptosis contributing to ovarian follicular atresia in the Nile tilapia. Mol Reprod Dev 86, 1592–1602. https://doi.org/10.1002/mrd.23245

Santos, H.B., Thomé, R.G., Arantes, F.P., Sato, Y., Bazzoli, N., Rizzo, E., 2008. Ovarian follicular atresia is mediated by heterophagy, autophagy, and apoptosis in *Prochilodus argenteus* and *Leporinus taeniatus* (Teleostei: Characiformes). Theriogenology 70, 1449–1460. https://doi.org/https://doi.org/10.1016/j.theriogenology.2008.06.091

Sária, M.P., Santos, M.M., Reis-Henriques, M.A., Vieira, N.M., Monteiro, N.M., 2011. The unpredictable effects of mixtures of androgenic and estrogenic chemicals on fish early life. Environ Int 37, 418–424. https://doi.org/10.1016/j.envint.2010.11.004

Schøyen, M., Green, N.W., Hjermann, D.Ø., Tveiten, L., Beylich, B., Øxnevad, S., Beyer, J., 2019. Levels and trends of tributyltin (TBT) and imposex in dogwhelk (*Nucella lapillus*) along the Norwegian coastline from 1991 to 2017. Mar Environ Res 144, 1–8. https://doi.org/10.1016/j.marenvres.2018.11.011

Schroeder, R., Schwingel, P.R., Correia, A.T., 2021. Population structure of the Brazilian sardine (*Sardinella brasiliensis*) in the Southwest Atlantic inferred from body morphology and otolith shape signatures. Hydrobiologia 7. https://doi.org/10.1007/s10750-021-04730-7

Schroeder, R., Schwingel, P.R., Pinto, E., Almeida, A., Correia, A.T., 2022. Stock structure of the Brazilian sardine *Sardinella brasiliensis* from Southwest Atlantic Ocean inferred from otolith elemental signatures. Fish Res 248, 106192. https://doi.org/10.1016/j.fishres.2021.106192

Schug, T.T., Johnson, A.F., Birnbaum, L.S., Colborn, T., Guillette, L.J., Crews, D.P., Collins, T., Soto, A.M., vom Saal, F.S., McLachlan, J.A., Sonnenschein, C., Heindel, J.J., 2016. Minireview: Endocrine Disruptors: past lessons and future directions. Molecular Endocrinology 30, 833–847. https://doi.org/10.1210/me.2016-1096

Scott, A.P., Sanders, M., Stentiford, G.D., Reese, R.A., Katsiadaki, I., 2007. Evidence for estrogenic endocrine disruption in an offshore flatfish, the dab (*Limanda limanda* L.). Mar Environ Res 64, 128–148. https://doi.org/10.1016/j.marenvres.2006.12.013

Selkoe, K.A., Toonen, R.J., 2006. Microsatellites for ecologists: A practical guide to using and evaluating microsatellite markers. Ecol Lett 9, 615–629. https://doi.org/10.1111/j.1461-0248.2006.00889.x

Serrat, A., Saborido-Rey, F., Garcia-Fernandez, C., Muñoz, M., Lloret, J., Thorsen, A., Kjesbu, O.S., 2019. New insights in oocyte dynamics shed light on the complexities associated with fish reproductive strategies. Sci Rep 9, 1–15. https://doi.org/10.1038/s41598-019-54672-3

Shahidul Islam, Md., Tanaka, M., 2004. Impacts of pollution on coastal and marine ecosystems including coastal and marine fisheries and approach for management: a review and synthesis. Mar Pollut Bull 48, 624–649. https://doi.org/10.1016/j.marpolbul.2003.12.004

Siskey, M.R., Lyubchich, V., Liang, D., Piccoli, P.M., Secor, D.H., 2016. Periodicity of strontium: Calcium across annuli further validates otolith-ageing for Atlantic bluefin tuna (*Thunnus thynnus*). Fish Res 177, 13–17. https://doi.org/10.1016/j.fishres.2016.01.004

Slate, J., Gratten, J., Beraldi, D., Stapley, J., Hale, M., Pemberton, J.M., 2009. Gene mapping in the wild with SNPs: guidelines and future directions. Genetica 136, 97–107. https://doi.org/10.1007/s10709-008-9317-z

Soeth, M., Spach, H.L., Daros, F.A., Adelir-Alves, J., de Almeida, A.C.O., Correia, A.T., 2019. Stock structure of Atlantic spadefish *Chaetodipterus faber* from Southwest Atlantic Ocean inferred from otolith elemental and shape signatures. Fish Res 211, 81–90. https://doi.org/https://doi.org/10.1016/j.fishres.2018.11.003

Soeth, M., Spach, H.L., Daros, F.A., Castro, J.P., Correia, A.T., 2020. Use of otolith elemental signatures to unravel lifetime movement patterns of Atlantic spadefish, *Chaetodipterus faber*, in the Southwest Atlantic Ocean. J Sea Res 158, 101873. https://doi.org/10.1016/j.seares.2020.101873

Sörengård, M., Campos-Pereira, H., Ullberg, M., Lai, F.Y., Golovko, O., Ahrens, L., 2019. Mass loads, source apportionment, and risk estimation of organic micropollutants from hospital and municipal wastewater in recipient catchments. Chemosphere 234, 931–941. https://doi.org/10.1016/j.chemosphere.2019.06.041

Steller, H., 1995. Mechanisms and genes of cellular suicide. Science (1979) 267, 1445–1449. https://doi.org/10.1126/science.7878463

Stransky, C., 2014. Morphometric Outlines, in: Stock Identification Methods. Elsevier, pp. 129–140. https://doi.org/10.1016/B978-0-12-397003-9.00007-2

Sturrock, A.M., Hunter, E., Milton, J.A., Johnson, R.C., Waring, C.P., Trueman, C.N., EIMF, 2015. Quantifying physiological influences on otolith microchemistry. Methods Ecol Evol 6, 806–816. https://doi.org/10.1111/2041-210X.12381

Sumpter, J.P., Jobling, S., 1995. Vitellogenesis as a biomarker for estrogenic contamination of the aquatic environment. Environ Health Perspect 103, 173–178. https://doi.org/10.1289/ehp.95103s7173

Szwejser, E., Verburg-van Kemenade, B.M.L., Maciuszek, M., Chadzinska, M., 2017. Estrogen-dependent seasonal adaptations in the immune response of fish. Horm Behav 88, 15–24. https://doi.org/10.1016/j.yhbeh.2016.10.007

Thambirajah, A.A., Koide, E.M., Imbery, J.J., Helbing, C.C., 2019. Contaminant and environmental influences on thyroid hormone action in amphibian metamorphosis. Front Endocrinol (Lausanne) 10. https://doi.org/10.3389/fendo.2019.00276

Therkildsen, N.O., Palumbi, S.R., 2017. Practical low-coverage genomewide sequencing of hundreds of individually barcoded samples for population and evolutionary genomics in nonmodel species. Mol Ecol Resour 17, 194–208. https://doi.org/10.1111/1755-0998.12593

Thomas, O.R.B., Ganio, K., Roberts, B.R., Swearer, S.E., 2017. Trace element–protein interactions in endolymph from the inner ear of fish: implications for environmental reconstructions using fish otolith chemistry. Metallomics 9, 239–249. https://doi.org/10.1039/C6MT00189K

Thomas, O.R.B.B., Swearer, S.E., 2019. Otolith Biochemistry—A Review. Reviews in Fisheries Science & Aquaculture 27, 458–489. https://doi.org/10.1080/23308249.2019.1627285

Thomé, R.G., Batista, H., Arantes, F.P., Prado, P.S., Flavio, F., Domingos, T., Sato, Y., Bazzoli, N., Rizzo, E., Domingos, F.F.T., Sato, Y., Bazzoli, N., Rizzo, E., 2006. Regression of postovulatory follicles in *Prochilodus costatus* Valenciennes, 1850 (Characiformes, Prochilodontidae). Brazillian Journal of Morphological Sciences 23, 495–500.

Thomé, R.G., Santos, H.B., Arantes, F.P., Domingos, F.F.T., Bazzoli, N., Rizzo, E., 2009. Dual roles for autophagy during follicular atresia in fish ovary. Autophagy 5, 117–119. https://doi.org/10.4161/auto.5.1.7302

Thorstad, E.B., Rikardsen, A.H., Alp, A., Okland, F., 2014. The use of electronic tags in fish research – An overview of fish telemetry methods. Turk J Fish Aquat Sci 13, 881–896. https://doi.org/10.4194/1303-2712-v13_5_13

Tilly, J.L., 1996. Apoptosis and ovarian function. Rev Reprod 1, 162–172. https://doi.org/10.1530/REVREPROD/1.3.162

Tiwari, M., Prasad, S., Tripathi, A., Pandey, A.N., Ali, I., Singh, A.K., Shrivastav, T.G., Chaube, S.K., 2015. Apoptosis in mammalian oocytes: A review. Apoptosis 20, 1019–1025. https://doi.org/10.1007/s10495-015-1136-y

Tyler, C.R., Jobling, S., 2008. Roach, sex, and gender-bending chemicals: The feminization of wild fish in English rivers. Bioscience 58, 1051–1059. https://doi.org/10.1641/B581108

Valencia, A., Rojo-Bartolomé, I., Bizarro, C., Cancio, I., Ortiz-Zarragoitia, M., 2017. Alteration in molecular markers of oocyte development and intersex condition in mullets impacted by wastewater treatment plant effluents. Gen Comp Endocrinol 245, 10–18. https://doi.org/10.1016/J.YGCEN.2016.06.017

Vignon, M., 2015. Extracting environmental histories from sclerochronological structures - Recursive partitioning as a mean to explore multi-elemental composition of fish otolith. Ecol Inform 30, 159–169. https://doi.org/10.1016/j.ecoinf.2015.10.002

Vignon, M., 2012. Ontogenetic trajectories of otolith shape during shift in habitat use: Interaction between otolith growth and environment. J Exp Mar Biol Ecol 420–421, 26–32. https://doi.org/10.1016/j.jembe.2012.03.021

Vignon, M., Morat, F., 2010. Environmental and genetic determinant of otolith shape revealed by a non-indigenous tropical fish. Mar Ecol Prog Ser 411, 231–241. https://doi.org/10.3354/meps08651

Vousden, K.H., Prives, C., 2009. Blinded by the Light: The Growing Complexity of p53. Cell 137, 413–431. https://doi.org/10.1016/j.cell.2009.04.037

Walther, B.D., Kingsford, M.J., O'Callaghan, M.D., McCulloch, M.T., 2010. Interactive effects of ontogeny, food ration and temperature on elemental incorporation in otoliths of a coral reef fish. Environ Biol Fishes 89, 441–451. https://doi.org/10.1007/s10641-010-9661-6

Ward, R.D., 2000. Genetics in fisheries management. Hydrobiologia 420, 191–201. https://doi.org/10.1023/A:1003928327503

Ward, R.D., Woodwark, M., Skibinski, O.F., 1994. A comparison of genetic diversity levels in marine, freshwater and anadromous fishes. J Fish Biol 44, 213–232.

Weist, P., Schade, F.M., Damerau, M., Barth, J.M.I., Dierking, J., André, C., Petereit, C., Reusch, T., Jentoft, S., Hanel, R., Krumme, U., 2019. Assessing SNP-markers to study population mixing and

ecological adaptation in Baltic cod. PLoS One 14, e0218127. https://doi.org/10.1371/journal.pone.0218127

White, J.W., Cole, B.J., Cherr, G.N., Connon, R.E., Brander, S.M., 2017. Scaling up endocrine disruption effects from individuals to populations: outcomes depend on how many males a population needs. Environ Sci Technol 51, 1802–1810. https://doi.org/10.1021/acs.est.6b05276

Whitfield, A.K., 2020. Fish species in estuaries-from partial association to complete dependency. J Fish Biol 97, 1262–1264. https://doi.org/10.1111/jfb.14476

Whitfield, A.K., Panfili, J., Durand, J.D., 2012. A global review of the cosmopolitan flathead mullet *Mugil cephalus* Linnaeus 1758 (Teleostei: Mugilidae), with emphasis on the biology, genetics, ecology and fisheries aspects of this apparent species complex, Reviews in Fish Biology and Fisheries. https://doi.org/10.1007/s11160-012-9263-9

Wood, A.W., Van Der Kraak, G.J., 2003. Yolk proteolysis in rainbow trout oocytes after serum-free culture: evidence for a novel biochemical mechanism of atresia in oviparous vertebrates. Mol Reprod Dev 65, 219–227. https://doi.org/10.1002/mrd.10272

Wood, A.W., Van Der Kraak, G.J., 2001. Apoptosis and ovarian function: novel perspectives from the teleosts. Biol Reprod 64, 264–271. https://doi.org/10.1095/biolreprod64.1.264

Xia, R., Durand, J.D., Fu, C., 2016. Multilocus resolution of Mugilidae phylogeny (Teleostei: Mugiliformes): Implications for the family's taxonomy. Mol Phylogenet Evol 96, 161–177. https://doi.org/10.1016/j.ympev.2015.12.010

Yamamoto, Y., Luckenbach, J.A., Young, G., Swanson, P., 2016. Alterations in gene expression during fasting-induced atresia of early secondary ovarian follicles of coho salmon, *Oncorhynchus kisutch*. Comp Biochem Physiol A Mol Integr Physiol 201, 1–11. https://doi.org/10.1016/j.cbpa.2016.06.016

Yang, Y., Wang, G., Li, Y., Hu, J., Wang, Y., Tao, Z., 2022. Oocytes skipped spawning through atresia is regulated by somatic cells revealed by transcriptome analysis in *Pampus argenteus*. Front Mar Sci 9, 1–14. https://doi.org/10.3389/fmars.2022.927548

Yang, Y.-J., Wang, Y., Li, Z., Zhou, L., Gui, J.-F., 2017. Sequential, divergent, and cooperative requirements of Foxl2a and Foxl2b in ovary development and maintenance of Zebrafish. Genetics 205, 1551–1572. https://doi.org/10.1534/genetics.116.199133

Yu, L., Liu, Y., Liu, J., 2020. Gene-associated microsatellite markers confirm panmixia and indicate a different pattern of spatially varying selection in the endangered Japanese eel *Anguilla japonica*. J Oceanol Limnol 38, 1572–1583. https://doi.org/10.1007/s00343-020-0048-z

Zhang, X., Li, Mengru, Ma, H., Liu, X., Shi, H., Li, Minghui, Wang, D., 2017. Mutation of foxl2 or cyp19a1a results in female to male sex reversal in XX Nile tilapia. Endocrinology 158, 2634–2647. https://doi.org/10.1210/en.2017-00127

Zoeller, T.R., Brown, T.R., Doan, L.L., Gore, A.C., Skakkebaek, N.E., Soto, A.M., Woodruff, T.J., Vom Saal, F.S., 2012. Endocrine-disrupting chemicals and public health protection: A statement of principles from the Endocrine Society. Endocrinology 153, 4097–4110. https://doi.org/10.1210/en.2012-1422

II. STATE OF THE ART, HYPOTHESIS AND OBJECTIVES

1. State of the art

The presence of contaminants in the aquatic environment, particularly xenoestrogens, has been a major concern in recent decades. These chemicals are readily bioavailable to aquatic organisms where they can exert several deleterious effects. Considering that the gonadal development and reproductive cycles of teleost fishes are dependent on endocrine communication between the brain, pituitary gland and gonads, chemical contaminants affecting this complex communicational network pose severe risks to the development, reproduction and survival of fish. In this way, exposure to xenobiotics have been proved to result in increased ovarian atresia, altered gonadal development and sex reversal (either feminisation or masculinisation) of fish populations inhabiting polluted water bodies. Effects of such exposures during specific developmental windows have been first identified at the molecular level in the form of altered gene expression patterns that in several studies have been proved to lead to phenotypic consequences at the physiological, developmental, organismal and population levels.

The production of oocytes in fish is an energetically demanding process that must be balanced with the energetic requirements of other processes necessary for survival such as growth and maintenance. During each reproductive cycle many fish species tend to recruit more oocytes into vitellogenesis than those that will finally be spawned, so oocytes destined for ovulation that cannot be spawned are diverted to atresia. In this way, follicles can be resorbed to facilitate the redistribution of energy-rich materials such as yolk, etc. Atresia is usually the consequence of the selection of dominant follicles for ovulation under the fine control of gonadotropins, steroid hormones, growth factors, and cytokines. Skipped spawning allows fish to adjust the number of eggs produced to the affordable amount of stored energy and show resilience in the presence of environmental stressors. In this regard, skipped spawning even to the extent of completely failing to spawn in a given year takes special relevance as a mechanism to save previously spent energy, obviously decreases the final number of ovulated eggs and alters fecundity of individuals and populations, with important consequences in fish stock management.

In fish chronically exposed to contaminated waters, atresia has been observed in ovarian follicles and has been applied as a biomarker of pollution exposure in fish ecotoxicology. In any case, fish follicular atresia has received quite little scientific attention in scenarios of exposure to endocrine disrupting chemical compounds opposite to the literacy piling up in

relation to the feminisation of fish male gonads. In this regard, little we know of the molecular and cellular mechanisms that regulate follicular atresia in fish ovaries exposed to these compounds. The Cell Biology in Environmental Toxicology and One Health (CBET+) consolidated research group of the University of the Basque Country (UPV/EHU) has described in Gernika and in several estuaries along the Basque coast, a relatively high percentage of male thicklip grey mullets *Chelon labrosus* showing oocytes within their sperm follicles, in a condition that is referred as intersex condition. Although this intersex condition can in principle be in the opposite direction, feminisation under exposure to xenoestrogenic compounds is the most often described consequence worldwide and mainly in riparian and estuarine environments. This feminising "intersex" phenomenon is associated with the high bioavailability of oestrogenic chemical compounds, often resulting at the molecular level in the production of vitellogenin (Vtg), an egg yolk precursor protein, that appears in the blood of male fish. Other molecular alterations in the form of altered expression of sex differentiation master-genes can redirect the process of differentiation of the sperm-line cells into oocytes. On the other hand, the production of differentiated oocytes in testes can also be molecularly monitored due to the extraordinary capacity of oocytes to produce 5S rRNA and accompanying proteins that signal the presence of mainly previtellogenic oocytes in any tissue.

Chronic long-term exposure to xenoestrogens through the life history of a fish causing gonadal alterations such as increased prevalence of atresia and intersex condition as evidenced through histopathological studies suggests possible impacts on population dynamics. While several studies have looked at the effects of endocrine disruption on fish, monitoring wild fish populations, the assessment of the spatial and temporal effects of chronic long-term exposure is quite difficult. This is so because the life history traits of teleost fish species are varied, the complex interactions of multiple biotic and abiotic factors that are characteristic of the aquatic systems they inhabit introduce an extra layer of uncertainty. Many diadromous species often undergoe complex migratory movements often linked to reproductive behaviours with life history patterns that impose distinct habitat use needs during different stages of their life. In this respect, while some species show highly structured populations, others such as the European eel, *Anguilla anguilla* on the other end show panmixia and high levels of gene flow across the whole of the European continent.

Therefore, this study was directed towards understanding the molecular mechanisms underlying atresia in teleosts, and the development of gonad alterations in thicklip grey

mullet *C. labrosus* populations with respect to their population dynamics and life history of exposure to chemicals in their estuaries of residence (exposure during the juvenile or adult stages). Species spawning in near-shore and marine environments, such as *C. labrosus* have life-trait characteristics allowing for genetic flow at the microgeographic level, that may result in low to non-existent genetic structure among the different groups among nearby estuaries independent of their pollution burdens. The genetic patterns of the population or populations and the processes that structure them, although complex, could explain their history of fidelity and homing to a certain estuary and therefore reveal the historical level of exposure to environmental stressors and contaminated continental waters. In relation to the population connectivity of mullets, otolith microstructure and microchemistry could determine whether a single interconnected population or a meta-population structure exists or otherwise different estuaries house distinct subpopulations of adult individuals. In addition, the study of migratory patterns and habitat use within and among estuaries could be studied, to determine whether individuals are lifelong residents of the estuaries they inhabit. A multidisciplinary approach combining complimentary analytical methods could provide knowledge on the underlying molecular mechanisms involved in the generation of the gonad alterations that are observed in estuaries of the southern Bay of Biscay such Gernika or Pasaia, and whether they are the consequence of a life-long exposure due to early recruitment and homing to these particular estuaries for life.

2. Hypothesis

Differing levels of intersex condition and follicular atresia identified in thicklip grey mullets (*Chelon labrosus*) across different estuaries within the southern Bay of Biscay are the consequence of the lack of connectivity between the distinct populations of mullets inhabiting each estuary and the differing life-long history of exposure to the xenoestrogens discharged into these disconnected water bodies.

3. Objectives

To test this hypothesis, the present work aimed at investigating the molecular and cellular mechanisms that regulate ovarian follicular atresia in fish to identify its true relevance in *C. labrosus* mullets exposed to xenoestrogens in some estuaries of the southern Bay of Biscay and understand the life trait characteristics (connectivity, population structure and history of reproductive migrations) that could be affecting such phenotypic alterations. This general objective were tackled through a multidisciplinary approach, combining complimentary analytical methods that were led by the following specific objectives:

1. To identify and describe molecular and cellular mechanisms involved in follicular atresia, throughout oogenesis, in teleost fish.
    1.1. To describe the morphological characteristics of follicular atresia as a possible result of environmental alterations in biotic and abiotic factors in European hakes *Merluccius merluccius* of the southern Bay of Biscay and after exposure to endocrine disrupting chemicals (EDCs) in thicklip grey mullets *C. labrosus* from Gernika.
    1.2. To analyse the transcription levels of apoptosis (*p53, caspase-3, mdm2, bcl-2, rpl11, rpl5*) and autophagy (*beclin-1, ptenb, cathepsin d, dapk1*) marker genes in a commercial fish species showing periodical episodes of skipped spawning due to different environmental circumstances, the European hake *M. merluccius*.
    1.3. To analyse the prevalence of follicular atresia and the transcription levels of apoptosis (*p53, caspase-3, mdm2, bcl-2, rpl11, rpl5*) and autophagy (*beclin-1, ptenb, cathepsin d, dapk1*) marker genes in thicklip grey mullets *C. labrosus* from the estuary of Gernika where high levels of intersex condition have been reported.
    1.4. To analyse the expression at the protein level of apoptosis (p53, MDM2, RPL5 and RPL11) markers involved in 5S rRNA nuclear traffic in the atretic ovaries of the European hake *M. merluccius* and the thicklip grey mullet *C. labrosus*.

2. To analyse the connectivity, and possible genetic structure of the thicklip grey mullets *C. labrosus* inhabiting different Basque estuaries with different chemical burdens within the southern Bay of Biscay.
   2.1. To define the population structure of euryhaline and marine reproducing thicklip grey mullets and determine whether Basque estuaries house different *C. labrosus* population units through microsatellite analyses.
   2.2. To define the mobility patterns of *C. labrosus* between and within estuaries, and between estuaries and oceanic waters in the Basque coast to better understand whether reproductive behaviours may affect the level and extent of exposure to xenoestrogens through otolith shape and elemental analyses.
3. To evaluate whether *C. labrosus* individuals from two estuaries in the Bay of Biscay, one with a high incidence of intersex condition (Gernika), and the other one pristine (Plentzia), are lifelong residents of these estuaries.
   3.1. To describe the migration patterns, habitat use, residency and life history attributes of *C. labrosus* using otolith core-to-edge trace element analyses.
   3.2. To determine whether exposure to xenoestrogens is impairing reproduction because of life-long residency in xenoestrogen-contaminated waters.

III. RESULTS

Chapter 1

Apoptosis and autophagy-related gene transcription during ovarian follicular atresia in European hake *(Merluccius merluccius)*

ARTICLE

Nzioka, A., Valencia, A., Atxaerandio-Landa, A., Diaz de Cerio, O., Hossain, M.A., Korta, M., Ortiz-Zarragoitia, M., Cancio, I., 2023. Apoptosis and autophagy-related gene transcription during ovarian follicular atresia in European hake (*Merluccius merluccius*). Mar. Environ. Res. 183, 105846. https://doi.org/10.1016/j.marenvres.2022.105846

CONGRESS

20th Pollutant Responses in Marine Organisms (PRIMO20) Conference, 18th – 22nd May 2019, Charleston, SC, USA. Oihane Diaz de Cerio, Aitor Achaerandio, **Anthony Nzioka**, Hossain Mohammed Amzad, Ainara Valencia, Maria Korta, Maren Ortiz-Zarragoitia and Ibon Cancio (2019). "Molecular Markers of apoptosis and autophagocytosis to study ovarian atresia in European hake (*Merluccius merluccius*)." Oral Communication.

XIII Congress of Iberian Association for Comparative Endocrinology – AIEC, 16th – 17th September 2021, Faro, Portugal. **Anthony Nzioka**, Maren Ortiz-Zarragoitia, Oihane Diaz de Cerio and Ibon Cancio (2021). "Molecular pathways involved in ovarian follicular atresia in European hake (*Merluccius merluccius*)." Oral Communication.

NUCLEOTIDE SEQUENCES PUBLISHED IN GENBANK: ACCESSION NUMBERS

Merluccius merluccius E3 ubiquitin-protein ligase (mouse double minute 2, *mdm2*)*:* OR672056
Merluccius merluccius B-cell lymphoma 2 (*bcl2*): OR672057
Merluccius merluccius ribosomal protein L5 (*rpl5*): OR672058

Resumen

La atresia folicular es un proceso de reabsorción de ovocitos que ahorra energía y puede permitir la supervivencia de las hembras de peces cuando las condiciones ambientales son desfavorables y a expensas de la fecundidad. Este estudio investigó los niveles de transcripción de genes relacionados con la apoptosis y la autofagia durante la atresia en la merluza europea, que puede mostrar episodios de aumento de la atresia folicular a lo largo del ciclo reproductivo. Se recolectaron 169 hembras en el Golfo de Vizcaya y se analizaron los ovarios mediante métodos histológicos y moleculares. Se detectaron histológicamente diferentes niveles de atresia en el 73,7% de los ovarios analizados y el ensayo TUNEL identificó núcleos apoptóticos en folículos tanto de estadios previtelogénicos como vitelogénicos. Los transcritos de *beclin-1* y ptenb estaban regulados al alza en los ovarios que contenían folículos atrésicos, mientras que *p53*, *caspasa-3*, *catepsina D* y *dapk1* estaban regulados al alza sólo en los ovarios que presentaban folículos atrésicos vitelogénicos. Nuestros resultados indican diferentes implicaciones de los procesos apoptóticos frente a los autofágicos que conducen a la atresia durante el desarrollo ovocitario, siendo la vitelogénesis el momento de máxima actividad apoptótica y autofágica en las merluzas atrésicas. Los genes analizados podrían proporcionar biomarcadores de alerta temprana para identificar la atresia folicular en peces y evaluar la fecundidad en poblaciones de peces.

Palabras clave: *Apoptosis; Autofagia; Biomarcador; merluza europea; Pesca; Atresia folicular; ARNm; ciclo reproductivo*

Abstract

Follicular atresia is an energy-saving oocyte resorption process that can allow the survival of female fish when environmental conditions are unfavourable and at the expense of fecundity. This study investigated the transcription levels of apoptosis and autophagy-related genes during atresia in the European hake that can show episodes of increased follicular atresia throughout the reproductive cycle. 169 female individuals were collected from the Bay of Biscay, and the ovaries were analysed using histological and molecular methods. Different levels of atresia were histologically detected in 73.7% of the ovaries analysed and the TUNEL assay identified apoptotic nuclei in follicles from both previtellogenic and vitellogenic stages. Transcripts of *beclin-1* and *ptenb* were up-regulated in the ovaries containing atretic follicles, whereas *p53*, *caspase-3, cathepsin D* and *dapk1* were up-regulated only in ovaries presenting vitellogenic atretic follicles. Our results indicate different implications of apoptotic vs autophagic processes leading to atresia during oocyte development, vitellogenesis being the moment of maximal apoptotic and autophagic activity in atretic hakes. The analysed genes could provide early warning biomarkers to identify follicular atresia in fish and evaluate fecundity in fish stocks.

Keywords: *Apoptosis; Autophagy; Biomarker; European hake; Fisheries; Follicular atresia; mRNA; Reproductive cycle*

Abbreviations

ANOVA, analysis of variance
BLAST, Basic Local Alignment Search Tool
BSA, bovine serum albumin
cDNA, complementary DNA
cds, coding domain sequences
DNA, deoxyribonucleic acid
ECAE, Ethics Committee for Animal Experimentation
EDTA, ethylenediaminetetraacetic acid
H&L, heavy and light chains
HCl, hydrochloric acid
HE, haematoxylin-eosin
HRP, horseradish peroxidase
IgG, Immunoglobulin G
mRNA, messenger RNA
NBF, neutral buffered formalin
PCR, polymerase chain reaction
qPCR, quantitative PCR
RNA, ribonucleic acid
rRNA, ribosomal RNA
SDS-PAGE, sodium dodecyl sulphate–polyacrylamide gel electrophoresis
ssDNA, single-strand cDNA
TBS-T, tris-buffered saline with Tween
TUNEL, terminal deoxynucleotide transferase (TdT) dUTP nick-end labelling

1. Introduction

The reproductive potential of most female fishes establishes the capacity of wild populations to sustain their numbers and to face increased mortality associated with natural factors (food deprivation, disease, predation, competition, ageing, etc.) or unsustainable fishing activity (Cadima, 2003; Jørgensen et al., 2008; Jørgensen and Holt, 2013; McBride et al., 2015). As part of the policy to improve fisheries management, the assignment of maturity and estimation of fecundity of fish populations are key exercises in the assessment of fish stocks. Many fisheries managers calculate maturity through the macroscopic evaluation of the gonads and assigning proportions of mature individuals, hence estimating the proportion of mature females in fish stocks (Vitale et al., 2005). Fecundity in fish is very much limited by the capacity of females to produce sufficient and good-quality oocytes (McBride et al., 2015) and environmental stressors might interfere with oocyte development. Food deprivation, contaminant exposure, unfavourable temperature or photoperiod regimes and suboptimal water quality may disrupt the endocrine system and induce follicular atresia, a degenerative process in which the oocytes and their follicles are reabsorbed (Corriero et al., 2021; Kjesbu, 2009; Saidapur, 1978; Serrat et al., 2019).

During each reproductive cycle, fish species tend to recruit more oocytes into vitellogenesis than those that will finally be spawned, irrespective of the reproductive strategy they show (Kjesbu, 2009). In some circumstances, fish oocytes in vitellogenesis destined for ovulation cannot be spawned so they are diverted to atresia and follicles are resorbed to facilitate the redistribution of energy-rich yolk materials (Janz and Van Der Kraak, 1997; Kjesbu, 2009; Miranda et al., 1999; Wood and Van Der Kraak, 2003, 2001). This allows the fish to interrupt its normal reproductive cycle by skipping a batch of oocytes during their recruitment, thereby adjusting the number of eggs produced to an affordable amount of stored energy (Kennedy et al., 2009). This can have a strong impact on fecundity calculations if the reduction in the number of secondary follicles by atresia is not considered during fish stock analyses.

Follicular atresia is an evolutionarily conserved process that is essential for the maintenance of ovarian homeostasis in vertebrates including fish (Bhardwaj and Sharma, 2012; Corriero et al., 2021; Guraya, 1986; Krysko et al., 2008; Saidapur, 1978). In birds and mammals, most of the oocytes recruited during ovarian development lose their integrity and are eliminated before ovulation by follicular atresia (Bhardwaj and Sharma, 2012; Krysko

et al., 2008; Saidapur, 1978). In teleost fishes, follicular atresia is frequently associated with environmental stress or changes in hormonal levels (Habibi and Andreu-Vieyra, 2007) and has been observed irrespective of the differentiation stage between previtellogenesis and final maturation in the (Guraya, 1986; Janz and Van Der Kraak, 1997; Miranda et al., 1999; Rizzo and Bazzoli, 1995; Wood and Van Der Kraak, 2001).

Apoptosis is an evolutionarily conserved process of programmed cell death characterized by biochemical and morphological changes that remodel, differentiate and degenerate tissues to maintain the number of cells (Steller, 1995; Tilly, 1996a). In teleost fish, apoptosis is involved in selecting and recruiting follicles for vitellogenesis (Janz and Van Der Kraak, 1997) and postovulatory regression after spawning (Santos et al., 2008; Thomé et al., 2006; Wood and Van Der Kraak, 2001). The first morphological signs of apoptosis-mediated atresia are the disintegration of the oocyte nucleus and other cytoplasmic organelles such as the mitochondria, cortical alveoli and annulate lamellae, followed by the fragmentation of the zona pellucida and hypertrophy of the follicle cells (Janz and Van Der Kraak, 1997; Miranda et al., 1999; Saidapur, 1978; Wood and Van Der Kraak, 2001). The follicle cells accompany the process by incorporating and digesting the proteins that the dying oocyte had previously accumulated (Lubzens et al., 2010). However, increasing evidence suggests that apoptosis is not the exclusive mechanism, and that autophagy represents an alternative non-apoptotic process that contributes to the efficient elimination of granulosa cells and oocytes (Cassel et al., 2017; Corriero et al., 2021; Morais et al., 2016, 2012; Sales et al., 2019; Santos et al., 2008; Thomé et al., 2009). Recently, a review paper by Bhardwaj et al. (2022) has reported the implication of autophagy marker genes also in the process of atresia in mammals and involving all cell types forming the follicle. Autophagy recycles nutrients from degraded cell organelles in the follicle, and hence could provide the energy that may be required for future oocyte and egg production in vertebrates (Bhardwaj et al., 2022). Whereas in mammals, apoptosis in cells that form the ovarian follicles is considered the main cellular mechanism mediating early ovarian atresia (Hsueh et al., 1994; Matsuda et al., 2012; Tilly, 1996a, 1996b; Tiwari et al., 2015), in fish, apoptosis is accompanied by autophagy at least during the late stages of follicular atresia (Miranda et al., 1999; Morais et al., 2012); thus suggesting the existence of another novel pathway during follicular atresia (Yang et al., 2022).

While follicular atresia is a common degenerative process in fish ovaries, it has been mainly described histologically, and much of its molecular and cellular mechanisms are

poorly understood. A recent literature review identified a list of 20 different genes that play a potential role in follicular atresia in teleost fish (González-Kother et al., 2020). Although some of these genes participate in processes such as lipid or oxidative metabolism, most of them are usual suspects that participate in regulating apoptotic and autophagic mechanisms (González-Kother et al., 2020). For instance, the sequential activation of caspases essential for proteolytic cleavage and apoptosis-mediated cell death (Andreu-Vieyra and Habibi, 2000) has been demonstrated during follicular atresia in fasted coho salmon (Yamamoto et al., 2016). In the freshwater fishes, *Astyanax bimaculatus*, *Leporium obtusidens* and *Prochilodus argenteus* overexpression of apoptotic and autophagy marker genes *caspase-3*, Bcl2 protein family genes *bcl2* and *bax*, *cathepsin D* and *beclin-1* has been demonstrated in follicular and theca cells during early and advanced ovarian regression (Morais et al., 2012). In the Japanese flounder *Paralichthys olivaceus*, the phosphatase and tensin homolog B (ptenb) has been implicated in the process of follicular atresia through its relationship with Beclin-1 and the initiation of autophagy and apoptosis (Li et al., 2020).

p53, a main regulator of both apoptotic and autophagic pathways, has not received enough attention in relation to the phenomenon of follicular atresia in teleosts. Its role in controlling the fate of ovarian follicles of fish is envisaged to be very relevant as demonstrated by the process of zebrafish sex differentiation (Rodríguez-Marí et al., 2010). All zebrafish after hatching develop a juvenile ovary that in males is degenerated to allow the formation of testis in substitution. This process is regulated mainly through p53 activation that triggers the resorption of immature oocytes (Rodríguez-Marí et al., 2010). In this sense, it has been reported that during previtellogenesis oocytes in all teleost fish produce immense amounts of 5S ribosomal RNA (5S rRNA) in preparation for ribosomal assembly during early embryonic development (Diaz De Cerio et al., 2012; Rojo-Bartolomé et al., 2016). In mammalian cells under ribosomal stress, 5S rRNA in conjunction with some ribosomal proteins is known to regulate p53 activity and trigger apoptosis (Deisenroth and Zhang, 2010; Donati et al., 2013; Sloan et al., 2013) and in ovaries this could make of 5S rRNA and p53 a regulatory switch deciding between oocyte survival and death.

The present study evaluated the role that apoptosis and autophagy-related genes and proteins may play in regulating follicular atresia in the European hake (*Merluccius merluccius*). This is a commercially important fish species with indeterminate fecundity and asynchronous oocyte development which experiences periods of a high incidence of follicular atresia linked to environmental changes as it was for instance in the Prestige oil

spill in 2002 (Díez et al., 2011; Murua and Motos, 2006). Since the European hake northern stock assessment considers maturity and not fecundity, developed early oocyte atresia molecular markers could be applied in potentially useful fishery-independent methods such as the daily egg production method proposed (Murua et al., 2010) for the European hake.

2. Materials and methods

2.1. Study area, fish and tissue sample collection

The Biscay Bay is a gulf of the northeast Atlantic Ocean located south of the Celtic Sea (44° 14' 23" N°, 4° 52' 45.9" W) defined as major fishing area 27.8 by the International Council for the Exploration of the Sea (ICES). Samples were fished in subarea 8 (divisions 8b and 8c). In total, 169 adult European hakes (*M. merluccius*) were obtained from landings of commercial longline fishing vessels in the Bay of Biscay between March and July (2016-2018). From these, 76 mature female individuals were selected and studied (Mean fork length = 58.41±3.78 cm; Mean body weight = 1,863.61±360.24 g). The ovaries were analysed using histological and molecular biology techniques. Ovaries were dissected and weighed (to the nearest 0.1 g) within 24 hours of landing. One portion of the ovarian tissue of each individual was fixed in 10% neutral buffered formalin (NBF) containing 1% glutaraldehyde at 4ºC. Another portion of the same ovarian tissue was placed in RNAlater® Stabilization Solution (Ambion™, ThermoFisher Scientific, Waltham, Massachusetts, USA) for 5-10 min, frozen in liquid nitrogen and stored at -80ºC until further analysis. All chemicals were of analytical grade and were obtained from Sigma-Aldrich (St. Louis, Missouri, USA) unless otherwise specified. Ethical approval from the Ethics Committee for Animal Experimentation (ECAE) of the University of the Basque Country (UPV/EHU) was not necessary because the fish samples were obtained from landings of commercial fishing vessels. Genetic material was collected and utilized according to the Access and Benefit Sharing Legislation in place in Spain and under the Internationally Recognized Certificate of Compliance (ABSCH-IRCC-ES-258968-1).

2.2. Histological analysis, ovary development staging and atresia identification

After 24 hours, the fixed ovarian tissue samples were dehydrated in a graded ethanol series (80, 96 and 100%) and embedded in paraffin using the Leica ASP300 S Automated Vacuum Tissue Processor (Leica Biosystems, Nussloch, Germany). For sectioning, paraffin blocks were cooled rapidly on a PF100 cooling plate (Bio-Optica Milano, Milano, Italy) and

cut into 5 µm tissue sections on a Leica RM 2125RT Rotary Microtome (Leica Biosystems, Germany). Sections were mounted onto albumin-coated 90º frosted-end microscope slides (BPB019 RS France, Wissous, France). Haematoxylin-Eosin (HE) staining (Gamble, 2008) was performed using a Leica Autostainer XL (Leica Biosystems, Germany). An Olympus BX50 light microscope (Olympus Corporation, Tokyo, Japan) was used to analyse the tissue sections. The gametogenic stages of each individual were determined according to Murua and Motos (2006) and Korta et al. (2010) and as explained in Table 1. The presence of a single oocyte in the most advanced stage of development was used to label the ovary as being in that exact phase of development, without taking into consideration the prevalence of the oocyte developmental stage in the ovary (West, 1990). Ovaries of each individual that had at least one oocyte in a state of cellular structural disorganisation were classified for our study as atretic (Hunter and Macewicz, 1985). Although different stages (alpha, beta, gamma and delta) of atresia have been described (Hunter and Macewicz, 1985), the alpha stage being an earlier stage at which the oocyte begins to become irregular in shape and granulosa cells phagocytize the oocyte yolk, and the delta stage is the last stage when granulosa cells reduce in numbers and are no longer surrounded by thecal cells and blood vessels (Corriero et al., 2021; Hunter and Macewicz, 1985), no distinction among the different atretic stages was done. High-resolution histological images were captured with a Nikon DS-Fi2 digital camera (Nikon Instruments Inc., Tokyo, Japan).

Table 1
Oocyte developmental staging in European hake ovaries during histological analysis (adapted from Murua and Motos (2006) and Korta et al. (2010)).

Ovary phase	**Developmental stage**	**Main histological characteristic**
Previtellogenic	Previtellogenesis	Lightened basophilic cytoplasm with no cytoplasmic inclusions
	Cortical alveoli	Presence of cortical alveoli vesicles in the cytoplasm with lipid droplets accumulating in the cytoplasm
Vitellogenic	Early vitellogenic	Yolk proteins arranged in the periphery of the ooplasm with more lipid droplets present in the cytoplasm
	Vitellogenic	Yolk proteins present in the cytoplasm with an equal amount of lipid droplets
	Late vitellogenic	Further accumulation of yolk proteins in the cytoplasm with fewer lipid droplets present
Maturation	Maturing	Nuclear migration, fusion of lipids droplets and yolk proteins, germinal vesicle breakdown and hydration

2.3. In-situ TUNEL assay and apoptosis

Apoptotic cells in hake ovaries were detected using a DeadEnd Colorimetric in-situ terminal deoxynucleotide transferase (TdT) dUTP nick-end labelling (TUNEL) assay kit (Promega, Madison, WI, USA) following the manufacturers' instructions. Tissue sections, 5 μm thick, were mounted on silanized microscope slides. The slides were deparaffinised with xylene, rehydrated with a series of ethanol dilutions and then washed at room temperature in 0.85% NaCl (5 min), phosphate buffer solution (PBS) (5 min), followed by a fixation step in 4% paraformaldehyde (15 min). After the slides were washed twice in PBS (5 min each), 100 μL of proteinase K solution was added to each slide and incubated for 20 min. Slides were washed with PBS (5 min) and re-fixed in 4% paraformaldehyde (5 min). Sections were treated with TdT equilibration buffer at room temperature for 10 min before being incubated with rTdT enzyme in a humidified chamber for 1 hour at 37ºC equilibration buffer for 10 min. TdT was removed and sections were stained at room temperature for 10 min with 10% DAB staining solution (1X) after being rinsed in PBS. Slides were rinsed several times in de-ionized water and mounted in glycerol (Kaiser's glycerol gelatine – for microscopy; Merck KgaA, Darmstadt, Germany). The sections were observed under an Olympus BX50 light microscope, and the images were captured with a Nikon DS-Fi2 digital camera.

2.4. Total RNA extraction, quantification and 5S/18S rRNA ratio calculation

Total RNA was extracted from the remaining portion of the same ovarian tissue taken for histology using TRIzol Reagent® Solution (Ambion®, ThermoFisher Scientific, Massachusetts, USA) following the manufacturer´s instructions. After histological analysis, oocyte developmental staging and atresia identification, 46 ovaries showing extensive follicular atresia (21 previtellogenic, 25 vitellogenic) and 22 ovaries without signs of atresia (11 previtellogenic, 11 vitellogenic) were selected. RNA yield of each sample was assessed using a cuvette photometer (Biophotometer plus, Eppendorf, Hamburg, Germany) using a 1:50 dilution (or appropriate dilution factor) (Rojo-Bartolomé et al., 2016).

The quantity and quality of the RNA were then determined by capillary electrophoresis using the Agilent RNA 6000 Nano Kits Assay Protocol (Agilent Technologies, Santa Clara, California, USA). The Bioanalyzer (Agilent 2100 Bioanalyzer; Agilent Technologies) electropherograms were used to quantify the concentration of the bands corresponding to 5S and 18S ribosomal RNAs (rRNAs) in each sample. The Time-Corrected-Area of each

peak was used to calculate the 5S/18S rRNA ratio and the Log2 of this value was used to develop a 5S/18S rRNA ratio, in order to rank ovaries according to their different developmental phases (Rojo-Bartolomé et al., 2016).

2.5. Gene transcription analyses by qPCR

First-Strand cDNA was synthesised using Affinity Script Multiple Temperature cDNA Synthesis Kit (Agilent Technologies) in a 2720 Applied Biosystems Thermal Cycler (Applied Biosystems, Foster City, California, USA). Total RNA was reverse transcribed to cDNA using random primers following the manufacturer´s instructions (2 µg total RNA in a reaction volume of 20 µL for a final theoretical cDNA concentration of 100 $ng.\mu L^{-1}$). The cDNA was stored at -40ºC for subsequent PCR amplification and gene expression analysis. Single-strand cDNA (ssDNA) concentrations were quantified by measuring fluorescence in a Synergy HT Multi-Mode Microplate Reader (Biotek, Winoosky, USA) using Quant-iT™ OliGreen® Kit (Life Technologies™, ThermoFisher Scientific, Waltham, Massachusetts, USA). The quantification was run in triplicate, in a reaction volume of 100 µL with a theoretical cDNA concentration of 0.2 $ng.\mu L^{-1}$ (Rojo-Bartolomé et al., 2017). The fluorescence was measured at standard fluorescein excitation and emission wavelengths of 480 nm and 520 nm respectively. Real cDNA concentration was calculated using a five-point standard curve according to the manufacturer's instructions and the exact amount of cDNA loaded in qPCR reactions was calculated, adjusting dilutions used for each gene (Rojo-Bartolomé et al., 2017).

Gene sequences for European hake *p53* (DQ146942), *beclin-1* (KY771082), *caspase-3* (*casp3*) (KY771084), *fshr* (KY178270.1) and l*hr* (KY178271.1) were obtained from Genbank in the NCBI database. The sequence for other target genes (*mdm2, rpl11, rpl5, bcl2, ptenb, ctsd* and *dapk1*) were obtained from querying the draft genome assembly produced for *M. merluccius* in a broad comparative genomic study of gadoid fish species published in the Dryad Digital Repository (Malmstrøm et al., 2016a, 2016b). To identify the coding domain sequences (cds) of each target gene, a BLAST (BlastN) against ortholog sequences of *Danio rerio* and *Gadus morhua* available in the NCBI database was run. Scaffolds with the best hits were selected and a local BLAST (BlastN and BlastX) ran. Primer pairs for each target gene were designed using Eurofins online tools and their specificity was verified by conventional PCR amplification on at least two independent cDNA samples of each tissue (Table 2). The PCR programme for each target gene was as

follows: 94°C for 2 min, denaturation at 94°C for 30 s, annealing step (temperature for each primer set in Table 2) for 30 s, and elongation at 72°C for 30 s. PCR was finalised at 72°C for 8 min (2720 thermal cycler, Applied Biosystems, USA). All PCR products/amplicons were visualized in 1.5% (w/v) agarose gels stained with ethidium bromide and sequenced at the Sequencing and Genotyping Service of the University of the Basque Country (SGIker-UPV/EHU).

The relative transcription levels for the target genes in all the atretic and non-atretic individual samples were determined by real-time quantitative PCR (qPCR) amplifications performed in a final volume of 20 µL with 10 µL FastStart Universal SYBR Green Master (Rox) (Roche Diagnostics, Mannheim, Germany), 2 µL appropriately diluted cDNA, 7.94 µL or 7.88 µL of nuclease-free water and 0.03 µL (6.25 pmol.µl^{-1}) or 0.06 µL (12.5 pmol.µl^{-1}) of primer pair respectively (Rojo-Bartolomé et al., 2016). Optimal concentrations of primers and samples were used for each gene (Table 2). Samples were run in triplicate on 96-well reaction plates using the 7300 PCR thermal cycler (Applied Biosystems, Forster City, California, USA). A no-template control (NTC) was also run in triplicate in each plate using the same reaction conditions. The amplification protocol was set up to follow an initial denaturation and activation at 50ºC for 2 minutes and 95ºC for 10 minutes, followed by 40 cycles at 95ºC for 15 seconds and an annealing step of 60 s at the appropriate primer pair temperature (Table 2). To obtain a dissociation curve, the amplification reaction was followed by a dissociation step carried out at 95ºC for 15 seconds, 60ºC for 15 seconds and 95ºC for 15 seconds. The reaction efficiencies for each plate were estimated by generating a standard curve for each primer pair from a 2-fold serial dilution of a pool of first-strand cDNA templates from all samples as described (Rojo-Bartolomé et al., 2017):

$$E = (10^{(-1/m)}) - 1 \quad (1)$$

Where E = amplification efficiency of the qPCR reaction and m = slope of the standard curve of the qPCR reaction. The standard curve represented the cycle threshold (C_t) of the sample as a function of the logarithm of the number of copies generated.

The delta C_t (ΔC_t) method adapted from the delta-delta C_t ($\Delta\Delta C_t$) normalization method ($\Delta C_t = C_t$ sample $- C_t$ Intercept) was used to normalize (Log_2) the relative quantity (RQ) of all gene transcription levels to the amount of cDNA in nanograms per sample used in the qPCR, with the C_t intercept of the standard curve when the logarithm of the number of copies generated is zero (Rojo-Bartolomé et al., 2016):

$$RQ = Log_2 [(1 + E)^{-\Delta Ct}/\text{ng cDNA}] \quad (2)$$

Where RQ = relative quantity of each gene transcription level in the sample, E = amplification efficiency of the qPCR reaction, ΔC_t = difference between the C_t values of the gene of interest and the C_t value of the standard curve when the logarithm of the number of copies generated is zero in the sample and ng cDNA = amount of cDNA in nanograms per sample used in the qPCR.

No reference or housekeeping gene was used to normalize the target gene transcription and instead, the total amount of input cDNA was used (Libus and Štorchová, 2006; Mittelholzer et al., 2007; Rojo-Bartolomé et al., 2016; Valencia et al., 2020). Considering that fish ovaries undergo profound changes in terms of cell composition, physiological status, hydration levels or meiotic stage, their mRNA content varies enormously throughout growth and maturation. In these circumstances, it is hard to conceive the existence of any valid reference gene.

Table 2

Nucleotide sequences of forward (F) and reverse (R) primer pairs with the temperatures (T_A = annealing temperature) used for the qPCR. GenBank accession numbers are available in the International Nucleotide Sequence Database and the scaffold numbers in the draft genome assembly produced for *M. merluccius* in the Dryad Digital Repository (Malmstrøm et al., 2016a, 2016b).

Target gene	GenBank Accession No./ Scaffold No.	Primer Sequence (5' – 3')	T_A (^{0}C)	Primer concentration (pmol µl^{-1})	Sample dilution factor
p53	DQ146942	F:GAGCCAGAGGGTCCAGT	58.0	12.5	1:40
		R:CATGAGCTGTTGCACATG	58.0		
mdm2	Scf718000323709	F:GAAGAGGAGGCGSTCTGATAG	59.0	6.25	1:200
		R:ACCTGGTCRTCCCCAGATARC	59.0		
rpl11	Scf7180003655120	F:CTGGAGAAGGGACTCAAGGT	55.0	12.5	1:50
		R:CCAGAACCACCACGTAGAAG	55.0		
rpl5	Scf7180005283183	F:CAAGAGGTACAGGTCAAGTTC	55.0	6.25	1:200
		R:GCRTCCAGGTAGCAKGTGA	55.0		
caspase-3	KY771084	F:CGGTGCGTCATCATCAAC	59.0	12.5	1:200
		R:GAACGGCTGTGATCTTCCATC	59.0		
bcl2	Scf7180005228352	F:AGCTTCGAGARCGTGATGGAY	55.0	6.25	1:200
		R:CASGGSTSRATGGTTGTCCAG	55.0		
beclin-1	KY771082	F:GAGGAGGAGATGCTGGT	59.0	6.25	1:200
		R:TCCAGCTCCAGCTGCTGC	59.0		
ptenb	Scf7180003609668	F:GCATGTGGAGAGGCTGGAAA	59.0	12.5	1:50
		R:GAGAGCACCAAGAAGTCCCG	59.0		
ctsd	Scf7180003655488	F:GGTGAGCTGTGACAAGATCC	57.0	6.25	1:200
		R:TGGCCAATGAATACATCTCC	57.0		
dapk1	Scf7180003611438	F:CTCTGTGAGCATCTCCAACC	57.0	6.25	1:200
		R:CACCGTTGATGTTGGTGTTC	57.0		
fshr	KY178270.1	F:GCATGGCCGTGCTCATCTTC	58.0	6.25	1:40 & 1:50
		R:GCGTACAGGAAGGGGTTGG	58.0		
lhr	KY178271.1	F:GTCAGCGAGTTGGACATGGA	56.0	6.25	1:10
		R:ATGACCCAGGTGAGAAAGCG	56.0		

2.6. Immunoblotting

Total protein was extracted from a portion of frozen ovarian tissue taken for molecular biology analysis. 12 ovaries showing extensive follicular atresia (6 previtellogenic, 6 vitellogenic) and 12 ovaries without signs of atresia (6 previtellogenic, 6 vitellogenic) identified from histological analysis, oocyte developmental staging and atresia identification were selected. Two sets of the same thawed frozen tissue samples (~100 mg each) were homogenized, while in ice, using a Potter S Homogenizer (B. Braun Biotech International, GmbH, Melsungen, Germany) in 4X sample volume (~400 µL) ice cold lysis buffer freshly supplemented with an EDTA-free protease inhibitor cocktail tablet (cOmplete Tablets Mini EDTA-free EASYpack, Roche Diagnostics). One set of the samples were homogenized in ice-cold TrisHCl-Triton X-100 lysis buffer (50 mM Tris-HCl, 150mM NaCl, 1 mM EDTA, 0.1% Triton X-100) (Buffer A), and the other in ice cold Triton X-100 lysis buffer (1 mM NaHCO3, 1 mM EDTA, 0.1% absolute ethanol, 0.1% Triton X-100) (Buffer B). The lysis buffers were evaluated in downstream immunoblot analysis for the target proteins p53, MDM2, RPL5 and RPL11. Buffer A was used for p53 immunoblotting while Buffer B, for MDM2, RPL5 and RPL11. After homogenisation, the homogenate was incubated on ice for 10 min and centrifuged at 8,000 rpm, for 10 min at 4ºC using an Eppendorf 5415R centrifuge (Eppendorf AG, Hamburg, Germany) to obtain the supernatant (protein sample lysate). The total protein concentration in the sample lysate was analysed using Bio-Rad´s Quick Start Bradford assay kit (Bio-Rad Laboratories Inc.) following the manufacturer's instructions. Absorbance was measured at 595 nm in Thermo Scientific Multikscan® Spectrum Spectrophotometer (Thermo Fisher Scientific Oy Microplate Instrumentation, Vantaa, Finland) and values from a protein standard curve obtained using Bio-Rad´s Quick Start Bovine Serum Albumin (BSA) standards kit (Bio-Rad Laboratories Inc.) were used to calculate total protein concentration (mg mL^{-1}) in the samples.

Total protein was electrophoretically separated per lane on a 12% SDS-PAGE pre-cast gel (BIORAD Mini-PROTEAN® TGX, Bio-Rad Laboratories Inc.) using the Mini-PROTEAN® Tetra Vertical Electrophoresis Cell and Mini Trans-Blot® Module (Bio-Rad Laboratories Inc.) at 200V for 30 – 45 min and blotted onto 0.45 µm nitrocellulose blotting membrane (Amersham™ Protran™ Premium, Catalogue No.: 10600096, GE Healthcare Bio-Sciences AB, Uppsala, Sweden), with a positive atretic (AT, "+") and no protein load control ("-"). Loaded amounts per lane: 15 and 10 µg of total protein was separated per lane and blotted onto the membranes for the target protein p53, and for MDM2, RPL5 and RPL11

respectively. Non-specific binding sites were blocked with 5% Non-fat dry milk in Tris-buffered saline with Tween 20 (TBS-T) for p53 and MDM2, and 3% bovine serum albumin (BSA: A9647-100G; Sigma-Aldrich, Missouri, USA) in TBS-T for RPL5 and RPL11. Blotting membranes were probed with rabbit polyclonal antibodies for all target proteins (Abcam, Cambridge, UK) and were appropriately diluted in blocking solution overnight, followed by another 1 h incubation in horseradish peroxidase (HRP)-conjugated goat anti-rabbit IgG H&L (Table 3). The protein bands were visualized under chemiluminescence light using BIORAD ChemiDoc XRS System (Bio-Rad Laboratories Inc.) after treating the sample membranes for 2 min with ~ 600 µL (1:1 ratio) of Clarity™ Western ECL Substrate detection kit (Catalogue No.: 170-5060) (Bio-Rad Laboratories Inc.).

Table 3
Target protein(s) antibodies used for immunoblotting of hake ovarian tissue samples. Catalogue numbers for primary and secondary antibodies used are provided for in parentheses. Lot number (Lot #) for each antibody is also provided. Concentration [µg mL^{-1}] and corresponding dilutions (in parentheses) used for each antibody is provided.

Primary antibody (Rabbit polyclonal)	**Lot number (Lot #)**	**Concentration [µg mL^{-1}] (Dilution)**	**Secondary antibody**	**Concentration [µg mL^{-1}] (Dilution)**
Anti-p53 (ab131442)	GR316086-46	5 (1:200)	Goat Anti-Rabbit IgG H&L (HRP) (ab205718), Lot #: GR3269880-7	0.2 (1:10000)
Anti-MDM2 (ab38618)	GR3172855-11	4 (1:500)		0.4 (1:5000)
Anti-RPL5 (ab137617)	GR3206161-7	0.85 (1:1000)		0.4 (1:5000)
Anti-RPL11 (ab79352)	GR3224424-1	1 (1:200)		0.2 (1:10000)

The protein band image shape in each lane was quantified in Image Studio™ Lite Version 5.2.5 Quantification Software (LI-COR Biosciences, Lincoln, Nebraska, USA). Background signal was subtracted to accurately calculate the signal intensity from the protein band image shape(s) using the lane background subtraction method and applying a "Median background correction" to each lane. The relative density (RD: no units) of the target protein(s) were then calculated from the signal values of the sample and the atretic positive normalization sample using the formula:

$$\text{Relative Density, RD} = \frac{Target\ Protein\ Signal}{Target\ Protein\ Atretic\ Positive\ \ Signal} \quad (3)$$

2.7. Statistical analysis

Statistical analysis was performed on *R* using the base *R stats* package (R Core Team, 2020) and the packages *Tidyverse* (Wickham et al., 2019) and *YaRrr* (Phillips, 2017) with all data expressed as the median with upper and lower limits and 95% confidence interval. First and second-order correlations (linear-quadratic regressions) were performed, and a two-way ANOVA test was applied for multiple comparisons in all the data (Zar, 2010). Relative quantification values for each gene in each individual were plotted against the 5S/18S rRNA ratio either on a regression curve for the statistically significant coefficient of correlations or in a constant representing the median of the total values. Protein analyses data were checked for normality (Shapiro-Wilk test, $p > 0.05$) and homogeneity of variances (Levene's test, $p > 0.05$). When these assumptions were not met, the non-parametric Mann-Whitney U test was performed. Once these assumptions were met, a parametric two-samples students t-test was performed to compare means. All *p*-values were corrected using Benjamini-Hochberg (BH) method to control the false discovery rate (i.e., falsely rejecting the null hypotheses). The *onewaytests* (Dag et al., 2018), *car* (Fox and Weisberg, 2019), and *ggstatsplot* (Patil, 2021) packages were also used. The statistically significant difference was set at $p < 0.05$.

3. Results

3.1. Histological analysis, gonad developmental staging and atresia identification

Histological analysis of the ovaries of European hakes obtained from landings of commercial longline fishing vessels fishing the Bay of Biscay between March and July (2016 – 2018) showed different ovarian developmental stages ranging from previtellogenesis to maturation that were ranked according to Korta et al. (2010) (Table 1). While we were able to examine non-atretic oocytes in some of the ovaries (Figures 1A – 1D), atresia was identified in oocytes in any stage of development and was characterized by some level of disorganization of the cellular structure of the oocyte (Figures 1E – 1H) according to Hunter and Macewicz (1985). The presence of atresia was identified in 73.7% of mature females analysed, with atresia being most prevalent in vitellogenic oocytes in comparison to previtellogenic ones or oocytes transitioning from cortical alveoli to early vitellogenesis. Hereby, we did not attempt to study the prevalence of atresia in the hake population analysed, nor compare the situation between studied years. This was conceived

as a mechanistic study to develop tools that could be utilized to identify atresia and not a fisheries study.

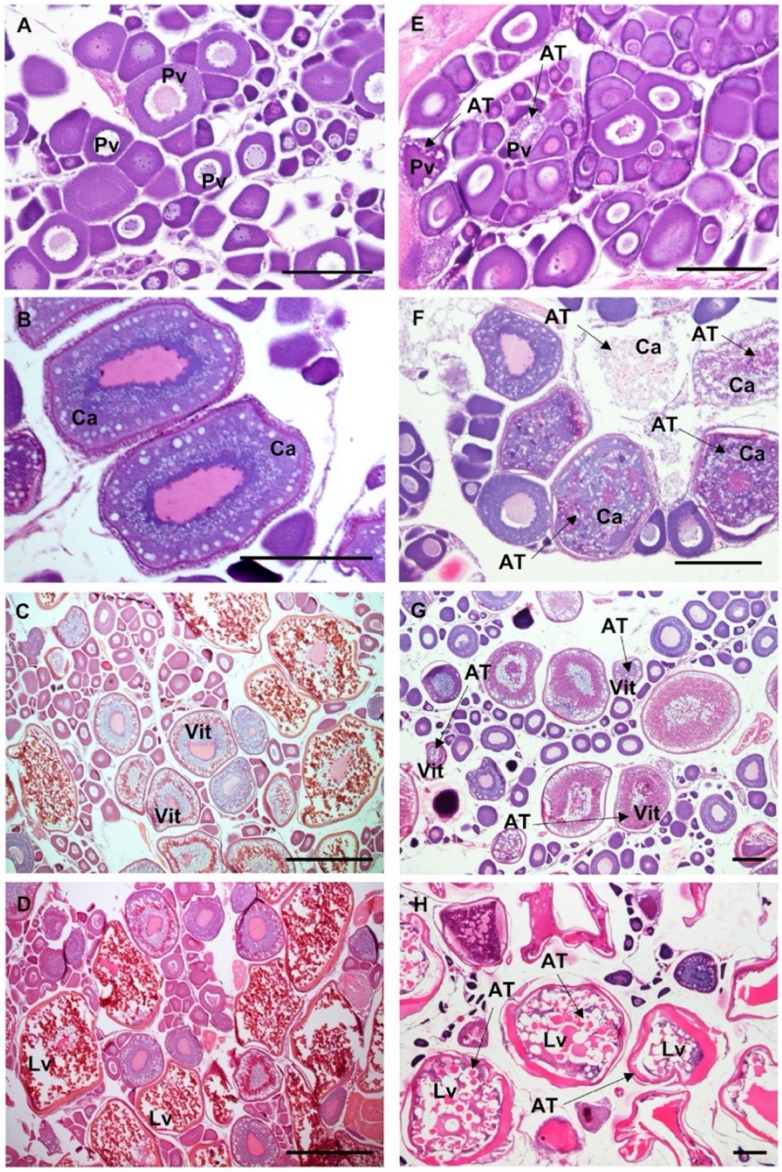

Figure 1
Histological analysis and ovary development staging in European hake. Asynchronous developing ovaries in European hake with oocytes at different developmental stages: (A to D) ovaries with non-atretic oocytes at different stages of development (Pv = Previtellogenic oocytes; Ca = Cortical alveoli; Vit = Vitellogenic oocytes; Lv = Late vitellogenic oocytes). (E–H) Ovaries with atretic oocytes in all stages of development (AT = Atretic). Bars = 100 µm in all micrographs except C and D where bars = 500 µm.

3.2. In-situ TUNEL assay and apoptosis

In-situ TUNEL analysis of histological sections of European hake ovarian tissue revealed TUNEL-positive cells with a distinct staining and displaying stained nuclei in contrast to the TUNEL negative controls devoid of any staining (Figure 2B).

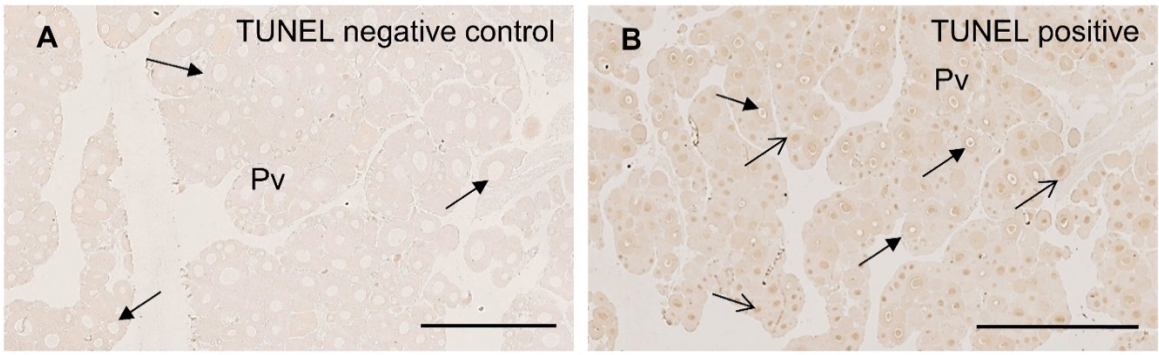

Figure 2
In-situ TUNEL staining in ovaries of European hake. (A) TUNEL assay negative control. Bar = 500 µm; (B) TUNEL-positive staining in cells of ovarian follicles. Bar = 1 mm. Open arrows show positively labelled previtellogenic oocyte (Pv) nuclei and full arrows indicate unstained oocyte nuclei in this early developmental stage ovary.

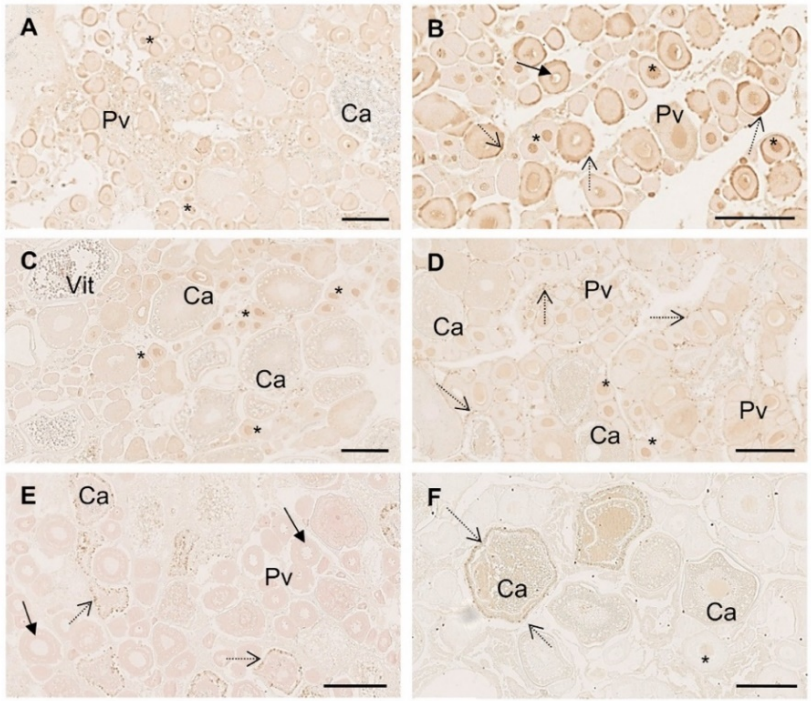

Figure 3
In-situ TUNEL staining in ovaries of the asynchronous developing European hake**.** Apoptotic oocytes with TUNEL-positive staining can be observed. Asterisks show positively labelled oocyte nuclei all of them at previtellogenic stage (Pv). Broken arrows label positively labelled follicular cells mainly around cortical alveoli (Ca) and vitellogenic (Vit) stage oocytes. Full arrows mark non-apoptotic and unlabelled oocyte nuclei. Bars = 250 µm.

Positively stained nuclei were identified in atretic previtellogenic oocytes although labelling was also conspicuous in nuclei of hypertrophied granulosa cells (Figures 2B and 3B-3D) whereas oocytes in normal non-atretic follicles were TUNEL-negative (Figures 2B and 3B). Atresia in follicles at more advanced developmental stages resulted in TUNEL-positive staining of theca and follicular cells but it was not evident in oocytes themselves (Figure 3D-3F).

3.3. 5S/18S rRNA ratio calculation

The 5S/18S rRNA ratio was useful to discreetly identify the level of development of the ovaries in European hake. Ovaries were classified as containing mainly previtellogenic oocytes when they displayed the highest 5S/18S rRNA ratio values (Rojo-Bartolomé et al., 2017, 2016). Values decreased as the ovaries contained more oocytes that had entered the vitellogenesis stage that is characterised by a high production of 18S and 28S rRNA's. The lowest values were observed when ovaries contained many oocytes reaching final maturation (Figure 4). Hake ovary develops asynchronously (Figures 1 and 3), and our histological ranking of development took into consideration the presence of at least one oocyte in the most advanced developmental stage without distinguishing which is the most dominant oocyte developmental stage in each moment. With the 5S/18S rRNA ratio, a fine-grain continuous numerical ranking of ovarian development was made possible, thus eliminating the possibility of bias with histological staging. Within the developmental continuum from early development to full maturity this ranking system matched well with the histological staging that was previously done. In all cases, there were individuals showing ratio values that would rank them outside their histologically assigned developmental stage.

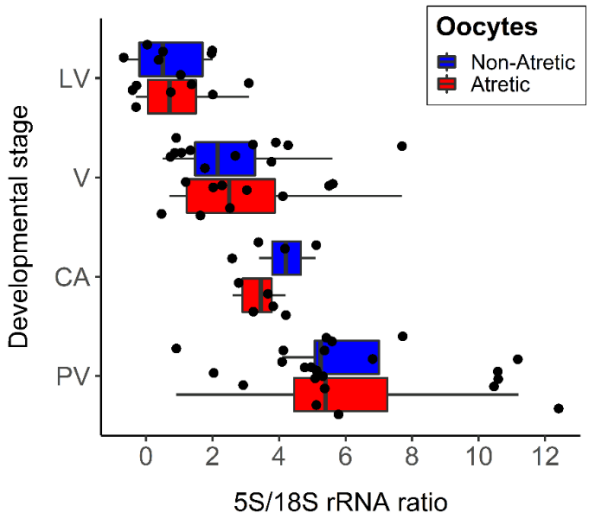

Figure 4
5S/18S rRNA ratio values during ovarian development in the European hake (atretic and non-atretic). The developmental stages include previtellogenic (PV; atretic n = 14, non-atretic n = 7), cortical alveoli (CA; atretic n = 6, non-atretic n = 3), vitellogenic (V; atretic n =19, non-atretic n = 5), late vitellogenic and maturing (LV; atretic n = 7, non-atretic n = 7) and were assigned according to the presence of the most advanced developmental stage present in the ovary. Boxplots represent the data within the 25th and 75th percentiles, with the median indicated by a line, and bottom and top whiskers representing minimum and maximum values, respectively. Each dot corresponds to an individual.

3.4. Gene transcription analyses

Relative transcription levels in each individual were plotted against their individual 5S/18S rRNA ratio comparing transcription levels between ovaries identified histologically as atretic or non-atretic. The ratio classified the asynchronous ovaries in European hake in terms of their stage of development and was used to plot the qPCR values along ovarian development. Lower 5S/18S rRNA ratio values identified ovaries with oocytes in vitellogenesis and entering final maturation, while higher values identified ovaries with oocytes in previtellogenesis. The histological classification ranks in the same group an ovary with only one vitellogenic oocyte and another one with most of its oocytes in vitellogenesis (vitellogenic); whereas the ratio reflects the gonad development stage along a numerical continuum. The trends in relative transcription levels of *p53* and *caspase-3* (*casp3*) (Figure 5) and *cathepsin D* (*ctsd*) and *death-associated protein kinase 1* (*dapk1*) (Figure 6) were identical. Significant differences in *p53* transcription levels were observed between vitellogenic atretic follicles and non-atretic follicles with 5S/18S index values ranging from 3.01 and 10.65, with *p53* transcripts being upregulated in atretic oocytes. However, *p53* showed no transcription level differences in atretic vs. non-atretic follicles during very early previtellogenesis and late vitellogenesis. The same expression patterns were observed for *casp3*, *ctsd* and *dapk1* transcripts but this time in between 5S/18S rRNA ratio values of 2.95–10.01, 3.24–10.25 and 3.47–10.21 respectively. In the case of *beclin-1* and *ptenb*, upregulation was observed in atretic follicles along their whole developmental spectrum, including very early previtellogenesis and late vitellogenesis (Figure 6). For *mdm2*, *rpl11*, *rpl5*, *bcl2*, *fshr* and *lhr*, no significant transcription level differences were observed between atretic and non-atretic follicles.

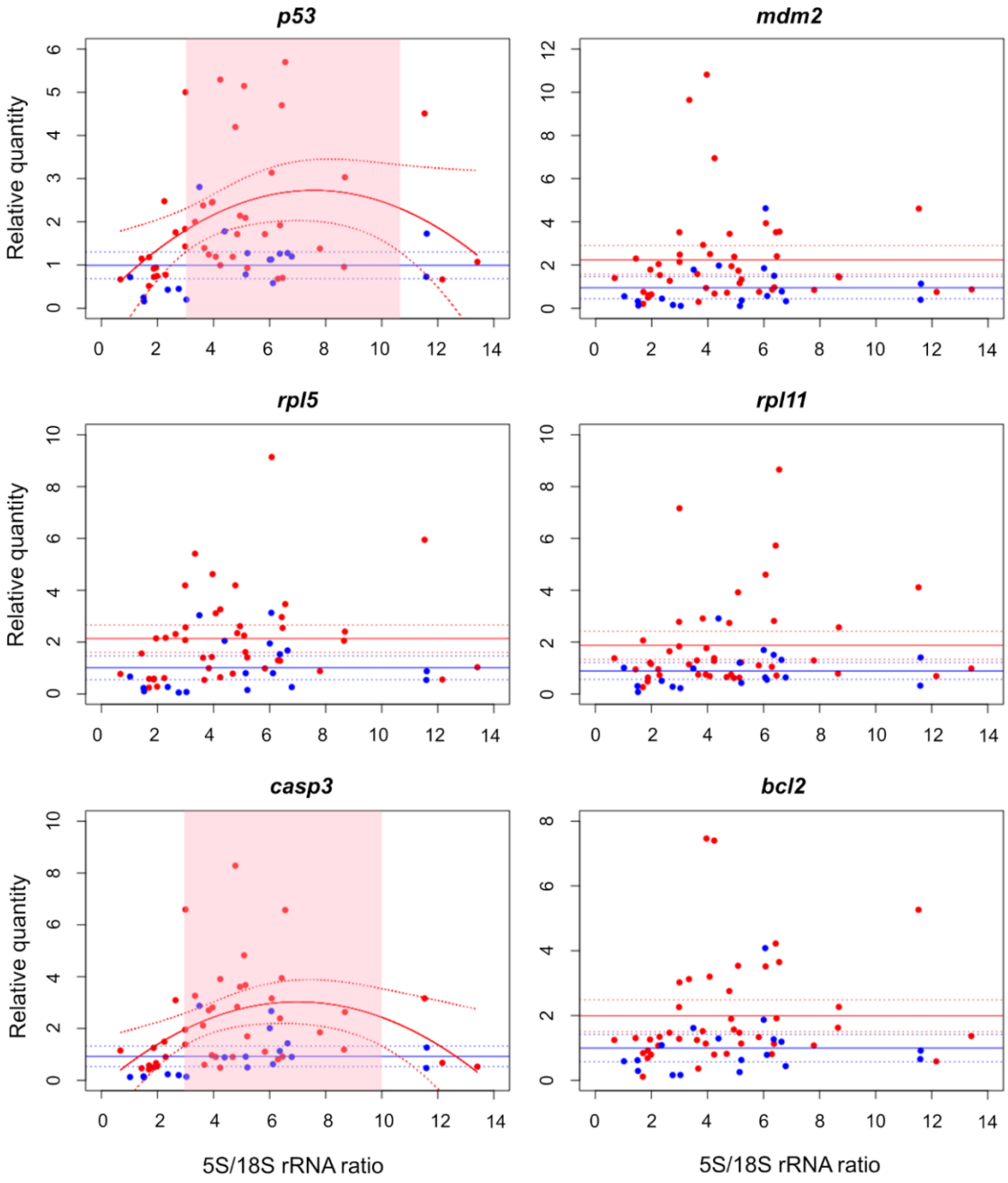

Figure 5
Transcription levels of genes related to apoptosis and autophagy in ovaries of the European hake at different developmental stages. 5S/18S rRNA ratio indicates the level of maturity of the ovaries analysed ranging from ovaries with oocytes in vitellogenesis (values tending to 0) to pre-vitellogenesis (values tending to 14). Each dot represents one individual. Red dots represent ovaries with atretic follicles and blue dots represent ovaries with non-atretic follicles. Red and blue lines represent the regression curves (continuous lines) and 95% confidence intervals (dashed lines) of ovaries with atretic and non-atretic follicles respectively. Pink shading covers the rank of individuals along the developmental continuum as staged by the 5S/18S rRNA ratio that shows significant differences between atretic and non-atretic individuals ($p < 0.05$).

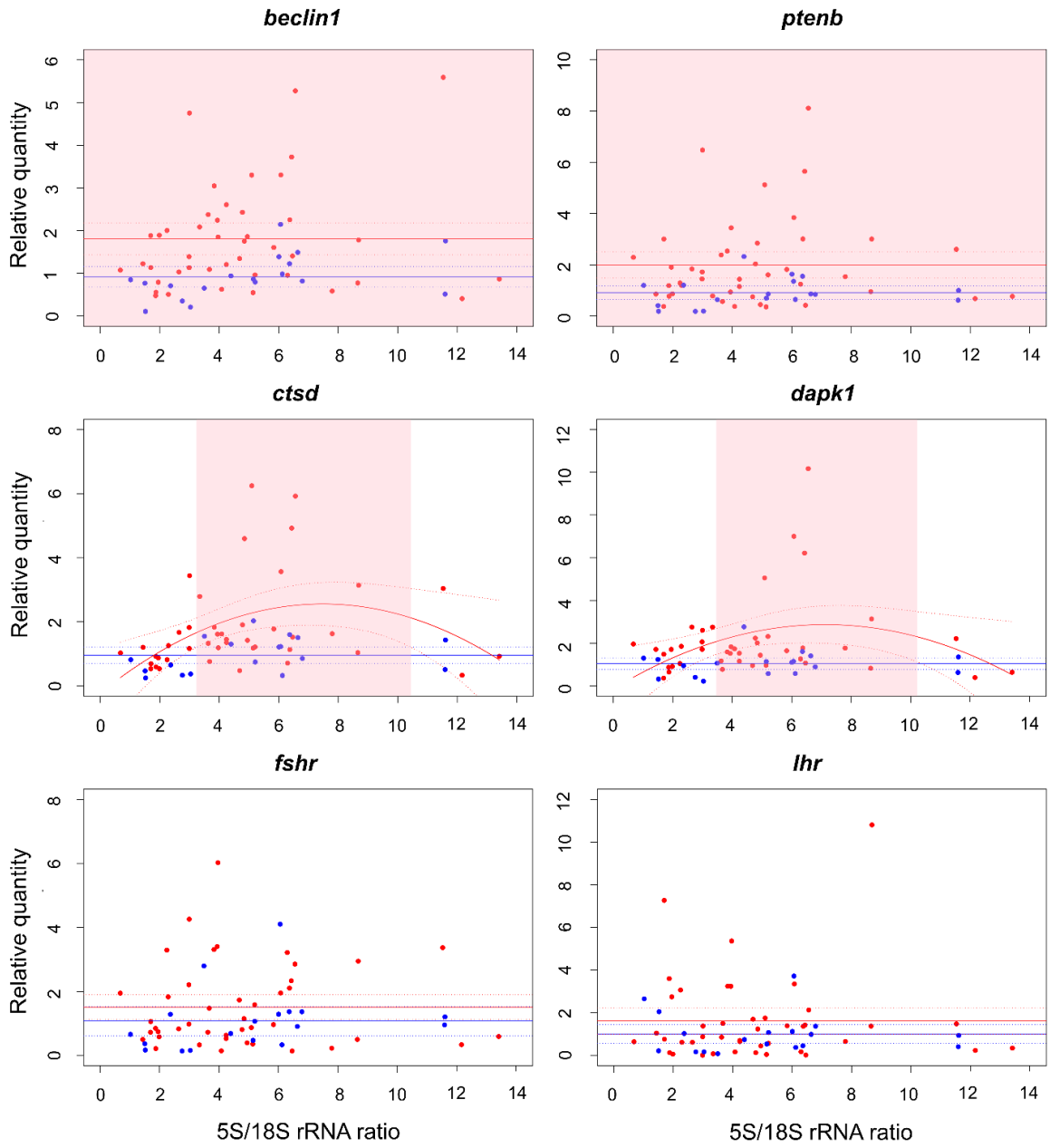

Figure 6
Transcription levels of genes related to apoptosis and autophagy in ovaries of the European hake at different developmental stages. 5S/18S rRNA ratio indicates the level of maturity of the ovaries analysed ranging from ovaries with oocytes in vitellogenesis (values tending to 0) to pre-vitellogenesis (values tending to 14). Each dot represents one individual. Red dots represent ovaries with atretic follicles and blue dots represent ovaries with non-atretic follicles. Red and blue lines represent the regression curves (continuous lines) and 95% confidence intervals (dashed lines) of ovaries with atretic and non-atretic follicles respectively. Pink shading covers the rank of individuals along the developmental continuum as staged by the 5S/18S rRNA ratio that shows significant differences between atretic and non-atretic individuals ($p < 0.05$).

3.5. Protein expression analysis: immunoblotting

Specific cross-labelling was observed for hake proteins in previtellogenic and vitellogenic atretic and non-atretic follicular tissue using antibodies against mammalian proteins of p53, MDM2, RPL5 and RPL11 proteins. Specific bands of 53 kDa, 55 kDa, 34 kDa and 22 kDa were labelled in European hake corresponding respectively to the typical molecular mass of p53, MDM2, RPL5 and RPL11 in vertebrates (Figure 7A).

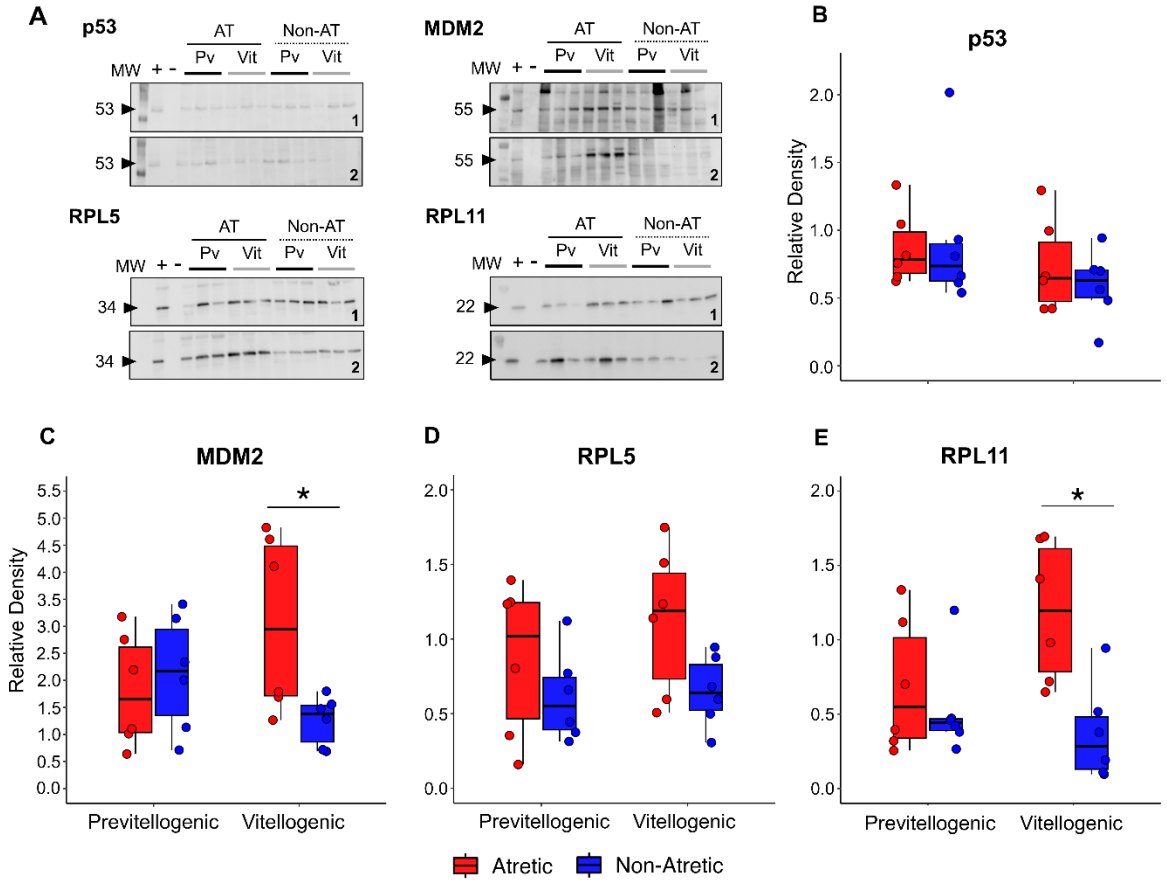

Figure 7
Western blots of hake ovarian tissue samples revealing the expression of target proteins related to apoptosis and autophagy during follicular atresia. (A) Cropped blots (1 and 2) for p53, MDM2, RPL5 and RPL11 with predicted molecular weights (MW) of 53 kDa, 55 kDa, 34 kDa and 22 kDa respectively. Total number of individuals analysed per protein was 24 (blot 1 and 2). Full-length western blots are shown in supplementary material (Figure S1). (+) represents positive (atretic) sample used for normalization across blots and (-) represents negative no-protein load control. Pv = ovaries in previtellogenesis and Vit = ovary in vitellogenesis. AT = ovaries with atretic previtellogenic (n = 6) and vitellogenic (n = 6) follicles. Non-AT = ovaries with non-atretic previtellogenic (n = 6) and vitellogenic (n = 6) follicles. (B, C, D and E) Quantification of each target protein based on their relative labelling densities. Boxplots represent the data within the 25th and 75th percentiles, with the median indicated by a line, and bottom and top whiskers representing minimum and maximum values, respectively. Asterisks (*) above bars indicate statistically significant different results ($p < 0.05$).

Stronger immunoreactivity was found for MDM2 and RPL11 proteins in ovaries with atretic vs. non-atretic follicles and quantification (Figures 7C and 7E) showed that significant differences exist in vitellogenic ovaries (Students t-test, $p < 0.05$). For p53 and RPL5, no significant differences were observed between atretic and non-atretic previtellogenic and vitellogenic ovaries (Figures 7B and 7D).

4. Discussion

The focus of the present study was to understand the molecular mechanisms governing follicular atresia in fish ovaries to develop early warning biomarkers of atresia and interruption of the normal oogenic cycle that could eventually be applied to better monitor fish stock fecundity. The transcriptional profile of apoptosis and autophagy-related genes (*p53*, *mdm2*, *rpl11*, *rpl5*, *caspase-3*, *bcl2*, *ptenb*, *fshr*, *lhr*, *beclin-1*, *ctsd*, *dapk1*) were analysed in the ovaries of the European hake (*Merluccius merluccius*), a species whose ovaries develop asynchronously and that shows episodes of enhanced oocyte atresia. Ovarian developmental stages were ranked histologically and inferred molecularly by applying the 5S/18S rRNA ratio (Rojo-Bartolomé et al., 2016) and TUNEL assay was used to histologically identify apoptosis. Immunoblotting analysis of p53, MDM2, RPL5 and RPL11 proteins was also performed.

Histological analysis revealed the presence of atretic follicles in the ovaries of a high percentage of the hakes analysed, the atresia becoming evident in follicles at any stage of development. It must be noted that individuals were captured from March to July after the peak winter spawning period and this could help explain the high prevalence of atresia identified in the study population. In European hake, oocyte recruitment is a continuous process, with oocytes of different sizes and stages coexisting in an ovary during maturity (Korta et al., 2010). Ranking the developmental stage of an ovary as vitellogenic due to the presence of a single oocyte in vitellogenesis and thus disregarding the predominance of cortical alveoli and previtellogenesis stage oocytes (West, 1990) may not reflect the relative maturity stage of the individual ovary. Instead of taking a stereological approach to quantify the extent of coverture of each type of oocyte in each ovary, we aimed to rank the developmental stage of the study ovaries more granularly using the 5S/18S rRNA ratio.

The 5S/18S rRNA ratio has been proposed as a good quantitative and unbiased proxy to establish the ovarian developmental stage of any teleost species (Rojo-Bartolomé et al.,

2016). This is so because 5S rRNA levels are very high in previtellogenic oocytes while 18S rRNA (and 28S rRNA) levels begin to increase after the cortical alveoli stage (Rojo-Bartolomé et al., 2017, 2016). Growing oocytes require rRNAs to synthesise new ribosomes for the proper development of the embryo after fertilisation and they initiate the process with the production of the less energy-demanding 5S rRNA molecule. Larger molecules begin to accumulate during vitellogenesis and secondary oocyte growth (Diaz De Cerio et al., 2012; Rojo-Bartolomé et al., 2017, 2016; Shen et al., 2016). Due to the dynamics of production of the ribosomal intermediates, the 5S/18S rRNA ratio ranks ovarian developmental status efficiently in synchronous species although it has been proved also to work in asynchronous species such as Atlantic, chub and horse mackerels, blue whiting, European anchovy and pilchard and bluegill and largemouth bass (Rojo-Bartolomé et al., 2016; Shen et al., 2016). Therefore, considering the dynamics of 5S and 18S rRNA production, the 5S/18S rRNA ratio proved to be a useful numerical and non-biased approach to rank ovaries, integrating the developmental stage of the pool of oocytes in each gonad. The results aligned quite well with the histological staging, but instead of creating four discrete groups (previtellogenic, cortical alveoli, vitellogenic, late-vitellogenic) identified each ovary along the continuum of the maturation process.

There is evidence that apoptosis plays a key role in gonad development and reproduction in birds and mammals, but also in fish (Habibi and Andreu-Vieyra, 2007; Janz and Van Der Kraak, 1997; Matsuda et al., 2012; Nozu et al., 2013; Tilly, 1996a; Tiwari et al., 2015; Wood and Van Der Kraak, 2001; Yamamoto et al., 2011; Yang et al., 2022). In birds and mammals, for example, the dominant follicle is normally recruited to the ovulatory pool, while the remaining follicles are eliminated through atresia, mediated by apoptosis initiated within granulosa cells (Andreu-Vieyra and Habibi, 2000; Bhardwaj and Sharma, 2012; Matsuda et al., 2012). In fish, widespread apoptosis-mediated atresia occurs when of the thousands of oocytes normally recruited, the vitellogenic oocytes fail to mature in a spawning season and regression occurs in preparation for a new reproductive cycle (Guraya, 1986; Miranda et al., 1999; Nozu et al., 2013; Rizzo and Bazzoli, 1995; Yamamoto et al., 2011). Results of the TUNEL assay demonstrate that apoptosis occurs in hake previtellogenic oocytes and their surrounding follicular cells. Apoptosis was additionally observed in cortical alveoli and vitellogenic follicles, but not within the oocytes. In such cases, apoptosis was limited to the nuclei of the surrounding follicular cells. Similar responses in advanced-stage follicles were observed in other asynchronous developing species, the goldfish (*Carassius auratus*) (Wood

and Van Der Kraak, 2001) and farmed Nile tilapia (*Oreochromis niloticus*) (Qiang et al., 2021). This points to an atresia process that is directed from outside to inside in the follicular structure, as has been suggested for other fish species (Qiang et al., 2022; Wood et al., 2005). Previous studies of atresia in ovaries of non-mammalian vertebrates showed that the degeneration of follicular cells takes place only after the resorption of vitellogenic materials from vitellogenic oocytes is completed (Saidapur, 1978); thus, facilitating the efficient recycling of oocyte contents (Wood and Van Der Kraak, 2001).

The molecular mechanisms that control follicular atresia in teleost fishes may open avenues for early assessment of the onset of the process under environmental stress and in this respect, a set of core genes involved in apoptosis and autophagocytosis have been highlighted as potential markers across teleost species (González-Kother et al., 2020), although some others may exist. Reproductive hormones in teleosts closely integrate physiological status and environmental cues to direct gonad development (Habibi and Andreu-Vieyra, 2007; Juntti and Fernald, 2016; Qiang et al., 2022). In this way, increased levels of follicle-stimulating (FSH) and luteinizing (LH) hormone are known to promote oocyte development and maturation (Qiang et al., 2022), with FSH controlling apoptosis-mediated atresia in ovaries (Lubzens et al., 2010; Shen et al., 2016). In this study, the transcript levels of genes encoding the receptors of both gonadotropins (*fshr* and *lhr*) did not change in ovaries with atretic follicles. Nonetheless, the role of FSH as an anti-apoptotic hormone has been clearly demonstrated in the Coho salmon (*Oncorhynchus kisutch*) and the Nile tilapia, and upregulation of *fshr* and *lhr* has been reported in connection with reduced apoptosis-mediated follicular atresia (Guzmán et al., 2014).

p53 is the guardian of the cell cycle both in its functions as a tumour suppressor and regulator of apoptosis and its transcriptional regulation has often been studied as a marker of stress (Rau Embry et al., 2006) although not in relation to follicular atresia. Its role in triggering apoptosis in fish oocytes is proved by its role in sex differentiation in *Danio rerio*. All newly hatched zebrafish develop a juvenile ovary with previtellogenic oocytes and this ovary regresses in the case of males for the development of testis. This sex reversal process is triggered by p53 and executed by caspase-3, causing apoptosis of oocytes (Rodríguez-Marí et al., 2010). In hake, we observed an upregulation of the apoptosis-related gene *p53* in ovaries with atretic vitellogenic (5S/18S index 3.01 to 10.65) follicles and no difference in transcription and protein expression levels between ovaries with atretic and non-atretic

follicles when these were early previtellogenic or late vitellogenic. In these two cases, differences in p53 activities cannot be ruled out since p53 is largely regulated post-transcriptionally through ubiquitination and proteolytic cleavage via the E3 ubiquitin ligase MDM2 (Boehme and Blattner, 2009; Deisenroth and Zhang, 2010; Rau Embry et al., 2006; Shi and Gu, 2012). Another gene corroborates the preponderance of apoptotic response in atresia affecting vitellogenic stage follicles in opposition to those in previtellogenesis or late vitellogenesis. Transcript levels of caspase-3 were also significantly higher in ovaries with vitellogenic (5S/18S rRNA ratio 3 to 10) atretic follicles, without differences atretic vs non-atresia in ovaries histologically ranked as previtellogenic or late vitellogenic. Caspase-3 largely mediate the apoptotic response triggered by p53 and its proteolytic activity, also in fish oocytes (Rodríguez-Marí et al., 2010). p53 controls the proteolytic cascade by regulating the transcription of anti-apoptotic Bcl2 whose function is to stabilise the mitochondrial membrane. When this membrane is destabilised, cytochrome c is released to the cytosol and caspase-3 is activated (Donati et al., 2013; Maiuri et al., 2007). However, even if *bcl2* transcriptional regulation has been reported in some teleost species suffering atresia (González-Kother et al., 2020), transcription levels were similar in hake ovaries with and without atretic follicles.

As already said MDM2 is the major regulator of p53 through ubiquitination but no differences in *mdm2* transcription levels were observed between ovaries with atretic and non-atretic follicles at any stage. A strict relationship could exist between p53, MDM2 and 5S rRNA, considering the enormous amount of 5S rRNA in fish oocytes that could account for a major mechanism deciding the fate of oocytes during development in fish ovaries. In conjunction with ribosomal proteins L5 (RPL5) and L11 (RPL11), 5S rRNA has been demonstrated to bind MDM2 in mammalian cells suffering ribosomal stress. Such binding rescues p53 from ubiquitination and degradation and results in its activation in such circumstances (Deisenroth and Zhang, 2010; Donati et al., 2013; Sloan et al., 2013). Chakraborty et al. (2009) observed that in *Danio rerio* embryos, the loss of RPL11 results in a decreased production of mature 18S rRNA molecules, activation of p53 and impaired ribosome biogenesis. In this study, however, the transcription levels of *rpl5* and *rpl11* followed a pattern similar to that of *mdm2* without significant transcriptional regulation with regard to atresia. Obviously, the mechanism does not need to be regulated at the transcriptional level. At the protein level, higher levels of MDM2 and RPL11 were observed in vitellogenic ovaries with atretic follicles compared to those not presenting atresia.

Autophagy is another mechanism that may lead to cell death in atretic follicles in fish (Maiuri et al., 2007; Thomé et al., 2009). Autophagy can be triggered as a stress response to degrade damaged cell proteins and organelles (Maiuri et al., 2007; Thomé et al., 2009). Beclin-1, an important autophagy marker, is responsible for forming the isolation membrane that engulfs cytoplasmic material to form the autophagosomes that initiate autophagy (Bhardwaj et al., 2022), and it has been implicated in the process of follicular atresia in different freshwater fish species (Morais et al., 2012). Our study observed that both *beclin-1* and *ptenb* were continuously upregulated in atretic follicles irrespective of their developmental stage. Ptenb protein, a transcriptional target of p53, is known to negatively regulate the PI3K/AKT/mTOR signalling pathway, which in turn affects autophagy as it has been reported in Japanese flounder suffering from a pathogen infection (Li et al., 2020).

In vitellogenic oocytes of the European hake, autophagy and also phagocytosis by follicular cells could help to digest oocyte yolk material during atresia. In this way, we have observed the upregulation of *ctsd* and *dapk1* in ovaries with vitellogenic (5S/18S rRNA ratio 3 to 10) atretic follicles. Cathepsin D (*ctsd*) is well known for its key role in oocyte development in fish, amphibians and birds, cleaving vitellogenin into smaller molecules for yolk formation and in turn, oocyte growth and maturation (Carnevali et al., 2006). Several studies have observed that the cleavage of vitellogenin occurs during the early stages of atresia, coinciding with the presence of cathepsin D and preceding the formation of autophagic vacuoles (Guzmán et al., 2014; Mayo and Donner, 2002). These studies reinforce the suggestion that *ctsd* is necessary for vitellogenin cleavage to occur before atresia can proceed (Chang et al., 2003; Janz and Van Der Kraak, 1997). At the same time, Dapk1 is known for its role in stress signalling, regulating cell death and autophagy processes through caspase activation (Gozuacik et al., 2008; Singh et al., 2016). Taking this into account, our study suggests that the overexpression of *beclin-1* and *ptenb* promotes autophagy and transcription of proteolytic enzymes to facilitate the removal of organelles and proteins, therefore recycling macromolecules during nutrient deprivation or energy deficiency. This would allow the recovery of the energy invested in oogenesis previous to follicle resorption through apoptosis-mediated atresia. Comparatively, apoptosis seems to take the leading role in regulating atresia in mammals while in fish as seen hereby, autophagy also plays an important role, especially in somatic cells surrounding the vitellogenic oocytes (Yang et al., 2022). Nonetheless, recent revision of follicular atresia in

mammals points also to an important role of autophagy with special mention to molecular markers such as Beclin-1 as in the present study in hake.

5. Conclusions

It can be concluded that the 5S/18S rRNA ratio can be used as a useful non-biased method to rank the overall development stage in the asynchronous developing ovaries of the European hake. The novelty of the study stands in that we can relate the levels of transcription and protein expression of atresia marker genes in relation to the exact developmental stage of the ovaries. In this way, we observed that apoptosis marker genes *p53* and *caspase-3* are upregulated in hake ovaries displaying atresia during vitellogenesis and at the same time MDM2 and RPL11 protein levels are higher. In addition, autophagocytosis marker genes *ctsd* and *dapk1* are upregulated. The upregulation of *beclin-1* and *ptenb* transcripts in atretic follicles, occurred irrespective of their developmental stage, suggesting that autophagy is strongly involved in follicular atresia along the whole process of oogenesis. The upregulation of *p53*, *caspase-3*, *ctsd* and *dapk1* transcripts, and the high protein expression of MDM2 and RPL11 only during atresia affecting vitellogenic follicles, would suggest that vitellogenesis is the moment at which both apoptosis and autophagy are at their highest (Yang et al., 2022). Hereby a set of marker genes and proteins for the early estimation of atresia in female European hakes (that could be extended to other fish species) is provided. These marker genes could be studied for a better estimation of hake stock fecundity but deeper analysis at the protein level should be carried out to confirm our observations.

Acknowledgements

SGIker technical support (University of the Basque Country) is greatly acknowledged. This work was funded by the Spanish Ministry of Science, Innovation and Universities (ATREoVO AGL2015-63936-R and BORN2bEGG PGC2018-101442-B-I00) and by the Basque Government (Grant to consolidated research groups IT1302-19). A.N. is a recipient of a pre-doctoral grant from the University of the Basque Country (UPV/EHU).

References

Andreu-Vieyra, C.V., Habibi, H.R., 2000. Factors controlling ovarian apoptosis. Can J Physiol Pharmacol 78, 1003–1012. https://doi.org/10.1139/y00-101

Bhardwaj, J.K., Paliwal, A., Saraf, P., Sachdeva, S.N., 2022. Role of autophagy in follicular development and maintenance of primordial follicular pool in the ovary. J Cell Physiol 237, 1157–1170. https://doi.org/10.1002/JCP.30613

Bhardwaj, J.K., Sharma, R.K., 2012. Apoptosis and ovarian follicular atresia in mammals, in: García, M.-D. (Ed.), Zoology. IntechOpen, pp. 185–206.

Boehme, K., Blattner, C., 2009. Regulation of p53 - insights into a complex process. Crit Rev Biochem Mol Biol 44, 367–392. https://doi.org/10.3109/10409230903401507

Cadima, E.L., 2003. Fish stock assessment manual, FAO Fisheries Technical Paper. No. 393. Rome, FAO. 2003. 161p. Rome.

Carnevali, O., Cionna, C., Tosti, L., Lubzens, E., Maradonna, F., 2006. Role of cathepsins in ovarian follicle growth and maturation. Gen Comp Endocrinol 146, 195–203. https://doi.org/10.1016/j.ygcen.2005.12.007

Cassel, M., de Paiva Camargo, M., Oliveira de Jesus, L.W., Borella, M.I., 2017. Involution processes of follicular atresia and post-ovulatory complex in a characid fish ovary: a study of apoptosis and autophagy pathways. J Mol Histol 48, 243–257. https://doi.org/10.1007/s10735-017-9723-6

Chakraborty, A., Uechi, T., Higa, S., Torihara, H., Kenmochi, N., 2009. Loss of ribosomal protein L11 affects zebrafish embryonic development through a p53-dependent apoptotic response. PLoS One 4, e4152. https://doi.org/10.1371/journal.pone.0004152

Chang, F., Lee, J.T., Navolanic, P.M., Steelman, L.S., Shelton, J.G., Blalock, W.L., Franklin, R.A., McCubrey, J.A., 2003. Involvement of PI3K/Akt pathway in cell cycle progression, apoptosis, and neoplastic transformation: A target for cancer chemotherapy. Leukemia 17, 590–603. https://doi.org/10.1038/sj.leu.2402824

Corriero, A., Zupa, R., Mylonas, C.C., Passantino, L., 2021. Atresia of ovarian follicles in fishes, and implications and uses in aquaculture and fisheries. J Fish Dis 44, 1271–1291. https://doi.org/10.1111/JFD.13469

Dag, O., Dolgun, A., Konar, N.M., 2018. Onewaytests: An R package for one-way tests in independent groups designs. R Journal 10, 175–199. https://doi.org/10.32614/rj-2018-022

Deisenroth, C., Zhang, Y., 2010. Ribosome biogenesis surveillance: probing the ribosomal protein-Mdm2-p53 pathway. Oncogene 29, 4253–4260. https://doi.org/10.1038/onc.2010.189

Diaz De Cerio, O., Rojo-Bartolomé, I., Bizarro, C., Ortiz-Zarragoitia, M., Cancio, I., 2012. 5S rRNA and accompanying proteins in gonads: powerful markers to identify sex and reproductive endocrine disruption in fish. Environ Sci Technol 46, 7763–7771. https://doi.org/10.1021/es301132b

Díez, G., Díaz, E., Arregi, L., Sagarminaga, Y., Irigoien, X., Álvarez, P., Cotano, U., Murua, H., Santos, M., Murillas, A., 2011. Impact assessment in the life cycle and demographic structure of commercial and ecological interest species after the Prestige oil spill. Revista de Investigación Marina (Marine Research Journal) 18, 92–133.

Donati, G., Peddigari, S., Mercer, C.A., Thomas, G., 2013. 5S ribosomal RNA is an essential component of a nascent ribosomal precursor complex that regulates the Hdm2-p53 checkpoint. Cell Rep 4, 87–98. https://doi.org/10.1016/j.celrep.2013.05.045

Fox, J., Weisberg, S., 2019. An R Companion to Applied Regression, Third. ed. Sage, Thousand Oaks, CA.

González-Kother, P., Oliva, M.E., Tanguy, A., Moraga, D., 2020. A review of the potential genes implicated in follicular atresia in teleost fish. Mar Genomics 50, 100704. https://doi.org/10.1016/j.margen.2019.100704

Gozuacik, D., Bialik, S., Raveh, T., Mitou, G., Shohat, G., Sabanay, H., Mizushima, N., Yoshimori, T., Kimchi, A., 2008. DAP-kinase is a mediator of endoplasmic reticulum stress-induced caspase

activation and autophagic cell death. Cell Death Differ 15, 1875–1886. https://doi.org/10.1038/cdd.2008.121

Guraya, S.S., 1986. The cell and molecular biology of fish oogenesis, Monographs in Developmental Biology, Vol. 18, Monographs in Developmental Biology. Karger, Basel.

Guzmán, J.M., Luckenbach, J.A., Yamamoto, Y., Swanson, P., 2014. Expression profiles of fsh-regulated ovarian genes during oogenesis in Coho Salmon. PLoS One 9, e114176. https://doi.org/10.1371/journal.pone.0114176

Habibi, H.R., Andreu-Vieyra, C. V., 2007. Hormonal regulation of follicular atresia in teleost fish, in: Babin, P.J., Cerdà, J., Lubzens, E. (Eds.), The Fish Oocyte: From Basic Studies to Biotechnological Applications. Springer Netherlands, pp. 235–253. https://doi.org/10.1007/978-1-4020-6235-3_9

Hsueh, A.J.W., Billig, H., Tsafriri, A., 1994. Ovarian follicle atresia: a hormonally controlled apoptotic process. Endocr Rev 15, 707–724. https://doi.org/10.1210/edrv-15-6-707

Hunter, J.R., Macewicz, B.J., 1985. Rates of atresia in the ovary of captive and wild northern anchovy, Engraulis mordax. Fishery Bulletin 83, 119–136.

Janz, D.M., Van Der Kraak, G.J., 1997. Suppression of apoptosis by gonadotropin, 17β-estradiol, and epidermal growth factor in rainbow trout preovulatory ovarian follicles. Gen Comp Endocrinol 105, 186–193. https://doi.org/10.1006/gcen.1996.6820

Jørgensen, C., Dunlop, E.S., Frugå, A., Opdal, R.D., Fiksen, Ø., Opdal, A.F., Fiksen, Ø., 2008. The evolution of spawning migrations: State dependence and fishing-induced changes. Ecology 89, 3436–3448. https://doi.org/10.1890/07-1469.1

Jørgensen, C., Holt, R.E., 2013. Natural mortality: Its ecology, how it shapes fish life histories, and why it may be increased by fishing. J Sea Res 75, 8–18. https://doi.org/10.1016/j.seares.2012.04.003

Juntti, S.A., Fernald, R.D., 2016. Timing reproduction in teleost fish: Cues and mechanisms. Curr Opin Neurobiol 38, 57–62. https://doi.org/10.1016/j.conb.2016.02.006

Kennedy, J., Gundersen, A.C., Boje, J., 2009. When to count your eggs: Is fecundity in Greenland halibut (*Reinhardtius hippoglossoides* W.) down-regulated? Fish Res 100, 260–265. https://doi.org/https://doi.org/10.1016/j.fishres.2009.08.008

Kjesbu, O.S., 2009. Applied fish reproductive biology: contribution of individual reproductive potential to recruitment and fisheries management, in: Jakobsen, T., Forgarty, M., Megrey, Bernard.A., Moksness, E. (Eds.), Fish Reproductive Biology: Implications for Assessment and Management. Wiley-Blackwell, pp. 293–332. https://doi.org/10.1002/9781444312133.ch8

Korta, M., Murua, H., Kurita, Y., Kjesbu, O.S., 2010. How are the oocytes recruited in an indeterminate fish? Applications of stereological techniques along with advanced packing density theory on European hake (*Merluccius merluccius* L.). Fish Res 104, 56–63. https://doi.org/10.1016/j.fishres.2010.01.010

Krysko, D. V., Diez-Fraile, A., Criel, G., Svistunov, A.A., Vandenabeele, P., D'Herde, K., 2008. Life and death of female gametes during oogenesis and folliculogenesis. Apoptosis 13, 1065–1087. https://doi.org/10.1007/s10495-008-0238-1

Li, W., Guan, X., Sun, L., 2020. Phosphatase and tensin homolog (Pten) of japanese flounder—its regulation by miRNA and role in autophagy, apoptosis and pathogen infection. Int J Mol Sci 21, 1–18. https://doi.org/10.3390/ijms21207725

Libus, J., Štorchová, H., 2006. Quantification of cDNA generated by reverse transcription of total RNA provides a simple alternative tool for quantitative RT-PCR normalization. Biotechniques 41, 156–164. https://doi.org/10.2144/000112232

Lubzens, E., Young, G., Bobe, J., Cerdà, J., 2010. Oogenesis in teleosts: How fish eggs are formed. Gen Comp Endocrinol 165, 367–389. https://doi.org/10.1016/j.ygcen.2009.05.022

Maiuri, M.C., Zalckvar, E., Kimchi, A., Kroemer, G., 2007. Self-eating and self-killing: Crosstalk between autophagy and apoptosis. Nat Rev Mol Cell Biol 8, 741–752. https://doi.org/10.1038/nrm2239

Malmstrøm, M., Matschiner, M., Tørresen, O.K., Star, B., Snipen, L.G., Hansen, T.F., Baalsrud, H.T., Nederbragt, A.J., Hanel, R., Salzburger, W., Stenseth, N.C., Jakobsen, K.S., Jentoft, S., 2016a. Evolution of the immune system influences speciation rates in teleost fishes. Nat Genet 48, 1204–1210. https://doi.org/10.1038/ng.3645

Malmstrøm, M., Matschiner, M., Tørresen, O.K., Star, B., Snipen, L.G., Hansen, T.F., Baalsrud, H.T., Nederbragt, A.J., Hanel, R., Salzburger, W., Stenseth, N.C., Jakobsen, K.S., Jentoft, S., 2016b. Data from: Evolution of the immune system influences speciation rates in teleost fishes. Nat Genet 48, 1204–1210. https://doi.org/10.5061/dryad.326r8

Matsuda, F., Inoue, N., Manabe, N., Ohkura, S., 2012. Follicular growth and atresia in mammalian ovaries: Regulation by survival and death of granulosa cells. Journal of Reproduction and Development 58, 44–50. https://doi.org/10.1262/jrd.2011-012

Mayo, L.D., Donner, D.B., 2002. The PTEN, MDM2, p53 tumor suppressor–oncoprotein network. Trends Biochem Sci 27, 462–467. https://doi.org/10.1016/S0968-0004(02)02166-7

McBride, R.S., Somarakis, S., Fitzhugh, G.R., Albert, A., Yaragina, N.A., Wuenschel, M.J., Alonso-Fernández, A., Basilone, G., 2015. Energy acquisition and allocation to egg production in relation to fish reproductive strategies. Fish and Fisheries 16, 23–57. https://doi.org/10.1111/faf.12043

Miranda, A.C.L., Bazzoli, N., Rizzo, E., Sato, Y., 1999. Ovarian follicular atresia in two teleost species: a histological and ultrastructural study. Tissue Cell 31, 480–488. https://doi.org/10.1054/tice.1999.0045

Mittelholzer, C., Andersson, E., Consten, D., Hirai, T., Nagahama, Y., Norberg, B., 2007. 20β-hydroxysteroid dehydrogenase and CYP19A1 are differentially expressed during maturation in Atlantic cod (Gadus morhua). J Mol Endocrinol 39, 319–328. https://doi.org/10.1677/JME-07-0070

Morais, R.D.V.S., Thomé, R.G., Lemos, F.S., Bazzoli, N., Rizzo, E., 2012. Autophagy and apoptosis interplay during follicular atresia in fish ovary: a morphological and immunocytochemical study. Cell Tissue Res 347, 467–478. https://doi.org/10.1007/s00441-012-1327-6

Morais, R.D.V.S., Thomé, R.G., Santos, H.B., Bazzoli, N., Rizzo, E., 2016. Relationship between bcl-2, bax, beclin-1, and cathepsin-D proteins during postovulatory follicular regression in fish ovary. Theriogenology 85, 1118–1131. https://doi.org/10.1016/j.theriogenology.2015.11.024

Murua, H., Ibaibarriaga, L., Álvarez, P., Santos, M., Korta, M., Santurtun, M., Motos, L., 2010. The daily egg production method: A valid tool for application to European hake in the Bay of Biscay? Fish Res 104, 100–110. https://doi.org/10.1016/j.fishres.2009.06.007

Murua, H., Motos, L., 2006. Reproductive strategy and spawning activity of the European hake Merluccius merluccius (L.) in the Bay of Biscay. J Fish Biol 69, 1288–1303. https://doi.org/10.1111/j.1095-8649.2006.01169.x

Nozu, R., Horiguchi, R., Murata, R., Kobayashi, Y., Nakamura, M., 2013. Survival of ovarian somatic cells during sex change in the protogynous wrasse, *Halichoeres trimaculatus*. Fish Physiol Biochem 39, 47–51. https://doi.org/10.1007/s10695-012-9632-2

Patil, I., 2021. Visualizations with statistical details: The "ggstatsplot" approach. J Open Source Softw 6, 3167. https://doi.org/10.21105/joss.03167

Phillips, N.D., 2017. YaRrr! The Pirate's Guide to R [WWW Document]. URL https://bookdown.org/ndphillips/YaRrr/YaRrr.pdf

Qiang, J., Duan, X.J., Zhu, H.J., He, J., Tao, Y.F., Bao, J.W., Zhu, X.W., Xu, P., 2021. Some 'white' oocytes undergo atresia and fail to mature during the reproductive cycle in female genetically improved farmed tilapia (Oreochromis niloticus). Aquaculture 534, 736278. https://doi.org/10.1016/j.aquaculture.2020.736278

Qiang, J., Tao, Y.-F., Zhu, J.-H., Lu, S.-Q., Cao, Z.-M., Ma, J.-L., He, J., Xu, P., 2022. Effects of heat stress on follicular development and atresia in Nile tilapia (*Oreochromis niloticus*) during one reproductive cycle and its potential regulation by autophagy and apoptosis. Aquaculture 555, 738171. https://doi.org/10.1016/j.aquaculture.2022.738171

Rau Embry, M., Billiard, S.M., Di Giulio, R.T., Embry, M.R., Giulio, R.T. Di, 2006. Lack of p53 induction in fish cells by model chemotherapeutics. Oncogene 25, 2004–2010. https://doi.org/10.1038/sj.onc.

Rizzo, E., Bazzoli, N., 1995. Follicular atresia in curimatá-pioa *Prochilodus affinis* Reinhardt, 1874 (Pisces, Characiformes). Rev Bras Biol 55, 697–703.

Rodríguez-Marí, A., Cañestro, C., BreMiller, R.A., Nguyen-Johnson, A., Asakawa, K., Kawakami, K., Postlethwait, J.H., 2010. Sex reversal in zebrafish fancl mutants is caused by Tp53-mediated germ cell apoptosis. PLoS Genet 6, 1–14. https://doi.org/10.1371/journal.pgen.1001034

Rojo-Bartolomé, I., Diaz de Cerio, O., Diez, G., Cancio, I., 2016. Identification of sex and female's reproductive stage in commercial fish species through the quantification of ribosomal transcripts in gonads. PLoS One 11, e0149711. https://doi.org/10.1371/journal.pone.0149711

Rojo-Bartolomé, I., Martínez-Miguel, L., Lafont, A., Vílchez, M.C., Asturiano, J.F., Pérez, L., Cancio, I., 2017. Molecular markers of oocyte differentiation in European eel during hormonally induced oogenesis. Comp Biochem Physiol A Mol Integr Physiol 211, 17–25. https://doi.org/10.1016/j.cbpa.2017.05.018

Saidapur, S.K., 1978. Follicular atresia in the ovaries of nonmammalian vertebrates, in: International Review of Cytology. Academic Press, pp. 225–244. https://doi.org/10.1016/S0074-7696(08)60169-2

Sales, C.F., Melo, R.M.C., Pinheiro, A.P.B., Luz, R.K., Bazzoli, N., Rizzo, E., 2019. Autophagy and Cathepsin D mediated apoptosis contributing to ovarian follicular atresia in the Nile tilapia. Mol Reprod Dev 86, 1592–1602. https://doi.org/10.1002/mrd.23245

Santos, H.B., Thomé, R.G., Arantes, F.P., Sato, Y., Bazzoli, N., Rizzo, E., 2008. Ovarian follicular atresia is mediated by heterophagy, autophagy, and apoptosis in *Prochilodus argenteus* and *Leporinus taeniatus* (Teleostei: Characiformes). Theriogenology 70, 1449–1460. https://doi.org/https://doi.org/10.1016/j.theriogenology.2008.06.091

Serrat, A., Saborido-Rey, F., Garcia-Fernandez, C., Muñoz, M., Lloret, J., Thorsen, A., Kjesbu, O.S., 2019. New insights in oocyte dynamics shed light on the complexities associated with fish reproductive strategies. Sci Rep 9, 1–15. https://doi.org/10.1038/s41598-019-54672-3

Shen, M., Jiang, Y., Guan, Z., Cao, Y., Sun, S., Liu, H., 2016. FSH protects mouse granulosa cells from oxidative damage by repressing mitophagy. Sci Rep 6, 38090. https://doi.org/10.1038/srep38090

Shi, D., Gu, W., 2012. Dual roles of MDM2 in the regulation of p53: ubiquitination dependent and ubiquitination independent mechanisms of MDM2 repression of p53 activity. Genes Cancer 3, 240–248. https://doi.org/10.1177/1947601912455199

Singh, P., Ravanan, P., Talwar, P., 2016. Death associated protein kinase 1 (DAPK1): a regulator of apoptosis and autophagy. Front Mol Neurosci 9, 46. https://doi.org/10.3389/fnmol.2016.00046

Sloan, K.E., Bohnsack, M.T., Watkins, N.J., 2013. The 5S RNP Couples p53 Homeostasis to Ribosome Biogenesis and Nucleolar Stress. Cell Rep 5, 237–247. https://doi.org/10.1016/j.celrep.2013.08.049

Steller, H., 1995. Mechanisms and genes of cellular suicide. Science (1979) 267, 1445–1449. https://doi.org/10.1126/science.7878463

Thomé, R.G., Batista, H., Arantes, F.P., Prado, P.S., Flavio, F., Domingos, T., Sato, Y., Bazzoli, N., Rizzo, E., Domingos, F.F.T., Sato, Y., Bazzoli, N., Rizzo, E., 2006. Regression of postovulatory follicles in *Prochilodus costatus* Valenciennes, 1850 (Characiformes, Prochilodontidae). Brazillian Journal of Morphological Sciences 23, 495–500.

Thomé, R.G., Santos, H.B., Arantes, F.P., Domingos, F.F.T., Bazzoli, N., Rizzo, E., 2009. Dual roles for autophagy during follicular atresia in fish ovary. Autophagy 5, 117–119. https://doi.org/10.4161/auto.5.1.7302

Tilly, J.L., 1996a. Apoptosis and ovarian function. Rev Reprod 1, 162–172. https://doi.org/10.1530/REVREPROD/1.3.162

Tilly, J.L., 1996b. The molecular basis of ovarian cell death during germ cell attrition, follicular atresia, and luteolysis. Frontiers in Bioscience-Landmark 1, 1–11. https://doi.org/10.2741/A111

Tiwari, M., Prasad, S., Tripathi, A., Pandey, A.N., Ali, I., Singh, A.K., Shrivastav, T.G., Chaube, S.K., 2015. Apoptosis in mammalian oocytes: A review. Apoptosis 20, 1019–1025. https://doi.org/10.1007/s10495-015-1136-y

Valencia, A., Andrieu, J., Nzioka, A., Cancio, I., Ortiz-Zarragoitia, M., 2020. Transcription pattern of reproduction relevant genes along the brain-pituitary-gonad axis of female, male and intersex thicklip grey mullets, *Chelon labrosus*, from a polluted harbor. Gen Comp Endocrinol 287, 113339. https://doi.org/10.1016/j.ygcen.2019.113339

Vitale, F., Cardinale, M., Svedäng, H., 2005. Evaluation of the temporal development of the ovaries in Gadus morhua from the Sound and Kattegat, North Sea. J Fish Biol 67, 669–683. https://doi.org/10.1111/j.0022-1112.2005.00767.x

West, G., 1990. Methods of assessing ovarian development in fishes: A review. Mar Freshw Res 41, 199–222. https://doi.org/10.1071/MF9900199

Wickham, H., Averick, M., Bryan, J., Chang, W., McGowan, L., François, R., Grolemund, G., Hayes, A., Henry, L., Hester, J., Kuhn, M., Pedersen, T., Miller, E., Bache, S.M., Müller, K., Ooms, J., Robinson, D., Seidel, D.P., Spinu, V., Takahashi, K., Vaughan, D., Wilke, C., Woo, K., Yutani, H., D', L., Mcgowan, A., François, R., Grolemund, G., Hayes, A., Henry, L., Hester, J., Kuhn, M., Lin Pedersen, T., Miller, E., Bache, S.M., Müller, K., Ooms, J., Robinson, D., Seidel, D.P., Spinu, V., Takahashi, K., Vaughan, D., Wilke, C., Woo, K., Yutani, H., 2019. Welcome to the Tidyverse. J Open Source Softw 4, 1686. https://doi.org/10.21105/JOSS.01686

Wood, A.W., Janz, D.M., Van Der Kraak, G.J., 2005. Chapter 11 Cell death: investigation and application in fish toxicology, in: Mommsen, T.P., Moon, T.W. (Eds.), Biochemistry and Molecular Biology of Fishes. Elsevier, pp. 303–328. https://doi.org/10.1016/S1873-0140(05)80014-1

Wood, A.W., Van Der Kraak, G.J., 2003. Yolk proteolysis in rainbow trout oocytes after serum-free culture: evidence for a novel biochemical mechanism of atresia in oviparous vertebrates. Mol Reprod Dev 65, 219–227. https://doi.org/10.1002/mrd.10272

Wood, A.W., Van Der Kraak, G.J., 2001. Apoptosis and ovarian function: novel perspectives from the teleosts. Biol Reprod 64, 264–271. https://doi.org/10.1095/biolreprod64.1.264

Yamamoto, Y., Luckenbach, J.A., Goetz, F.W., Young, G., Swanson, P., 2011. Disruption of the salmon reproductive endocrine axis through prolonged nutritional stress: changes in circulating hormone levels and transcripts for ovarian genes involved in steroidogenesis and apoptosis. Gen Comp Endocrinol 172, 331–343. https://doi.org/10.1016/j.ygcen.2011.03.017

Yamamoto, Y., Luckenbach, J.A., Young, G., Swanson, P., 2016. Alterations in gene expression during fasting-induced atresia of early secondary ovarian follicles of coho salmon, *Oncorhynchus kisutch*. Comp Biochem Physiol A Mol Integr Physiol 201, 1–11. https://doi.org/10.1016/j.cbpa.2016.06.016

Yang, Y., Wang, G., Li, Y., Hu, J., Wang, Y., Tao, Z., 2022. Oocytes skipped spawning through atresia is regulated by somatic cells revealed by transcriptome analysis in *Pampus argenteus*. Front Mar Sci 9, 1–14. https://doi.org/10.3389/fmars.2022.927548

Zar, J.H., 2010. Biostatistical Analysis, 5th ed. Pearson Education Inc., Upper Saddle River, New Jersey, USA.

SUPPLEMENTARY MATERIAL

Obtained cDNA sequences with corresponding deduced proteins sequences are presented. The open reading frame (ORF) for each protein sequence is shaded in red.

>seq1 [organisms = Merluccius merluccius] E3 ubiquitin-protein ligase Mdm2 mRNA, partial cds
GAAGAGGAGGCGcTCTGATAGCTTCTCACTAACCTTTGATGACAGCTTATCCTGGTGTGTGATTGG
TGGACTCAGAAATGACACTAGACTAGGCCACGGCCACTCnCTGACACACACCAGTATGGTGAGTGA
TAACTTCAGnGTGGAGTTTGAGGTGGAGTCTCTGGACTCTGATGATTACAGTGATGAAGAAACGTC
GCTATCTGGGGACGACCAGGTAA

KRRRSDSFSLTFDDSLSWCVIGGLRNDTRLGHGHXLTHTSMVSDNFXVEFEVESLDSDDYSDEETS
LSGDDQV

>seq2 [organisms = Merluccius merluccius] B-cell lymphoma 2 (bcl2) mRNA, partial cds
GCTTCGAGGAGGCGTGATGGACGAGGTGTCACGGCGACCAGCAGTCAAACCTGGGGCCCGCAGAGG
TCGGCACTGTTTGCGTCGCGGCGGAAGCCGCCTGTGCGTGGAAGGTGCTGTGGAGAAGGAGATGAG
CCTACGACTTGGTTGCGCCGGGCGATGCGCGCGACGTGGGATGACCAGTGCTACCTGGACACCAAT
CTCACCCCCCTG

LRGGVMDEVSRRPAVKPGARRGRHCLRRGGSRLCVEGAVEKEMSLRLGCAGRCARRGMTSATWTPI
SPP

>seq3 [organisms = Merluccius merluccius] ribosomal protein L5 (rpl5) Mdm2 mRNA, partial cds
TCAAGAGGTAACAGTCAAGTTCAGGAGGAGGAGAGAGGGAAAAACCGACTTCTTCGCCCGCAAGCG
CCTGGTCATCCAGGACAAGAACAAGTACAACACACCCAAGTACAGGATGATCGTCCGTTTCTCCAA
CAGGGACATCGTATGCCAGATCGCCTACGCCAAAATCGAGGGTGACATGATCGTGTGCGCTGCCTA
CTCGCATGAGCTGCCCAAGTATGGCGTGACAGTTGGTCTGACGAACTACGCAGCGGCCTACTGCAC
GGGTCTGCTGGTGGCTCGCAGGCTGCTCAACAAGTTCAAACTGGACAAGGTCTACGAGGGCCAGGT
GGAGGTGACCGGTGACGAGTTCAATGTGGAGAGCGTGGACGATCAGCCCGGTGCCTTCACATGCTC
CCTGGACGCA

QEVTVKFRRRREGKTDFFARKRLVIQDKNKYNTPKYRMIVRFSNRDIVCQIAYAKIEGDMIVCAAY
SHELPKYGVTVGLTNYAAAYCTGLLVARRLLNKFKLDKVYEGQVEVTGDEFNVESVDDQPGAFTCS
LDA

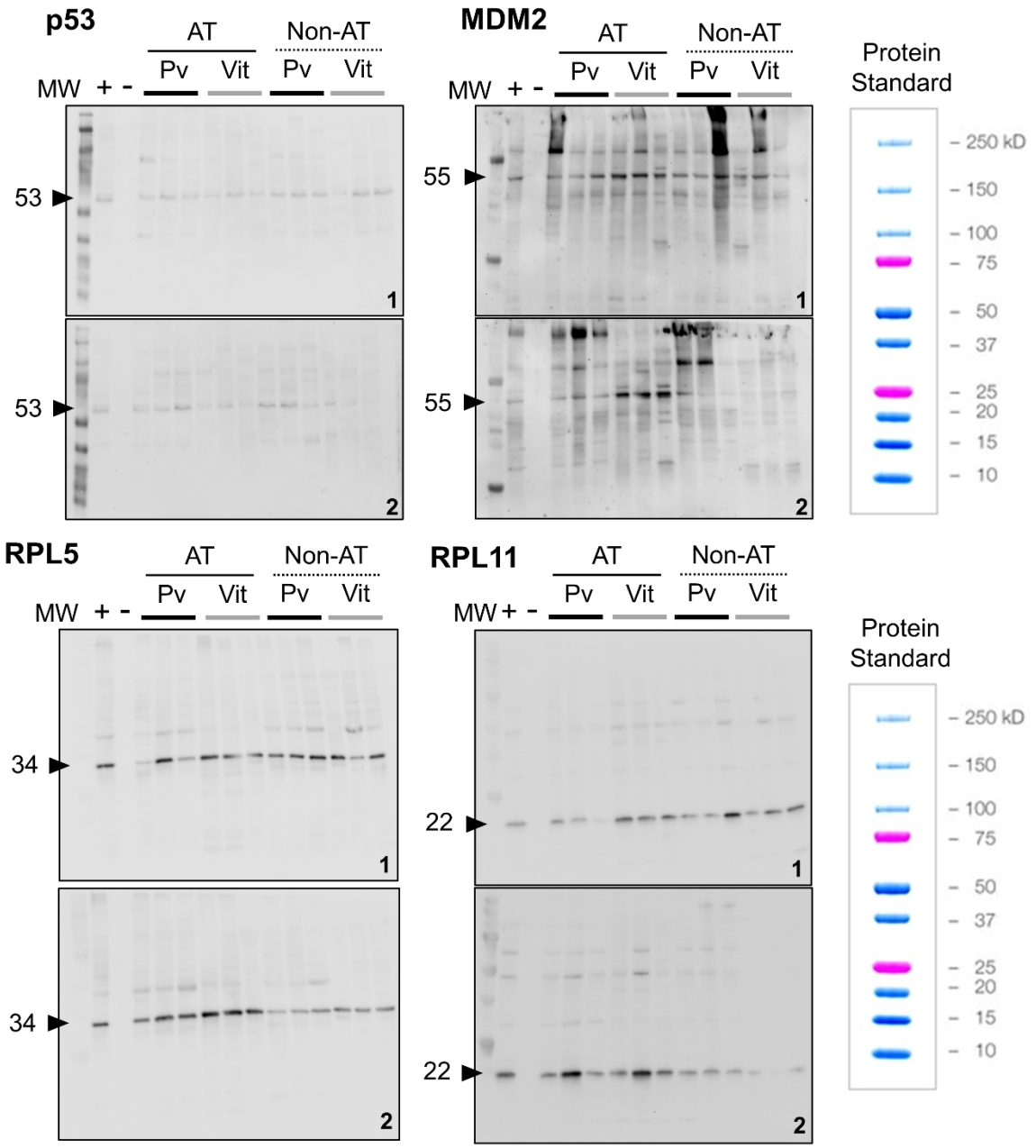

Figure S1

Full-length western blots of hake ovarian tissue samples revealing the expression of target proteins related to apoptosis and autophagy during follicular atresia. Plates represents cropped blots (1 and 2) for p53, MDM2, RPL5 and RPL11 with predicted molecular weights (in kilodaltons, kDa) of 53 kDa, 55 kDa, 34 kDa and 22 kDa respectively. 1 and 2 represent the number of blots used for each target protein to analyse a sample size of n = 24. MW represents the protein standards molecular weights, (+) represents positive (atretic) sample used for normalization across blots and (-) represents negative no-protein load control. Pv = previtellogenic follicles and Vit = Vitellogenic follicles. AT = previtellogenic (n = 6) and vitellogenic (n = 6) atretic follicles. Non-AT = previtellogenic (n = 6) and vitellogenic (n = 6) atretic follicles. Precision Plus Dual Colour Protein Standard (Catalogue #161-0374, Bio-Rad Laboratories Inc.) used as the ladder is shown to the right of the western blot plots.

Chapter 2

Molecular markers of follicular atresia in thicklip grey mullets *(Chelon labrosus)* inhabiting an estuary (Gernika) with high burdens of xenoestrogens

ARTICLE

Nzioka, A., Valencia, A., Rojo-Bartolomé, I., Lekube, X., Ortiz-Zarragoitia, M., Diaz de Cerio, O., Cancio, I., 2023. "Molecular markers of follicular atresia in thicklip grey mullets (*Chelon labrosus*) inhabiting an estuary (Gernika) with high burdens of xenoestrogens. Journal of Experimental Marine Biology and Ecology (in prep.).

CONGRESS

XIV AIEC Congress of the Iberian Association for Comparative Endocrinology, 11th – 13th September 2023, Bilbao, Spain. **Anthony Nzioka**, Ainara Valencia, Iratxe Rojo-Bartolomé, Xabier Lecube, Maren Ortiz-Zarragoitia, Oihane Diaz de Cerio and Ibon Cancio (2023). "Molecular markers of follicular atresia in thicklip grey mullets (*Chelon labrosus*) inhabiting an estuary (Gernika) with high burdens of xenoestrogens." Poster Communication.

Resumen

La atresia folicular es un proceso degenerativo que implica mecanismos relacionados con la apoptosis y la autofagia y que es esencial para el mantenimiento de la homeostasis ovárica en peces teleósteos. Este fenómeno común durante la oogénesis es responsable del estado físico de los peces y está asociado a factores ambientales, cambios en los niveles hormonales o el final de la temporada de desove. Dado que se han descrito efectos xenoestrogénicos en poblaciones de mubles de labios gruesos de estuarios contaminados del Golfo de Vizcaya, este estudio investigó los cambios morfológicos y los niveles de expresión de varios genes y proteínas implicados en la apoptosis y la autofagia durante la atresia folicular. Se analizaron histológicamente 31 hembras de muble muestreadas durante el verano aguas abajo de la planta de tratamiento de aguas residuales de Gernika desde 2014 hasta 2019 para identificar la prevalencia de atresia en esta población expuesta a xenoestrógenos. Los ovarios estaban siempre en previtelogénesis y sin embargo, la identificación atresia histológicamente y molecularmente. El análisis histopatológico reveló una elevada prevalencia de atresia (hasta el 100%) en los folículos ováricos previtelogénicos, con folículos ováricos que mostraban un elevado número de núcleos basófilos y ovocitos encogidos desprendidos de los folículos vecinos y del tejido conjuntivo circundante. Los transcritos de los genes relacionados con la apoptosis y la autofagia *p53*, *mdm2*, *rpl5*, *caspasa-3* y *beclin-1* no revelaron diferencias significativas en los ovarios previtelogénicos con o sin folículos atrésicos. El análisis de inmunoblot reveló diferencias significativas en el contenido proteico tanto de p53 como de RPL11 en ovarios con o sin folículos atrésicos. Los resultados muestran que la atresia folicular no sólo afecta a los folículos ováricos previtelogénicos, sino que p53 desempeña un papel clave en la atresia mediada por apoptosis en teleósteos y su activación se regula muy probablemente de forma post-transcripcional. Aún no está claro si estos efectos tendrán implicaciones sobre la capacidad reproductiva de las poblaciones de muble.

Palabras clave: *Apoptosis; Autofagia; Biomarcador; Chelón labrosus; Atresia folicular; ARNm; ciclo reproductivo*

Abstract

Follicular atresia is a degenerative process involving apoptosis and autophagy related mechanisms that is essential for the maintenance of ovarian homeostasis in teleost fish. This common phenomenon during oogenesis is responsible for the fish fitness and is associated with environmental factors, changes in hormonal levels or the end of spawning season. With xenoestrogenic effects having been reported in populations of thicklip grey mullets from contaminated estuaries in the Bay of Biscay, this study investigated the morphological changes and expression levels of various genes and proteins involved in apoptosis and autophagy during follicular atresia. 31 female mullets sampled during summer downstream of the wastewater treatment plant of Gernika from 2014 to 2019 were analysed histologically to identify the prevalence of atresia in this population exposed to xenoestrogens. Ovaries were always in previtellogenesis and yet, identifying atresia histologically and molecularly. Histopathological analysis revealed a high prevalence of atresia (up to 100%) in previtellogenic ovarian follicles, with ovarian follicles showing a high number of basophilic nuclei and shrunk oocytes detached from neighbouring follicles and the surrounding connective tissue. Transcripts of apoptosis and autophagy-related genes *p53, mdm2, rpl5, caspase-3* and *beclin-1* revealed no significant differences in previtellogenic ovaries with or without atretic follicles. Immunoblot analysis revealed significant differences in protein content of both p53 and RPL11 in ovaries with or without atretic follicles. The results show that not only does follicular atresia affects previtellogenic ovarian follicles, but p53 has a key role to play in apoptosis-mediated atresia in teleosts and its activation is most probably regulated post-transcriptionally. Whether these effects will have implications on the reproductive capacity of mullet populations remains unclear.

Keywords: *Apoptosis; Autophagy; Biomarker; Chelon labrosus; Follicular atresia; mRNA; Reproductive cycle*

Abbreviations

BBEB, Biscay Bay Environmental Biospecimen Bank
cDNA, complementary deoxyribonucleic acid
cds, coding domain sequences
DNA, deoxyribonucleic acid
E_2, oestradiol
ECAE, Ethics Committee for Animal Experimentation
EDC, endocrine disrupting compounds
EDTA, ethylenediaminetetraacetic acid
EE_2, 17α-ethinylestradiol
GADM, global administrative areas (database**)**
H&L, heavy and light chains
HCl, hydrochloric acid
HE, haematoxylin-eosin
HPG, hypothalamus-pituitary-gonadal
HRP, horseradish peroxidase
IgG, Immunoglobulin G
mRNA, messenger RNA
NBF, neutral buffered formalin
NCBI, national centre for biotechnology information
NP, nonylphenols
PAH, polycyclic aromatic hydrocarbons
PCR, polymerase chain reaction
QGIS, quantum geographic information system (software)
qPCR, quantitative PCR
RD, relative density
RNA, ribonucleic acid
RQ, relative quantity
rRNA, ribosomal RNA
SDS-PAGE, sodium dodecyl sulphate–polyacrylamide gel electrophoresis
ssDNA, single-strand cDNA
TBS-T, tris-buffered saline with Tween
WWTP, wastewater treatment plant

1. Introduction

Ovarian follicle development in vertebrates is a dynamic process that involves the sequential development of primordial follicles into first primary, then secondary and finally mature follicles through different recruitment and selection steps (Bhardwaj et al., 2022; McGee and Horne, 2018; Qiang et al., 2022). In mammals, a large number of primordial follicles are produced, more than those that will be required for maturation, with most follicles arresting development and degenerating through atresia (Bhardwaj and Sharma, 2012; Krysko et al., 2008; McGee and Horne, 2018). In fish, irrespective of their reproductive strategy, ovarian development follows annual cycles which in many species results in the recruitment into vitellogenesis of more oocytes than those that will finally be spawned (Kjesbu, 2009). The vitellogenic oocytes that cannot be spawned go to atresia, facilitating the re-distribution of energy-rich yolk material (Janz and Van Der Kraak, 1997; Miranda et al., 1999; Wood and Van Der Kraak, 2003, 2001). Follicle resorption seems to be more important in teleosts than in other vertebrates due to the large amounts of yolk accumulated during oocyte development (Cassel et al., 2017).

Follicular atresia is physiologically important as it also allows for selection of good-quality oocytes, limiting the number of eggs produced during each reproductive cycle (Kjesbu, 2009). In teleost fish, atresia mainly affects follicles containing vitellogenic oocytes though several studies have observed its occurrence in previtellogenic follicles (Corriero et al., 2021; Nzioka et al., 2023). In this respect, atresia has been described to be responsible for the selection and recruitment of the follicles from the available pool that will proceed into vitellogenesis (Janz and Van Der Kraak, 1997) and regulating in this way fecundity (Corriero et al., 2021; Kennedy et al., 2009; Rideout and Tomkiewicz, 2011).

Although a physiological phenomenon especially at the end of the spawning season, atresia in fish is usually associated with environmental stress (starvation, contaminant exposure, confinement, unfavourable temperature or photoperiod regimes, sub-optimal water quality) and changes in hormonal levels (Corriero et al., 2021; Guzmán et al., 2013; Serrat et al., 2019; Yamamoto et al., 2016). An increase in the rate of atresia in previtellogenic ovarian follicles in the presence of environmental stressors, may be an important indicator of response to stress and/or pathology (Bromley et al., 2000; Janz et al., 2001; Blazer, 2002; Sato et al., 2005). In coastal waters contaminated with endocrine disrupting compounds (EDCs), increased follicular atresia has been observed in the white

croaker (*Genyonemus lineatus*) off Southern California (Cross and Hose, 1989) and in the English sole (*Parophyrs vetulus*) from Puget Sound, Washington (Johnson et al., 2008), resulting in impaired reproduction. Furthermore, ovarian follicular atresia has also been reported in zebrafish (*Danio rerio*), fathead minnow (*Pimephalus promelas*) and common carp (*Cyprinus carpio*) after laboratory exposure to EDCs (Altun et al., 2017; Jensen et al., 2004; Van den Belt et al., 2002).

The morphological description of atretic previtellogenic and vitellogenic follicles has been published in captive *Prochildus affinis* (Rizzo and Bazzoli, 1995), *Astyanax bimaculatus lacustris* and *Leporinus reinhardti* (Miranda et al., 1999). Histologically four stages can be distinguished during atresia; (1) oocyte fragmentation and hypertrophy of follicles or granulosa cells, (2) invasion of the ooplasm with follicular/phagocytic cells and elimination of cell residues, (3) degeneration of the granulosa cells and changes in pigmentation and, (4) degeneration of the follicle (Corriero et al., 2021; Habibi and Andreu-Vieyra, 2007). However, much of the cellular and molecular mechanisms responsible for the observed morphological changes remain poorly understood (Nzioka et al., 2023). In mammals, apoptotic cell death has long been considered the main molecular mechanism leading ovarian follicular atresia (Matsuda et al., 2012; Tiwari et al., 2015). Apoptosis is an evolutionarily conserved process involving biochemical and morphological changes that remodel tissue cell content and homeostasis (Krysko et al., 2008; Steller, 1995; Tilly, 1996). The role of apoptosis in follicular atresia has been studied in teleosts (Janz and Van Der Kraak, 1997; Wood and Van Der Kraak, 2001) and the evidence excludes the possibility of apoptosis being the trigger mechanism. Autophagy is an alternative mechanism that contributes to the efficient elimination of all cell types conforming the ovarian follicle in vertebrates (Cassel et al., 2017; Corriero et al., 2021; Morais et al., 2012; Sales et al., 2019; Santos et al., 2008; Thomé et al., 2009; Bhardwaj et al. 2022). Nutrients from degraded cell organelles in the follicle are recycled through autophagocytosis, providing the much-needed energy required for future oocyte production (Bhardwaj et al., 2022). In teleosts in particular, it has been observed that apoptosis is accompanied by autophagy (Miranda et al., 1999; Morais et al., 2012; Yang et al., 2022).

A recent review of the literature identified a list of 20 different genes that play a potential role in ovarian follicular atresia in teleost fish either through lipid metabolism, oxidative metabolism and immune cell processes, but also through apoptotic and autophagic mechanisms (González-Kother et al., 2020). Sequential activation of caspases has been

observed to be important for proteolytic cleavage and apoptosis-mediated cell death during follicular atresia in fasted coho salmon (Yamamoto et al., 2016). In the freshwater fishes *P. affinis, A. bimaculatus lacustris* and *L. reinhardti*, the overexpression of apoptotic (*caspase-3*) and autophagocytotic (*beclin-1*) genes have been demonstrated in ovarian follicular and theca cells during atresia (Morais et al., 2012). p53 has received little attention in relation to its role in follicular atresia in teleosts. p53, a regulator of both apoptotic and autophagic pathways (Levine et al., 2006; Levine and Oren, 2009; Vousden and Prives, 2009), plays a very important role in controlling the fate of ovarian follicles in teleost fishes. This has been demonstrated in fasted coho salmon (Yamamoto et al., 2016), the spotted knifejaw *Oplegnathus punctatus* (Du et al., 2017). The role of p53 is for instance very clear during zebrafish sex differentiation. All zebrafish develop a juvenile ovary after hatching which in males regresses to allow the formation of testis, in a process that is regulated through the activation of p53 to trigger the resorption of immature oocytes (Rodríguez-Marí et al., 2010).

Thicklip grey mullets (*Chelon labrosus*) from contaminated estuaries along the Basque coast have been reported to suffer strong xenoestrogenic effects mainly linked to exposure to alkylphenols, pesticides and other xenoestrogens from wastewater treatment plant (WWTP) effluents that are discharged into estuaries, resulting in the development of intersex testes in males (Bizarro et al., 2014; Ortiz-Zarragoitia et al., 2014; Puy-Azurmendi et al., 2013). The majority of studies have focused their attention on males with varying prevalence of intersex condition depending on the estuary (Bizarro et al., 2014; Diaz De Cerio et al., 2012; Ortiz-Zarragoitia et al., 2014; Puy-Azurmendi et al., 2013; Valencia et al., 2017). However, less attention has been placed on females. This study assesses the follicular atresia in *C. labrosus* from the Urdaibai estuary in Gernika based on morphological observations, and gene transcription and protein expression analysis in previtellogenic ovaries displaying follicular atresia. The aim was to uncover the underlying molecular mechanisms regulating follicular atresia and reveal the morphological characteristics of atresia as a possible result of exposure to EDCs.

2. Materials and methods

2.1. Study area

The Urdaibai estuary (43°19′26.389″ N, 2°40′25.46″ W) located between the towns of Genika and Mundaka and declared a Biosphere Reserve by UNESCO in 1984 was the

sampling area (Figure 1). It is a shallow (mean depth of 3 m) meso-macrotidal estuary that is 12.5 km long and receives freshwater input from the Oka River (Iriarte et al., 2015). Major impacts can be attributed to the direct discharge of effluent from the Gernika WWTP at a narrow and very shallow stretch of the Oka River within the estuary (Mijangos et al., 2018). This old WWTP receives domestic and industrial waste from the town of Gernika and its surrounding areas (~26,000 inhabitants) and all fish were angled in the estuary in the vicinity of the effluent of the WWTP.

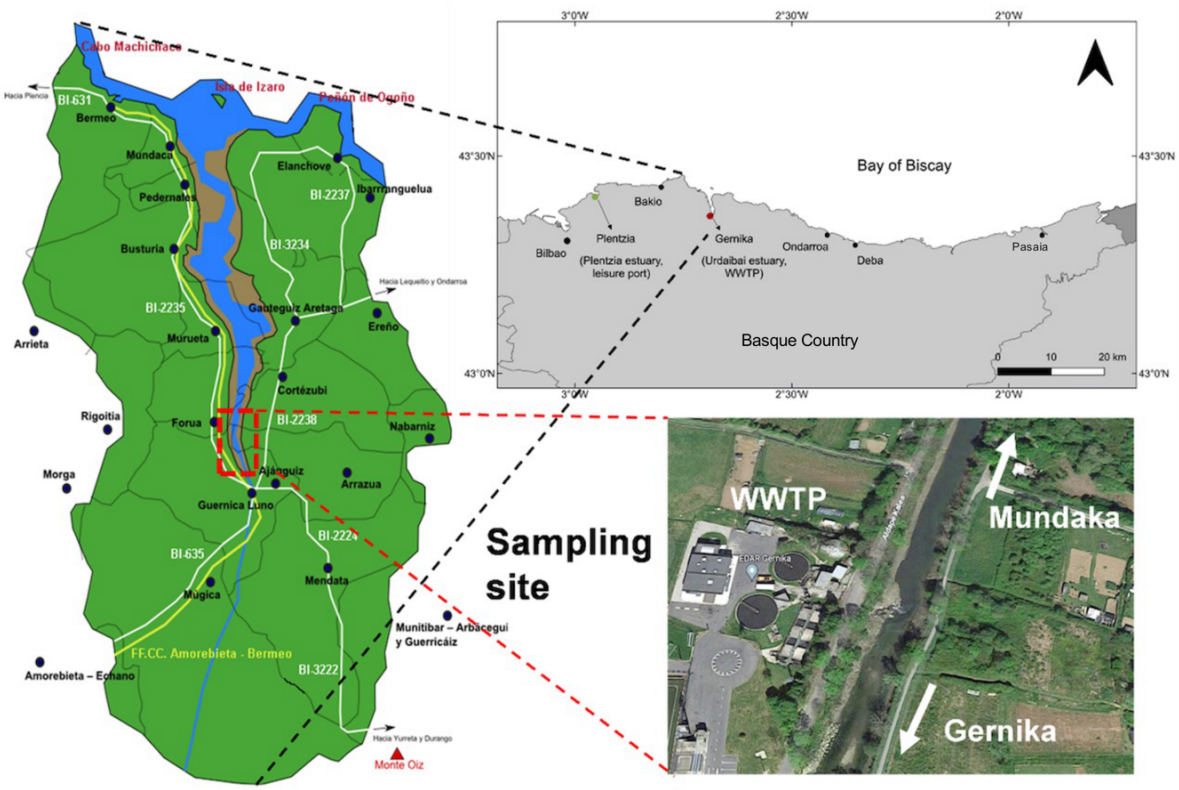

Figure 1
Sampling site of the thicklip grey mullet *Chelon labrosus* along the Basque coast within the Urdaibai estuary at Gernika and nearby a wastewater treatment plant (WWTP). Part of this figure was produced with the GADM database (www.gadm.org), version 4.1, 16 July 2022 and QGIS version 3.18.0-Zürich.

2.2. Fish sampling

Adult thicklip grey mullets (*Chelon labrosus*) used in the study were obtained from the annual sampling campaigns of the Biscay Bay Environmental Biospecimen Bank (BBEBB) conducted every June (2014 – 2019). The sampling campaigns were generally conducted at the end of the spawning period and mullets (> 20 cm) were captured using a fishing rod. The fish were anaesthetized in a saturated benzocaine/seawater bath and individuals were measured for total length (TL, 1 mm), and weighed (W, 1 g). Individuals were immediately

dissected, and their gonad tissue weighed (to the nearest 0.1 g). A portion of the gonads was fixed in 10% neutral buffered formalin (NBF) containing 1% glutaraldehyde at 4ºC and another portion placed in RNAlater® Stabilization Solution (Ambion™, ThermoFisher Scientific, Waltham, Massachusetts, USA) for 5-10 min before being frozen in liquid nitrogen and stored at -80ºC until further downstream analysis. All chemicals were of analytical grade and were obtained from Sigma-Aldrich (St. Louis, Missouri, USA) unless otherwise specified. All fishing activities and handling procedures were carried out in accordance with the Ethics Committee for Animal Experimentation (ECAE) of the UPV/EHU and with the permission for sampling activities of the regional authorities.

2.3. Ovarian development staging and atresia identification

After a 24-h period, the fixed gonad tissue samples were dehydrated in a graded ethanol series (70, 90 and 96%) and embedded in paraffin using the Leica ASP300 S Automated Vacuum Tissue Processor (Leica Biosystems, Nussloch, Germany). For sectioning, paraffin blocks were cooled rapidly on a PF100 cooling plate (Bio-Optica Milano, Milano, Italy) and cut into 5 µm tissue sections on a Leica RM 2125RT Rotary Microtome (Leica Biosystems). Sections were mounted onto albumin-coated 90º frosted-end microscope slides (BPB019 RS France, Wissous, France). Haematoxylin-Eosin (HE) staining was performed using a Leica Autostainer XL (Leica Biosystems). A high-speed, high-resolution whole-slide NanoZoomer S210 Digital slide scanner (Hamamatsu Photonics K.K., Hamamatsu, Japan) was used to analyse the tissue sections.

The gametogenic stages of each individual was determined according to McDonough et al. (2005). From all the individuals collected during BBEBB annual sampling campaigns (2014-2019), 31 were identified as females and they all were in the previtellogenic stage of development. Ovaries of each individual that had at least one oocyte in a state of cellular structural disorganisation were classified for our study as atretic (Hunter and Macewicz, 1985). The number of normal (non-atretic) and atretic previtellogenic oocytes ($n > 100$) was counted in histological sections. No distinction among alpha, beta, gamma and delta atresia was done. Since atretic oocytes are smaller than non-atretic oocytes due to size-specific selection (Witthames and Greer Walker, 1995), shrinkage or both, all oocytes both with and without nuclei were counted to eliminate bias and avoid underestimation of atresia (Kurita et al., 2003). Three indices of atresia – relative intensity (*Ia*), prevalence (*Pa*) and average

relative intensity (*AIa*) – were calculated biannually (2014 – 2019), with the *AIa* index indicating the relative intensity of atresia at the group/population level (Kurita et al., 2003):

$$\text{Relative intensity, } Ia = \frac{Number\ of\ atretic\ oocytes}{Total\ number\ of\ normal{+}atretic\ oocytes\ in\ an\ individual\ fish} \quad (1)$$

$$\text{Prevalence, } Pa = \frac{Number\ of\ fish\ with\ atresia}{Total\ number\ of\ examined\ fish} \quad (2)$$

$$\text{Average relative intensity, } AIa = Geometric\ mean\ of\ Ia \times Pa \quad (3)$$

2.4. Total RNA extraction, quantification and 5S/18S rRNA ratio calculation

Total RNA was extracted from the -80ºC RNAlater® stored ovary (~ 100 mg) using TRIzol Reagent® Solution (Ambion®, ThermoFisher Scientific, Massachusetts, USA) following the manufacturer´s instructions. After oocyte developmental staging and atresia identification, a total of five ovaries showing follicular atresia (labelled as AT) and nine ovaries without signs of atresia (non-AT) were selected. The RNA yield (concentration and quality) of each sample was assessed using a cuvette photometer (Biophotometer plus, Eppendorf, Hamburg, Germany). All samples with A260/280 absorbance ratios between 1.8 and 2.2 were selected for downstream analysis.

The quality of the RNA was then determined by capillary electrophoresis using the Agilent RNA 6000 Nano Kits Assay Protocol (Agilent Technologies, Santa Clara, California, USA). The Bioanalyzer electropherograms were used to quantify the concentration of the bands corresponding to 5S and 18S ribosomal RNAs (rRNAs) in each sample. The Time-Corrected-Area of each peak was used to calculate the 5S/18S rRNA ratio and the Log_2 of this value was used to develop a 5S/18S rRNA ratio for each sample (Rojo-Bartolomé et al., 2016).

2.5. Gene transcription analyses by qPCR

First-Strand cDNA was synthesised using Affinity Script Multiple Temperature cDNA Synthesis Kit (Agilent Technologies) in a 2720 Applied Biosystems Thermal Cycler (Applied Biosystems, Foster City, California, USA). Total RNA was reverse transcribed

using random primers following the manufacturer´s instructions (2 μg total RNA in a reaction volume of 20 μL for a final theoretical cDNA concentration of 100 ng μL^{-1}). The cDNA was stored at -40ºC for subsequent gene expression analysis. Single-strand cDNA (ssDNA) concentrations were quantified by measuring fluorescence in a Synergy HT Multi-Mode Microplate Reader (Biotek, Winoosky, USA) using Quant-iT™ OliGreen® Kit (Life Technologies™, ThermoFisher). The quantification was run in triplicate, in a reaction volume of 100 μL with a theoretical cDNA concentration of 0.2 ng μL^{-1} (Rojo-Bartolomé et al., 2017). The fluorescence was measured at standard fluorescein excitation and emission wavelengths of 480 nm and 520 nm respectively. Real cDNA concentration was calculated using a five-point standard curve according to the manufacturer's instructions and the exact amount of cDNA loaded in qPCR reactions was calculated, adjusting dilutions used for each gene (Rojo-Bartolomé et al., 2017).

Gene sequences for *p53*, *mdm2, caspase-3,* and *beclin-1* were obtained from Genbank in the NCBI database, whereas for *rpl5*, the partial sequence obtained by MiSeq Illumina RNASeq analysis of mullet gonads (unpublished data) was used (Table 1). Primer pairs for each target gene were designed using Integrated DNA Technologies (IDT) OligoAnalyzer™ and Eurofins Genomics PCR Primer Design online tools, and their specificity was verified by conventional PCR amplification on at least two independent cDNA samples of each tissue. The PCR programme for each target gene was as follows: 94°C for 2 min, denaturation at 94°C for 30 s, annealing step (temperature for each primer set in Table 1) for 30 s, and elongation at 72°C for 30 s. PCR was finalised at 72°C for 8 min (2720 thermal cycler, Applied Biosystems, USA). All PCR products/amplicons were visualized in 1.5% (w/v) agarose gels stained with ethidium bromide and sequenced at the Sequencing and Genotyping Service of the University of the Basque Country (SGIker-UPV/EHU).

Table 1
Nucleotide sequences of forward (F) and reverse (R) primer pairs with the annealing temperatures (T_A) used for PCR and the PCR product size in base pairs (bp). GenBank accession numbers for sequences of thicklip grey mullet are available in the International Nucleotide Sequence Database.

Target gene	GenBank Accession No.	Primer Sequence (5' – 3')	T_A (^{0}C)	PCR product size (bp)
p53	DQ146943	F:TCTTCAGAGTGGAGGGCAC R:CAGCAGGATGGTCGTCATTTC	59.0	136
mdm2	KX758587	F:TCGACAGCTTCTCTGTTAAGAG R:CTGGCTGCTGCTTTGTGTTTG	59.0	127
rpl5	MK331988	F:ACTGACTACTTTGCTCGCAAAGC R:TGTCACCCTCAATCTTGGCATAG	60.0	150
caspase-3	JF732773	F:TCGTGGAACTGAAGTAC R:CTGTCCGTTTCAATCCCTGGA	60.0	130
beclin-1	KY771085	F:CACAGAGGAGCTACAGTACCA R:GTACCAAACTGTCCGCTGTG	60.0	176

The relative transcription levels for the target genes in all the atretic and non-atretic individual samples were determined by real-time quantitative PCR (qPCR) amplifications performed in a final volume of 20 µL, with 10 µL FastStart Universal SYBR Green Master (Rox) (Roche Diagnostics, Mannheim, Germany), 2 µL appropriately diluted cDNA, 7.94 µL or 7.88 µL of nuclease-free water and 0.03 µL (6.25 pmol μl^{-1}) or 0.06 µL (12.5 pmol μl^{-1}) of primer pair respectively (Rojo-Bartolomé et al., 2016). Optimal concentrations of primers and samples were used for each gene. Samples were run in triplicate on 96-well reaction plates using the 7300 PCR thermal cycler (Applied Biosystems). A no-template control (NTC) was also run in triplicate in each plate using the same reaction conditions. The amplification protocol was set up to follow an initial denaturation and activation at 50ºC for 2 minutes and 95ºC for 10 minutes, followed by 40 cycles at 95ºC for 15 seconds and an annealing step of 60 s at the appropriate primer pair temperature. To obtain a dissociation curve, the amplification reaction was followed by a dissociation step carried out at 95ºC for 15 seconds, 60ºC for 15 seconds and 95ºC for 15 seconds. The reaction efficiencies for each plate were estimated by generating a standard curve for each primer pair from a 2-fold serial dilution of a pool of first-strand cDNA templates from all samples as described and the relative quantity (RQ) of all gene transcription levels normalized to the amount of cDNA in nanograms per sample used in the qPCR (Rojo-Bartolomé et al., 2016). No reference or housekeeping gene was used since it is difficult to imagine the existence of any reliable reference gene for fish ovaries undergoing significant variations in cell composition,

physiological status, hydration levels, and meiotic stage, their mRNA concentration varies greatly during growth and maturation (Libus and Štorchová, 2006; Mittelholzer et al., 2007; Rojo-Bartolomé et al., 2016; Valencia et al., 2020).

2.6. Immunoblotting

Total protein was extracted from part of the remaining portion of the same frozen ovarian tissue taken for molecular biology analysis. Two sets of the same thawed frozen tissue samples (~100 mg each) were homogenized in 4X sample volume (~400 µL) lysis buffer, while in ice, using a Potter S Homogenizer (B. Braun Biotech International, GmbH, Melsungen, Germany). One set of the sample was homogenized in one type of ice-cold TrisHCl-Triton X-100 lysis buffer (50 mM Tris-HCl, 150mM NaCl, 1 mM EDTA, 0.1% Triton X-100), herein referred to as Buffer A, and the other in ice cold Triton X-100 lysis buffer (1 mM $NaHCO_3$, 1 mM EDTA, 0.1% absolute ethanol, 0.1% Triton X-100), herein referred to as Buffer B. Both lysis buffers were freshly supplemented with an EDTA-free protease inhibitor cocktail tablet (cOmplete Tablets Mini EDTA-free EASYpack, Roche Diagnostics). The lysis buffers were evaluated in downstream western blot analysis for the target proteins p53, MDM2, RPL5 and RPL11. Buffer A worked well for p53 western blot analysis while Buffer B worked better for MDM2, RPL5 and RPL11. Following homogenization, the homogenate was incubated on ice for 10 min, and centrifuged at 8,000 rpm, for 10 min at 4ºC using an Eppendorf 5415R centrifuge (Eppendorf AG, Hamburg, Germany). The supernatant (protein sample lysate) was removed, and the total protein concentration was analysed using the method of Bradford (1976) with Bio-Rad´s Quick Start Bradford assay kit (Bio-Rad Laboratories Inc.) following the manufacturer's instructions. Absorbance was measured at 595 nm in Thermo Scientific Multikscan® Spectrum Spectrophotometer (Thermo Fisher Scientific Oy Microplate Instrumentation, Vantaa, Finland). Values from a protein standard curve obtained using Bio-Rad´s Quick Start Bovine Serum Albumin (BSA) standards kit (Bio-Rad Laboratories Inc.) were used to calculate total protein concentration (mg mL^{-1}) in the samples.

Total protein was separated per lane on a 12% SDS-PAGE pre-cast gel (BIORAD Mini-PROTEAN® TGX, Bio-Rad Laboratories Inc.) and blotted onto 0.45 µm nitrocellulose blotting membrane (Amersham™ Protran™ Premium, Catalogue No.: 10600096, GE Healthcare Bio-Sciences AB, Uppsala, Sweden), with a positive atretic ("+") sample used for normalization across blots and no protein load control ("-"). For p53, 15 µg of total

protein were separated per lane and blotted onto the membranes, while for MDM2, RPL5 and RPL11, 10 µg of total protein were separated per lane and blotted. Non-specific binding sites were blocked with 5% Non-fat dry milk in Tris-buffered saline with Tween 20 (TBS-T) for p53 and MDM2, and 3% bovine serum albumin (BSA: A9647-100G; Sigma-Aldrich, Missouri, USA) in TBS-T for RPL5 and RPL11. The membranes were probed with rabbit polyclonal antibodies for human p53 (ab131442, Lot# GR316086-46), human MDM2 (ab38618, Lot# GR3172855-11), mammalian RPL5 (ab137617, Lot# GR3206161-7) and human, zebrafish RPL11 (ab79352, Lot# GR3224424-1) (Abcam, Cambridge, UK) diluted 1:200 (5 µg mL^{-1}; p53), 1:500 (4 µg mL^{-1}; MDM2), 1:1000 (0.85 µg mL^{-1}; RPL5) and 1:200 (1 µg mL^{-1}; RPL11) in blocking solution overnight. They were then incubated in horseradish peroxidase (HRP)-conjugated goat anti-rabbit IgG H&L (ab205718, Lot# GR3269880-7) (Abcam) secondary antibodies (1:5000 or 0.4 µg mL^{-1} for RPL5 and MDM2; 1:10000 or 0.2 µg mL^{-1} for p53 and RPL11) for another 1 h. The protein bands were visualized under chemiluminescence light using BIORAD ChemiDoc XRS System (Bio-Rad Laboratories Inc.) after treating the sample membranes for 2 min with ~ 600 µL (1:1 ratio) of Clarity™ Western ECL Substrate detection kit (Catalogue No.: 170-5060) (Bio-Rad Laboratories Inc.).

The protein band image shape in each lane was quantified in Image Studio™ Lite Version 5.2.5 Quantification Software (LI-COR Biosciences, Lincoln, Nebraska, USA). Background signal was subtracted to accurately calculate the signal intensity from the protein band image shape(s) using the lane background subtraction method and applying a "Median background correction" to each lane. The relative density (RD: no units) of the target protein(s) were then calculated from the signal values of the sample and the atretic positive normalization sample using the formula:

$$\text{Relative Density, RD} = \frac{Target\ Protein\ Signal}{Target\ Protein\ Atretic\ Positive\ \ Signal} \quad (4)$$

2.7. Statistical analysis

Statistical analyses were done using *R 4.0.2* (R Core Team, 2023), the *Tidyverse* (Wickham et al., 2019), the *onewaytests* (Dag et al., 2018), the *car* (Fox and Weisberg, 2019), the *ggstatsplot* (Patil, 2021), the *effectsize* (Hervé, 2022) and the *RVAideMemoire* (Hervé, 2022) packages. Data (relative intensity of atresia, *Ia*) were $\log_{10}(x+1)$ transformed to allow for comparisons of geometric means and Fisher's ANOVA used to determine if there were significant associations between studied biannual periods and the average relative intensity among fish with atresia (*Ia*) followed by post-hoc pairwise students t-test. Pearson's chi-squared test was used to determine if there were significant associations between studied biannual periods and prevalence of atresia followed by post-hoc pairwise Fisher's exact or proportion tests. Gene transcription and protein analyses data were checked for normality (Shapiro-Wilk test, $p > 0.05$) and homogeneity of variances (Levene's test, $p > 0.05$). When these assumptions were not met, the non-parametric Mann-Whitney U test was performed, followed by a measure of effect size (rank bi-serial correlation coefficient) where significant differences were detected. Once these assumptions were met, a parametric two-samples students t-test was performed to compare means. All p-values were corrected using Benjamini-Hochberg (BH) method to control the false discovery rate (i.e., falsely rejecting the null hypotheses). Data are presented as means ± S.E. and the statistically significant difference was set at $p < 0.05$.

3. Results

3.1. Histological analysis, gonad developmental staging and atresia identification

Histological analysis of the ovaries of thicklip grey mullets from the annual sampling campaigns of the BBEBB of June 2014 to 2019 showed that they all were in the previtellogenic stage (Figure 2). In ovaries classified as atretic, shrinkage of the ooplasm, detachment of zona pellucida, the disintegration of the oocyte nucleus and other ooplasmic organelles, hypertrophy of the follicle cells, presence of basophilic nuclei and the invasion of the ooplasm with phagocytic cells were observed in follicles containing previtellogenic oocytes. In this case, phagocytosis was observed to occur from the outer to the inner side of the oocyte (Figures 2B-D).

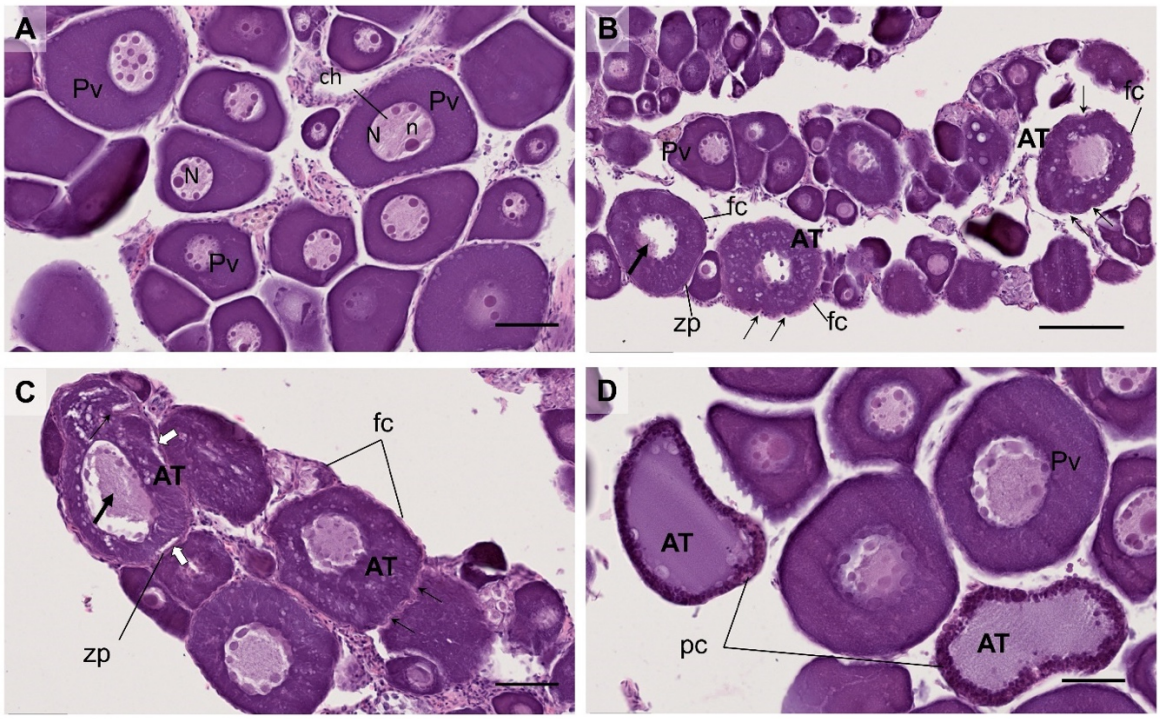

Figure 2
Micrographs of ovary sections from adult thicklip grey mullets *Chelon labrosus.* Synchronous developing ovaries in thicklip grey mullet *Chelon labrosus* with non-atretic follicles (A) and atretic follicles (B-D) at the previtellogenic developmental stage. (A) Ovaries showing no signs of atresia (Pv = Previtellogenic). (B) Initial atresia – intact zona pellucida, condensation of the chromatin (thick black arrow) and the proliferation of follicular cells and inward folding (thin black arrows) towards the ooplasm. (C) Medium atresia – progression of inward folding (thin black arrow) towards the ooplasm, chromatin condensation (thick black arrow), detachment of the zona pellucida (white arrows) and (D) Medium-to-Advanced atresia – follicle shrinks, nucleus degraded, phagocytic cells remaining as an organized layer and ooplasmic material reabsorbed. AT = Atretic; ch = chromatin; fc = follicle cells; n = nucleolus; N = nucleus; pc = phagocytic cells; zp = zona pellucida. Bars = 50 µm in all micrographs except B where bars = 100 µm.

Summary of the prevalence and intensity of atresia in studied thicklip grey mullets is provided in Table 2. The average relative intensity (*Ia*) was highest in 2018-2019 (31.7%) and lowest in 2016-2017 (19.9%) among fish with atresia, and no statistically significant differences were found between studied biannual periods (Fisher's ANOVA, $p = 0.455$). The prevalence of atresia (*Pa*) for the thicklip grey mullet over the six studied years was 77.4%. Prevalence was high in 2014-2015 (90%) and 2016-2017 (100%) and decreased to 54% in 2018-2019 (Table 2). Similarly, the opposite was true for normal non-atretic ovaries. Although there were within-group significant differences in prevalence between atretic and normal non-atretic ovaries in 2014-2015 (Chi-squared test, $p < 0.05$) and 2016-2017 (Chi-squared test, $p < 0.05$), pairwise comparisons between the studied bi-annual periods were non-significant ($p > 0.05$).

Table 2
Characteristics of atresia from annual June samplings (2014 – 2019) for thicklip grey mullets (TL > 20 cm). *Ia* represents the geometric mean of relative intensity for fish with atresia and *AIa* represents the geometric mean of relative intensity for fish with atresia multiplied by prevalence. Pairwise comparisons between the studied bi-annual periods revealed non-significant differences in prevalence ($p > 0.05$) and average relative intensity among fish with atresia ($p > 0.05$).

Year	Number of females	Prevalence (%)	Average relative intensity (%)	
			Among fish with atresia (*Ia*)	Among all fish (*AIa*)
2014 - 2015	10	90	26.0	23.4
2016 - 2017	8	100	19.9	22.3
2018 - 2019	13	54	31.7	17.1

3.2. 5S/18S rRNA ratio calculation

Similar 5S/18S rRNA ratio levels were observed in the ovaries showing atretic vs non-atretic ovarian follicles (Figure 3). The ovaries always contained previtellogenic oocytes, and accordingly individuals showed high ratio values corresponding to this developmental stage.

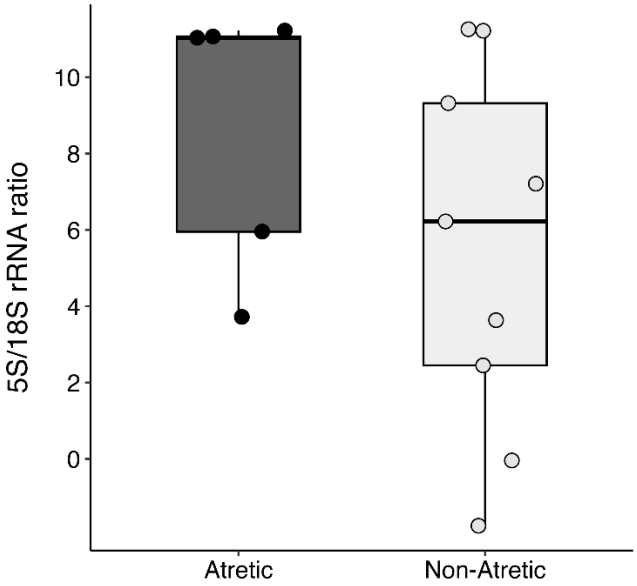

Figure 3
5S/18S rRNA ratio values during ovarian development in thicklip grey mullets. Pre-vitellogenic atretic (dark grey; n = 5) and non-atretic (light grey; n = 9) ovarian follicles. Boxplots represent the data within the 25th and 75th percentiles, with the median indicated by a line, and bottom and top whiskers representing minimum and maximum values, respectively. Each dot corresponds to an individual.

3.3. Gene transcription analyses

Relative transcription levels of genes related to atresia (*p53, mdm2, rpl5, caspase-3,* and *beclin-1*) in each individual were compared between ovarian follicles identified histologically as atretic or non-atretic (Figure 4) and no transcription level differences were observed between them.

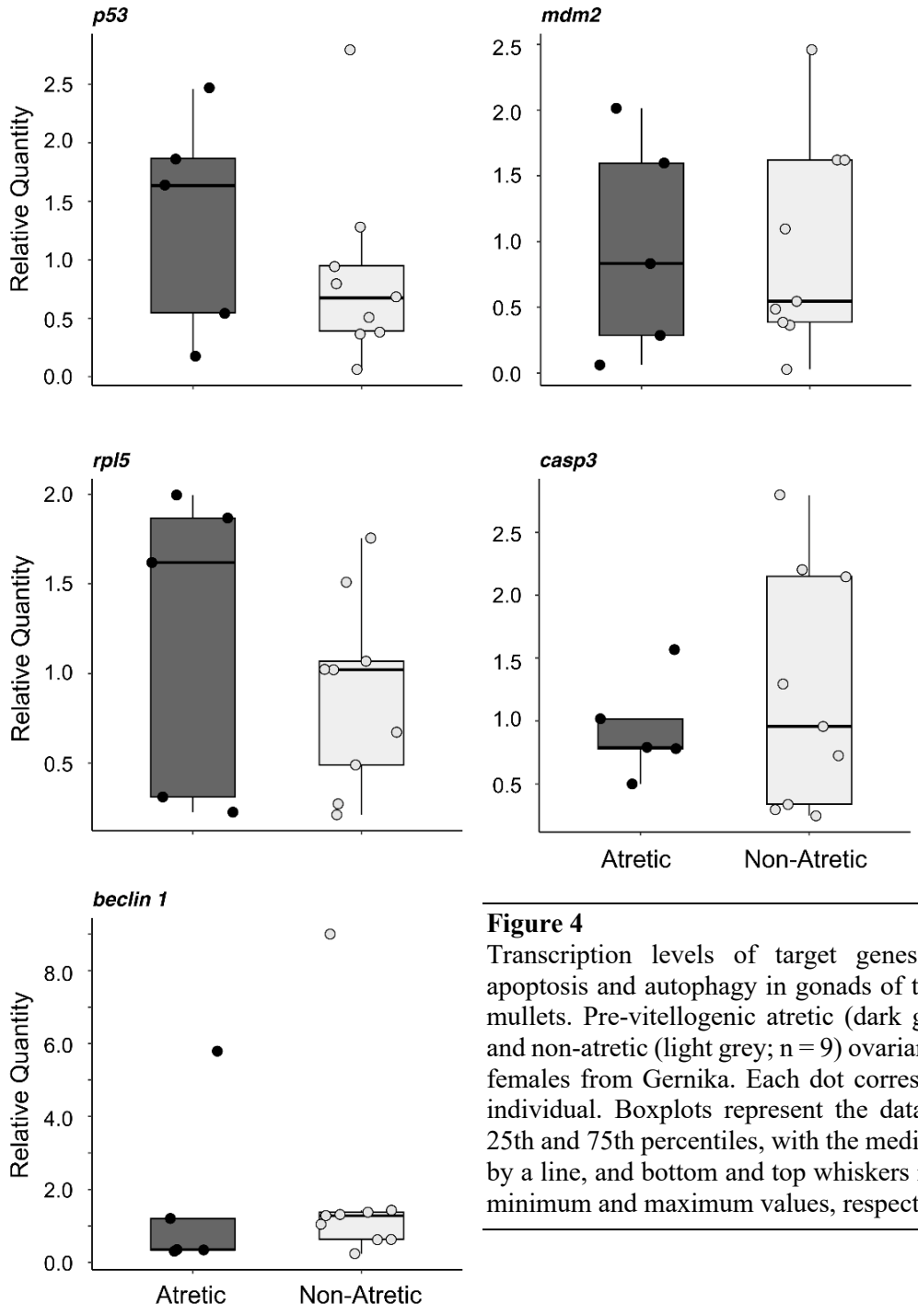

Figure 4
Transcription levels of target genes related to apoptosis and autophagy in gonads of thicklip grey mullets. Pre-vitellogenic atretic (dark grey; n = 5) and non-atretic (light grey; n = 9) ovarian follicles of females from Gernika. Each dot corresponds to an individual. Boxplots represent the data within the 25th and 75th percentiles, with the median indicated by a line, and bottom and top whiskers representing minimum and maximum values, respectively.

3.4. Immunoblotting

To determine the protein expression pattern of p53, MDM2, RPL5 and RPL11 proteins in atretic and non-atretic follicular tissue of thicklip grey mullet, western blotting analyses were performed with antibodies against mammalian proteins that showed specific cross-labelling for mullet proteins. Specific bands of 53 kDa, 55 kDa, 34 kDa and 22 kDa were labelled in thicklip grey mullets corresponding respectively to the typical molecular mass

of p53, MDM2, RPL5 and RPL11 in vertebrates (top plate; Figure 5A). Stronger immunoreactivity was found for p53 protein in ovaries with atretic vs. non-atretic follicles and quantification (Figure 5) showed that significant differences exist (Mann-Whitney U test, $p < 0.05$). For MDM2 and RPL5, no significant differences were observed between atretic and non-atretic ovaries, whereas for RPL11, significant differences appeared that were in the opposite direction as for p53 (Figures 5B - D) (Students t-test, $p < 0.05$).

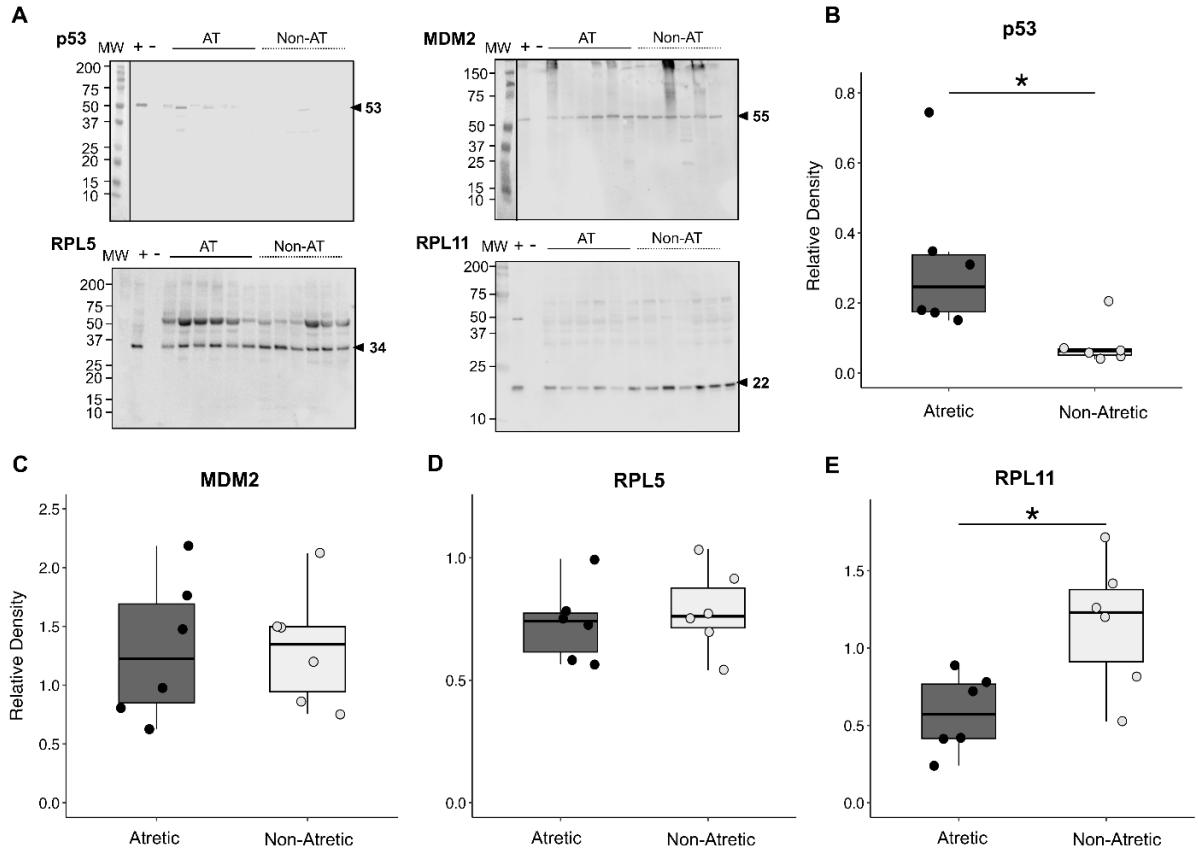

Figure 5

Expression of target proteins related to apoptosis and autophagy and their relative density in gonads of thicklip grey mullets by Western blotting analysis. (A) Plate represents blots for p53, MDM2, RPL5 and RPL11 with predicted molecular weights of 53 kDa, 55 kDa, 34 kDa and 22 kDa respectively. MW represents the molecular weights, (+) represents positive (atretic) sample used for normalization across blots and (-) represents negative no-protein load control. AT represents previtellogenic atretic follicles (n = 6) and non-AT represents previtellogenic non-atretic follicles (n = 6). (B, C, D and E) Associated quantification of each target protein based on their relative densities in atretic (dark grey; n = 6) and non-atretic (light grey; n = 6) ovarian follicles of female individuals from Gernika. Each dot corresponds to an individual. Boxplots represent the data within the 25th and 75th percentiles, with the median indicated by a line, and bottom and top whiskers representing minimum and maximum values, respectively. Asterisks (*) above bars indicate statistically significant different results $p < 0.05$).

4. Discussion

The focus of the study was to understand the molecular mechanisms governing follicular atresia in thicklip grey mullets (*Chelon labrosus*), a species inhabiting estuaries with high burdens of xenoestrogens in the Southeast Bay of Biscay. Ovarian development stages were ranked histologically and inferred molecularly using the 5S/18S rRNA ratio (Rojo-Bartolomé et al., 2016) confirming that all ovaries studied were in the previtellogenic stage of development. A high prevalence of ovarian follicular atresia was observed but the transcriptional profiling of apoptosis and autophagy-related genes (*p53, mdm2, rpl5, caspase-3,* and *beclin-1*) revealed no significant differences between atretic and non-atretic ovaries. However, immunoblotting analysis of p53, MDM2, RPL5 and RPL11 revealed significant differences in the expression of both p53 and RPL11 proteins between ovaries displaying atresia and those without signs of atresia.

Ovarian maturation is synchronous in thicklip grey mullets, with the oocyte recruitment process occurring in a single event and all oocytes in an ovary belonging to the same developmental stage (González-Castro and Minos, 2016). In previtellogenic oocytes, 5S rRNA levels are usually very high while 18S rRNA (and 28S rRNA) levels, initially low, increase after the cortical alveoli stage (Rojo-Bartolomé et al., 2017, 2016). The high levels of 5S rRNA observed in previtellogenic ovaries of thicklip grey mullets, were similar when comparing ovaries with atretic vs. non-atretic follicles (Figure 3).

Several factors have been described as being the cause of follicular atresia in fish. These include food deprivation, contaminant exposure, unfavourable temperature or photoperiod regimes and confinement (Corriero et al., 2021; Kjesbu, 2009; Serrat et al., 2019). In teleost fish, atresia mainly affects follicles containing vitellogenic oocytes, although it has also been observed in follicles containing previtellogenic oocytes (Corriero et al., 2021), as it has been the case in the present study in *C. labrosus*. Studied individuals presented previtellogenic follicles undergoing degeneration, with clear signs of shrinkage of the ooplasm, vacuolated areas appearing close to the nucleus, hypertrophied follicle cells, presence of basophilic nuclei and the invasion of the ooplasm with phagocytic cells, all in accordance with other studies (Corriero et al., 2021; Miranda et al., 1999; Rizzo and Bazzoli, 1995). The high prevalence of atresia in the studied population from Gernika could be explained by the exposure of *C. labrosus* individuals to xenoestrogens that have been reported to cause development of intersex testes in the males inhabiting the same area

(Bizarro et al., 2014; Ortiz-Zarragoitia et al., 2014; Puy-Azurmendi et al., 2013; Ros et al., 2015). In synchronous developing wild roach (*Rutilus rutilus*) and largemouth bass (*Micropterus salmoides*), a high prevalence of atresia has also been reported in fish (Baldigo et al., 2006; Jobling et al., 2002). Several studies have shown that laboratory exposure to endocrine disrupting chemicals (EDCs) such as 17α-ethinylestradiol (EE_2), nonylphenols (NPs) or the anti-androgen flutamide result in follicular atresia in female medaka (*Oryzias latipes*) (Weber et al., 2002), zebrafish (*Danio rerio*) (Van den Belt et al., 2002), fathead minnow (*Pimephales promelas*) (Jensen et al., 2004) or sheepshead minnows (*Cyprinodon variegatus*) (Zillioux et al., 2001). Exposure of pre-spawning White sucker (*Catostomus commersonii*) females to paper mill effluents with elevated oestradiol (E_2) levels led to very high rates of apoptosis-mediated atresia in ovarian follicles, possibly as a result of physiologically low E_2 levels that is characteristic of pre-spawning *C. commersonii* (Janz et al., 1997). Exposing the same population to high concentrations of polycyclic aromatic hydrocarbons (PAHs) also resulted in similarly high rates of apoptosis-mediated atresia. (Janz et al., 1997) suggested the possibility of effluent-induced apoptosis of ovarian follicles initiated through the alteration of hormone levels along the hypothalamus-pituitary-gonadal (HPG) axis. Considering that the estuary in Gernika receives a direct discharge of effluent from the local WWTP, and that previous studies on mullet individuals from the area have reported high concentrations of EDCs, the high prevalence of follicular atresia in the ovaries of mullet could be indicative of exposure to EDCs.

Several genes involved in apoptosis and autophagocytosis have been highlighted as potential markers of ovarian follicular atresia across teleost fish (González-Kother et al., 2020). The apoptosis and autophagocytosis-related genes studied in the present study showed similar transcription levels in mullet ovaries with or without atretic follicles. In some fish such as rainbow trout (*Oncorhynchus mykiss*) and the Senegalese sole (*Solea senegalensis*), a constant transcription pattern of apoptotic-related genes has been observed, with no differences between ovaries with or without atretic follicles irrespective of developmental stage (Cerdà et al., 2008; Tingaud-Sequeira et al., 2009; Von Schalburg et al., 2005). In asynchronous developing European hake (*Merluccius merluccius*) contrary to our synchronous developing mullets, upregulation of apoptosis-marker genes *p53* and *caspase-3* was observed in vitellogenic ovaries with atretic follicles, together with autophagocytosis marker genes cathepsin-D (*ctsd*) and death-associated protein kinase (*dapk1*), suggesting vitellogenesis to be the moment at which both apoptosis and autophagy

are at their highest (Nzioka et al., 2023; Yang et al., 2022).

The tumour suppressor gene *p53*, a guardian of the cell cycle, functions both as a tumour suppressor and regulator of apoptosis and is often studied as a marker of stress (Rau Embry et al., 2006). In zebrafish, *p53* has been shown to play a major role in sex differentiation, triggering apoptosis in previtellogenic oocytes that is executed by Caspase-3 during male differentiation as all individuals develop first juvenile ovaries that regress to allow testis development (Rodríguez-Marí et al., 2010). In the presence of physiological or environmental stress factors, p53 can be activated to trigger apoptotic and autophagocytotic cellular responses (Gump and Thorburn, 2011; Haupt et al., 2003). The presence of EDCs in Gernika (Bizarro et al., 2014; Puy-Azurmendi et al., 2013; Ros et al., 2015) could be linked to a basal high transcription level of *p53* and *caspase-3* in previtellogenic ovaries. Caspase-3 mediates the apoptotic response triggered by p53 and its proteolytic activity in fish oocytes (Rodríguez-Marí et al., 2010) and it is only activated when the mitochondrial membrane is destabilized, releasing cytochrome *c* to the cytosol (Donati et al., 2013; Maiuri et al., 2007). The results obtained in ovaries from Gernika would suggest a Caspase-3 activation may be promoted by the activation of p53, considering the significantly higher p53 protein levels observed in previtellogenic atretic ovaries when compared to non-atretic ovaries. Thus, the activation of p53 would enhance apoptosis through downstream activation of Caspase-3.

The upregulation of *p53* transcript levels, together with *mdm2*, has been observed after exposure of zebrafish larvae and embryos to the EDCs acetochlor and pretilachlor respectively, suggesting the potential of such substances as apoptosis inducers (Jiang et al., 2016, 2015). p53 is a pre-apoptotic protein under the regulation of MDM2 through binding, ubiquitination and proteolytic cleavage (Haupt et al., 2003). The higher p53 protein levels observed in this study suggest that indeed, p53 is largely regulated post-transcriptionally in principle via the E3 ubiquitin ligase MDM2 (Boehme and Blattner, 2009; Deisenroth and Zhang, 2010; Rau Embry et al., 2006) although no regulation of mdm2 or MDM2 has been observed hereby. 5S rRNA and ribosomal proteins L5 (RPL5) and L11 (RPL11) form a ribosomal nucleoprotein complex (RNP) that can under certain conditions bind to MDM2 in mammalian cells, rescuing p53 from ubiquitination and degradation, resulting in its activation (Deisenroth and Zhang, 2010; Donati et al., 2013; Sloan et al., 2013). The interaction between 5S RNP with RPL5 and RPL11 increases when ribosomal biogenesis is blocked (Sloan et al., 2013). Transcription levels of *rpl5* were observed to follow a pattern

similar to that of *mdm2* without significant transcriptional regulation with regard to atresia, the results being similar to that of European hake (Nzioka et al., 2023). A similar trend was observed at the protein level. While we did not measure *rpl11* transcription patterns, but RPL11 protein levels were significantly lower in previtellogenic ovaries with atretic follicles than in those with non-atretic follicles. In *Danio rerio*, the loss of RPL11 resulted in the activation of p53 and impaired ribosome biogenesis (Chakraborty et al., 2009). Therefore, in the absence of transcriptional regulation of pro-apoptotic p53-related pathways post-transcriptional regulation might be envisaged.

Autophagy is also involved in cell death and atresia in fish. It is a cell process that can be triggered as a stress response (nutrient starvation, contaminant exposure, hypoxia, confinement) to degrade damaged cell proteins and organelles (Maiuri et al., 2007; Thomé et al., 2009). Beclin-1, an important autophagy marker, appeared not to be upregulated in previtellogenic ovaries with atretic follicles, and there was no statistically significant differences between atretic and non-atretic ovaries (Figure 3). Beclin-1 is responsible for forming the isolation membrane that engulfs cytoplasmic material and form autophagosomes at the initial stages of autophagy (Bhardwaj et al., 2022). In European hake, transcripts of *beclin-1*, and another autophagocytosis-related gene *ptenb*, were observed to be upregulated continuously in atretic follicles irrespective of development stage (Nzioka et al., 2023). In the case of synchronous developing Nile tilapia (*Oreochromis niloticus*), while there was no significant difference in transcript levels of *caspase-3* and *beclin-1* among experimental groups during early oocyte development, *beclin-1* were observed to be significantly upregulated during one reproductive cycle, with both *caspase-3* and *beclin-1* transcript levels being significantly higher during late oogenesis (Qiang et al., 2021). The dynamics of Caspase-3 and Beclin-1 have been studied in several teleost species (Cassel et al., 2017; Morais et al., 2016), suggesting that an increase in Beclin-1 levels during the beginning of follicular atresia leads to a later increase in Caspase-3 levels. In the absence of Beclin-1, cells are unable to activate autophagy in response to stress (Gozuacik et al., 2008). Autophagy may thus induce an increase in the transcription of apoptotic *caspase-3* in teleost fish ovaries (Qiang et al., 2021; Sales et al., 2019), suggesting that both apoptotic and autophagic processes act in a coordinated manner. This cannot be ruled out in the ovaries of mullets from Gernika, considering the similar patterns in transcription observed for *caspase-3* and *beclin-1* observed.

5. Conclusions

In summary, atresia has been observed in the previtellogenic ovaries of thicklip grey mullets from Gernika where they are exposed to high concentrations of xenoestrogens. The mullets used in this study, with previtellogenic oocytes, showed elevated levels of follicular atresia despite having characteristically high physiological levels of E_2 (Sardi et al., 2015). Exposure to EDCs may have affected the HPG axis in mullets resulting in changes in hormone levels subsequently leading to effluent-induced apoptosis and the observed atresia in ovarian follicles. Although the transcriptional profiles of apoptosis and autophagy-related genes (*p53, mdm2, rpl5, caspase-3* and *beclin-1*) revealed no significant differences between atretic and non-atretic ovarian follicles, the over-expression of p53 and downregulation of RPL11 proteins in ovaries with atresia was observed. The low number of samples studied was a limiting factor, considering the range of variation in gene expression present between individuals. Nevertheless, p53 appears to play a major role in apoptosis-mediated atresia in teleosts and the mechanisms related to its activation are most probably regulated post-transcriptionally.

Acknowledgements

SGIker technical support (University of the Basque Country) is greatly acknowledged. This work was funded by the Spanish Ministry of Science, Innovation and Universities (ATREoVO AGL2015-63936-R and BORN2bEGG PGC2018-101442-B-I00) and by the Basque Government (Grant to consolidated research groups IT1302-19 and IT1743-22). A.N. is a recipient of a pre-doctoral grant (PIF17/172) from the University of the Basque Country (UPV/EHU).

References

Altun, S., Özdemir, S., Arslan, H., 2017. Histopathological effects, responses of oxidative stress, inflammation, apoptosis biomarkers and alteration of gene expressions related to apoptosis, oxidative stress, and reproductive system in chlorpyrifos-exposed common carp (*Cyprinus carpio* L.). Environmental Pollution 230, 432–443. https://doi.org/10.1016/j.envpol.2017.06.085

Baldigo, B.P., Sloan, R.J., Smith, S.B., Denslow, N.D., Blazer, V.S., Gross, T.S., 2006. Polychlorinated biphenyls, mercury, and potential endocrine disruption in fish from the Hudson River, New York, USA. Aquat Sci 68, 206–228. https://doi.org/10.1007/s00027-006-0831-8

Bhardwaj, J.K., Paliwal, A., Saraf, P., Sachdeva, S.N., 2022. Role of autophagy in follicular development and maintenance of primordial follicular pool in the ovary. J Cell Physiol 237, 1157–1170. https://doi.org/10.1002/JCP.30613

Bhardwaj, J.K., Sharma, R.K., 2012. Apoptosis and ovarian follicular atresia in mammals, in: García, M.-D. (Ed.), Zoology. IntechOpen, pp. 185–206.

Bizarro, C., Ros, O., Vallejo, A., Prieto, A., Etxebarria, N., Cajaraville, M.P., Ortiz-Zarragoitia, M., 2014. Intersex condition and molecular markers of endocrine disruption in relation with burdens of emerging pollutants in thicklip grey mullets (*Chelon labrosus*) from Basque estuaries (South-East Bay of Biscay). Mar Environ Res 96, 19–28. https://doi.org/10.1016/j.marenvres.2013.10.009

Boehme, K., Blattner, C., 2009. Regulation of p53 - insights into a complex process. Crit Rev Biochem Mol Biol 44, 367–392. https://doi.org/10.3109/10409230903401507

Bradford, M.M., 1976. A rapid and sensitive method for the quantitation of microgram quantities of protein utilizing the principle of protein-dye binding. Anal Biochem 72, 248–254. https://doi.org/10.1016/0003-2697(76)90527-3

Bromley, P.J., Ravier, C., Witthames, P.R., 2000. The influence of feeding regime on sexual maturation, fecundity and atresia in first-time spawning turbot. J Fish Biol 56, 264–278. https://doi.org/10.1006/jfbi.1999.1162

Cassel, M., de Paiva Camargo, M., Oliveira de Jesus, L.W., Borella, M.I., 2017. Involution processes of follicular atresia and post-ovulatory complex in a characid fish ovary: a study of apoptosis and autophagy pathways. J Mol Histol 48, 243–257. https://doi.org/10.1007/s10735-017-9723-6

Cerdà, J., Bobe, J., Babin, P.J., Admon, A., Lubzens, E., 2008. Functional genomics and proteomic approaches for the study of gamete formation and viability in farmed finfish. Reviews in Fisheries Science 16, 54–70. https://doi.org/10.1080/10641260802324685

Chakraborty, A., Uechi, T., Higa, S., Torihara, H., Kenmochi, N., 2009. Loss of ribosomal protein L11 affects zebrafish embryonic development through a p53-dependent apoptotic response. PLoS One 4, e4152. https://doi.org/10.1371/journal.pone.0004152

Corriero, A., Zupa, R., Mylonas, C.C., Passantino, L., 2021. Atresia of ovarian follicles in fishes, and implications and uses in aquaculture and fisheries. J Fish Dis 44, 1271–1291. https://doi.org/10.1111/JFD.13469

Cross, J.N., Hose, J.E., 1989. Reproductive impairment in two species of fish from contaminated areas off southern California, in: Proceedings OCEANS. IEEE, pp. 382–384. https://doi.org/10.1109/OCEANS.1989.586744

Dag, O., Dolgun, A., Konar, N.M., 2018. Onewaytests: An R package for one-way tests in independent groups designs. R Journal 10, 175–199. https://doi.org/10.32614/rj-2018-022

Deisenroth, C., Zhang, Y., 2010. Ribosome biogenesis surveillance: probing the ribosomal protein-Mdm2-p53 pathway. Oncogene 29, 4253–4260. https://doi.org/10.1038/onc.2010.189

Diaz De Cerio, O., Rojo-Bartolomé, I., Bizarro, C., Ortiz-Zarragoitia, M., Cancio, I., 2012. 5S rRNA and accompanying proteins in gonads: powerful markers to identify sex and reproductive endocrine disruption in fish. Environ Sci Technol 46, 7763–7771. https://doi.org/10.1021/es301132b

Donati, G., Peddigari, S., Mercer, C.A., Thomas, G., 2013. 5S ribosomal RNA is an essential component of a nascent ribosomal precursor complex that regulates the Hdm2-p53 checkpoint. Cell Rep 4, 87–98. https://doi.org/10.1016/j.celrep.2013.05.045

Du, X., Wang, B., Liu, Xiumei, Liu, Xiaobing, He, Y., Zhang, Q., Wang, X., 2017. Comparative transcriptome analysis of ovary and testis reveals potential sex-related genes and pathways in spotted knifejaw Oplegnathus punctatus. Gene 637, 203–210. https://doi.org/10.1016/j.gene.2017.09.055

González-Castro, M., Minos, G., 2016. Sexuality and reproduction of Mugilidae, in: Crosetti, D., Blaber, S. (Eds.), Biology, Ecology and Culture of Grey Mullets (Mugilidae). CRC Press, pp. 227–263.

González-Kother, P., Oliva, M.E., Tanguy, A., Moraga, D., 2020. A review of the potential genes implicated in follicular atresia in teleost fish. Mar Genomics 50, 100704. https://doi.org/10.1016/j.margen.2019.100704

Gozuacik, D., Bialik, S., Raveh, T., Mitou, G., Shohat, G., Sabanay, H., Mizushima, N., Yoshimori, T., Kimchi, A., 2008. DAP-kinase is a mediator of endoplasmic reticulum stress-induced caspase activation and autophagic cell death. Cell Death Differ 15, 1875–1886. https://doi.org/10.1038/cdd.2008.121

Gump, J.M., Thorburn, A., 2011. Autophagy and apoptosis: What is the connection? Trends Cell Biol 21, 387–392. https://doi.org/10.1016/j.tcb.2011.03.007

Guzmán, J.M., Adam Luckenbach, J., Swanson, P., 2013. Molecular characterization and quantification of sablefish (*Anoplopoma fimbria*) gonadotropins and their receptors: Reproductive dysfunction in female captive broodstock. Gen Comp Endocrinol 193, 37–47. https://doi.org/10.1016/j.ygcen.2013.07.007

Habibi, H.R., Andreu-Vieyra, C. V., 2007. Hormonal regulation of follicular atresia in teleost fish, in: Babin, P.J., Cerdà, J., Lubzens, E. (Eds.), The Fish Oocyte: From Basic Studies to Biotechnological Applications. Springer Netherlands, pp. 235–253. https://doi.org/10.1007/978-1-4020-6235-3_9

Haupt, S., Berger, M., Goldberg, Z., Haupt, Y., 2003. Apoptosis - The p53 network. J Cell Sci 116, 4077–4085. https://doi.org/10.1242/jcs.00739

Hervé, M., 2022. RVAideMemoire: Testing and plotting procedures for biostatistics.

Hunter, J.R., Macewicz, B.J., 1985. Rates of atresia in the ovary of captive and wild northern anchovy, *Engraulis mordax*. Fishery Bulletin 83, 119–136.

Iriarte, A., Villate, F., Uriarte, I., Alberdi, L., Intxausti, L., 2015. Dissolved Oxygen in a Temperate Estuary: the Influence of Hydro-climatic Factors and Eutrophication at Seasonal and Inter-annual Time Scales. Estuaries and Coasts 38, 1000–1015. https://doi.org/10.1007/s12237-014-9870-x

Janz, D.M., McMaster, M.E., Munkittrick, K.R., Van Der Kraak, G., 1997. Elevated ovarian follicular apoptosis and heat shock protein-70 expression in white sucker exposed to bleached kraft pulp mill effluent. Toxicol Appl Pharmacol 147, 391–398. https://doi.org/10.1006/taap.1997.8283

Janz, D.M., McMaster, M.E., Weber, L.P., Munkittrick, K.R., Van Der Kraak, G., 2001. Recovery of ovary size, follicle cell apoptosis, and HSP70 expression in fish exposed to bleached pulp mill effluent. Canadian Journal of Fisheries and Aquatic Sciences 58, 620–625. https://doi.org/10.1139/cjfas-58-3-620

Janz, D.M., Van Der Kraak, G.J., 1997. Suppression of apoptosis by gonadotropin, 17β-estradiol, and epidermal growth factor in rainbow trout preovulatory ovarian follicles. Gen Comp Endocrinol 105, 186–193. https://doi.org/10.1006/gcen.1996.6820

Jensen, K.M., Kahl, M.D., Makynen, E.A., Korte, J.J., Leino, R.L., Butterworth, B.C., Ankley, G.T., 2004. Characterization of responses to the antiandrogen flutamide in a short-term reproduction assay with the fathead minnow. Aquatic Toxicology 70, 99–110. https://doi.org/10.1016/j.aquatox.2004.06.012

Jiang, J., Chen, Y., Yu, R., Zhao, X., Wang, Q., Cai, L., 2016. Pretilachlor has the potential to induce endocrine disruption, oxidative stress, apoptosis and immunotoxicity during zebrafish embryo development. Environ Toxicol Pharmacol 42, 125–134. https://doi.org/10.1016/j.etap.2016.01.006

Jiang, J., Wu, S., Liu, X., Wang, Y., An, X., Cai, L., Zhao, X., 2015. Effect of acetochlor on transcription of genes associated with oxidative stress, apoptosis, immunotoxicity and endocrine disruption in the early life stage of zebrafish. Environ Toxicol Pharmacol 40, 516–523. https://doi.org/10.1016/j.etap.2015.08.005

Jobling, S., Coey, S., Whitmore, J.G., Kime, D.E., Van Look, K.J.W., McAllister, B.G., Beresford, N., Henshaw, A.C., Brighty, G., Tyler, C.R., Sumpter, J.P., 2002. Wild intersex roach (*Rutilus rutilus*) have reduced fertility. Biol Reprod 67, 515–524. https://doi.org/10.1095/biolreprod67.2.515

Johnson, L.L., Lomax, D.P., Myers, M.S., Olson, O.P., Sol, S.Y., O'Neill, S.M., West, J., Collier, T.K., 2008. Xenoestrogen exposure and effects in English sole (*Parophrys vetulus*) from Puget Sound, WA. Aquatic Toxicology 88, 29–38. https://doi.org/10.1016/j.aquatox.2008.03.001

Kennedy, J., Gundersen, A.C., Boje, J., 2009. When to count your eggs: Is fecundity in Greenland halibut (*Reinhardtius hippoglossoides* W.) down-regulated? Fish Res 100, 260–265. https://doi.org/https://doi.org/10.1016/j.fishres.2009.08.008

Kjesbu, O.S., 2009. Applied fish reproductive biology: contribution of individual reproductive potential to recruitment and fisheries management, in: Jakobsen, T., Forgarty, M., Megrey, Bernard.A., Moksness, E. (Eds.), Fish Reproductive Biology: Implications for Assessment and Management. Wiley-Blackwell, pp. 293–332. https://doi.org/10.1002/9781444312133.ch8

Krysko, D. V., Diez-Fraile, A., Criel, G., Svistunov, A.A., Vandenabeele, P., D'Herde, K., 2008. Life and death of female gametes during oogenesis and folliculogenesis. Apoptosis 13, 1065–1087. https://doi.org/10.1007/s10495-008-0238-1

Kurita, Y., Meier, S., Kjesbu, O.S., 2003. Oocyte growth and fecundity regulation by atresia of Atlantic herring (*Clupea harengus*) in relation to body condition throughout the maturation cycle. J Sea Res 49, 203–219. https://doi.org/10.1016/S1385-1101(03)00004-2

Levine, A.J., Feng, Z., Mak, T.W., You, H., Jin, S., 2006. Coordination and communication between the p53 and IGF-1-AKT-TOR signal transduction pathways. Genes Dev 20, 267–275. https://doi.org/10.1101/gad.1363206

Levine, A.J., Oren, M., 2009. The first 30 years of p53: Growing ever more complex. Nat Rev Cancer 9, 749–758. https://doi.org/10.1038/nrc2723

Libus, J., Štorchová, H., 2006. Quantification of cDNA generated by reverse transcription of total RNA provides a simple alternative tool for quantitative RT-PCR normalization. Biotechniques 41, 156–164. https://doi.org/10.2144/000112232

Maiuri, M.C., Zalckvar, E., Kimchi, A., Kroemer, G., 2007. Self-eating and self-killing: Crosstalk between autophagy and apoptosis. Nat Rev Mol Cell Biol 8, 741–752. https://doi.org/10.1038/nrm2239

Matsuda, F., Inoue, N., Manabe, N., Ohkura, S., 2012. Follicular growth and atresia in mammalian ovaries: Regulation by survival and death of granulosa cells. Journal of Reproduction and Development 58, 44–50. https://doi.org/10.1262/jrd.2011-012

McDonough, C.J., Roumillat, W.A., Wenner, C.A., 2005. Sexual differentiation and gonad development in striped mullet (*Mugil cephalus* L.) from South Carolina estuaries. Fishery Bulletin 103, 601–619.

McGee, E.A., Horne, J., 2018. Follicle atresia, Second Edi. ed, Encyclopedia of Reproduction. Elsevier. https://doi.org/10.1016/B978-0-12-801238-3.64395-7

Mijangos, L., Ziarrusta, H., Ros, O., Kortazar, L., Fernández, L.A., Olivares, M., Zuloaga, O., Prieto, A., Etxebarria, N., 2018. Occurrence of emerging pollutants in estuaries of the Basque Country: Analysis of sources and distribution, and assessment of the environmental risk. Water Res 147, 152–163. https://doi.org/10.1016/j.watres.2018.09.033

Miranda, A.C.L., Bazzoli, N., Rizzo, E., Sato, Y., 1999. Ovarian follicular atresia in two teleost species: a histological and ultrastructural study. Tissue Cell 31, 480–488. https://doi.org/10.1054/tice.1999.0045

Mittelholzer, C., Andersson, E., Consten, D., Hirai, T., Nagahama, Y., Norberg, B., 2007. 20β-hydroxysteroid dehydrogenase and CYP19A1 are differentially expressed during maturation in Atlantic cod (*Gadus morhua*). J Mol Endocrinol 39, 319–328. https://doi.org/10.1677/JME-07-0070

Morais, R.D.V.S., Thomé, R.G., Lemos, F.S., Bazzoli, N., Rizzo, E., 2012. Autophagy and apoptosis interplay during follicular atresia in fish ovary: a morphological and immunocytochemical study. Cell Tissue Res 347, 467–478. https://doi.org/10.1007/s00441-012-1327-6

Morais, R.D.V.S., Thomé, R.G., Santos, H.B., Bazzoli, N., Rizzo, E., 2016. Relationship between bcl-2, bax, beclin-1, and cathepsin-D proteins during postovulatory follicular regression in fish ovary. Theriogenology 85, 1118–1131. https://doi.org/10.1016/j.theriogenology.2015.11.024

Nzioka, A., Valencia, A., Atxaerandio-Landa, A., Diaz de Cerio, O., Hossain, M.A., Korta, M., Ortiz-Zarragoitia, M., Cancio, I., 2023. Apoptosis and autophagy-related gene transcription during ovarian follicular atresia in European hake (*Merluccius merluccius*). Mar Environ Res 183, 105846. https://doi.org/10.1016/j.marenvres.2022.105846

Ortiz-Zarragoitia, M., Bizarro, C., Rojo-Bartolomé, I., de Cerio, O.D., Cajaraville, M.P., Cancio, I., 2014. Mugilid fish are sentinels of exposure to endocrine disrupting compounds in coastal and estuarine environments. Mar Drugs 12, 4756–4782. https://doi.org/10.3390/md12094756

Patil, I., 2021. Visualizations with statistical details: The "ggstatsplot" approach. J Open Source Softw 6, 3167. https://doi.org/10.21105/joss.03167

Puy-Azurmendi, E., Ortiz-Zarragoitia, M., Villagrasa, M., Kuster, M., Aragón, P., Atienza, J., Puchades, R., Maquieira, A., Domínguez, C., López de Alda, M., Fernandes, D., Porte, C., Bayona, J.M., Barceló, D., Cajaraville, M.P., 2013. Endocrine disruption in thicklip grey mullet (*Chelon labrosus*) from the Urdaibai Biosphere Reserve (Bay of Biscay, Southwestern Europe). Science of the Total Environment. https://doi.org/10.1016/j.scitotenv.2012.10.078

Qiang, J., Duan, X.J., Zhu, H.J., He, J., Tao, Y.F., Bao, J.W., Zhu, X.W., Xu, P., 2021. Some 'white' oocytes undergo atresia and fail to mature during the reproductive cycle in female genetically improved farmed tilapia (Oreochromis niloticus). Aquaculture 534, 736278. https://doi.org/10.1016/j.aquaculture.2020.736278

Qiang, J., Tao, Y.-F., Zhu, J.-H., Lu, S.-Q., Cao, Z.-M., Ma, J.-L., He, J., Xu, P., 2022. Effects of heat stress on follicular development and atresia in Nile tilapia (*Oreochromis niloticus*) during one reproductive cycle and its potential regulation by autophagy and apoptosis. Aquaculture 555, 738171. https://doi.org/10.1016/j.aquaculture.2022.738171

R Core Team, 2023. R: A language and environment for statistical computing. R Foundation for Statistical Computing, Vienna, Austria.

Rau Embry, M., Billiard, S.M., Di Giulio, R.T., Embry, M.R., Giulio, R.T. Di, 2006. Lack of p53 induction in fish cells by model chemotherapeutics. Oncogene 25, 2004–2010. https://doi.org/10.1038/sj.onc.

Rideout, R.M., Tomkiewicz, J., 2011. Skipped spawning in fishes: More common than you might think. Marine and Coastal Fisheries 3, 176–189. https://doi.org/10.1080/19425120.2011.556943

Rizzo, E., Bazzoli, N., 1995. Follicular atresia in curimatá-pioa *Prochilodus affinis* Reinhardt, 1874 (Pisces, Characiformes). Rev Bras Biol 55, 697–703.

Rodríguez-Marí, A., Cañestro, C., BreMiller, R.A., Nguyen-Johnson, A., Asakawa, K., Kawakami, K., Postlethwait, J.H., 2010. Sex reversal in zebrafish fancl mutants is caused by Tp53-mediated germ cell apoptosis. PLoS Genet 6, 1–14. https://doi.org/10.1371/journal.pgen.1001034

Rojo-Bartolomé, I., Diaz de Cerio, O., Diez, G., Cancio, I., 2016. Identification of sex and female's reproductive stage in commercial fish species through the quantification of ribosomal transcripts in gonads. PLoS One 11, e0149711. https://doi.org/10.1371/journal.pone.0149711

Rojo-Bartolomé, I., Martínez-Miguel, L., Lafont, A., Vílchez, M.C., Asturiano, J.F., Pérez, L., Cancio, I., 2017. Molecular markers of oocyte differentiation in European eel during hormonally induced oogenesis. Comp Biochem Physiol A Mol Integr Physiol 211, 17–25. https://doi.org/10.1016/j.cbpa.2017.05.018

Ros, O., Vallejo, A., Blanco-Zubiaguirre, L., Olivares, M., Delgado, A., Etxebarria, N., Prieto, A., 2015. Microextraction with polyethersulfone for bisphenol-A, alkylphenols and hormones determination in water samples by means of gas chromatography-mass spectrometry and liquid chromatography-tandem mass spectrometry analysis. Talanta 134, 247–255. https://doi.org/10.1016/j.talanta.2014.11.015

Sales, C.F., Melo, R.M.C., Pinheiro, A.P.B., Luz, R.K., Bazzoli, N., Rizzo, E., 2019. Autophagy and Cathepsin D mediated apoptosis contributing to ovarian follicular atresia in the Nile tilapia. Mol Reprod Dev 86, 1592–1602. https://doi.org/10.1002/mrd.23245

Santos, H.B., Thomé, R.G., Arantes, F.P., Sato, Y., Bazzoli, N., Rizzo, E., 2008. Ovarian follicular atresia is mediated by heterophagy, autophagy, and apoptosis in *Prochilodus argenteus* and *Leporinus taeniatus* (Teleostei: Characiformes). Theriogenology 70, 1449–1460. https://doi.org/https://doi.org/10.1016/j.theriogenology.2008.06.091

Sardi, A.E., Bizarro, C., Cajaraville, M.P., Ortiz-Zarragoitia, M., 2015. Steroidogenesis and phase II conjugation during the gametogenesis of thicklip grey mullet (*Chelon labrosus*) from a population showing intersex condition. Gen Comp Endocrinol 221, 144–155. https://doi.org/10.1016/j.ygcen.2015.01.005

Sato, Y., Bazzoli, N., Rizzo, E., Boschi, M.B., Miranda, M.O.T., 2005. Influence of the Abaeté River on the reproductive success of the neotropical migratory teleost *Prochilodus argenteus* in the São Francisco River, downstream from the Três Marias Dam, southeastern Brazil. River Res Appl 21, 939–950. https://doi.org/10.1002/rra.859

Serrat, A., Saborido-Rey, F., Garcia-Fernandez, C., Muñoz, M., Lloret, J., Thorsen, A., Kjesbu, O.S., 2019. New insights in oocyte dynamics shed light on the complexities associated with fish reproductive strategies. Sci Rep 9, 1–15. https://doi.org/10.1038/s41598-019-54672-3

Sloan, K.E., Bohnsack, M.T., Watkins, N.J., 2013. The 5S RNP couples p53 homeostasis to ribosome biogenesis and nucleolar stress. Cell Rep 5, 237–247. https://doi.org/10.1016/j.celrep.2013.08.049

Steller, H., 1995. Mechanisms and genes of cellular suicide. Science (1979) 267, 1445–1449. https://doi.org/10.1126/science.7878463

Thomé, R.G., Santos, H.B., Arantes, F.P., Domingos, F.F.T., Bazzoli, N., Rizzo, E., 2009. Dual roles for autophagy during follicular atresia in fish ovary. Autophagy 5, 117–119. https://doi.org/10.4161/auto.5.1.7302

Tilly, J.L., 1996. Apoptosis and ovarian function. Rev Reprod 1, 162–172. https://doi.org/10.1530/REVREPROD/1.3.162

Tingaud-Sequeira, A., Chauvigné, F., Lozano, J., Agulleiro, M.J., Asensio, E., Cerdà, J., 2009. New insights into molecular pathways associated with flatfish ovarian development and atresia revealed by transcriptional analysis. BMC Genomics 10, 434. https://doi.org/10.1186/1471-2164-10-434

Tiwari, M., Prasad, S., Tripathi, A., Pandey, A.N., Ali, I., Singh, A.K., Shrivastav, T.G., Chaube, S.K., 2015. Apoptosis in mammalian oocytes: A review. Apoptosis 20, 1019–1025. https://doi.org/10.1007/s10495-015-1136-y

Valencia, A., Andrieu, J., Nzioka, A., Cancio, I., Ortiz-Zarragoitia, M., 2020. Transcription pattern of reproduction relevant genes along the brain-pituitary-gonad axis of female, male and intersex thicklip grey mullets, Chelon labrosus, from a polluted harbor. Gen Comp Endocrinol 287, 113339. https://doi.org/10.1016/j.ygcen.2019.113339

Valencia, A., Rojo-Bartolomé, I., Bizarro, C., Cancio, I., Ortiz-Zarragoitia, M., 2017. Alteration in molecular markers of oocyte development and intersex condition in mullets impacted by wastewater treatment plant effluents. Gen Comp Endocrinol 245, 10–18. https://doi.org/10.1016/j.ygcen.2016.06.017

Van den Belt, K., Verheyen, R., Witters, H., 2002. Reproductive effects of ethynylestradiol and 4t-octylphenol on the zebrafish (*Danio rerio*). Environ Toxicol Chem 21, 767–775. https://doi.org/10.1007/s002440010272

Von Schalburg, K.R., Rise, M.L., Brown, G.D., Davidson, W.S., Koop, B.F., 2005. A comprehensive survey of the genes involved in maturation and development of the rainbow trout ovary. Biol Reprod 72, 687–699. https://doi.org/10.1095/biolreprod.104.034967

Vousden, K.H., Prives, C., 2009. Blinded by the Light: The Growing Complexity of p53. Cell 137, 413–431. https://doi.org/10.1016/j.cell.2009.04.037

Weber, L.P., Kiparissis, Y., Hwang, G.S., Niimi, A.J., Janz, D.M., Metcalfe, C.D., 2002. Increased cellular apoptosis after chronic aqueous exposure to nonylphenol and quercetin in adult medaka (*Oryzias latipes*). Comparative Biochemistry and Physiology - C Toxicology and Pharmacology 131, 51–59. https://doi.org/10.1016/S1532-0456(01)00276-9

Wickham, H., Averick, M., Bryan, J., Chang, W., McGowan, L., François, R., Grolemund, G., Hayes, A., Henry, L., Hester, J., Kuhn, M., Pedersen, T., Miller, E., Bache, S., Müller, K., Ooms, J., Robinson, D., Seidel, D., Spinu, V., Takahashi, K., Vaughan, D., Wilke, C., Woo, K., Yutani, H., 2019. Welcome to the Tidyverse. J Open Source Softw 4, 1686. https://doi.org/10.21105/joss.01686

Witthames, P.R., Greer Walker, M., 1995. Determinacy of fecundity and oocyte atresia in sole (*Solea solea*) from the Channel, the North Sea and the Irish Sea . Aquat Living Resour 8, 91–109. https://doi.org/10.1051/alr:1995007

Wood, A.W., Van Der Kraak, G.J., 2003. Yolk proteolysis in rainbow trout oocytes after serum-free culture: evidence for a novel biochemical mechanism of atresia in oviparous vertebrates. Mol Reprod Dev 65, 219–227. https://doi.org/10.1002/mrd.10272

Wood, A.W., Van Der Kraak, G.J., 2001. Apoptosis and ovarian function: novel perspectives from the teleosts. Biol Reprod 64, 264–271. https://doi.org/10.1095/biolreprod64.1.264

Yamamoto, Y., Luckenbach, J.A., Young, G., Swanson, P., 2016. Alterations in gene expression during fasting-induced atresia of early secondary ovarian follicles of coho salmon, *Oncorhynchus kisutch*. Comp Biochem Physiol A Mol Integr Physiol 201, 1–11. https://doi.org/10.1016/j.cbpa.2016.06.016

Yang, Y., Wang, G., Li, Y., Hu, J., Wang, Y., Tao, Z., 2022. Oocytes skipped spawning through atresia is regulated by somatic cells revealed by transcriptome analysis in *Pampus argenteus*. Front Mar Sci 9, 1–14. https://doi.org/10.3389/fmars.2022.927548

Zillioux, E.J., Johnson, I.C., Kiparissis, Y., Metcalfe, C.D., Wheat, J. V., Ward, S.G., Liu, H., 2001. The sheepshead minnow as an in vivo model for endocrine disruption in marine teleosts: A partial life-cycle test with 17α-ethynylestradiol. Environ Toxicol Chem 20, 1968–1978. https://doi.org/10.1002/etc.5620200915

Chapter 3

Lack of genetic structure in the euryhaline thicklip grey mullet *(Chelon labrosus)* inhabiting estuaries with high burdens of xenoestrogens in the Southern Bay of Biscay

ARTICLE

Nzioka, A., Madeira, M.J., Kokokiris, L., Ortiz-Zarrogoitia, M., Diaz de Cerio, O., Cancio, I., 2023. Lack of genetic structure in euryhaline Chelon labrosus from the estuaries under anthropic pressure in the Southern Bay of Biscay to the coastal waters of the Mediterranean Sea. Mar. Environ. Res. 189, 106058. https://doi.org/10.1016/j.marenvres.2023.1060

CONGRESS

21st Pollutant Responses in Marine Organisms (PRIMO21) Conference, 22nd – 25th May 2022, Gothenburg, Sweden. **Anthony Nzioka**, Oihane Diaz de Cerio, Marie-Jose Madeira, Lambros Kokoris, Maren Ortiz-Zarragoitia, Alberto Teodorico Correia and Ibon Cancio (2022). "Population structure of catadromous thicklip grey mullet in the Basque coast in connection to estuarine homing, exposure to xenoestrogens and development of intersex condtion." Oral Communication.

Resumen

En la última década se han descrito efectos xenoestrogénicos en poblaciones de muble *Chelon labrosus* procedentes de estuarios contaminados del Golfo de Vizcaya, que han dado lugar a la aparición de intersexualidad. Para entender el nivel de flujo genético en los individuos afectados por xenoestrógenos de algunos estuarios vascos, se utilizaron marcadores microsatélites para evaluar la estructura poblacional y la conectividad *de C. labrosus* de estuarios de la costa vasca. Se ensayaron 46 microsatélites y se validaron 10 para el análisis de 204 individuos recolectados en 5 estuarios vascos seleccionados y en 2 grupos externos de la Bahía de Cádiz y el Golfo Termánico. Los microsatélites polimórficos revelaron 74 alelos totales, 2 - 19 alelos por locus. La heterocigosidad media observada (0,49 ± 0,02) fue inferior a la esperada (0,53 ± 0,01). No había indicios de diferenciación genética (F_{ST} = 0,0098, p = 0,0000) entre individuos o lugares. El análisis bayesiano de agrupación reveló la existencia de una única población en todos los lugares muestreados. Los resultados de este estudio indican una homogeneidad genética generalizada y panmixia de *C. labrosus* en las zonas de muestreo actuales que abarcan las cuencas atlántica y mediterránea. Por tanto, la hipótesis de la panmixia podría estar bien apoyada, de modo que los individuos que habitan estuarios con alta carga de xenoestrógenos y prevalencia de condición intersexual deberían considerarse miembros del mismo grupo genético único que los que habitan estuarios adyacentes sin incidencia de xenoestrogenicidad.

Palabras clave: *Chelon labrosus, microsatélites de ADN, estuarios, peces, genética, migración, panmixia, genética de poblaciones, estructura poblacional*

Abstract

Over the last decade, xenoestrogenic effects have been reported in populations of thicklip grey mullet *Chelon labrosus* from contaminated estuaries in the Bay of Biscay, resulting in intersex condition. To understand the level of gene flow in xenoestrogen-affected individuals of some Basque estuaries, microsatellite markers were used to evaluate the population structure and connectivity of *C. labrosus* from estuaries of the Basque coast. 46 microsatellites were tested and 10 validated for the analysis of 204 individuals collected from 5 selected Basque estuaries and 2 outgroups in the Bay of Cadiz and Thermaic Gulf. The polymorphic microsatellites revealed 74 total alleles, 2 – 19 alleles per locus. The mean observed heterozygosity (0.49 ± 0.02) was lower than the expected one (0.53 ± 0.01). There was no evidence of genetic differentiation (F_{ST} = 0.0098, p = 0.0000) among individuals or sites. Bayesian clustering analysis revealed a single population in all sampled locations. The results of this study indicate widespread genetic homogeneity and panmixia of *C. labrosus* across the current sampling areas spanning the Atlantic and Mediterranean basins. The hypothesis of panmixia could therefore be well supported so individuals inhabiting estuaries with high xenoestrogen burdens and prevalence of intersex condition should be considered as members of the same single genetic group as those inhabiting adjacent estuaries without incidence of xenoestrogenicity.

Keywords: *Chelon labrosus, DNA microsatellites, estuaries, fish, genetics, migration, panmixia, population genetics, population structure*

Abbreviations

AFLP, amplified fragment length polymorphisms
AMOVA, analysis of molecular variance
BOC, Bay of Cadiz
BPA, bisphenol-A
DNA, deoxyribonucleic acid
E_2, 17β-oestradiol
ECAE, Ethical approval from the Ethics Committee for Animal Experimentation
ENA, excluding null alleles
GADM, global administrative areas (database**)**
H_E, estimated heterozygosity
H_O, observed heterozygosity
HW, Hardy-Weinberg
HWE, Hardy-Weinberg Equilibrium
IBD, Isolation-by-Distance
LD, linkage disequilibrium
MCMC, Markov Chain Monte Carlo
MT, 17α-methyltestosterone
mtDNA, mitochondrial DNA
N_A, number of alleles
NP, nonylphenol
OP, octylphenol
PCoA, Principal Coordinate Analysis
QGIS, quantum geographic information system (software)
RFLP, restricted fragment length polymorphisms
SBB, Southern Bay of Biscay
SNP, single nucleotide polymorphisms
TGM, Thermaic Gulf
WWTP, wastewater treatment plant
β-HCH, β-hexachlorocyclohexane

1. Introduction

The thicklip grey mullet *Chelon labrosus* (Risso, 1827) is a member of the Mugilid family which consists of approximately 25 genera and 80 species (Crosetti and Blaber, 2016; Xia et al., 2016) widely distributed along the Northeast Atlantic Ocean and the Mediterranean and Black Seas (Crosetti and Blaber, 2016; Froese and Pauly, 2022). It is a euryhaline fish that exhibits a high degree of residency within coastal systems, using estuaries as nursery and foraging habitats, migrating up and down estuaries with the moving tide (Crosetti and Blaber, 2016; Froese and Pauly, 2022; Whitfield, 2020). Adults migrate and spawn offshore in marine waters during winter (December-February), with the pelagic planktonic eggs hatching within 3-4 days and the planktonic larval stage lasting approximately 4 weeks (Crosetti and Blaber, 2016). Post-larvae juveniles of these marine reproducing mugilids form dense schools that migrate to inshore coastal waters and shallow estuaries in the first and second month of life where they remain until they reach the adult stage (Crosetti and Blaber, 2016; Crosetti and Cataudella, 1995; Mićković et al., 2010). *C. labrosus* individuals can survive in highly polluted aquatic environments where their benthic feeding habits make them particularly susceptible to bioaccumulation of contaminants. Therefore, the thicklip grey mullet is considered a good choice for use as an estuarine pollution sentinel species (Crosetti and Blaber, 2016; Ortiz-Zarragoitia et al., 2014).

In *C. labrosus*, xenoestrogenic effects have been reported in individuals from contaminated estuaries along the Basque coast (Bizarro et al., 2014; Diaz De Cerio et al., 2012; Ortiz-Zarragoitia et al., 2014; Puy-Azurmendi et al., 2013; Valencia et al., 2017). This has been mainly linked to exposure to alkylphenols, pesticides and other xenoestrogens in wastewater treatment plant (WWTP) effluents that are discharged into estuaries (Bizarro et al., 2014; Ortiz-Zarragoitia et al., 2014; Puy-Azurmendi et al., 2013). Intersex testes have been identified in up to 83% of the males in estuaries like the one of Gernika, while males in other nearby estuaries have always shown normally developing testes (Ortiz-Zarragoitia et al., 2014). Thicklip grey mullets and mugilids in general are considered gonochoristic with separate sexes maintained throughout their 25-years lifespan (Devlin and Nagahama, 2002). Males and females reach sexual maturity between 2 and 3 years respectively (Sostoa, 1983), so early sex differentiation occurs in continental waters, and in polluted estuaries in close contact to xenoestrogens when they are bioavailable. Early exposure of *D. rerio*

embryos to 17β-oestradiol (E_2) and 17α-methyltestosterone (MT) results in the generation of both female and male single-sex groups, proving that full feminisation can also occur during early sex differentiation (Rojo-Bartolomé et al., 2020). While feminised genetic males could develop testes after withdrawal from oestrogenic compounds (Baumann et al., 2014; Nash et al., 2004), exposure during gonad differentiation in the early life stages would generate intersex condition and could make the process irreversible (Rojo-Bartolomé et al., 2020).

The environmental factor most intimately related to fish sex differentiation temperature and normally out of unusual high temperatures can result in masculinization (Devlin and Nagahama, 2002). In most fish species tested, the offspring of sex reversed neomales show higher sensitivity to masculinizing temperatures (Piferrer and Anastasiadi, 2021). This suggests some kind of epigenetic mechanism such as DNA methylation of sex control genes that would render the offspring of these neomales more susceptible to sex reversal (Piferrer and Anastasiadi, 2021). With time DNA hypermethylation of some regions of the genome could lead to accumulation of mutations due to the propensity of methylated cytosines to spontaneously mutate into thymines. Whether this occurs in xenoestrogen driven intersex individuals is not known, but it has multiple implications depending on whether the thicklip grey mullets maintain fidelity to their estuary of origin and their larvae too.

Based on the early life-history characteristics of *C. labrosus*, there appears to be a high potential for reproduction occurring between adults of different estuaries of provenance in the sea and for larval geographical dispersal (Pereira et al., 2023). The yearly oceanic reproductive migration in the species can generate different patterns of genetic structuring; from a total panmixia (genetic homogenization) to a moderate structuring due to isolation, either reproductive or geographical. While the most extreme catadromous species tend to show panmixia throughout their distribution area (Avise et al., 1986; Dannewitz et al., 2005), the possibility of genetic structure among the different groups of *C. labrosus* from estuary-to-estuary in the Basque coast cannot be ruled out. In any case, the catadromous thinlip grey mullet *Chelon ramada*, with residence in freshwaters in contrast to the more estuarine *C. labrosus* (Crosetti and Blaber, 2016), has been recently identified through a microsatellite study of 457 individuals from 16 locations to form a panmictic population with high connectivity along its distribution from the Northeast Atlantic coast to the Mediterranean Sea (Pereira et al., 2023).

Mugilids can be candidate species for diversification of aquaculture in Europe and recently different protocols have been published for the induction of spawning, reproduction and culture of different representative species (García-Márquez et al., 2021; Ramos-Júdez et al., 2022; Vallainc et al., 2022). C. labrosus is in fact, a nominee fish species for diversification in Spain due to two of its most notorious biological traits, its omnivore and euryhaline nature (García-Márquez et al., 2021). However, significant knowledge gaps on the biology and ecology of the species remain. In this sense, nothing is known of the genetic structure of the population(s) in European waters which should be taken into account before allowing future intensive aquaculture initiatives across regional basins.

Understanding the population structure of these migratory fish is important, especially in the face of site-specific anthropogenic pollution and habitat loss (Collins et al., 2013; Halpern et al., 2007; Hoegh-Guldberg and Bruno, 2010). In the context of our work, it is important to know the population structure of our pollution sentinel species to understand their history of exposure to xenoestrogens leading to the effects observed in some local estuaries in male individuals that develop intersex testes. The most adequate methodological approach to understand this would require physical tagging (implanted internal or external tags) of adults in winter to follow their reproductive migration and analyse whether they return to the same estuary of origin and whether at sea they encounter individuals from other estuaries (Pepping et al., 2020). The cliff dominated orography of the Basque coast does not recommend the use of internally implanted tags (recapture) or pop-up archival tags (washed into the shore) that would never be recovered, while pop-up satellite archival tags are normally suitable for larger species and may impact fish performance (Musyl et al., 2011). The utilization of PIT-tags (passive integrated transponders) or radiotelemetry would help us to spot episodes of exit and entry into estuaries where we could place permanent antenna installations (Cooke et al., 2022), but without informing us where the fish went for reproduction and who they reproduced with. At this stage, it seems relevant at least to understand whether we are facing a single genetic population or multiple populations each associated to one estuary without genetic flow among them.

To date, most genetic studies conducted on Mugilids that inhabit the North-East (NE) Atlantic coast of Europe have primarily used mitochondrial markers or microsatellites to provide information about the ancient history of populations and their evolutionary processes (Durand et al., 2013, 2012b; Pereira et al., 2023; Xia et al., 2016). To the best of our knowledge, this study is the first to investigate the population genetics of *C. labrosus*,

employing microsatellite marker analysis to detect patterns of genetic structure. Microsatellite nuclear markers provide information on diversity and contemporary population processes due to their abundance in the genome and high degree of polymorphism (Durand et al., 2013; Pacheco-Almanzar et al., 2017; Pereira et al., 2023). This study aims to evaluate the population genetic structure of *C. labrosus* in the Bay of Biscay using microsatellites to understand the level of gene flow in the individuals of our xenoestrogen effects biomonitoring program and begin to answer the question of whether individuals from an estuary reproduce with individuals of the same estuary and test the hypothesis of panmixia.

2. Materials and methods

2.1. Sampling details

In all, 204 *C. labrosus* individuals that had been collected in five estuaries along the Basque coast in the Southeast Bay of Biscay (December 2010 – October 2015) and stored in the cryobank of the Biscay Bay Environmental Biospecimen Bank (BBEBB) were analysed. Additionally, individuals were sampled in two outgroup locations, one in the Bay of Cadiz (February 2019) and the other in the Mediterranean Sea within Thermaic Gulf at Thessaloniki, Greece (February 2020) (Table 1; Figure 1). The fish were obtained by angling with a rod (Basque coast) and from commercial captures (Cadiz and Thermaic Gulf). Brain, gonad and/or liver tissues of *C. labrosus* from the Bay of Biscay were collected in RNA later solution (Ambion™, ThermoFisher Scientific, Waltham, Massachusetts, USA) and frozen in liquid nitrogen until arrival at the laboratory where they were immediately stored in -80ºC. In mullets from Cadiz and Thessaloniki muscle and/or gills were dissected from fresh fish, preserved in 98% ethanol immediately after sampling and stored at -80ºC on arrival at the laboratory. Ethical approval from the Ethics Committee for Animal Experimentation (ECAE) of the University of the Basque Country (UPV/EHU) was not necessary, with all fishing activities and handling procedures done in accordance with the ECAE – UPV/EHU and regional authorities. According to the Access and Benefit Sharing Legislation in place in Spain, the present analysis to study population structure means no utilization of Spanish genetic resources.

Table 1
Provenance of the thicklip grey mullets (*C. labrosus*) analysed in this study. The names and abbreviations of the sampling locations are indicated (five in the Southeast Bay of Biscay, one in the South of Spain in the Bay of Cadiz, and one in the Mediterranean Sea, Greece) together with the sample size (*N*) and geographical coordinates (latitude and longitude) in decimal degrees.

Country	Location (ID)	*N*	Latitude	Longitude
Spain	Pasaia (PA)	28	43.321940	-1.931670
Spain	Ondarroa (ON)	30	43.320000	-2.431110
Spain	Gernika (GE)	30	43.323890	-2.673610
Spain	Plentzia (PL)	30	43.407220	-2.946110
Spain	Bilbao (BI)	29	43.336110	-3.016390
Spain	Cadiz (CA)	30	36.538063	-6.301807
Greece	Thermaic Gulf (TG)	27	40.634975	22.927675

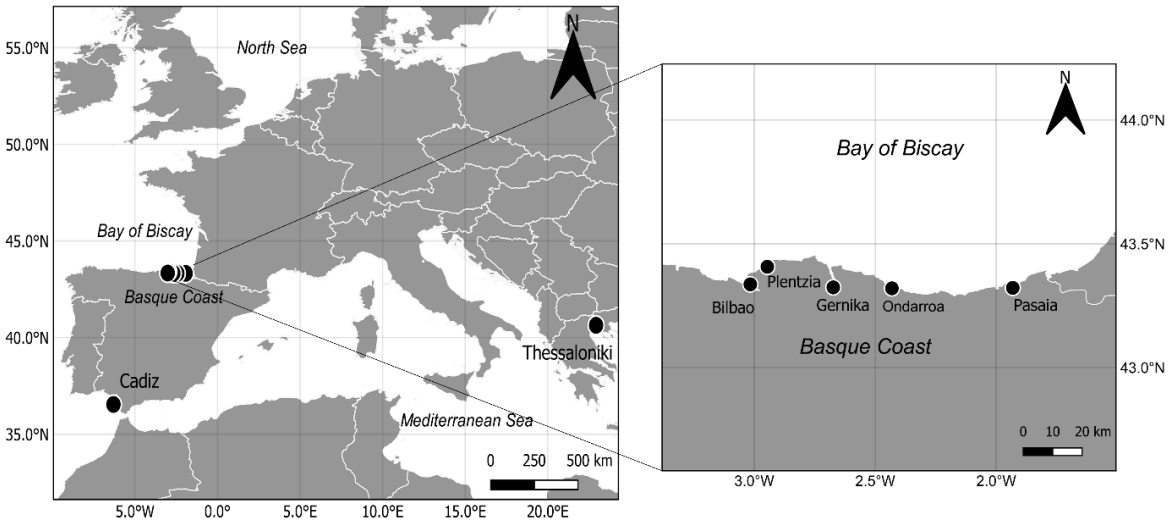

Figure 1
Sampling locations of *C. labrosus* (black dots) across five locations along the Basque coast (inset, Southeast Bay of Biscay), one location in the Bay of Cadiz (South of the Iberian Peninsula, Spain) and one location in the Mediterranean Sea, Greece. This figure was produced with the GADM database (www.gadm.org), version 2.5, July 2015 and QGIS version 3.18.0-Zürich.

2.2. DNA isolation and amplification of microsatellites

Total genomic DNA was extracted from 25 mg of tissue (brain, gonad, liver, muscle or gill) using DNeasy® Blood & Tissue Kit following the manufacturer's instructions (Cat. No.: 69504, QIAGEN, Hilden, Germany). The quality of the extracted DNA was assessed using gel electrophoresis (1% agarose gels), with clear high molecular weight bands on gels used as a selection criterion and subsequently stored at -20ºC until use.

A set of 46 microsatellite loci previously described for the *Mugil cephalus* complex (Miggiano et al., 2005; Shen et al., 2010; Xu et al., 2009, 2010) were screened on a representative sample of 30 individuals randomly selected from different locations under study to test the PCR amplification effectiveness on *C. labrosus* (Supplementary material, Table S1). All PCR analyses contained 10 – 100 ng DNA, 10X PCR reaction buffer, 20 µM of each primer, 100 mM $MgCl_2$, 10 mM dNTPs, 10 µg bovine serum albumin (BSA, REF: 10711454001, Roche Diagnostics GmbH, Mannheim, Germany) and 1.25 U BIOTAQ™ DNA polymerase (BIO-21040, Bioline GmbH, Luckenwalde, Germany). PCR profiles for amplification of microsatellites were conducted as follows: initial denaturation at 95ºC for 15 min, followed by 35 cycles at 94ºC for 30 s, annealing step (temperature for each primer set in Table 2) for 90 s and 72ºC for 60 s, and a final extension at 60ºC for 30 min (Bio-Rad C1000 Touch Thermal Cycler, Bio-Rad Laboratories Inc., Hercules, California, USA). The quality of the PCR products and the allele size range were evaluated using GelRed® stained 2% agarose gels (Biotium GelRed® 10,000X in water, Catalogue No. 41003; Biotium Inc., Freemont, California, USA). A selection of usable loci was done, based on the presence of polymorphism and good multiplexing PCRs capabilities (Table 2; Supplementary Table S1 bold and underlined). Forward primers for each selected locus were labelled with FAM, PET, VIC or NED fluorescent dyes. A total of 147 individuals from 5 locations along the Basque coast, 30 individuals from Cadiz, and 27 individuals from Thessaloniki were genotyped (Table 1). The following cycling conditions for amplification of microsatellites using multiplex PCR according to QIAGEN® Multiplex PCR Kit (Cat. No: 206143, QIAGEN, Hilden, Germany) were used: initial denaturation at 95ºC for 15 min, followed by 35 cycles at 94ºC for 30 s, annealing step of 57ºC for 90 s and extension of 72ºC for 60 s, and a final extension at 60ºC for 30 min (Bio-Rad C1000 Touch Thermal Cycler, Bio-Rad Laboratories Inc., Hercules, California, USA). PCR products were checked electrophoretically on GelRed® stained 2% agarose gels (Biotium Gel Red®; Biotium Inc., USA) before being sent for capillary electrophoresing (Macrogen SPAIN; Macrogen Inc., Seoul, South Korea). The microsatellite marker profiles were scored using Geneious Prime v.2019 software (Biomatters Ltd., Auckland, New Zealand), with LIZ-500 Size Standard (Applied Biosystems, Foster City, California, USA) to calibrate product size. Alleles were recorded as three-digit genotypes.

Table 2
Characteristics of 10 amplified microsatellite loci used to study the genetic diversity and population structure of the thicklip grey mullet (*C. labrosus*). Locus name (Locus), forward (F) and reverse(R) primer sequences, information of repeated Motif, used florescence label, how primers were multiplexed (the same number belongs to the same multiplexing group), multiplexing annealing PCR temperature T_A (ºC), resulting allelic size length (bp) and the GenBank accession number of each selected locus. Loci Muce and its respective primers were reported by Xu et al. (2010), loci Muso and its respective primers were reported by Xu et al. (2009) and loci Mce and its respective primers were reported by Shen et al. (2010) (All of them were applied by the authors for *Mugil cephalus* and *Mugil so-iuy*, and here were validated for *C. labrosus*). Five loci (in bold) were monomorphic in all studied individuals and were not used in further downstream analyses.

Locus	Primer Sequence (5´- 3´)	Repeat Motif	Fluorescent label	Multiplex Panel	T_A (ºC)	Allelic sizes (bp)	GenBank Accession No.
Muce44	F: GCTTCGGAGGACCAAC R: CGACAGCCACTGTTATG	$(CA)_5(GA)_4$	FAM	I	57	285 - 311	HM060975
Mce6	F: GAGGAGGCTCGGAGGATT R: CGGGGCTTGTGACAGTTT	$(CA)_{15}$	PET	II	57	187 - 229	HM004328
Mce11	F: ATTAGCCAGGGCCACCAG R: CAGAAGCCAAAAGGACGG	$(TG)_{14}$	VIC	II	57	151 - 163	HM004332
Mce25	F: TCGGCATGTATATGAAAGCAC R: ACATAACTCTGCCACTGCTTG	$(TG)_{14}$	NED	II	57	123 - 125	HM004346
Muce38	F: GCACCAACATCTCACCTG R: CCTACCATTTACCCCTCT	$(GA)_5(GGAGA)_4$	FAM	III	57	231 - 251	HM060974
Mce10	F: CCACTGTAGGGCTGTATGC R: GGGAGGAGGATTTCTCAA	$(TG)_{12}$	VIC	III	57	124 - 140	HM004331
Muce26	F: TGCGGAGACAATGTAAAC R: AAATGAAACAATCCACCC	$(ACAA)_3$	FAM	IV	57	266 - 268	HM060972
Mce2	F: AGCCAAAGTTCCTGTAAGTACG R: TCAGATTAGGACCCGACCATA	$(GT)_{30}$	VIC	IV	57	134 - 168	HM004324
Muso32	F: GCAGTGCACATGGTAACAAAA R: CGCCTACAGCATCAGACAAG	$(AC)_9$	PET	V	57	193 - 197	EU570307
Muso19	F: CACCACTATGGCATCCTTCA R: AACCCCTTTTCTTGCTCAAA	$(AC)_9$	VIC	V	57	142 - 162	EU570294
Muso25	**F: ATGAAAAGGGAGGGGCAATA R: CTGCTCACCTTGCGTTTACA**	**$(CA)_{11}$**	**PET**	**I**	**57**	**204**	**EU570300**
Muso36	**F: TCCTTTATGGGGAGACGATG R: CCCAATAGCCACAAATGTCC**	**$(GT)_3GA(GT)_6$**	**VIC**	**I**	**57**	**192**	**EU570311**
Mce27	**F: ACTGTGCACTTCTGGTTTCC R: ACATCTTTGAGGTTGCCC**	**$(CA)_{12}$**	**NED**	**I**	**57**	**126**	**HM004348**
Muso22	**F: TGATGAGAATGGTGGTGACG R: TTTTGGGCTGCTTGTCTCTC**	**$(GT)_{17}$**	**PET**	**III**	**57**	**189**	**EU570297**
Mce8	**F: AGGGATTGGGTTTAGGCG R: GTGCTCGACACTTTAGACTGAT**	**$(CA)_{20}$**	**PET**	**IV**	**57**	**175**	**HM004330**

2.3. Data analysis

2.3.1. Loci assessment and genetic diversity

Calculations of allele frequency for each marker, the number of alleles (N_A), estimated heterozygosity (H_E), and observed heterozygosity (H_O) for each locus and locality were estimated using the GenAlEx v. 6.5 computer program (Peakall and Smouse, 2006, 2012). Deviations from the Hardy-Weinberg equilibrium (HWE) at each locus using Fisher´s exact test, under Markov Chain Monte Carlo (MCMC) algorithms (Guo and Thompson, 1992), with 10,000 dememorizations, 10,000 batches (treatments per location), and 100,000 iterations per batch were calculated by GENEPOP 4.7.5 software (Raymond and Rousset, 1995). The same package was used to assess linkage disequilibrium (LD) between pairs of loci using Fisher´s exact test according to (Pacheco-Almanzar et al., 2017) (10,000 dememorizations, 100 batches, 1,000 iterations per batch), with probability values for both tests (HWE & LD) corrected with Bonferroni multiple comparison test at $p \leq 0.05$ (Rice, 1989). GENEPOP 4.7.5 was further used to calculate Wright´s *F* statistics (Wright, 1978, 1965) using allele frequency-based correlations (F_{ST} & F_{IS}) at each locus according to (Weir and Cockerham, 1984). The program Micro-Checker v 2.2.3 (Van Oosterhout et al., 2004) was used to examine large allele dropout, stuttering, and null alleles as potential sources of error.

2.3.2. Genetic structure analysis

F_{ST} values between pairs of locations calculated from Wright´s *F* statistics (Weir and Cockerham, 1984) were used to calculate the genetic differentiation of the entire population with values of (Cavalli-Sforza and Edwards, 1967). We estimated null allele frequencies (Table 3) and F_{ST} (Table 4) using the FreeNA software (Chapuis and Estoup, 2007) with the number of replicates fixed at 25,000. We ran this analysis using the ENA correction method to efficiently correct for the positive bias induced by the presence of null alleles on F_{ST} estimation and, so, to provide an accurate estimation of F_{ST}. FreeNA provided F_{ST} values and confidence intervals with and without correction (excluding null alleles (ENA) correction), relative to the null alleles (Chapuis and Estoup, 2007) and a Chi-square test was performed to compare the values. If significant differences were observed in F_{ST} value comparisons, loci with null alleles present were to be discarded. The program ARLEQUIN version 3.5.2.2 was then used to perform a hierarchical analysis of molecular variance (AMOVA) to assess the presence of a differential genetic structure (Excoffier et al., 2005)

across the total sample range and among putative regional groupings of samples. Genetic clusters in HW were determined using the program STRUCTURE v2.3.4 (Pritchard et al., 2009, 2000) using the admixture model. As the presence of null alleles introduces potential ambiguity around the true underlying genotype, we ran the program under two conditions; RECESSIVEALLELES set to 0 in which no ambiguity is assumed; and RECESSIVEALLELES set to 1 where missing data are assigned as recessive to better account for null alleles (Falush et al., 2007). To estimate the number of *K* populations, 20 independent runs were done for each *K* from *K* = 1 to *K* = 10, using a burn-in of 100,000 and 1,000,000 iterations of MCMC. The ΔK statistics (Evanno et al., 2005) were used to detect the uppermost hierarchical level of the population structure, based on the rate of change between successive *K* values. The best estimate of *K* (Δ*K*) was calculated using the web-based STRUCTURE HARVESTER program (Earl and VonHoldt, 2012).

2.3.3. Estimation of genetic divergence

The GenAlEx 6.5 software (Peakall and Smouse, 2006, 2012) was used to perform a Principal Coordinate Analysis (PCoA) procedure to reveal patterns of genetic relationship, if any, among the 7 populations of *C. labrosus*. To test for Isolation-by-Distance (IBD), the same software was used to perform a Mantel test. The Mantel test investigates the relationship between the pairwise population F_{ST} values and geographic distance. The correlation between the geographic coordinates (longitude, latitude) and the genetic diversity parameters was studied.

3. Results

3.1. Microsatellite loci and genetic diversity

Of the 46 microsatellites selected from the literature previously used for the analysis of the dynamics of populations of *Mugil cephalus* (Shen et al., 2010; Xu et al., 2009, 2010), 18 loci amplified well in *C. labrosus* (Supplementary material, Table S1). 31 loci were excluded from further analysis either because of lack of allelic variations, poor amplification of alleles or poor multiplexing possibilities (Supplementary material, Table S1). Out of the remaining 15 loci, 5 were monomorphic and were not selected for the analyses (Table 2; Supplementary table S1 bold and underlined).

Summary statistics for the 10 microsatellite loci in the seven populations from the South-East Bay of Biscay to the Mediterranean are shown in Table 3. A total of 74 alleles ranging

from 123 to 311 bp in length were observed. The number of alleles per locus varied considerably from 2 in loci Mce25, Muce26, and Muso32 to 19 in locus Mce6, depending on the location. The highest level of polymorphism was observed in loci Muce44, Mce11, Mce6, Muce38, Mce10 and Mce 2 (Table 3). The number of alleles per population varied slightly, with 51 (in mullets from Ondarroa-ON) to 54 (Plentzia-PL) alleles for populations from the Basque coast and 58 to 63 alleles for mullets from Thessaloniki (TG) and Cadiz (CA) respectively. There was no evidence of large allele dropout at any loci. Stuttering was identified as a potential issue at two loci (Mce6 and Mce25). Significant LD (Fisher´s method; $P < 0.05$) was found for six different combinations of loci (Supplementary material, Tables S2 and S3, $P < 0.05$). Loci showing potential stuttering or LD were retained in the dataset as genuine stuttering and LD are expected to affect all sites equally. After adjusting for multiple comparisons, none of the mullet populations deviated from HWE at any loci after Bonferroni correction (Table 3). The average H_O per population (mean ± standard error) ranged from 0.44 ± 0.09 (Pasaia-PA and Gernika-GE) to 0.56 ± 0.08 (ON), while the average H_E by location ranged from 0.48 ± 0.08 (CA) to 0.56 ± 0.08 (ON). The fixation index (F) averaged across all loci ranged from 0.08 (ON) to 0.28 (PA) (Table 3). In most sampling locations, there were more homozygous genotypes than expected (F positive), but there was no significant evidence of an excess of homozygotes at any location. Significant and high F_{IS} values were observed for 3 loci, indicating a heterozygotic deficiency (loci Muce 38, Muce 26 and Muso 19) (Table 3). In terms of null allele frequencies, the overall frequency estimate was 5%, and ranged from 2% (ON), to 6% (PA, CA and TG) (Table 4).

Table 3
Population genetic parameters for 204 individuals of *C. labrosus* sampled across five locations along the Basque coast, one location in the Bay of Cadiz and one location in the Mediterranean Sea, as analysed by 10 microsatellite loci. *N* - Sample size; N_A - Allele number per locus; HWE - Hardy-Weinberg equilibrium after Bonferroni correction; H_O - Observed heterozygosity; H_E - Expected heterozygosity; *F* - fixation index (Weir and Cockerham, 1984). Hyphen - no values, Mean represents mean values across 10 polymorphic loci. Significant adjusted nominal level was 0.001.

Location		**Microsatellite Loci**										**Mean**
		Muce44	**Mce11**	**Mce25**	**Mce6**	**Muce38**	**Mce10**	**Muce26**	**Mce2**	**Muso19**	**Muso32**	
Pasaia	*N*	26	28	28	28	24	28	26	27	28	26	26.9
	N_A	5	5	2	12	3	6	2	9	1	2	4.7
	HWE	0.00	0.16	0.02	0.00	0.11	0.66	0.06	0.38	-	0.64	0.23
	H_O	0.42	0.54	0.00	0.68	0.25	0.79	0.04	0.74	-	0.50	0.44
	H_E	0.51	0.61	0.07	0.85	0.34	0.75	0.11	0.76	-	0.49	0.50
	F	0.19	0.14	1.00	0.21	0.29	-0.03	0.66	0.04	-	0.01	0.28
Ondarroa	*N*	30	30	30	30	29	29	30	30	30	28	29.6
	N_A	5	5	1	12	4	6	2	8	1	2	4.6
	HWE	0.84	0.75	-	0.19	0.40	0.56	0.00	0.66	-	0.88	0.54
	H_O	0.63	0.67	-	0.73	0.34	0.76	0.03	0.73	-	0.57	0.56
	H_E	0.56	0.63	-	0.83	0.35	0.71	0.21	0.70	-	0.49	0.56
	F	-0.12	-0.05	-	0.14	0.04	-0.05	0.84	-0.04	-	-0.15	0.08
Gernika	*N*	30	30	30	30	29	30	28	27	30	30	29.4
	N_A	7	5	1	13	3	6	2	7	1	2	4.7
	HWE	0.94	0.46	-	0.60	0.00	0.41	0.18	0.12	-	0.17	0.36
	H_O	0.60	0.67	-	0.80	0.21	0.73	0.11	0.63	-	0.37	0.51
	H_E	0.53	0.66	-	0.76	0.41	0.70	0.16	0.69	-	0.47	0.55
	F	-0.13	0.00	-	-0.04	0.51	-0.04	0.36	0.10	-	0.24	0.13
Plentzia	*N*	30	30	30	30	28	30	29	30	30	30	29.7
	N_A	7	4	1	13	3	8	2	8	1	2	4.9
	HWE	0.40	0.81	-	0.01	0.01	0.00	0.00	0.48	-	0.38	0.26

Table 3 continued…

Location		Microsatellite Loci										Mean
		Muce44	**Mce11**	**Mce25**	**Mce6**	**Muce38**	**Mce10**	**Muce26**	**Mce2**	**Muso19**	**Muso32**	
	H_O	0.50	0.60	-	0.73	0.07	0.63	0.03	0.73	-	0.43	0.47
	H_E	0.56	0.54	-	0.86	0.19	0.75	0.21	0.77	-	0.49	0.55
	F	0.12	-0.10	-	0.17	0.64	0.18	0.84	0.07	-	0.13	0.26
Bilbao	N	29	29	29	29	25	29	29	29	29	29	28.6
	N_A	7	5	1	11	4	6	2	8	1	3	4.8
	HWE	0.58	0.43	-	0.86	0.00	0.94	0.05	0.05	-	0.42	0.42
	H_O	0.66	0.55	-	0.90	0.24	0.76	0.03	0.76	-	0.34	0.53
	H_E	0.64	0.58	-	0.83	0.48	0.68	0.10	0.75	-	0.37	0.55
	F	0.00	0.06	-	-0.06	0.51	-0.01	0.66	0.00	-	0.10	0.16
Cadiz	N	30	30	30	30	30	30	30	30	30	30	30
	N_A	7	6	2	15	4	5	2	12	3	2	5.8
	HWE	0.01	0.01	0.05	0.14	0.07	0.59	0.03	0.31	0.01	1.00	0.22
	H_O	0.57	0.53	0.03	0.87	0.23	0.70	0.10	0.83	0.03	0.70	0.46
	H_E	0.63	0.64	0.10	0.86	0.31	0.65	0.21	0.78	0.13	0.50	0.48
	F	0.12	0.18	0.66	0.01	0.27	-0.05	0.53	-0.04	0.74	-0.40	0.20
Thermaic Gulf	N	27	27	27	27	13	27	27	27	27	27	25.6
	N_A	7	5	1	12	5	6	2	9	3	3	5.3
	HWE	0.01	0.17	-	0.14	0.00	0.23	0.01	0.72	0.02	0.82	0.23
	H_O	0.41	0.44	-	0.67	0.23	0.74	0.04	0.78	0.04	0.59	0.44
	H_E	0.60	0.48	-	0.79	0.62	0.74	0.17	0.74	0.07	0.52	0.53
	F	0.34	0.09	-	0.18	0.65	-0.02	0.79	-0.04	0.50	-0.13	0.26

Table 4
Null allele frequency estimates using EM algorithm (Dempster et al., 1977) with FreeNA software (25,000 replicates).

Loci	PA	ON	GE	PL	BI	CA	TG	Mean
Muce44	0.097	0.000	0.000	0.000	0.000	0.067	0.112	0.039
Mce11	0.043	0.000	0.000	0.000	0.000	0.076	0.029	0.021
Mce25	0.128	0.001	0.001	0.001	0.001	0.110	0.001	0.035
Mce6	0.094	0.019	0.000	0.071	0.000	0.015	0.037	0.034
Muce38	0.088	0.015	0.167	0.149	0.179	0.083	0.242	0.132
Mce10	0.000	0.000	0.000	0.085	0.000	0.000	0.016	0.015
Muce26	0.116	0.188	0.083	0.191	0.111	0.126	0.162	0.139
Mce2	0.000	0.000	0.043	0.000	0.025	0.000	0.000	0.010
Muso19	0.001	0.001	0.001	0.001	0.001	0.117	0.001	0.018
Muso32	0.000	0.000	0.074	0.036	0.025	0.000	0.000	0.019
Mean	**0.057**	**0.022**	**0.037**	**0.053**	**0.034**	**0.059**	**0.060**	**0.046**
Frequency estimates (%)	**6**	**2**	**4**	**5**	**3**	**6**	**6**	**5**

3.2. Genetic structure

As indicated by F_{ST} values, very low but significant genetic differences were found at nuclear loci between Pasaia (PA) and Bilbao (BI), Gernika (GE) and BI + Thermaic Gulf (TG), and BI and Cadiz (CA) + TG populations (Table 5). However, estimates of the global F_{ST} values both with (F_{ST} = 0.011250) and without (F_{ST} = 0.007908) correction relative to null alleles showed little genetic differentiation for all loci.

Table 5
Pairwise population F_{ST} values (below diagonal) (Weir and Cockerham, 1984) and their corresponding p-values (above diagonal) for comparisons of *C. labrosus* populations among the seven sampling locations based on 10 polymorphic microsatellite loci. Values in **bold** indicate significant comparisons ($p < 0.05$).

Location	PA	ON	GE	PL	BI	CA	TG
Pasaia (PA)	-	0.703	0.072	0.982	**0.027**	0.279	0.081
Ondarroa (ON)	0.002	-	0.757	0.496	0.135	0.486	0.072
Gernika (GE)	0.009	0.005	-	0.063	**0.027**	0.252	**0.018**
Plentzia (PL)	0.010	0.001	0.011	-	0.063	0.189	0.126
Bilbao (BI)	**0.015**	0.006	**0.013**	0.010	-	**0.000**	**0.000**
Cadiz (CA)	0.004	0.000	0.004	0.006	**0.020**	-	0.324
Thermaic Gulf (TG)	0.010	0.011	**0.018**	0.010	**0.027**	0.004	-

The overall AMOVA results showed that only 0.98% of the variation was distributed between the origin locales, while 99.02% was allocated within locations (F_{ST} = 0.00976, p = 0.0000) (Table 6). This was further supported by global pairwise F_{ST} comparisons of *C.*

labrosus populations extracted from AMOVA, indicating that the mullets from each location are not genetically different from each other.

Table 6
Results of the global analysis of molecular variance (AMOVA) as a weighted average of 10 polymorphic loci (AMOVA, F_{ST} = 0.00976, p = 0.0000, n = 204).

Source of variation	Sum of squares	Variance of components	Percentage variation
Among populations	21.359	0.023	0.976
Within populations	901.691	2.292	99.024
Total	923.050	2.315	

In STRUCTURE, there were no appreciable differences in optimum values of *K* or assignment of individuals to each cluster when RECESSIVEALLELES was set to 0 or 1, therefore we only report results as per RECESSIVEALLELES set to 0. No loci were dropped due to the presence of null alleles to minimise power loss, as when dealing with a low number of loci, it is generally preferable to account for null alleles rather than exclude loci (Wagner et al., 2006). Although the application of the Evanno test to the results of Bayesian clustering analysis of the entire data set conducted in STRUCTURE revealed a peak at K = 2 in the plot of estimated Delta K versus K, the Delta K value was very low (Supplementary Material, Fig S1), an indication that the strength of the signal detected in STRUCTURE is weak (Evanno et al., 2005); hence the non-existence of different population clusters in *C. labrosus* samples. Assignment tests in STRUCTURE revealed that we have one main population (K = 1) across all the sampled locations (Figure 2).

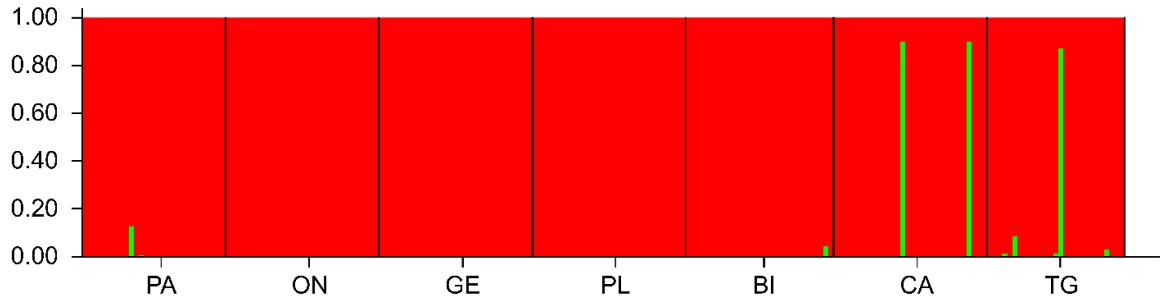

Figure 2
STRUCTURE plots from microsatellite data for *C. labrosus* using an LOCPRIOR admixture model. Presence of a single group is represented by a single red colour, with the proportion of each bar assigned to a single colour representing the probability that an individual belongs to that group (Supplementary material Fig S2). See **Table 1** for additional information on sample names.

3.3. Genetic divergence and isolation-by-distance (IBD)

The PCoA indicated that there may be some form of genetic structure and the possibility of IBD, with 77.43 of variation being explained by the first 2 axes. The Mantel test of the correlation coefficient showed a low and not significant correlation between geographic distance and pairwise F_{ST} values ($R = -0.051$, $p = 0.590$; $R^2 = 0.0026$). There was no pattern of IBD since there was no indication of the existence of a distinct geographical structure in the studied locations, nor was a longitudinal trend of genetic variation detected.

4. Discussion

The study evaluated the genetic diversity and population structure of genetic connectivity as a consequence of reproductive migration patterns in thicklip grey mullet *Chelon labrosus* from estuaries of the Basque coast in the Southern Bay of Biscay (SBB). 46 microsatellite markers were tested and 15 validated for the analysis of 204 individuals from 5 estuaries in the SBB and 2 outgroups in the Bay of Cadiz (BOC) and Thermaic Gulf (TGM). The results of this study indicate widespread genetic homogeneity and panmixia of *C. labrosus* across the current sampling areas spanning the Atlantic and Mediterranean basins. There was no evidence of genetic structure for *C. labrosus* across ~5000 km of coastline, despite the use of ten highly variable microsatellite loci. F_{ST} values indicate that the thicklip grey mullets from each location are not genetically different from each other. Furthermore, Bayesian clustering analysis of the microsatellite data supported the single population group findings, suggesting the absence of genetic differentiation between sampling locations. Since there was no evidence of genetic differentiation, these populations should be grouped as belonging to a single genetic group.

The microsatellite primers tested were developed for *Mugil cephalus* and *Mugil so-iuy*; however, of the 18 primers that amplified well, only 15 allowed for multiplexing in PCR, from which 10 were used for further analyses of genetic structure and diversity of *C. labrosus* (Supplementary material, Table S1). These markers amplified well due to the close phylogenetic relationship between these mugilid species (Durand et al., 2012b, 2012a; Xia et al., 2016). Although microsatellite diversity levels in *C. labrosus* differed depending on the loci compared, a lower number of alleles were observed in the sample analysed when compared to the populations of *M. cephalus* and *M. so-iuy* (Supplementary material, Table S2) (Shen et al., 2010; Xu et al., 2009, 2010), except for loci Mce6, Mce10 and Muce44. For example, the loci Mce8, Mce27, Muso22, Muso25 and Muso36 which are monomorphic

in *C. labrosus* display 4-8 alleles and 5-12 alleles for loci Mce8 and Mce27 in samples of *M. cephalus* from Taiwan, Peru, East Australia, and Spain (Shen et al., 2010), and four alleles each for loci Muso22, Muso25, and Muso36 in samples of *M. so-iuy* from China (Xu et al., 2009). At polymorphic loci Muce26 and Muce38, two and five alleles were obtained respectively in *C. labrosus* compared to 3 and 6 alleles in samples of both *M. so-iuy* and *M. cephalus* (Shen et al., 2010). To illustrate this difference between species, when comparing *Chelon ramada* and *Mugil liza*, three alleles were observed at the Mce27 locus of *C. ramada* from South Africa (Shen et al., 2010) but 10-11 alleles in samples of *M. liza* from Brazil and Argentina (Mai et al., 2014). Comparatively, more alleles were observed in *C. labrosus* samples on loci Mce6 (19 alleles), Mce10 (9 alleles) and Muce44 (9 alleles) (Table 2) compared to the 4-9 alleles at Mce6 and 4-6 alleles at Mce10 described in *M. cephalus*, and the 5 alleles at Muce44 described in both *M. cephalus* and *M so-iuy* (Shen et al., 2010). At the same time different allele numbers were found in *C. labrosus* vs *C. ramada* sampled in the same distribution range (Pereira et al., 2023) for Mce27 (1 allele vs 11 alleles), Mce10 (10 vs 17), Muso19 (3 vs 4) and Mce12 (13 vs 7) (Pereira et al., 2023). In samples of *M. curema* from the Gulf of Mexico, loci Mce6 and Mce10 only displayed 2-5 alleles each (Pacheco-Almanzar et al., 2017).

The average heterozygosity observed (0.49±0.02) was lower than the one declared for 12 marine fish species (0.77±0.19) reported by (DeWoody and Avise, 2000) in a review study which compared the genetic diversity in fishes occupying different habitats. Compared to other mugilid species, the average mean values of observed heterozygosity (H_O) in *C. labrosus* (0.437 – 0.559) (Table 2) were within the range observed for *M. curema* (0.372 – 0.530) (Pacheco-Almanzar et al., 2017), for *M. cephalus* (0.588 – 0.760 and 0.425 – 0.975) (Colín et al., 2020; Shen et al., 2010), for *C. ramada* (averaged 0.547 – 0.655 and 0.033 – 0.900) (Pereira et al., 2023 and Shen et al., 2010), for *Chelon auratus* (averaged 0.033 - 0.743) (Behrouz et al., 2018) and for *M. liza* (0.654 – 0.716) (Mai et al., 2014). The same trend was observed with the average values of expected heterozygosity (H_E). Furthermore, the observed heterozygosity values in *C. labrosus* were not only comparable to other mugilid species but were within the range reported in anadromous salmonids and brackish water fish and fell between the higher and lower genetically diverse marine and freshwater fish, respectively (DeWoody and Avise, 2000; Martinez et al., 2018). In all locations except for Ondarroa, the H_O in *C. labrosus* was lower than the expected H_E. Generally, with lower H_O than H_E, reduction in allelic variation and the existence of low-

frequency alleles may be due to changes in the marine ecosystems associated with anthropogenic climate change, pollution, habitat loss, and overexploitation (Collins et al., 2013; Halpern et al., 2007; Hoegh-Guldberg and Bruno, 2010). Such changes result in a reduction of the species' reproductive potential. However, this does not seem to be the case for *C. labrosus* in the SBB, a species that remains unexploited and thrives in polluted aquatic environments.

The presently validated molecular markers (ten heterozygous microsatellite loci) studied on 204 individuals did not find any significant genetic variation among individuals from the 7 different geographical origins studied. Five weak and marginally significant pairwise comparisons were recorded: BI – PA (F_{ST} = 0.0147, p = 0.0027), BI – GE (F_{ST} = 0.0128, p = 0.0027), CA – BI (F_{ST} = 0.0120, p = 0.0000), TG – GE (F_{ST} = 0.0176, p = 0.0181) and TG – BI (F_{ST} = 0.0269, p = 0.0000). These significant and small F_{ST} comparisons may be a product of temporal instability in gene frequencies (Dannewitz et al., 2005). In any case, the pairwise F_{ST} comparisons are very close to 0 and suggest that no genetic distinctions can be drawn between any two compared localities. More precisely, a lack of spatial genetic differentiation was observed in an AMOVA analysis (F_{ST} = 0.0098, p = 0.0000), where most of the variance was attributed from within the populations rather than from among populations (Table 6). The K = 1 gene pools depicted with the Bayesian clustering approach supported the single population group findings, reinforcing the lack of genetic differentiation between sampling locations (Figure 2).

This absence of genetic structuring in *C. labrosus* has been reported in many marine species that share similar biology. In *M. cephalus,* a lack of genetic and phylogeographic structure was reported in populations from the Gulf of Mexico and Atlantic Coasts (Rocha-Olivares et al., 2000) and along ~550 km of the Queensland coastline in Australia (Huey et al., 2013), despite using mtDNA and six highly polymorphic microsatellite loci, respectively. Typical panmictic populations show similar results. This is the case of *Anguilla anguilla* from southern and northern Europe (6 microsatellite loci and mtDNA sequences) (Palm et al., 2009; Ragauskas et al., 2014), *Anguilla japonicus* from East Asia (8 microsatellite loci and SNPs) (Gong et al., 2019; Yu et al., 2020), *Acanthopagrus australis* from Australia (6 microsatellite loci) (Roberts and Ayre, 2010), *Balaenoptera physalus* from the NE Atlantic (10 microsatellite loci) (Quintela et al., 2014) and most significantly in the related mugilid, catadromous and geographically close species *C. ramada* (11 microsatellite loci) (Pereira et al., 2023). In the Iberian Peninsula and the

Mediterranean, analysis of the genetic structure of 3 *Trachurus* species using restriction fragment length polymorphisms (RFLPs) on individuals from Atlantic and Mediterranean samples did not find any genetic variation among samples within *T. picturatus* and *T. mediterraneus* or European samples of *T. picturatus* (Comesaña et al., 2008; Karaiskou et al., 2004). These results were consistent with recent evaluations of *T. picturatus* population genetic structure in the same area when mtDNA and 10 polymorphic microsatellite loci were applied (Moreira et al., 2020, 2019). Furthermore, in two species belonging to the family Sparidae, mtDNA displayed little to no genetic differentiation in *Pagellus bogaraveo* and *Pagrus pagrus* when comparing Atlantic and Mediterranean individuals (Bargelloni et al., 2003). Such absence in genetic structuring in various marine fishes is commonly associated with two factors, *i.e.* a large effective population size that narrows the impact of genetic drift and life history traits that promote dispersal and high gene flow among populations either through passive dispersal of eggs and planktonic larvae or active migration of adults and or juveniles (Carvalho and Hauser, 1998; DeWoody and Avise, 2000; Martinez et al., 2018; Moreira et al., 2020; Pereira et al., 2023). *C. labrosus* exhibits those life history traits, synchronising spawning during winter (December – February) when spawning- or reproductive migrations involve the movement of maturing individuals from foraging areas in freshwater and estuarine environments into marine waters where they will spawn (Ortiz-Zarragoitia et al., 2014). The life-history and dispersal strategy along the Iberian coast suggests a metapopulation scenario, with a high season-related gene flow among the sampled locations preventing any stable genetic drift (Moreira et al., 2020; Pereira et al., 2023).

Several studies have shown that along the Basque coastline, individuals of *C. labrosus* inhabiting different contaminated estuaries exhibit varying levels of xenoestrogenicity (Bizarro et al., 2014; Ortiz-Zarragoitia et al., 2014; Puy-Azurmendi et al., 2013; Valencia et al., 2017). These individuals are geographically separated and are differentially exposed to xenoestrogens in their estuaries of residence. Prevalence of intersex (ovotestis) has been found all along the annual reproductive cycle, with percentages ranging from 3 to 83 of analysed males. Although no intersex has been recorded in individuals from Plentzia, the Pasaia and Gernika sites have been defined as xenoestrogenic pollution “hotspots” with an intersex prevalence of up to 56 and 83 respectively (Ortiz-Zarragoitia et al., 2014). Xenoestrogen concentrations measured in bile from individuals from Gernika have been as high as 7,942 ng g^{-1} nonylphenol (NPs) and 95 ng g^{-1} octylphenol (OPs) (Puy-Azurmendi

et al., 2013), and on average, 177.5 ng mL^{-1} bisphenol-A (BPA) and 1,508 ng mL^{-1} β-hexachlorocyclohexane (β-HCH) (Ros et al., 2015). In addition, intersex males at varying levels have been reported in other estuaries such as those of Bilbao, Ondarroa and Deba (Bizarro et al., 2014; Diaz De Cerio et al., 2012; Puy-Azurmendi et al., 2013; Rojo-Bartolomé et al., 2017; Valencia et al., 2017) while intersex has not been reported in individuals for other locations including BOC and TGM. Although the studies showed that different geographical population units were under different pressures of xenoestrogen pollution, pollution and the gonad phenotype that it generates do not define the different population units and the current microsatellite data does not support the existence of such discrete units.

F_{ST} and Bayesian clustering analysis show the population dynamics of *C. labrosus* in the SBB has been in synchrony, suggesting the contribution of gene flow to the lack of genetic partitioning of these populations. If free-swimming planktonic *Chelon* larvae are transported by oceanic currents in spring-summer from open waters to the coast randomly, if adults returning to estuaries after reproduction do not return to their estuary of origin and if reproduction occurs among adults of different estuaries, then a long-distance dispersal and gene flow over a wide geographic scale will be promoted (Whitfield, 2020; Whitfield et al., 2012). This is evidenced by the limited genetic structure observed (Pereira et al., 2023; Teodósio et al., 2016). Experimental evidence on such synergy is lacking for *C. labrosus,* though several coastal species have congeners or populations with this kind of distribution (Gandra et al., 2021; Huey et al., 2013; Liao et al., 2021; Moreira et al., 2020; Pereira et al., 2023; Rocha-Olivares et al., 2000). Regardless of the forces determining connectivity among *C. labrosus* in the Iberian Peninsula, the current microsatellites show that restrictions to gene flow seem to be unlikely. The lack of genetic differentiation found between the Atlantic Ocean and the Mediterranean Sea for other marine species (Comesaña et al., 2008; Debes et al., 2008; Karaiskou et al., 2004; Pereira et al., 2023) suggests that active barriers to connectivity seem to be non-functional on *C. labrosus,* confirming that the transition from the Atlantic to the Mediterranean might not be an efficient phylogeographic break for all species. The hypothesis of panmixia could therefore be well supported by these observations although spawning or breeding grounds for the species remains unknown.

Fish population genetic structure is often analysed using a variety of different molecular and statistical methods including RFLPs, mtDNA sequences, genotyping DNA microsatellites, amplified fragment length polymorphisms (AFLPs) and SNPs, and such an

approach banking on a battery of methodologies could help to improve our understanding of *Chelon labrosu*s populations. However, we need to adopt the use of other non-genetic population markers such as those based on the analysis of otolith shape and chemical signatures. Otoliths may inform about the life history of the fish within each estuary in the absence of genetic differences (Moreira et al., 2020, 2019).

5. Conclusions

In conclusion, our data set of ten microsatellites revealed a lack of spatial genetic structuring in 204 individuals of *C. labrosus* sampled at five locations along the SBB and two outgroup locations in the Bay of Cadiz and the Mediterranean Sea. The microsatellite results suggest that *C. labrosus* comprises a single panmictic population. None the less, it is important to highlight that greater geographical coverage and sampling size would be beneficial to support the existence of a unique genetic stock. However, panmixia does not rule out the possibility of adults always returning to their estuary of origin after reproductive migration to sea nor the probable existence of local population units. Genetic markers are more conservative at broad spatiotemporal scales than markers that are based on environmentally-dependent phenotypic traits (Moreira et al., 2020). Otolith elemental composition can be used to distinguish between groups of fishes that have experienced long-term separation because of varied environmental conditions such as water temperature, salinity, habitat and feeding conditions (Correia et al., 2011, 2014) and to tell us whether mullets migrating for reproduction from the xenoestrogen polluted estuary of Gernika always return to Gernika.

Acknowledgements

This work was funded by the Spanish Ministry of Science. Innovation and Universities and EU-FEDER/ERDF (BORN2bEGG PGC2018-101442-B-I00) and the Basque Government (Grants to consolidated research groups IT1302-19 and IT1743-22). A.N. is a recipient of a pre-doctoral grant PIF17/172 from the University of the Basque Country (UPV/EHU).

References

Avise, J.C., Helfman, G.S., Saunders, N.C., Hales, L.S., 1986. Mitochondrial DNA differentiation in North Atlantic eels: Population genetic consequences of an unusual life history pattern. Proceedings of the National Academy of Sciences 83, 4350–4354. https://doi.org/10.1073/pnas.83.12.4350

Bargelloni, L., Alarcon, J.A., Alvarez, M.C., Penzo, E., Magoulas, A., Reis, C., Patarnello, T., 2003. Discord in the family Sparidae (Teleostei): Divergent phylogeographical patterns across the Atlantic-Mediterranean divide. J Evol Biol 16, 1149–1158. https://doi.org/10.1046/j.1420-9101.2003.00620.x

Baumann, L., Knörr, S., Keiter, S., Nagel, T., Rehberger, K., Volz, S., Oberrauch, S., Schiller, V., Fenske, M., Holbech, H., Segner, H., Braunbeck, T., 2014. Persistence of endocrine disruption in zebrafish (*Danio rerio*) after discontinued exposure to the androgen 17β-trenbolone. Environ Toxicol Chem 33, 2488–2496. https://doi.org/10.1002/etc.2698

Behrouz, M., Norouzi, M., Samiei, M.H., Heshmatzad, P., 2018. Microsatellite analysis of golden grey mullet *Chelon auratus* (Risso, 1810) in the fereydoon - kenar and ramsar coasts (South Caspian Sea, Iran). Ribarstvo, Croatian Journal of Fisheries 76, 35–40. https://doi.org/10.2478/cjf-2018-0004

Bizarro, C., Ros, O., Vallejo, A., Prieto, A., Etxebarria, N., Cajaraville, M.P., Ortiz-Zarragoitia, M., 2014. Intersex condition and molecular markers of endocrine disruption in relation with burdens of emerging pollutants in thicklip grey mullets (*Chelon labrosus*) from Basque estuaries (South-East Bay of Biscay). Mar Environ Res 96, 19–28. https://doi.org/10.1016/j.marenvres.2013.10.009

Carvalho, G.R., Hauser, L., 1998. Advances in the molecular analysis of fish population structure. Italian Journal of Zoology 65, 21–33. https://doi.org/10.1080/11250009809386791

Cavalli-Sforza, L.L., Edwards, A.W.F., 1967. Phylogenetic analysis. Models and estimation procedures. Am J Hum Genet 19, 233–257. https://doi.org/10.2307/2406616

Chapuis, M.P., Estoup, A., 2007. Microsatellite null alleles and estimation of population differentiation. Mol Biol Evol 24, 621–631. https://doi.org/10.1093/molbev/msl191

Colín, A., Hernández-Pérez, Z., Guevara-Chumacero, L.M., Castañeda-Rico, S., Serrato-Díaz, A., Ibáñez, A.L., 2020. Are striped mullet (*Mugil cephalus*) philopatric? Mar Biol 167, 1–15. https://doi.org/10.1007/s00227-019-3622-1

Collins, S.M., Bickford, N., McIntyre, P.B., Coulon, A., Ulseth, A.J., Taphorn, D.C., Flecker, A.S., 2013. Population Structure of a Neotropical Migratory Fish: Contrasting Perspectives from Genetics and Otolith Microchemistry. Trans Am Fish Soc 142, 1192–1201. https://doi.org/10.1080/00028487.2013.804005

Comesaña, A.S., Martínez-Areal, M.T., Sanjuan, A., 2008. Genetic variation in the mitochondrial DNA control region among horse mackerel (*Trachurus trachurus*) from the Atlantic and Mediterranean areas. Fish Res 89, 122–131. https://doi.org/10.1016/j.fishres.2007.09.014

Cooke, S.J., Brooks, J.L., Raby, G.D., Thorstad, E.B., Brownscombe, J.W., Vandergoot, C.S., Lennox, R.J., Bulte, G., Bino, G., Thiem, J.D., 2022. Electronic Tagging and Tracking of Animals in Inland Waters, in: Tockner, K., Mehner, T. (Eds.), Encyclopedia of Inland Waters, Second Edition. Elsevier, pp. 699–712. https://doi.org/10.1016/B978-0-12-819166-8.00061-X

Correia, A.T., Pipa, T., Gonçalves, J.M.S., Erzini, K., Hamer, P.A., 2011. Insights into population structure of *Diplodus vulgaris* along the SW Portuguese coast from otolith elemental signatures. Fish Res 111, 82–91. https://doi.org/10.1016/j.fishres.2011.06.014

Correia, A.T.T., Hamer, P., Carocinho, B., Silva, A., 2014. Evidence for meta-population structure of *Sardina pilchardus* in the Atlantic Iberian waters from otolith elemental signatures of a strong cohort. Fish Res 149, 76–85. https://doi.org/10.1016/j.fishres.2013.09.016

Crosetti, D., Blaber, S. (Eds.), 2016. Biology, ecology and culture of grey mullets (Mugilidae), 1st ed. CRC Press. https://doi.org/10.1201/b19927

Crosetti, D., Cataudella, S., 1995. Grey mullet culture, in: Nash, C.E. (Ed.), World Animal Science 34B: Production of Aquatic Animals. Elsevier BV: Burlington, MA, USA, pp. 271–288.

Dannewitz, J., Maes, G.E., Johansson, L., Wickström, H., Volckaert, F.A.M., Järvi, T., 2005. Panmixia in the European eel: A matter of time... Proceedings of the Royal Society B: Biological Sciences 272, 1129–1137. https://doi.org/10.1098/rspb.2005.3064

Debes, P. V., Zachos, F.E., Hanel, R., 2008. Mitochondrial phylogeography of the European sprat (*Sprattus sprattus* L., Clupeidae) reveals isolated climatically vulnerable populations in the Mediterranean Sea and range expansion in the northeast Atlantic. Mol Ecol 17, 3873–3888. https://doi.org/10.1111/j.1365-294X.2008.03872.x

Dempster, A.P., Laird, N.M., Rubin, D.B., 1977. Maximum Likelihood from incomplete data via the EM algorithm. Journal of the Royal Statistical Society. Series B (Methodological) 39, 1–38. https://doi.org/10.1111/j.2517-6161.1977.tb01600.x

Devlin, R.H., Nagahama, Y., 2002. Sex determination and sex differentiation in fish: an overview of genetic, physiological, and environmental influences. Aquaculture 208, 191–364. https://doi.org/10.1016/S0044-8486(02)00057-1

DeWoody, J.A., Avise, J.C., 2000. Microsatellite variation in marine, freshwater and anadromous fishes compared with other animals. J Fish Biol 56, 461–473. https://doi.org/10.1006/jfbi.1999.1210

Diaz De Cerio, O., Rojo-Bartolomé, I., Bizarro, C., Ortiz-Zarragoitia, M., Cancio, I., 2012. 5S rRNA and accompanying proteins in gonads: powerful markers to identify sex and reproductive endocrine disruption in fish. Environ Sci Technol 46, 7763–7771. https://doi.org/10.1021/es301132b

Durand, J.D., Blel, H., Shen, K.N., Koutrakis, E.T., Guinand, B., 2013. Population genetic structure of *Mugil cephalus* in the Mediterranean and Black Seas: A single mitochondrial clade and many nuclear barriers. Mar Ecol Prog Ser 474, 243–261. https://doi.org/10.3354/meps10080

Durand, J.D., Chen, W.J., Shen, K.N., Fu, C., Borsa, P., 2012a. Genus-level taxonomic changes implied by the mitochondrial phylogeny of grey mullets (Teleostei: Mugilidae). C R Biol 335, 687–697. https://doi.org/10.1016/j.crvi.2012.09.005

Durand, J.D., Shen, K.N., Chen, W.J., Jamandre, B.W., Blel, H., Diop, K., Nirchio, M., Garcia de León, F.J., Whitfield, A.K., Chang, C.W., Borsa, P., 2012b. Systematics of the grey mullets (Teleostei: Mugiliformes: Mugilidae): Molecular phylogenetic evidence challenges two centuries of morphology-based taxonomy. Mol Phylogenet Evol 64, 73–92. https://doi.org/10.1016/j.ympev.2012.03.006

Earl, D.A., VonHoldt, B.M., 2012. STRUCTURE HARVESTER: a website and program for visualizing STRUCTURE output and implementing the Evanno method. Conserv Genet Resour 4, 359–361. https://doi.org/10.1007/s12686-011-9548-7

Evanno, G., Regnaut, S., Goudet, J., 2005. Detecting the number of clusters of individuals using the software STRUCTURE: A simulation study. Mol Ecol 14, 2611–2620. https://doi.org/10.1111/j.1365-294X.2005.02553.x

Excoffier, L., Laval, G., Schneider, S., 2005. Arlequin (version 3.0): An integrated software package for population genetics data analysis. Evolutionary Bioinformatics 1, 117693430500100. https://doi.org/10.1177/117693430500100003

Falush, D., Stephens, M., Pritchard, J.K., 2007. Inference of population structure using multilocus genotype data: Dominant markers and null alleles. Mol Ecol Notes 7, 574–578. https://doi.org/10.1111/j.1471-8286.2007.01758.x

Froese, R., Pauly, D., 2022. FishBase [WWW Document]. World Wide Web electronic publication. URL https://www.fishbase.se/search.php (accessed 6.15.22).

Gandra, M., Assis, J., Martins, M.R., Abecasis, D., 2021. Reduced global genetic differentiation of exploited marine fish species. Mol Biol Evol 38, 1402–1412. https://doi.org/10.1093/molbev/msaa299

García-Márquez, J., Galafat, A., Alarcón, F.J., Figueroa, F.L., Martínez-Manzanares, E., Arijo, S., Abdala-Díaz, R.T., 2021. Cultivated and Wild Juvenile Thick-Lipped Grey Mullet, *Chelon labrosus*: A Comparison from a Nutritional Point of View. Animals 11, 2112. https://doi.org/10.3390/ani11072112

Gong, X., Davenport, E.R., Wang, D., Clark, A.G., 2019. Lack of spatial and temporal genetic structure of Japanese eel (*Anguilla japonica*) populations. Conservation Genetics 20, 467–475. https://doi.org/10.1007/s10592-019-01146-8

Guo, S.W., Thompson, E.A., 1992. Performing the Exact Test of Hardy-Weinberg proportion for multiple alleles. Biometrics 48, 361—372. https://doi.org/10.2307/2532296

Halpern, B.S., Silliman, B.R., Olden, J.D., Bruno, J.P., Bertness, M.D., 2007. Incorporating positive interactions in aquatic restoration and conservation. Front Ecol Environ 5, 153–160. https://doi.org/10.1890/1540-9295(2007)5[153:IPIIAR]2.0.CO;2

Hoegh-Guldberg, O., Bruno, J.F., 2010. The impact of climate change on the British Isles. New Sci (1956) 206, 49. https://doi.org/10.1016/s0262-4079(10)61509-6

Huey, J.A., Espinoza, T., Hughes, J.M., 2013. Regional panmixia in the mullet *Mugil cephalus* along the coast of Eastern Queensland; revealed using six highly polymorphic microsatellite loci. Proceedings of the Royal Society of Queensland 118, 7–15. https://doi.org/10.3316/ielapa.684745616782467

Karaiskou, N., Triantafyllidis, A., Triantaphyllidis, C., 2004. Shallow genetic structure of three species of the genus *Trachurus* in European waters. Mar Ecol Prog Ser 281, 193–205. https://doi.org/10.3354/meps281193

Liao, T.-Y., Lu, P.-L., Yu, Y.-H., Huang, W.-C., Shiao, J.-C., Lin, H.-D., Jhuang, W.-C., Chou, T.-K., Li, F., 2021. Amphidromous but endemic: Population connectivity of Rhinogobius gigas (Teleostei: Gobioidei). PLoS One 16, 1–14. https://doi.org/10.1371/journal.pone.0246406

Mai, A.C.G., Miño, C.I., Marins, L.F.F., Monteiro-Neto, C., Miranda, L., Schwingel, P.R., Lemos, V.M., Gonzalez-Castro, M., Castello, J.P., Vieira, J.P., 2014. Microsatellite variation and genetic structuring in *Mugil liza* (Teleostei: Mugilidae) populations from Argentina and Brazil. Estuar Coast Shelf Sci 149, 80–86. https://doi.org/10.1016/j.ecss.2014.07.013

Martinez, A.S., Willoughby, J.R., Christie, M.R., 2018. Genetic diversity in fishes is influenced by habitat type and life-history variation. Ecol Evol 8, 12022–12031. https://doi.org/10.1002/ece3.4661

Mićković, B., Nikčević, M., Hegediš, A., Regner, S., Gačić, Z., Krpo-Ćetković, J., 2010. Mullet Fry (Mugilidae) in coastal waters of montenegro, their spatial distribution and migration phenology. Arch Biol Sci. https://doi.org/10.2298/ABS1001107M

Miggiano, E., Lyons, R.E., Li, Y., Dierens, L.M., Crosetti, D., Sola, L., 2005. Isolation and characterization of microsatellite loci in the striped mullet, *Mugil cephalus*. Mol Ecol Notes 5, 323–326. https://doi.org/10.1111/j.1471-8286.2005.00915.x

Moreira, C., Correia, A.T., Vaz-Pires, P., Froufe, E., 2019. Genetic diversity and population structure of the blue jack mackerel *Trachurus picturatus* across its western distribution. J Fish Biol 94, 725–731. https://doi.org/10.1111/jfb.13944

Moreira, C., Presa, P., Correia, A.T., Vaz-Pires, P., Froufe, E., 2020. Spatio-temporal microsatellite data suggest a multidirectional connectivity pattern in the *Trachurus picturatus* metapopulation from the Northeast Atlantic. Fish Res 225, 105499. https://doi.org/10.1016/j.fishres.2020.105499

Musyl, M.K., Domeier, M.L., Nasby-Lucas, N., Brill, R.W., McNaughton, L.M., Swimmer, J.Y., Lutcavage, M.S., Wilson, S.G., Galuardi, B., Liddle, J.B., 2011. Performance of pop-up satellite archival tags. Mar Ecol Prog Ser 433, 1–28. https://doi.org/10.3354/meps09202

Nash, J.P., Kime, D.E., Van der Ven, L.T.M., Wester, P.W., Brion, F., Maack, G., Stahlschmidt-Allner, P., Tyler, C.R., 2004. Long-term exposure to environmental concentrations of the pharmaceutical

ethynylestradiol causes reproductive failure in fish. Environ Health Perspect 112, 1725–1733. https://doi.org/10.1289/ehp.7209

Ortiz-Zarragoitia, M., Bizarro, C., Rojo-Bartolomé, I., De Cerio, O.D., Cajaraville, M.P., Cancio, I., 2014. Mugilid fish are sentinels of exposure to endocrine disrupting compounds in coastal and estuarine environments. Mar Drugs 12, 4756–4782. https://doi.org/10.3390/md12094756

Pacheco-Almanzar, E., Ramírez-Saad, H., Velázquez-Aragón, J.A., Serrato, A., Ibáñez, A.L., 2017. Diversity and genetic structure of white mullet populations in the Gulf of Mexico analyzed by microsatellite markers. Estuar Coast Shelf Sci 198, 249–256. https://doi.org/10.1016/j.ecss.2017.09.015

Palm, S., Dannewitz, J., Prestegaard, T., Wickström, H., 2009. Panmixia in European eel revisited: No genetic difference between maturing adults from southern and northern Europe. Heredity (Edinb) 103, 82–89. https://doi.org/10.1038/hdy.2009.51

Peakall, R., Smouse, P., 2006. GENALEX 6: Genetic analysis in Excel. Population genetic software for teaching and research. Mol Ecol Notes 6, 288–295. https://doi.org/10.1111/j.1471-8286.2005.01155.x

Peakall, R., Smouse, P.E., 2012. GenAlEx 6.5: genetic analysis in Excel. Population genetic software for teaching and research—an update. Bioinformatics 28, 2537–2539. https://doi.org/10.1093/bioinformatics/bts460

Pepping, M.Y., O'Rourke, S.M., Huang, C., Katz, J.V.E.E., Jeffres, C., Miller, M.R., 2020. Rapture facilitates inexpensive and high-throughput parent-based tagging in salmonids. PLoS One 15, 1–17. https://doi.org/10.1371/journal.pone.0239221

Pereira, E., Mateus, C.S., Alves, M.J., Almeida, R., Pereira, J., Quintella, B.R., Almeida, P.R., 2023. Connectivity patterns and gene flow among *Chelon ramada* populations. Estuar Coast Shelf Sci 281, 108209. https://doi.org/10.1016/j.ecss.2022.108209

Piferrer, F., Anastasiadi, D., 2021. Do the offspring of sex reversals have higher sensitivity to environmental perturbations? Review Article Sex Dev 15, 134–147. https://doi.org/10.1159/000515192

Pritchard, J.K., Stephens, M., Donnelly, P., 2000. Inference of population structure using multilocus genotype data. Genetics 155, 945–959. https://doi.org/10.1093/genetics/155.2.945

Pritchard, J.K., Wen, X., Falush, D., 2009. Documentation for structure software: Version 2.3 [WWW Document]. URL http://web.stanford.edu/group/pritchardlab/structure_software/release_versions/v2.3.2/structure_doc.pdf (accessed 2.9.21).

Puy-Azurmendi, E., Ortiz-Zarragoitia, M., Villagrasa, M., Kuster, M., Aragón, P., Atienza, J., Puchades, R., Maquieira, A., Domínguez, C., López de Alda, M., Fernandes, D., Porte, C., Bayona, J.M., Barceló, D., Cajaraville, M.P., 2013. Endocrine disruption in thicklip grey mullet (*Chelon labrosus*) from the Urdaibai Biosphere Reserve (Bay of Biscay, Southwestern Europe), Science of the Total Environment. Elsevier. https://doi.org/10.1016/j.scitotenv.2012.10.078

Quintela, M., Skaug, H.J., Øien, N., Haug, T., Seliussen, B.B., Solvang, H.K., Pampoulie, C., Kanda, N., Pastene, L.A., Glover, K.A., 2014. Investigating population genetic structure in a highly mobile marine organism: The minke whale *Balaenoptera acutorostrata acutorostrata* in the North East Atlantic. PLoS One 9, 108640. https://doi.org/10.1371/journal.pone.0108640

Ragauskas, A., Butkauskas, D., Sruoga, A., Kesminas, V., Rashal, I., Tzeng, W.-N.N., 2014. Analysis of the genetic structure of the European eel *Anguilla anguilla* using the mtDNA D-loop region molecular marker. Fisheries Science 80, 463–474. https://doi.org/10.1007/s12562-014-0714-1

Ramos-Júdez, S., Giménez, I., Gumbau-Pous, J., Arnold-Cruañes, L.S., Estévez, A., Duncan, N., 2022. Recombinant Fsh and Lh therapy for spawning induction of previtellogenic and early spermatogenic arrested teleost, the flathead grey mullet (*Mugil cephalus*). Sci Rep 12, 6563. https://doi.org/10.1038/s41598-022-10371-0

Raymond, M., Rousset, F., 1995. GENEPOP (Version 1.2): Population Genetics Software for Exact Tests and Ecumenicism. Journal of Heredity 86, 248–249. https://doi.org/10.1093/oxfordjournals.jhered.a111573

Rice, W.R., 1989. Analyzing tables of statistical tests. Evolution (N Y) 43, 223–225. https://doi.org/10.1111/j.1558-5646.1989.tb04220.x

Roberts, D.G., Ayre, D.J., 2010. Panmictic population structure in the migratory marine sparid *Acanthopagrus australis* despite its close association with estuaries. Mar Ecol Prog Ser 412, 223–230. https://doi.org/10.3354/meps08676

Rocha-Olivares, A., Garber, N.M., Stuck, K.C., 2000. High genetic diversity, large inter-oceanic divergence and historical demography of the striped mullet. J Fish Biol 57, 1134–1149. https://doi.org/10.1006/jfbi.2000.1379

Rojo-Bartolomé, I., de Souza, J.E.S., de Cerio, O.D., Cancio, I., 2020. Duplication and subfunctionalisation of the general transcription factor IIIA (gtf3a) gene in teleost genomes, with ovarian specific transcription of gtf3ab. PLoS One 15, 1–21. https://doi.org/10.1371/journal.pone.0227690

Rojo-Bartolomé, I., Martínez-Miguel, L., Lafont, A., Vílchez, M.C., Asturiano, J.F., Pérez, L., Cancio, I., 2017. Molecular markers of oocyte differentiation in European eel during hormonally induced oogenesis. Comp Biochem Physiol A Mol Integr Physiol 211, 17–25. https://doi.org/10.1016/j.cbpa.2017.05.018

Ros, O., Vallejo, A., Blanco-Zubiaguirre, L., Olivares, M., Delgado, A., Etxebarria, N., Prieto, A., 2015. Microextraction with polyethersulfone for bisphenol-A, alkylphenols and hormones determination in water samples by means of gas chromatography-mass spectrometry and liquid chromatography-tandem mass spectrometry analysis. Talanta 134, 247–255. https://doi.org/10.1016/j.talanta.2014.11.015

Shen, K.N., Chen, C.Y., Tzeng, W.N., Chen, J.D., Knibb, W., Durand, J.D., 2010. Development and characterization of 13 GT/CA microsatellite loci in cosmopolitan flathead mullet Mugil cephalus. In permanent genetic resources added to molecular ecology resources database 1 April 2010 – 31 May 2010 database. Mol Ecol Resour 10, 1098–1105. https://doi.org/doi: 10.1111/j.1755-0998.2010.02898.x

Sostoa, A., 1983. Las Comunidades de peces del Delta del Ebro. Universitat de Barcelona.

Teodósio, M.A., Paris, C.B., Wolanski, E., Morais, P., 2016. Biophysical processes leading to the ingress of temperate fish larvae into estuarine nursery areas: A review. Estuar Coast Shelf Sci 183, 187–202. https://doi.org/10.1016/j.ecss.2016.10.022

Valencia, A., Rojo-Bartolomé, I., Bizarro, C., Cancio, I., Ortiz-Zarragoitia, M., 2017. Alteration in molecular markers of oocyte development and intersex condition in mullets impacted by wastewater treatment plant effluents. Gen Comp Endocrinol 245, 10–18. https://doi.org/10.1016/j.ygcen.2016.06.017

Vallainc, D., Concu, D., Loi, B., Pitzalis, A., Frongia, C., Chindris, A., Carboni, S., 2022. Spawning induction and larval rearing in the thinlip gray mullet (*Chelon ramada*): The use of the slow release gonadotropin releasing hormone analog (GnRHa) preparation, leuprorelin acetate. Anim Reprod Sci 247, 107145. https://doi.org/10.1016/j.anireprosci.2022.107145

Van Oosterhout, C., Hutchinson, W.F., Wills, D.P.M., Shipley, P., 2004. MICRO-CHECKER : software for identifying and correcting genotyping errors in microsatellite data. Mol Ecol Notes 4, 535–538. https://doi.org/10.1111/j.1471-8286.2004.00684.x

Wagner, A.P., Creel, S., Kalinowski, S.T., 2006. Estimating relatedness and relationships using microsatellite loci with null alleles. Heredity (Edinb) 97, 336–345. https://doi.org/10.1038/sj.hdy.6800865

Weir, B.S., Cockerham, C.C., 1984. Estimating F-Statistics for the Analysis of Population Structure. Evolution (N Y) 38, 1358. https://doi.org/10.2307/2408641

Whitfield, A.K., 2020. Fish species in estuaries-from partial association to complete dependency. J Fish Biol 97, 1262–1264. https://doi.org/10.1111/jfb.14476

Whitfield, A.K., Panfili, J., Durand, J.D., 2012. A global review of the cosmopolitan flathead mullet *Mugil cephalus* Linnaeus 1758 (Teleostei: Mugilidae), with emphasis on the biology, genetics, ecology and fisheries aspects of this apparent species complex, Reviews in Fish Biology and Fisheries. https://doi.org/10.1007/s11160-012-9263-9

Wright, S., 1978. Variability within and among natural populations, in: Evolution and the Genetics of Populations. University of Chicago Press.

Wright, S., 1965. The interpretation of population structure by F-statistics with special regard to systems of mating. Evolution (N Y) 19, 395–420. https://doi.org/10.1111/j.1558-5646.1965.tb01731.x

Xia, R., Durand, J.D., Fu, C., 2016. Multilocus resolution of Mugilidae phylogeny (Teleostei: Mugiliformes): Implications for the family's taxonomy. Mol Phylogenet Evol 96, 161–177. https://doi.org/10.1016/j.ympev.2015.12.010

Xu, G., Shao, C., Liao, X., Tian, Y., Chen, S., 2009. Isolation and charaterization of polymorphic microsatellite loci from so-iuy mullet (*Mugil soiuy* Basilewsky 1855). Conservation Genetics 10, 653–655. https://doi.org/10.1007/s10592-008-9602-5

Xu, T.-J., Sun, D.-Q., Shi, G., Wang, R.-X., 2010. Development and characterization of polymorphic microsatellite markers in the gray mullet (*Mugil cephalus*). Genetics and molecular research 9, 1791–1795. https://doi.org/10.4238/vol9-3gmr909

Yu, L., Liu, Y., Liu, J., 2020. Gene-associated microsatellite markers confirm panmixia and indicate a different pattern of spatially varying selection in the endangered Japanese eel *Anguilla japonica*. J Oceanol Limnol 38, 1572–1583. https://doi.org/10.1007/s00343-020-0048-z

SUPPLEMENTARY MATERIAL

Table S1 Set of 46 microsatellite primers previously described for the *Mugil cephalus* complex Miggiano et al. (2005), Xu et al. (2009), Xu et al. (2010) and Shen et al. (2010) that were screened on a representative sample of 30 individuals from different locations under study. Polymorphic loci are in bold and underlined, monomorphic loci are in bold and loci that worked but were not selected are in bold and asterisks.

Table S2 Number of alleles based on 15 microsatellite loci for *C. labrosus* compared to the number of alleles previously described for the *Mugil cephalus* complex Miggiano et al. (2005), Xu et al. (2009), Xu et al. (2010) and Shen et al. (2010).

Table S3 Genotypic linkage disequilibrium for each validated locus among populations ($P < 0.05$).

Table S4 Genotypic linkage disequilibrium for each locus pair across all populations (Fisher´s method; $P < 0.05$).

Table S5 Estimated null allele frequencies for all loci in *C. labrosus* populations Two loci show evidence for a null allele. The population is possibly in Hardy Weinberg equilibrium with loci Mce25, Mce6, showing signs of a null allele (MICROCHECKER).

Table S6 Mantel test table geographic distance. X is the geographic distance (km) and Y the pairwise F_{ST} values for locations categorized in Sample 1 vs Sample 2. The numerical numbers 1 – 7 represent the locations from which samples were collected from. 1 = Pasaia, 2 = Ondarroa, 3 = Gernika, 4 = Plentzia, 5 = Bilbao, 6 = Cadiz and 7 = Thermaic Gulf.

Figure S1 Delta *K* plot of Evanno test based on STRUCTURE analysis for ten microsatellites in samples of *Chelon labrosus.* A very low Delta *K* value was observed, with a peak at $K = 2$ in the plot of estimated Delta *K* versus *K*.

Figure S2 STRUCTURE plots from microsatellite data for *C. labrosus* using an admixture model with LOCPRIOR. Presence of a single group is represented by a singl e red colour, with the proporition of each bar assigned to a single colour representing the probability that an individual belongs to that group.

Table S1

Set of 46 microsatellite primers previously described for the *Mugil cephalus* complex Miggiano et al. (2005), Xu et al. (2009), Xu et al. (2010) and Shen et al. (2010) that were screened on a representative sample of 30 individuals from different locations under study. Polymorphic loci are in bold and underlined, monomorphic loci are in bold and loci that worked but were not selected are in bold and asterisks.

No.	Locus	Primer Sequence	T_A	PCR Size	Accession #	Reference
1	*Mcs2FH-F*	GCAGTGAAATAAACAGGCACCTCTCA	65	191-267	AY770925	Miggiano et. al., 2005
	Mcs2FH-R	TGTGGGGTATGAAGTCCTCTTGCTC				
2	*Mcs17FM-F*	TCACCTCTAACCACTACTCCACAGCTTC	65	184-277	AY770932	
	Mcs17FM-R	ATTCCCGTCAGTAACGGCGGATG				
3	*Mcs16EM-F*	CAGATTGTTGTTCGGGAGGGCAGA	65	270-347	AY770930	
	Mcs16EM-R	GTCATGATGCTGCTATCAGGCAAA				
4	*Mcs1EH-F*	ACCGGGCTTTAGGCTGTTGGTCA	63	271-334	AY770926	
	Mcs1EH-R	TGAGACACATCCCATCACTGCCTACG				
5	*Mcs2DM-F*	CATGGGCATCTTTATCGCTCTCAA	63	191-267	AY770922	
	Mcs2DM-R	CAACTTAATTTCCCTTCGGGGATGA				
6	*Mcs6DM-F*	GACAACCTAATTTACCTTTGGGGATGA	60	226-341	AY770923	
	Mcs6DM-R	TGCTTCGTGTTTGATGGGGAATTTG				
7	*Mcs16GM-F*	CACTGTGTGGACGTGAACACGTTATG	64	215-283	AY770931	
	Mcs16GM-R	CGGTAGCTAGTCGCTGCTATGGACA				
8	*Mcs4GH-F*	GACATCCCCAAAACAGAAAGCAGA	63	229-337	AY770924	
	Mcs4GH-R	GCGTGGACTAACCCAAGCTGTGTC				
9	*Mcs15AM-F*	GAGCCAAACTGGTCACATGAAAGAGA	63	186-338	AY770927	
	Mcs15AM-R	ACTTTCAGTGCAGCGCCCAGTGTT				
10	*Mcs15CM-F*	GGATTAGTGGCGGACTTCTGTGAA	60	156-257	AY770928	
	Mcs15CM-R	CTCTTTCAATTATGTCAGTGGTATGGCTTC				
11	*Mcs16DM-F*	ACAAATACTAGATGCTTTGCACACCCTTAC	63	144-205	AY770929	
	Mcs16DM-R	GGCCTACAGATTTCCTTCTTTATGCTAGGC				
12	*Muso08-F*	CACAGCAAACACAGCCTGAT	53	342–346	EU570283	Xu et al., 2009
	Muso08-R	AGAGAGGGAGCAAGGGAAAG				
13	*Muso09-F*	TCGCTGAAGGCACTAAATCA	53	156–162	EU570284	
	Muso09-R	CGAGCTCACGTACAGCAAAT				
14	*Muso10-F*	TTGCTCAGGGAACACATTGA	53	236–252	EU570285	
	Muso10-R	CAAACAGAGACGTGATGCAAA				

Table S1 continued…

No.	Locus	Primer Sequence	T_A	PCR Size	Accession #	Reference
15	*Muso16-F*	TGAACTGTGACCCTCGTTGA	57	234–250	EU570291	
	Muso16-R	GGAGAGGTTGGCTCGTCATA				
16	***Muso19-F***	CACCACTATGGCATCCTTCA	57	146–158	EU570294	
	Muso19-R	AACCCCTTTTCTTGCTCAAA				
17	***Muso22-F***	TGATGAGAATGGTGGTGACG	57	194–212	EU570294	
	Muso22-R	TTTTGGGCTGCTTGTCTCTC				
18	***Muso25-F***	ATGAAAAGGGAGGGGCAATA	57	184–190	EU570300	
	Muso25-R	CTGCTCACCTTGCGTTTACA				
19	****Muso27-F***	CTTGGCTGCCTGTATCCTGT	57	164–172	EU570302	
	****Muso27-R***	CCTGAGAGTGAGGGGTCAAC				
20	***Muso32-F***	GCAGTGCACATGGTAACAAAA	57	182–186	EU570307	
	Muso32-R	CGCCTACAGCATCAGACAAG				
21	***Muso36-F***	TCCTTTATGGGGAGACGATG	57	190–198	EU570311	
	Muso36-R	CCCAATAGCCACAAATGTCC				
22	*Muce-9-F*	ATAAAGACTTGAAGGGAA	48	100~134	HM060969	T-J Xu et al., 2010
	Muce-9-R	GTTGAGGTAGTTAGGAGC				
23	*Muce-14-F*	AGTGACACCGTATCTGGTC	50	284~334	HM060970	
	Muce-14-R	CTCCGTAGTAGTAACAATGAAA				
24	*Muce-16-F*	TGGCTGGGTCCGTTAGAT	48	166~178	HM060971	
	Muce-16-R	TGGCGTCACAAGAACATTAG				
25	***Muce-26-F***	TGCGGAGACAATGTAAAC	50	244~274	HM060972	
	Muce-26-R	AAATGAAACAATCCACCC				
26	*Muce-37-F*	TACTCAGCCAGCAGGTGT	47	228~248	HM060973	
	Muce-37-R	AATACAGGGTTGTTGTCG				
27	***Muce-38-F***	GCACCAACATCTCACCTG	50	259~337	HM060974	
	Muce-38-R	CCTACCATTTACCCCTCT				
28	***Muce-44-F***	GCTTCGGAGGACCAAC	51	183~203	HM060975	
	Muce-44-R	CGACAGCCACTGTTATG				
29	*Muce-51-F*	TGTCCGTTTTGGTAAGC	49	159~169	HM060976	
	Muce-51-R	TCGCCTTTTCATCTCA				
30	*Muce-55-F*	AGAAGAAGACAGGGACTC	47	74~136	HM060977	
	Muce-55-R	AGAAATACTCTGCTAACCT				

Table S1 continued…

No.	Locus	Primer Sequence	T_A	PCR Size	Accession #	Reference
31	*Muce-57-F*	GCGATCATCTCCACAATA	50	117~121	HM060978	
	Muce-57-R	CGTTCACAGTGCGTAACAG				
32	***Muce-74-F**	GACCCGTCGGCTATGTAA	50	111~241	HM060979	
	***Muce-74-R**	GATTTGTTGCTCCGTATCT				
33	***Muce-80-F**	ACTGGGTTCAGATAGAAAT	49	198~238	HM060980	
	***Muce-80-R**	CTCGTGGAGGAAACATAA				
34	***Mce-2-F***	AGCCAAAGTTCCTGTAAGTACG	58	143	HM004324	Shen et al., 2010
	Mce-2-R	TCAGATTAGGACCCGACCATA				
35	*Mce-3-F*	GGAGGACTAGGATTTCGTG	54	159	HM004325	
	Mce-3-R	CTTATCCCTGACCTTCTCAT				
36	*Mce-4-F*	TCGCACGCCCGTAATAGC	58	185	HM004326	
	Mce-4-R	TACCGCCCTCCCTCCAAC				
37	***Mce-6-F***	GAGGAGGCTCGGAGGATT	54	197	HM004328	
	Mce-6-R	CGGGGCTTGTGACAGTTT				
38	*Mce-7-F*	GCCCCGAGATGGAGAAGA	58	196	HM004329	
	Mce-7-R	AAGATGGAACAAGGCAAAGAG				
39	***Mce-8-F***	AGGGATTGGGTTTAGGCG	58	176	HM004330	
	Mce-8-R	GTGCTCGACACTTTAGACTGAT				
40	***Mce-10-F***	CCACTGTAGGGCTGTATGC	54	138	HM004331	
	Mce-10-R	GGGAGGAGGATTTCTCAA				
41	***Mce-11-F***	ATTAGCCAGGGCCACCAG	58	165	HM004332	
	Mce-11-R	CAGAAGCCAAAAGGACGG				
42	*Mce-14-F*	TAATACGATGTGCTTTGTCCC	58	159	HM004335	
	Mce-14-R	CATAACCTCCACCTGCTGAC				
43	*Mce-22-F*	ACGCATTGAGCAGACATGAACT	58	122	HM004343	
	Mce-22-R	TGACCCTACGTACGTATCAG				
44	*Mce-24-F*	AAAGTCTGAATGGAGCGCAG	58	121	HM004345	
	Mce-24-R	TCCTGAATCTCTGGTGACAGC				
45	***Mce-25-F***	TCGGCATGTATATGAAAGCAC	58	141	HM004346	
	Mce-25-R	ACATAACTCTGCCACTGCTTG				
46	***Mce-27-F***	ACTGTGCACTTCTGGTTTCC	58	135	HM004348	
	Mce-27-R	ACATCTTTGAGGTTGCCC				

Table S2
Number of alleles based on 15 microsatellite loci for *C. labrosus* compared to the number of alleles previously described for the *Mugil cephalus* complex Miggiano et al. (2005), Xu et al. (2009), Xu et al. (2010) and Shen et al. (2010).

	Chelon labrosus	***Mugil so-iuy***		***Mugil cephalus***				***Liza ramada***
Locus	**Northeast Atlantic & Mediterranean Sea (This study)**	**China (Xu et al., 2009)**	**China (Xu et al., 2010)**	**Taiwan (Shen et al., 2010)**	**Peru (Shen et al., 2010)**	**East Australia (Shen et al., 2010)**	**Spain (Shen et al., 2010)**	**South Africa (Shen et al., 2010)**
Muce44	9	5	5	-	-	-	-	-
Muso25	1	4	-	-	-	-	-	-
Muso36	1	4	-	-	-	-	-	-
Mce27	1	-	-	12	6	5	7	3
Mce6	19	-	-	9	4	8	7	7
Mce11	6	-	-	5	7	6	5	-
Mce25	2	-	-	14	5	-	16	1
Muce38	5	6	6	-	-	-	-	-
Muso22	1	4	-	-	-	-	-	-
Mce10	9	-	-	6	4	-	5	12
Muce26	2	3	3	-	-	-	-	-
Mce8	1	-	-	4	6	8	6	3
Mce2	13	-	-	32	10	8	16	8
Muso32	3	3	-	-	-	-	-	-
Muso19	3	8	-	-	-	-	-	-

Table S3
Genotypic linkage disequilibrium for each validated locus among populations ($p < 0.05$).

Pop	Locus#1	Locus#2	P-Value	S.E.	Switches
PA	Muce44	Mce10	0.03636	0.008017	6083
PA	Muce44	Muso32	0.04414	0.004159	22865
PA	Mce10	Muso32	0.04180	0.003573	21395
ON	Muce38	Muso32	0.00601	0.001002	23774
GE	Muce44	Mce6	0.00468	0.004680	1934
GE	Muce44	Muce38	0.03027	0.005912	5885
PL	Muce26	Muso32	0.04907	0.001948	30291
BI	Mce11	Muce26	0.00608	0.001577	4446
BI	Muce38	Muso32	0.01731	0.001936	14464
CA	Muce44	Mce11	0.03907	0.008244	3558
CA	Muce44	Mce25	0.03681	0.005256	3324
CA	Mce25	Muce26	0.02218	0.001673	6883
CA	Muce44	Muso19	0.03821	0.004844	3287
CA	Mce25	Muso19	0.00140	0.000357	2834
CA	Muce26	Muso19	0.02156	0.001715	6847
TG	Mce6	Muce38	0.03090	0.005958	4804
TG	Muce38	Mce2	0.04367	0.006094	5428
TG	Muce26	Muso32	0.00523	0.000732	13271
TG	Muso19	Muso32	0.03793	0.001620	11711

Table S4
Genotypic linkage disequilibrium for each locus pair across all populations (Fisher´s method; $p < 0.05$).

Locus pair	Chi-square test (χ^2)	df	*p*-value
Muce44 & Mce25	6.603971	2	0.036810
Muce44 & Mce10	23.974834	14	0.046144
Mce25 & Muso19	13.142566	2	0.001400
Muce26 & Muso19	12.001914	4	0.017337
Muce38 & Muso32	27.737252	14	0.015414
Muso19 & Muso32	11.625710	4	0.020363

Table S5
Estimated null allele frequencies for all loci in *C. labrosus* populations Two loci show evidence for a null allele. The population is possibly in Hardy Weinberg equilibrium with loci Mce25, Mce6 which are in bold, showing signs of a null allele (MICROCHECKER).

Locus	Null Present	Oosterhout	Chakraborty	Brookfield 1	Brookfield 2
Muce44	no	0.0557	0.0942	0.0582	0.2311
Muso36	no	0	0	0	0
Mce27	no	0	0	0	0
Muso25	no	0	0	0	0
Mce11	no	0.0524	0.0625	0.0444	0.0444
Mce25	yes	0.1710	1.0000	0.0644	0.0644
Mce6	yes	0.0960	0.1093	0.0902	0.0902
Muce38	no	0.1121	0.1579	0.0698	0.3615
Mce10	no	-0.0227	-0.0228	-0.0200	0.0000
Muso22	no	0	0	0	0
Muce26	no	0.1569	0.4774	0.0634	0.2837
Mce2	no	0.0106	0.0105	0.009	0.1056
Mce8	no	0	0	0	0
Muso19	no	0	0	0	0
Muso32	no	-0.0068	-0.0067	-0.0045	0.1945

Table S6
Mantel test table geographic distance. X is the geographic distance (km) and Y the pairwise F_{ST} values for locations categorized in Sample 1 vs Sample 2. The numerical numbers 1 – 7 represent the locations from which samples were collected from: 1 = Pasaia, 2 = Ondarroa, 3 = Gernika, 4 = Plentzia, 5 = Bilbao, 6 = Cadiz and 7 = Thermaic Gulf.

X	Y	Sample 1	Sample 2
40.499	0.002	1	2
60.159	0.009	1	3
19.667	0.005	2	3
82.741	0.010	1	4
42.838	0.001	2	4
23.940	0.011	3	4
87.957	0.015	1	5
47.485	0.006	2	5
27.823	0.013	3	5
9.736	0.010	4	5
765.934	0.004	1	6
774.548	0.000	2	6
780.055	0.004	3	6
795.216	0.006	4	6
789.413	0.020	5	6
306.762	0.010	1	7
318.694	0.011	2	7
326.717	0.018	3	7
344.697	0.010	4	7
340.416	0.027	5	7
459.762	0.004	6	7

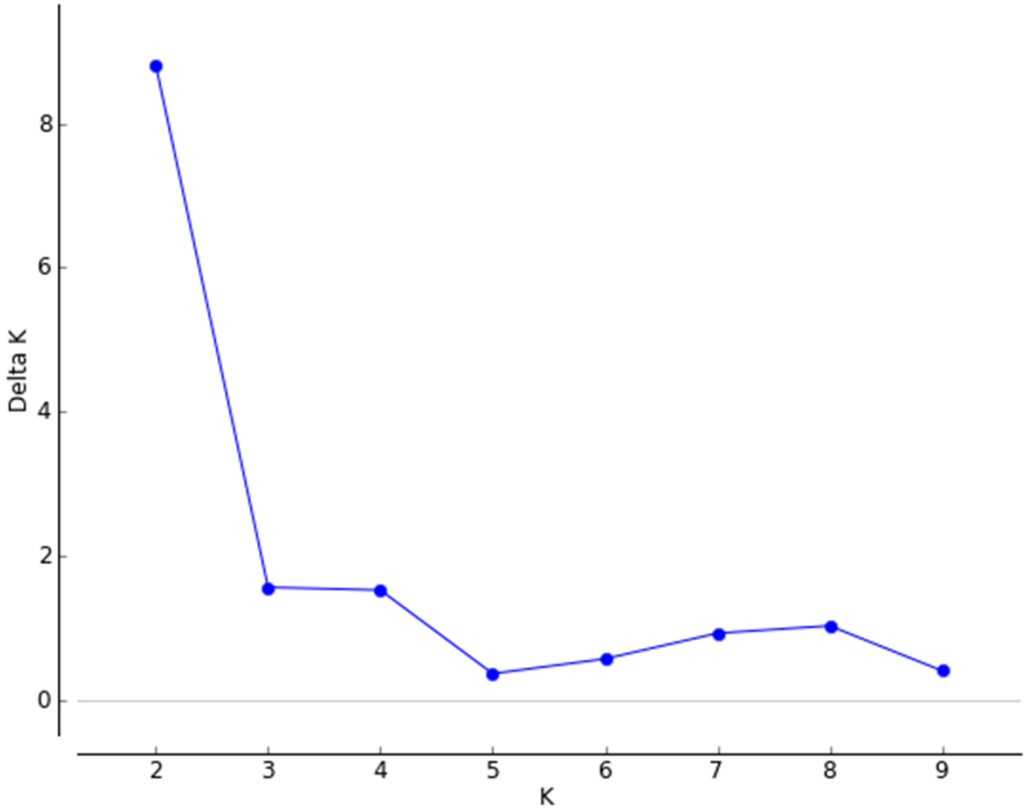

Figure S1
Delta *K* plot of Evanno test based on STRUCTURE analysis for ten microsatellites in samples of *Chelon labrosus*. A very low Delta *K* value was observed, with a peak at *K* = 2 in the plot of estimated Delta *K* versus *K*.

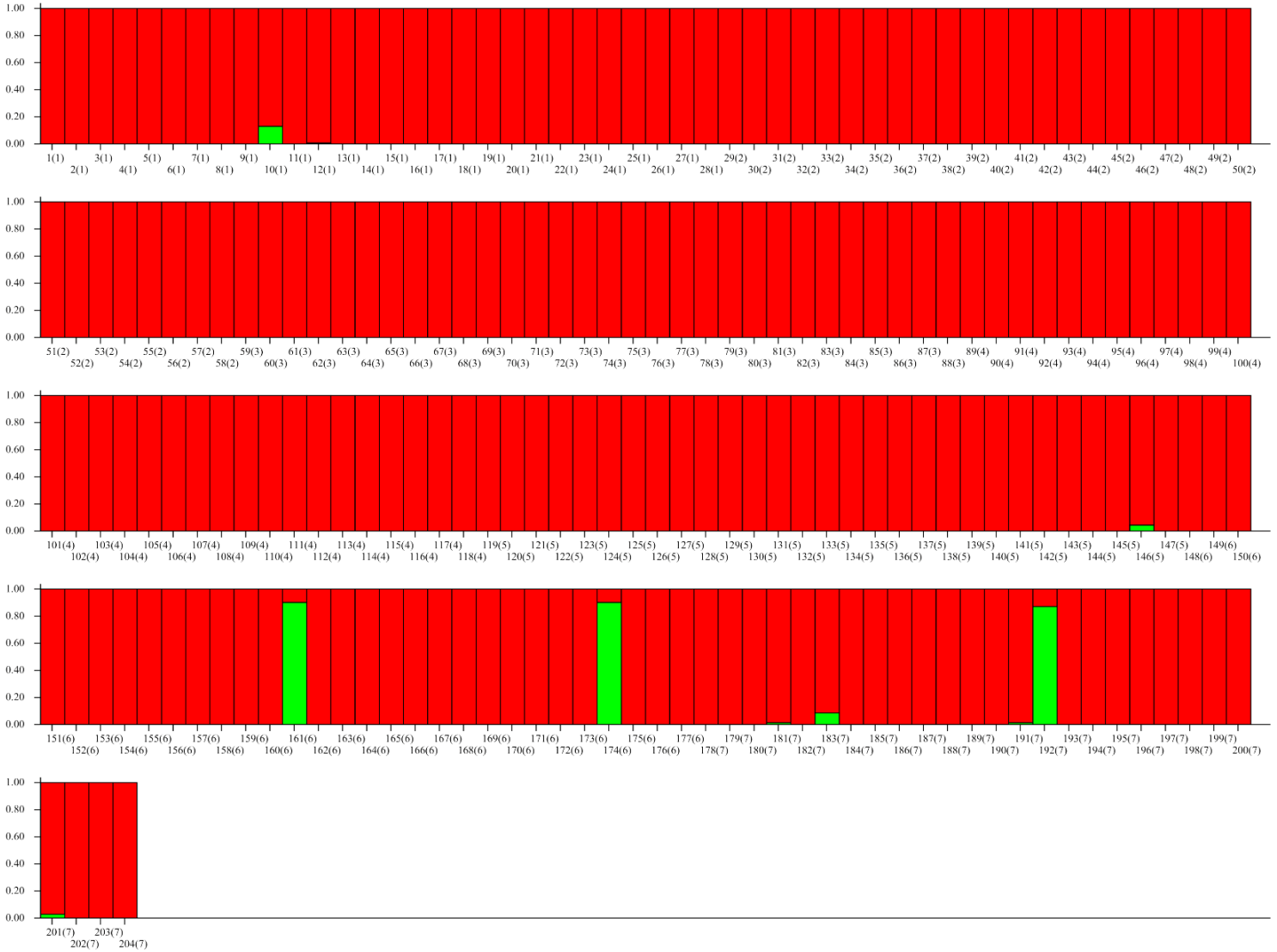

Figure S2
STRUCTURE plots from microsatellite data for *C. labrosus* using an admixture model with LOCPRIOR. Presence of a single group is represented by a single red colour, with the proportion of each bar assigned to a single colour representing the probability that an individual belongs to that group.

Chapter 4

Otolith shape and elemental signatures provide insights into the connectivity of euryhaline (*Chelon labrosus*) inhabiting two close estuaries with different burdens of xenoestrogens in the Southern Bay of Biscay

ARTICLE

Nzioka, A., Cancio, I., Diaz de Cerio, O., Pinto, E., Almeida, A., Correia, A.T., 2023. Otolith shape and elemental signatures provide insights into the connectivity of euryhaline *Chelon labrosus* inhabiting two close estuaries with different burdens of xenoestrogens in the Southern Bay of Biscay. Mar. Environ. Res. 189, 106075. https://doi.org/10.1016/j.marenvres.2023.106075

CONGRESS

IX Iberian Congress of Ichthyology (SIBIC2022), 20th – 23rd JUNE 2022, Porto, Portugal. **Anthony Nzioka**, Ibon Cancio, Oihane Diaz de Cerio, Maren Ortiz-Zarragoitia, Edgar Pinto, Agostinho Almeida and Alberto Teorodico Correia (2022). "Use of otolith shape and elemental signatures to infer the population structure of the thicklip grey mullet *Chelon labrosus* in the Southern Bay of Biscay." Poster Communication. https://doi.org/10.3390/blsf2022013071

ASSEMBLE Plus Conference 2022 – Marine Biological Research at the Frontier, 13th – 24th June 2022, online. **Anthony Nzioka,** Oihane Diaz de Cerio, Alberto Teodorico Correia, Ibon Cancio. (2022). "Otolith microstructure and microchemistry analyses to evaluate the population structure of the thicklip grey mullet, *Chelon labrosus*, in the Southern Bay of Biscay – FISHOTOTRACKING." Oral Communication.

ASSEMBLE Plus Closing Assembly, 14th – 15th September 2022, Paris, France. **Anthony Nzioka**, Ibon Cancio, Oihane Diaz de Cerio, Maren Ortiz-Zarragoitia, Edgar Pinto, Agostinho Almeida and Alberto Teorodico Correia (2022). "Otolith microstructure and microchemistry analyses to evaluate the population structure of the thicklip grey mullet, *Chelon labrosus*, in the Southern Bay of Biscay – FISHOTOTRACKING." Poster Communication.

Resumen

Se han observado gónadas intersexuales en el muble *Chelon labrosus*, que habita estuarios con altas cargas de xenoestrógenos en el sureste del Golfo de Vizcaya, pero se carece de conocimientos sobre la conectividad poblacional entre estuarios para esta especie de pez euryhalino. Este estudio investiga la estructura poblacional de *C. labrosus* utilizando la forma de los otolitos y las firmas elementales de 60 adultos (longitud total ~ 38 cm) de dos estuarios separados por 21 millas náuticas, uno con una alta incidencia de condición intersexual (Gernika), y el otro prístino (Plentzia). Los análisis de la forma de los otolitos se realizaron mediante descriptores elípticos de Fourier, mientras que las firmas elementales de los sagittae enteros se obtuvieron mediante espectrofotometría de masas con plasma acoplado inductivamente. Se aplicaron estadísticas univariantes y multivariantes para determinar si las firmas de los otolitos mostraban patrones de homogeneidad entre estuarios. Los datos indicaron diferencias significativas en la forma del otolito y la composición elemental entre los mubles de Gernika y Plentzia. Las diferencias elementales se debieron principalmente a Sr, Li (ambos más altos en Plentzia) y Ba (más alto en Gernika). La tasa de éxito en la reclasificación del 98% obtenida a partir del análisis de la función discriminante lineal por pasos sugiere que los individuos de Gernika y Plentzia forman unidades de población separadas. La limitada conectividad entre estos dos estuarios cercanos indicaría una historia vital diferente de exposición a sustancias químicas, lo que podría explicar la alta prevalencia de la condición intersexual en Gernika y su ausencia en Plenztia.

Palabras clave: *Historia de contaminación, peces, Mugilidae, etiquetas naturales, historia de vida, poblaciones*

Abstract

Intersex gonads have been observed in thicklip grey mullet *Chelon labrosus*, inhabiting estuaries with high burdens of xenoestrogens in the Southeast Bay of Biscay, but knowledge of population connectivity among estuaries is lacking for this euryhaline fish species. This study investigates the population structure of *C. labrosus* using otolith shape and elemental signatures of 60 adults (overall length ~ 38 cm) from two estuaries 21 nautical miles apart, one with a high incidence of intersex condition (Gernika), and the other one pristine (Plentzia). Otolith shape analyses were performed using elliptical Fourier descriptors, while elemental signatures of whole sagittae were obtained by inductively coupled plasma mass spectrophotometry. Univariate and multivariate statistics were applied to determine if otolith signatures show patterns of homogeneity between estuaries. The data indicated significant differences in the otolith shape and elemental composition between mullets of Gernika and Plentzia. Elemental differences were mainly driven by Sr, Li (both higher in Plentzia) and Ba (higher in Gernika). The 98% re-classification success rate obtained from stepwise linear discriminant function analysis suggests that Gernika and Plentzia individuals form separated population units. The limited connectivity between these two close estuaries would indicate a different life history of exposure to chemicals, which might explain the high prevalence of intersex condition in Gernika and its absence in Plenztia.

Keywords: *Contamination history, fish, Mugilidae, natural tags, life history, populations*

Abbreviations

ANOVA, Analysis of variance
BPA, bisphenol-A
CRM, Certified Reference Material
E_2, 17β-oestradiol
ECAE, Ethics Committee for Animal Experimentation
EFD, elliptic Fourier descriptors
GADM, global administrative areas (database**)**
HNO_3, nitric acid
ICP-MS, Inductively Coupled Plasma Mass Spectrometry
MANOVA, Multivariate analysis of variance
MES, multi-elemental signatures
mtDNA, mitochondrial DNA
NIES, National Institute for Environmental Studies
NP, nonylphenol
QGIS, quantum geographic information system (software)
RR, recovery rate
RSD, relative standard deviation
SBB, Southern Bay of Biscay
SLDFA, Stepwise linear discriminant function analysis
SNP, single nucleotide polymorphism
UNESCO, United Nations Educational, Scientific and Cultural Organisation
WWTP, wastewater treatment plant

1. Introduction

Otoliths are paired metabolically inert bio-mineralized crystalline-organic complex structures found in the inner ears of teleost fishes which are used for balance and hearing (Thomas and Swearer, 2019). They are mainly composed of calcium carbonate (~98%) and an organic matrix (~2%), and grow continuously, resulting in conspicuous growth bands generated by seasonal variations in the aragonitic matrix as they grow (Hüssy et al., 2021). During growth, otoliths incorporate different minor and trace elements from the local aquatic environment through which a fish passes during its lifetime, thus providing a record of their life history and habitat residency (Hüssy et al., 2021; Thomas and Swearer, 2019). Otolith shape and elemental composition may show intra-specific geographic variations depending on the genetics, environmental conditions (water temperature, salinity and others), feeding regime, fish condition, growth, maturation and reproduction (Hüssy et al., 2021; Izzo et al., 2018; Sturrock et al., 2015). However, the extent to which these processes influence otolith chemistry is still poorly understood (Hoff et al., 2022; Moreira et al., 2018; Reis-Santos et al., 2018). Differences in shape and elemental composition in otoliths provide a method to unravel the population structure and habitat connectivity of fish that may reflect the level of connectivity between different individuals of one single species (Moreira et al., 2022; Schroeder et al., 2022; Soeth et al., 2019).

The thicklip grey mullet *Chelon labrosus* (Risso, 1827) is a member of the family Mugilidae, which consists of approximately 25 genera and 80 species widely distributed around the world in tropical and temperate regions (Xia et al., 2016). It is a long-lived and slow-growing euryhaline demersal fish species broadly distributed along the eastern Atlantic Ocean from southern Scandinavia and Iceland to Senegal and Cape Verde, and across the Mediterranean and Black Seas (Freyhof and Kottelat, 2008; Froese and Pauly, 2022; Turan, 2016). It occupies inshore areas, estuaries, rivers, coastal lagoons and seas, thereby supporting artisanal and recreational fisheries (Freyhof and Kottelat, 2008; Froese and Pauly, 2022; Turan, 2016) *C. labrosus* is known to use estuaries as nursery areas or foraging habitats, migrating daily in and out of the estuaries with the tidal regime (Froese and Pauly, 2022; Whitfield, 2020). It is catadromous, spawning yearly at sea in coastal surface waters during the winter season (December – February), and pelagic eggs hatch in 3-4 days, with the pelagic larval stage lasting approximately four weeks (González-Castro and Minos, 2016). In coastal environments, juveniles form dense schools, migrating to inshore coastal waters and shallow estuaries, that in the Mediterranean Sea, occurs during

the first and second month of life for *C. labrosus* (Crosetti and Cataudella, 1995; Hickling, 1970; Koutrakis, 2016; Mićković et al., 2010). The species can survive in highly polluted environments, making it a good choice as an estuarine pollution sentinel organism (Ortiz-Zarragoitia et al., 2014).

Strong xenoestrogenic effects have been reported in *C. labrosus* individuals from contaminated estuaries along the Basque coast (Bizarro et al., 2014; Diaz De Cerio et al., 2012; Ortiz-Zarragoitia et al., 2014; Puy-Azurmendi et al., 2013; Valencia et al., 2017). This has been mainly linked to exposure to alkylphenols, pesticides and other xenoestrogens from wastewater treatment plant (WWTP) effluents that are discharged into estuaries, resulting in the development of intersex individuals (Bizarro et al., 2014; Ortiz-Zarragoitia et al., 2014; Puy-Azurmendi et al., 2013). Intersex gonads show the simultaneous occurrence of male and female reproductive stages in a gonochoristic species, mostly characterized by the presence of oocytes in testicular tissue (ovotestes) (Bahamonde et al., 2013). An abnormally high number of intersex testes (up to 83%) has been identified in *C. labrosus* males sampled in the Urdaibai estuary near Gernika, and these individuals have also shown accumulation of xenoestrogenic compounds such as bisphenol A (BPA; up to 177.5 ng mL^{-1}), oestradiol (E_2; up to 27 ng mL^{-1}) and nonylphenol (NPs; up to 1142 ng mL^{-1}) (Bizarro et al., 2014; Ortiz-Zarragoitia et al., 2014; Puy-Azurmendi et al., 2013; Ros et al., 2015). Additionally, varying prevalence of intersex condition have been reported in *C. labrosus* males captured from Bilbao (Nerbioi-Ibaizabal estuary), near the WWTP of Galindo (9%) and the Arriluze marina (10%), the fishing port of Ondarroa (50%), the port of Deba (20%) and the industrial harbour of Pasaia (56%) at the mouth of Oiartzun River (Bizarro et al., 2014; Diaz De Cerio et al., 2012; Ortiz-Zarragoitia et al., 2014; Puy-Azurmendi et al., 2013; Ros et al., 2015; Valencia et al., 2017). However, mullets sampled from the leisure port of Plentzia have shown normally developing testes with no incidences of intersex condition (Bizarro et al., 2014; Ortiz-Zarragoitia et al., 2014; Ros et al., 2015). The development of intersex condition thus appears to be estuarine-specific depending on the pollution load present in each estuary (Bizarro et al., 2014; Diaz De Cerio et al., 2012; Ortiz-Zarragoitia et al., 2014; Puy-Azurmendi et al., 2013).

The limited knowledge about the population structure and connectivity of *C. labrosus* in the Southern Bay of Biscay (SBB), prevents the understanding of the history of chemical exposure and the development of gonadal alterations in mullets. It could be perfectly feasible that an adult mullet from Plentzia might travel to Gernika after any of its yearly

reproductive migrations. Several methods, including natural tags (body morphometrics and meristics, otoliths, scales count, presence of parasites, population genetic structure) and applied or artificial markers (mark-recapture), can be used to identify and discriminate fish population (Cadrin et al., 2014; Marengo et al., 2017). In genetic approaches, highly polymorphic microsatellite DNA markers provide great resolution for identifying population structure (Durand et al., 2013; Ward, 2000), however, genetic variation between population groups may be inadequate, especially where low and inconsistent levels of genetic differentiation exist (Marengo et al., 2017; Moreira et al., 2019a; Ward, 2000). For such marine fish populations, with long larval stages, without physical barriers and high genetic flow, other approaches such as those studying otoliths might be useful in distinguishing geographically separated populations by discriminating the heterogeneous environmental conditions the fish has lived in (Correia et al., 2012; Marengo et al., 2017; Soeth et al., 2019).

Thus, the use of otolith shape and elemental signatures could provide insights into whether *C. labrosus* constitute a single interconnected population in the Basque coast or whether a meta-population structure exists. Interpreting the migratory patterns of *C. labrosus* within and among estuaries may unravel the time during which fish are first exposed to xenoestrogens and intersex condition is developed. Therefore, it is important to define the mobility pattern of *C. labrosus* between and within estuaries in the Basque coast to better understand the reproductive constraints that exposure to xenoestrogens at the local level could have on the populations.

2. Materials and methods

2.1. Study area

Two estuaries located in the Basque coast in the SBB in northern Spain (*c.* 21 nautical miles apart) were selected as the sampling areas: the Plentzia estuary (43°24′25.794″ N, 2°56′46.921″ W) located in the resort town of Plentzia, and the Urdaibai estuary (43°19′26.389″ N, 2°40′25.46″ W) located within the Urdabai Biosphere Reserve (declared by UNESCO in 1984) in the town of Gernika (Figure 1). In between these two estuaries, there lies a small estuary (*c.* 9 miles from Plentzia and *c.* 12 miles from Gernika) in the town of Bakio (43° 25′51″ N, 2° 48′40″ W) that is drained inland by the river Estepona (Marigómez et al., 2013).

Plentzia estuary is a relatively shallow meso-tidal estuary (tidal variation ~2.5 m) that forms the tidal part of the 7.9 km long Butron River (Leorri et al., 2013), and has a small leisure port near the tidal inlet and the adjacent beaches of Plentzia and Gorliz. Pollution inputs are minimal and the local WWTP that collects urban wastewater from ~10,0000 inhabitants discharge its effluent outside the estuary through a submarine pipe extending ~1 km offshore at a depth of ~18 m (Mijangos et al., 2018). Urdaibai estuary is also a shallow (mean depth of 3 m) meso-macrotidal estuary that is 12.5 km long and receives freshwater input from the Oka River (Iriarte et al., 2015). Major impacts can be attributed to the direct discharge of effluent from the Gernika WWTP at a narrow and very shallow stretch of the river within the estuary. This old WWTP receives domestic and industrial wastes from the town of Gernika and its surrounding areas (~26,000 inhabitants).

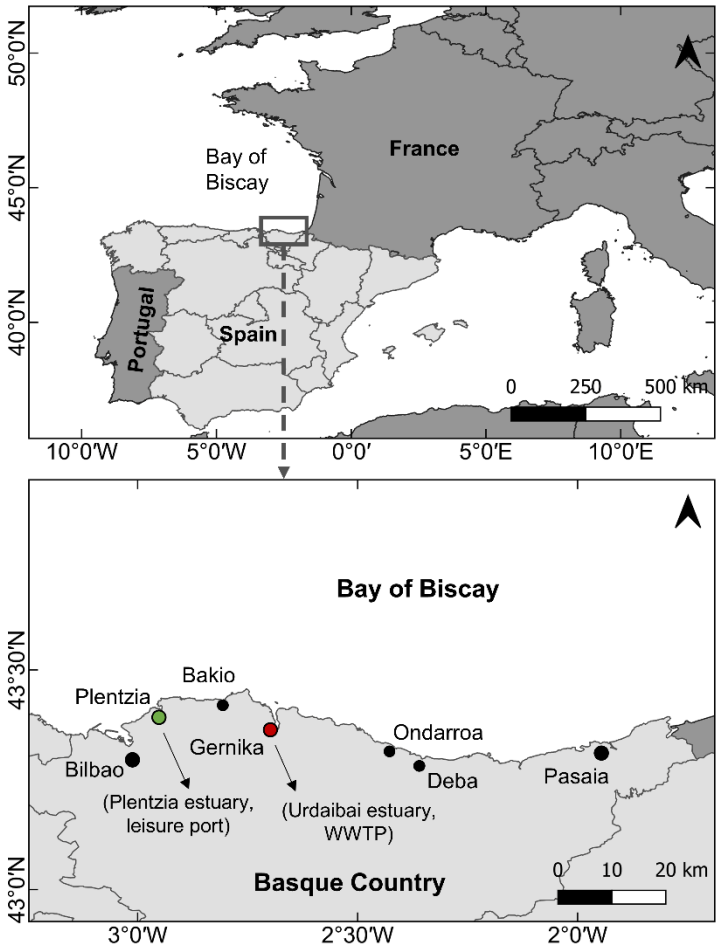

Figure 1
Overview of sampling locations for *Chelon labrosus* along the Basque coast. Brackets indicate the main activity in the location and nearby wastewater treatment plants (WWTP) indicated. The green dot marks the location with no prevalence of intersex conditions (Plentzia) while the red dot marks the location where intersex condition was prevalent (Gernika). This figure was produced with the GADM database (www.gadm.org), version 4.1, 16 July 2022 and QGIS version 3.18.0-Zürich.

2.2. Sample collection

Adult thicklip grey mullets (*Chelon labrosus*) were caught using a fishing rod in Plentzia (PL; n = 30) and Gernika (GE; n = 30) within a period of three weeks in June 2020. The fish were anaesthetized in a saturated benzocaine/seawater bath and preserved in ice before being taken to be processed in the laboratory. The individuals were measured for total length (TL, 1 mm) and weighed (W, 1 g). The mean total length and weight of individuals selected (± Standard Error) were 38.41 ± 0.70 cm and 778.07 ± 36.00 g for Gernika, and 37.45 ± 0.93 cm and 617.13 ± 37.49 g and for Plentizia. The mean Fulton's condition factor, K_F = [100*(W/TL^3)], of the selected individuals, was 1.37 ± 0.05 for Gernika and 1.15 ± 0.04 for Plentzia. Sagittal otoliths from each fish were removed using plastic forceps to avoid metallic contamination, cleaned of any adherent tissues with ultrapure water (Milli-Q water, 0.52 μS cm^{-1}) and air-dried in clean and labelled Eppendorf tubes. The right otolith was used for shape analysis, while the left otolith was used for microchemistry analysis. All fishing activities and handling procedures were carried out in accordance with the Ethics Committee for Animal Experimentation of the UPV/EHU and with the permission for sampling activities of the regional authorities.

2.3. Otolith shape analysis (elliptic Fourier descriptors)

Right sagittal otoliths were placed with the sulcus acusticus up (convex side down) and the rostrum to the left side. Orthogonal two-dimensional digital images were captured using a stereomicroscope at 10× magnification (Meiji Techno EMZ-13TR, Meiji Techno Co. Ltd, Saitama, Japan) coupled to a USB digital camera (Olympus SC30) with the analySIS getIT software (Olympus Soft Imaging Solutions GmBH, Münster, Germany). Full colour (*.jpg) and high-resolution (2048 × 1532) microphotographs of each otolith were captured using reflected light against a dark background (Figure 2A).

To determine whether the shape of the otoliths varied between locations, elliptic Fourier descriptors (EFD) was used to describe the shape outline of each otolith. EFD fits a closed curve to an ordered set of data points and decomposes the contour into a sum of harmonically related ellipses (Kuhl and Giardina, 1982) giving consistent results suitable for use in statistical comparisons between samples (Mérigot et al., 2007; Moura et al., 2020; Muniz et al., 2021).

The digitized otolith images were analysed using the R package *shapeR* (Libungan and Pálsson, 2015). The outlines were detected by transforming the images into grey-scale and

converting them to black and white images using a threshold pixel value. The outlines were later superimposed on the original image to verify consistency and a weighted moving average over three successive coordinate points used to eliminate pixel noise from the captured outline (Figure 2B) (Libungan and Pálsson, 2015). Mean EFD were obtained by rotating all otoliths positioned horizontally along the longest axis, setting the area equal in all otoliths and drawing a polar axis (radial) horizontally from the otolith centroid to the right which corresponds to the 0° angle of the otolith outline (Figure 2C). Fourier coefficients standardized to otolith size (i.e., otolith length) were used to obtain the normalized EFD (Libungan and Pálsson, 2015). A level of 95% of accumulated variance was used to select the minimum number of harmonics. The first 12 harmonics reached >95% of the cumulative power and gave 45 normalized Fourier coefficients (48 – 3 = 45), with the first three coefficients (a1, b1 and c1) omitted due to standardisation in relation to size, rotation and starting point. One coefficient showed significant interactions between populations and otolith length ($p < 0.05$) (i.e., otolith length having an effect on site-specific differences) and was thus excluded from further analysis. While applying the Bonferroni adjustment to account for increased alpha error due to multiple testing of the different coefficients (Sokal and Rohlf, 1995), all coefficients were included. The inclusion of the one coefficient did not affect the results of the overall analysis.

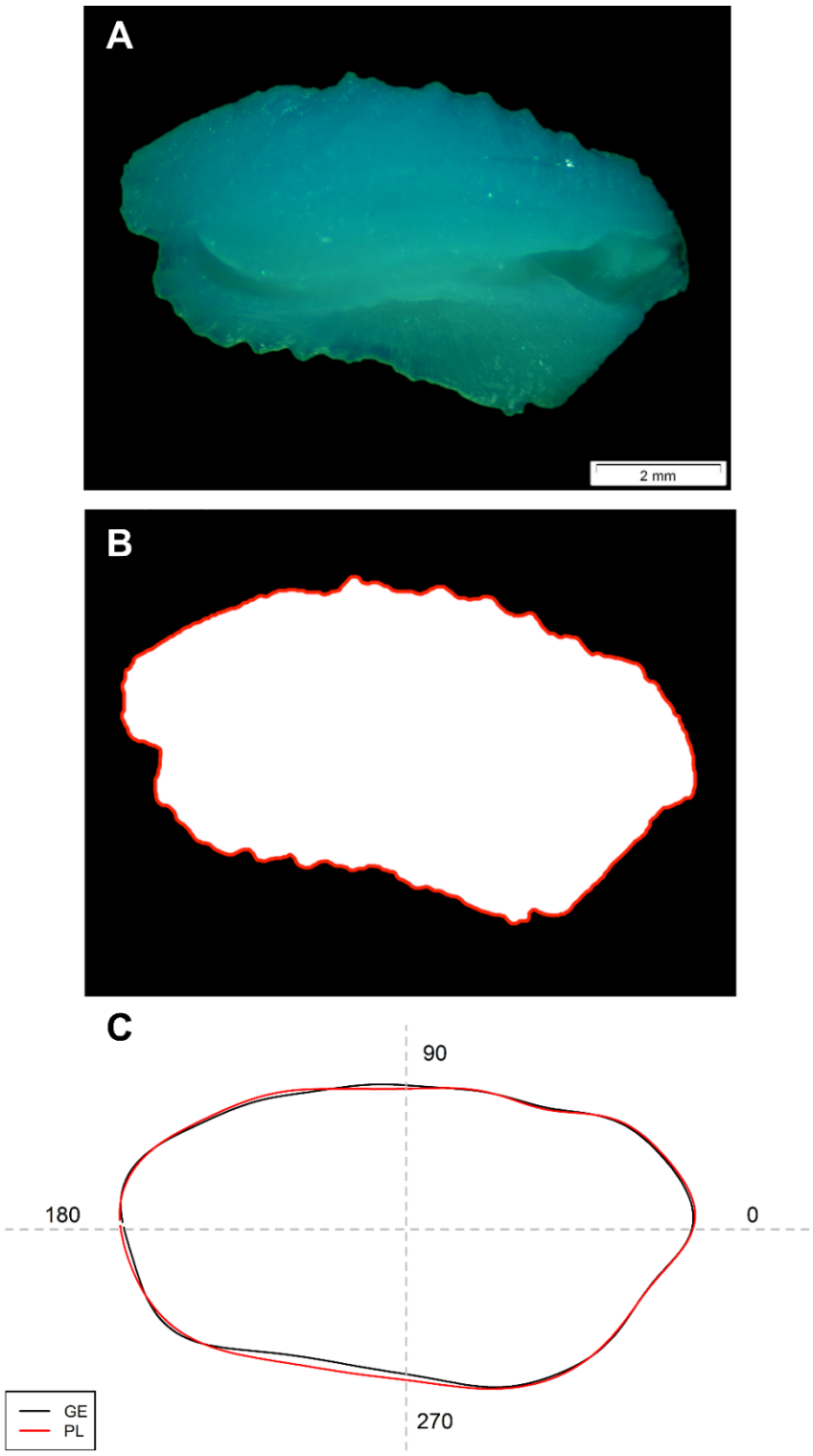

Figure 2
Medial view of the right sagittal otolith microphotograph of *Chelon labrosus*: (A) the original image with ×10 magnification, (B) the corresponding binary image and (C) the averaged outlined contour for each location based on Elliptical Fourier Descriptor (EFD) reconstructions. (GE = Gernika; PL = Plentzia; Scale bar = 2.0 mm).

2.4. Otolith elemental analyses (element:Ca)

Right otoliths were cleaned in an ultrasonic bath for 5 min in ultrapure water (Thermo Scientific, Lab Tower EDI 15, Thermo Electron LED GmbH, Langenselbold, Germany), followed by immersion in 200 µL of 3% analytical grade hydrogen peroxide solution (H_2O_2, Fluka Analytical) for 15 min to remove any adherent biological tissues. The otoliths were then rinsed in ultrapure 1% nitric acid (HNO_3) solution (Fluka Trace Select, > 69%) for 10 s and triple-washed in ultrapure water for 5 min to remove the acid (Rooker et al., 2001). Finally, otoliths were stored in pre-decontaminated Falcon tubes and allowed to dry overnight in a laminar flow hood (Moura et al., 2020; Patterson et al., 1999; Rooker et al., 2001). The decontaminated otoliths were then weighed (otolith mass: OM, 0.00001 g) on an analytical balance (Secura225D-1S, Sartorius Lab Instruments GmbH, Goettingen, Germany), dissolved for 15 min in 300 µL of ultrapure nitric acid (HNO_3, Fluka Trace Select, > 69%) and then diluted with ultrapure water to a final volume of 15 mL [2% HNO_3 (v/v) and 0.02% TDS (m/v)] before stirring with a vortex (Moura et al., 2020).

Twelve elements (^{137}Ba, ^{43}Ca, ^{111}Cd, ^{59}Co, ^{65}Cu, ^{7}Li, ^{26}Mg, ^{55}Mn, ^{60}Ni, ^{208}Pb, ^{88}Sr, ^{66}Zn), were analysed by Inductively Coupled Plasma Mass Spectrometry (ICP-MS) using an iCAP™ Q (Thermo Fisher Scientific, Bremen, Germany) instrument equipped with a concentric glass nebulizer, a Peltier-cooled baffled cyclonic spray chamber, a standard quartz torch and a two-cone interface design (nickel sample and skimmer cones). Argon of high-purity (99.9997%, Gasin II, Leça da Palmeira, Portugal) was used as the nebulizer and plasma gas. The Qtegra™ software (Thermo Fisher Scientific, Bremen, Germany) was used for instrument control and data acquisition. The instrument was operated under the following conditions: RF power, 1550 W; argon flow rate, 14 L min^{-1}; auxiliary argon flow rate, 0.8 L min^{-1}; nebulizer flow rate, 0.98 L min^{-1}. Indium (^{115}In), Scandium (^{45}Sc), Yttrium (^{89}Y) and Terbium (^{159}Tb) were monitored as internal standards. Otolith samples were analysed in random order to avoid possible sequence effects.

Procedural blanks and Fish Otolith Certified Reference Material (CRM; NIES 22, National Institute for Environmental Studies; https://www.nies.go.jp/) were similarly prepared for blank corrections, accuracy of calculations and quality precision of the analysis of selected trace elements in fish otolith. The precision of individual elements was determined from the percentage of the relative standard deviation (RSD, %) of three replicate measurements. The accuracy, expressed as a percentage of the recovery rate (RR,

%), was checked using the NIES22. The limit of detection (LOD) were obtained from the individual calibration of the curves using the three sigma criteria. Nine elements (^{137}Ba, ^{43}Ca, ^{59}Co, ^{65}Cu, ^{7}Li, ^{26}Mg, ^{55}Mn, ^{60}Ni, ^{88}Sr) were consistently above the LOD: Ba (0.021 µg L^{-1}), Ca (8630 µg L^{-1}), Co (0.016 µg L^{-1}), Cu (0.060 µg L^{-1}), Li (0.013 µg L^{-1}), Mg (0.096 µg L^{-1}), Mn (0.016 µg L^{-1}), Ni (0.014 µg L^{-1}) and Sr (0.025 µg L^{-1}). The precision expressed as the relative standard deviation (RSD) ranged between 0.98% and 3.49%, and the accuracy expressed as the recovery rate (RR) varied from 82% to 110%; both values (RSD and RR) are within the analytical accepted values (Dove et al. 1996: RSD: <20% and RR: 75%-125%). The trace element concentrations, originally in µg element/L solution, were thereafter transformed to µg element/g otolith and finally to µg element/g calcium (Higgins et al., 2013).

2.5. Data analysis

The mean EFD reconstruction was used to evaluate the main differences in otolith contours among the two different locations (Libungan and Pálsson, 2015). Spatial differences in otolith shape variability were visualized using the otolith mean length-standardized elliptic Fourier descriptors with the Canonical Analysis of Principal Coordinates (CAP) (Anderson and Willis, 2003) using the *vegan* package (Oksanen et al., 2022) in R software (R Core Team, 2023). CAP analyses were based on Euclidean distance (modified Gower dissimilarity index) and an ANOVA-like permutation test for Canonical Correspondence Analysis (CCA), also in *vegan*, was used to test the partition of variation among groups (Libungan and Pálsson, 2015). P-values were generated using 1000 permutations.

Before any statistical analyses, elemental signatures (element:Ca) were checked for normality (Shapiro-Wilk test, $P > 0.05$) and homogeneity of variances (Levene's test, $p > 0.05$), and the few outliers that were detected and trunked using Grubb´s test. Ba:Ca, Mg:Ca and Mn:Ca were log(x+1) transformed to meet these assumptions. To ensure that site-specific differences in otolith chemistry were not confounded by otolith mass (OM) (Gerard and Muhling, 2010), the relationship between elemental ratios and OM was evaluated using analysis of covariance (ANCOVA), with OM as a covariate and location as a fixed factor (Campana et al., 2000; Correia et al., 2021; Moura et al., 2020). This relationship was significant for Ba:Ca (positive relationship, $r^2 = 0.347$, $p = 0.000$), Mg:Ca (negative relationship, $r^2 = 0.240$, $p = 0.065$), Mn:Ca (negative relationship, $r^2 = 0.294$, $p = 0.184$) and

Sr:Ca (positive relationship, $r^2 = 0.76$, $p = 0.000$). The effect of OM on otolith chemistry was thus removed by subtracting the product of the common within-group linear slope and OM from the observed elemental ratios:

$$[X]D = [X] - (b \times covariate) \quad (1)$$

where $[X]_D$ is the detrended elemental concentration, $[X]$ the original element concentration and b the ANCOVA slope value (Campana et al., 2000).

Analysis of variance (ANOVA) was used to explore differences in individual shape and elemental variables between the two locations ($p < 0.05$). Multivariate analysis of variance (MANOVA) was used to test for differences in the otolith shape and multi-elemental signatures from different locations and approximate F-ratio statistic (Pillai's trace) was reported for MANOVA (Correia et al., 2021, 2012). Stepwise linear discriminant function analysis (SLDFA) was used to visualize differences in locations and to examine the re-classification accuracy of fish to their original location, verified through the percentage of correct re-classification of the discriminant functions using a jack-knifed ("leave one out") matrix (Correia et al., 2021, 2014). All statistical analyses were performed using open access R software version 3.6.3 (R Core Team, 2020) and Systat v.12 software (SYSTAT Software Inc., San Jose, CA, USA). A level of significance (α) level of 0.05 was used for all two-tailed statistical tests, with data presented as means ± standard errors (SE).

3. Results

3.1. Otolith shape analysis (elliptic Fourier analyses)

Three individual EFD (c2, a5 and c5) (Table 1) presented significant differences between individuals from Gernika and Plentzia (One-Way ANOVA, $p < 0.05$). MANOVA statistical tests performed on the EFD showed significant differences between Gernika and Plentzia (MANOVA, Pillai´s Trace $F_{2.101} = 0.48$, $p < 0.05$). The canonical analysis of principal coordinates (CAP) plot displayed a clear separation between individuals from Gernika and Plentzia (Figure 3A), identifying two groups (One-Way ANOVA, $p < 0.05$). CAP and stepwise linear discriminant function analysis (SLDFA) showed distinct population units of *C. labrosus* from Gernika and Plentzia, although two individuals from Gernika were re-classified by the SLDFA to Plentzia and one individual the other way around (Table 2).

Table 1
C. labrosus otolith elliptic Fourier descriptors (EFD) values for Gernika and Plentzia sampling locations. Eighteen EFD at 95% accumulation were selected, with the first three (a1, b1 and c1 constants) excluded. For each EFD, overall significant differences between Gernika and Plentzia populations (One-Way ANOVA, $p < 0.05$) were highlighted in bold. Data are presented as mean values ± SE.

Variable	Gernika	Plentzia	One-Way ANOVA	
			F-statistic	P-value
EFD				
d1	−0.587 ± 0.005	−0.596 ± 0.006	1.233	0.271
a2	−0.012 ± 0.003	−0.009 ± 0.002	0.760	0.387
b2	−0.004 ± 0.003	−0.014 ± 0.005	3.052	0.086
c2	0.015 ± 0.002	0.028 ± 0.005	4.505	**0.038**
d2	0.007 ± 0.002	0.001 ± 0.003	1.354	0.249
a3	−0.061 ± 0.002	−0.063 ± 0.002	1.164	0.285
b3	−0.001 ± 0.002	−0.005 ± 0.002	2.004	0.162
c3	−0.024 ± 0.002	−0.023 ± 0.002	0.516	0.475
d3	−0.058 ± 0.002	−0.057 ± 0.002	0.015	0.902
a4	0.002 ± 0.001	0.000 ± 0.001	1.072	0.305
b4	0.008 ± 0.001	0.008 ± 0.001	0.024	0.877
c4	0.010 ± 0.002	0.007 ± 0.002	1.928	0.170
d4	−0.015 ± 0.001	−0.012 ± 0.002	1.981	0.165
a5	−0.011 ± 0.001	−0.014 ± 0.001	4.965	**0.030**
b5	−0.002 ± 0.001	−0.003 ± 0.001	0.291	0.591
c5	0.012 ± 0.001	0.007 ± 0.001	6.399	**0.014**
d5	−0.006 ± 0.001	−0.004 ± 0.002	1.461	0.232
a6	0.007 ± 0.001	0.006 ± 0.001	0.215	0.644

3.3. Otolith elemental analyses (element:Ca)

Significant differences among locations for Ba:Ca, Li:Ca and Sr:Ca (One-Way ANOVAs, $p < 0.05$) were observed (Figure 4). Ba:Ca showed lower mean ratio values for Plentzia, while Li:Ca and Sr:Ca showed higher mean ratio values (Figure 4). No significant differences were found between the locations for Co:Ca, Cu:Ca, Mg:Ca, Mn:Ca, and Ni:Ca (Figures 4B, 4C and 4E – 4G) (One-Way ANOVAs, $p < 0.05$).

3.4. Otolith shape and elemental analyses

Stepwise linear discriminant function analysis (SLDFA) (Table 2) for otolith shape analyses (EFD). otolith elemental analyses (MES) and all data combined (EFD + MES) showed a clear separation between individuals from Gernika and Plentzia. Jack-knife re-classification accuracies for EFD showed a good overall re-classification success of 75% of individuals to the estuary of origin, with individuals from Gernika (77%) showing the best re-classification success (Table 2A). Regarding MES, a better overall jack-knife re-

classification success (97%) was observed, with individuals from Plentzia showing the best re-classification success of 100% (Table 2B). Using both otolith shape and elemental analyses, the allocation of samples increased the overall re-classification success to 98%. Full discrimination was obtained for individuals from Plentzia (100%) with a 97% re-classification success for Gernika (Table 2C). The canonical analysis of principal coordinates (CAP) plot displayed a clear distinction between individuals from Gernika and Plentzia using EFD+MES (Figure 3C).

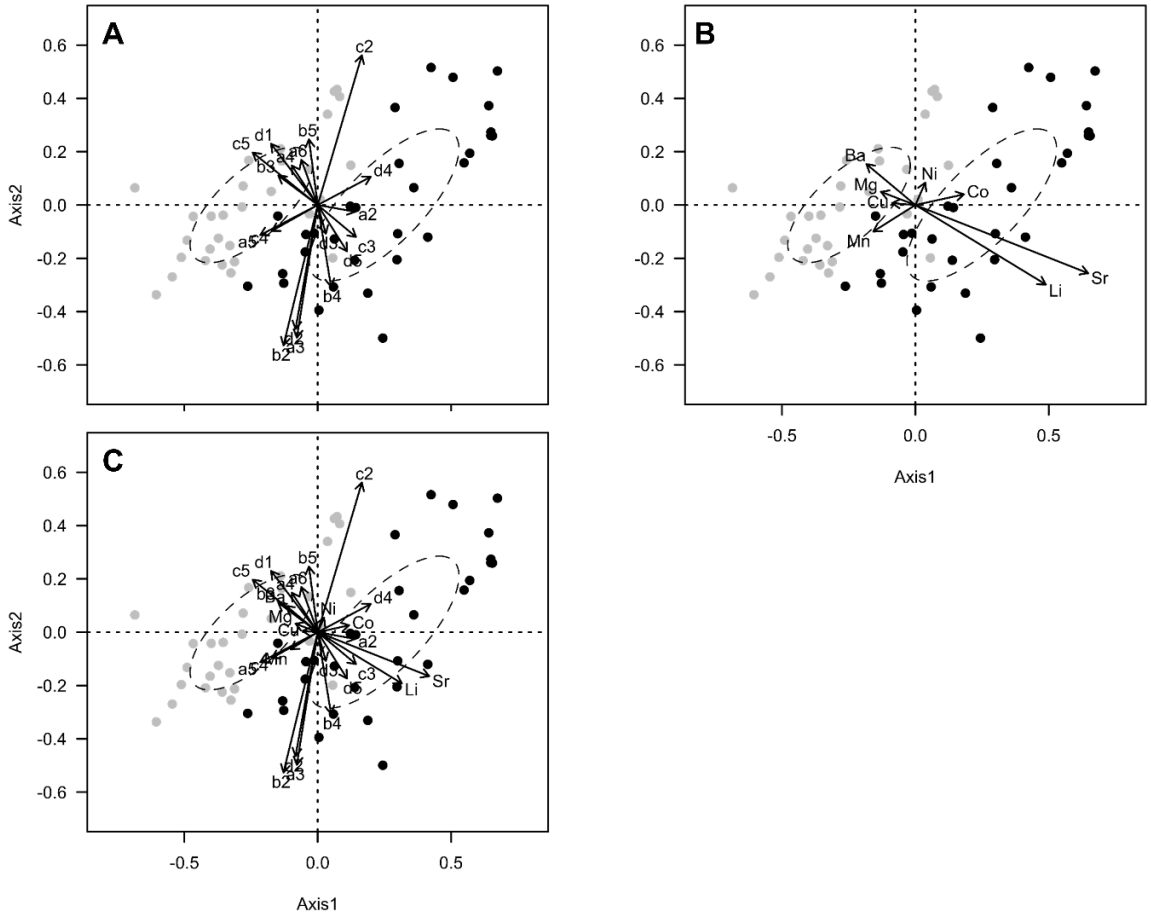

Figure 3
Canonical analysis of principal coordinates (CAP) plots for otolith shape analyses (EFD) and otolith elemental analyses (MES) from *C. labrosus* individuals collected from the estuaries of Gernika (GE) and Plentzia (PL). (A) CAP with EFD, (B) CAP with MES and (C) CAP with EFD and MES. Ellipses represent 95% confidence intervals. Each data point represents an individual fish from Gernika (grey dots) and Plentzia (black dots).

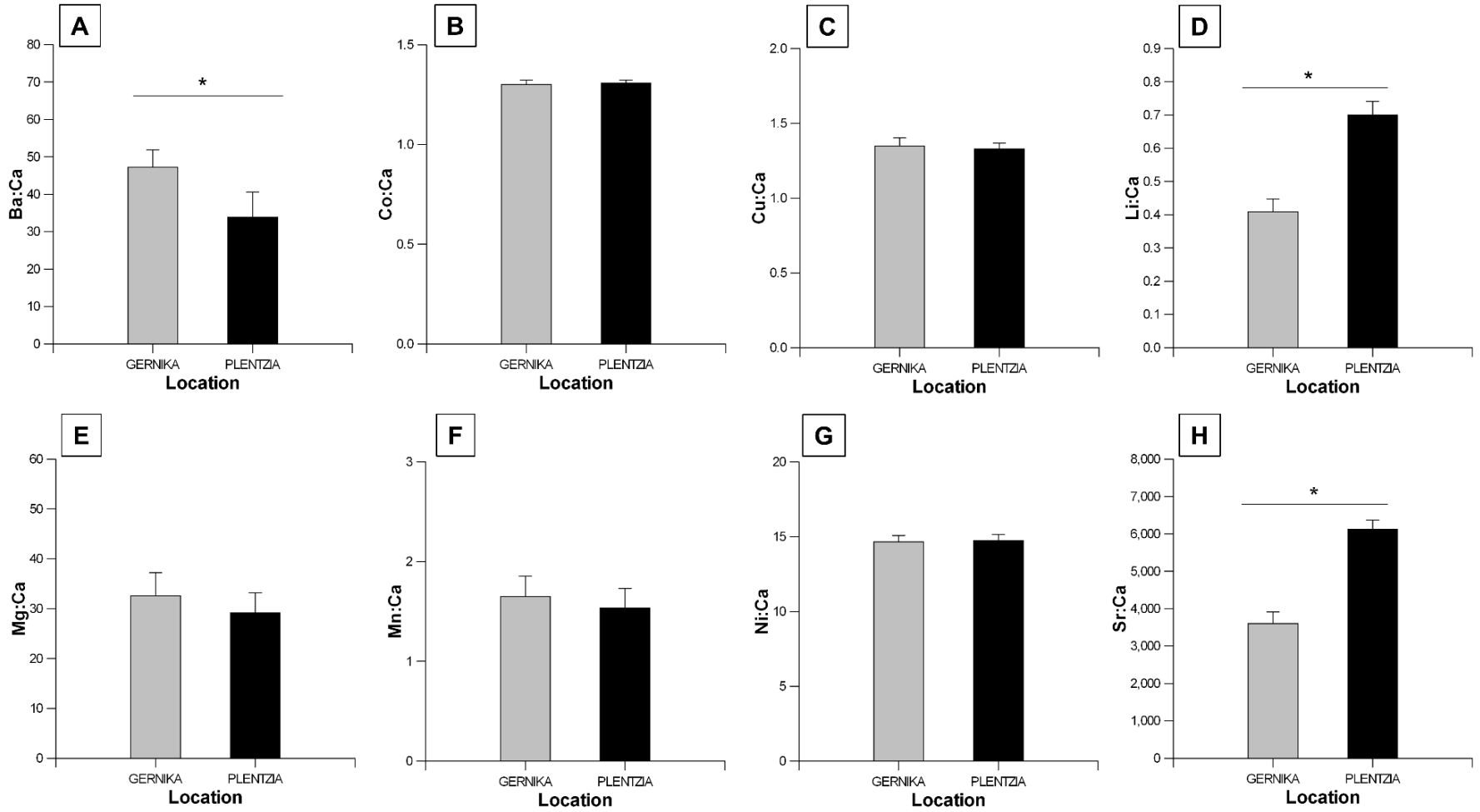

Figure 4

Element:Ca ratios in whole otoliths of *C. labrosus* collected in the Southeast Bay of Biscay. Unit of measurement is given as µg element g^{-1} calcium. An asterisk (*) above the bars indicates statistically significant different results (One-Way ANOVA, $p < 0.05$). For Ba:Ca, Mg:Ca, Mn:Ca and Sr:Ca detrended values were shown. Data are presented as mean values ± SE.

Table 2
Jack-knifed re-classification matrix resulting from stepwise discriminant linear function analyses (SLDFA) using elliptical Fourier descriptors (EFD). multi-elemental signatures (MES) and a combination of both (EFD and MES) for *Chelon labrosus* populations from the Bay of Biscay (correct reclassification in bold).

Original Location	**N**	**Predicted Location**		**% Correct**
		Gernika	**Plentzia**	
A. EFD				
Gernika	30	**23**	7	77
Plentzia	30	8	**22**	73
Total	60	31	29	**75**
B. MES				
Gernika	30	**28**	2	93
Plentzia	30	0	**30**	100
Total	60	28	32	**97**
C. EFD + MES				
Gernika	30	**29**	1	97
Plentzia	30	0	**30**	100
Total	60	29	31	**98**

4. Discussion

This study aimed at examining differences in otolith shape and elemental signatures of *C. labrosus* individuals inhabiting two estuaries with distinct burdens of xenoestrogens in the Southern Bay of Biscay, and to assess their potential to delineate the structure of *C. labrosus* populations. Elliptic Fourier descriptors (EFD) and multi-elemental signatures (MES) of whole otoliths distinguished individuals from the two estuaries sampled, suggesting that there is more than one local population unit along the Basque coast. Moreover, univariate tests on MES indicate that the differences between the two locations were largely driven by Ba, Li and Sr content. These results suggest that the individuals from Gernika and Plentzia have limited connectivity despite their geographical proximity.

Otolith shape and elemental analyses provide powerful means to characterise the natal origin and movements of fish (Adelir-Alves et al., 2018; Moura et al., 2020; Soeth et al., 2019) and to distinguish between groups of fish experiencing geographic separation (Correia et al., 2011, 2014; Smoliński et al., 2020). even when no significant genetic differences can be found (Correia et al., 2012; Marengo et al., 2017; Moreira et al., 2019a). Polymorphic microsatellite DNA markers provide great resolution for identifying

population structure (Durand et al., 2013; Moreira et al., 2020; Ward, 2000); however, genetic variation between population groups may be so low that individuals appear as members of a single interbreeding population (Marengo et al., 2017; Moreira et al., 2019b; Ward, 2000). Recently, *C. labrosus* individuals from five Basque estuaries were analysed by applying 10 different microsatellite markers and by comparing them with two out-groups from the Southern Atlantic Ocean and the Mediterranean Sea; however, no genetic differences were found, suggesting that all mullets from the SBB to the Greek Mediterranean form a single panmictic population (personal observation). This geographically-extense gene flow could be due to the existence of common spawning grounds at sea with high dispersion rates of adult individuals and long larval stages with high dispersion rates on homing into estuaries in the absence of physical barriers (DeWoody and Avise, 2000; Karaiskou et al., 2004; Martinez et al., 2018; Moreira et al., 2018). Despite this, *C. labrosus* mullets display phenotypic differences associated to the estuaries they live within the Biscay Bay. In this sense, male mullets from the Gernika estuary show up to 83% prevalence of intersex condition due to the exposure to xenoestrogens discharged by the WWTP of Gernika, while in the nearby pristine Plentzia estuary, not a single case has been reported (Bizarro et al., 2014; Ortiz-Zarragoitia et al., 2014; Valencia et al., 2017). The absence of genetic differences between Plentzia and Gernika individuals does not rule out the possibility that individuals in such estuaries are not lifelong residents of such estuaries, and that migration to the sea, for instance, for reproduction, is always followed by a return to the same estuary, with intersex individuals always returning to the xenoestrogenic loaded environment.

Some studies have been able to establish site-specific differences in otolith shape, even in the presence of limited genetic heterogeneity (Marengo et al., 2017; Neves et al., 2021; Soeth et al., 2019). Reef species such as the yellowstripe goatfish *Mulloidichthys flavolineatus* from the South-West Indian Ocean show recruitment back into native reefs and this is reflected in site-specific differences in otolith morphometric features observed in two population units sampled in two close sites in Reunion Island (Pothin et al., 2006). Genetic differences influence otolith shape, but environmental conditions have been shown to alter otolith growth rates, which in turn affected otolith shape. For instance, in the case of the Atlantic cod *Gadus morhua* from the Faroe Islands (Cardinale et al., 2004), Atlantic cod individuals were significantly separated into Bank and Plateau stocks with environment-linked classification rates above 85% depending on the age class (Cardinale et al., 2004).

In the absence of genetic differences, environment-related differences in otolith shape have also allowed the identification of different stocks/groups of the Brazillian sardine (*Sardinella brasiliensis*) in the South-West Atlantic (Schroeder et al., 2021), the common dentex (*Dentex dentex*) in the Mediterranean Sea (Marengo et al., 2017), the blue jack mackerel (*Trachurus picturatus*) (Moreira et al., 2019a), the chub mackerel (*Scomber colias*) (Muniz et al., 2020) and the European sardine (*Saldina pilchardus*) in the North-East Atlantic Ocean (Neves et al., 2021). However, few studies have explored the effect of local habitat variability (physical and chemical) on otolith shape over short geographical distances in the absence of genetic differences (Vignon, 2012). In the catadromous and panmictic European eel (*Anguilla anguilla*), otolith shape differences in adult individuals have been attributed to variability in environmental factors, with local population units being successfully separated into brackishwater estuarine and riverine freshwater population units in Italy (Capoccioni et al., 2011) and in waters of the North-West Iberian Peninsula (Moura et al., 2022). The difference in shape among the two locations studied hereby (only 21 miles apart) provided an overall re-classification accuracy of 75% (Table 2), a value considered acceptable for separating different fish populations (Stransky et al., 2008). Otolith shapes are generally more uniform and linked to fish size during the early life history stages due to an ontogenetically determined development and show a more divergent and constant pattern in relation to fish size once fish reach sexual maturity (Capoccioni et al., 2011; Vignon, 2012). Considering that otolith grow by incremental layers through the deposition of calcium carbonate, differential otolith growth rates as a result of environmental factors that strongly influence fish growth (salinity, water temperature, substrate type and feeding regime) will have a strong influence on otolith shape (Capoccioni et al., 2011; Soeth et al., 2019; Vignon, 2012). *C. labrosus* used in this study were mature adults (overall total length ~ 38 cm) (Tsikliras and Stergiou, 2014) and thus, the observed variations in otolith shape comparing mullets between the close estuaries of Gernika and Plentzia probably results from the influences of local environmental conditions (Capoccioni et al., 2011; Cardinale et al., 2004; Correia et al., 2014; Hüssy, 2008; Vignon and Morat, 2010). In any case, this reflects different habitat residencies and life histories for the individuals collected in the two estuaries.

The concentration of five elements (Co, Cu, Mg, Mn and Ni) in the otoliths of *C. labrosus* individuals from the two sampled locations did not show any significant differences between Gernika and Plentzia. These elements (including Cd, Pb and Zn, which

were below the LOD) are usually found in domestic and industrial wastes and occur naturally in freshwater terrestrial run-off (Gillanders and Kingsford, 1996). They are well suited for otolith elemental fingerprint studies, as they could be reflecting the distinctive geology in an estuary and/or the level of exposure to domestic and industrial wastewater effluents (Søndergaard et al., 2015; Vasconcelos et al., 2011; Vrdoljak et al., 2020). However, differences between Gernika and Plentzia and their environmental concentrations have not greatly affected the chemical element composition in otoliths of *C. labrosus*. Instead, elemental signatures of Ba, Li and Sr resulted in a clear separation of individuals from Gernika and Plentzia (overall re-classification accuracy of 95%. Table 2) into two distinct population units.

Incorporation of Ba, Li and Sr in otoliths is influenced by water temperature, salinity and primary productivity and growth rate (Bath et al., 2000; Grammer et al., 2017; Hüssy et al., 2021; Sturrock et al., 2015; Walther and Thorrold, 2006). Sr and Li are positively correlated with salinity, hence higher Sr and Li concentrations reflect higher salinities as a result of greater marine water influence relative to freshwater (Bath et al., 2000; Hicks et al., 2010; Hüssy et al., 2021). In this study, the higher Sr and Li concentrations observed in Plentzia is to be expected, considering that mullets in Plentzia were sampled in the small leisure port in the outer part of the relatively shallow estuary of the Butron river. This estuary experiences strong wave energy fluxes in its tidal range with strong tidal currents during ebb and flood that generate an equilibrium in the tidal inlet and bay area (Leorri et al., 2013; Lomonaco et al., 2003). Although growth and reproduction have also been shown to affect Sr:Ca ratios in marine fish (Grammer et al., 2017; Hüssy et al., 2021; Sturrock et al., 2015), these factors do not seem to establish differences within each of the studied population units. On the other hand, the lower Sr and Li and higher Ba otolith contents in Gernika may be due to freshwater input and terrestrial enrichment influencing changes in water chemistry. The sampling area is known to have a low-salinity water lens formed by a stronger axial gradient towards the head, where it receives freshwater input from the Oka River, as well as effluent discharges from the Gernika WWTP (Iriarte et al., 2016, 2015; Villate et al., 2008). Ba has been linked to terrestrial run-off and freshwater/river discharge in estuaries (Elsdon and Gillanders, 2004; Hicks et al., 2010), and some studies report an inverse relationship between Ba:Ca otolith content and water salinity (Hüssy et al., 2021; Izzo et al., 2018; Moreira et al., 2018), consistent with the Ba results found in the present study.

5. Conclusions

Genetic markers identified one single *Chelon labrosus* population from the Southern Bay of Biscay to the Thermoikos Gulf in the Mediterranean, indicating that individuals from the Basque estuaries may reproduce among themselves. However, the high overall re-classification success of 98% (Table 2) obtained from combining both shape and elemental signatures in otoliths of mullets from Gernika and Plentzia indicated the presence of discrete and spatially structured phenotypic groups, which suggests that individuals passed enough time in distinct water compartments even if separated only by 21 miles of sea. Therefore, these mullets could be regarded as belonging to two different population units. A finer spatial structure was also found for whitemouth croaker (*Micropogonias furnieri*) populations along the Rio de Janeiro coast, Brazil, when using otolith's shape and elemental signatures compared with nuclear microsatellites (Franco et al., 2023). These results, even with the spatial sampling limitations of this study, indicate restricted connectivity between mullets and suggest a limited degree of mixing of adults among estuaries in the Southern Bay of Biscay. This could also suggest that mullets migrating to the sea for reproduction every year would always return to their native estuary (the one they recruited to as larvae) and that the intersex condition that has been observed in Gernika is probably due to life-long exposure to xenoestrogens. However, the selection of only two locations is a limiting factor, considering the broader range of estuaries available for the species as nursery grounds. Future works should address the variations in informative minor and trace elements along the growth increments, from the otolith's core (natal origin) to the edge (moment of capture), to better understand the yearly pattern of brackishwater-marine migrations in *C. labrosus*. This could help us unravel the real fidelity of the adult individuals to their native estuary of recruitment.

Acknowledgements

This work was funded by the Spanish Ministry of Science. Innovation and Universities and EU-FEDER/ERDF (BORN2bEGG PGC2018-101442-B-I00), the Basque Government (Grants to consolidated research groups IT1302-19 and IT1743-22) and a transnational access project of the Horizon-2020 project ASSEMBLE PLUS. 730984). This study was also partially supported by the Strategic Funding UID/Multi/04423/2019 through national funds provided by FCT and European Regional Development Fund (ERDF) in the framework of the program PT2020. A. N. is a recipient of a pre-doctoral grant from the

University of the Basque Country (UPV/EHU).

References

Adelir-Alves, J., Daros, F.A.L.M., Spach, H.L., Soeth, M., Correia, A.T., 2018. Otoliths as a tool to study reef fish population structure from coastal islands of South Brazil. Marine Biology Research 14, 973–988. https://doi.org/10.1080/17451000.2019.1572194

Anderson, M.J., Willis, T.J., 2003. Canonical analysis of principal coordinates: A useful method of constrained ordination for ecology. Ecology 84, 511–525. https://doi.org/10.1890/0012-9658(2003)084[0511:CAOPCA]2.0.CO;2

Bahamonde, P.A., Munkittrick, K.R., Martyniuk, C.J., 2013. Intersex in teleost fish: Are we distinguishing endocrine disruption from natural phenomena? Gen Comp Endocrinol 192, 25–35. https://doi.org/10.1016/j.ygcen.2013.04.005

Bath, G.E., Thorrold, S.R., Jones, C.M., Campana, S.E., McLaren, J.W., Lam, J.W.H., 2000. Strontium and barium uptake in aragonitic otoliths of marine fish. Geochim Cosmochim Acta. https://doi.org/10.1016/S0016-7037(99)00419-6

Bizarro, C., Ros, O., Vallejo, A., Prieto, A., Etxebarria, N., Cajaraville, M.P., Ortiz-Zarragoitia, M., 2014. Intersex condition and molecular markers of endocrine disruption in relation with burdens of emerging pollutants in thicklip grey mullets (*Chelon labrosus*) from Basque estuaries (South-East Bay of Biscay). Mar Environ Res 96, 19–28. https://doi.org/10.1016/j.marenvres.2013.10.009

Cadrin, S.X., Karr, L.A., Mariani, S., 2014. Stock Identification Methods, in: Stock Identification Methods. Elsevier, pp. 1–5. https://doi.org/10.1016/B978-0-12-397003-9.00001-1

Campana, S.E., Chouinard, G.A., Hanson, J.M., Fréchet, A., Brattey, J., 2000. Otolith elemental fingerprints as biological tracers of fish stocks. Fish Res 46, 343–357.

Capoccioni, F., Costa, C., Aguzzi, J., Menesatti, P., Lombarte, A., Ciccotti, E., 2011. Ontogenetic and environmental effects on otolith shape variability in three Mediterranean European eel (*Anguilla anguilla*, L.) local stocks. J Exp Mar Biol Ecol 397, 1–7. https://doi.org/10.1016/j.jembe.2010.11.011

Cardinale, M., Doering-Arjes, P., Kastowsky, M., Mosegaard, H., 2004. Effects of sex, stock, and environment on the shape of known-age Atlantic cod (*Gadus morhua*) otoliths. https://doi.org/10.1139/F03-151

Correia, A.T., Moura, A., Triay-Portella, R., Santos, P.T., Pinto, E., Almeida, A.A., Sial, A.N., Muniz, A.A., 2021. Population structure of the chub mackerel (*Scomber colias*) in the NE Atlantic inferred from otolith elemental and isotopic signatures. Fish Res 234, 105785. https://doi.org/10.1016/j.fishres.2020.105785

Correia, A.T., Pipa, T., Gonçalves, J.M.S., Erzini, K., Hamer, P.A., 2011. Insights into population structure of *Diplodus vulgaris* along the SW Portuguese coast from otolith elemental signatures. Fish Res 111, 82–91. https://doi.org/10.1016/j.fishres.2011.06.014

Correia, A.T., Ramos, A.A., Barros, F., Silva, G., Hamer, P., Morais, P., Cunha, R.L., Castilho, R., 2012. Population structure and connectivity of the European conger eel (*Conger conger*) across the north-eastern Atlantic and western Mediterranean: Integrating molecular and otolith elemental approaches. Mar Biol 159, 1509–1525. https://doi.org/10.1007/s00227-012-1936-3

Correia, A.T.T., Hamer, P., Carocinho, B., Silva, A., 2014. Evidence for meta-population structure of *Sardina pilchardus* in the Atlantic Iberian waters from otolith elemental signatures of a strong cohort. Fish Res 149, 76–85. https://doi.org/10.1016/j.fishres.2013.09.016

Crosetti, D., Cataudella, S., 1995. Grey mullet culture, in: Nash, C.E. (Ed.), World Animal Science 34B: Production of Aquatic Animals. Elsevier BV: Burlington, MA, USA, pp. 271–288.

DeWoody, J.A., Avise, J.C., 2000. Microsatellite variation in marine, freshwater and anadromous fishes compared with other animals. J Fish Biol 56, 461–473. https://doi.org/10.1006/jfbi.1999.1210

Diaz De Cerio, O., Rojo-Bartolomé, I., Bizarro, C., Ortiz-Zarragoitia, M., Cancio, I., 2012. 5S rRNA and accompanying proteins in gonads: powerful markers to identify sex and reproductive endocrine disruption in fish. Environ Sci Technol 46, 7763–7771. https://doi.org/10.1021/es301132b

Durand, J.D., Blel, H., Shen, K.N., Koutrakis, E.T., Guinand, B., 2013. Population genetic structure of *Mugil cephalus* in the Mediterranean and Black Seas: A single mitochondrial clade and many nuclear barriers. Mar Ecol Prog Ser 474, 243–261. https://doi.org/10.3354/meps10080

Elsdon, T.S., Gillanders, B.M., 2004. Fish otolith chemistry influenced by exposure to multiple environmental variables. J Exp Mar Biol Ecol 313, 269–284. https://doi.org/10.1016/j.jembe.2004.08.010

Franco, T.P., Vilasboa, A., Araújo, F.G., Gama, J.M., Correia, A.T., 2023. Identifying whitemouth croaker (*Micropogonias furnieri*) populations along the Rio de Janeiro coast, Brazil, through microsatellites and otoliths analyses. Biology (Basel) In Press.

Freyhof, J., Kottelat, M., 2008. Chelon labrosus ,Thicklip Grey Mullet [WWW Document]. IUCN Red List. https://doi.org/10.2305/IUCN.UK.2008.RLTS.T135689A4182365.en

Froese, R., Pauly, D., 2022. FishBase [WWW Document]. World Wide Web electronic publication. URL https://www.fishbase.se/search.php (accessed 6.15.22).

Gerard, T., Muhling, B., 2010. Variation in the isotopic signatures of juvenile gray snapper (*Lutjanus griseus*) from five southern Florida regions. Fishery Bulletin 108, 98–105.

Gillanders, B.M., Kingsford, M.J., 1996. Elements in otoliths may elucidate the contribution of estuarine recruitment to sustaining coastal reef populations of a temperate reef fish. Mar Ecol Prog Ser 141, 13–20. https://doi.org/10.3354/meps141013

González-Castro, M., Minos, G., 2016. Sexuality and reproduction of Mugilidae, in: Crosetti, D., Blaber, S. (Eds.), Biology, Ecology and Culture of Grey Mullets (Mugilidae). CRC Press, pp. 227–263.

Grammer, G.L., Morrongiello, J.R., Izzo, C., Hawthorne, P.J., Middleton, J.F., Gillanders, B.M., 2017. Coupling biogeochemical tracers with fish growth reveals physiological and environmental controls on otolith chemistry. Ecol Monogr 87, 487–507. https://doi.org/10.1002/ecm.1264

Hickling, C.F., 1970. A contribution to the natural history of the English grey mullets [Pisces, Mugilidae]. Journal of the Marine Biological Association of the United Kingdom 50, 609–633. https://doi.org/10.1017/S0025315400004914

Hicks, A.S., Closs, G.P., Swearer, S.E., 2010. Otolith microchemistry of two amphidromous galaxiids across an experimental salinity gradient: A multi-element approach for tracking diadromous migrations. J Exp Mar Biol Ecol 394, 86–97. https://doi.org/10.1016/j.jembe.2010.07.018

Higgins, R., Isidro, E., Menezes, G., Correia, A., 2013. Otolith elemental signatures indicate population separation in deep-sea rockfish, *Helicolenus dactylopterus* and *Pontinus kuhlii*, from the Azores. J Sea Res 83, 202–208. https://doi.org/10.1016/j.seares.2013.05.014

Hoff, N.T., Dias, J.F., Pinto, E., Almeida, A., Schroeder, R., Correia, A.T., 2022. Past and contemporaneous otolith fingerprints reveal potential anthropogenic interferences and allows refinement of the population structure of *Isopisthus parvipinnis* in the South Brazil Bight. Biology (Basel) 11, 1005. https://doi.org/10.3390/biology11071005

Hüssy, K., 2008. Otolith shape in juvenile cod (*Gadus morhua*): Ontogenetic and environmental effects. J Exp Mar Biol Ecol 364, 35–41. https://doi.org/10.1016/j.jembe.2008.06.026

Hüssy, K., Limburg, K.E., de Pontual, H., Thomas, O.R.B., Cook, P.K., Heimbrand, Y., Blass, M., Sturrock, A.M., 2021. Trace element patterns in otoliths: The role of biomineralization. Reviews in Fisheries Science and Aquaculture 29, 445–477. https://doi.org/10.1080/23308249.2020.1760204

Iriarte, A., Villate, F., Uriarte, I., Alberdi, L., Intxausti, L., 2015. Dissolved oxygen in a temperate estuary: the influence of hydro-climatic factors and eutrophication at seasonal and inter-annual time scales. Estuaries and Coasts 38, 1000–1015. https://doi.org/10.1007/s12237-014-9870-x

Iriarte, A., Villate, F., Uriarte, I., Arranz, S., 2016. Assessment of the climate and human impact on estuarine water environments in two estuaries of the Bay of Biscay. Oceanol Hydrobiol Stud 45, 505–523. https://doi.org/10.1515/ohs-2016-0043

Izzo, C., Reis-Santos, P., Gillanders, B.M., 2018. Otolith chemistry does not just reflect environmental conditions: A meta-analytic evaluation. Fish and Fisheries 19, 441–454. https://doi.org/10.1111/faf.12264

Karaiskou, N., Triantafyllidis, A., Triantaphyllidis, C., 2004. Shallow genetic structure of three species of the genus *Trachurus* in European waters. Mar Ecol Prog Ser 281, 193–205. https://doi.org/10.3354/meps281193

Koutrakis, E., 2016. Biology and ecology of fry and juveniles of Mugilidae, in: Crosetti, D., Blaber, S. (Eds.), Biology, Ecology and Culture of Grey Mullets (Mugilidae). CRC Press, pp. 264–292.

Kuhl, F.P., Giardina, C.R., 1982. Elliptic Fourier features of a closed contour. Computer Graphics and Image Processing 18, 236–258. https://doi.org/10.1016/0146-664X(82)90034-X

Leorri, E., Cearreta, A., García-Artola, A., Irabien, M.J., Blake, W.H., 2013. Relative sea-level rise in the Basque coast (N Spain): Different environmental consequences on the coastal area. Ocean Coast Manag 77, 3–13. https://doi.org/10.1016/j.ocecoaman.2012.02.007

Libungan, L.A., Pálsson, S., 2015. ShapeR: An R package to study otolith shape variation among fish populations. PLoS One 10, 1–12. https://doi.org/10.1371/journal.pone.0121102

Lomonaco, P., Medina, R., Gyssels, P., Vidal, C., 2003. Application of a long-term morphologic evolution model to the Plencia tidal inlet and its adjacent beaches, in: Proc. 3rd IAHR Symposium on Rivers, Coastal and Estuarine Morphodynamics. pp. 401–413.

Marengo, M., Baudouin, M., Viret, A., Laporte, M., Berrebi, P., Vignon, M., Marchand, B., Durieux, E.D.H., 2017. Combining microsatellite, otolith shape and parasites community analyses as a holistic approach to assess population structure of *Dentex dentex*. J Sea Res 128, 1–14. https://doi.org/10.1016/j.seares.2017.07.003

Marigómez, I., Garmendia, L., Soto, M., Orbea, A., Izagirre, U., Cajaraville, M.P., 2013. Marine ecosystem health status assessment through integrative biomarker indices: A comparative study after the Prestige oil spill "mussel Watch." Ecotoxicology 22, 486–505. https://doi.org/10.1007/s10646-013-1042-4

Martinez, A.S., Willoughby, J.R., Christie, M.R., 2018. Genetic diversity in fishes is influenced by habitat type and life-history variation. Ecol Evol 8, 12022–12031. https://doi.org/10.1002/ece3.4661

Mérigot, B., Letourneur, Y., Lecomte-Finiger, R., 2007. Characterization of local populations of the common sole *Solea solea* (Pisces, Soleidae) in the NW Mediterranean through otolith morphometrics and shape analysis. Mar Biol 151, 997–1008. https://doi.org/10.1007/s00227-006-0549-0

Mićković, B., Nikčević, M., Hegediš, A., Regner, S., Gačić, Z., Krpo-Ćetković, J., 2010. Mullet Fry (Mugilidae) in coastal waters of montenegro, their spatial distribution and migration phenology. Arch Biol Sci. https://doi.org/10.2298/ABS1001107M

Mijangos, L., Ziarrusta, H., Ros, O., Kortazar, L., Fernández, L.A., Olivares, M., Zuloaga, O., Prieto, A., Etxebarria, N., 2018. Occurrence of emerging pollutants in estuaries of the Basque Country: Analysis of sources and distribution, and assessment of the environmental risk. Water Res 147, 152–163. https://doi.org/10.1016/j.watres.2018.09.033

Moreira, C., Correia, Alberto T., Vaz-Pires, P., Froufe, Elsa, 2019a. Genetic diversity and population structure of the blue jack mackerel *Trachurus picturatus* across its western distribution. J Fish Biol 94, 725–731. https://doi.org/10.1111/jfb.13944

Moreira, C., Froufe, E., Sial, A.N., Caeiro, A., Vaz-Pires, P., Correia, A.T., 2018. Population structure of the blue jack mackerel (*Trachurus picturatus*) in the NE Atlantic inferred from otolith microchemistry. Fish Res 197, 113–122. https://doi.org/10.1016/j.fishres.2017.08.012

Moreira, C., Froufe, E., Vaz-Pires, P., Correia, A.T., 2019b. Otolith shape analysis as a tool to infer the population structure of the blue jack mackerel, *Trachurus picturatus*, in the NE Atlantic. Fish Res 209, 40–48. https://doi.org/10.1016/j.fishres.2018.09.010

Moreira, C., Froufe, E., Vaz-Pires, P., Triay-Portella, R., Méndez, A., Pisonero Castro, J., Correia, A.T., 2022. Unravelling the spatial-temporal population structure of *Trachurus picturatus* across the North-East Atlantic using otolith fingerprinting. Estuar Coast Shelf Sci 272, 107860. https://doi.org/10.1016/j.ecss.2022.107860

Moreira, C., Presa, P., Correia, A.T., Vaz-Pires, P., Froufe, E., 2020. Spatio-temporal microsatellite data suggest a multidirectional connectivity pattern in the *Trachurus picturatus* metapopulation from the Northeast Atlantic. Fish Res 225, 105499. https://doi.org/10.1016/j.fishres.2020.105499

Moura, A., Dias, E., López, R., Antunes, C., 2022. Regional population structure of the European eel at the southern limit of its distribution revealed by otolith shape signature. Fishes 7, 135. https://doi.org/10.3390/FISHES7030135/S1

Moura, A., Muniz, A.A., Mullis, E., Wilson, J.M., Vieira, R.P., Almeida, A.A., Pinto, E., Brummer, G.J.A., Gaever, P.V., Gonçalves, J.M.S., Correia, A.T., 2020. Population structure and dynamics of the Atlantic mackerel (*Scomber scombrus*) in the North Atlantic inferred from otolith chemical and shape signatures. Fish Res 230, 105621. https://doi.org/10.1016/j.fishres.2020.105621

Muniz, A.A., Moura, A., Triay-Portella, R., Moreira, C., Santos, P.T., Correia, A.T., 2021. Population structure of the chub mackerel (*Scomber colias*) in the North-east Atlantic inferred from otolith shape and body morphometrics. Mar Freshw Res 72, 341–352. https://doi.org/10.1071/MF19389

Muniz, A.A., Moura, A., Triay-Portella, R., Moreira, C., Santos, P.T., Correia, A.T., 2020. Population structure of the chub mackerel (*Scomber colias*) in the North-east Atlantic inferred from otolith shape and body morphometrics. Mar Freshw Res 72, 341–352. https://doi.org/10.1071/MF19389

Neves, J., Silva, A.A., Moreno, A., Veríssimo, A., Santos, A.M., Garrido, S., 2021. Population structure of the European sardine *Sardina pilchardus* from Atlantic and Mediterranean waters based on otolith shape analysis. Fish Res 243. https://doi.org/10.1016/j.fishres.2021.106050

Oksanen, J., Simpson, G.L., Blanchet, F.G., Kindt, R., Legendre, P., Minchin, P.R., O'Hara, R.B., Solymos, P., Stevens, M.H.H., Szoecs, E., Wagner, H., Barbour, M., Bedward, M., Bolker, B., Borcard, D., Carvalho, G., Chirico, M., De Caceres, M., Durand, S., Evangelista, H.B.A., FitzJohn, R., Friendly, M., Furneaux, B., Hannigan, G., Hill, M.O., Lahti, L., McGlinn, D., Ouellette, M.-H., Ribeiro Cunha, E., Smith, T., Stier, A., Ter Braak, C.J.F., Weedon, J., 2022. vegan: Community Ecology Package.

Ortiz-Zarragoitia, M., Bizarro, C., Rojo-Bartolomé, I., De Cerio, O.D., Cajaraville, M.P., Cancio, I., 2014. Mugilid fish are sentinels of exposure to endocrine disrupting compounds in coastal and estuarine environments. Mar Drugs 12, 4756–4782. https://doi.org/10.3390/md12094756

Patterson, H.M., Thorrold, S.R., Shenker, J.M., 1999. Analysis of otolith chemistry in Nassau grouper (*Epinephelus striatus*) from the Bahamas and Belize using solution-based ICP-MS. Coral Reefs 18, 171–178. https://doi.org/10.1007/s003380050176

Pothin, K., Gonzalez-Salas, C., Chabanet, P., Lecomte-Finiger, R., 2006. Distinction between *Mulloidichthys flavolineatus* juveniles from Reunion Island and Mauritius Island (south-west Indian Ocean) based on otolith morphometrics. J Fish Biol 69, 38–53. https://doi.org/10.1111/j.1095-8649.2006.01047.x

Puy-Azurmendi, E., Ortiz-Zarragoitia, M., Villagrasa, M., Kuster, M., Aragón, P., Atienza, J., Puchades, R., Maquieira, A., Domínguez, C., López de Alda, M., Fernandes, D., Porte, C., Bayona, J.M., Barceló, D., Cajaraville, M.P., 2013. Endocrine disruption in thicklip grey mullet (*Chelon labrosus*) from the

Urdaibai Biosphere Reserve (Bay of Biscay, Southwestern Europe). Science of The Total Environment 443, 233–244. https://doi.org/10.1016/J.SCITOTENV.2012.10.078

R Core Team, 2023. R: A language and environment for statistical computing. R Foundation for Statistical Computing, Vienna, Austria.

Reis-Santos, P., Vasconcelos, R.P., Tanner, S.E., Fonseca, V.F., Cabral, H.N., Gillanders, B.M., 2018. Extrinsic and intrinsic factors shape the ability of using otolith chemistry to characterize estuarine environmental histories. Mar Environ Res. https://doi.org/10.1016/j.marenvres.2018.06.002

Rooker, J.R., Zdanowicz, V.S., Secor, D.H., 2001. Chemistry of tuna otoliths: Assessment of base composition and postmortem handling effects. Mar Biol 139, 35–43. https://doi.org/10.1007/s002270100568

Ros, O., Vallejo, A., Blanco-Zubiaguirre, L., Olivares, M., Delgado, A., Etxebarria, N., Prieto, A., 2015. Microextraction with polyethersulfone for bisphenol-A, alkylphenols and hormones determination in water samples by means of gas chromatography-mass spectrometry and liquid chromatography-tandem mass spectrometry analysis. Talanta 134, 247–255. https://doi.org/10.1016/j.talanta.2014.11.015

Schroeder, R., Schwingel, P.R., Correia, A.T., 2021. Population structure of the Brazilian sardine (*Sardinella brasiliensis*) in the Southwest Atlantic inferred from body morphology and otolith shape signatures. Hydrobiologia 7. https://doi.org/10.1007/s10750-021-04730-7

Schroeder, R., Schwingel, P.R., Pinto, E., Almeida, A., Correia, A.T., 2022. Stock structure of the Brazilian sardine *Sardinella brasiliensis* from Southwest Atlantic Ocean inferred from otolith elemental signatures. Fish Res 248, 106192. https://doi.org/10.1016/j.fishres.2021.106192

Smoliński, S., Schade, F.M., Berg, F., 2020. Assessing the performance of statistical classifiers to discriminate fish stocks using Fourier analysis of otolith shape. Canadian Journal of Fisheries and Aquatic Sciences 77, 674–683. https://doi.org/10.1139/cjfas-2019-0251

Soeth, M., Spach, H.L., Daros, F.A., Adelir-Alves, J., de Almeida, A.C.O., Correia, A.T., 2019. Stock structure of Atlantic spadefish *Chaetodipterus faber* from Southwest Atlantic Ocean inferred from otolith elemental and shape signatures. Fish Res 211, 81–90. https://doi.org/https://doi.org/10.1016/j.fishres.2018.11.003

Sokal, R.R., Rohlf, F.J., 1995. Biometry: The Principles and Practice of Statistics in Biological Research, Third. ed. W. H. Freeman, New York.

Søndergaard, J., Halden, N., Bach, L., Gustavson, K., Sonne, C., Mosbech, A., 2015. Otolith chemistry of common sculpins (*Myoxocephalus scorpius*) in a mining polluted greenlandic fiord (Black Angel Lead-Zinc Mine, West Greenland). Water Air Soil Pollut 226. https://doi.org/10.1007/s11270-015-2605-1

Stransky, C., Murta, A.G., Schlickeisen, J., Zimmermann, C., 2008. Otolith shape analysis as a tool for stock separation of horse mackerel (*Trachurus trachurus*) in the Northeast Atlantic and Mediterranean. Fish Res 89, 159–166. https://doi.org/10.1016/j.fishres.2007.09.017

Sturrock, A.M., Hunter, E., Milton, J.A., Johnson, R.C., Waring, C.P., Trueman, C.N., EIMF, 2015. Quantifying physiological influences on otolith microchemistry. Methods Ecol Evol 6, 806–816. https://doi.org/10.1111/2041-210X.12381

Thomas, O.R.B., Swearer, S.E., 2019. Otolith Biochemistry — A Review. Reviews in Fisheries Science & Aquaculture 27, 1–32. https://doi.org/10.1080/23308249.2019.1627285

Tsikliras, A.C., Stergiou, K.I., 2014. Size at maturity of Mediterranean marine fishes. Rev Fish Biol Fish 24, 219–268. https://doi.org/10.1007/s11160-013-9330-x

Turan, C., 2016. Biogeography and distribution of Mugilidae in the Mediterranean and the Black Sea, and North-East Atlantic, in: Crosetti, D., Blaber, S. (Eds.), Biology, Ecology and Culture of Grey Mullets (Mugilidae). CRC Press, pp. 116–127.

Valencia, A., Rojo-Bartolomé, I., Bizarro, C., Cancio, I., Ortiz-Zarragoitia, M., 2017. Alteration in molecular markers of oocyte development and intersex condition in mullets impacted by wastewater treatment plant effluents. Gen Comp Endocrinol 245, 10–18. https://doi.org/10.1016/j.ygcen.2016.06.017

Vasconcelos, R.P., Reis-Santos, P., Costa, M.J., Cabral, H.N., 2011. Connectivity between estuaries and marine environment: Integrating metrics to assess estuarine nursery function. Ecol Indic 11, 1123–1133. https://doi.org/10.1016/j.ecolind.2010.12.012

Vignon, M., 2012. Ontogenetic trajectories of otolith shape during shift in habitat use: Interaction between otolith growth and environment. J Exp Mar Biol Ecol 420–421, 26–32. https://doi.org/10.1016/j.jembe.2012.03.021

Vignon, M., Morat, F., 2010. Environmental and genetic determinant of otolith shape revealed by a non-indigenous tropical fish. Mar Ecol Prog Ser 411, 231–241. https://doi.org/10.3354/meps08651

Villate, F., Aravena, G., Iriarte, A., Uriarte, I., 2008. Axial variability in the relationship of chlorophyll a with climatic factors and the North Atlantic oscillation in a Basque coast estuary, Bay of Biscay (1997-2006). J Plankton Res 30, 1041–1049. https://doi.org/10.1093/plankt/fbn056

Vrdoljak, D., Matić-Skoko, S., Peharda, M., Uvanović, H., Markulin, K., Mertz-Kraus, R., 2020. Otolith fingerprints reveals potential pollution exposure of newly settled juvenile *Sparus aurata*. Mar Pollut Bull 160, 111695. https://doi.org/10.1016/j.marpolbul.2020.111695

Walther, B.D., Thorrold, S.R., 2006. Water, not food, contributes the majority of strontium and barium deposited in the otoliths of a marine fish. Mar Ecol Prog Ser 311, 125–130. https://doi.org/10.3354/meps311125

Ward, R.D., 2000. Genetics in fisheries management. Hydrobiologia 420, 191–201. https://doi.org/10.1023/A:1003928327503

Whitfield, A.K., 2020. Fish species in estuaries-from partial association to complete dependency. J Fish Biol 97, 1262–1264. https://doi.org/10.1111/jfb.14476

Xia, R., Durand, J.D., Fu, C., 2016. Multilocus resolution of Mugilidae phylogeny (Teleostei: Mugiliformes): Implications for the family's taxonomy. Mol Phylogenet Evol 96, 161–177. https://doi.org/10.1016/j.ympev.2015.12.010

Chapter 5

Tracing life history patterns from chemical signatures in otoliths of thicklip grey mullets inhabiting two adjacent estuaries with different xenoestrogenic pressures along the Southern Bay of Biscay

ARTICLE

Nzioka, A., Cancio, I., Diaz de Cerio, O., Daros, F., Mendez-Vincente, A., Correia, A.T., 2023. Tracing life history patterns from chemical signatures in otoliths of thicklip grey mullets inhabiting two adjacent estuaries with different xenoestrogenic pressures along the Southern Bay of Biscay. Ecological Indicators (in prep.)

CONGRESS

IX Iberian Congress of Ichthyology (SIBIC2022), 20th – 23rd JUNE 2022, Porto, Portugal. **Anthony Nzioka**, Ibon Cancio, Oihane Diaz de Cerio, Maren Ortiz-Zarragoitia, Edgar Pinto, Agostinho Almeida and Alberto Teorodico Correia (2022). "Use of otolith shape and elemental signatures to infer the population structure of the thicklip grey mullet *Chelon labrosus* in the Southern Bay of Biscay." Poster Communication.

ASSEMBLE Plus Conference 2022 – Marine Biological Research at the Frontier, 13th – 24th June 2022, online. **Anthony Nzioka**, Oihane Diaz de Cerio, Alberto Teodorico Correia, Ibon Cancio. (2022). "Otolith microstructure and microchemistry analyses to evaluate the population structure of the thicklip grey mullet, *Chelon labrosus*, in the Southern Bay of Biscay – FISHOTOTRACKING." Oral Communication.

ASSEMBLE Plus Closing Assembly, 14th – 15th September 2022, Paris, France. **Anthony Nzioka**, Ibon Cancio, Oihane Diaz de Cerio, Maren Ortiz-Zarragoitia, Edgar Pinto, Agostinho Almeida and Alberto Teorodico Correia (2022). "Otolith microstructure and microchemistry analyses to evaluate the population structure of the thicklip grey mullet, *Chelon labrosus*, in the Southern Bay of Biscay – FISHOTOTRACKING." Poster Communication.

XIV AIEC Congress of the Iberian Association for Comparative Endocrinology, 11th – 13th September 2023, Bilbao, Spain. **Anthony Nzioka**, Ainara Valencia, Iratxe Rojo-Bartolomé, Xabier Lecube, Maren Ortiz-Zarragoitia, Oihane Diaz de Cerio and Ibon Cancio (2023). "Molecular markers of follicular atresia in thicklip grey mullets (*Chelon labrosus*) inhabiting an estuary (Gernika) with high burdens of xenoestrogens." Oral Communication.

Resumen

El muble, *Chelon labrosus*, es una especie que puede soportar ambientes acuáticos altamente contaminados y, por lo tanto, se utiliza como especie centinela de la contaminación en los estuarios del Sur del Golfo de Vizcaya (SGV). Los mubles expuestos a xenoestrógenos han mostrado signos de alteración endocrina y deterioro del desarrollo de las gónadas, lo que a veces conduce a una condición intersexual. Se ha detectado una alta prevalencia de testículos intersexuales en la ría de Urdaibai de Gernika debido al mal funcionamiento de su depuradora de aguas residuales. Para comprender la historia de la exposición a xenoestrógenos de estos peces que habitan en estuarios, pero se reproducen en el mar, necesitamos saber si la migración reproductiva marina resulta en un retorno al estuario de origen contaminado. En este estudio, se utilizó espectrometría de masas de plasma acoplado inductivamente por ablación láser para analizar la composición química de los otolitos durante toda la vida de 60 mubles muestreados en dos estuarios adyacentes con diferentes presiones xenoestrogénicas. Los patrones de migración de mubles reconstruidos a partir de perfiles elementales de Sr:Ca y Ba:Ca de núcleo a borde de otolitos (edad estimada en el rango de 6 a 23) revelaron dos historias de vida principales y distintas: residentes de estuarios y migrantes marinos. En Gernika, el análisis de otolitos de 30 individuos mostró que el 83% de ellos podían ser considerados residentes, el 20% realizando movimientos repetidos desde la ría al mar, el 17% realizando patrones de movimiento irregulares entre la ría y el mar y el 64% residiendo únicamente en la ría. toda su vida tras la etapa juvenil. En Plentzia, sólo el 53% se consideran residentes, de los cuales el 37,5% presenta patrones de movimiento repetidos/cíclicos entre la ría y el mar, en contraste con los patrones de movimiento irregular del resto. Ninguno de los individuos de Plentzia vivía únicamente en ambientes estuarinos antes de su captura. Los resultados muestran falta de conectividad entre los estuarios adyacentes estudiados. Es muy posible que el comportamiento de residencia observado por *C. labrosus* sea consecuencia de la fidelidad a la ría del primer reclutamiento y por lo tanto la exposición a xenoestrógenos en Gernika resultando en el desarrollo de testículos intersexuales sería de por vida.

Palabras clave: *Historia de contaminación, peces, Mugilidae, etiquetas naturales, historia de vida, microquímica de otolitos, estuarios, poblaciones*

Abstract

The thicklip grey mullet, *Chelon labrosus*, is a species that can endure highly polluted aquatic environments and is therefore used as a pollution sentinel species in estuaries in the Southern Bay of Biscay (SBB). Mullets exposed to xenoestrogens have shown signs of endocrine disruption and impaired gonad development, sometimes leading to intersex condition. High intersex testes prevalence have been detected in the Urdaibai estuary of Gernika due to the malfunctioning of its wastewater treatment plant. To understand the history of xenoestrogen exposure of these fish which inhabit estuaries but reproduce at sea, we need to know whether marine reproductive migration results in return to the polluted estuary of origin. In this study, laser ablation inductively coupled plasma mass spectrometry was used to analyse the chemical composition of otoliths throughout the entire life of 60 mullets sampled from two adjacent estuaries with different xenoestrogenic pressures. The mullet migration patterns reconstructed from otolith (age estimated in the range 6 to 23) core-to-edge Sr:Ca and Ba:Ca elemental profiles revealed two main and distinct life histories: estuarine-residents and marine-migrants. In Gernika, otolith analysis of 30 individuals showed that 83% of them could be considered resident, 20% making repeated movements from estuaries to the sea, 17% making irregular movement patterns between the estuary and the sea and 64% solely residing in the estuary their entire life following the juvenile stage. In Plentzia, only 53% were considered residents of which 37.5% displayed repeated/cyclical movement patterns between the estuary and the sea, in contrast to the irregular movement patterns of the rest. None of the individuals from Plentzia lived solely in estuarine environments before their capture. Results show lack of connectivity between the studied adjacent estuaries. It is quite possible that the residency behaviour observed by *C. labrosus* is as a result of fidelity to the estuary of the first recruitment and therefore xenoestrogen exposure in Gernika resulting in intersex testes development would be life-long.

Keywords: *estuaries, Mugilidae, life history, otolith microchemistry, population structure, xenoestrogen exposure*

Abbreviations

ECAE, Ethics Committee for Animal Experimentation
GADM, global administrative areas (database**)**
GE, Gernika
LA-ICP-MS, laser ablation-inductively coupled plasma-mass spectrometry
NIST, National Institute of Standards and Technology
PIT, passive-integrated responder tag
PL, Plentzia
PSAT, pop-up satellite archival tag
QGIS, quantum geographic information system (software)
r_s**,** Spearman's rank correlation
SRM, standard reference material
UNESCO, United Nations Educational, Scientific and Cultural Organisation
WWTP, wastewater treatment plant

1. Introduction

The movement and life history of many diadromous euryhaline fishes is often complex because of the variable habitat use patterns at different stages of their vital cycle (Crosetti and Blaber, 2016). Many fish species spawn in marine waters and migrate to estuaries for variable periods for one reason or another, completing their life cycle in estuaries while others use the estuaries as a transitory migration route to and from spawning grounds at sea (Potter et al., 2015). These ontogenetic movements offer access to different habitats and resources. For instance, a migration pattern of grey mullets, between primarily brackish waters during youth and maturation, moving to the open sea for spawning, onshore migration of larvae and settlement in surf zones as juveniles, and movement of juvenile schools to coastal lagoons or estuarine waters, is widely accepted (Crosetti and Blaber, 2016). Although mullets perform annual spawning runs from estuarine and coastal waters into the open sea, the spawning grounds for most mullet species remain poorly documented (Crosetti and Blaber, 2016). On the other hand, some individuals have been observed to remain in estuaries without migrating to spawn, while permanent marine-living populations have also been observed (Whitfield et al., 2012). Accurately estimating the movement and life history of diadromous euryhaline fishes is crucial (Crook et al., 2017) to understand connectivity as this is directly linked to population dynamics, productivity, and resilience, particularly in the face of changing environmental conditions and anthropogenic impacts (Xuan and Wang, 2023).

Although several methods such as mark-recapture tagging and animal tracking technology (telemetry) have been used to study the migration patterns of fish (Cooke et al., 2022; Pepping et al., 2020), otolith chemistry analysis has gained popularity in the reconstruction of fish movements (Izzo et al., 2018; Reis-Santos et al., 2022; Walther, 2019). Mark-recapture (internally or externally implanted), passive-integrated responder (PIT) tags, acoustic or radio telemetry tags and pop-up archival tags or pop-up satellite archival tags (PSATs) though routinely used, are unable to provide lifetime insights on movement because these methods either depend on fishing effort for recapture, tag retention and recovery rates, may alter behaviours and decrease swimming performance upon tagging or, they may be unsuitable for small-sized fish species (Hedger et al., 2017; Jepsen et al., 2015; Thorstad et al., 2014). Otoliths, which are paired metabolically inert bio-mineralized crystalline-organic complex structures that chronologically precipitate calcium carbonate onto the organic matrix throughout the entire life of the fish, serve instead as natural tags

that avoid many of these issues (Hüssy et al., 2021; Xuan and Wang, 2023). As otoliths grow incrementally, minor and trace elements are incorporated at proportions roughly proportionate to those in the surrounding environment, under the influence of the genetics and physiology of the particular fish species (Hüssy et al., 2021; Izzo et al., 2018; Sturrock et al., 2015).

Reconstructing the environmental history of fish from otolith chemistry relies on the concentration of elements changing predictably with environmental variables (Elsdon and Gillanders, 2004). Barium (Ba) and strontium (Sr) are often used as proxies to reconstruct migratory patterns between environments of different salinity (Elsdon et al., 2008; Hüssy et al., 2021; Menezes et al., 2021), though other elements, such as magnesium (Mg) or manganese (Mn), have proven useful in reflecting multiple responses of individual fish to surrounding ambient water conditions (Hüssy et al., 2021; Sturrock et al., 2015; Wang, 2014).

The thicklip grey mullet, *Chelon labrosus* (Risso, 1827), is one of five species of mullets belonging to two genera, *Chelon* and *Mugil* that inhabit the North-East Atlantic Ocean (Crosetti and Blaber, 2016; Froese and Pauly, 2022; Thieme et al., 2022). Thicklip grey mullets are euryhaline demersal fish species with a high degree of residency within estuarine systems, utilising estuaries as nursery grounds or foraging habitats, travelling up and downstream with the tidal regime daily (Crosetti and Blaber, 2016; Froese and Pauly, 2022; Whitfield, 2020). Individuals of this species are consistently present in estuaries of the southern Bay of Biscay, often occurring in large numbers. Every winter (December - February), adults spawn in oceanic coastal surface waters as it is observed by their gametogenic cycle showing. Pelagic eggs hatch 3-4 days after spawning and fertilisation and the pelagic larval stage lasts about four weeks before metamorphosing into the juvenile stage (Besbes et al., 2020; Boglione et al., 1992; Crosetti and Blaber, 2016). While spawning locations are unknown in the ocean, schooling juveniles in coastal habitats migrate inshore into shallow estuaries during the first and second months of their lives (Crosetti and Blaber, 2016; Hickling, 1970; Mićković et al., 2010).

The ability of *C. labrosus* to survive highly polluted aquatic environments has made them excellent pollution sentinel species (Crosetti and Blaber, 2016; Ortiz-Zarragoitia et al., 2014). They have been shown to bioaccumulate contaminants such as alkylphenols, pesticides, pharmaceuticals and other chemicals discharged from wastewater treatment

plant (WWTP) effluents into estuaries resulting in the development of intersex condition (i.e., the appearance of oocytes in testicular tissue) in individuals from several estuaries in the Basque Autonomous Region (Bizarro et al., 2014; Ortiz-Zarragoitia et al., 2014; Puy-Azurmendi et al., 2013). Intersex prevalence levels in male individuals vary from ~10% in Bilbao (Nerbioi-Ibaizabal estuary) to 83% in the Urdaibai estuary of Gernika. Instead, males captured from the leisure port of Plentzia have consistently shown normally developing testes with no incidence of intersex condition (Bizarro et al., 2014; Diaz De Cerio et al., 2012; Valencia et al., 2017). It has been hypothesised that early sex differentiation takes place after recruitment into the estuaries and attained at 2 and 3 years for males and females, respectively (Sostoa, 1983) so if xenoestrogens were present and bioavailable this would have an impact in gonad development. Given the early life-history characteristics of *C. labrosus*, migration patterns and life history attributes can provide useful insights into the history of xenoestrogen exposure, to understand the effects observed in males with intersex testes from some estuaries. The movement of thicklip grey mullets between habitats shapes the spatial and temporal xenoestrogen exposure windows.

Even though thicklip grey mullets in the Biscay Bay can be considered as a single panmictic population (Nzioka et al., 2023b), a recent study using otolith shape and whole elemental signatures from individuals captured from two close estuaries, Plentzia and Gernika, showed distinct and estuary-specific phenotypic groupings (Nzioka et al., 2023a). However, a deeper understanding of the life history of these individuals could be obtained by analysing the fluctuations in otolith elemental profiles during growth, from the otolith's core (natal origin) to the edge (moment of capture). Among other things, this would allow a better comprehension of the yearly pattern of migration between brackish and marine waters. This information could critically establish the true fidelity of the adult individuals to their original estuary of recruitment, this being polluted or pristine, and whether migration to the sea for reproduction is always followed by a return to the same estuary.

Therefore, this study aims to evaluate whether *C. labrosus* individuals from two estuaries in the Bay of Biscay, one with a high incidence of intersex condition (Gernika), and the other one pristine (Plentzia), are lifelong residents of these estuaries using otolith elemental signatures. More specifically, using Laser Ablation-Inductively Coupled Plasma-Mass Spectrometry (LA-ICP-MS) (Avigliano et al., 2017; Fowler et al., 2016; Xuan and Wang, 2023), quantifying otolith Sr:Ca and Ba:Ca concentrations from hatching to capture

we want to describe the migration patterns, habitat use, residency and life history attributes of *C. labrosus*, to understand whether intersex condition reported in Gernika may be due to life-long residency in xenoestrogen-contaminated waters.

2. Materials and methods

2.1. Study area

The Urdabai estuary (43°19′26.389″ N, 2°40′25.46″ W), located in the town of Gernika within the Urdaibai Biosphere Reserve (designated by UNESCO in 1984), and the Plentzia estuary (43°24′25.794″ N, 2°56′46.921″ W), located in the town of Plentzia, were chosen as the sampling areas. They are both situated approximately 21 miles apart (Figure 1). A small estuary in the village of Bakio (43° 25′51″ N, 2° 48′40″ W) is located between these two estuaries about nine miles from Plentzia and twelve from Gernika (Marigómez et al., 2013).

The Plentzia estuary, which is 7.9 km long and has a tidal variation of ± 2.5 m, is a relatively shallow meso-tidal estuary (Leorri et al., 2013) with a small recreational port close to the tidal entrance and the nearby beach of Plentzia-Gorliz. The WWTP, which gathers urban wastewater from about 10,000 residents, releases its effluent beyond the estuary through a submarine pipe that extends about 1 km offshore at a depth of about 18 m (Mijangos et al., 2018) disconnected from our sampling point and with limited pollutant discharges. The Oka River provides freshwater input to the 12.5 km long meso-macrotidal and shallow (mean depth of 3 m) Urdaibai estuary (Iriarte et al., 2015). There are substantial impacts from the direct discharge of wastewater from the Gernika WWTP onto a small and extremely shallow part of the estuary where mullets were captured. This outdated WWTP receives domestic and industrial wastes from the neighbouring town of Gernika which has ~ 26,000 inhabitants.

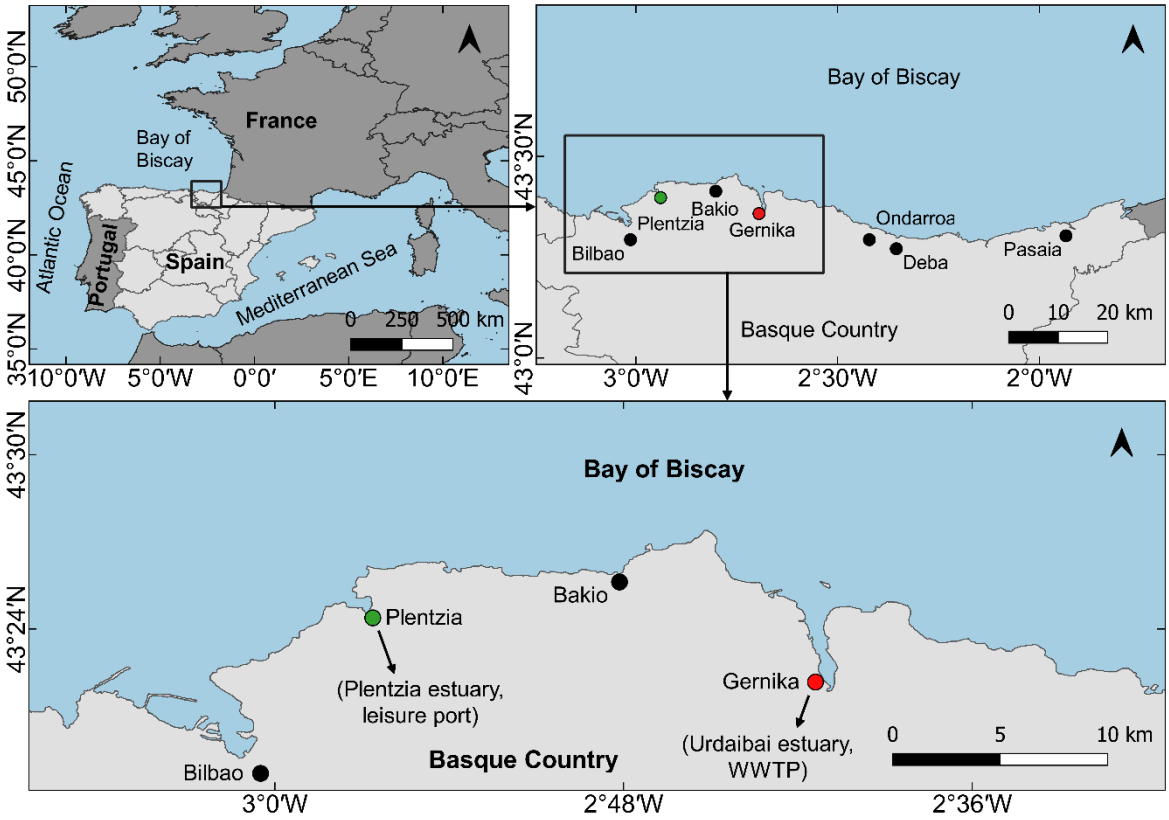

Figure 1
An overview of sampling locations for *Chelon labrosus* along the Basque coast. (A) Location of Spain in Europe, (B) the Basque coast in the southern Bay of Biscay and (C) where 60 individuals of *C. labrosus* were selected for otolith microchemistry at Gernika (red point, N=30) and the estuary of Plentzia (green point, N=30). Black points indicate locations of estuaries along the Basque coast. This figure was produced with the GADM database (www.gadm.org), version 4.1, 16 July 2022 and QGIS version 3.18.0-Zürich.

2.2. Fish sample collection

Adult thicklip grey mullets (Chelon labrosus) were captured using a fishing rod in Plentzia (PL; N=30) and Gernika (GE; N=30) over a three-week period in June 2020. Before being transported to be processed in the lab, the fish were anesthetized in a saturated benzocaine/seawater bath and kept in ice. The individuals were measured for total length (TL, 1 mm), weighed (W, 1 g) and the gonads examined macroscopically to identify sex. Sagittal otoliths from each fish were removed, cleaned of any adherent tissues with ultrapure water (Milli-Q water, 0.52 µS cm^{-1}) and air-dried in clean and labelled tubes. The approval of the UPV/EHU Ethics Committee for Animal Experimentation (ECAE) and the regional authorities was obtained for all fishing and fish handling operations.

2.3. Otolith processing

Right sagittal otoliths were embedded in transparent epoxy resin (EpoThin™ 2; Buehler, IL, USA) and transversely sectioned (~ 0.5 mm slices) through the core region using a precision metallographic diamond saw (IsoMet Low-Speed Saw; Buehler, USA). The slices were grinded with 1000, 2400 and 4000 grit waterproof Silicon Carbide paper (200 mm diameter SiC-Paper; Struers, Copenhagen, Denmark) to expose the primordium and further polished with 6-, 3- and 1-micron diamond polishing compound (MetaDi® II; Buehler, USA) (Correia et al., 2012). The transverse otolith sections were mounted onto glass slides with epoxy resin (EpoThin™ 2; Buehler, IL, USA), cleaned in an ultrasonic bath with ultrapure water (Thermo Scientific, Lab Tower EDI 15, Thermo Electron LED GmbH, Langenselbold, Germany) for 5 min and allowed to dry overnight in a laminar flow hood (Correia et al., 2012).

2.4. Elemental determination by LA-ICP-MS analysis

Otolith elemental concentrations were obtained using a 193-nm ArF* Excimer Laser Ablation System (Photon Machines Analyte G2) coupled to an ICP-MS, Agilent 7700 ICP-MS (Agilent Technologies, Santa Clara, USA) running the ICP-MS MassHunter Workstation software at University of Oviedo, Spain. A continuous line scan ablation was used to obtain elemental profiles from the core to the edge of each otolith (spot diameter: 30 μm, nominal fluence: 2.5 J cm^{-2} or ~ 46% energy, repetition rate: 100 Hz, scan speed: 20 μm s^{-1}). To compensate for any variation in ablation yield along the laser transect and to improve the reliability of the measurements, the Microanalytical Carbonate Standard (MACS-3; ^{43}Ca) was used as the internal standard (Campana, 1999). External calibration was performed using standard reference material (SRM) NIST610 and NIST612 silicate glass (www.nist.gov) and the accuracy expressed as the recovery rate (RR) varying from 71% to 110% within the analytical accepted values (Dove et al. 1996: RSD: 75%-125%). All operating conditions (spot size, laser frequency, laser energy/pulse and gas flows) were kept constant in both reference material and otoliths. Pre-ablation using a spot diameter of 40 μm, nominal fluence 0.22 J cm^{-2} (~ 12% energy), repetition rate 20 Hz, and scan speed of 200 μm s^{-1} was done to avoid any surface contamination. Laser transects were measured and ablation time from the initial (otolith core) and final (otolith edge) laser positions was converted to distance from core-to-edge (Figure 2). The otoliths were analysed in a random

order to eliminate any bias resulting from instrument drift (Avigliano et al., 2017; Bailey et al., 2015).

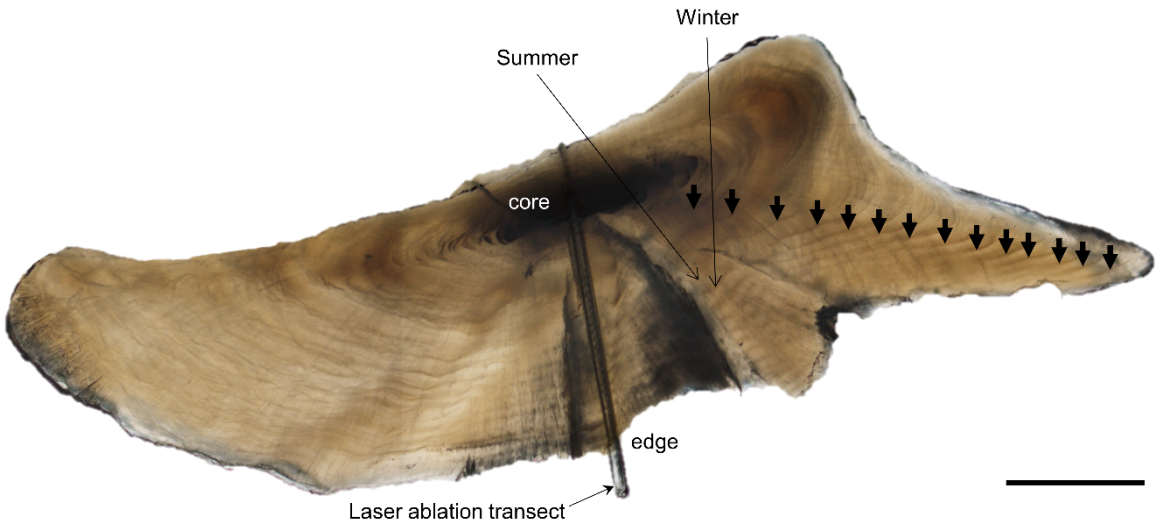

Figure 2
Complete transverse section of a left sagittal otolith from Chelon labrosus (TL = 39.0 cm). A laser transect from the core and edge of the otolith section is shown. Alternating opaque and transparent ring-like structures (annuli) in otoliths representing annual slow (Winter– opaque) and fast (Summer– transparent) growth segments. Black arrows indicate the annuli position used in age estimation. Scale bar = 500 µm.

The Iolite software (Paton et al., 2011) was used to process the data and determine element concentration abundances. Counts-per-second data for all elements were converted to elemental concentrations by subtracting background counts, standardizing to the external reference standard (NIST612) and normalizing to the internal standard (^{43}Ca) to obtain the ablation yield (Avigliano et al., 2017; Fowler et al., 2016). Along the continuous transects, concentrations of each element were determined every 12 µm. The trace element concentration (element:Ca ratios) were expressed as molar ratios in mmol mol^{-1} to account for material loss during the preparation process and any fluctuations in the amount of material analysed (Avigliano et al., 2017; Bailey et al., 2015). High-resolution images of the ablated otolith sections were captured with a Nikon DS-Fi2 digital camera (Nikon Instruments Inc., Tokyo, Japan) with NIS Elements software mounted on an Olympus BX50 light microscope (Olympus Corporation, Tokyo, Japan). Fiji Image-J image analysis software (Schindelin et al., 2012) was used to measure age estimates of transverse otolith sections along transect lines, counting the growth annuli in each section 3 times, assuming an annual growth periodicity as has been validated for other mugilid species (Ellender et al., 2012).

2.5. Life history reconstruction, migration classification and data analysis

The study assumed that there is a positive correlation between otolith Sr and habitat salinities, hence the Sr:Ca ratio was utilized to categorize patterns of migration between estuaries and marine environments (Hüssy et al., 2021). Otolith Sr:Ca ratio values are generally higher in marine waters than in brackish estuarine waters, whereas Ba:Ca ratio values are lower in marine waters than in brackish water estuarine environments. Therefore, the mean Sr:Ca ratio of the last three otolith edge readings plus one standard deviation (mean + 1*SD) was assumed to represent the capture environment when calculating the transition threshold between estuarine and marine environments, hence the most recent months of growth (Avigliano et al., 2017; Tabouret et al., 2010). This value was extracted and averaged over all fish collected in Gernika (N=30), empirically providing a reference baseline without being able to quantitatively detect changes in the environment (Xuan et al., 2022).

Since fluctuations in otolith elemental profiles could be used to predict habitat changes during the fish's entire life, Change-Point Analysis (CPA) was performed to estimate the number of habitat changes that fish experienced throughout their life history (Avigliano et al., 2017. The Prune Exact Linear Time (PELT) algorithm (Killick et al., 2012) was used to detects multiple changes cross a time series based on mean of otolith elemental ratios. Similar Sr:Ca and Ba:Ca ratios within a segment were thought to be associated with quiescent stages in similar habitats, and the multiple changes defined by CPA were assumed to indicate fish movement between different environments (Vignon, 2015; Xuan and Wang, 2023). Otolith core-to-edge profiles of Sr:Ca and Ba:Ca ratios were analysed for each individual fish and the existence of habitat use patterns displayed by *C. labrosus* individuals evaluated and inferred from the Sr:Ca transition threshold value. The *changepoint* package version 2.2.4 (Killick et al., 2012) in *R* programming language (R Core Team, 2023) was utilized for CPA. Elemental signatures of the first and last 10 readings of the otolith core and edge along the transect element profile were used to represent and define the natal origin and most recent months of growth (Mai et al., 2018; Menezes et al., 2021).

All data were checked for normality (Shapiro-Wilk test, $p > 0.05$) and homogeneity of variances (Levene's test, $p > 0.05$). In case these assumptions were violated, non-parametric Mann-Whitney U test was used. Once these assumptions were met, a Two-Sample student t-test was performed to compare differences in means. Spearman's rank correlation was computed to assess the relationship between Ba:Ca and Sr:Ca ratios observed. *Tidyverse*

(Wickham et al., 2019), *onewaytests* (Dag et al., 2018), *car* (Fox and Weisberg, 2019), *ggstatsplot* (Patil, 2021), and *ggpubr* (Kassambara, 2023) packages were used to complete all statistical analysis in *R* programming software. Data are presented as means ± S.E. or medians and the statistically significant difference was set at $p < 0.05$.

3. Results

3.1. Age estimation

Total length (TL) and age estimates of Chelon labrosus sampled ranged from 28.8 to 50.0 cm and 6 to 23 years (Table 1). Annuli from all otolith's transverse sections (Gernika, GE) and (Plentzia, PL) were easily readable and the estimation of age successfully performed (Table 1).

Table 1
Summary of sample size (N), total length (TL), and age of *Chelon labrosus* sampled in Gernika (GE) and Plentzia (PL). Values represent mean (± SD, standard deviation) and range (minimum and maximum).

Site	N	TL (cm)		Age (years)	
		Mean ± SD	Range	Mean ± SD	Range
GE	30	38.4 ± 3.8	30.2-50.0	10.2 ± 3.4	6-21
PL	30	37.5 ± 5.1	28.8-46.0	11.1 ± 4.2	6-23

3.2. Otolith trace elemental profiles

Otolith Sr:Ca ratio values ranged from 0.6719 to 5.8924 mmol mol^{-1} (median 2.3325 mmol mol^{-1}) and 0.8917 to 5.6132 mmol mol^{-1} (median 3.1323 mmol mol^{-1}) for GE and PL, respectively, while Ba:Ca ratio values ranged from 0.0010 to 0.1351 mmol mol^{-1} (median 0.0072 mmol mol^{-1}) for GE, and 0.0005 to 0.1345 mmol mol^{-1} (median 0.0049 mmol mol^{-1}) for PL. The mean Sr:Ca ratios based on the last 3 edge readings of otoliths from individuals of GE was 2.71 ± 0.86 mmol mol^{-1}, so the threshold value for movements between the estuarine and marine environment was set at 3.57 mmol mol^{-1} (mean ± 1*SD). Sr:Ca ratio values above 3.75 mmol mol^{-1} were considered to correspond to marine/saline water environments and below 3.75 mmol mol^{-1} to estuarine/brackish environments.

Spearman's rank correlation (r_s) computed to assess the relationship between Ba:Ca and Sr:Ca ratios showed that there was significant and weak negative correlation between the two variables for all sites combined (r_s = -0.35, p = 0.0058). A moderately positive

relationship was found between age and Sr:Ca ratios (r_s = 0.46, p = 0.0002) and between age and the number of change points (r_s = 0.57, p = 0.0000018). Otolith Sr:Ca ratios were negatively correlated with otolith Mg:Ca, and Mn:Ca ratios in GE and PL (r_s, $p < 0.05$) (Table 2). Mg:Ca, and Mn:Ca ratios were negatively correlated with otolith Ba:Ca ratios except for GE where negative correlation was not significant (Table 2).

Table 2
Spearman's rank correlation (r_s) rho coefficients between otolith element:Ca ratios of *Chelon labrosus* sampled in Gernika (GE) and Plentzia (PL). Significant correlations at $p < 0.05$ is indicated with an asterisk (*).

Variable	GE	PL
Sr:Ca vs Ba:Ca	-0.07	0.29
Sr:Ca vs Mg:Ca	-0.38*	-0.43*
Sr:Ca vs Mn:Ca	-0.58*	-0.52*
Mg:Ca vs Ba:Ca	-0.52*	-0.52*
Mn:Ca vs Ba:Ca	-0.16	-0.44*

The Sr:Ca ratio in the otolith core were similar for GE and PL (Student Two Sample t-test, p = 0.25), averaging approximately 2.09 ± 0.06 mmol mol^{-1} and 2.17 ± 0.04 mmol mol^{-1}, respectively (Figure 3). However, otolith edge Sr:Ca ratio values were higher in PL than in GE (Mann-Whitney U-test, $p < 0.05$) (Figure 3B). Otolith core Ba:Ca ratios were also similar in both estuaries (Mann-Whitney U-test, p = 0.31), while the edge values in GE were higher than in PL (Mann-Whitney U-test, $p < 0.05$) (Figure 3A). For Mg:Ca and Mn:Ca, ratios were high in the otolith core, decreasing with increasing distance from the core in both estuaries (Figure 4).

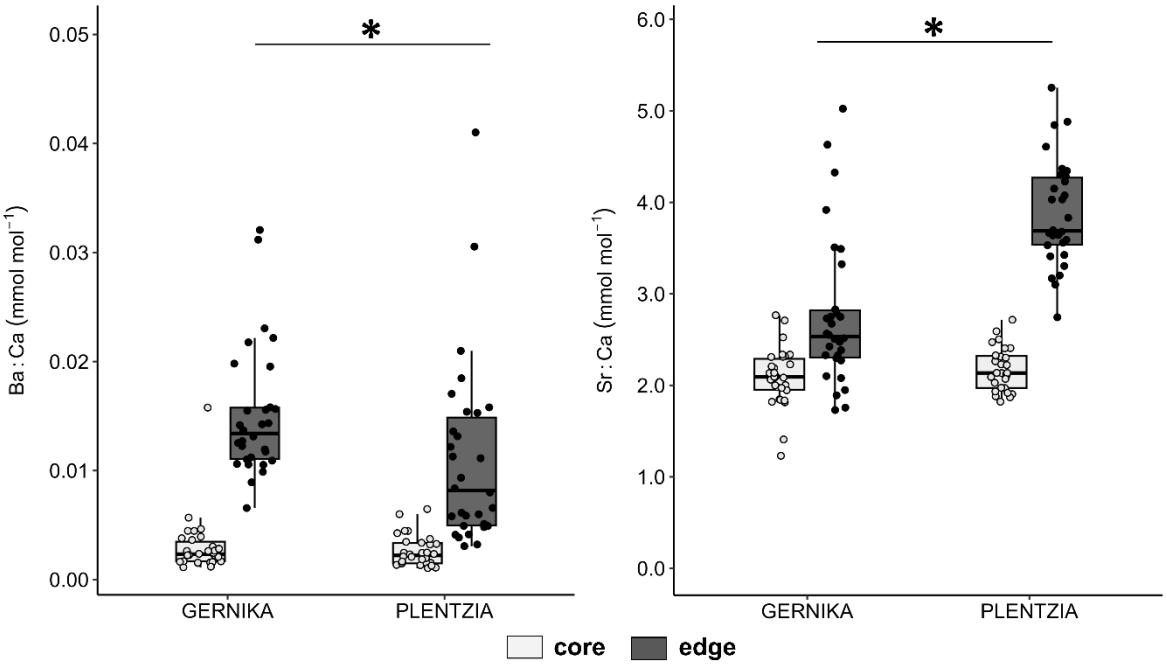

Figure 3
Otolith Ba:Ca and Sr:Ca ratio values at the core and edges of *Chelon labrosus* individuals from Gernika (N=30) and Plentzia (N=30). Data points are mean values of the first and last 10 core and edge readings respectively for each individual. Boxplots represent the data within the 25th and 75th percentiles, with the median indicated by a line, and bottom and top whiskers representing minimum and maximum values, respectively. An asterisk above represents statistically significant different results (Mann Whitney U test and Student Two Sample t-test, $p < 0.05$).

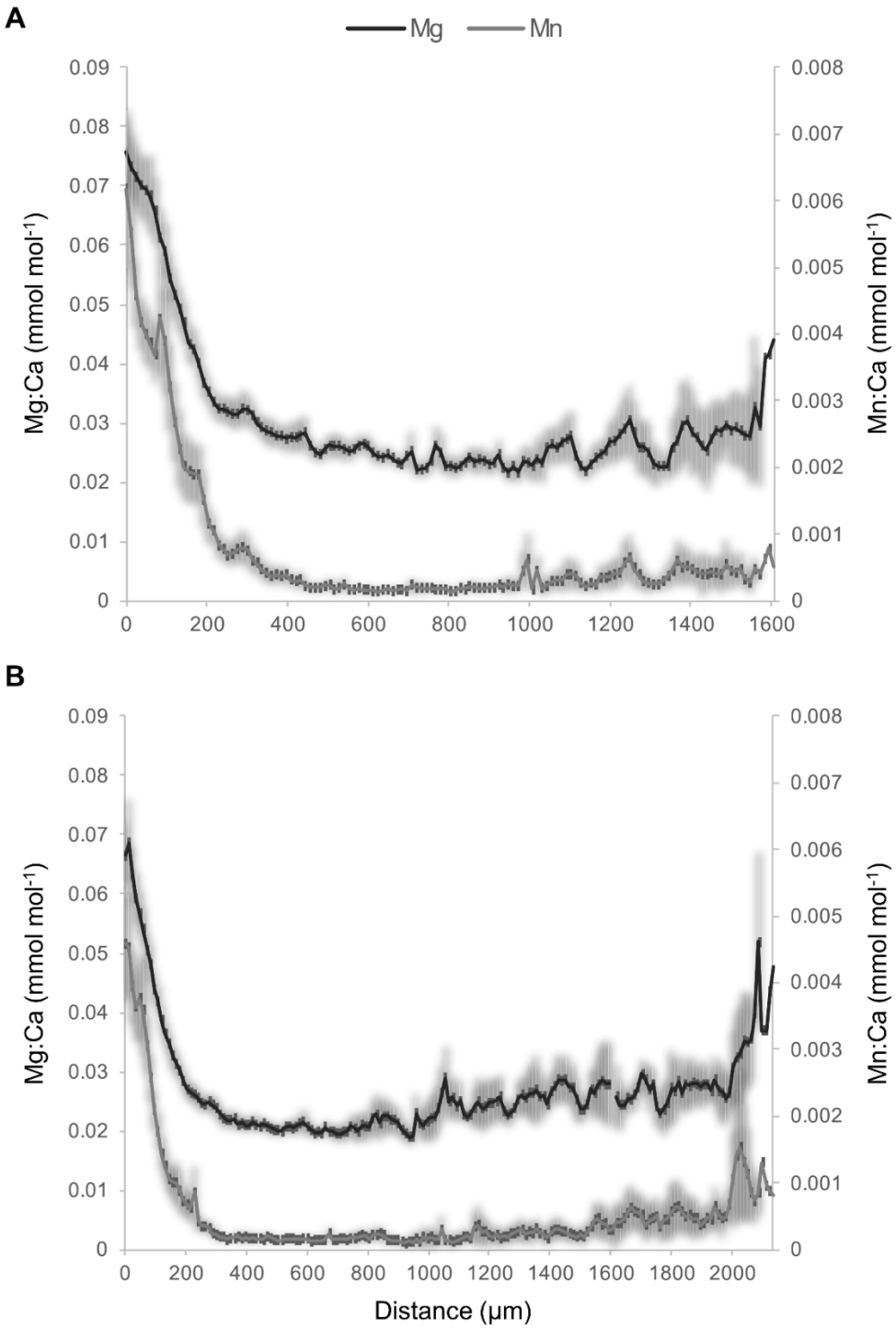

Figure 4
Core to edge otolith elemental Mg:Ca and Mn:Ca ratios in *Chelon labrosus* from GE and PL. Scatter straight lines indicate otolith mean (± SE) values for Mg:Ca (black) and Mn:Ca (grey) ratio values from the core to the edge of individuals from (A) Gernika (N=30) and (B) Plentzia (N=30). Grey shaded area indicates standard error (SE).

3.3. Life history reconstruction and migration classification

A summary on the life histories of 60 *Chelon labrosus* individuals captured from two Basque estuaries is provided (Table 3). 83 and 53% of the fish caught in GE and PL, respectively, showed values below the Sr:Ca threshold value of 3.75 mmol mol^{-1} (1.63 – 5.44 mmol mol^{-1}), while the remaining individuals (17% GE and 47% PL) showed values above this threshold value. Based on this data, the reconstructed migration patterns of *C. labrosus* from otolith core-to-edge elemental profiles revealed two distinct life histories (Figures 5 and 6): (1) fish that mostly resided in the estuarine environment (estuarine-residents), and (2) fish that residing in the estuaries during their early life stages later migrated to the marine environment (marine-migrants).

In terms of the quantification of changes in the life history of *C. labrosus*, the average number of changes in transects for Sr:Ca ratio in GE is 1.5 ± 0.2 (range: 0-4) while in PL was 2.2 ± 0.2 (range: 1-6). There were no statistically significant differences between both estuaries.

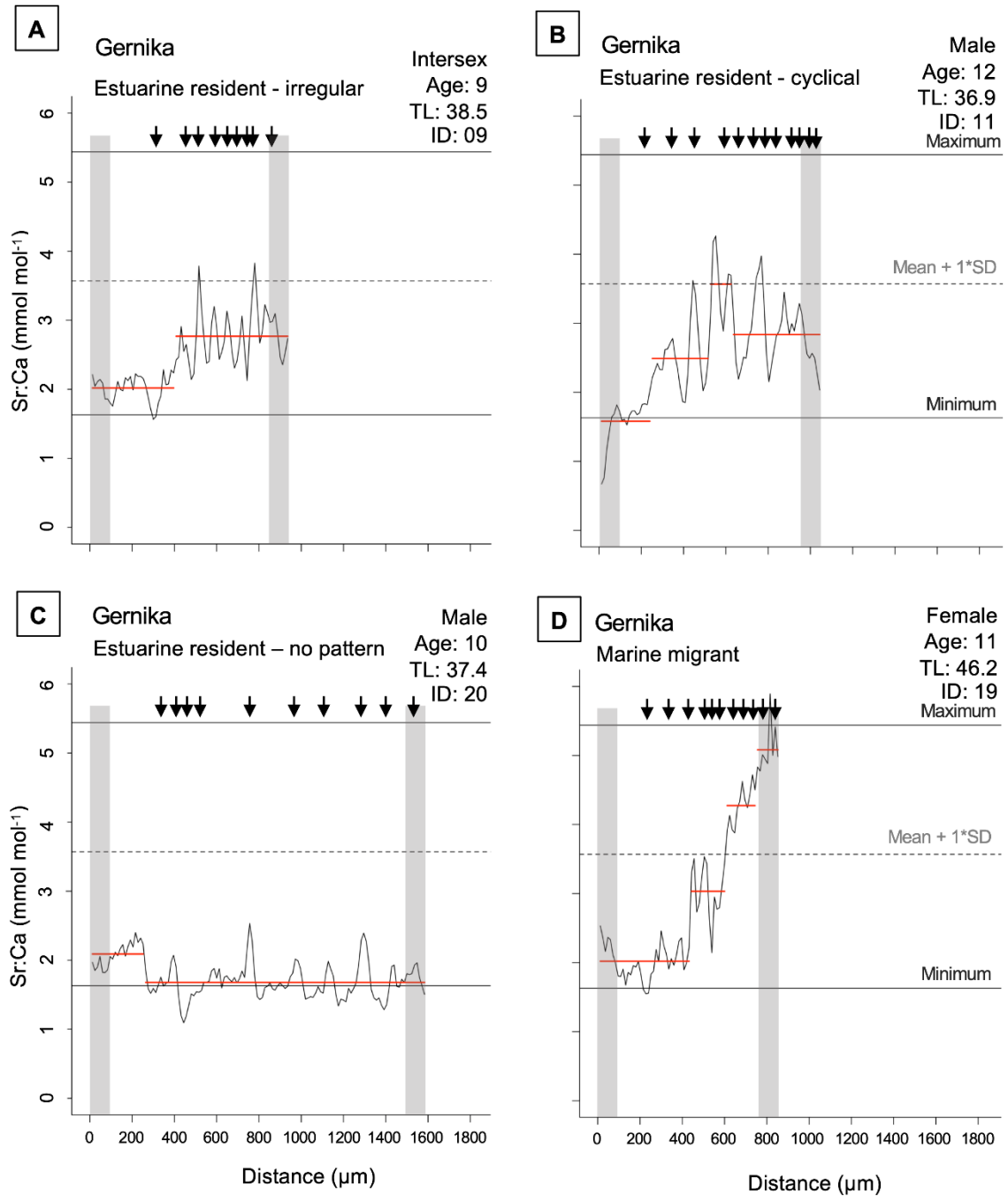

Figure 5
Core to edge otolith elemental signatures of *Chelon labrosus* from Gernika. The grey dashed horizontal line indicates the upper (marine) and lower (estuarine) thresholds for Sr:Ca ratio, black horizontal straight lines indicate the minimum and maximum values for Sr:Ca and the vertical arrows indicate otolith *annuli* (age). Horizontal red lines illustrate stable signatures identified from change-point analysis for Sr:Ca ratio. TL = total length and ID = fish/sample number.

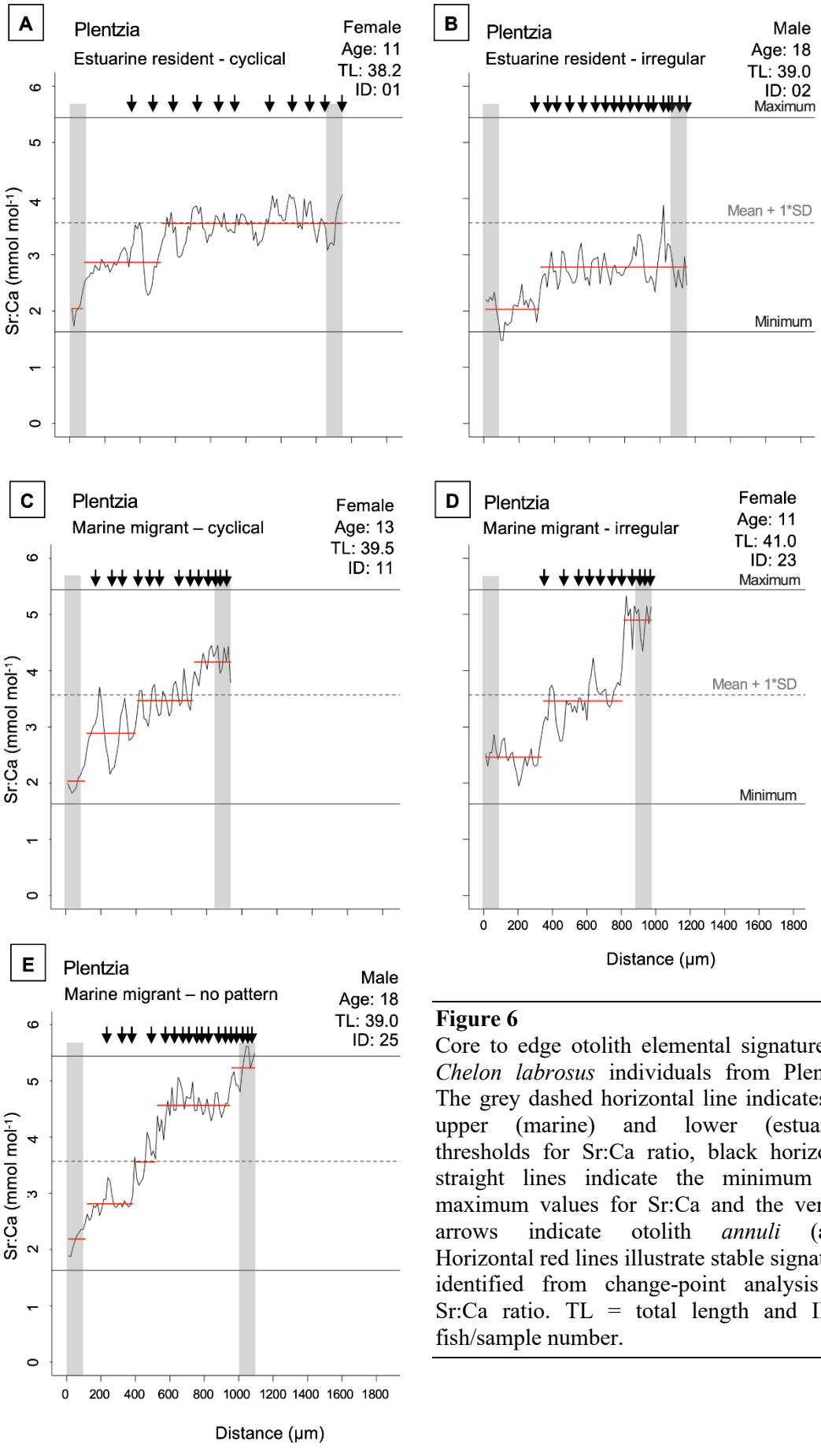

Figure 6
Core to edge otolith elemental signatures of *Chelon labrosus* individuals from Plentzia. The grey dashed horizontal line indicates the upper (marine) and lower (estuarine) thresholds for Sr:Ca ratio, black horizontal straight lines indicate the minimum and maximum values for Sr:Ca and the vertical arrows indicate otolith *annuli* (age). Horizontal red lines illustrate stable signatures identified from change-point analysis for Sr:Ca ratio. TL = total length and ID = fish/sample number.

Table 3
Life histories of 60 *Chelon labrosus* individuals captured from Gernika (displaying intersex condition males) and the other in Plentzia. Habitat and migratory patterns were assessed after the larval/early juvenile stage (< 2 years) and prior to capture according to Fowler et al. (2016). Migratory patterns: migratory irregular – movements between salinity environments but no demonstrable regular movements; migratory cyclical – at least 3 repeated movements between estuarine and marine environments at regular time intervals (e.g., 1 year). Migratory classification: Marine migrants – estuarine use in the early life history stages and later moving to marine or higher salinity waters and Estuarine residents – most frequent use of estuarine or brackish water environments.

Fish ID	Location	Sex	Age (years)	Habitat use		Migratory Pattern	Migratory Classification
				Estuarine	Marine		
GE01	GERNIKA	Intersex	12	Yes	Yes	migratory - irregular/marine	Marine Migrant
GE02	GERNIKA	Intersex	10	Yes	Yes	migratory - irregular	Estuarine Resident
GE03	GERNIKA	Male	7	Yes	No	resident - estuary	Estuarine Resident
GE04	GERNIKA	Male	9	Yes	No	resident - estuary	Estuarine Resident
GE05	GERNIKA	Male	8	Yes	No	resident - estuary	Estuarine Resident
GE06	GERNIKA	Female	13	Yes	Yes	migratory - cyclical	Estuarine Resident
GE07	GERNIKA	NA	10	Yes	Yes	migratory - irregular	Estuarine Resident
GE08	GERNIKA	Intersex	7	Yes	No	resident - estuary	Estuarine Resident
GE09	GERNIKA	Intersex	9	Yes	Yes	migratory - irregular	Estuarine Resident
GE10	GERNIKA	Intersex	8	Yes	No	resident - estuary	Estuarine Resident
GE11	GERNIKA	Male	12	Yes	Yes	migratory - cyclical	Estuarine Resident
GE12	GERNIKA	Intersex	9	Yes	No	resident - estuary	Estuarine Resident
GE13	GERNIKA	Male	6	Yes	No	resident - estuary	Estuarine Resident
GE14	GERNIKA	Male	8	Yes	No	resident - estuary	Estuarine Resident
GE15	GERNIKA	Male	8	Yes	No	resident - estuary	Estuarine Resident
GE16	GERNIKA	Male	8	Yes	No	resident - estuary	Estuarine Resident
GE17	GERNIKA	Male	7	Yes	No	resident - estuary	Estuarine Resident
GE18	GERNIKA	Intersex	8	Yes	Yes	migratory - irregular	Estuarine Resident
GE19	GERNIKA	Female	11	Yes	Yes	migratory - marine	Marine Migrant
GE20	GERNIKA	Male	10	Yes	No	resident - estuary	Estuarine Resident
GE21	GERNIKA	Male	17	Yes	Yes	migratory - cyclical	Estuarine Resident
GE22	GERNIKA	Male	15	Yes	Yes	migratory - irregular	Estuarine Resident
GE23	GERNIKA	Male	8	Yes	No	resident - estuary	Estuarine Resident

Table 3 continued…

Fish ID	Location	Sex	Age (years)	Habitat use		Migratory Pattern	Migratory Classification
				Estuarine	Marine		
GE24	GERNIKA	Female	11	Yes	Yes	migratory - cyclical/marine	Marine Migrant
GE25	GERNIKA	Male	7	Yes	No	resident - estuary	Estuarine Resident
GE26	GERNIKA	Intersex	12	Yes	Yes	migratory - marine	Marine Migrant
GE27	GERNIKA	Male	15	Yes	No	resident - estuary	Estuarine Resident
GE28	GERNIKA	Male	11	Yes	Yes	migratory - cyclical	Estuarine Resident
GE29	GERNIKA	Female	21	Yes	Yes	migratory - marine	Marine Migrant
GE30	GERNIKA	Male	8	Yes	No	resident - estuary	Estuarine Resident
PL01	PLENTZIA	Female	11	Yes	Yes	migratory - cyclical	Estuarine Resident
PL02	PLENTZIA	Male	18	Yes	Yes	migratory - irregular	Estuarine Resident
PL03	PLENTZIA	Female	8	Yes	Yes	migratory - marine	Marine Migrant
PL04	PLENTZIA	Female	11	Yes	Yes	migratory - irregular/marine	Marine Migrant
PL05	PLENTZIA	Female	8	Yes	Yes	migratory - cyclical	Estuarine Resident
PL06	PLENTZIA	Female	7	Yes	Yes	migratory - irregular	Estuarine Resident
PL07	PLENTZIA	Female	11	Yes	Yes	migratory - irregular	Estuarine Resident
PL08	PLENTZIA	Female	11	Yes	Yes	migratory - irregular	Estuarine Resident
PL09	PLENTZIA	Female	8	Yes	Yes	migratory - cyclical	Estuarine Resident
PL10	PLENTZIA	Male	8	Yes	Yes	migratory - irregular	Estuarine Resident
PL11	PLENTZIA	Female	13	Yes	Yes	migratory - cyclical/marine	Marine Migrant
PL12	PLENTZIA	Male	23	Yes	Yes	migratory - cyclical/marine	Marine Migrant
PL13	PLENTZIA	Female	8	Yes	Yes	migratory - irregular	Estuarine Resident
PL14	PLENTZIA	Female	12	Yes	Yes	migratory - irregular/marine	Marine Migrant
PL15	PLENTZIA	Female	8	Yes	Yes	migratory - irregular	Estuarine Resident
PL16	PLENTZIA	Female	6	Yes	Yes	migratory - cyclical	Estuarine Resident
PL17	PLENTZIA	Female	7	Yes	Yes	migratory - irregular/marine	Marine Migrant
PL18	PLENTZIA	Male	6	Yes	Yes	migratory - cyclical	Estuarine Resident
PL19	PLENTZIA	Male	12	Yes	Yes	migratory - irregular/marine	Marine Migrant
PL20	PLENTZIA	Female	13	Yes	Yes	migratory - irregular/marine	Marine Migrant
PL21	PLENTZIA	Female	21	Yes	Yes	migratory - marine	Marine Migrant

Table 3 continued…

Fish ID	Location	Sex	Age (years)	Habitat use		Migratory Pattern	Migratory Classification
				Estuarine	Marine		
PL22	PLENTZIA	Female	9	Yes	Yes	migratory - marine	Marine Migrant
PL23	PLENTZIA	Female	11	Yes	Yes	migratory - irregular/marine	Marine Migrant
PL24	PLENTZIA	Female	11	Yes	Yes	migratory - irregular/marine	Marine Migrant
PL25	PLENTZIA	Male	18	Yes	Yes	migratory - marine	Marine Migrant
PL26	PLENTZIA	Male	10	Yes	Yes	migratory - cyclical	Estuarine Resident
PL27	PLENTZIA	Female	11	Yes	Yes	migratory - irregular	Estuarine Resident
PL28	PLENTZIA	Female	12	Yes	Yes	migratory - marine	Marine Migrant
PL29	PLENTZIA	Male	8	Yes	Yes	migratory - irregular	Estuarine Resident
PL30	PLENTZIA	Female	10	Yes	Yes	migratory - irregular	Estuarine Resident

4. Discussion

The current study sought to evaluate whether *Chelon labrosus* individuals from two estuaries in the southern Bay of Biscay (SBB), one with a high incidence of intersex condition (GE), and the other one pristine (PL), are lifelong residents of these estuaries despite their cyclic spawning migrations to the sea. Differences in otolith edge values for both Ba and Sr were observed among individuals from GE and PL. Reconstructed mullet migration patterns from otolith core-to-edge elemental profiles obtained by LA-ICP-MS techniques revealed two distinct life histories within the two estuaries and different diadromous movement behaviours. In both estuaries, individuals with the most frequent use of estuaries were classified as estuarine-residents, while those that used the estuary during their early life history stages to later move regularly or irregularly to the marine environment were classified as marine-migrants. Mullet from GE were mostly estuarine residents while nearly 50% of the PL individuals showed periodic migration to the sea. These results agree with those reported by Nzioka et al. (2023a), which strongly suggested that individuals from GE and PL could be divided into two distinct groups belonging to their respective estuaries.

Recently, the analysis of 10 microsatellite markers in *C. labrosus* individuals from estuaries along the Basque Autonomous Region (Bay of Biscay) compared to two out-groups from the Gulf of Cádiz (southwest of the Iberian Peninsula) and Thermaic Gulf (Mediterranean Sea) could not find any genetic differences among individuals, suggesting that the species forms a single panmictic population across the whole studied area (Nzioka et al., 2023b). Despite this lack of genetic divergence in *C. labrosus*, otolith shape and multi-elemental signature analyses revealed that *C. labrosus* from the estuaries of GE and PL form, in fact, two distinct subpopulations units (Nzioka et al., 2023a). In terms of multi-elemental analyses, the differences between the two estuaries were largely driven by barium (Ba), lithium (Li) and strontium (Sr) content (Nzioka et al., 2023a).

In most otolith microchemistry studies, Ba and Sr are often used as proxies to track fish movements and habitat use. These elements accumulate differentially depending on the surrounding water and physico-chemical characteristics (Elsdon et al., 2008; Hüssy et al., 2021; Menezes et al., 2021). Element incorporation into otoliths is a complex process influenced not only by elemental concentration but also by ambient salinity, temperature and the physiology and genetics of the fish (Elsdon and Gillanders, 2004; Hüssy et al.,

2021). For most species, the relation between otolith Sr content and salinity is positive, despite obvious species-specific differences in rates of incorporation (Brown and Severin, 2009; Hüssy et al., 2021). In the case of grey mullets, Sr:Ca ratios are the preferred proxies to track estuarine-marine migrations, with other elements requiring validation experiments under controlled conditions before being used to identify dispersal in aquatic environments or fidelity to certain coastal areas (Crosetti and Blaber, 2016). For instance, the effectiveness of Sr in reconstructing the migratory history of mullets has been shown in recent studies of *M. cephalus* (Callicó Fortunato et al., 2017; Fowler et al., 2016; Wang, 2014), *M. curema* and *M. liza* (Avigliano et al., 2021; Mai et al., 2018). On the other hand, Ba:Ca ratios have also shown to be useful proxies in coastal systems where the presence of marine water in estuarine and adjacent systems impede the occurrence of specific Sr:Ca signatures (Menezes et al., 2021).

In this study, the results from otolith Sr:Ca ratio analysis of transverse otolith sections using LA-ICP-MS were identified different migration patterns between environments of different salinity performing better than Ba:Ca ratios to trace mullet movement patterns within Basque continental and oceanic transition zones. The Sr:Ca ratio threshold value used to identify movements between the estuarine and marine environments (3.57 mmol mol^{-1}) was comparatively lower than that pointed out for *Mugil cephalus* (6.40 mmol mol^{-1}) from the Australian east coast (Fowler et al., 2016), but within range to values observed in *Mugil curema* (3.46 – 4.75 mmol mol^{-1}) from Neotropical Pacific and Atlantic waters (Avigliano et al., 2021). On the other hand, otolith Ba:Ca ratios were consistently low, thus less reliable in distinguishing estuarine and marine environments especially for values < 0.020 mmol mol^{-1} (Fowler et al., 2016; Wang et al., 2010). Despite an attempt to combine both Ba:Ca and Sr:Ca ratio profiles, Ba:Ca ratio values did not allow discriminating between the two environments. Thus, without more information on ambient Ba concentrations in estuaries and the nearshore marine environment, it is not possible to improve the classifications made using otolith Sr:Ca ratios (Fowler et al., 2016). This was further corroborated by change-point analysis studies showing that Ba:Ca ratio values were not suitable for assigning individuals to different salinity environments. The number of changes for transects of Sr:Ca ratios were found to be similar in mullets from GE and PL, suggesting that on average, the number of fish movements is similar in both estuaries. Therefore, in the context of this study, habitat use of *C. labrosus* was based only on Sr:Ca ratios that fluctuated consistently throughout the otolith growth axis and allowed for the detection of habitat changes.

The movement of *C. labrosus* into the marine environment is assumed to be indicated by high Sr:Ca ratio values (Tabouret et al., 2010) regardless of the habitat use patterns. Despite all individuals being caught in estuarine systems, typical marine values of Sr:Ca were recorded at the otolith edge in 13% of the individuals from GE and in 57% of the individuals from PL. This could be due to undetected short-term but rapid movements between salinity environments, resulting in delayed uptake of Sr:Ca into the otolith during movement into estuaries, despite the fact that elemental profiles indicating most spawning migration movements between estuarine and marine environments being easily detectable (Fowler et al., 2016). The elemental signatures (Ba and Sr) of the last 10 readings of the otolith edge along the transect element profile indicated that individuals from GE were different from individuals from PL, 21 miles away (Fig. 3), confirming a lack of population connectivity between these two estuaries as reported by Nzioka et al. (2023a).

While all existing evidence suggests that spawning of *C. labrosus* occurs in the marine environment (Crosetti and Blaber, 2016), there was a lack of marine Sr:Ca values recorded near the otolith core. Similar results have been observed with *M. cephalus* (Fowler et al., 2016). That study suggested that the earliest larval increment structure is rarely exposed during otolith sectioning, despite the resulting thickness of sections passing through the core being ~300 – 500 µm. Alternatively, it is quite possible that low Sr:Ca values near the core in *C. labrosus* are physiologically-related, possibly dependant on feeding behaviour. This could result in non-uptake of Sr during the early larval stages. Moreover, pelagic eggs and larvae are susceptible to changing oceanographic conditions, thus the estuarine-level Sr:Ca signatures recorded near the otolith core may be as a result of fertilized eggs spawned offshore being transported into onshore waters with lower salinity, promoting the rapid entry of larvae and juveniles into estuaries. This is a pattern commonly observed in life cycles of most estuarine-associated species (Ibáñez et al., 2012; Secor and Rooker, 2005).

The observed high otolith Mg:Ca and Mn:Ca ratio values observed near the core showed a similar trend to other marine species in the northern Atlantic region. In the Atlantic cod (*Gadus morhua*), the Baltic Sea herring (*Clupea harengus membras*) and the catadromous European eel (*Anguilla Anguilla*), high Mg:Ca and Mn:Ca ratios have also been observed in the otolith core region, corresponding to the winter growth season and declining with the increasing size/growth of the fish (Hüssy et al., 2016; Limburg et al., 2018). A similar result was also reported for *M. cephalus* in Taiwanese coastal waters (Wang, 2014) and in a variety

of species from different regions and habitats, suggesting a general ontogenetic pattern (high levels during early life, decreasing to lower levels later in life with increasing age/size) especially in cold water temperate species (Limburg et al., 2018). However, otolith Mg and Mn are not suitable tracers of environmental concentrations for tracking the movement and migratory history of fish (Hüssy et al., 2021; Soeth et al., 2020; Wang, 2014), at least for *C. labrosus*. The elevated levels of Mg and Mn in the core region observed in *C. labrosus* samples in the present study may reflect the winter spawning migrations with spawning taking place at sea (high Mg and Mn levels in the otolith core suggesting natal waters at sea), with larvae and/or juveniles migrating into nearshore coastal waters and estuaries (low levels of Mg and Mn with increasing age). Thus, the ontogenetic patterns in otolith Mg and Mn would confirm spawning, fertilization and hatching in marine environments for *C. labrosus* in the SBB.

Previous studies using Sr:Ca ratios have revealed different habitat use patterns and behaviours in mullet populations (Bae and Kim, 2020; Callicó Fortunato et al., 2017; Chang et al., 2004; Fowler et al., 2016; Ibáñez et al., 2012; Wang, 2014). *M. cephalus* has been shown to present partial migration on the Australian east coast (Fowler et al., 2016) and diverse migratory life patterns on the Spanish Mediterranean coast (Callicó Fortunato et al., 2017). In this study, temporal changes in otolith Sr:Ca signatures indicate that *C. labrosus* movements could be divided into two groups, one that presented most frequent use of the estuarine environment (estuarine-residents) and the other that made use of the estuarine environment in the early life history stages before later moving to the marine environment (marine-migrants). In GE, of the 83% of mullets (N = 25) considered estuarine-residents, 20% (N = 5) made repeated cyclical movements from the estuary to the open ocean, possibly corresponding with annual spawning migrations, 17% (N = 4) made irregular movement patterns between the estuary and the sea and 64% (N = 16) solely resided in the estuary during their life following the juvenile stage. For PL, out of the 53% estuarine-residents (N = 16), 37.5% (N = 6) regularly moved (repeated/cyclical pattern) between the estuary and the marine environment, compared to 62.5% (N = 10) with irregular movement patterns between the two salinities. None of the individuals from Plentzia lived solely in estuarine environments before their capture.

Considering all core-to-edge Sr:Ca ratio values, majority of migrant fish made their first migration run to the marine environment after 2 – 3 years spent in the estuary. There appears

to be high mobility right after the juvenile stages and the fish should be considered to be mature. This study further observed that while some individuals migrated to the marine environment possibly during the spawning season, most individuals (residents and irregular migrants), especially from Urdaibai estuary in GE remained behind and likely did not spawn. This behaviour is consistent with other studies that have assessed migration patterns in mullets (Avigliano et al., 2021; Fowler et al., 2016; Wang, 2014). Despite that fact, we cannot say for sure whether skipped spawning is common in *C. labrosus*; though individuals used in this study were mature adults (overall total length ~ 38 cm; > 6 years) (Tsikliras and Stergiou, 2014). In GE, 64% of mullets had not entered the marine environment prior to capture compared to PL where all individuals had shown migration to the sea. This suggests that a large proportion of mullets from GE has never migrated for spawning and thus has never reproduced.

Previous studies in GE estuary, have identified an abnormally high number of intersex testes (up to 83%) in *C. labrosus* males, while mullets from PL have consistently shown normally developing testes with no evidence of intersex (Bizarro et al., 2014; Diaz De Cerio et al., 2012; Ortiz-Zarragoitia et al., 2014; Puy-Azurmendi et al., 2013). Given the predominant use of the estuarine environment in GE by *C. labrosus*, and that the development of intersex appears to be estuarine-specific and dependent on their pollutant load, it is quite possible that the residency behaviour observed by *C. labrosus* may be as a result of fidelity to the estuary of the first recruitment. By not moving out of the estuary, GE mullets are continuously exposed to xenoestrogens. On the other hand, it could also be concluded that exposure to xenoestrogens does not allow final reproductive maturation, resulting in that fish never initiated reproductive migration. As such, it could be considered that most GE mullets have never reproduced.

5. Conclusions

Otolith microchemistry analysis allowed to gain important insights into life history and population connectivity of *C. labrosus* in the SBB. Although we still do not know the processes through which juveniles are incorporated into estuaries along the Basque coast, our results demonstrate that after early migration into inshore coastal waters and estuaries, mullets show a diversity of life history patterns, but clearly showing that in both studied locations estuaries served as nursery habitats. After spawning migrations, adult mullets showed site fidelity, returning as larvae and/or juveniles to their estuary of first recruitment.

This was indicated by otolith Ba and Sr trace elemental composition that was significantly different for individuals from GE and PL. In addition, no migration to the sea was observed in most mullets from GE so most likely they did not spawn or reproduce due to the effects of exposure to xenoestrogen preventing final maturation of individual fish. We propose that *C. labrosus* is a marine estuarine-dependent species in the Basque coast that seems to be conducive to successful habitation and in this way, young juveniles rely on protected and resources rich waters of estuaries for providing a suitable nursery habitat.

Acknowledgements

The Scientific Technical Support (STS) service of the Environmental Testing Unit (University of Oviedo) is greatly acknowledged. This work was funded by the Spanish Ministry of Science, Innovation and Universities and EU-FEDER/ERDF (BORN2bEGG PGC2018-101442-B-I00), the Basque Government (Grants to consolidated research groups IT1302-19 and IT1743-22) and a transnational access project of the Horizon-2020 project ASSEMBLE PLUS, 730984). This study was also partially supported by the Strategic Funding UID/Multi/04423/2019 through national funds provided by FCT and European Regional Development Fund (ERDF) in the framework of the program PT2020. A.N. is a recipient of a pre-doctoral grant (PIF17/172) from the University of the Basque Country (UPV/EHU).

References

Avigliano, E., Ibañez, A., Fabré, N., Callicó Fortunato, R., Méndez, A., Pisonero, J., Volpedo, A. V., 2021. Unravelling the complex habitat use of the white mullet, *Mugil curema*, in several coastal environments from Neotropical Pacific and Atlantic waters. Aquat Conserv 31, 789–801. https://doi.org/10.1002/aqc.3486

Avigliano, E., Leisen, M., Romero, R., Carvalho, B., Velasco, G., Vianna, M., Barra, F., Volpedo, A.V., 2017. Fluvio-marine travelers from South America: cyclic amphidromy and freshwater residency, typical behaviors in *Genidens barbus* inferred by otolith chemistry. Fish Res 193, 184–194. https://doi.org/10.1016/J.FISHRES.2017.04.011

Bae, S.E., Kim, J.K., 2020. Otolith microchemistry reveals the migration patterns of the flathead grey mullet *Mugil cephalus* (Pisces: Mugilidae) in Korean waters. J Ecol Environ 44. https://doi.org/10.1186/s41610-020-00164-9

Bailey, D.S., Fairchild, E.A., Kalnejais, L.H., 2015. Microchemical Signatures in Juvenile Winter Flounder Otoliths Provide Identification of Natal Nurseries. Trans Am Fish Soc 144, 173–183. https://doi.org/10.1080/00028487.2014.982259

Besbes, R., Benseddik, A.B., Kokokiris, L., Changeux, T., Hamza, A., Kammoun, F., Missaoui, H., 2020. Thicklip (*Chelon labrosus*) and flathead (*Mugil cephalus*) grey mullets fry production in Tunisian aquaculture. Aquac Rep 17, 100380. https://doi.org/10.1016/j.aqrep.2020.100380

Bizarro, C., Ros, O., Vallejo, A., Prieto, A., Etxebarria, N., Cajaraville, M.P., Ortiz-Zarragoitia, M., 2014. Intersex condition and molecular markers of endocrine disruption in relation with burdens of emerging pollutants in thicklip grey mullets (*Chelon labrosus*) from Basque estuaries (South-East Bay of Biscay). Mar Environ Res 96, 19–28. https://doi.org/10.1016/j.marenvres.2013.10.009

Boglione, C., Bertolini, B., Russiello, M., Cataudella, S., 1992. Embryonic and larval development of the thicklipped mullet (*Chelon labrosus*) under controlled reproduction conditions. Aquaculture 101, 349–359. https://doi.org/10.1016/0044-8486(92)90037-L

Brown, R.J., Severin, K.P., 2009. Otolith chemistry analyses indicate that water Sr:Ca is the primary factor influencing otolith Sr:Ca for freshwater and diadromous fish but not for marine fish. Canadian Journal of Fisheries and Aquatic Sciences 66, 1790–1808. https://doi.org/10.1139/F09-112

Callicó Fortunato, R., Reguera Galán, A., García Alonso, I., Volpedo, A., Benedito Durà, V., 2017. Environmental migratory patterns and stock identification of *Mugil cephalus* in the Spanish Mediterranean Sea, by means of otolith microchemistry. Estuar Coast Shelf Sci 188, 174–180. https://doi.org/10.1016/j.ecss.2017.02.018

Campana, S.E., 1999. Chemistry and composition of fish otoliths: Pathways, mechanisms and applications. Mar Ecol Prog Ser 188, 263–297. https://doi.org/10.3354/meps188263

Chang, C.W., Iizuka, Y., Tzeng, W.N., 2004. Migratory environmental history of the grey mullet *Mugil cephalus* as revealed by otolith Sr:Ca ratios. Mar Ecol Prog Ser 269, 277–288. https://doi.org/10.3354/meps269277

Cooke, S.J., Brooks, J.L., Raby, G.D., Thorstad, E.B., Brownscombe, J.W., Vandergoot, C.S., Lennox, R.J., Bulte, G., Bino, G., Thiem, J.D., 2022. Electronic Tagging and Tracking of Animals in Inland Waters, in: Tockner, K., Mehner, T. (Eds.), Encyclopedia of Inland Waters, Second Edition. Elsevier, pp. 699–712. https://doi.org/10.1016/B978-0-12-819166-8.00061-X

Correia, A.T., Gomes, P., Gonçalves, J.M.S., Erzini, K., Hamer, P.A., 2012. Population structure of the black seabream *Spondyliosoma cantharus* along the south-west Portuguese coast inferred from otolith chemistry. J Fish Biol 80, 427–443. https://doi.org/10.1111/j.1095-8649.2011.03186.x

Crook, D.A., Lacksen, K., King, A.J., Buckle, D.J., Tickell, S.J., Woodhead, J.D., Maas, R., Townsend, S.A., Douglas, M.M., 2017. Temporal and spatial variation in strontium in a tropical river: implications for otolith chemistry analyses of fish migration. Canadian Journal of Fisheries and Aquatic Sciences 74, 533–545. https://doi.org/10.1139/cjfas-2016-0153

Crosetti, D., Blaber, S. (Eds.), 2016. Biology, ecology and culture of grey mullets (Mugilidae), 1st ed. CRC Press. https://doi.org/10.1201/b19927

Dag, O., Dolgun, A., Konar, N.M., 2018. Onewaytests: An R package for one-way tests in independent groups designs. R Journal 10, 175–199. https://doi.org/10.32614/rj-2018-022

Diaz De Cerio, O., Rojo-Bartolomé, I., Bizarro, C., Ortiz-Zarragoitia, M., Cancio, I., 2012. 5S rRNA and accompanying proteins in gonads: powerful markers to identify sex and reproductive endocrine disruption in fish. Environ Sci Technol 46, 7763–7771. https://doi.org/10.1021/es301132b

Ellender, B., Taylor, G., Weyl, O., 2012. Validation of growth zone deposition rate in otoliths and scales of flathead mullet *Mugil cephalus* and freshwater mullet *Myxus capensis* from fish of known age. Afr J Mar Sci 34, 455–458. https://doi.org/10.2989/1814232X.2012.725518

Elsdon, T.S., Gillanders, B.M., 2005. Alternative life-history patterns of estuarine fish: barium in otoliths elucidates freshwater residency. Canadian Journal of Fisheries and Aquatic Sciences 62, 1143–1152. https://doi.org/10.1139/f05-029

Elsdon, T.S., Gillanders, B.M., 2004. Fish otolith chemistry influenced by exposure to multiple environmental variables. J Exp Mar Biol Ecol 313, 269–284. https://doi.org/10.1016/j.jembe.2004.08.010

Elsdon, T.S., Wells, B.K., Campana, S.E., Gillanders, B.M., Jones, C.M., Limburg, K.E., Secor, D.H., Thorrold, S.R., Walther, B.D., 2008. Otolith chemistry to describe movements and life -history parameters of fishes: hypotheses, assumptions, limitations and inferences, in: Gibson, R.N., Atkinson, R.J.A., Gordon, D.M. (Eds.), Oceanography and Marine Biology. CRC Press, pp. 303–336. https://doi.org/10.1201/9781420065756-9

Fowler, A.M., Smith, S.M., Booth, D.J., Stewart, J., 2016. Partial migration of grey mullet (*Mugil cephalus*) on Australia's east coast revealed by otolith chemistry. Mar Environ Res 119, 238–244. https://doi.org/10.1016/j.marenvres.2016.06.010

Fox, J., Weisberg, S., 2019. An R Companion to Applied Regression, Third. ed. Sage, Thousand Oaks, CA.

Froese, R., Pauly, D., 2022. FishBase [WWW Document]. World Wide Web electronic publication. URL https://www.fishbase.se/search.php (accessed 6.15.22).

Hedger, R.D., Rikardsen, A.H., Thorstad, E.B., 2017. Pop-up satellite archival tag effects on the diving behaviour, growth and survival of adult Atlantic salmon *Salmo salar* at sea. J Fish Biol 90, 294–310. https://doi.org/10.1111/jfb.13174

Hickling, C.F., 1970. A contribution to the natural history of the English grey mullets [Pisces, Mugilidae]. Journal of the Marine Biological Association of the United Kingdom 50, 609–633. https://doi.org/10.1017/S0025315400004914

Higgins, R., Isidro, E., Menezes, G., Correia, A., 2013. Otolith elemental signatures indicate population separation in deep-sea rockfish, *Helicolenus dactylopterus* and *Pontinus kuhlii*, from the Azores. J Sea Res 83, 202–208. https://doi.org/10.1016/j.seares.2013.05.014

Hsu, C.-C., Tzeng, W.-N., 2009. Validation of annular deposition in scales and otoliths of flathead mullet *Mugil cephalus*. Zool Stud 48, 640–648.

Hüssy, K., Gröger, J., Heidmann, F., Hinrichsen, H.-H., Marohn, L., 2016. Slave to the rhythm: seasonal signals in otolith microchemistry reveal age of eastern Baltic cod (*Gadus morhua*). ICES Journal of Marine Science 73, 1019–1032. https://doi.org/10.1093/icesjms/fsv247

Hüssy, K., Limburg, K.E., de Pontual, H., Thomas, O.R.B., Cook, P.K., Heimbrand, Y., Blass, M., Sturrock, A.M., 2021. Trace element patterns in otoliths: The role of biomineralization. Reviews in Fisheries Science and Aquaculture 29, 445–477. https://doi.org/10.1080/23308249.2020.1760204

Ibáñez, A., Chang, C., Hsu, C., Wang, C., Iizuka, Y., Tzeng, W., 2012. Diversity of migratory environmental history of the mullets *Mugil cephalus* and *M. curema* in Mexican coastal waters as indicated by otolith Sr:Ca ratios. Cienc Mar 38, 73–87. https://doi.org/10.7773/cm.v38i1A.1905

Iriarte, A., Villate, F., Uriarte, I., Alberdi, L., Intxausti, L., 2015. Dissolved Oxygen in a Temperate Estuary: the Influence of Hydro-climatic Factors and Eutrophication at Seasonal and Inter-annual Time Scales. Estuaries and Coasts 38, 1000–1015. https://doi.org/10.1007/s12237-014-9870-x

Izzo, C., Reis-Santos, P., Gillanders, B.M., 2018. Otolith chemistry does not just reflect environmental conditions: A meta-analytic evaluation. Fish and Fisheries 19, 441–454. https://doi.org/10.1111/faf.12264

Jepsen, N., Thorstad, E.B., Havn, T., Lucas, M.C., 2015. The use of external electronic tags on fish: An evaluation of tag retention and tagging effects. Animal Biotelemetry 3. https://doi.org/10.1186/s40317-015-0086-z

Kassambara, A., 2023. ggpubr: "ggplot2" Based Publication Ready Plots [WWW Document]. R package version 0.6.0. URL https://cran.r-project.org/package=ggpubr

Killick, R., Fearnhead, P., Eckley, I.A., 2012. Optimal detection of changepoints with a linear computational cost. J Am Stat Assoc 107, 1590–1598. https://doi.org/10.1080/01621459.2012.737745

Leorri, E., Cearreta, A., García-Artola, A., Irabien, M.J., Blake, W.H., 2013. Relative sea-level rise in the Basque coast (N Spain): Different environmental consequences on the coastal area. Ocean Coast Manag 77, 3–13. https://doi.org/10.1016/j.ocecoaman.2012.02.007

Limburg, K.E., Wuenschel, M.J., Hüssy, K., Heimbrand, Y., Samson, M., 2018. Making the Otolith Magnesium Chemical Calendar-Clock Tick: Plausible Mechanism and Empirical Evidence. Reviews in Fisheries Science and Aquaculture 26, 479–493. https://doi.org/10.1080/23308249.2018.1458817

Lin, Y.-J., Jessop, B.M., Weyl, O.L.F., Iizuka, Y., Lin, S.-H., Tzeng, W.-N., 2015. Migratory history of African longfinned eel *Anguilla mossambica* from Maningory River, Madagascar: discovery of a unique pattern in otolith Sr:Ca ratios. Environ Biol Fishes 98, 457–468. https://doi.org/10.1007/s10641-014-0275-2

Mai, A.C.G., Santos, M.L. dos, Lemos, V.M., Vieira, J.P., 2018. Discrimination of habitat use between two sympatric species of mullets, *Mugil curema* and *Mugil liza* (Mugiliformes: Mugilidae) in the rio Tramandaí Estuary, determined by otolith chemistry. Neotropical Ichthyology 16, 1–8. https://doi.org/10.1590/1982-0224-20170045

Marigómez, I., Garmendia, L., Soto, M., Orbea, A., Izagirre, U., Cajaraville, M.P., 2013. Marine ecosystem health status assessment through integrative biomarker indices: A comparative study after the Prestige oil spill "mussel Watch." Ecotoxicology 22, 486–505. https://doi.org/10.1007/s10646-013-1042-4

Menezes, R., Moura, P.E.S., Santos, A.C.A., Moraes, L.E., Condini, M. V., Rosa, R.S., Albuquerque, C.Q., 2021. Habitat use plasticity by the dog snapper (*Lutjanus jocu*) across the Abrolhos Bank shelf, eastern Brazil, inferred from otolith chemistry. Estuar Coast Shelf Sci 263, 107637. https://doi.org/10.1016/j.ecss.2021.107637

Mićković, B., Nikčević, M., Hegediš, A., Regner, S., Gačić, Z., Krpo-Ćetković, J., 2010. Mullet Fry (Mugilidae) in coastal waters of Montenegro, their spatial distribution and migration phenology. Arch Biol Sci. https://doi.org/10.2298/ABS1001107M

Mijangos, L., Ziarrusta, H., Ros, O., Kortazar, L., Fernández, L.A., Olivares, M., Zuloaga, O., Prieto, A., Etxebarria, N., 2018. Occurrence of emerging pollutants in estuaries of the Basque Country: Analysis of sources and distribution, and assessment of the environmental risk. Water Res 147, 152–163. https://doi.org/10.1016/j.watres.2018.09.033

Nzioka, A., Cancio, I., Diaz de Cerio, O., Pinto, E., Almeida, A., Correia, A.T., 2023a. Otolith shape and elemental signatures provide insights into the connectivity of euryhaline *Chelon labrosus* inhabiting two close estuaries with different burdens of xenoestrogens in the Southern Bay of Biscay. Mar Environ Res 189, 106075. https://doi.org/10.1016/j.marenvres.2023.106075

Nzioka, A., Madeira, M.J., Kokokiris, L., Ortiz-Zarrogoitia, M., Diaz de Cerio, O., Cancio, I., 2023b. Lack of genetic structure in euryhaline *Chelon labrosus* from the estuaries under anthropic pressure in the Southern Bay of Biscay to the coastal waters of the Mediterranean Sea. Mar Environ Res 189, 106058. https://doi.org/10.1016/j.marenvres.2023.106058

Ortiz-Zarragoitia, M., Bizarro, C., Rojo-Bartolomé, I., de Cerio, O.D., Cajaraville, M.P., Cancio, I., 2014. Mugilid fish are sentinels of exposure to endocrine disrupting compounds in coastal and estuarine environments. Mar Drugs 12, 4756–4782. https://doi.org/10.3390/md12094756

Patil, I., 2021. Visualizations with statistical details: The "ggstatsplot" approach. J Open Source Softw 6, 3167. https://doi.org/10.21105/joss.03167

Paton, C., Hellstrom, J., Paul, B., Woodhead, J., Hergt, J., 2011. Iolite: Freeware for the visualisation and processing of mass spectrometric data. J Anal At Spectrom 26, 2508. https://doi.org/10.1039/c1ja10172b

Payne Wynne, M.L., Wilson, K.A., Limburg, K.E., 2015. Retrospective examination of habitat use by blueback herring (*Alosa aestivalis*) using otolith microchemical methods. Canadian Journal of Fisheries and Aquatic Sciences 72, 1073–1086. https://doi.org/10.1139/cjfas-2014-0206

Pepping, M.Y., O'Rourke, S.M., Huang, C., Katz, J.V.E.E., Jeffres, C., Miller, M.R., 2020. Rapture facilitates inexpensive and high-throughput parent-based tagging in salmonids. PLoS One 15, 1–17. https://doi.org/10.1371/journal.pone.0239221

Potter, I.C., Tweedley, J.R., Elliott, M., Whitfield, A.K., 2015. The ways in which fish use estuaries: a refinement and expansion of the guild approach. Fish and Fisheries 16, 230–239. https://doi.org/10.1111/faf.12050

Puy-Azurmendi, E., Ortiz-Zarragoitia, M., Villagrasa, M., Kuster, M., Aragón, P., Atienza, J., Puchades, R., Maquieira, A., Domínguez, C., López de Alda, M., Fernandes, D., Porte, C., Bayona, J.M., Barceló, D., Cajaraville, M.P., 2013. Endocrine disruption in thicklip grey mullet (*Chelon labrosus*) from the Urdaibai Biosphere Reserve (Bay of Biscay, Southwestern Europe). Science of The Total Environment 443, 233–244. https://doi.org/10.1016/J.SCITOTENV.2012.10.078

R Core Team, 2023. R: A language and environment for statistical computing. R Foundation for Statistical Computing, Vienna, Austria.

Reis-Santos, P., Gillanders, B.M., Sturrock, A.M., Izzo, C., Oxman, D.S., Lueders-Dumont, J.A., Hüssy, K., Tanner, S.E., Rogers, T., Doubleday, Z.A., Andrews, A.H., Trueman, C., Brophy, D., Thiem, J.D., Baumgartner, L.J., Willmes, M., Chung, M.T., Johnson, R.C., Heimbrand, Y., Limburg, K.E., Walther, B.D., 2022. Reading the biomineralized book of life: expanding otolith biogeochemical research and applications for fisheries and ecosystem-based management, Reviews in Fish Biology and Fisheries. Springer International Publishing. https://doi.org/10.1007/s11160-022-09720-z

Schindelin, J., Arganda-Carreras, I., Frise, E., Kaynig, V., Longair, M., Pietzsch, T., Preibisch, S., Rueden, C., Saalfeld, S., Schmid, B., Tinevez, J.Y., White, D.J., Hartenstein, V., Eliceiri, K., Tomancak, P., Cardona, A., 2012. Fiji: An open-source platform for biological-image analysis. Nat Methods 9, 676–682. https://doi.org/10.1038/nmeth.2019

Secor, H., Rooker, J.R., 2005. Connectivity in the life histories of fishes that use estuaries. Estuar Coast Shelf Sci 64, 1–3. https://doi.org/10.1016/j.ecss.2005.02.001

Soeth, M., Spach, H.L., Daros, F.A., Castro, J.P., Correia, A.T., 2020. Use of otolith elemental signatures to unravel lifetime movement patterns of Atlantic spadefish, *Chaetodipterus faber*, in the Southwest Atlantic Ocean. J Sea Res 158, 101873. https://doi.org/10.1016/j.seares.2020.101873

Sostoa, A., 1983. Las Comunidades de peces del Delta del Ebro. Universitat de Barcelona.

Sturrock, A.M., Hunter, E., Milton, J.A., Johnson, R.C., Waring, C.P., Trueman, C.N., EIMF, 2015. Quantifying physiological influences on otolith microchemistry. Methods Ecol Evol 6, 806–816. https://doi.org/10.1111/2041-210X.12381

Tabouret, H., Bareille, G., Claverie, F., Pécheyran, C., Prouzet, P., Donard, O.F.X., 2010. Simultaneous use of strontium:calcium and barium:calcium ratios in otoliths as markers of habitat: Application to the European eel (*Anguilla anguilla*) in the Adour basin, South West France. Mar Environ Res 70, 35–45. https://doi.org/10.1016/j.marenvres.2010.02.006

Thieme, P., Bogorodsky, S. V., Alpermann, T.J., Whitfield, A.K., Freitas, R., Durand, J.-D., 2022. Contributions to the taxonomy of the mugilid genus *Chelon* Artedi (Teleostei: Mugilidae), with a major review of the status of *C. persicus* Senou, Randall & Okiyama, 1995. Zootaxa 5188, 1–42. https://doi.org/10.11646/zootaxa.5188.1.1

Thorstad, E.B., Rikardsen, A.H., Alp, A., Okland, F., 2014. The use of electronic tags in fish research – An overview of fish telemetry methods. Turk J Fish Aquat Sci 13, 881–896. https://doi.org/10.4194/1303-2712-v13_5_13

Tsikliras, A.C., Stergiou, K.I., 2014. Size at maturity of Mediterranean marine fishes. Rev Fish Biol Fish 24, 219–268. https://doi.org/10.1007/s11160-013-9330-x

Valencia, A., Rojo-Bartolomé, I., Bizarro, C., Cancio, I., Ortiz-Zarragoitia, M., 2017. Alteration in molecular markers of oocyte development and intersex condition in mullets impacted by wastewater treatment plant effluents. Gen Comp Endocrinol 245, 10–18. https://doi.org/10.1016/J.YGCEN.2016.06.017

Vignon, M., 2015. Extracting environmental histories from sclerochronological structures - Recursive partitioning as a mean to explore multi-elemental composition of fish otolith. Ecol Inform 30, 159–169. https://doi.org/10.1016/j.ecoinf.2015.10.002

Walther, B.D., 2019. The art of otolith chemistry: Interpreting patterns by integrating perspectives. Mar Freshw Res 70, 1643–1658. https://doi.org/10.1071/MF18270

Wang, C.H., 2014. Otolith elemental ratios of flathead mullet *Mugil cephalus* in Taiwanese waters reveal variable patterns of habitat use. Estuar Coast Shelf Sci 151, 124–130. https://doi.org/10.1016/j.ecss.2014.08.024

Wang, C.H., Hsu, C.C., Chang, C.W., You, C.F., Tzeng, W.N., 2010. The migratory environmental history of freshwater resident flathead mullet *Mugil cephalus* L. in the Tanshui River, northern Taiwan. Zool Stud 49, 504–514.

Whitfield, A.K., 2020. Fish species in estuaries-from partial association to complete dependency. J Fish Biol 97, 1262–1264. https://doi.org/10.1111/jfb.14476

Whitfield, A.K., Panfili, J., Durand, J.D., 2012. A global review of the cosmopolitan flathead mullet *Mugil cephalus* Linnaeus 1758 (Teleostei: Mugilidae), with emphasis on the biology, genetics, ecology and fisheries aspects of this apparent species complex, Reviews in Fish Biology and Fisheries. https://doi.org/10.1007/s11160-012-9263-9

Wickham, H., Averick, M., Bryan, J., Chang, W., McGowan, L., François, R., Grolemund, G., Hayes, A., Henry, L., Hester, J., Kuhn, M., Pedersen, T., Miller, E., Bache, S., Müller, K., Ooms, J., Robinson, D., Seidel, D., Spinu, V., Takahashi, K., Vaughan, D., Wilke, C., Woo, K., Yutani, H., 2019. Welcome to the Tidyverse. J Open Source Softw 4, 1686. https://doi.org/10.21105/joss.01686

Xuan, Z., Wang, W.X., 2023. Diversity of life history and population connectivity of threadfin fish *Eleutheronema tetradactylum* along the coastal waters of Southern China. Sci Rep 13, 1–17. https://doi.org/10.1038/s41598-023-31174-x

Xuan, Z., Wang, X., Hajisamae, S., Tsim, K., Yang, J., Wang, W., 2022. Otolith microchemistry reveals different environmental histories for two endangered fourfinger threadfin species. Mar Ecol Prog Ser 700, 161–178. https://doi.org/10.3354/meps14187

SUPPLEMENTARY MATERIAL

Figure S1 Core to edge otolith elemental signatures of *Chelon labrosus* estuarine residents (no movement to the sea) from Gernika. The grey dashed horizontal line indicates the upper (marine) and lower (estuarine) thresholds for Sr:Ca ratio, black horizontal straight lines indicate the minimum and maximum values for Sr:Ca and the vertical arrows indicate otolith *annuli* (age). Horizontal red lines illustrate stable signatures identified from change-point analysis for Sr:Ca ratio. TL = total length and ID = fish/sample number.

Figure S2 Core to edge otolith elemental signatures of *Chelon labrosus* estuarine residents (no movement pattern to the sea) from Gernika. The grey dashed horizontal line indicates the upper (marine) and lower (estuarine) thresholds for Sr:Ca ratio, black horizontal straight lines indicate the minimum and maximum values for Sr:Ca and the vertical arrows indicate otolith *annuli* (age). Horizontal red lines illustrate stable signatures identified from change-point analysis for Sr:Ca ratio. TL = total length and ID = fish/sample number.

Figure S3 Core to edge otolith elemental signatures of *Chelon labrosus* estuarine residents (irregular and regular movement patterns to the sea) from Gernika. The grey dashed horizontal line indicates the upper (marine) and lower (estuarine) thresholds for Sr:Ca ratio, black horizontal straight lines indicate the minimum and maximum values for Sr:Ca and the vertical arrows indicate otolith *annuli* (age). Horizontal red lines illustrate stable signatures identified from change-point analysis for Sr:Ca ratio. TL = total length and ID = fish/sample number.

Figure S4 Core to edge otolith elemental signatures of *Chelon labrosus* estuarine residents (irregular and regular movement patterns to the sea) and marine migrants from Gernika. The grey dashed horizontal line indicates the upper (marine) and lower (estuarine) thresholds for Sr:Ca ratio, black horizontal straight lines indicate the minimum and maximum values for Sr:Ca and the vertical arrows indicate otolith *annuli* (age). Horizontal red lines illustrate stable signatures identified from change-point analysis for Sr:Ca ratio. TL = total length and ID = fish/sample number.

Figure S5 Core to edge otolith elemental signatures of *Chelon labrosus* estuarine residents (with irregular movement patterns to the sea) from Plentzia. The grey dashed horizontal line indicates the upper (marine) and lower (estuarine) thresholds for Sr:Ca ratio, black horizontal straight lines indicate the minimum and maximum values for Sr:Ca and the vertical arrows indicate otolith *annuli* (age). Horizontal red lines illustrate stable signatures identified from change-point analysis for Sr:Ca ratio. TL = total length and ID = fish/sample number.

Figure S6 Core to edge otolith elemental signatures of *Chelon labrosus* estuarine residents from Plentzia with irregular and regular movements patterns to the sea. The grey dashed horizontal line indicates the upper (marine) and lower (estuarine) thresholds for Sr:Ca ratio, black horizontal straight lines indicate the minimum and maximum values for Sr:Ca and the vertical arrows indicate otolith *annuli* (age). Horizontal red lines illustrate stable signatures identified from change-point analysis for Sr:Ca ratio. TL = total length and ID = fish/sample number.

Figure S7 Core to edge otolith elemental signatures of *Chelon labrosus* marine migrants from Plentzia with initial irregular and regular movements patterns to the sea. The grey dashed horizontal line indicates the upper (marine) and lower (estuarine) thresholds for Sr:Ca ratio, black horizontal straight lines indicate the minimum and maximum values for Sr:Ca and the vertical arrows indicate otolith *annuli* (age). Horizontal red lines illustrate stable signatures identified from change-point analysis for Sr:Ca ratio. TL = total length and ID = fish/sample number.

Figure S8 Core to edge otolith elemental signatures of *Chelon labrosus* marine migrants from Plentzia with initial irregular and regular movements patterns to the sea. The grey dashed horizontal line indicates the upper (marine) and lower (estuarine) thresholds for Sr:Ca ratio, black horizontal straight lines indicate the minimum and maximum values for Sr:Ca and the vertical arrows indicate otolith *annuli* (age). Horizontal red lines illustrate stable signatures identified from change-point analysis for Sr:Ca ratio. TL = total length and ID = fish/sample number.

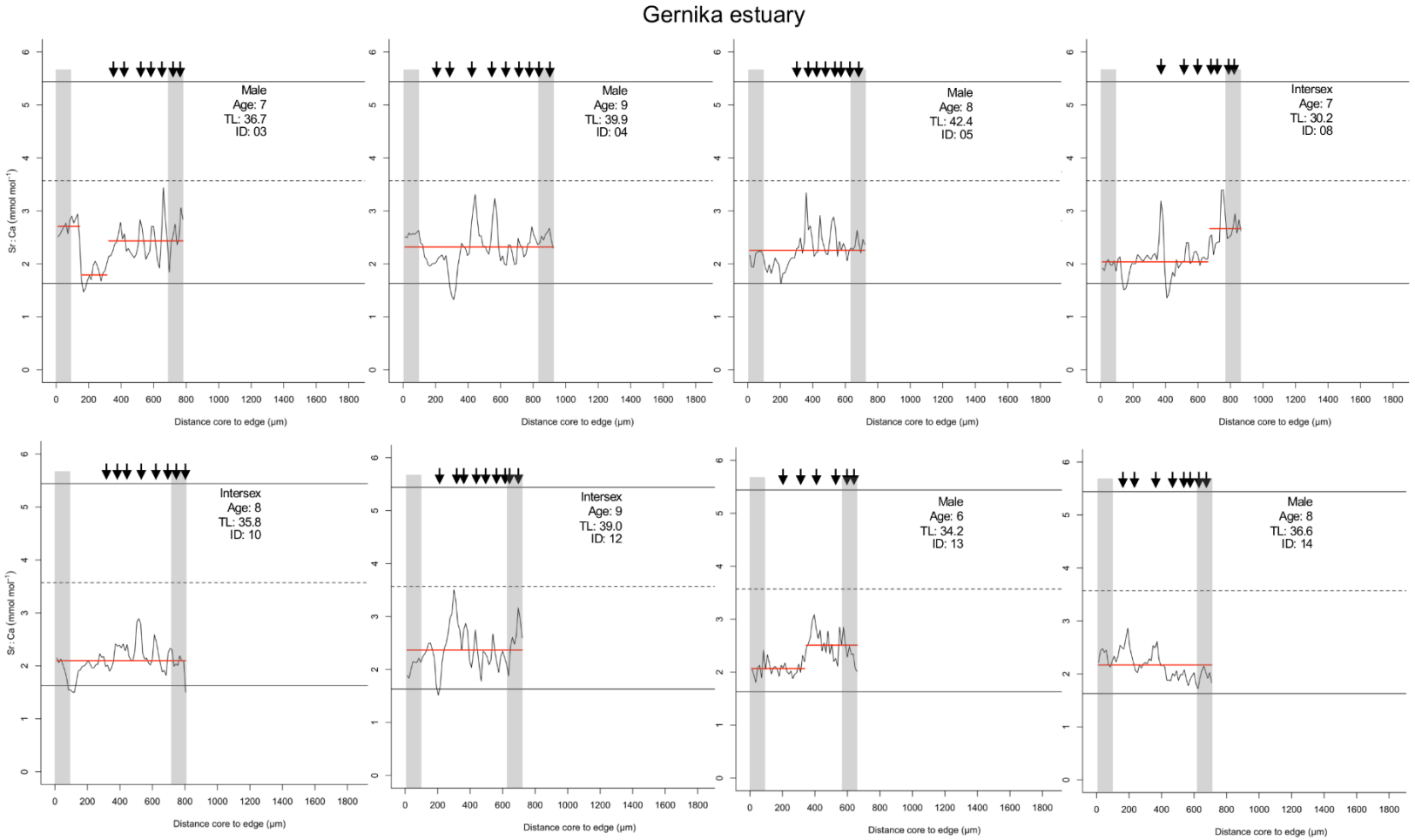

Figure S1

Core to edge otolith elemental signatures of *Chelon labrosus* estuarine residents (no movement to the sea) from Gernika. The grey dashed horizontal line indicates the upper (marine) and lower (estuarine) thresholds for Sr:Ca ratio, black horizontal straight lines indicate the minimum and maximum values for Sr:Ca and the vertical arrows indicate otolith *annuli* (age). Horizontal red lines illustrate stable signatures identified from change-point analysis for Sr:Ca ratio. TL = total length and ID = fish/sample number.

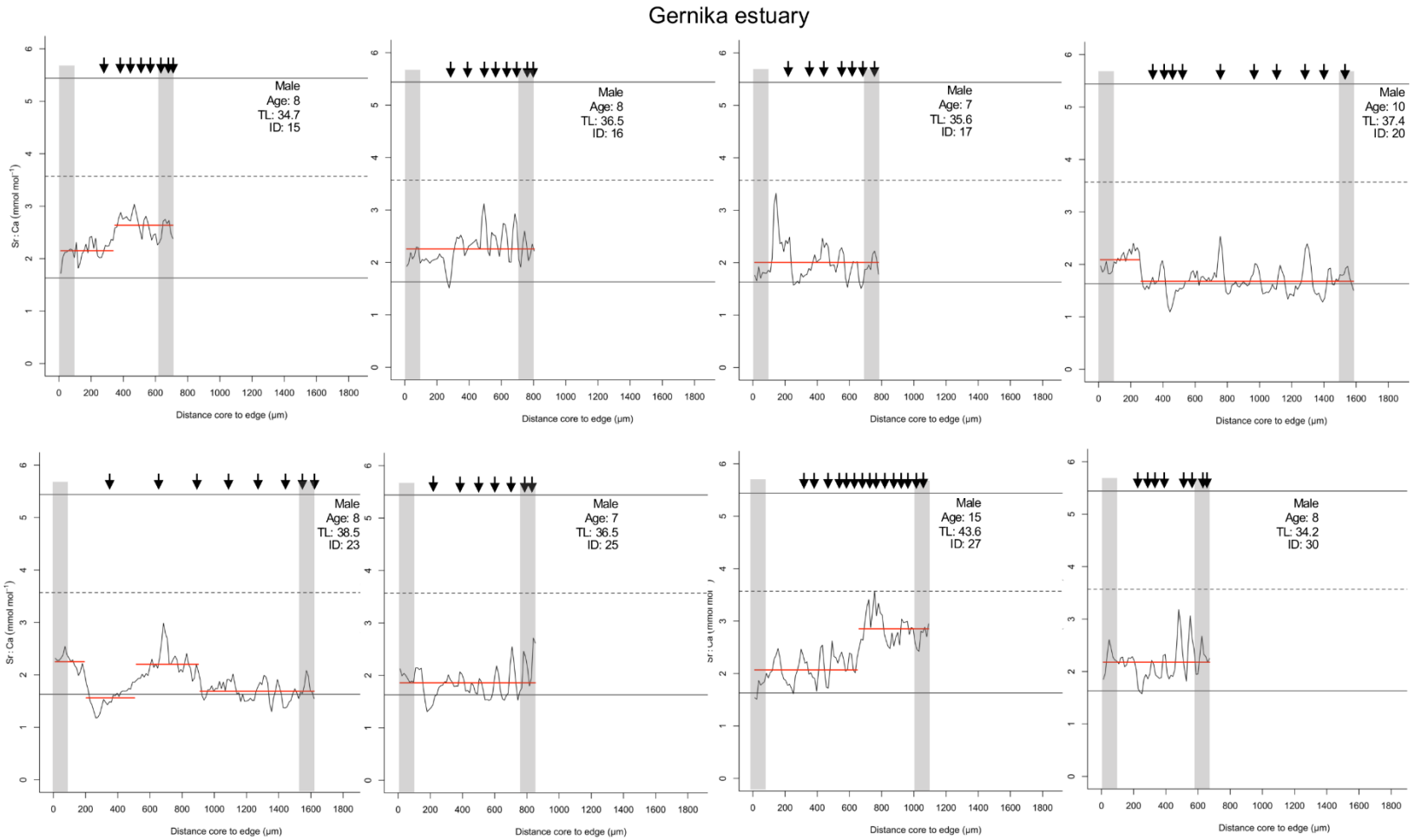

Figure S2

Core to edge otolith elemental signatures of *Chelon labrosus* estuarine residents (no movement to the sea) from Gernika. The grey dashed horizontal line indicates the upper (marine) and lower (estuarine) thresholds for Sr:Ca ratio, black horizontal straight lines indicate the minimum and maximum values for Sr:Ca and the vertical arrows indicate otolith *annuli* (age). Horizontal red lines illustrate stable signatures identified from change-point analysis for Sr:Ca ratio. TL = total length and ID = fish/sample number.

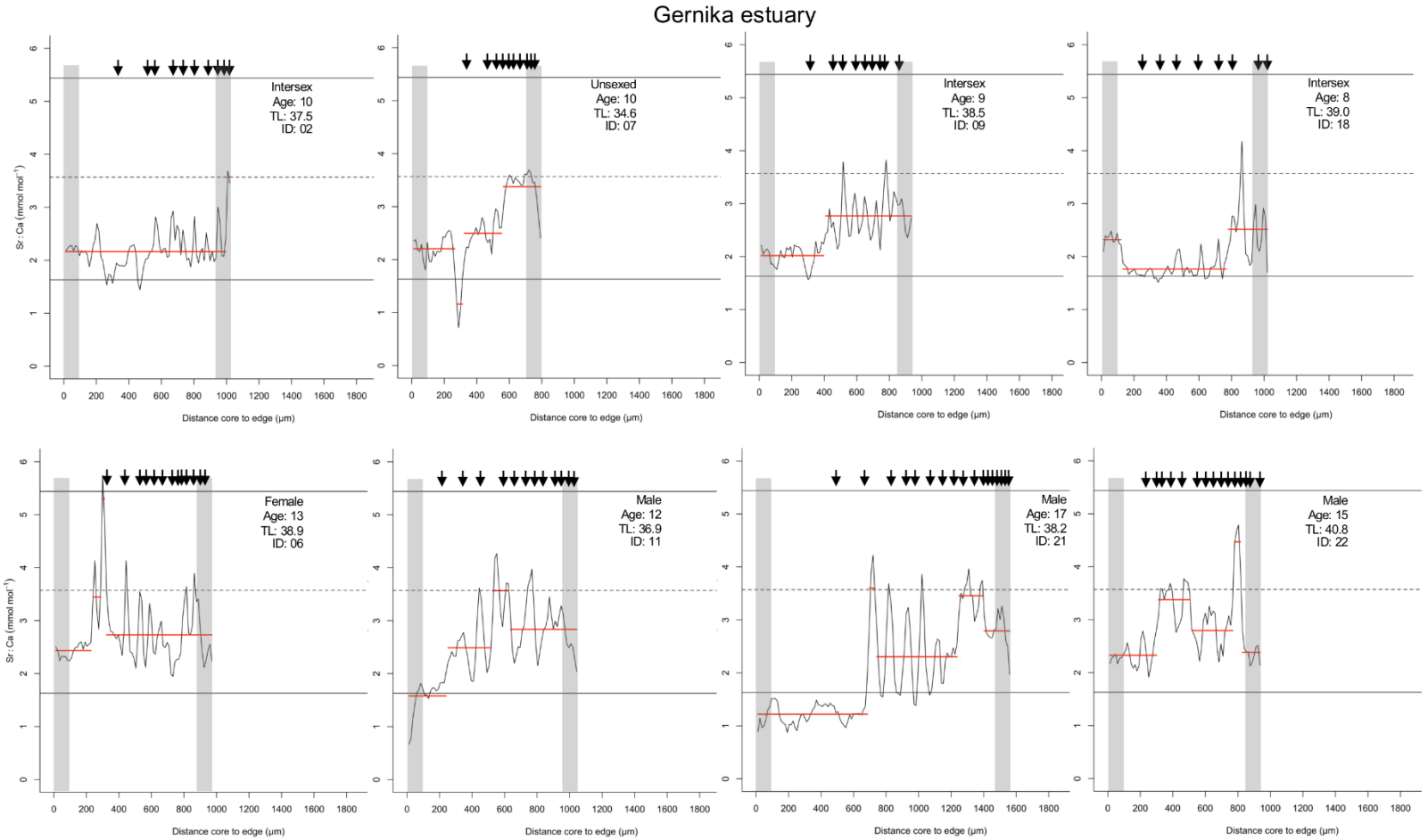

Figure S3
Core to edge otolith elemental signatures of *Chelon labrosus* estuarine residents (irregular and regular movements to the sea) from Gernika. The grey dashed horizontal line indicates the upper (marine) and lower (estuarine) thresholds for Sr:Ca ratio, black horizontal straight lines indicate the minimum and maximum values for Sr:Ca and the vertical arrows indicate otolith *annuli* (age). Horizontal red lines illustrate stable signatures identified from change-point analysis for Sr:Ca ratio. TL = total length and ID = fish/sample number.

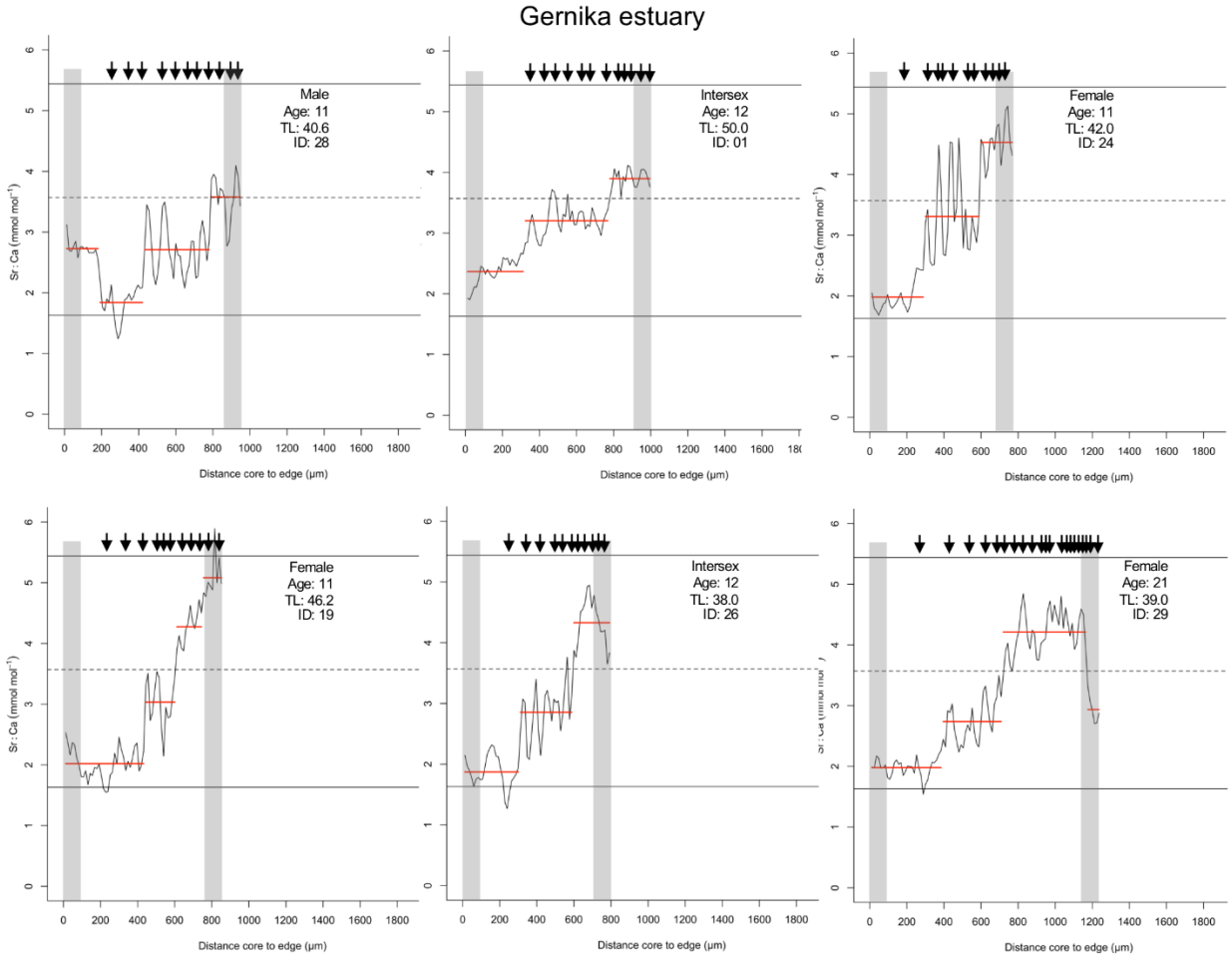

Figure S4

Core to edge otolith elemental signatures of *Chelon labrosus* estuarine residents (irregular and regular movements to the sea) and marine migrants from Gernika. The grey dashed horizontal line indicates the upper (marine) and lower (estuarine) thresholds for Sr:Ca ratio, black horizontal straight lines indicate the minimum and maximum values for Sr:Ca and the vertical arrows indicate otolith *annuli* (age). Horizontal red lines illustrate stable signatures identified from change-point analysis for Sr:Ca ratio. TL = total length and ID = fish/sample number.

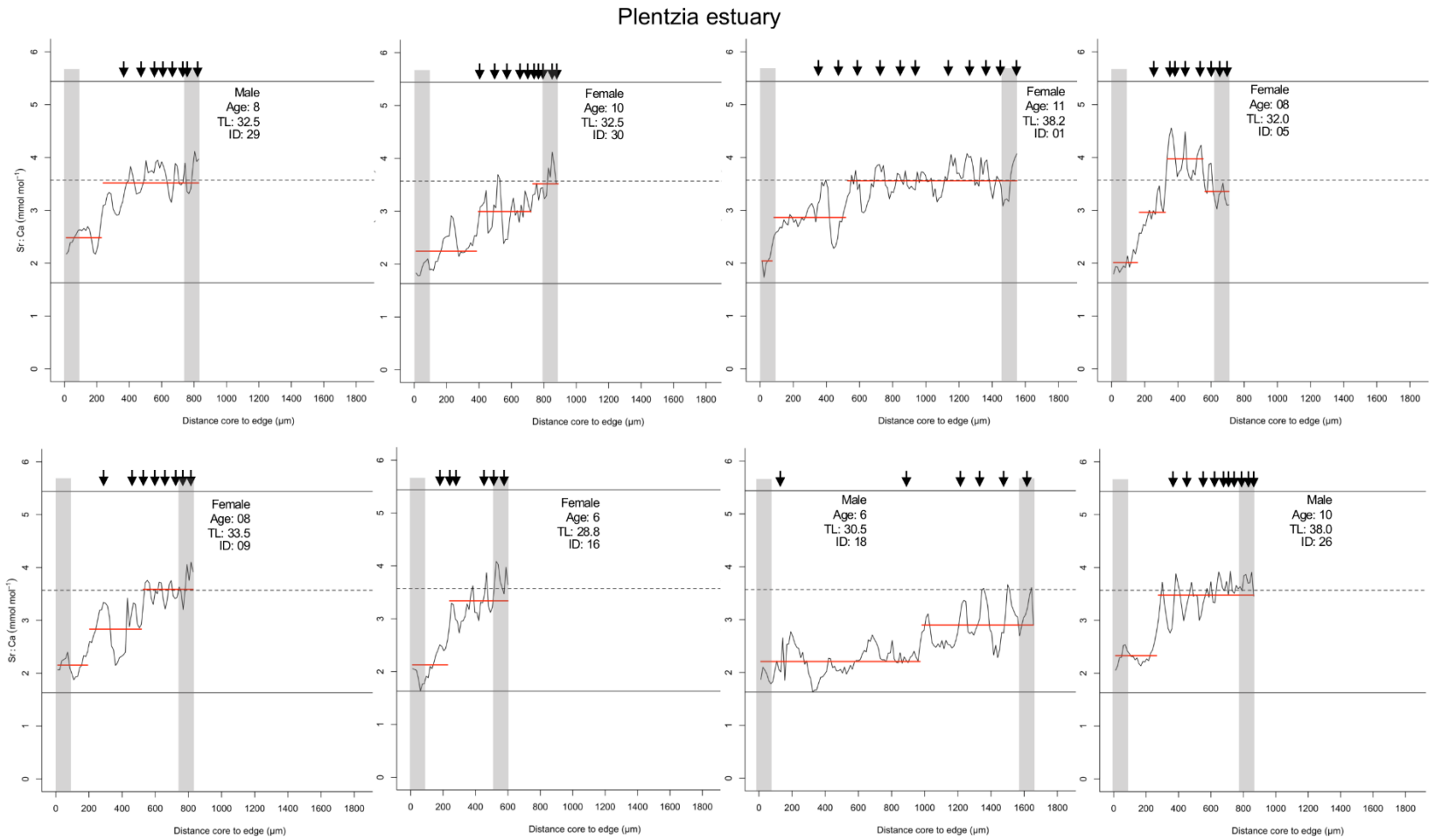

Figure S5

Core to edge otolith elemental signatures of *Chelon labrosus* estuarine residents (with irregular movements to the sea) from Plentzia. The grey dashed horizontal line indicates the upper (marine) and lower (estuarine) thresholds for Sr:Ca ratio, black horizontal straight lines indicate the minimum and maximum values for Sr:Ca and the vertical arrows indicate otolith *annuli* (age). Horizontal red lines illustrate stable signatures identified from change-point analysis for Sr:Ca ratio. TL = total length and ID = fish/sample number.

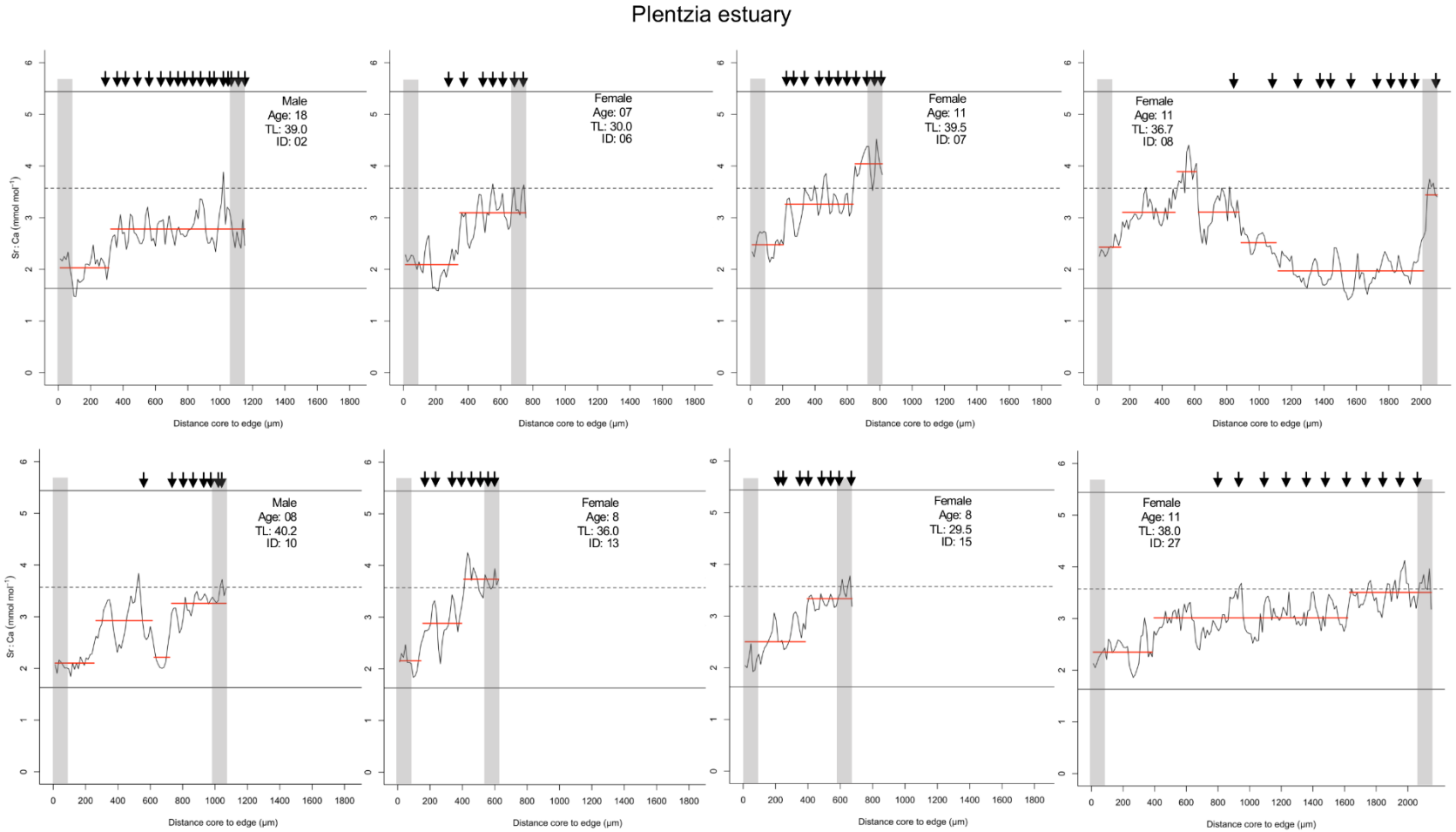

Figure S6

Core to edge otolith elemental signatures of *Chelon labrosus* estuarine residents from Plentzia with irregular and regular movements patterns to the sea. The grey dashed horizontal line indicates the upper (marine) and lower (estuarine) thresholds for Sr:Ca ratio, black horizontal straight lines indicate the minimum and maximum values for Sr:Ca and the vertical arrows indicate otolith *annuli* (age). Horizontal red lines illustrate stable signatures identified from change-point analysis for Sr:Ca ratio. TL = total length and ID = fish/sample number.

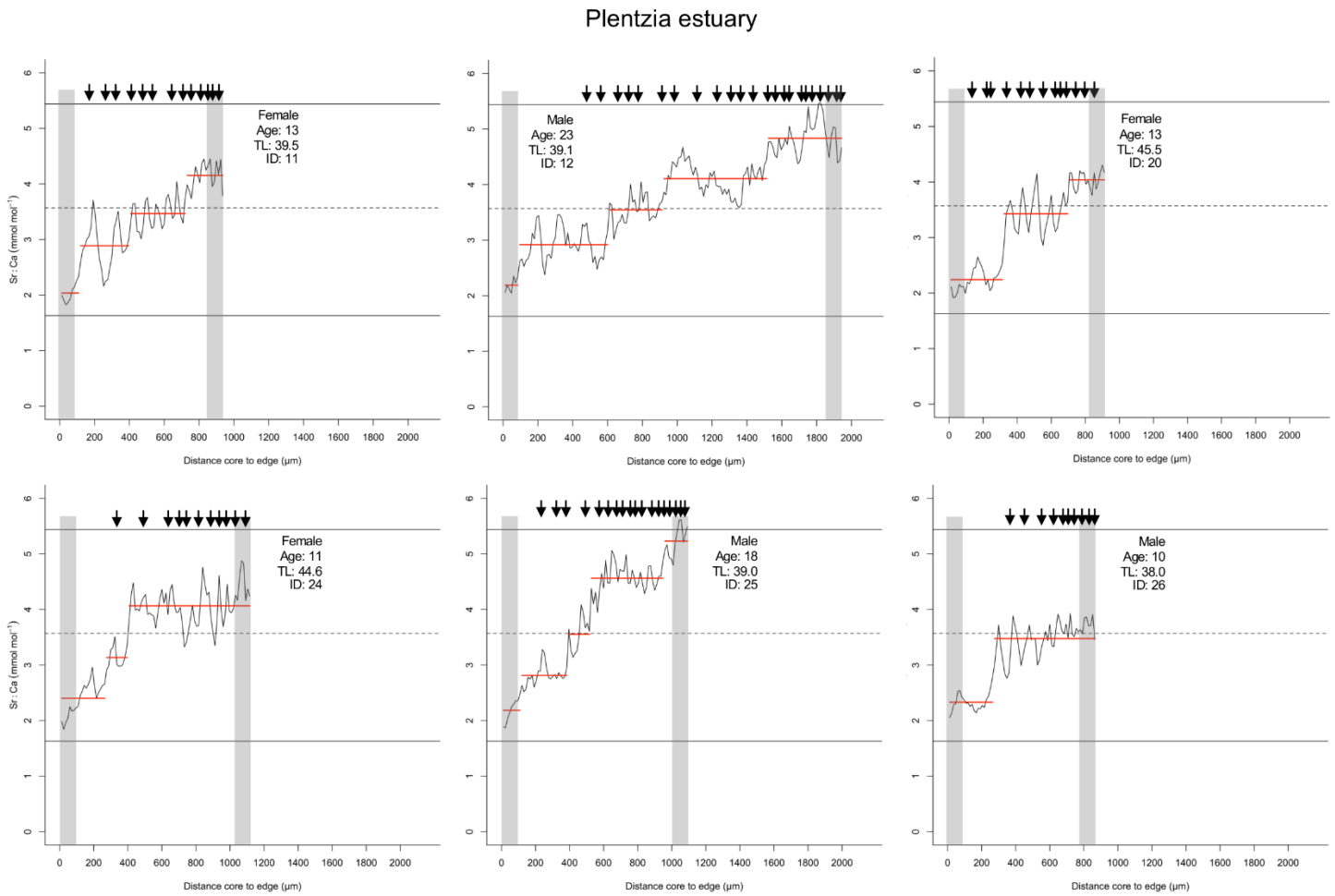

Figure S7

Core to edge otolith elemental signatures of *Chelon labrosus* marine migrants from Plentzia with initial irregular and regular movements patterns to the sea. The grey dashed horizontal line indicates the upper (marine) and lower (estuarine) thresholds for Sr:Ca ratio, black horizontal straight lines indicate the minimum and maximum values for Sr:Ca and the vertical arrows indicate otolith *annuli* (age). Horizontal red lines illustrate stable signatures identified from change-point analysis for Sr:Ca ratio. TL = total length and ID = fish/sample number.

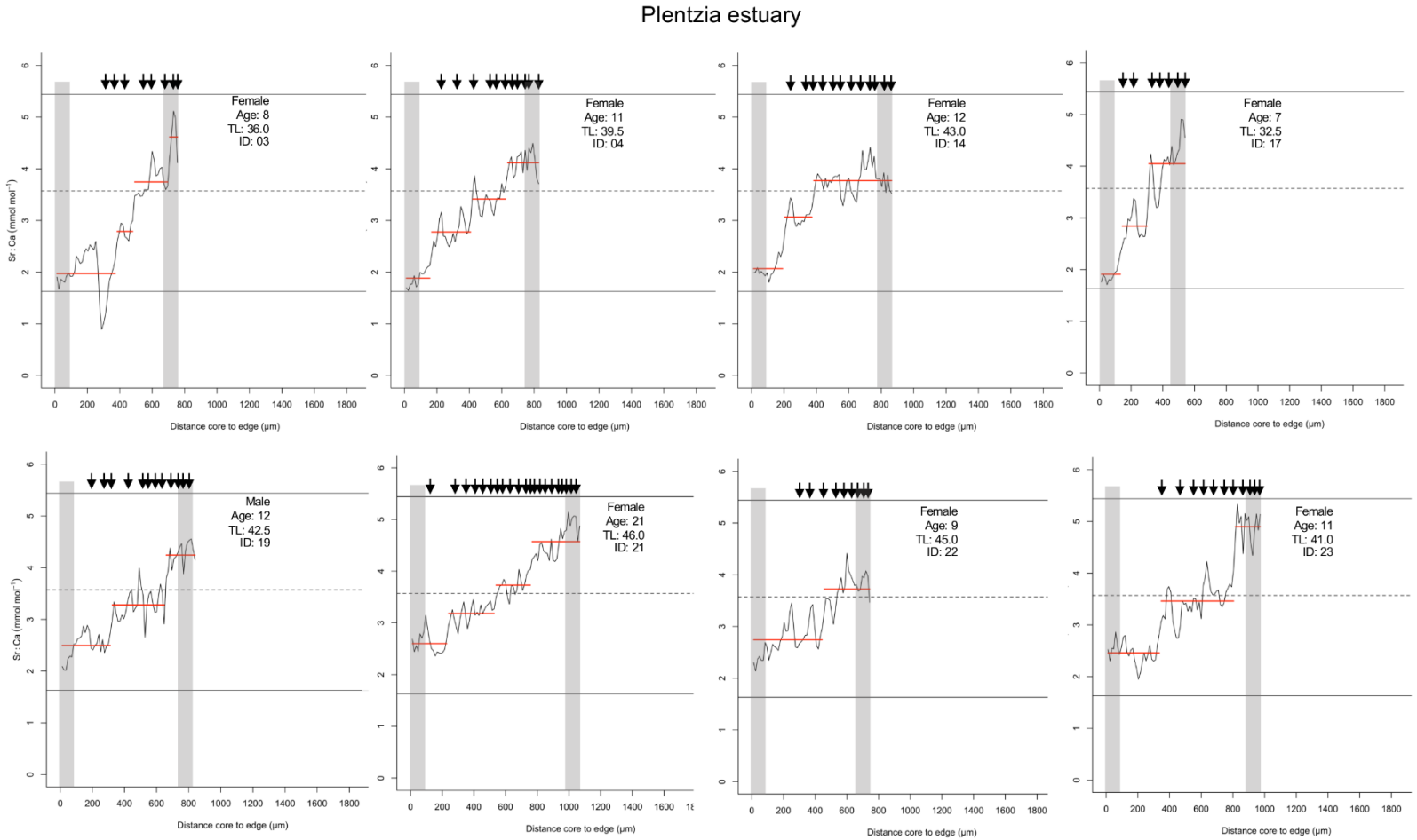

Figure S8

Core to edge otolith elemental signatures of *Chelon labrosus* marine migrants from Plentzia with initial irregular and regular movements patterns to the sea. The grey dashed horizontal line indicates the upper (marine) and lower (estuarine) thresholds for Sr:Ca ratio, black horizontal straight lines indicate the minimum and maximum values for Sr:Ca and the vertical arrows indicate otolith *annuli* (age). Horizontal red lines illustrate stable signatures identified from change-point analysis for Sr:Ca ratio. TL = total length and ID = fish/sample number.

IV. GENERAL DISCUSSION

Aquatic ecosystems frequently accumulate chemical contaminants from both urban and industrial discharges, which can disrupt the normal functioning of the endocrine systems of marine animals. Most notably, exposure to some endocrine disrupting compounds has been shown to result in altered gonadal development, increased ovarian atresia, and feminisation or masculinisation of fish populations (Corriero et al., 2021; King Heiden et al., 2006; Puy-Azurmendi et al., 2013; Tyler and Jobling, 2008). Most attention has been focused on xenoestrogenic compounds that trigger female specific vitellogenin expression in male fish and in some instances development of oocytes in testes. Understanding how and when chemicals impact wild fish populations and the level of exposure or the geographical scale at which populations may be affected during their life history becomes increasingly important when faced with site-specific exposure to xenoestrogens. This is especially relevant because altered gonad development as a consequence of exposure may disrupt the reproductive potential of the impacted individuals/populations. Several studies have found that effects of xenoestrogens may occur immediately after exposure but may differ in nature and intensity throughout the development and sex differentiation of affected fish (Delbes et al., 2022; Brander, 2013; Goksøyr, 2006).

Fish gonad development through early sex differentiation (gonadogenesis) but also through the annual reproductive cycle in adults is species-specific and controlled by different factors which may promote or limit reproductive success. Principal roles are played by steroid hormones, under the control of the expression of key genes involved in steroidogenesis (e.g., ovarian aromatase, *cyp19a* in the case of females or the antimüllerian hormone, *amh* in the case of males). This has been studied in a wide range of fish species, with different reproductive strategies and oocyte recruitment patterns (asynchronous vs synchronous spawners) (Cowan et al., 2017). Asynchronous spawners such as the European hake (*Merluccius merluccius*) have ovaries displaying oocytes at all development stages, releasing batches of such oocytes when mature over varying periods of time (Murua and Motos, 2006; Murua and Saborido-Rey, 2003). In synchronous spawning fish such as the catadromous European eel (*Anguilla anguilla*) and thicklip grey mullets (*Chelon labrosus*), all oocytes develop and ovulate at the same time in a single event or over a short period of time as part of a single episode (Ganias and Lowerre-Barbieri, 2018; Murua and Saborido-Rey, 2003). Thus, all oocytes develop synchronously in the ovary and spawning usually takes place when there is potential for reproductive success.

The Cell Biology in Environmental Toxicology and One Health (CBET+) Research Group works towards the development of early warning biomarkers of exposure to and effects of pollutants in sentinel organisms such as the thicklip grey mullet *Chelon labrosus*. During its sampling campaigns, CBET+ has reported strong xenoestrogenic effects in this euryhaline fish inhabiting estuaries in the southern Bay of Biscay (SBB), histologically describing gonad alterations such as intersex condition. Exposure to alkylphenols, pesticides, and other xenoestrogens, principally from wastewater treatment plant (WWTP) effluents has been reported to result in the production of oocytes in the testes of male individuals (Bizarro et al., 2014; Diaz De Cerio et al., 2012; Ortiz-Zarragoitia et al., 2014; Puy-Azurmendi et al., 2013; Valencia et al., 2017). On the other hand, and after the Prestige oil spill occurred in 2002, increased incidence of ovarian atresia was reported in the European hake *Merluccius merluccius* population in the vicinity of the Basque coast (Díez et al., 2011; Murua and Motos, 2006). These two species are of particular importance in the Basque coast, the European hake being a commercially important fish species, and the thicklip grey mullet, a pollution sentinel species strategically placed in the coastal environment to be profited in ecosystem health monitoring. We should not forget that mullets also possess a potential economic value with different species candidate for aquaculture diversification in Spain and the rest of Europe (García-Márquez et al., 2021; Ramos-Júdez et al., 2022; Vallainc et al., 2022).

The molecular pathways underlining the activation of such developmental effects on gonads driven by xenoestrogen exposure is still the issue of much research. Atresia is a complex process involving stress-related responses that include apoptotic and autophagic processes (Corriero et al., 2021; Miranda et al., 1999; Morais et al., 2012; Yang et al., 2022). Increased follicular atresia in fish ovaries may be an important indicator of stress response and/or pathology (Bromley et al., 2000; Janz et al., 2001; Blazer, 2002; Sato et al., 2005). For an asynchronous developing species such as the European hake, atresia could just be a physiological phenomenon to interrupt spawning when necessary during each reproductive cycle facilitating the resorption and re-distribution of energy-rich yolk material incorporated into the growing oocytes (Wood and Van Der Kraak, 2003, 2001). This could result in skipped spawning events which could be of great importance in fisheries fecundity studies, since it could be overestimating the productivity of a given stock if the bulk of oocytes not finalising maturation is not considered in the analyses. The advance detection of skipped spawning events and possible description of early warning biomarkers could have great

scientific and economic impact. The first two chapters of this thesis focused on molecularly deciphering such pathways, paying special attention to specifically selected target genes, and focusing first on the European hake as a species where seasonal episodes of follicular atresia are common. Then, learned lessons were applied into the pollution sentinel species *C. labrosus* inhabiting the area in the vicinity of the WWTP of Gernika. Mechanistically, we were interested in the analysis of the role that 5S rRNA related pathways could have in the regulation of follicular atresia. 5S rRNA accumulates to enormous concentrations in the ooplasm of growing oocytes representing the most important transcript in the previtellogenic oocytes of fish (Diaz de Cerio et al., 2012, Ortiz-Zarragoitia et al., 2014; Rojo-Bartolomé et al., 2016). Interestingly, 5S rRNA in combination with different ribosomal proteins (RPL5 and RPL11) is known to interact in mammalian cancer cells with the protein that under normal conditions ubiquitinises p53 into proteolysis (MDM2). Thus, 5S rRNA could be involved upregulating both apoptosis and autophagocytosis through p53.

Standard qPCR methods were used to analyse the transcription levels of distinct apoptosis and autophagy markers genes in ovaries of European hakes that histologically were identified as containing atretic follicles (Chapter 1). A significant proportion of ovaries of European hake displayed atretic follicles, irrespective of the follicular development stage. Applying the TUNEL assay, we identified that apoptosis is a mechanism involved in this response and that it affects previtellogenic, cortical alveoli stage and vitellogenic follicles at a similar level (Figure 1). This being so, in previtellogenic oocytes all cell types in the follicle were affected (follicular cells and the oocyte they contain) while in vitellogenic oocytes positively stained nuclei were restricted to the follicular cells. Target genes related to apoptosis (*p53* and *caspase-3*) and autophagy (*ctsd* and *dapk1*) were upregulated in ovaries with atretic vitellogenic follicles (Chapter 1), suggesting that both apoptosis and autophagy are at their highest during atresia at vitellogenesis (Yang et al., 2022). In addition, autophagy-related genes *beclin-1* and *ptenb* were also upregulated in ovaries presenting atretic follicles at any developmental stage, suggesting that autophagy is strongly involved in follicular atresia throughout the entire process of oocyte differentiation along oogenesis (Figure 1). At the protein level, higher expression levels of MDM2 and RPL11 were observed in atretic vs. non-atretic vitellogenic ovaries, suggesting that *mdm2* and *rpl11* are activated to regulate p53 levels (Figure 1).

The thicklip grey mullet has been shown to bioaccumulate contaminants from several estuaries along the Basque coast, resulting in the development of intersex condition in male

individuals (Bizarro et al., 2014; Ortiz-Zarragoitia et al., 2014; Puy-Azurmendi et al., 2013) and this has been shown (Chapter 2) to result in increased ovarian atresia. In an estuary that discharges into open oceanic waters at the leisure port of Plentzia, male mullets have consistently shown normally developing testes with no incidence of intersex condition (Bizarro et al., 2014; Diaz De Cerio et al., 2012; Valencia et al., 2017). Most studies conducted on mullets inhabiting contaminated estuaries along the Basque coast focused more on male gonads (Bizarro et al., 2014; Diaz De Cerio et al., 2012; Ortiz-Zarragoitia et al., 2014; Puy-Azurmendi et al., 2013; Valencia et al., 2017) than on the effects experienced by the ovaries in female mullets exposed to the same compounds. In such mullet's disruption of the hypothalamus-pituitary-gland (HPG) axis may contribute to trigger follicular atresia. In reality, this has been observed in mullet samples obtained from the annual summer sampling campaigns of the Biscay Bay Environmental Biospecimen Bank (Chapter 2). In the Basque coast, in summer, mullets are in previtellogenic stage but in estuaries such as the one of Gernika they characteristically display high physiological levels of oestradiol (E_2) (Sardi et al., 2015). Indeed, many other species inhabiting xenoestrogen-contaminated waters have also displayed atresia in ovaries associated to high E_2 plasma levels (Agbohessi et al., 2015). Nonetheless, in some species, follicular atresia has been observed to occur also in individuals with low E_2 plasma levels (Aguilar et al., 2007; Au, 2004; Jobling et al., 2002; Mayon et al., 2006) caused by the inhibition of gonadotropin-releasing hormone (GtH) and subsequent suppression of steroid synthesis (Corriero et al., 2021).

No significant differences in the transcriptional profiles of apoptosis and autophagy-related genes (*p53, mdm2, rpl5, caspase-3* and *beclin-1*) was found in mullets with atretic vs non-atretic ovaries (Chapter 2 and Figure 1). The protein p53 was found to be upregulated in atretic previtellogenic ovaries. In both hake and mullet, downregulation of RPL11 in atretic previtellogenic ovaries was observed, with RPL11 being upregulated in non-atretic previtellogenic ovaries and in hake atretic vitellogenic ovaries (Figure 1). Therefore, p53 appears to play a significant role in ovarian follicular atresia in fish, and the mechanisms regulating its activation are most likely post-transcriptional.

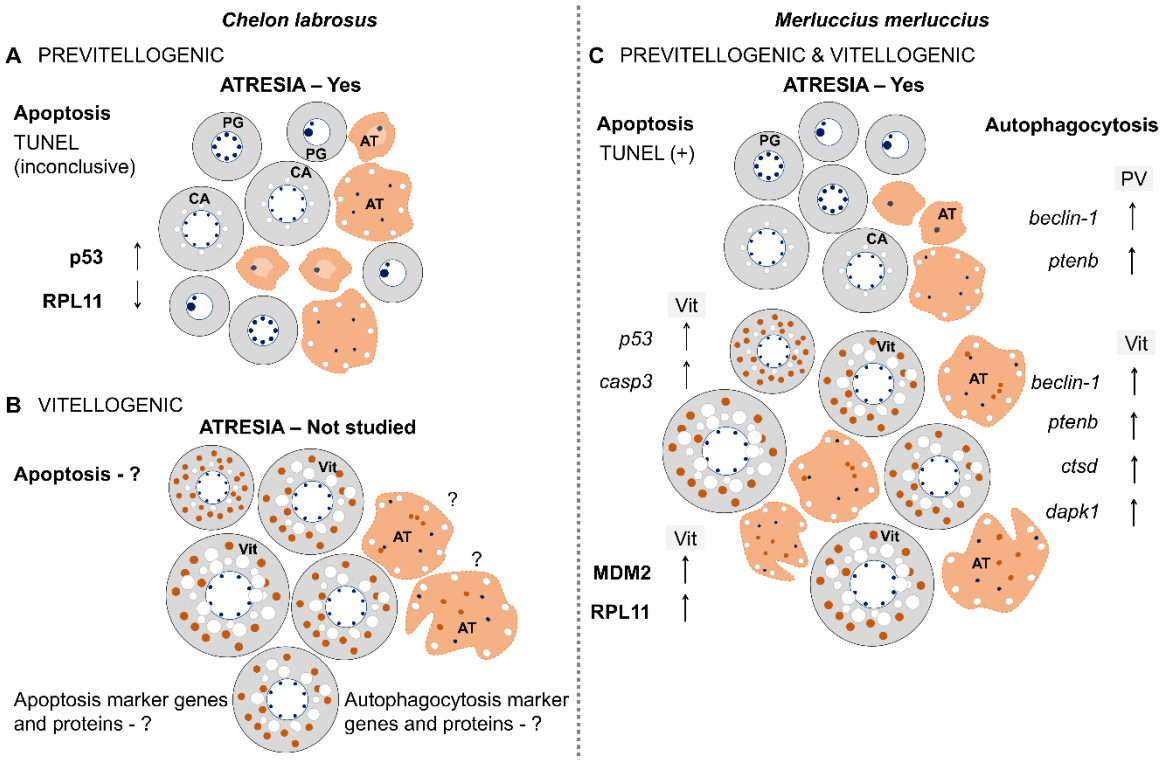

Figure 1
Schematic representation of follicular atresia in synchronous spawning *Chelon labrosus* (A and B) and asynchronous *Merluccius merluccius* (C). (A) Atretic ovary with oocytes in previtellogenesis in *C. labrosus.* TUNEL assay results were inconclusive and upregulation of p53 and downregulation of RPL11 were observed at the protein level. (B) Atretic ovary with oocytes in vitellogenesis. TUNEL assay results for apoptosis and the upregulation or downregulation of target genes and proteins remain unknown. The question mark (?) means that they were not studied. (C) Atretic synchronous ovaries with oocytes of *M. merluccius* with atresia occurring at all stages of oocyte development. TUNEL positive (+) results indicate apoptosis in oocytes at all developmental stages. Target apoptosis genes and proteins (*p53, casp3,* MDM2, RPL11) were upregulated in ovaries displaying vitellogenic atretic follicles while autophagocytic genes (*beclin-1* and *ptenb*) were upregulated when both previtellogenic and vitellogenic atretic follicles were present. Autophagocytosis genes *ctsd* and *dapk1* were upregulated only when atretic vitellogenic oocytes were present. Target genes are represented in *italics* while proteins are represented in **bold**. AT = atresia, CA = cortical alveolar, PG = Primary growth, PV = previtellogenic and Vit = vitellogenic.

Given the strong xenoestrogenic effects experienced by thicklip grey mullets in the estuaries of the southern Bay of Biscay which result in high prevalence of intersex testes and increased follicular atresia in females, it is crucial to gain knowledge on the life history characteristics and genetic connectivity of the species. The history of exposure to pollutants could have important implications for the gonad alterations observed in these organisms with implications for their possible reproductive success. Considering the yearly oceanic reproductive migratory behaviour of *C. labrosus* from the estuaries where they live and feed and that sexual maturity for males and females is attained at two and three years, respectively (Sostoa, 1983), it is quite possible that sex differentiation in mullets takes place after recruitment into estuaries, where the presence and bioavailability of xenoestrogens

could have an impact on sex determination and gonad development. Furthermore, because mullets can move between habitats (estuarine into marine and back into estuarine but not necessarily the same estuary), recognising the periods of exposure to xenoestrogens (associated to life in the estuaries) is important. A multidisciplinary approach was used to estimate the levels of genetic diversity, population structure (Chapter 3) and migratory pattern (Chapters 4 and 5) of *C. labrosus*. With this purpose complementary analytical methodologies were applied.

A battery of 46 microsatellites was tested in order to compare the population structure and possible connectivity of mullets from five different estuaries in the Basque Country using two populations as outgroups in the comparison, one from Cadiz and the other one from the Mediterranean in Greece (Chapter 3). The results of 10 polymorphic microsatellites studied indicated that *C. labrosus* displays widespread genetic homogeneity and panmixia across the sampled area, suggesting a single reproductive population from the SBB (Figure 2) all the way to the Thermaikos gulf. This is not unique to *C. labrosus* since many marine species with similar biology where one extreme could be the European eel *Anguilla anguilla* (Palm et al., 2009; Ragauskas et al., 2014) or *Mugil cephalus* (Huey et al., 2013; Rocha-Olivares et al., 2000) and the catadromous and geographically close species *C. ramada* (Pereira et al., 2023) also show a lack of genetic structure in their European populations. This could be due to the fact that large populations of many marine species are greatly influenced by genetic drift and life-history traits that promote dispersal and high gene flow, either as a consequence of large dispersal capacity of eggs, planktonic larvae and/or juveniles and/or active migration of adults that would allow mating between individuals of distant origins (Carvalho and Hauser, 1998; DeWoody and Avise, 2000; Martinez et al., 2018; Moreira et al., 2020; Pereira et al., 2023). Indeed, *C. labrosus* individuals seem to belong to a single panmictic population; hence, individuals inhabiting contaminated estuaries with a high prevalence of intersex condition, such as Gernika, are part of the same genetic group as those living in adjacent estuaries with no incidence of xenoestrogenicity.

However, genetic markers are more conservative (low mutation rates and less influenced by natural selection) at broad spatiotemporal scales than markers based on environmental-dependent phenotypic traits such as otoliths (Moreira et al., 2020). The possibility of adult mullet individuals always returning to their estuary of origin after reproductive migration to sea or the probable existence of local subpopulation units cannot be ruled out. In this case,

identified panmixia would be fully resulting from reproduction between adults coming from different estuaries and broad dispersion capacity of resulting offspring. Otolith shape and elemental chemical signatures of studied mullet individuals inhabiting two estuaries with distinct burdens of xenoestrogens, Gernika and Plentzia (with no signs of xenoestrogenicity), showed distinct local subpopulation groupings (Chapter 4). Discriminant function analysis confirmed the presence of discrete and spatially structured phenotypic groups of mullets from both estuaries when results of shape and elemental signatures were combined (98% re-classification success). The connectivity between both mullet subpopulations appeared to be restricted, suggesting a limited degree of mixing of adults among estuaries, even between two estuaries so close one to each other. Thus, the mullets studied here could be regarded as belonging to two different subpopulation units.

To determine the true fidelity of the adult individuals to their native estuary of recruitment, fluctuations in otolith elemental profiles all along their growth increments, from the core (natal origin) to edge (moment of capture) were evaluated using laser ablation-inductively coupled plasma-mass spectrometry (LA-ICP-MS) techniques (Avigliano et al., 2017; Fowler et al., 2016; Xuan and Wang, 2023) in Chapter 5. Such elemental profiles revealed two distinct life histories in the studied fish with different diadromous movement behaviours when comparing both estuaries. The two migratory patterns revealed mullets that were estuarine residents (individuals with the most frequent use of estuaries) and marine migrants (individuals that used the estuary during their early life and later moving to the marine environment). While some individuals from Plentzia migrated to the ocean after spending their first 2 – 3 years in the estuary, possibly for spawning, most mullets from Gernika were estuarine residents, and only some migrate to the ocean (Figure 2). This migratory behaviour is consistent with other studies that have assessed migration patterns in mullets (Avigliano et al., 2021; Fowler et al., 2016; Wang, 2014). The migratory patterns exhibited by *C. labrosus* seem to suggest a behaviour consistent with fidelity to the estuary of first recruitment. Given that *C. labrosus* mostly prefers the estuarine environment in Gernika and that exposure to xenoestrogens occurs in association to WWTP discharges within the estuary, it is entirely possible that exposure to xenoestrogens does not allow for final maturation. This would imply that most fish from Gernika studied in this thesis have never reproduced (Figure 2).

The findings of this thesis add to our understanding of the reproductive constraints that may arise from altered gonad development in fish because of local exposure to chemical

contaminants during their life history. Skipped spawning events and enhanced follicular atresia may be a common strategy during reproduction in times of environmental stress in asynchronous developing fish species with indeterminate fecundity, such as the European hake, not only as an energy-saving mechanism but also as a way to ensure offspring survivability by selectively regulating gonad development and subsequent egg release. In synchronous developing mullets, skipped spawning events may also be common. Nonetheless, the molecular mechanisms regulating follicular atresia in both hake and mullet appear to be regulated post-transcriptionally. The results in this thesis further showed that despite thicklip grey mullets from southern Europe exhibiting panmixia, individuals migrating to the sea for reproduction appear to return to their estuary of origin, the one they recruited to as larvae, and that the intersex condition observed in contaminated estuaries such as Gernika is most likely the result of life-long exposure to xenoestrogens. Considering the high prevalence of intersex and follicular atresia observed in mullets, it is also quite possible that exposure to xenoestrogens may inhibit the activation of reproductive cues promoting normal gonadal development, but also prevent some individuals from partaking in the annual reproductive migration to spawn in the open ocean, resulting in absence of reproduction.

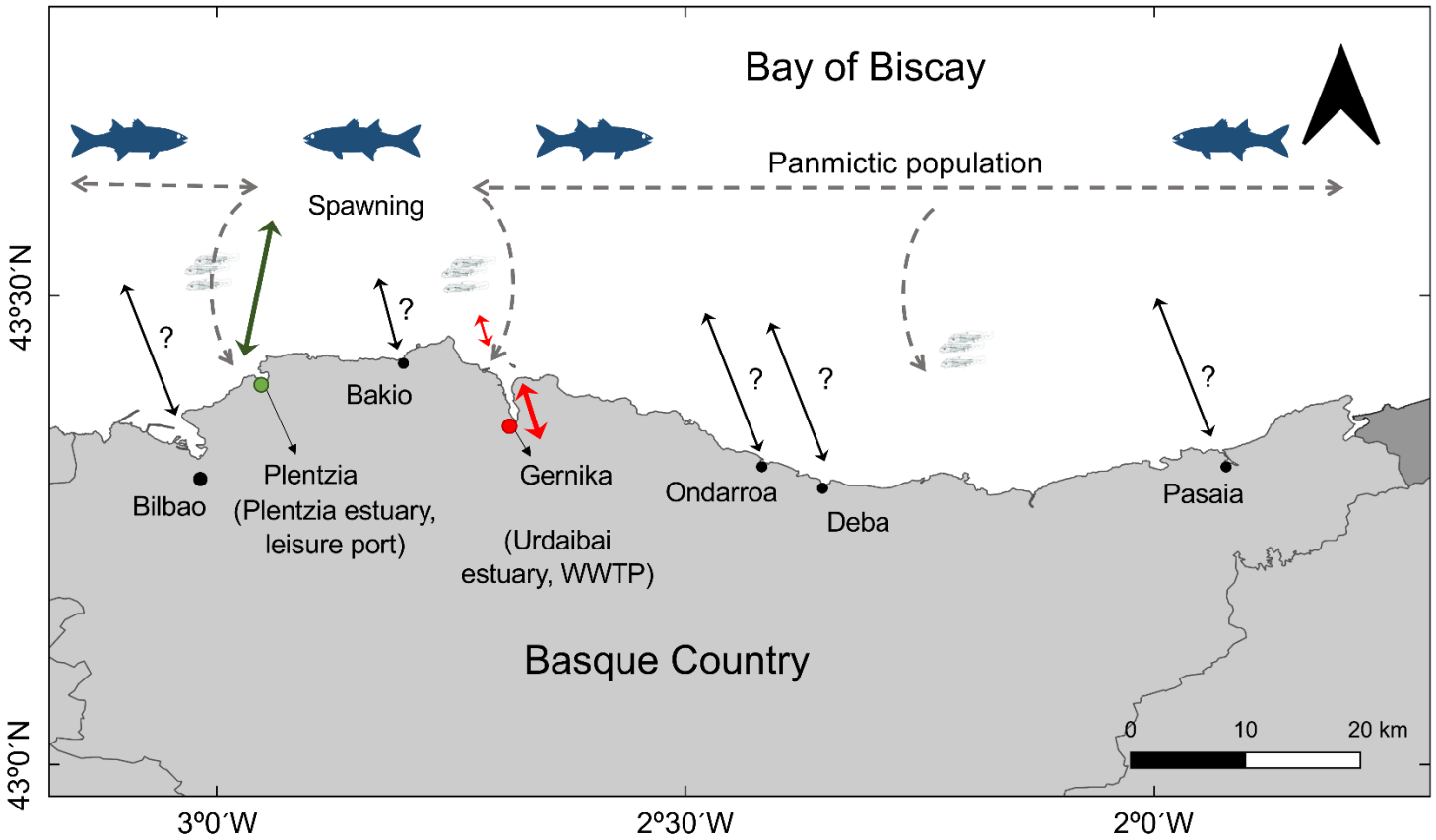

Figure 2

Map showing the life history characteristics of *Chelon labrosus* in the Basque coast. Dashed straight lines with double arrow heads represent panmictic mullet populations that reproduce at sea, forming a single population. Dashed curved lines with single arrowhead represents larvae and/or juveniles exhibiting a broad migration capacity entering coastal waters and estuaries. Green double arrowhead line represents possible adult migration between spawning grounds and their estuary of residence (Green point, Plentzia). Red double arrowhead line represents possible adult migrations within their habitual estuary (Red point, Gernika). Short thin red double arrowhead line represents possible adult migrations between spawning grounds and their estuary of residence (Red point, Gernika). Black double arrowhead lines with question mark (?) show adult reproductive migration to and from spawning grounds.

References

Agbohessi, P.T., Imorou Toko, I., Ouédraogo, A., Jauniaux, T., Mandiki, S.N.M., Kestemont, P., 2015. Assessment of the health status of wild fish inhabiting a cotton basin heavily impacted by pesticides in Benin (West Africa). Science of the Total Environment 506–507, 567–584. https://doi.org/10.1016/j.scitotenv.2014.11.047

Aguilar, C., González-Sansón, G., Hernández, I., MacLatchy, D.L., Munkittrick, K.R., 2007. Effects-based assessment in a tropical coastal system: Status of bicolor damselfish (*Stegastes partitus*) on the north shore of Cuba. Ecotoxicol Environ Saf 67, 459–471. https://doi.org/10.1016/j.ecoenv.2006.05.004

Au, D.W.T., 2004. The application of histo-cytopathological biomarkers in marine pollution monitoring: A review. Mar Pollut Bull 48, 817–834. https://doi.org/10.1016/j.marpolbul.2004.02.032

Avigliano, E., Leisen, M., Romero, R., Carvalho, B., Velasco, G., Vianna, M., Barra, F., Volpedo, A.V., 2017. Fluvio-marine travelers from South America: cyclic amphidromy and freshwater residency, typical behaviors in *Genidens barbus* inferred by otolith chemistry. Fish Res 193, 184–194. https://doi.org/10.1016/J.FISHRES.2017.04.011

Bizarro, C., Ros, O., Vallejo, A., Prieto, A., Etxebarria, N., Cajaraville, M.P., Ortiz-Zarragoitia, M., 2014. Intersex condition and molecular markers of endocrine disruption in relation with burdens of emerging pollutants in thicklip grey mullets (*Chelon labrosus*) from Basque estuaries (South-East Bay of Biscay). Mar Environ Res 96, 19–28. https://doi.org/10.1016/j.marenvres.2013.10.009

Bromley, P.J., Ravier, C., Witthames, P.R., 2000. The influence of feeding regime on sexual maturation, fecundity and atresia in first-time spawning turbot. J Fish Biol 56, 264–278. https://doi.org/10.1006/jfbi.1999.1162

Carvalho, G.R., Hauser, L., 1998. Advances in the molecular analysis of fish population structure. Italian Journal of Zoology 65, 21–33. https://doi.org/10.1080/11250009809386791

Corriero, A., Zupa, R., Mylonas, C.C., Passantino, L., 2021. Atresia of ovarian follicles in fishes, and implications and uses in aquaculture and fisheries. J Fish Dis 44, 1271–1291. https://doi.org/10.1111/JFD.13469

Cowan, M., Azpeleta, C., López-Olmeda, J.F., 2017. Rhythms in the endocrine system of fish: a review. J Comp Physiol B 187, 1057–1089. https://doi.org/10.1007/s00360-017-1094-5

Delbes, G., Blázquez, M., Fernandino, J.I., Grigorova, P., Hales, B.F., Metcalfe, C., Navarro-Martín, L., Parent, L., Robaire, B., Rwigemera, A., Van Der Kraak, G., Wade, M., Marlatt, V., 2022. Effects of endocrine disrupting chemicals on gonad development: Mechanistic insights from fish and mammals. Environ Res 204. https://doi.org/10.1016/j.envres.2021.112040

DeWoody, J.A., Avise, J.C., 2000. Microsatellite variation in marine, freshwater and anadromous fishes compared with other animals. J Fish Biol 56, 461–473. https://doi.org/10.1006/jfbi.1999.1210

Diaz De Cerio, O., Rojo-Bartolomé, I., Bizarro, C., Ortiz-Zarragoitia, M., Cancio, I., 2012. 5S rRNA and accompanying proteins in gonads: powerful markers to identify sex and reproductive endocrine disruption in fish. Environ Sci Technol 46, 7763–7771. https://doi.org/10.1021/es301132b

Fowler, A.M., Smith, S.M., Booth, D.J., Stewart, J., 2016. Partial migration of grey mullet (*Mugil cephalus*) on Australia's east coast revealed by otolith chemistry. Mar Environ Res 119, 238–244. https://doi.org/10.1016/j.marenvres.2016.06.010

Ganias, K., Lowerre-Barbieri, S., 2018. Oocyte recruitment and fecundity type in fishes: Refining terms to reflect underlying processes and drivers. Fish and Fisheries 19, 562–572. https://doi.org/10.1111/faf.12267

García-Márquez, J., Galafat, A., Alarcón, F.J., Figueroa, F.L., Martínez-Manzanares, E., Arijo, S., Abdala-Díaz, R.T., 2021. Cultivated and Wild Juvenile Thick-Lipped Grey Mullet, *Chelon labrosus*: A Comparison from a Nutritional Point of View. Animals 11, 2112. https://doi.org/10.3390/ani11072112

Huey, J.A., Espinoza, T., Hughes, J.M., 2013. Regional panmixia in the mullet *Mugil cephalus* along the coast of Eastern Queensland; revealed using six highly polymorphic microsatellite loci. Proceedings of the Royal Society of Queensland 118, 7–15. https://doi.org/10.3316/ielapa.684745616782467

Janz, D.M., McMaster, M.E., Weber, L.P., Munkittrick, K.R., Van Der Kraak, G., 2001. Recovery of ovary size, follicle cell apoptosis, and HSP70 expression in fish exposed to bleached pulp mill effluent. Canadian Journal of Fisheries and Aquatic Sciences 58, 620–625. https://doi.org/10.1139/cjfas-58-3-620

Jobling, S., Beresford, N., Nolan, M., Rodgers-Gray, T., Brighty, G.C., Sumpter, J.P., Tyler, C.R., 2002. Altered sexual maturation and gamete production in wild roach (*Rutilus rutilus*) living in rivers that receive treated sewage effluents. Biol Reprod 66, 272–281. https://doi.org/10.1095/biolreprod66.2.272

King Heiden, T., Carvan, M.J., Hutz, R.J., 2006. Inhibition of follicular development, vitellogenesis, and serum 17β-estradiol concentrations in zebrafish following chronic, sublethal dietary exposure to 2,3,7,8-tetrachlorodibenzo-p-dioxin. Toxicological Sciences 90, 490–499. https://doi.org/10.1093/toxsci/kfj085

Martinez, A.S., Willoughby, J.R., Christie, M.R., 2018. Genetic diversity in fishes is influenced by habitat type and life-history variation. Ecol Evol 8, 12022–12031. https://doi.org/10.1002/ece3.4661

Mayon, N., Bertrand, A., Leroy, D., Malbrouck, C., Mandiki, S.N.M., Silvestre, F., Goffart, A., Thomé, J.P., Kestemont, P., 2006. Multiscale approach of fish responses to different types of environmental contaminations: A case study. Science of the Total Environment 367, 715–731. https://doi.org/10.1016/j.scitotenv.2006.03.005

Miranda, A.C.L., Bazzoli, N., Rizzo, E., Sato, Y., 1999. Ovarian follicular atresia in two teleost species: a histological and ultrastructural study. Tissue Cell 31, 480–488. https://doi.org/10.1054/tice.1999.0045

Morais, R.D.V.S., Thomé, R.G., Lemos, F.S., Bazzoli, N., Rizzo, E., 2012. Autophagy and apoptosis interplay during follicular atresia in fish ovary: a morphological and immunocytochemical study. Cell Tissue Res 347, 467–478. https://doi.org/10.1007/s00441-012-1327-6

Moreira, C., Presa, P., Correia, A.T., Vaz-Pires, P., Froufe, E., 2020. Spatio-temporal microsatellite data suggest a multidirectional connectivity pattern in the *Trachurus picturatus* metapopulation from the Northeast Atlantic. Fish Res 225, 105499. https://doi.org/10.1016/j.fishres.2020.105499

Murua, H., Motos, L., 2006. Reproductive strategy and spawning activity of the European hake *Merluccius merluccius* (L.) in the Bay of Biscay. J Fish Biol 69, 1288–1303. https://doi.org/10.1111/j.1095-8649.2006.01169.x

Murua, H., Saborido-Rey, F., 2003. Female reproductive strategies of marine fish species of the North Atlantic. Journal of Northwest Atlantic Fishery Science 33, 23–31.

Ortiz-Zarragoitia, M., Bizarro, C., Rojo-Bartolomé, I., De Cerio, O.D., Cajaraville, M.P., Cancio, I., 2014. Mugilid fish are sentinels of exposure to endocrine disrupting compounds in coastal and estuarine environments. Mar Drugs 12, 4756–4782. https://doi.org/10.3390/md12094756

Palm, S., Dannewitz, J., Prestegaard, T., Wickström, H., 2009. Panmixia in European eel revisited: No genetic difference between maturing adults from southern and northern Europe. Heredity (Edinb) 103, 82–89. https://doi.org/10.1038/hdy.2009.51

Pereira, E., Mateus, C.S., Alves, M.J., Almeida, R., Pereira, J., Quintella, B.R., Almeida, P.R., 2023. Connectivity patterns and gene flow among *Chelon ramada* populations. Estuar Coast Shelf Sci 281, 108209. https://doi.org/10.1016/j.ecss.2022.108209

Puy-Azurmendi, E., Ortiz-Zarragoitia, M., Villagrasa, M., Kuster, M., Aragón, P., Atienza, J., Puchades, R., Maquieira, A., Domínguez, C., López de Alda, M., Fernandes, D., Porte, C., Bayona, J.M., Barceló, D., Cajaraville, M.P., 2013. Endocrine disruption in thicklip grey mullet (*Chelon labrosus*) from the Urdaibai Biosphere Reserve (Bay of Biscay, Southwestern Europe), Science of the Total Environment. Elsevier. https://doi.org/10.1016/j.scitotenv.2012.10.078

Ragauskas, A., Butkauskas, D., Sruoga, A., Kesminas, V., Rashal, I., Tzeng, W.-N.N., 2014. Analysis of the genetic structure of the European eel *Anguilla anguilla* using the mtDNA D-loop region molecular marker. Fisheries Science 80, 463–474. https://doi.org/10.1007/s12562-014-0714-1

Ramos-Júdez, S., Giménez, I., Gumbau-Pous, J., Arnold-Cruañes, L.S., Estévez, A., Duncan, N., 2022. Recombinant Fsh and Lh therapy for spawning induction of previtellogenic and early spermatogenic arrested teleost, the flathead grey mullet (*Mugil cephalus*). Sci Rep 12, 6563. https://doi.org/10.1038/s41598-022-10371-0

Rocha-Olivares, A., Garber, N.M., Stuck, K.C., 2000. High genetic diversity, large inter-oceanic divergence and historical demography of the striped mullet. J Fish Biol 57, 1134–1149. https://doi.org/10.1006/jfbi.2000.1379

Sardi, A.E., Bizarro, C., Cajaraville, M.P., Ortiz-Zarragoitia, M., 2015. Steroidogenesis and phase II conjugation during the gametogenesis of thicklip grey mullet (*Chelon labrosus*) from a population showing intersex condition. Gen Comp Endocrinol 221, 144–155. https://doi.org/10.1016/j.ygcen.2015.01.005

Sato, Y., Bazzoli, N., Rizzo, E., Boschi, M.B., Miranda, M.O.T., 2005. Influence of the Abaeté River on the reproductive success of the neotropical migratory teleost Prochilodus argenteus in the São Francisco River, downstream from the Três Marias Dam, southeastern Brazil. River Res Appl 21, 939–950. https://doi.org/10.1002/rra.859

Sostoa, A., 1983. Las Comunidades de peces del Delta del Ebro. Universitat de Barcelona.

Tyler, C.R., Jobling, S., 2008. Roach, sex, and gender-bending chemicals: The feminization of wild fish in English rivers. Bioscience 58, 1051. https://doi.org/10.1641/B581108

Valencia, A., Rojo-Bartolomé, I., Bizarro, C., Cancio, I., Ortiz-Zarragoitia, M., 2017. Alteration in molecular markers of oocyte development and intersex condition in mullets impacted by wastewater treatment plant effluents. Gen Comp Endocrinol 245, 10–18. https://doi.org/10.1016/j.ygcen.2016.06.017

Vallainc, D., Concu, D., Loi, B., Pitzalis, A., Frongia, C., Chindris, A., Carboni, S., 2022. Spawning induction and larval rearing in the thinlip gray mullet (*Chelon ramada*): The use of the slow release gonadotropin releasing hormone analog (GnRHa) preparation, leuprorelin acetate. Anim Reprod Sci 247, 107145. https://doi.org/10.1016/j.anireprosci.2022.107145

Wood, A.W., Van Der Kraak, G.J., 2003. Yolk proteolysis in rainbow trout oocytes after serum-free culture: evidence for a novel biochemical mechanism of atresia in oviparous vertebrates. Mol Reprod Dev 65, 219–227. https://doi.org/10.1002/mrd.10272

Wood, A.W., Van Der Kraak, G.J., 2001. Apoptosis and ovarian function: novel perspectives from the teleosts. Biol Reprod 64, 264–271. https://doi.org/10.1095/biolreprod64.1.264

Xuan, Z., Wang, W.X., 2023. Diversity of life history and population connectivity of threadfin fish *Eleutheronema tetradactylum* along the coastal waters of Southern China. Sci Rep 13, 1–17. https://doi.org/10.1038/s41598-023-31174-x

Yang, Y., Wang, G., Li, Y., Hu, J., Wang, Y., Tao, Z., 2022. Oocytes skipped spawning through atresia is regulated by somatic cells revealed by transcriptome analysis in *Pampus argenteus*. Front Mar Sci 9, 1–14. https://doi.org/10.3389/fmars.2022.927548

V. CONCLUSIONS AND THESIS

Conclusions

1. A significant proportion of asynchronous developing ovaries of European hake *Merluccius merluccius* displayed atretic follicles in all the development stages, with apoptosis clearly (TUNEL positive) playing a role in follicular atresia in previtellogenic, cortical alveoli stage and vitellogenic follicles, involving follicular cells and oocytes during early oogenic stages and only follicular cells in vitellogenic ones.
2. The 5S/18S rRNA ratio proved to be a useful numerical and non-biased approach to rank asynchronous developing *M. merluccius* ovaries across oogenesis, integrating oocyte development along the continuum of the maturation process, and to determine the moments along oogenesis at which follicular atresia, identified through transcriptional profiling of atresia marker genes, was most common.
3. The transcriptional regulation of *p53, caspase-3, ctsd, dapk1, beclin-1* and *ptenb*, and protein expression of MDM2 and RPL11 along oogenesis point to the differential regulation of follicular atresia through apoptosis and autophagocytosis in *M. merluccius*.
   a. In ovaries with vitellogenic atretic follicles, molecular markers of autophagy and apoptosis pathways (*p53, caspase-3*, *ctsd* and *dapk1*) are simultaneously upregulated in comparison to those without atresia.
   b. *beclin-1* and *ptenb* are upregulated in atretic follicles in every oogenic stage, indicating that autophagy mechanisms are active during the whole oogenesis process.
4. Annual sampling campaigns (2014 – 2019) in Gernika (Urdaibai estuary) showed atresia is common in previtellogenic ovaries of thicklip grey mullets (*Chelon labrosus*).
5. Transcriptional profiles of apoptosis and autophagy-related genes (*p53, mdm2, rpl5, caspa*se-*3, and beclin-1*) revealed no significant differences between ovaries with atretic and non-atretic follicles. However, differences detected at the protein level, over-expression of p53 and downregulation of RPL11 in atretic ovaries implies that p53 plays a significant role in follicular atresia and that the mechanisms regulating its activation are most likely regulated post-transcriptionally.
6. In both hake and mullets, the molecular mechanisms regulating follicular atresia appear to work differently and thus it is not possible to apply the same atresia markers for both species. Whether these differences are related to the different developmental patterns of the ovaries in both species (synchronous vs asynchronous) remains to be elucidated.

7. Microsatellite analysis indicated that *C. labrosus* display widespread genetic homogeneity and panmixia across the southern Bay of Biscay (SBB) all the way to the Thermaikos gulf in Greece, suggesting a single reproductive population and the existence of significant gene flow among mullet subpopulations in the estuaries of the studied area.
8. Otolith shape and chemical (barium, lithium and strontium) composition showed significant differences between *C. labrosus* mullets of Gernika and Plentzia suggesting a lack of connectivity and geographical separation between individuals from both estuaries allowing to conclude that they could be regarded as two different subpopulation units.
9. Fluctuations in otolith manganese and magnesium profiles all along the growth increments of *C. labrosus* mullets from Gernika and Plentzia, (core-to-edge laser transects) evaluated using laser ablation-inductively coupled plasma-mass spectrometry (LA-ICP-MS) revealed that all individuals were born in oceanic waters to return early in their development to estuarine waters. This suggests that the thicklip grey mullet is a marine estuarine-dependent species in the Basque coast and that young juveniles rely on protected and resources rich waters of estuaries for providing a suitable nursery habitat.
10. Fluctuations in otolith core-to-edge strontium profiles evaluated using laser ablation-inductively coupled plasma-mass spectrometry (LA-ICP-MS) revealed that the individuals from Plentzia could display two distinct life histories with different diadromous movement behaviours estuarine residents (individuals with the most frequent use of estuaries) and marine migrants (individuals that use the estuary during their early life and later move to the marine environment). In turn, individuals from Gernika were exclusively estuarine residents suggesting that exposure to xenoestrogens jeopardises normal gonadal development and final maturation of individual fish, so they never migrate to the sea for spawning and reproduction. Xenoestrogenic exposure in Gernika resulting in intersex condition and increased follicular atresia is probably life-long.
11. The migratory patterns and residency behaviour of *C. labrosus* suggest a behaviour consistent with site-fidelity with mullets from Plentzia and Gernika possibly spawning at sea after spending their first 2 – 3 years in the estuary but always returning back to the same estuary.

Thesis

The thicklip grey mullet (*Chelon labrosus*) is a marine-estuarine dependent species that shows genetic homogeneity and panmixia across the southern Bay of Biscay (SBB) as a result of significant gene flow among mullet subpopulations. Mullets forming a single genetic population in the SBB appear to show fidelity to the estuary of first recruitment suggesting that the high prevalence of intersex condition and follicular atresia observed in subpopulations exposed to xenoestrogens in some estuaries may be the result of limited migration between estuaries and continuous exposure during their life within one single polluted estuary as it is the case of Gernika where mullets show complete failure to migrate for reproduction.

APPENDIX

TRIZOL PROTOCOL (TOTAL RNA EXTRACTION)

**Protocol follows manufacturer's instructions (Ambion®) with some modifications.*

Reagents and materials needed:

- *TRIzol® Reagent Solution (Ambion, Cat. #15596-026)*
- *Chloroform, synthesis grade (Scharlau, Cat. #CL01982500)*
- *Isopropanol /2 propanol (Scharlau, Cat. #AL03101000)*
- *75% ethanol (Panreac, Cat. #221086 Ethanol absolute – HPLC-gradient grade in RNase-free water)*
- *RNase-free water*
- *1.0 mm Zirconia/Silica beads (BioSpec, Cat. #11079110z)*
- *RNaseZAP™ RNase decontamination solution (Sigma, R2020-250 mL)*
- *Glass-Teflon® or power homogenizer (Precellys 24 lysis & tissue homogenizer, Bertin technologies).*
- *Refrigerated Centrifuge (Eppendorf Centrifuge 5415R)*
- *Cuvette Spectrophotometer (Eppendorf Biophotometer plus) or*
- *NanoDrop One Spectrophotometer (ThermoScientific)*
- *Bioanalyzer (Agilent 2100 Bioanalyzer)*
- *Polypropylene micro-centrifuge tubes*
- *Water bath or heat block (55 – 60ºC) (ACCUBLOCK™ Digital Dry Bath, Labnet International, Inc.)*
- *Sterile nuclease-free filter tips and non-filter tips (1 – 10 µL, 10 – 100 µL, 100 – 1000 µL)*
- *Pipettes (1 – 10 µL, 10 – 100 µL, 100 – 1000 µL)*

Notes/guidelines:

- *Perform on fresh sample (immediately after sample collection) or on quick frozen samples stored in liquid nitrogen or at -80ºC.*
- *Decontaminate all work/bench surfaces, centrifuges and pipettes with RNaseZAP™ at least once a month and with 75% ethanol (non-analytical grade) prior to beginning the procedure and regularly as need while performing the procedure.*
- *Perform all steps at room temperature (20-25ºC) unless otherwise noted.*
- *Use cold TRIzol if starting material contains high levels of RNase (e.g., spleen, pancreas)*

Procedure:

A. Homogenization/lysis of samples

1. Prepare 1.0 mm Zirconia/Silica beads in 1.5 mL RNase-free microcentrifuge tubes.
2. Weigh 50 – 100 mg of tissue and immediately place in the 1.5 mL RNase-free microcentrifuge tubes containing the 1.0 mm Zirconia/Silica beads.
3. Add 1 mL (1000 µL) of TRIzol® Reagent per 50 – 100 mg of tissue sample to the tissue sample.
4. Homogenize (at room temperature) the tissue twice (2X) for 15 sec each at 5,000 m/s using the tissue homogenizer (*5,500 – 2 ×20 s is also ok*).

5. Transfer the homogenized sample to new 1.5 mL RNase-free microcentrifuge tubes absent the 1.0 mm Zirconia/Silica beads.

Proceed to **phase separation or immediately freeze the homogenized sample. (Samples can be stored @ 4ºC overnight or @ -20ºC for up to 1 year).*

B. Phase Separation

6. Incubate for 5 min (at room temperature) to permit complete dissociation of the nucleoprotein complex.
7. Add 0.2 mL (200 µL) chloroform per 1 mL (1000 µL) of TRIzol® Reagent used for homogenisation, securely cap the tube and *shake vigorously by hand for 15 sec. *(*Critical step*).
8. Incubate for 2 – 3 min (at room temperature).
9. Centrifuge samples at 12,000 × *g* (11,400 rpm) for 15 min @ 4ºC. (*Mixture seperates into a colourless upper aqueous phase, an interphase and lower red phenol-chloroform phase. Repeat centrifuge step if this does not occur or add a bit more chloroform and centrifuge again*).

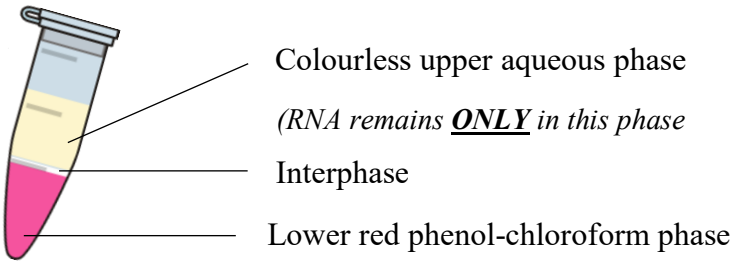

10. Transfer the upper aqueous phase containing the RNA into a new tube by angling the tube at a 45º angle and *carefully pipetting out the upper aqueous phase. (**Critical step: Avoid transferring any of the interphase or organic layer into the pipette since this will affect the quality of your RNA*).

Proceed directly to **RNA Isolation Procedure.*

C. RNA Isolation

11. Add 0.5 mL of 100% isopropanol to the aqueous phase, per 1.0 mL (1000 µL) of TRIzol® Reagent used for homogenization.
12. Incubate for 10 min (at room temperature).
13. Centrifuge at 12,000 × *g* (11,400 rpm) for 10 min @ 4ºC. (*Total RNA precipate forms a white gel-like pellet at the bottom of the tube*).
14. Discard the supernatant with a pipette or micropipettor.
15. Resuspend the pellet in 1.0 mL of 75% ethanol (analytical grade), per 1.0 mL (1000 µL) of TRIzol® Reagent used for homogenization. (*RNA can be stored @ -20ºC for up to 1 year or @ -4ºC for one week*).
16. Vortex briefly and centrifuge at 7,500 × *g* (9,000 rpm) for 5 min @ 4ºC.
17. Discard the supernatant with a pipette.

18. Air dry the RNA pellet for 5 – 10 min. (*Keep it covered with aluminium foil to avoid accidental contamination. Do not let the RNA pellet dry to ensure total solubilization of the RNA*).
19. Resuspend the RNA pellet in 20 – 50 µL of RNase-free water by pipetting up and down.
20. Incubate in a water bath or heat block at 55- 60ºC for 10 – 15 min.

Summary of Total RNA extraction

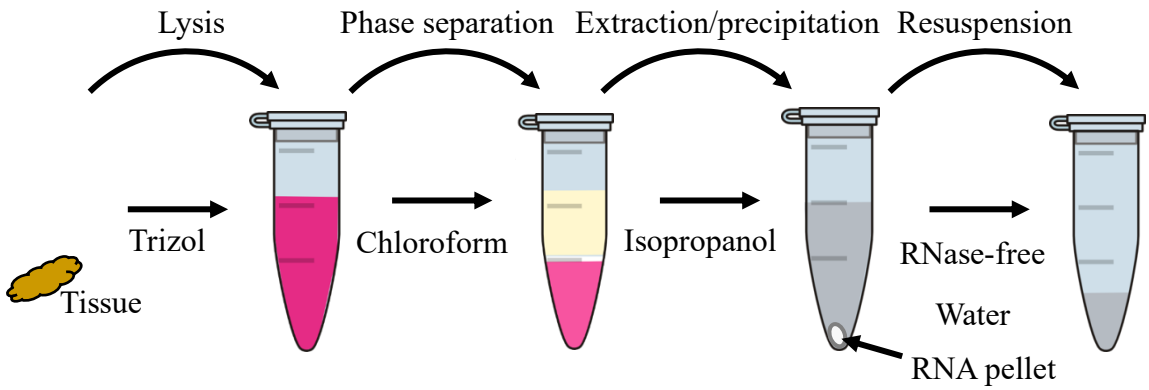

D. RNA Yield Determination

21. Determine RNA yield by measuring Absorbance at 260 nm (A_{260}) (for total nucleic acid content) and 280 nm (for sample purity determination) as follows:
    i. If using the cuvette Spectrophotometer (Biophotometer plus) method:
        a. dilute 2 µL of RNA in 98 µL RNase-free water to get 1:50 dilution, then measure absorbance at 260 nm (A_{260}) and 280 nm (A_{280}).
        b. Calculate RNA concentration using the formula A260 × dilution × 40 = µg RNA/mL.
        c. Calculate the A_{260}/A_{280} ratio. A ratio of ~ 2 is considered pure.
    ii. If using the NanoDrop One Spectrophotometer, refer to the instrument's instruction.

TOTAL RNA QUALITY ANALYSIS

Reagents and materials needed:

- *Agilent RNA 6000 Nano Kit (Agilent Technologies, #5067-1511*
- *Agilent RNA 6000 Nano Reagents (#5067-1512) and Supplies*
- *Safe-Lock Eppendorf tubes PCR clean (nuclease-free) for gel-dye mix*
- *Agilent 2100 Bioanalyzer*
- *IKA vortexer (model MS3)*
- *Sterile nuclease-free filter tips (1 – 10 µL, 10 – 100 µL)*
- *Pipettes (0.5 – 10 µL, 10 – 100 µL)*

Procedure:

1. Refer to Agilent RNA 6000 Nano Kit Quick Start Guide for detailed instructions.
2. *When loading the Ladder and Samples, remember to heat denature the samples for 1 min at 70ºC before pipetting into the wells of the Nano Chips.

RETROTRANSCRIPTION (cDNA SYNTHESIS) PROTOCOL

Reagents and materials needed:

- *AffinityScript Multiple Temperature cDNA Synthesis Kit, 50 reactions (Cat. #600107)*
- *PCR Thermal Cycler (2720 Applied Biosystems Thermal Cycler)*
- *RNase-free water*
- *Sterile nuclease-free filter tips (1 – 10 µL, 10 – 100 µL)*
- *Pipettes (0.5 – 10 µL, 10 – 100 µL)*
- *Sterile 0.2 mL (200 µL) nuclease-free PCR tubes*

Procedure:

1. Add the following components in order, to a 0.2 mL (200 µL) nuclease-free PCR tube to a total volume of 13.7 µL. (***note:*** **100 ng/µL of random primers = 0.1 µg/µL*). For example, assuming an RNA concentration of 2 µg/µL.

i.	1.0 µL	Total RNA (~ 2 µg)
ii.	9.7 µL	RNase-free water
iii.	3.0 µL	Random primers (300 ng)
	13.7 µL	**Total**

2. **Pre-RT:** In a PCR Thermal Cycler, set cycling conditions as follows:
   i. Incubation at 65ºC for 5 min.
   ii. Cool down at 25ºC (room temperature) for 10 min to allow primers to anneal to RNA.
   iii. Keep at 4ºC as you move to step 3.

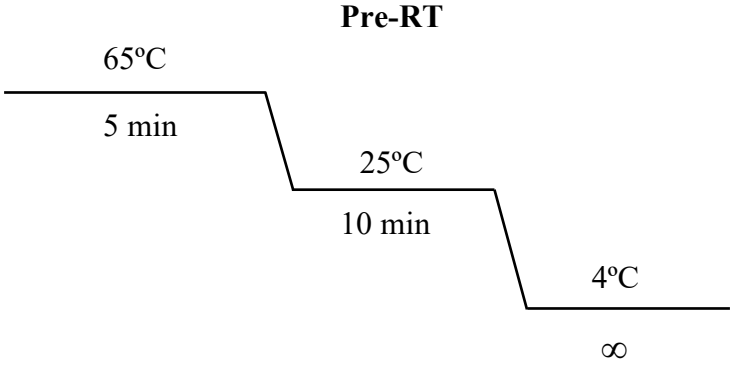

3. Add the following 4 components to the mixture to get a final reaction volume of 20 µL.

i.	2.0 µL	10x AffinityScript RT Buffer
ii.	2.0 µL	100 mM DTT
iii.	0.8 µL	100 mM dNTP mix
iv.	0.5 µL	RNase Block (40 U/µL)
v.	1.0 µL	AffinityScript Multiple Temperature Reverse Transcriptase
	20.0 µL	**Total**

** Gently mix.*

4. **RT:** In a PCR Thermal Cycler, set cycling conditions as follows:
    i. Pre-incubation at 25ºC for 10 min.
    ii. Incubate at 42 – 55ºC (50ºC seems to work well) for 1 hr (60 min).
    iii. Inactivate the reaction at 70ºC for 15 min and keep cDNA on ice or at -40ºC for subsequent use as a template in PCR.

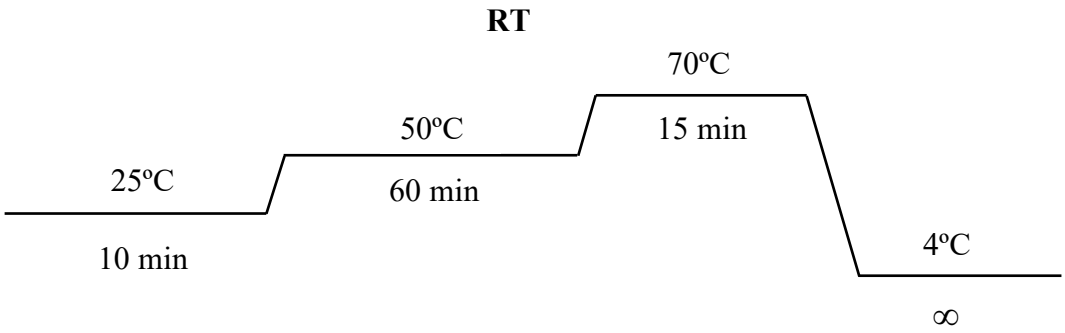

STANDARD PCR PROTOCOL

Reagents and materials needed:

- *Target lyophilized (freeze-dried) primer pairs (forward and reverse primers)*
- *Nuclease-free water*
- *10x PCR reaction buffer (without magnesium chloride)*
- *50mM magnesium chloride*
- *10 mM dNTP mix*
- *Forward primer (200 pmol/µL)*
- *Reverse primer (200 pmol/µL)*
- *Taq DNA Polymerase*
- *PCR Thermal Cycler (2720 Applied Biosystems Thermal Cycler)*
- *Heidolph Reax top mixer/vortex instrument*
- *Mini Centrifuges (Sprout Plus 120610 & 120611)*
- *Sterile nuclease-free filter & non-filter tips (1 – 10 µL, 10 – 100 µL, 100 – 1000 µL)*
- *Pipettes (1 – 10 µL, 10 – 100 µL, 100 – 1000 µL)*
- *Sterile 0.2 mL (200 µL) nuclease-free PCR tubes*
- *Assorted nuclease-free Eppendorf tubes (1.5 mL, 2.0 mL and/or 5.0 mL)*

Procedure:

A. Primer solution preparation

**All reactions to be performed on ice and use filter tips.*

1. Briefly spin tube containing lyophilized (freeze-dried) form of the primers before opening the cap to avoid loss of the primer (oligonucleotide) pellet.
2. Dissolve and dilute the primer in nuclease-free water to make a primer stock working solution of 200 pmol/µL (**Use filter tips*).

E.g., if **196 µL nuclease-free water** is required to make **100 pmol/µL** of primer solution (**primer-dependent:** see volume required to make 100 pmol/µL from the primer Oligo Synthesis Report):

$$\frac{\mathbf{196\ \mu L}}{\mathbf{2}} = \mathbf{98\ \mu L}$$

So, **98 µL nuclease-free water** required to make **200 pmol/µL** i.e., half the volume.

3. Briefly vortex and spin the prepared primer stock solution for a few seconds.
4. Keep refrigerated until ready for use *(*@4ºC ≤ 1 year or 20ºC for ≥ 2 years*).

B. Setting up the PCR reactions

1. Prepare the PCR Master Mix (+ 10% more) for each primer pair by adding/assembling the components starting from the **highest volume** component **to** the **lowest volume** component in a single Eppendorf tube. (******Easier to prepare 5x reactions since you are sure all components are in the mixture*).
2. Briefly mix (vortex) and spin (centrifuge) gently.

Reagents/Components	***Volume x1 (µL)***	***Volume x5 (µL)***	***Volume x10 (µL)***
Nuclease-free H_2O	39.6	198.0	396.0
10x PCR Reaction Buffer (without $MgCl_2$)	5.0	25.0	50.0
50 mM $MgCl_2$	1.5	7.5	15.0
10 mM dNTP Mix	1.0	5.0	10.0
Forward Primer	0.2	1.0	2.0
Reverse Primer	0.2	1.0	2.0
**Taq Polymerase*	0.5	2.5	5.0
Total	**48.0**	**240.0**	**480.0**

******Add Taq Polymerase **LAST** but **BEFORE** the **sample**.*

3. Add 48 µL of the PCR Master Mix to each 0.2 mL (200 µL) PCR tube.
4. Add 2 µL of template cDNA sample to the PCR Master Mix mixture in the PCR tubes for a total volume of 50.0 µL.
5. *Prepare a negative control (No Template Control or NTC) by adding 2 µL of nuclease-free water instead of the template cDNA sample to one PCR tube with the PCR Master Mix mixture for a total volume of 50.0 µL. *(*To verify no DNA contamination to PCR reagents*).
6. Briefly mix (vortex) and spin (centrifuge) the PCR tubes.

C. Standard PCR

1. Turn on the thermal cycler and set up/program cycling conditions as follows:

Step		*Temperature*	*Time*
Initial denaturation		95ºC	2 min
3-step cycling	*Denaturation*	95ºC	30 sec
(35 cycles)	*Annealing*	50-60ºC (Primer Temp.)	30 sec
	Extension	72ºC	30 sec
Final extension		72ºC	8 min
Stop/halt reaction (cooling)		4ºC	∞

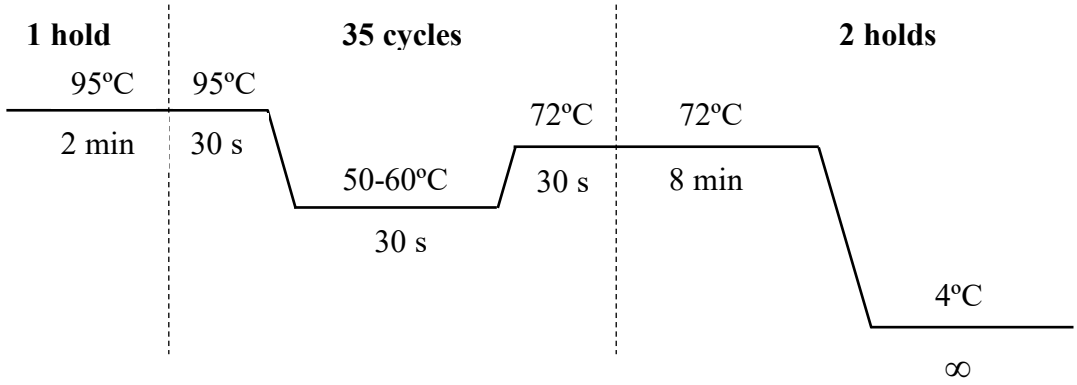

2. Place the PCR tubes in the thermal cycler and start the cycling program.
3. Remove the PCR product once thermal cycling is complete.
4. Evaluate the PCR product by gel electrophoresis (~1.5% agarose gel). (**Store at 20ºC for future use*).

GEL ELECTROPHORESIS OF PCR PRODUCT PROTOCOL

Reagents and materials needed:

- *Agarose powder for gel electrophoresis (Agarose D1 Low EEO)*
- *Tris-Acetate-EDTA (TAE) Buffer (offers faster migration of linear DNA & better resolution of supercoiled DNA)*
- *Ethidium Bromide (10 mg/mL)*
- *10X Gel Loading Buffer/Blue Juice (Bromophenol Blue).*
- *100 bp DNA Ladder*
- *Microwave*
- *Sub-Cell GT Horizontal Electrophoresis System with gel caster (UV transparent tray) and casting gates (Bio-Rad)*
- *UV transparent tray*
- *Sub-Cell GT Horizontal Electrophoresis Cell with PowerPac Basic Power Supply (Bio-Rad)*
- *E-Box V5 Gel Documentation Imaging System*
- *Sterile nuclease-free filter & non-filter tips (1 – 10 µL, 10 – 100 µL, 100 – 1000 µL)*
- *Pipettes (1 – 10 µL, 10 – 100 µL, 100 – 1000 µL)*
- *Parafilm*

Procedure:

A. Casting Agarose Gel slabs preparation

1. Level the gel caster using the levelling feet present and levelling bubble provided.
2. Disengage and slide the movable wall to the open end of the gel caster by turning and lifting the cam peg upwards.
3. Place the open edge of the UV transparent tray against the fixed wall of the gel caster.
4. Select the movable wall against the edge of the UV transparent tray and engage the cam peg to seal the open ends of the tray. (*Standard lab tape can be used to seal edges of the gel tray if gel caster is not available*).
5. Place the well comb(s) into the appropriate slots of the tray.

B. Gel preparation and electrophoresis

6. Add 1.5 g Agarose powder to a 250 mL Erlenmeyer flask or Duran lab bottle.
7. Add 100 mL 1x TAE electrophoresis buffer to the flask and swirl gently to suspend the agarose powder in the buffer.
8. Heat in microwave for 1 min 30 sec (1:30) at high settings.
9. Allow to cool in the microwave for ~ 10 min.
10. Transfer to fume hood chamber and add 10 µL of 10 mg/mL ethidium bromide. Gently swirl to mix.
11. Slowly pour the molten 1.5% agarose solution onto the UV transparent tray between the gates of the gel caster from one end or corner. Pop any bubbles with a pipette tip.
12. Let the agarose solution solidify into a gel, ~30 min @ room temperature.
13. Submerge the solidified gel in 1x TAE electrophoresis buffer inside a levelled Sub-Cell Base of the Sub-Cell GT Horizontal Cell System and carefully remove the well comb(s). The sample wells should be near the **cathode** (**Black**). PCR product will migrate from the cathode towards the **anode** (**Red**). (*Use a greater depth overlay by increasing the buffer volume with increasing voltage to avoid pH and overheating effects*).
14. Pipette 1.0 µL of 10x Gel Loading Buffer (Bromphenol Blue) onto parafilm for each sample, no template control (NTC) and DNA Ladder.
15. Add 8.0 µL PCR product and NTC to each 1 µL 10x Gel Loading Buffer.
16. Add 4.0 µL DNA Ladder to its corresponding 1 µL 10x Gel Loading Buffer on the parafilm.
17. Pipette 4.0 µL of DNA Ladder from the parafilm into the first (1st) and last lanes of the Agarose gel wells.
18. Pipette 4.0 µL of PCR product and NTC from the parafilm into the wells in between the 1st and last lane which have the DNA Ladder.
19. Connect the electrodes to the power source and turn-on the Sub-Cell GT Horizontal Cell System.
20. Run the electrophoresis on the Sub-Cell GT Horizontal Cell System, @ 100V for 30 min (10V/cm).
21. Turn-off the power, disconnect electrodes from the power source and carefully remove the gel from the Sub-Cell Base.
22. Visualize DNA fragments in the gel under UV light.

GENERAL PROTOCOL FOR WESTERN BLOTTING (IMMUNOBLOTTING)
STANDARD STOCK SOLUTIONS USED

**Prepare all stock solutions beforehand. Store all at 4ºC (including freshly made Ponceau S) to avoid microbial growth. Recommend using within 3 months for optimum results.*

0.1M EDTA (250 mL)

EDTA.Na_2.2H_2O (MW: 367.24 g/mol)	9.3 g
Milli-Q®/double-distilled H_2O (up to)	250.0 mL

**Mix for 20 – 30 min = pH ~4.0*
**Adjust pH to 8.0 slowly using NaOH pellets (~6 pellets or ~3.0 g, pH = ~7.3)*
**Autoclave solution for 15 – 20 min (121 – 124ºC) and store at 4ºC*

Lysis buffer A (Stock Solution): *50 mM Tris-HCl, 150 mM NaCl, 1 mM EDTA, 0.1% Triton X-100*

NaCl	8.8 mg
1M Tris-HCl (pH 7.6)	25.0 mL
0.1M EDTA	10.0 mL
Triton X-100 (10%)	1.0 mL
Milli-Q® H_2O (up to)	1000.0 mL

Lysis buffer B (Stock Solution): *50 mM $NaHCO_3$, 1 mM EDTA, 0.1% Absolute Ethanol, 0.1% Triton X-100*

$NaHCO_3$	84.0 mg
0.1M EDTA	10.0 mL
Absolute Ethanol (HPLC-grade)	1.0 mL
Triton X-100 (10%)	1.0 mL
Milli-Q®/double-distilled H_2O (up to)	1000.0 mL

10x Electrode running buffer (Stock Solution)

Tris-base (Trizma)	3.0 g
Glycine	14.2 g
SDS (Sodium Dodecyl Sulphate)	1.0 g
Distilled H_2O (up to)	1000.0 mL

1x Electrode running buffer (Working Solution)

10x Electrode running buffer	100.0 mL
Distilled H_2O (up to)	1000.0 mL

10x Transfer buffer (Stock Solution): *25mM Tris, 192mM glycine, pH 8.3*

Tris-base (Trizma)	30.0 g
Glycine	144.0 g
Distilled H_2O (up to)	1000.0 mL

**Adjust pH to 8.3*

1x Transfer buffer (Working Solution)

10x Transfer buffer	100.0 mL
Methanol, synthesis grade	200.0 mL
Distilled H_2O (up to)	700.0 mL

10x Tris-Buffered Saline (TBS) buffer (Stock Solution): *pH 8.0*

NaCl	87.0 g
Tris-base (Trizma)	12.0 g
Distilled H_2O (up to)	1000.0 mL

**Adjust pH to 8.0*

1x TBS with 0.05% Tween 20 (TBS-T) Wash buffer (Working Solution)

10x TBS buffer	100.0 mL
TWEEN 20	500.0 µL (0.5 mL)
Distilled H_2O (up to)	1000.0 mL

Blocking buffer (3% BSA in TBS-T)

Bovine Serum Albumin (BSA) (Sigma Aldrich, A9647-100G)	3.0 g
1x TBS-T buffer (working solution)	100.0 mL

**Do not stir or shake but allow BSA to slowly dissolve (15-30 min) @ 4ºC.*

Antibody diluent (TBS-T)

1x TBS-T buffer (working solution)	100.0 mL

Ponceau S Staining Solution (0.1% w/v in 5% acetic acid)

Ponceau S	1.0 g
Acetic Acid	50.0 mL
Milli-Q®/Deionized H_2O (up to)	1000.0 mL

Or:

Ponceau S Staining Solution (Sigma P7170)

0.1M NaOH Solution

NaOH	4.2 g
Distilled H_2O (up to)	1000.0 mL

10X Phosphate Buffered Saline (PBS) buffer (Stock Solution): *137 mM NaCl, 12 mM Phosphate, 2.7 mM KCl, pH 7.4*

NaCl	80.0 g
KCl	2.0 g
Na_2HPO_4 (dibasic anhydrous)	14.4 g **or**
$Na_2HPO_4 \cdot 2H_2O$ (dibasic dihydrate)	18.1 g **or**
$Na_2HPO_4 \cdot 7H_2O$ (dibasic heptahydrate)	27.2 g
KH_2PO_4 (monobasic anhydrous)	2.4 g
Distilled H_2O (up to)	1000.0 mL

**Adjust pH to 7.4*

1X PBS with 0.05% Tween 20 (PBS-T) Wash buffer (Working Solution)

10X PBS buffer	100.0 mL
TWEEN 20	500.0 µL (0.5 mL)
Distilled H_2O (up to)	1000.0 mL

Blocking buffer (3% BSA in PBS-T)

Bovine Serum Albumin (BSA) (Sigma Aldrich, A9647-100G)	3.0 g
1X PBS-T buffer (working solution)	100.0 mL

**Do not stir or shake but allow BSA to slowly dissolve (15-30 min) @ 4ºC.*

Antibody diluent (PBS-T)

1X TBS-T buffer (working solution)	100.0 mL

PROTEIN EXTRACTION/SAMPLE LYSATE PREPARATION PROTOCOL

Reagents needed:

- *Lysis buffer A or B*
- *EDTA-free protease inhibitor cocktail tablets (cOmplete Tablets Mini EDTA-free EASYpack).*

Procedure:

A. Tissue dissection (gonad, liver or brain)

1. Dissect the tissue on ice (2 – 8ºC), transfer to 1.5 mL round-bottomed micro-centrifuge tubes. Snap-freeze in liquid nitrogen before storing at -80ºC for future use.

B. Homogenization/lysis

1. Thaw the frozen gonad tissue samples at room temperature on ice.
2. Weigh the samples (~100mg) and place each in a 15 mL falcon tube ***sitting on/in ice***.
3. Add 4X sample volume (~400µL) ice cold **lysis buffer (A or B)** freshly supplemented with **EDTA-free protease inhibitor cocktail** (1 tablet/10 mL) into each 15 mL falcon tube with the sample.
4. Homogenize the sample, ***while in ice***, using a Tissue Grinder Potter-Elvehjem.
   i. Place the sample into a glass cylindrical mortar and place the mortar with sample into an ice bath.
   ii. Using the tissue grinder lever, lower the PTFE pestle into the glass mortar and power on the tissue grinder.
   iii. Hold the lever down, increase the speed to maximum (15,000) and slowly press the pestle onto the sample for 40 – 50 sec (*to ensure total homogenization*).
   iv. Once homogenization is complete, remove the homogenate from the glass mortar using a glass drop pipette and place into a 1.5 mL micro-centrifuge tube.
   v. Rinse the glass mortar with distilled water and wipe-down the pestle using a paper towel or tissue soaked in distilled water.
5. Repeat for subsequent samples.
6. Centrifuge the homogenate(s) for 10 min @ 4ºC, 6000 RCF (or 8,000rpm or 20 min, 4ºC 12,000 rpm) in a pre-cooled centrifuge (Eppendorf 5415R) and gently remove the micro-centrifuge tubes, ***place on ice***.
7. Transfer the supernatant (sample lysate) into fresh 1.5 mL micro-centrifuge tubes, also kept ***on ice.***
8. Mix/vortex the sample lysate before **aliquoting** (25 – 50 µL) into 0.2 mL micro-centrifuge tubes. (*Aliquoting avoids later freeze-thaw cycles. The sample lysates can now be stored @ -40ºC prior to further protein concentration analysis and SDS-PAGE if need be*).

PROTEIN CONCENTRATION ANALYSIS (LOWRY METHOD) PROTOCOL

Reagents needed:

- *Lysis buffer A or B*
- *Bio-Rad DC Protein Assay Kit (Catalogue No. 500-0116)*
- *Bovine gamma globulin (γ-Globulin) protein standard kit (Catalogue No. 500-0111)*

Procedure:

1. Prepare a **1:20 sample dilution** from the supernatant of each sample, using the same **lysis buffer** used for protein extraction.

   For **1:20 dilution**: $\frac{20}{1} = 20 = dilution\ factor$

   Since we will make a final volume of **100 µL** of sample diluted to **1:20**:

   $$\frac{100\ \mu L}{20} = 5\ \mu L$$

   5µL sample is added to **95 µL lysis buffer** to make a final total volume of **100 µL.**

2. Perform BIORAD DC Protein assay (Lowry Method) using the Microplate Assay Protocol following manufacturer's instructions (Bio-Rad Laboratories Inc.).
   i. Prepare the **working reagent A'** *(Add 20µL **reagent S** to each mL of **reagent A** that will be needed in the run. Since we only have 0.01M of EDTA (10mL EDTA in 1000mL lysis buffer) in the sample (from the buffer), this step can be omitted. If it was more than 0.025M EDTA, perform this step)*.
   ii. Prepare 3 – 5 (preferably 6 – 7) dilutions of **a protein standard** containing from 0.2mg/mL to about 1.5mg/mL protein (*we use gamma globulin (**γ-Globulin Standard**) in this example. A standard should be prepared for each assay to be performed and in the same buffer as the sample for the best of results. The linear range for **γ-Globulin is 125 – 1500 µg/mL.** *1.5 mg/mL = 1500 µg/mL = 1.5 µg/µL*).

Tube #	γ-Globulin Standard volume (µL)	Diluent (Lysis buffer) vol. (µL)	Final [Protein] (mg/mL)
0 Blank)	0	50	0
1	5	45	0.15
2	10	40	0.30
3	15	35	0.45
4	20	30	0.60
5	25	25	0.75
6	30	20	0.90
7	35	15	1.05
8	40	10	1.20
9	45	5	1,35
10	50	0	1.50

…Protein concentration analysis (Lowry method) cont'd

i. Pipette 5µL of each **protein standard dilution** and 5 µL of each **sample** into replicate wells in a clean dry microtiter plate.
ii. Add 25µL of **working reagent A'** or **reagent A** into each well.
iii. Add 200µL of **reagent B** into each well. *(If microreader has a mixing function, place plate in the reader and let the plate mix for 5s, if not, gently agitate the plate to mix the reagents. If bubbles form, pop them with a clean, dry pipette tip. Be careful to avoid cross contamination).*
iv. After 15min, **absorbance** can be read at **750nm** in a spectrophotometer (Thermo Scientific Multiskan® Spectrum) or **Nanodrop One** (*stable for 1 hour*).

	1	2	3	4	5	6	7	8	9	10	11	12
A	Blank	0.3 mg/mL	1.05 mg/mL	U	U	U	U	U	U	U	U	U
B	Blank	0.3 mg/mL	1.05 mg/mL	U	U	U	U	U	U	U	U	U
C	Blank	0.3 mg/mL	1.05 mg/mL	U	U	U	U	U	U	U	U	U
D	Blank	0.3 mg/mL	1.05 mg/mL	U	U	U	U	U	U	U	U	U
E	0.15 mg/mL	0.6 mg/mL	1.5 mg/mL	U	U	U	U	U	U	U	U	U
F	0.15 mg/mL	0.6 mg/mL	1.5 mg/mL	U	U	U	U	U	U	U	U	U
G	0.15 mg/mL	0.6 mg/mL	1.5 mg/mL	U	U	U	U	U	U	U	U	U
H	0.15 mg/mL	0.6 mg/mL	1.5 mg/mL	U	U	U	U	U	U	U	U	U

3. **Calculate** the protein concentration of the samples from the values obtained from the protein standards curve. (*If the spectrophotometer/multi-plate reader was not zeroed with the blank, average the blank values and subtract the average from the standard and unknown*).
4. Create a **Standard Curve** (plot Absorbance (nm) on y-axis vs. Concentration (mg/mL) on x-axis).
5. If the samples were diluted (e.g., 1:20), **adjust the final concentration** of the unknown samples by multiplying the concentration by the dilution factor used (e.g., 20 in this case).

PROTEIN CONCENTRATION ANALYSIS (BRADFORD METHOD) PROTOCOL

Reagents needed:

- *Lysis buffer A or B*
- *BioRad Quick Start™ Bradford 1x Dye Reagent (Cat. #500-0205)*
- *BioRad Quick Start™ Bovine Serum Albumin (BSA) Standard Set (Cat. # 500-0207)*

Procedure:

1. Prepare a 1:20 sample dilution from the supernatant of each sample, using the same **lysis buffer** used for protein extraction.

> For **1:20 dilution**: $\frac{\mathbf{20}}{\mathbf{1}} = \mathbf{20} = \boldsymbol{dilution\ factor}$
>
> Since we will make a final volume of **100 µL** of sample diluted to **1:20**:
>
> $$\frac{\mathbf{100}\ \mu\boldsymbol{L}}{\mathbf{20}} = \mathbf{5}\ \mu\boldsymbol{L}$$
>
> **5µL sample** is added to **95 µL lysis buffer** to make a final total volume of **100 µL.**

2. Perform BIORAD DC Protein assay (Bradford Method) using the **Quick Start™ Bradford Protein Assay Standard Protocol** following manufacturer's instructions (Bio-Rad Laboratories Inc.).
   i. Remove the **1x dye reagent** from 4ºC storage and let it warm to room temperature. Invert the **1x dye reagent** a few times before use.
   ii. Prepare 6 – 7 dilutions for protein standard BSA or γ-Globulin. For BSA (***Linear range for BSA is 125 – 1000 µg/mL*)**, prepare dilutions as follows:

Tube #	BSA Standard volume (µL)	Source of Standard	Diluent (Lysis Buffer) Vol. (µL)	Final [Protein] (µg/mL)
1	20	2mg/mL stock	0	2000
2	30	2mg/mL stock	10	1500
3	20	2mg/mL stock	20	1000
4	20	Tube 2	20	750
5	20	Tube 3	20	500
6	20	Tube 5	20	250
7	20	Tube 6	20	125
8	20	-	20	0

   iii. Pipette 5 µL of each **protein standard dilution** and 5 µL of each **sample** into replicate wells in a clean dry microtiter plate.
   iv. Add 250µL of **1x dye reagent** into each well.
   v. Incubate at room temperature for at least 5 min, **absorbance** can be read at **595 nm** in a spectrophotometer (Thermo Scientific Multiskan® Spectrum) or **Nanodrop One** (*stable for 1 hour*).

	1	2	3	4	5	6	7	8	9	10	11	12
A	Blank	250 µg/mL	750 µg/mL	U	U	U	U	U	U	U	U	U
B	Blank	250 µg/mL	750 µg/mL	U	U	U	U	U	U	U	U	U
C	Blank	250 µg/mL	750 µg/mL	U	U	U	U	U	U	U	U	U
D	Blank	250 µg/mL	750 µg/mL	U	U	U	U	U	U	U	U	U
E	125 µg/mL	500 µg/mL	1000 µg/mL	U	U	U	U	U	U	U	U	U
F	125 µg/mL	500 µg/mL	1000 µg/mL	U	U	U	U	U	U	U	U	U
G	125 µg/mL	500 µg/mL	1000 µg/mL	U	U	U	U	U	U	U	U	U
H	125 µg/mL	500 µg/mL	1000 µg/mL	U	U	U	U	U	U	U	U	U

vi. **Calculate** the protein concentration of the samples from the values obtained from the protein standards curve.
vii. Create a **Standard Curve** (plot Absorbance (nm) on y-axis vs. Concentration (mg/mL) on x-axis).
viii. If the samples were diluted (e.g., 1:20), **adjust the final concentration** of the unknown samples by multiplying the concentration by the dilution factor used (e.g., 20 in this case).

PROTEIN SEPARATION BY GEL ELECTROPHORESIS (SDS-PAGE) PROTOCOL

**Protocol follows manufacturer's instructions (Bio-Rad Laboratories Inc.) with some modifications.*

Reagents and materials needed:

- *1x Electrode running buffer (working solution)*
- *Beta (ß)-Mercapthanol (Sigma Aldrich, M-6250)*
- *2x Laemli Sample Buffer, SB (30 mL) (Bio-Rad, Cat. #161-0737)*
- *Precision Plus Protein Dual Colour Standard (500 µL) (Bio-Rad, Cat. #161-0374)*
- *Mini-PROTEAN® TGX pre-cast gels (12% 15µL, 15 well comb) (Bio-Rad, Cat. #.456-1046)*
- *Bio-Rad Mini-PROTEAN® Tetra Vertical Electrophoresis Cell for Mini Precast Gels, with Mini Trans-Blot® Module and PowerPac™ Basic Power Supply*
- *Protein/electrophoresis gel loading pipette tips (Bio-Rad, Cat. #2239915)*

Procedure:

A. Pre-treatment

1. Add 50 µL of **ß-Mercapthanol** to 950 µL **BIORAD 2x Laemli sample buffer** (*herein now called **sample buffer (SB)**. *It is recommended not to store ß-Mercapthanol with*

Laemli for best results, but to instead, add fresh ß-Mercapthanol to Laemli buffer each time. Use within 1 – 2 weeks and discard after 1 month).

2. Adjust the protein concentration in your sample lysate by preparing appropriate sample dilutions (**See example in table below*).
3. Add 15 µL **sample buffer (SB)** to 15 µL **BIORAD Protein Standard** for 25 µL sample volume (*1:1 ratio; if sample volume is 50 µL, mix 30 µL SB + 30 µL Standard. Extra volume is for possible loss during gel loading downstream*).
4. Add 25 µL of **sample buffer (SB)** to each 25 µL **sample lysate** (1:1 ratio) that has its protein concentration adjusted to the required final amount of protein needed when loading the sample tissue lysate into the wells of the gel **(e.g., 20 µg as shown).**

Sample #	C1 (µg/µL)	1:5 dilution conc. C1 (µg/µL)	Final Protein needed (100µg in 50µL)	C2 (µg/µL)	Final Sample Vol. V2. (µL)	Protein Volume. V1 (µL)	Lysis buffer Diluent Volume (µL)	2x Lameli buffer (Sample buffer, SB) (µL)	Final Protein in 10µL (µg)
35	28.27	5.65	50	2	50	17.7	7.3	25.0	20
36	25.47	5.09	50	2	50	19.6	5.4	25.0	20
39	25.04	5.01	50	2	50	20.0	5.0	25.0	20
40	31.37	6.27	50	2	50	15.9	9.1	25.0	20
41	22.68	4.54	50	2	50	22.0	3.0	25.0	20

5. **Boil** the standard and sample tissue **lysate in SB @ 95ºC** for **3 – 5 min**. *(*Remember to prick a hole on top of the tubes with a syringe needle to prevent the cap of the tubes from popping open when boiling*).
6. Centrifuge at 12,000 rpm in a micro-centrifuge for 1 min.

B. Gel preparation

1. **Soak** the commercial BIORAD Mini-PROTEAN® TGX **pre-cast gels** (12% 15µL, 15 well comb) in **1x Electrode running buffer** for at least 1 min.
2. **Remove the comb** by positioning your thumb on the indentation and pulling upwards in one smooth option.
3. **Remove the tape** from the bottom of the pre-cast gel cassette.

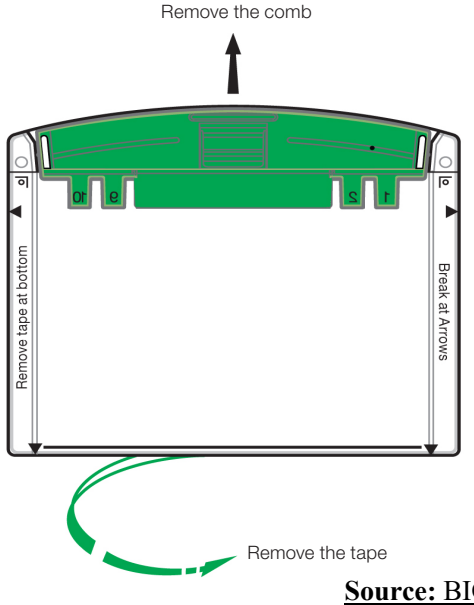

Source: BIO-RAD Laboratories Inc.

4. **Assemble the cassette** into the running module of the Mini-PROTEAN Tetra system. Add **1x Electrode running buffer** in the inner (~200 mL) and outer (~550 mL) chambers and rinse the wells with the **1x electrode running buffer** using a syringe or disposable pipette. (**Always use **FRESH** buffer*).

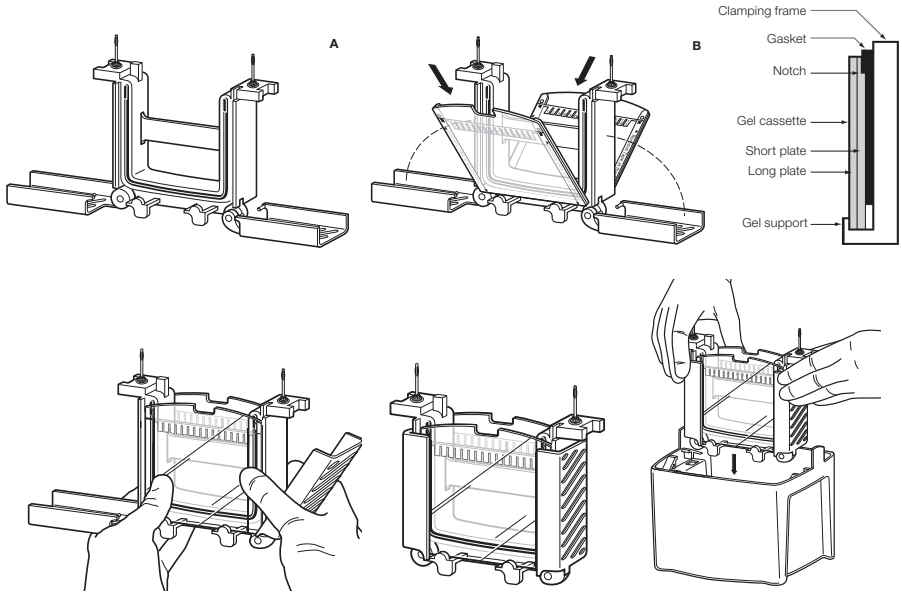

Source: BIO-RAD Laboratories Inc.

C. Running the gel

1. *Load the prepared 20 – 30 µg of the **sample lysate** (**10 µL**; **usually 10 – 15 µL or ⅔ of well volume to avoid sample lysate crossover*) and **standard** (**5 µL**; **usually half the volume of prepared samples, 7 µL for Precision Plus Dual Colour Standards*) into the wells using the gel loading tips for easier loading. Top up the wells with **1x electrode running buffer**.
2. **Run the electrophoresis** at 200V for ~30 – 45 min (*or until the dye front reaches the reference line*).
3. After completion of the run, disconnect the cell and remove the cassette.
4. **Open the cassette** by, inserting a lever between the cassette plates at indicated locations and apply downward pressure to break the seal. Do not twist the lever. Gently pull apart the two plates from the top of the cassette.

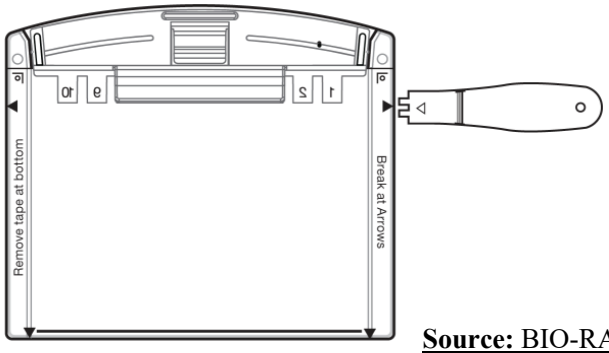

Source: BIO-RAD Laboratories Inc.

5. *Gently remove the gel from the cassette, cut away the wells from the gel and diagonally cut away a triangle gel piece next to lane 1. (**This will be your mark to remember which is lane 1*).

PROTEIN TRANSFER FROM GEL TO MEMBRANE (IMMUNOBLOTTING) PROTOCOL

Reagents and materials needed:

- *1x Transfer buffer (working solution)*
- *Methanol, synthesis grade (Scharlau, ME03000005L)*
- *Nitrocellulose membrane (Amersham™ Protran™ Premium, Cat. #10600096)*
- *Bio-Rad mini trans-blot foam pads (Cat. #1703933)*
- *Blot absorbent filter paper*
- *Bio-Rad mini trans-blot gel holder cassette*

Procedure:

1. **Equilibrate** the gels from the cassette, foam pad, filter paper and Mini Trans-Blot cassette plates in **freshly prepared 1x Transfer buffer working solution** for 10-20 min prior to blot assembly. (******Critical step:* to allow gel to shrink in methanol for 5 – 10 min to avoid ghost bands during transfer. Avoid using fresh Transfer buffer working solution due to air bubbles caused during transfer. Prepare 1 day before use*). Wet the nitrocellulose membrane just before assembly.
2. **Assemble** the Mini Trans-Blot cassette in a wet transfer system in contact with nitrocellulose membrane in the following transference order (**black plate > foam pad > filter paper > gel > nitrocellulose membrane > filter paper > foam pad > transparent or red plate**). (******Critical step:* Gel should always be closest to the black plate and membrane closet to the red plate of the cassette, with the ***cut edge for lane 1 on the right***. Cut off a triangle piece from the membrane and avoid moving the nitrocellulose membrane once placed carefully on the gel since protein will begin to blot immediately. Remember to remove air bubbles in between the gel and the membrane using a roller*).

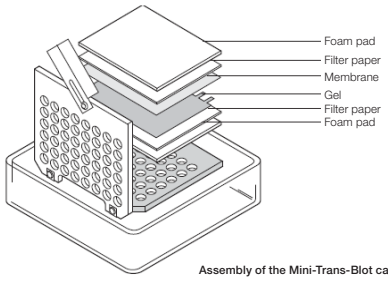

Assembly of the Mini-Trans-Blot cassette.

Source: BIO-RAD Laboratories Inc.

3. **Place** the assembled cassette **into** the **Mini Trans-Blot® transfer module and tank**. (*The transparent or red plate should face the red side of the transfer module*). Repeat steps (2) and (3) for a second blot, if needed.
4. Add the cooling unit and magnetic stir bar, fill the tank with **1x Transfer buffer working solution**. *(**Advisable not to use 1x Transfer buffer used for equilibrating the gel, etc).* Place the tank on a stir plate and begin stirring to maintain even buffer temperature and ion concentration during the transfer.
5. Connect the Mini Trans-Blot cell to a suitable power supply and begin transfer (*200 mA for 1 hour or 20V for 2.5 hours*).

IMMUNODETECTION (ANTI-BODY STAINING) PROTOCOL

Reagents and materials needed:

- *1x TBS with 0.05% Tween 20 (TBS-T) wash buffer (working solution)*
- *0.1M NaOH solution (optional but improves membrane visualization)*
- *Blocking buffer (3% BSA in TBS-T)*
- *Antibody diluent (1x TBS-T)*
- *Ponceau S Staining Solution*
- *Primary (1º) and Secondary (2º) antibodies*
- *Clarity™ Western ECL Substrate (Bio-Rad, Cat. #170-5060)*

Procedure:

1. Immediately after the transfer, carefully take out the membrane and **stain it** by placing **in Ponceau's Solution. Incubate** at **room temperature** for **5 min,** with **agitation** on a horizontal shaker. *(This is to confirm protein transfer).*
2. **Remove Ponceau's Solution** (*reusable up to 10x*) from your samples and rinse the membrane with deionized/distilled water for 20 sec (*to remove background dye*).
3. Remove the membrane from the deionized/distilled water and **visualize (take a photo).** The protein ladder and proteins should be **visibly stained red**, (*if not, there was possibly protein under-transfer or protein loss?*).
4. **Rinse the membrane in distilled water** and rapidly **immerse in** an aqueous solution of **0.1M NaOH**. Protein bands will start to disappear after 10 – 30 sec.
5. Rinse the membrane with running distilled water for 2 – 3 min before proceeding to the blocking step.
6. **Alternatively,** in the absence of 0.1M NaOH, **wash the membrane 3X** in **1x TBS-T Wash buffer** at room temperature with agitation on a horizontal shaker (gentle speed) until the red colour disappears **(5 min > 10 min > 5 min)**. Change the TBS-T after every wash cycle. (*However, you run the risk of producing non-specific background bands that are not your protein of interest. An alternative may be to use PBS as wash buffer instead of TBS-T if non-specific bands are present. Hence the preference for 0.1M NaOH*).
7. **Incubate** the membrane in **3% BSA in TBS-T blocking buffer (**5% BSA, 5% non-fat dry milk, 1% casein, or 1% gelatin can be used, but 3% BSA is usually optimum for most antibodies**)** for **1 hour** at **room temperature** with agitation on a horizontal shaker.
8. While the membrane is incubating, **dilute** the **primary (1º) antibodies** in **TBS-T** (or 1% BSA in TBS-T blocking buffer if the antibody is not so good) as specified by the manufacturer (*See below for calculations for antibody dilutions)* and **incubate** at room temperature with agitation for **1 hour** *(**vortex 20 sec. may be enough**).*

1º antibody dilutions

Volume-to-volume dilutions method

If 1:2000 dilution was suggested for western blot by manufacturer, this means 1 part of stock antibody to 999 parts of diluent (blocking buffer). For 1:2000 dilution:

$$\frac{\mathbf{2000}}{\mathbf{1}} = \mathbf{2000} = \boldsymbol{dilution\ factor}$$

If you need a final volume of 10 mL or 10,000 µL of antibody diluted to 1:2000 for your blot:

$$\frac{final\ volume\ you\ want}{dilution\ factor} = volume\ of\ stock\ antibody\ to\ add\ to\ your\ diluent$$

$$\frac{\mathbf{10,000\ \mu L}}{\mathbf{2000}} = \mathbf{5\ \mu L}$$

So, you want to add **5 µL** of **stock antibody** to **9,995 µL** of **diluent (blocking buffer)** for a final volume of **10,000 µL** or **10 mL of 1º antibody (1:2000).**

9. After incubating the membrane in blocking buffer, remove the blocking buffer from your sample.
10. **Wash the sample or membrane blot 3X** in **TBS-T Wash buffer** at room temperature with agitation (5 min > 10 min > 5 min).
11. Add enough **primary (1º) antibody** as prepared with appropriate dilutions (see example in step 8 above) to cover your sample and **incubate overnight (18 – 24 h) at 4ºC**. *(Sample can be incubated in zip-lock bags if the membrane was cut into small strips. You can put your experiment in the refrigerator until the following day).*
12. The following day, **dilute** the **secondary (2º) antibody in TBS-T** (or 1% BSA in TBS-T blocking buffer) as specified by the manufacturer (1:5000 – 1:20000 dilution) *(**Since rabbit antibody was used for 1º antibodies, in this case, recommended to use goat anti-rabbit 2º antibody. Incubate at room temperature with agitation for 1 hour. **vortex 20 sec. may be enough**).*

Since we already have **2º antibodies** diluted into **1:50 dilutions**, we need to make 10 mL or 10,000 µL of a **1:5000 dilution**.

$$\frac{Final\ dilution}{Initial\ dilution} = dilution\ factor \qquad \textbf{Thus,} \quad \frac{5000}{50} = 100$$

$$\frac{final\ volume\ you\ want}{dilution\ factor} = volume\ of\ stock\ 2º\ antibody\ (1{:}50)\ to\ add\ to\ your\ diluent$$

$$\frac{\mathbf{10,000\ \mu L}}{\mathbf{100}} = \mathbf{100\ \mu L}$$

Or,

$\boldsymbol{C1 \times V1 = C2 \times V2}$ $\qquad$ $\boldsymbol{Thus,}$ $\qquad \frac{1}{50} \times V1 = \frac{1}{5000} \times 10{,}000\ \mu L$

$$\boldsymbol{V1 = \frac{10,000\ \mu L}{5000} \times 50 = 100\ \mu L}$$

So, we need to add **100 µL** of **2º anti-Rb antibody (1:50)** to **9,900 µL TTBS** for a final volume of **10,000 µL** or **10 mL** of **2º antibody (1:5000)**.

13. **Remove** the 1º antibody staining solution from your samples (membrane).
14. **Wash** the 1º antibody-treated membrane 3X in **TBS-T Wash buffer** at room temperature with agitation (5 min > 10 min > 5 min). (*Remember to use a separate plastic container for each wash cycle to avoid remnants of 1º antibody that may have leached into the plastic, thereby providing for a cleaner blot).*
15. Add enough **secondary (2º) antibody staining** to cover your samples and incubate for 1 hour at room temperature.
16. **Wash** the 2º antibody-treated membrane 3X in **TBS-T Wash buffer** at room temperature with agitation (5 min > 10 min > 5 min).
17. ***Develop the blot** by treating the sample membrane for **2 min** with ~600 µL of **ECL reagent** detection kit (1:1 ratio) per membrane, enough to cover the entire surface of the membrane (300 µL Luminor/enhancer solution + 300 µL Peroxide solution). (1 min could be enough).
18. Place the membrane in-between two transparent plastic sheets and remove excess ECL. *(This is important to avoid pronounced background signal of ECL. Do not produce bubbles between the plastics and the membrane while doing this).*
19. Visualize and image your samples under chemiluminescence light. *(For the first trial, general exposure conditions are fine. However, manually adjust your time of exposure in the reader for each antibody/membrane).*
    *(*For total protein normalization, acquire image before developing the blot in step 17)*

IMAGING AND DATA ANALYSIS (CHEMIDOC XRS SYSTEM)

1. Set the lever position of the **BIORAD ChemiDoc XRS System** to WB (no filter) signifying western blot).
2. Open the system tray and insert plastic sheets with the membrane (s).
3. Go to **File** > **ChemiDoc XRS**
4. In ChemiDoc XRS,
    i. > **Step I – Select Application** > **Select…** > **Chemi Hi Sensitivity**
    ii. Check on the machine, that the following settings have been selected:
        a. **Lens control speed = SLOW**
        b. **Light Source = Epi-White**
    iii. > **Step II – Position Gel** > **Live Focus** (adjust the Iris, Zoom and Focus to capture the membrane image properly).
    iv. Click **Freeze.**
    v. > **Step III – Acquire Image** > **Live Acquire**
        a. Total Exposure = 200 sec
        b. Starting Exposure = 10 sec (*can be adjusted later as needed)*
        c. No. of exposures = 5
        d. **Turn-off** the light source **Epi-White** and **click OK.**
    vi. Choose location/directory to save your images on the computer.
    vii. Export the images acquired as **TIFF** and as **JPEG** to a **USB flash drive**.
5. **To check the ladder** and superimpose it on the one of the saved images.
    i. **Turn on** the light source **Epi-White**.
    ii. In **ChemiDoc XRS** application: > **Step III – Acquire Image >** Set Exposure value to **0.001** > **Then** click **Manual Acquire.**
    iii. Once the image opens, go to the menu bar on top > **Image > Transform >** Select **Invert display.** Your ladder image will now be visible.
    iv. Return to the menu bar > **View > Multichannel Viewer**
    v. A new window will open with 3 channels, Red, Green and Blue. We will only use the Red and Green channels.
        a. > Red Channel > select western blot image to display > Select **Display Red Channel.**
        b. > Green Channel > select the ladder image obtained from manual acquire ((iii) above) to display > Select **Display Green Channel.**
    vi. When the new window opens, maintain the settings, select **> Export TIFF > Save > DONE**. The image will be saved in the location/directory previously selected for all your images.

TOTAL GENOMIC DNA EXTRACTION PROTOCOL

**Protocol follows manufacturer's instructions (Qiagen) with some modifications.*

Reagents and materials needed:

- *DNeasy® Blood & Tissue Kit (Qiagen, Cat. #69504)*
- *Eppendorf® Thermomixer Compact*
- *Biofuge Pico Heraeus Ultracentrifuge*
- *Heidolph Reax top mixer/vortex instrument*
- *UVP CL-1000 UV Crosslinker*
- *Sterile nuclease-free filter & non-filter tips (1 – 10 µL, 10 – 100 µL, 100 – 1000 µL)*
- *Pipettes (1 – 10 µL, 10 – 100 µL, 100 – 1000 µL)*

Procedure:

**All centrifugation steps carried out at room temperature (15 – 25ºC).*

**All pipettes, tips and microcentrifuge should be sterilised in UVP CL-1000 UV Crosslinker for ~8 min prior to start of DNA extraction.*

1. Cut ≤ 25 mg of tissue (brain, gill, gonad, muscle or liver) into small pieces and place into pre-labelled 1.5 mL microcentrifuge tubes. (*Use a scalpel and forceps, applying aseptic techniques i.e., heat the scalpel blade in a flame and cool in distilled water before use*).

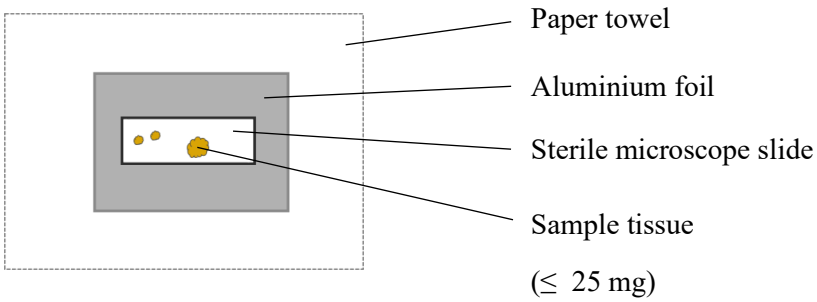

2. Add 180 µL Buffer ATL using sterile filter tips.
3. Add 25 µL Proteinase K.
4. Vortex and incubate overnight @ 56ºC in a thermomixer until completely lysed.
5. Label DNeasy mini spin columns and another set of 1.5 mL microcentrifuge tubes.
6. After overnight incubation (step 4), vortex samples for 15 sec.
7. Add 200 µL Buffer AL using sterile filter tips and mix thoroughly by vortexing.
8. Using non-filter tips, add 200 µL of analytical grade absolute ethanol (96 – 100%) and mix thoroughly by vortexing for 10 sec. (**precipitate does not interfere with DNeasy procedure and can be re-dissolved in Buffer AL and Buffer ATL*).
9. Pipette (non-filter tips) mixture into a DNeasy mini spin column placed in a 2.0 mL collection tube. Centrifuge for @ ≥ 6,000 $x\,g$ (8,000 rpm) for 3 min. Discard the flow-through and collection tube.
10. Place spin column into new 2.0 mL collection tube. Add 500 µL Buffer AW1. Centrifuge for 1 min @ 8,000 rpm. Discard the flow-through and collection tube.
11. Place spin column into new 2.0 mL collection tube. Add 500 µL Buffer AW2. Centrifuge for 3 min @ 13,000 rpm. Discard the flow-through and collection tube.

12. Transfer the spin column to new 1.5 mL or 2.0 mL microcentrifuge tubes.
13. Elute the DNA twice (2X):
    i. Elution I: Add 100 µL Buffer AE to the centre of the spin column membrane. Incubate 1 min @ room temperature (15 – 25ºC), centrifuge @ 8,000 rpm for 3 min.
    ii. Elution II: Add 100 µL Buffer AE to the centre of the spin column membrane. Incubate 1 min @ room temperature (15 – 25ºC), centrifuge @ 8,000 rpm for 3 min.
14. Discard the spin column. DNA will be in the 1.5 mL or 2.0 mL microcentrifuge tube.
15. **Proceed directly** to **gel electrophoresis** to assess DNA quality (**no PCR**). (*Samples can be stored overnight at 2 - 8ºC and proceed to gel electrophoresis the following day or at -20ºC for longer storage*).

2. EXTRACTED DNA QUALITY ASSESSMENT BY GEL ELECTROPHORESIS

CASTING AGAROSE GEL SLABS PREPARATION

Reagents and materials needed:

- *Sub-Cell GT Horizontal Electrophoresis System with gel caster and casting gates (Bio-Rad)*
- *Standard lab tape in lieu of gel caster*
- *UV transparent tray*

Procedure:

1. Level the gel caster using the levelling feet present and levelling bubble provided.
2. Disengage and slide the movable wall to the open end of the gel caster by turning and lifting the cam peg upwards.
3. Place the open edge of the UV transparent tray against the fixed wall of the gel caster.
4. Select the movable wall against the edge of the UV transparent tray and engage the cam peg to seal the open ends of the tray. (*Standard lab tape can be used to seal edges of the gel tray if gel caster is not available*).
5. Place the comb(s) into the appropriate slots of the tray.
6. Prepare the desired amount and concentration of agarose in 1x electrophoresis buffer.

DNA GEL PREPARATION AND GEL ELECTROPHORESIS

Reagents and materials needed:

- *Agarose powder for gel electrophoresis (Agarose D1 Low EEO)*
- *Tris-Borate-EDTA (TBE) Buffer (stronger buffering capacity for longer high voltage) or*
- *Tris-Acetate-EDTA (TAE) Buffer (offers faster migration of linear DNA & better resolution of supercoiled DNA)*

- *GelRed® Nucleic Acid Stain (0.5 mL) (Biotium GelRed® 10,000X in water, Cat. #41003) stock solution (Dilute to 1:3 or ¼ dilution and adjusted as necessary).*
- *Microwave*
- *Sub-Cell GT Horizontal Electrophoresis Cell with PowerPac Basic Power Supply (Bio-Rad)*
- *Gel imaging System*
- *Sterile nuclease-free filter & non-filter tips (1 – 10 µL, 10 – 100 µL, 100 – 1000 µL)*
- *Pipettes (1 – 10 µL, 10 – 100 µL, 100 – 1000 µL)*

Procedure:

1. Determine the amount of agarose (in grams) to make the desired agarose gel concentration.
2. For 1% Agarose Gel, add 1.0 g Agarose powder to a 250 mL Erlenmeyer flask or Duran lab bottle.
3. Add 100 mL 1x electrophoresis buffer (TBE Buffer) to the flask and swirl gently to suspend the agarose powder in the buffer.
4. Place the gel solution in the microwave, set medium-high settings and heat for 3 min. (*Fastest and safest way to dissolve agarose*).
5. Once all the agarose is dissolved, set aside and cool to 60ºC in a fume hood.
6. Add 1.0 µL GelRed (*1:3 or 1:4 diluted from stock solution*) to the 60ºC agarose solution and gently swirl ensuring no bubbles.
7. Slowly pour the molten agarose solution onto the UV transparent tray between the gates of the gel caster from one end or corner. Pop any bubbles with a pipette tip.
8. Let the agarose solution solidify into a gel, 20 – 40 min @ room temperature.
9. Carefully remove the comb(s) from the solidified gel.
10. Place the gel onto a levelled Sub-Cell Base of the Sub-Cell GT Horizontal Cell System so that the sample wells are near the **cathode** (**Black**). DNA will migrate from the cathode towards the **anode** (**Red**).
11. Submerge the gel beneath 2 – 6 mm of 1x electrophoresis buffer (TBE Buffer). (*Use a greater depth overlay (increase buffer volume) with increasing voltage to avoid pH and overheating effects*).
12. Carefully load or pipette 2.0 µL of your DNA (10 – 100 ng) samples into gel wells and run the electrophoresis on the Sub-Cell GT Horizontal Cell System, @ 150V for 90 min.
13. Turn-off the power, disconnect electrodes from the power source and carefully remove the gel from the Sub-Cell Base.
14. Visualize DNA fragments in the gel under UV light.

STANDARD PCR – MICROSATELLITE TESTING PROTOCOL

**All preparation work carried out in DNA/RNA UV cleaner chamber (BIOSAN UV/TC-AR DNA/RNA UV-cleaner box).*

Reagents and materials needed:

- *100 µM dNTP mix stock solution (Bioline, BIO-39053)*

- *Bovine Serum Albumin (BSA) Stock Solution (Roche Diagnostics, Ref # 10711454001)*
- *100 µM Forward and Reverse Primers stock solutions of each microsatellite*
- *Taq Polymerase (BIOTAQ™ DNA polymerase – BIO-21040)*
- *Bio-Rad C1000 Touch Thermal Cycler*
- *Heidolph Reax top mixer/vortex instrument*
- *Beckman Coulter Microfuge® 16 Centrifuge*
- *DNA/RNA UV cleaner chamber (BIOSAN UV/TC-AR DNA/RNA UV-cleaner box).*
- *Eppendorf centrifuge 5810R*
- *Sterile nuclease-free filter & non-filter tips (1 – 10 µL, 10 – 100 µL, 100 – 1000 µL)*
- *Pipettes (1 – 10 µL, 10 – 100 µL, 100 – 1000 µL)*
- *Finnpipette™ Novus Electronic Multichannel Pipette, 5 – 50 µL (Thermo Scientific, Cat. #46300300)*
- *Finnpipette™ Novus Electronic Single Channel Pipette, 5 – 50 µL (Thermo Scientific, Cat. #46200200)*
- *96-well PCR plates*
- *Eppendorf 5390 Plate Sealer*
- *Adhesive aluminium foil sheets for PCR plates (Thermofisher, Cat. #AB0626)*

Procedure:

9. Sterilise pipettes, 96-well PCR plates, filter tips microcentrifuge tubes and nuclease-free water under a DNA/RNA UV cleaner. Filter tip box and nuclease-free water bottle should be opened during this process.
10. Prepare 3 aliquots of 10 µM dNTPs mix from 100 µM dNTP mix stock solution (*should be enough, if not, more can be made later*):

30 µL dNTP mix (100 µM stock) + 270 µL nuclease-free H_2O = 300 µL dNTPs (10 µM)

11. Prepare 3 aliquots of BSA by diluting BSA stock solution with nuclease-free water (1:1). (*Should be enough, if not, more can be made later*).

50 µL BSA stock + 50 µL nuclease-free H_2O = 100 µL BSA

12. From 100 µM stock primer solution, prepare/aliquot 20 pmol (20 µM) primers in 50 µL nuclease-free water:

$$\boldsymbol{C1 \times V1 = C2 \times V2} \qquad \boldsymbol{Thus,} \qquad 100\ \cancel{\mu M} \times V1 = 20\ \cancel{\mu M} \times 50\ \mu L$$

$$\boldsymbol{V1 = \frac{1{,}000\ \mu L}{100} = 10\ \mu L}$$

10 µL Primer (100 µM stock) + 40 µL nuclease-free H_2O = 50 µL Primer (20 µM)

13. Prepare the PCR Master Mix for each primer pair as below in the order shown and remember to briefly vortex and spin.

Reagents/Components	***Volume x1 (µL)***	***Volume x10 (µL)***	***Volume x11 (µL)***
Nuclease-free H_2O	13.4	134.0	147.4
10 µM dNTPs mix	2.0	20.0	22.0
$MgCl_2$	1.25	12.5	13.75
10x Reaction Buffer	2.5	25.0	27.5
Forward Primer	0.3	3.0	3.3
Reverse Primer	0.3	3.0	3.3
BSA	1.0	10.0	11.0
**Taq Polymerase*	0.25	2.5	2.75
Sample DNA	1.0	-	-
Total	**22.0**		

Add Taq Polymerase **LAST but **BEFORE** the **sample**.*

14. Pipette 20 µL of the PCR Master Mix into each well of a sterile 96-well PCR plate (non-skirted). (*Perform this process under a UV cleaner chamber).*
15. Pipette 1.0 µL of DNA sample into the PCR Master Mix in each well of the 96-well PCR plate. *(On a separate bench, under a different UV cleaner chamber).*
16. Cover the plate with heat sealing adhesive aluminium foil sheets for PCR plates (heat seal ~ 20 sec using the Eppendorf 5390 Plate Sealer).
17. Briefly centrifuge the heat-sealed 96-well PCR plate at maximum speed or 4,000 rpm, few seconds.
18. Switch on thermal cycler and set up/program the cycling conditions as follows:

Step		***Temperature***	***Time***
Initial denaturation		95ºC	4 min
3-step cycling	*Denaturation*	94ºC	30 sec
(35 cycles)	*Annealing*	57ºC (Primer Temp.)	30 sec
	Extension	72ºC	45 sec
Final extension		72ºC	7 min
Stop/halt reaction (cooling)		4ºC	∞

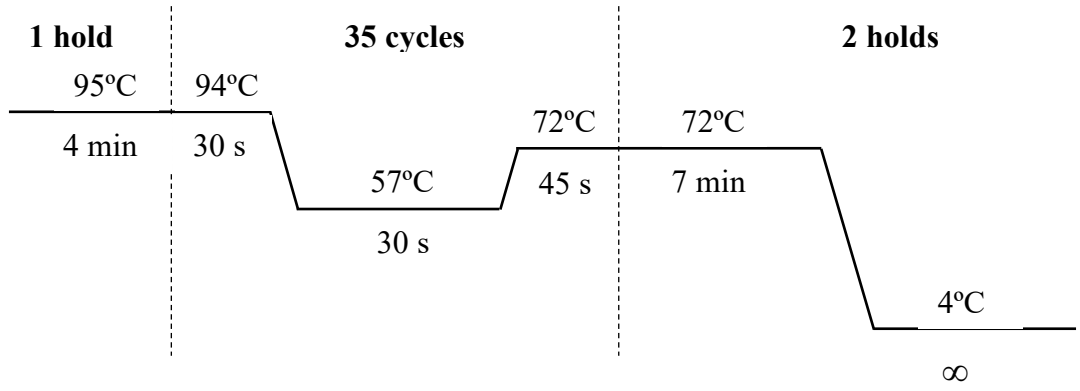

19. Place heat-sealed 96-well PCR plate with your sample in the thermal cycler and start the cycling program.
20. After amplification, proceed to gel electrophoresis (2% agarose gel). *(Store overnight at 2 - 8ºC and proceed to gel electrophoresis the following day or at -20ºC for longer storage).*

GEL ELECTROPHORESIS AFTER STANDARD PCR PROTOCOL

Reagents and materials needed:

- *Agarose powder for gel electrophoresis (Agarose D1 Low EEO)*
- *Tris-Borate-EDTA (TBE) Buffer*
- *GelRed® Nucleic Acid Stain (0.5 mL) (Biotium GelRed® 10,000X in water, Cat. #41003) stock solution (Dilute 1:1).*
- *10X Loading Buffer/Blue Juice (Takara Bio, SD0012).*
- *DNA Ladder, HyperLadder™ 100bp (Bioline, BIO-33056)*
- *Microwave*
- *Sub-Cell GT Horizontal Electrophoresis Cell with PowerPac Basic Power Supply (Bio-Rad)*
- *Gel imaging System*
- *Sterile nuclease-free filter tips & non-filter tips (1 – 10 µL, 10 – 100 µL, 100 – 1000 µL)*
- *Pipettes (1 – 10 µL, 10 – 100 µL, 100 – 1000 µL)*
- *Parafilm*

Procedure:

1. After setting up the casting tray, prepare 2% Agarose gel (*If using Sub-Cell GT, 3.2 g Agarose powder in 160 mL TBE buffer and if using the wide mini–Sub-Cell GT, 2.0 g Agarose in 100 mL TBE buffer*). Set medium-high settings in microwave and heat for 3 min). Allow the agarose solution to cool to 60ºC in a fume hood.
2. Add 1.1 µL GelRed (*1:1 diluted from stock solution*) to the 60ºC agarose solution, gently swirl slowly pour the molten agarose solution onto the UV transparent tray. Pop any bubbles with a pipette tip and allow the agarose solution to solidify into a gel, 15 min @ room temperature.
3. Carefully remove the comb(s) from the solidified gel submerged in 1x TBE electrophoresis buffer in a levelled Sub-Cell Base of the Sub-Cell GT Horizontal Cell System.
4. Pipette 1.5 µL of 10x Loading Buffer onto parafilm and add 2.0 µL DNA sample from PCR into the 10x Loading Buffer.
5. Pipette 2.0 µL of DNA Ladder into the first (1st) and last lanes of the Agarose gel wells.
6. Pipette 3.5 µL of DNA sample + 10x Loading Buffer Mix from the parafilm into the wells in between the 1st and last lane which have the DNA Ladder.
7. Connect the electrodes to the power source and turn-on the Sub-Cell GT Horizontal Cell System.
8. Run the electrophoresis on the Sub-Cell GT Horizontal Cell System, @ 150V for 90 min.
9. Turn-off the power, disconnect electrodes from the power source and carefully remove the gel from the Sub-Cell Base.
10. Visualize DNA fragments in the gel under UV light.